JAERI - M
89-026

NEANDC(J)-133"U"
INDC(JPN)-120/L

PROCEEDINGS OF THE 1988 SEMINAR ON NUCLEAR DATA

March 1989

(Ed.) Tsuneo NAKAGAWA and Atsushi ZUKERAN*

日 本 原 子 力 研 究 所
Japan Atomic Energy Research Institute

JAERI-Mレポートは，日本原子力研究所が不定期に公刊している研究報告書です。
入手の問合わせは，日本原子力研究所技術情報部情報資料課（〒319-11茨城県那珂郡東海村）あて，お申しこしください。なお，このほかに財団法人原子力弘済会資料センター（〒319-11 茨城県那珂郡東海村日本原子力研究所内）で複写による実費頒布をおこなっております。

JAERI-M reports are issued irregularly.
Inquiries about availability of the reports should be addressed to Information Division, Department of Technical Information, Japan Atomic Energy Research Institute, Tokai-mura, Naka-gun, Ibaraki-ken 319-11, Japan.

編集兼発行　日本原子力研究所
印　　刷　㈱原子力資料サービス

JAERI-M 89-026

Proceedings of the 1988 Seminar on Nuclear Data

(Ed.) Tsuneo NAKAGAWA and Atsushi ZUKERAN*

Japanese Nuclear Data Committee
Tokai Research Establishment
Japan Atomic Energy Research Institute
Tokai-mura, Naka-gun, Ibaraki-ken

(Received February 3, 1989)

The 1988 Seminar on Nuclear Data was held at Tokai Research Establishment of Japan Atomic Energy Research Institute, on December 8 and 9, 1988. This Seminar was organized by Japanese Nuclear Data Committee (JNDC) and Nuclear Data Center, JAERI. In an oral session, reviews of activities of JNDC and status of JENDL-3 were presented and problems on adjustment of cross-section data were discussed in connection with JENDL-3. In addition, several topical talks were also given. In a poster session, eighteen papers on evaluation and measurement were presented and fruitful discussions were made. In this proceedings, thirty-six papers given in the seminar are compiled.

Keywords: Nuclear Data, JENDL, Evaluation, Measurement, Adjustment, Proceedings

* Energy Research Laboratory, Hitachi Ltd.

JAERI－M 89－026

1988年核データ研究会報文集

日本原子力研究所東海研究所
シグマ研究委員会
(編)中川　庸雄・瑞慶覧　篤*

（1989年2月3日受理）

1988年核データ研究会は1988年12月8日と9日の両日，日本原子力研究所東海研究所において開催された。この研究会はシグマ委員会と原研核データセンターによって開かれたものである。口頭発表では，シグマ委員会の活動やＪＥＮＤＬ－３の現状が紹介され，ＪＥＮＤＬ－３との関連で断面積データの調整上の問題が議論された。さらに，トピックス的な講演もなされた。ポスターセッションでは，評価や測定に関する18件の報告があり有意義な議論がなされた。本報文集は研究会で報告された35件の論文をまとめたものである。

東海研究所：〒319－11 茨城県那珂郡東海村白方字白根２－４
＊（株）日立製作所

Purogram Committee

Atsushi ZUKERAN(Chairman)	(Energy Research Laboratory, Hitachi, Ltd.)
Tokio FUKAHORI	(Japan Atomic Energy Research Institute)
Kazuki HIDA	(Nippon Atomic Industry Group Co., Ltd)
Masayuki IGASHIRA	(Tokyo Institute of Technology)
Junichi KATAKURA	(Japan Atomic Energy Research Institute)
Katsuhei KITAO	(National Institute of Radiological Sciences)
Hiroshi MAEKAWA	(Japan Atomic Energy Research Institute)
Hiroyuki MATSUNOBU	(Sumitomo Atomic Energy Industries, Ltd.)
Motoharu MIZUMOTO	(Japan Atomic Energy Research Institute)
Tsuneo NAKAGAWA	(Japan Atomic Energy Research Institute)
Hisashi NAKAMURA	(Fuji Electric Co., Ltd.)
Masaharu NAKAZAWA	(University of Tokyo)
Makoto SASAKI	(Mitsubishi Atomic Power Industries, Ltd.)
Keiichi SHIBATA	(Japan Atomic Energy Research Institute)
Hideki TAKANO	(Japan Atomic Energy Research Institute)

プログラム委員会

瑞慶覧　篤（委員長）	((株）日立製作所エネルギー研究所)
深堀　智生	(日本原子力研究所)
肥田　和毅	(日本原子力事業（株）)
井頭　政之	(東京工業大学)
片倉　純一	(日本原子力研究所)
喜多尾憲助	(放射線医学総合研究所)
前川　　洋	(日本原子力研究所)
松延　廣幸	(住友原子力工業（株）)
水本　元治	(日本原子力研究所)
中川　庸雄	(日本原子力研究所)
中村　　久	(富士電機（株）)
中沢　正治	(東京大学)
佐々木　誠	(三菱原子力工業（株）)
柴田　恵一	(日本原子力研究所)
高野　秀機	(日本原子力研究所)

Contents

目　　次

1. Introduction

The 1988 Seminar on Nuclear Data was held at the Tokai Research Establishment of the Japan Atomic Energy Research Institute, on December 8 - 9, 1988. The program of the seminar is as follows:

December 8 (Thursday) Speaker

1. Opening Address

11:00 - 11:10 A. Zukeran (Hitachi)

2. 25th Anniversary of Japanese Nuclear Data Committee and JENDL

Chairman: R. Nakasima (Hosei Univ.)

11:10 - 11:40 2.1 Activities of Japanese Nuclear Data Committee for 25 years and Its Perspective S. Igarasi (JAERI)

11:40 - 12:00 2.2 Present Status of JENDL-3 K. Shibata (JAERI)

12:00 - 13:00 Lunch

3. Consistency between Microscopic Data and Integral Data

Chairman: Y. Kikuchi (JAERI)

13:00 - 13:25 3.1 Virtues of Cross-Section Adjustment Method and Present Status of the Utilization of the Method in Core Design T. Kamei (NAIG)

13:25 - 14:00 3.2 Application of Adjustment Method to JENDL-3T M. Takamoto (Osaka Univ.)

14:00 - 14:40 3.3 Experimental Error on Integral Data of Reactor Physics Experiments at FCA T. Osugi (JAERI)

14:40 - 15:10 3.4 On Uncertainties of Evaluated Nuclear Data Y. Kanda (Kyushu Univ.)

15:10 - 15:30 3.5 Comment on Uncertainties of Group Averaged Cross-sections M. Nakazawa (Univ. of Tokyo)

15:30 - 15:45 Coffee Break

4. Discussion

15:45 - 17:30 Chairman: A. Zukeran (Hitachi)

18:00 - 20:00 Reception (at the Akogigaura club)

December 9 (Friday) Speaker

5. Poster Session

9:00 - 10:20 (18 papers were presented)

6. Topics I: Present Status and Future of Databases

Chairman: M. Nakagawa (JAERI)

10:30 - 11:10 6.1 The Past and Future of Material Databases*
S. Iwata (Univ. of Tokyo)

11:10 - 11:50 6.2 Current Status of Database Development in JAERI
Y. Kikuchi (JAERI)

12:00 - 13:00 Lunch

7. Topics II: Theory and Evaluation of Nuclear Data

Chairman: S. Iwasaki (Tohoku Univ.)

13:00 - 13:45 7.1 Current Topics of Electromagnetic Transitions in Neutron Capture Reactions
H. Kitazawa (Tokyo Inst. of Technol.)

13:45 - 14:30 7.2 JENDL Special Purpose Data Files and Related Nuclear Data
S. Iijima (NAIG)

14:30 - 14:45 Coffee Break

8. Topics III: Others

Chairman: I. Kimura (Kyoto Univ.)

14:45 - 15:30 8.1 Experimental Analyses by Use of JENDL-3T for Joint PNC/USDOE Criticality Safety Experiments
N. Fukumura (PNC)

15:30 - 16:15 8.2 Synchrotron Radiation Project and Related Nuclear Data and Atomic and Molecular Data
Y. Nakai (JAERI)

9. Closing Address

16:15 - 16:20 S. Igarasi (JAERI)

In this proceedings, the papers and comments presented in the oral session are given in Chapter 2 and those in the poster session in Chapter 3. The paper of the presentation marked with an asterisk (*) is not included in this proceedings because it was not available by the deadline.

2. Papers Presented in Oral Session

2.1 25th Anniversary of Japanese Nuclear Data Committee, and JENDL

2.1.1 Activities of Japanese Nuclear Data Committee for Twenty-Five Years, and Its Perspective

Sin-iti IGARASI

Japan Atomic Energy Research Institute
Tokai-mura, Naka-gun, Ibaraki-ken

This year, 1988, is a commemorable year of 25th for the Japanese Nuclear Data Committee (JNDC) which was organized in 1963. It is also memorable that the International Conference on Nuclear Data for Science and Technology was held this year at Mito City. On these background, this Seminar was held with special plans for celebration of the 25th anniveresary of foundation of the JNDC. This report is one of the plans, and will try to review the activities of JNDC in the past, survey the present situation of the nuclear data field in the world, and propose some fearless plans for the future.

I. Introduction

This year, 1988, is a commemorable year of 25th for the Japanese Nuclear Data Committee (JNDC) which was organized in 1963 as a standing committee of the Atomic Energy Society of Japan (authorized on January 28, 1963) and a research committee of the Japan Atomic Energy Research Institute (authorized on February 28, 1963). It is also memorable that the International Conference on Nuclear Data for Science and Technology was held this year at Mito City, which would be an outstanding event in the brilliant history of the JNDC. On these background, the organizing committee of this Seminar made special plans for celebration of the 25th anniversary of foundation of the JNDC, and nominated the author to give an introductory commemorative talk.

Although the author does not always think he is the most appropriate person to play such honorable role as senior members do, he will try to review the activities of JNDC in the past, survey the present situation of the nuclear data field in the world, and propose some fearless plans for the future. In particular, he believes that it is important to discuss the future activities of the JNDC, and this Seminar must be a good occasion to do it seriously, because we should take heed in such a time of mirth as we could have two happy events.

In the next chapter of this report, a review of the activities in the JNDC is made together with some related matters. The activities in the recent ten years are described with particular emphasis. In this period, nuclear data evaluation for Japanese Evaluated Nuclear Data Library (JENDL) was carried out enthusiastically by the members of the JNDC, and the three versions of the JENDL were completed consecutively. Hence, the Chapter II is devoted mainly to introduce the activities for the JENDL.

Needless to say, circumstances of the nuclear energy fields are very severe in the world at present. In the nuclear data field, the situation is similar, and in particular the average age of the researchers becomes higher, because of few young researchers working in this field. The situation of the JNDC is the same as this world-wide tendency. In order to overcome this obstacle, international cooperation for nuclear data evaluation and measurement

becomes more and more important. In Chapter III, the present status of these circumstances will be taken to discuss what sort of cooperation the JNDC should do. It is, of course, necessary to raise our own ability and potential to do good cooperation and contribution. It is important also to promote our own plans. These matters will be discussed also.

II. Review of the JNDC Activities

As mentioned in the previous Chapter, the JNDC was organized in 1963, just one year before the Olympic Games was held in Tokyo. Research and development of fast breeder reactors was on the point of starting in Japan. In fact, a committee for this purpose was organized by the JAERI in this year. The first National Symposium on Atomic Energy was also held in Tokyo in this year. In these lively circumstances, the JNDC started quietly with the purpose of collection, compilation and evaluation of the nuclear data.

The first project of the JNDC was to obtain unknown nuclear data. This was supported by the government fund for peaceful use of nuclear energy. The JNDC made use of this fund to develop some nuclear model codes for calculation of the fast and thermal neutron cross sections, and to study various nuclear models, systematic trends of their parameters, etc.

From 1963 to 1966, Japan joined the international organizations and committees for nuclear data, and the JNDC could take part in the international activities of exchange of numerical data and information. After this period, some members of the JNDC made nuclear data evaluations individually for the total cross section of carbon[1], the $^{27}Al(n,\alpha)$, $^{56}Fe(n,p)$, $^{63}Cu(n,2n)$ and $^{65}Cu(n,2n)$ reaction cross sections[2], calculations[3] of the inelastic scattering cross sections for $^{238}U(n,n')$, capture cross sections[4] for Cr, Fe, Ni and Mo, etc. A part of these works was submitted to the International Conference held in Helsinki, 1970.

In 1971, the JNDC set up working groups to evaluate the nuclear data for ^{235}U, ^{238}U, ^{239}Pu, ^{240}Pu, Ni, Fe, Cr, Na and O, and for 28 important fission product nuclides. Work for preparation of data processing codes and a storage and retrieval system for experimental

data was started in this year to help the nuclear data evaluation work. Group cross sections for the fast breeder reactors[5] and of the fission product nuclides for thermal reactor calculations[6] were also studied. These studies for the nuclear data evaluation and group cross sections were followed by the work for JENDL-1[7] which started in 1973. Although the description on the JENDL-1 is omitted in this report, the JENDL-1 was released at October 1977, after testing its reliability through benchmark tests. It was very impressive that the community of nuclear data users in Japan consented to use the JENDL-1 as the domestic standard nuclear data library. This consensus is still available for JENDL-2 and JENDL-3.

Meanwhile, the Nuclear Data Laboratory of JAERI was established in April 1968, and was followed by the Nuclear Data Center in 1976. It has been playing a role of the domestic nuclear data center and of the window for international cooperation.

In recent ten years, the JNDC has exerted its efforts to make the JENDL-2 and the JENDL-3. The JENDL-2 was planned in 1977, and was completed in 1982.[8,9] It was planned so as to be applicable not only to fast breeder reactor, but to thermal reactor, fusion neutronics and shielding calculations. It was used in the analysis of Japan-USA joint research (JUPITER project) on mock-up experiments of large fast reactors, and achieved many fruitful results. The benchmark tests for fast reactor, thermal reactor and shielding calculations showed that the JENDL-2 was applicable to these problems. However, the nuclear data in the higher energy region were not yet satisfactory. Hence, the JENDL-2 is not always applicable to the fusion neutronics calculation. Besides, it does not have photon-production cross-section data which are needed in the calculation for the fusion reactors.

The nuclear data evaluation for the JENDL-3 was started at April 1982, in order to remedy the defects of the JENDL-2 and to make it a large general purpose nuclear data library. Compilation of the evaluated data for the JENDL-3 was almost finished at the end of 1987, and the first trial of the benchmark tests was carried out. Results of this trial showed some serious problems[10),11)], and reevaluation for some nuclear data has been made. Benchmark tests for these

revised data have also been tried. In this Seminar, reports about these matters will be presented and discussed.

Evaluation of nuclear structure and decay data has been promoted in the international cooperation network of mass chain evaluation. The JNDC joined this cooperation network in 1977, and took the evaluation of the data for A=118 - 129. The first cycle of the evaluation for these masses were completed by the end of 1984, and now, the second cycle is in progress.

JNDC Fission Product Decay Heat Library has been made for summation calculation of decay heat, since 1974. The first version[12] of the library includes the decay data for 1172 nuclides. This library gave very good agreement with the experimental beta- and gamma-ray components of the decay heat for ^{235}U and ^{239}Pu, except for a little discrepancy around cooling time of 1,000 sec. The JNDC is now making the second version of the library.

Table 1 shows a rough chronology of the JNDC activities together with some related matters. One can see from the Table that the circumstances around the JNDC have been changing gradually as well as its own stance. These may suggest direction of future activities of the JNDC.

III. Present and Future Roles of JNDC

It is really great that the JNDC has been actively doing various tasks in the nuclear data field for 25 years. These tasks have been taken and studied by the enthusiastic members who were 25 years younger in 1963 than they are over fifty-five years now, and most parts of the present activity of JNDC are still made by these Nestors. Although their expertise is valuable, we need fresh and young scientists to succeed the old specialists in order to hold and elevate the activities of JNDC.

Deficiency of manpower in the nuclear data field is one of the common problems in the world, especially a decrease in the population of young researchers. This must be due to not only the severe circumstances in the nuclear energy field, but also lack of attractive research subjects in the nuclear data field. The latter seems to

cover both nuclear data evaluation including theory and nuclear data measurements.

To overcome such difficulty and make plans for post-JENDL-3, the JNDC has tried to investigate users' requirements to nuclear data in wider research fields. Table 2 shows the summary of the users' requirements[13]. On the basis of the investigation, the JNDC expanded its research subjects so that the users in wider fields could approach the JNDC with their data requirements and some might join the working groups. In fact, the JNDC set up working groups on evaluation of the activation cross section and on the data file of the (α,n) reaction cross sections in 1987. Furthermore, three working groups on nuclear data files for photoreactions, DPA and high energy neutrons started this year. A part of these new activities will be presented in this Seminar.

In the recent NEANDC meeting held at LANL, a proposal for setting up a Task Force for Nuclear Data Evaluation Cooperation between JENDL, JEF and ENDF was accepted in connection with the necessity of surmounting manpower difficulty and accelerating international cooperation in the nuclear data field. This was one of the long-standing matters in the NEANDC since it was discussed in the 24th meeting of NEANDC in 1984. The objective of the Task Force is to help the existing nuclear data evaluation projects in NEA member countries to improve their data files, although the ultimate objective will be the convergence of the files.

This is an example of the international cooperative projects which will be more and more various. In fact, bilateral and multilateral cooperation between USA, Western European Countries and China are now in progress actively. We also have already some cooperative programs with them. Taking these varieties of international surroundings into account, the JNDC is now investigating strategy for better cooperation. We have not yet reached the conclusion, but, at least, to promote favorable cooperation, we must more develop our own potential so that we can make better plans of our own projects, carry out them and assume the leadership of some parts of the cooperative programs.

In this context, the JNDC will continue holding the JENDL project in which we will take as many subjects shown in Table 2 as possible to attract young scientists as well as users. Hence, it is favorable for us to set up such international cooperative projects as will foster the JENDL project. The JNDC should take the initiative in making such plans.

The world-wide cooperation in the nuclear data community has been outstandingly excellent in comparison with the other scientific communities. Nobody doubts that the community has owed easiness of collecting data and information to the four-center network of the NEA Data Bank, the IAEA/Nuclear Data Section, the BNL/National Nuclear Data Center and the Nuclear Data Center in Obninsk. For the future cooperation, the role of the network will be more important than that in the past. We wish the four centers to make more effort to keep the network.

Recent changes in the work of the NEA Data Bank, however, have given us anxiety about slowdown of the function of the four-center network. Reduction of manpower in the nuclear data service of the Data Bank may perhaps bring difficulty to the international cooperation. The IAEA/Nuclear Data Section seems to have the similar problem. Take FENDL (Fusion Evaluated Nuclear Data Library) for example, their leadership seems to be only the ruin of what it was. These expressions may be too strong, but increase in the bilateral and/or multilateral international cooperation seems to reflect these changes of situations.

Although the four-center network should be strongly supported, reorganization for the international cooperation may be needed in near future. It may be requested to investigate, in order to meet such change, what sort of contribution we can do, what type of cooperation we will take, etc. The JNDC should consider its own policy about the net-work cooperation, from now on, as well as its own research program. In particular, the cooperation with the researchers in the Asian-Pacific countries will be more and more important. It may be a dream that the JNDC will be expanded so that they can join it to work with us. Is it only a fancy?

IV. Conclusion

As a special talk for celebration of the 25th anniversary of foundation of the JNDC, a review of the past activities, a survey of the present situation and the future role of the JNDC were given. The benchmark tests for the JENDL-3 is now under way, and a part of the tests would be given in this Seminar.

Since it is important to take heed to the future role and activity, some fearless proposals were given. Many discussions about them should be made seriously. On the basis of these discussions, research subjects, plans of activity and perspectives of the JNDC will be put into shape.

References:

1) Nishimura K., Igarasi S., Fuketa T. and Tanaka S.: "Evaluation of the Total Cross Section of Carbon up to 2 MeV", JAERI 1218 (1971).
2) Nakasima R. and Kanda Y.: "Evaluation of Some Fast Neutron Cross Section Data", JAERI 1207 (1972).
3) Igarasi S., Nakamura H., Murata T. and Nishimura K.: "Analysis of Neutron Inelastic Scattering by ^{238}U", Proc. of Int. Conf. on Nucl. Data for Reactors, Helsinki 1970, Vol.2, 869 (1970).
4) Nishimura K., Asami T., Igarasi S., Hatchya M. and Nakamura H.: "Fast Neutron Capture Cross Sections of Cr, Fe, Ni and Mo", Proc. of Int. Conf. on Nucl. Data for Reactors, Helsinki 1970, Vol.2, 805 (1970).
5) Katsuragi S., Tone T. and Hasegawa A.: "JAERI Fast Reactor Group Constants Systems, Part I" JAERI 1195 (1970).
Katsuragi S., Ishiguro Y. Takano H. and Nakagawa M.: "JAERI Fast Reactor Group Constants Systems, Part II" JAERI 1199 (1970).
6) Iijima S., Kobayashi T. and Sakata H.: "Neutron Cross Sections of Fission Product Nuclides (in Japanese)", JAERI 1206 (1972).
7) Igarasi S., Nakagawa T., Kikuchi Y., Asami T. and Narita T.: "Japanese Evaluated Nuclear Data Library, Version-1 —— JENDL-1 ——", JAERI 1261 (1979).
8) Nakagawa T. (Ed.): "Summary of JENDL-2 General Purpose File", JAERI-M 84-103 (1984).

9) Kikuchi Y. and Members of JNDC: "Present Status and Benchmark Tests of JENDL-2", Proc. of Int. Conf. on Nucl. Data for Sci. and Technol., Antwerp 1982, 615 (1983).

10) Hasegawa A.: "Benchmark Testings of Evaluated Data Files on Fission Reactors and Shielding Problems", Proc. of Int. Conf. on Nucl. Data for Sci. and Technol., Mito 1988, 445 (1988).

11) Takeda T., Takamoto M., Takano H., Kaneko K. and Hasegawa A.: "Thermal and Fast Reactor Benchmark Test of JENDL-3T", Proc. of 1988 Int. Reactor Physics Conf., Jackson Hole 1988, I-271 (1988).

12) Tasaka K., Ihara H., Akiyama M., Yoshida T., Matumoto Z. and Nakasima R.: "JNDC Nuclear Data Library of Fission Products", JAERI 1287 (1983).

13) Nakazawa M., Hasegawa A., Katakura J., Mizumoto M., Nakagawa T. and Yoshida T.: "Proposals on Post-JENDL-3 Activity Programme for Japanese Nuclear Data Committee", JAERI-M 87-025, Proc. of 1986 Seminar on Nucl. Data, 9 (1987).

Table 1 Chronology of JNDC activities

Year	JNDC	Related Matters
1963	JNDC is organized, establishing study groups for calculations of unknown nuclear data, and collection of resonance parameters.	(1) INDSWG invited Japanese delegate. (2) JPDR attained criticality.
1964	(1) CINDA activity starts. (2) RENDA activity starts.	(1) ENEA/CCDN starts. (2) Japan joins OECD. (3) KUR attained criticality.
1965	(1) JNDC holds a Seminar on Fast Neutron Cross Sections. (2) Study group for group cross sections is established. (3) Many nuclear model codes for fast and thermal neutron cross section calculations are made.	(1) Japan becomes an associate member country of ENEA. (2) INDSWG is held in Tokyo. (3) INDC succeeds INDSWG. (4) Four center-network starts.
1966	(1) Second Seminar on Fast Neutron Cross Sections is held. (2) JNDC issues JNDC News.	(1) Japan joins EANDC, EACRP, ENEA/CCDN and ENEA/CPL. (2) Conference on Neutron Cross Section Technology at Washington. (3) IAEA Conference on Nuclear Data for Reactors at Paris.
1967	(1) Evaluation of carbon total cross section starts. (2) Evaluation of 14 MeV neutron reaction cross sections starts.	(1) PNC was established. (2) FCA and RAPSODIE attained criticality.
1968	(1) Nuclear Data Laboratory starts. (2) First Seminar on Neutron cross sections is held.	(1) Conference on Nuclear Cross Sections and Technology at Washington. (2) FACOM 230-60 started operation in JAERI.
1969	(1) JAERI-Fast Set is completed. (2) Storage and retrieval system for neutron experimental data is planned. (3) Second Seminar on Neutron Cross Sections is held.	(1) Panel on Nuclear Data Compilation at BNL. (2) JFT-1 started operation.

Year	JNDC	Related Matters
1970	(1) Group cross-section set of fission products for thermal reactors is completed. (2) Evaluations for $^{238}U(n,n')$ cross section and capture cross sections for Cr, Fe, Ni and Mo are made. (3) Collection and compilation of ^{235}U, ^{238}U, ^{239}Pu, ^{240}Pu, Ni, Fe, Cr, Na and O data for fast reactors start.	IAEA Conference on Nuclear Data for Reactors at Helsinki.
1971	(1) Nuclear data evaluation for ^{235}U, ^{238}U, ^{239}Pu, ^{240}Pu, O, Na, Cr, Fe, Ni, Ta starts. (2) Evaluation of 28 FP nuclides starts. (3) Neutron data storage and retrieval system (NESTOR) is completed. (4) Codes for nuclear data processing are prepared: (SPLINT, CRECT-J, etc.)	(1) Conference on Neutron Cross Sections and Technology at Knoxville. (2) Panel on Neutron Nuclear Data Evaluation at Vienna. (3) ENDF/B-III released. (4) YAYOI attained criticality.
1972	(1) Working group for JENDL-0 is organized. (2) Third Seminar on Neutron Cross Sections is held.	Japan becomes a member country of ENEA, and NEA succeeds ENEA.
1973	(1) Subcommittee on Nuclear Data for Safeguards is organized. (2) JENDL-1 project starts. (3) Data processing systems for group cross sections are developed. (4) Working group on nuclear data evaluation for safeguards is organized.	(1) Symposium on Application of Nuclear Data in Science and Technology at Paris. (2) Specialists meeting on Fission Product Nuclear Data at Bologna. (3) PHENIX attained criticality.
1974	(1) Compilation group for JENDL-1 is organized. (2) Working group on nuclear data for fusion reactors is organized. (3) Working group on evaluation of decay heat is organized.	(1) 17th meeting of EANDC is held at Tokyo. (2) ENDF/B-IV released. (3) Radiation leakage from Mutsu Reactor.

Year	JNDC	Related Matters
1975	(1) Evaluation of fission product nuclear data for 70 nuclides starts. (2) Compilation of JENDL-1 finished. (3) Chart of the Nuclides is published.	(1) Advisory Group Meeting on Transactinium Nuclear Data at KFK. (2) Conference on Nuclear Cross Section and Technology at Washington. (3) NEANDC and NEACRP succeed EANDC and EACRP respectively.
1976	(1) Working group on integral tests for JENDL-1 is organized. (2) Working group on group constants for shielding is organized. (3) Benchmark tests for JENDL-1 finished. (4) Nuclear Data News succeeds JNDC News. (5) Nuclear Data Center is set up.	(1) Advisory Group Meeting on Nuclear Structure and Decay Data at Vienna. (2) Specialists Meeting on Fast Neutron Fission Cross Section for ^{233}U, ^{235}U, ^{238}U and ^{239}Pu at ANL.
1977	(1) JENDL-1 released, and JENDL-2 starts. (2) Working group on nuclear structure data is organized, and Japan joins international cooperation for mass chain evaluation. (3) Nuclear Data Center becomes an official name.	(1) Advisory Group Meeting on Fission Product Nuclear Data at Petten. (2) Advisory Group Meeting on Nuclear Structure and Decay Data at ORNL. (3) Specialists Meeting on Structural Materials Nuclear Data at Geel. (4) JOYO attained criticality.
1978	(1) Working group on nuclear data for fuel cycle succeeds the working group on nuclear data evaluation for safeguards. (2) 1978 Seminar on Nuclear Data is held. (3) Sophisticated system for benchmark test is developed, and the JENDL-1 data are examined.	(1) Conference on Neutron Physics and Nuclear Data for Reactors and other Applied Purposes at Harwell. (2) 21st meeting of NEACRP is held at Tokai. (3) CCDN and CPL were amalgamated to NEA Data Bank. (4) FUGEN attained criticality.
1979	(1) Working group on nuclear data for photon production is organized. (2) 1979 Seminar on Nuclear Data is held. (3) JNDC FP decay data library for summation calculation of decay heat is completed.	(1) ENDF/B-V is completed, but not released. (2) Conference on Nuclear Cross Sections for Technology at Knoxville. (3) Advisory Group Meeting on Transactinium Nuclear Data at Cadarache. (4) Specialists Meeting on Fission Products Nuclear Data at Bologna. (5) TMI accident.

Year	JNDC	Related Matters
1980	(1) An ad hoc committee for JENDL-3 project is set up. (2) JENDL-2 is used for analyses of a large fast breeder mockup experiments. (3) 1980 Seminar on Nuclear Data is held. (4) Chart of the Nuclides (II) is published.	(1) NEACRP discussed JEF project, and organized an ad hoc committee for it. (2) Symposium on Neutron Cross Sections from 10 ~ 50 MeV, at BNL. (3) Japan and China signed agreement on Science and Technology Cooperation.
1981	(1) Working group on group constants for shielding includes activity on group constants for fusion. (2) Working group on nuclear data for fuel cycle terminated its activity. (3) An ad hoc committee is organized to survey potential needs of nuclear data for special purposes. Report submitted to JNDC in 1983. (4) 1981 Seminar on Nuclear Data.	(1) 2nd and 3rd meetings of JEF ad hoc committee. (2) Consultants Meeting on U and Pu Isotope Resonance Parameters at Vienna. (3) NEDAC was established.
1982	(1) Working group on evaluation for generation and depletion of nuclides is organized. (2) JENDL-2 is released, and JENDL-3 starts. (3) Working group on atomic, molecular and nuclear data for biomedical applications is organized. (4) Subcommittee on Nuclear Data reorganizes working groups for JENDL-3. (5) 1982 Seminar on Nuclear Data.	(1) JEF Scientific Coordination Group starts. (2) Advisory Group Meeting on Nuclear Structure and Decay Data at Zeist. (3) Conference on Nuclear Data for Science and Technology at Antwerp. (4) Decommission of JPDR was authorized.
1983	(1) Revised JNDC FP decay data library is released. (2) Sophisticated benchmark tests of JENDL-2 is promoted. (3) Nuclear data evaluation for fusion neutronics calculation is advanced. (4) 1983 Seminar on Nuclear Data.	(1) Advisory Group Meeting on Basic and Applied Problems of Nuclear Level Densities at BNL. (2) Conference on Radiation Shielding at Tokyo. (3) Consultants Meeting on Nuclear Data for Structural Materials at Vienna. (4) Specialists Meeting on Yields and Decay Data of Fission Product Nuclides at BNL. (5) Decommission of RAPSODIE.

Year	JNDC	Related Matters
1984	(1) Topical conference is held in coorperation with NEANDC. (2) Preparatory ad hoc committee is set up to explore possibility of holding 1988 International conference in Japan. (3) 1984 Seminar on Nuclear Data.	(1) 24th meeting of NEANDC is held at Tokai. (2) Advisory Group Meeting on Transactinium Isotope Nuclear Data at Uppsala. (3) Advisory Group Meeting on Nuclear Standard Reference Data at Geel. (4) JEF-1 released, and JEF-2 starts.
1985	(1) Specialists' Meeting on Nuclear Data for Fusion Neutronics is held at Tokai. (2) An ad hoc committee for exploring activities in post-JENDL-3 is set up. (3) Compilation group for JENDL-3 is organized. (4) 1985 Seminar on Nuclear Data, welcoming four Chinese and one Indonesian colleagues.	(1) Conference on Nuclear Data for Basic and Applied Science at Santa Fe. (2) Dr. R.S. Lasijo joins JAERI/NDC for three months under the auspices of the STA scientist exchange program (SEP). (3) NEANDC Specialists' Meeting on the Use of the Optical Model for the Calculation of Neutron Cross Sections below 20 MeV is held in Paris.
1986	(1) The ad hoc committee for post-JENDL-3 recommends several items for future activities. (2) A tentative version of JENDL-3 (JENDL-3T) is compiled. (3) 1986 Seminar on Nuclear Data, welcoming two Chinese and one Argentine.	(1) Organizing Committee for Nuclear Data Conference starts. (2) Dr. Liu Tingjin joins JAERI/NDC for six months under the auspices of the STASEP. (3) Specialist' Meeting on Covariance Methods and Practices in the Field of Nuclear Data is held in Rome. (4) Chernobyl accident.
1987	(1) Working group on special purpose nuclear data evaluation starts. (2) Benchmark tests of JENDL-3T is made. (3) International cooperation of nuclear data evaluation is discussed. (4) 1987 Seminar on Nuclear Data.	(1) Consultants' Meeting on Data Requirements for Medical Radioisotope Production in Tokyo. (2) Specialists' Meeting on Data for Decay Heat Predictions in Studsvik. (3) Reorientation of NEA Data Bank is accepted. (4) Dr. S. Wiboolsake joins JAERI/NDC for three months.

Year	JNDC	Related Matters
1988	(1) Reorientation of the working group on A & M·Nuclear Data for Medical Application is discussed. (2) An ad hoc committee on international cooperation of nuclear data evaluation is set up. (3) Second version of JNDC FP Decay Data Library is completed. (4) 1988 Seminar on Nuclear Data.	(1) Consultants' Meeting on the Physics of Neutron Emission in Fission at Mito. (2) Conference on Nuclear Data for Science and Technology at Mito. (3) 31st Meeting of NEACRP is held at Oarai. (4) Dr. Cai Shaohui joins JAERI/NDC for six months.

Table 2 Summary of nuclear data requirements

Areas	Requirements
Light Water Reactor	Little for present LWR, Actinide and FP nuclear data for high burn core calculation Every nuclear data for high conversion LWR, especially in resonance region
Fast Reactor	Critical benchmark testing by standard group constant, Adjustments of group constant
Fusion Reactor	Blanket neutronics of tritium breeding, nuclear heating, gamma-ray productions, activation cross-section and radiation damage, gamma-ray Production; covariance matrices (maybe JENDL-4)
Nuclear Fuel Cycle	Safety of criticality problem, Production and decay data of relating radioactive nuclides(more than 1000) X-ray emission and internal conversion electron yield of actinide (α,n) reactions
Accelerator	Neutron Production cross section Shielding and activation for high energy accelerator Charged particle data for advanced utilization of accelerators
Decommissioning of Nuclear Power Reactor	Activation cross-section of structural and impurity materials of nuclear power reactors
Radiation Damage	DPA, Kerma factor
Medical Application	Neutron production cross-section such as Be(d,n), Li(d,n), cross-section of collimator materials and human body elements, KERMA Cross section for heavy ion, proton, pion
RI Utilization	Practical hand book of activation, emitted gamma-ray spectra, nuclear structure
Enrichment by Laser	Ultra fine level & Isotope shift data, excitation, ionization, de-excitation cross-sections, life time & branching ratio of excited atoms
Charged Particle Data	Fusion reactor developments (α,n) reaction for spent fuel

2.1.2 Present Status of JENDL-3

Keiichi SHIBATA

Japan Atomic Energy Research Institute
Tokai-mura, Ibaraki-ken 319-11

Nuclear data evaluation has been made for JENDL-3. Its compilation work is now in the final stage. The number of nuclides to be stored in JENDL-3 will be 325 including 172 FP nuclides. In the general purpose file of JENDL-3, 172 nuclides will be included with 19 nuclides overlapping with the FP file. This paper presents the status of the evaluation and compilation for JENDL-3.

1. Introduction

A temporary file JENDL-3T[1] was prepared[2] for various benchmark tests in 1987. It contained evaluated data of 97 nuclides. For many nuclides, small or big problems were pointed out as a result of the tests. Modification of the evaluated data has been being performed. Furthermore, new evaluations have been being made for 75 nuclides which were not contained in JENDL-3T. A file including all these data is prepared and called JENDL-3T Rev.-1. The file made in 1987 is referred to as JENDL-3T Rev.-0 hereafter. The detailed benchmark tests of JENDL-3T Rev.-1 has already started.

The compilation for the general purpose (GP) file of JENDL-3 will be finished by the end of March, 1989. The number of nuclides to be stored in JENDL-3 will be 325 including 172 fission product (FP) nuclides. In the GP file, 172 nuclides will be included with 19 nuclides overlapping with the FP file.

This paper presents the status of the evaluation and compilation for the GP and FP files of JENDL-3.

2. General Purpose File

It is expected that the data of 38 nuclides in the Rev.-0 file will be assembled in the final JENDL-3 without any modification. Table 1 gives the list of the nuclides which do not need further modification. The data of 59 nuclides in the Rev.-1 file, which are given in Table 2, should be modified. Figure 1 shows the revised data[3] on the $^{7}Li(n,n_2)$ reaction, as an example. The inelastic scattering on iron and nickel isotopes was reanalyzed[4] with the coupled-channel theory by taking account of the 2-phonon states. As a result, the reproduction of the double-differential cross sections (DDXs) of iron and nickel was much improved. The ν_p value of ^{235}U was dereased[5] by 15% for 10 - 100 eV and 3% for 100 eV - 1 MeV compared with the Rev.-0 file, as shown in Fig.2.

In addition to the revised data, new evaluations for 75 nuclides have been made. The nuclides to be newly evaluated are listed in Table 3. As an example, the DDXs of ^{93}Nb are shown in Figs. 3 and 4. In this evaluation[6], the Kalbach-Mann systematics[7] were employed for the angular distribution of the continuum inelastic scattering. The evaluated data are in good agreement with the experimental data measured at Osaka University[8].

3. Fission Product File

The characteristics of the FP evaluation are given as follows:

1) Threshold reaction cross sections

   The calculations have been performed by using the PEGASUS code[9], and normalization is made by taking account of measurements or systematics.

2) Total, capture, elastic and inelastic scattering cross sections

   The cross sections were obtained from the CASTHY[10] calculations. The competing processes calculated with PEGASUS were considered.

3) Optical-model parameters

   The parameters were reexamined for all nuclides and improved.

4) Resolved resonance parameters

Recent measurements were taken into account as much as possible.

5) Unresolved resonance parameters

The parameters were searched for with the ASREP code[11] so as to fit to the capture cross section calculated by CASTHY or measured.

Concerning the resolved resonance, the evaluation has been almost finished. The thermal cross sections will be checked up soon. The unresolved resonance parameters were determined for 90% of the nuclides to be evaluated. Moreover, the PRGASUS and CASTHY calculations were almost completed. The calculated capture and (n,2n) cross sections are illustrated in Figs. 5 and 6, respectively.

4. Summary

The status of JENDL-3 was briefly described. The data of 59 nuclides in JENDL-3T Rev.-0 are being revised to improve the results on the integral tests. The evaluation and compilation work will be finished by the end of March, 1989.

References

1) JENDL Compilation Group (Nuclear Data Center, JAERI): JENDL-3T, private communication (1987).
2) Asami, T.: "An Outline of JENDL-3T", JAERI-M 88-065 (1988), p.4.
3) Chiba, S. Shibata, K.: "Revision and Status of the Neutron Nuclear Data of ^{6}Li and ^{7}Li", JAERI-M 88-164 (1988).
4) Eriguchi, M.: private communication (1988).
5) Matsunobu, H.: private communication (1988).
6) Kawai, M: private communication (1988).
7) Kalbach, C. Mann, F.M.: Phys. Rev., C3, 112, (1981).
8) Takahashi, A: private communication (1988).
9) Iijima, S., Sugi, T. Nakagawa, T., Nishigori, T.: "Program PEGASUS, A Precompound and Multi-step Evaporation Theory Code for Neutron Threshold Cross Section Calculation", JAERI-M 87-025, p.337 (1987).

10) Igarasi, S.: J. Nucl. Sci. Technol., 12, 67 (1975).
11) Kikuchi, Y.: praivate communication.

Table 1 Nuclides not to be modified in JENDL-3T, Rev.-0

H-1, 2, He-3, 4, Li-6, P-31, S-33, 34, 36,
K-nat, 39, 40, 41, Ca-nat, 40, 42, 43, 44, 46, 48,
Ni-61, 62, 64, Pa-231, U-232, 233, 234, Np-237, 239,
Pu-236, Am-242, 242m, Bk-249, 250,
Cf-249, 250, 251, 252

Table 2 Nuclides to be modified in JENDL-3T, Rev.-0

Li-7, Be-9, B-10, 11, C-12, N-14, O-16, Na-23,
Al-27, Si-nat, 28, 29, 30, S-nat, 32,
Cr-nat, 50, 52, 53, 54, Mn-55, Fe-nat, 54, 56, 57, 58,
Ni-nat, 58, 60, Cu-nat, 63, 65, Zr-nat, 90, 91, 92, 94, 96,
Mo-nat, Pb-nat, 204, 206, 207, 208, Th-228, 230, 232, 233,
234, Pa-233, U-235, 236, 238,
Pu-239, 240, 241, 242, Am-241, 243

Table 3 New data to be included in JENDL-3T, Rev.-1

N-15, F-19, Mg-nat, 24, 25, 26, Cl-nat, 35, 37,
Ar-40, Sc-45, Ti-nat, 46, 47, 48, 49, 50,
V-51, Co-59, Nb-93, Mo-92, 94, 95, 96, 97, 98, 100,
Ag-nat, 107, 109, Cd-nat, Sb-nat, 121, 123,
Eu-nat, 151, 153, Hf-nat, 174, 176, 177, 178, 179, 180,
Ta-181, W-nat, 182, 183, 184, 186, Bi-209,
Ra-223, 224, 225, 226, Ac-225, 226, 227,
Th-227, 229, Pa-232, Pu-238, Am-244, 244m,
Cm-241, 242, 243, 244, 245, 246, 250,
Cf-254, Es-254, 255, Fm-255

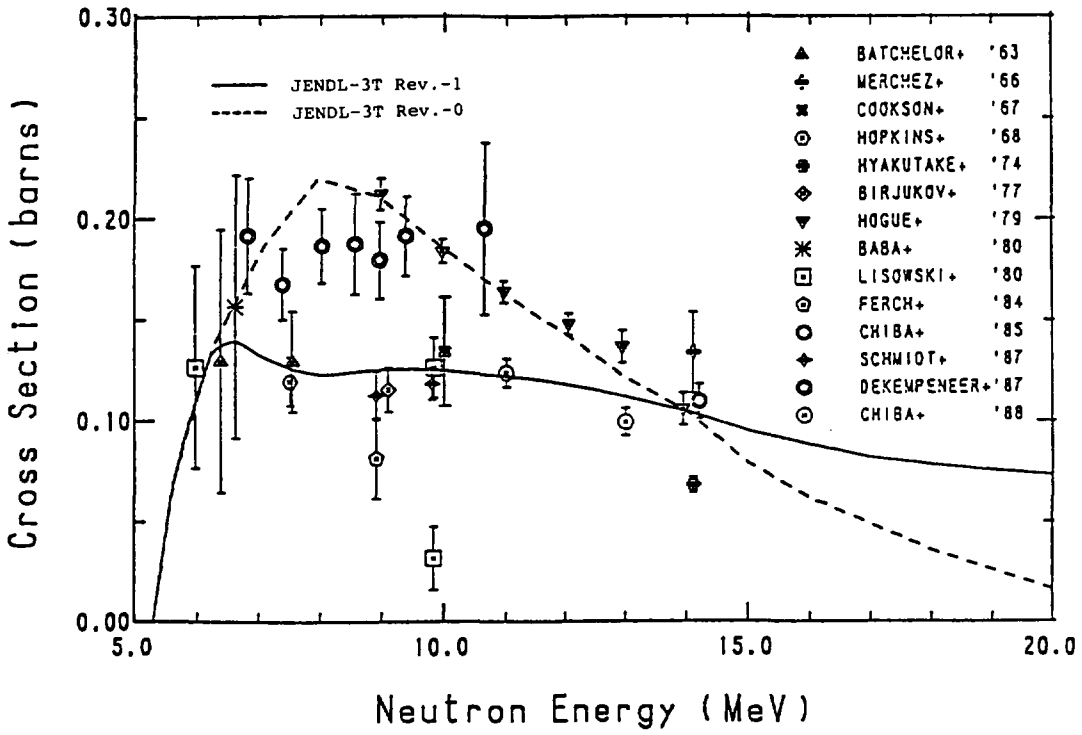

Fig. 1 $^{7}Li(n,n')\ Li^{*}$ (4.63 MeV) cross section.

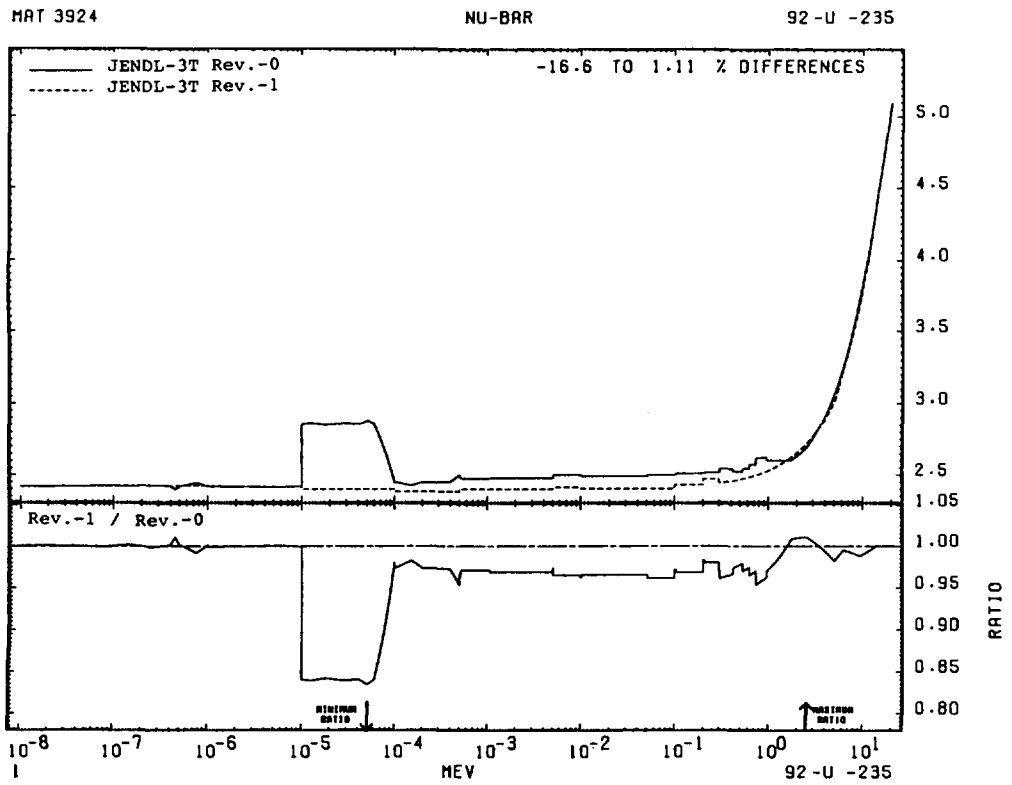

Fig. 2 ν_p of ^{235}U.

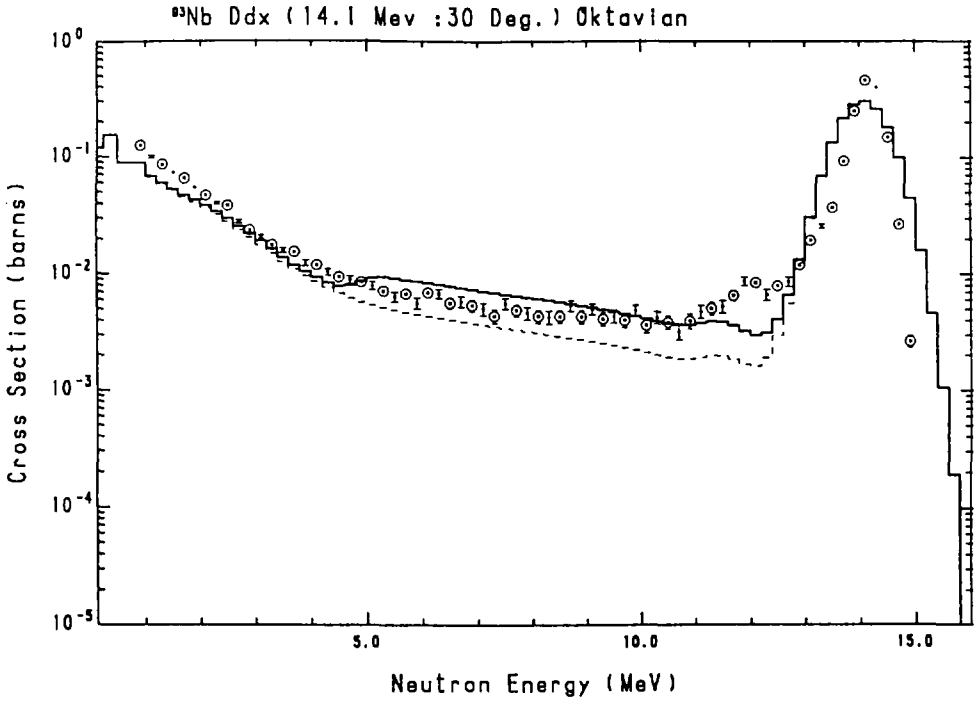

Fig. 3 DDX of ^{93}Nb at 30°.
The solid line was calculated by using the Kalbach-Mann systematics. An isotropic distribution was assumed for the dashed line.

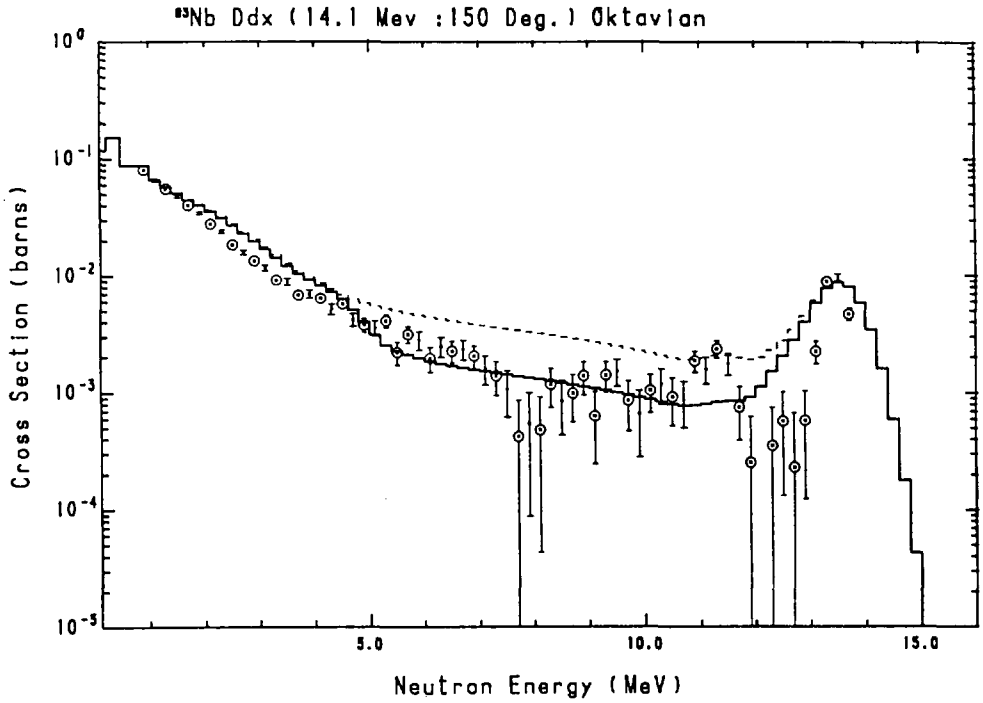

Fig. 4 DDX of ^{93}Nb at 150°.
See the caption of Fig. 3.

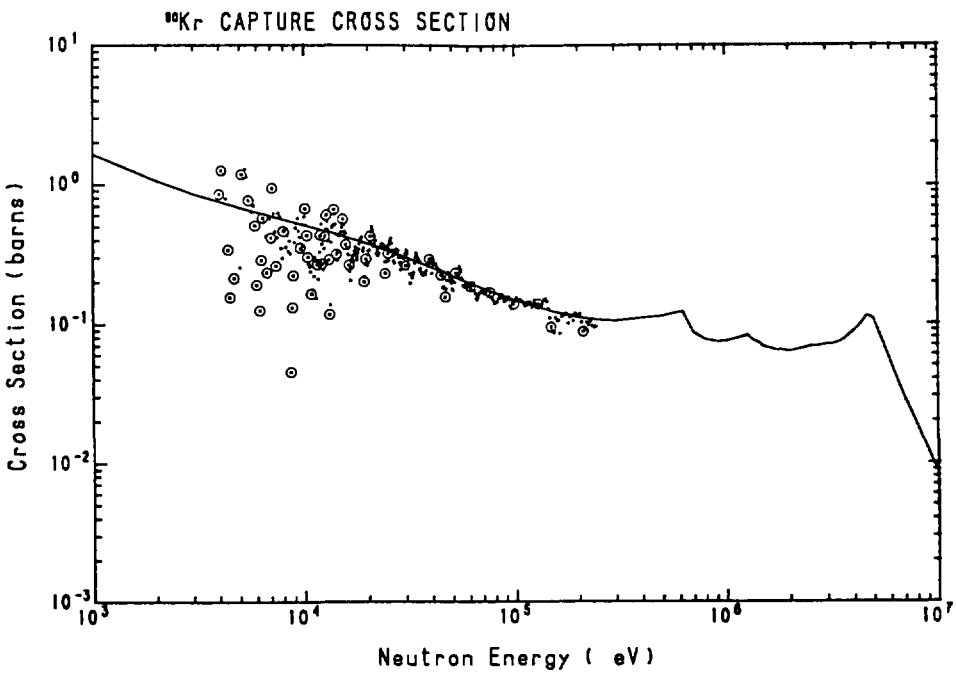

Fig. 5 Capture cross section of ^{80}Kr
The solid line was calculated with the CASTHY code.

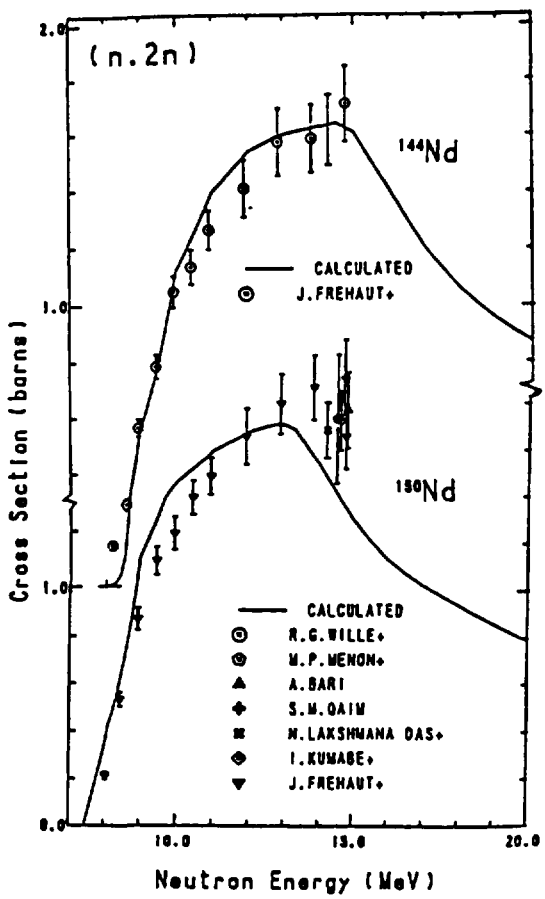

Fig. 6 (n,2n) cross sections of Nd isotopes.

2.2 Consistency between Microscopic Data and Integral Data

2.2.1 Virtues of Cross-section Adjustment Method and Present Status of the Utilization of the Method in Core Design

Takanobu Kamei
Nippon Atomic Industry Group Company, Ltd., NAIG Nuclear Research Laboratory
4-1 Ukishima-cho, Kawasaki-ku, Kawasaki-shi 210, Japan
and
Toshikazu Takeda
Osaka University, Department of Nuclear Engineering
2-1 Yamada-oka, Suita-shi 565, Japan

The prediction accuracies of key neutronics parameters including burnup property are improved by the use of the cross-section adjustment method. The effectiveness of the adjustment method are described through the authors' experience. The present status of the utilization of the method in the United States and France are also described in the present report.

1. Introduction

Efforts are made to decrease the prediction uncertainties of reactor performance parameters so that the reactor design might not necessitate excessive and expensive design margins. In order to decrease the prediction uncertainties, we heavily rely on experimental information from mock-up criticals.

The cross section adjustment method is an approach, in which cross sections are adjusted so that the calculation may reproduce the experimental results. With this method, experimental information is incorporated into adjusted group cross sections. The deviations between calculated and experimental results are expected to be narrowed with the use of the adjusted cross sections.

In the followings, we describe how the cross section adjustment method is effective in decreasing the prediction uncertainties of key neutronics parameters. The application example of the cross section adjustment method to decrease the C/E space dependence of control rod worth are described together with the application to the predictioin of burnup properties of a large LMFBRs.

2. Cross-section Adjustment Method and the Prediction Uncertainty of Key Neutronics Parameters

In the present section, we describe the cross-section adjustment method and compare the prediction uncertainties of key neutronics parameters before and after the application of the cross-section adjustment method.

Let us consider a set of microscopic cross-sections **T** with a covariance matrix **M**. Let there be measured integral quantities **I**. The **I** may be the effective multiplication factor, control rod worth, or reaction rate distribution, etc. The dependence of **I** on a partial change of **T** is expressed as the sensitivity matrix **G**. The cross-section adjustment is a method, in which the cross-section is corrected[1] to yield better agreement with experimental data obtained at critical facilities. The best-estimate cross section set **T'** and its covariance matrix **M'** can be obtained on the Bayes theorem. The adjusted vector **T'** is found as the vector that minimizes q^2;

$$q^2 = (\mathbf{T'}-\mathbf{T})^t\mathbf{M}^{-1}(\mathbf{T'}-\mathbf{T}) + (\mathbf{I'}-\mathbf{I}_e)^t\mathbf{U}^{-1}(\mathbf{I'}-\mathbf{I}_e) \quad (1)$$

where **I'** is the integral quantity obtained by using cross section set **T'**, $\mathbf{I}_e$ is the experimental value, and U is the uncertainty of C/E values or C-E values. The **T'** that minimized q^2 of Eq.(1) and the covariance matrix **M'** of a new cross section set **T'** are given as

$$\mathbf{T'} = \mathbf{T}+\mathbf{M'}\mathbf{G}^t\mathbf{U}^{-1}(\mathbf{I}_e-\mathbf{I}) \quad (2)$$

$$\mathbf{M'} = (\mathbf{M}^{-1}+\mathbf{G}^t\mathbf{U}^{-1}\mathbf{G})^{-1} \quad (3)$$

The prediction error in the case where an adjusted cross section library is employed is given by

$$\mathbf{V} = \mathbf{G}\mathbf{M'}\mathbf{G}^t \quad (4)$$

Note that the prediction error when the cross-section adjustment method is not employed is given by

$$\mathbf{V} = \mathbf{G}\mathbf{M}\mathbf{G}^{t} \tag{5}$$

Since $\mathbf{M}'$ is much smaller than $\mathbf{M}$, the prediction uncertainty can be decreased by applying the cross-section adjustment method.

3. Application of the Cross-Section Adjustment Method in the JUPITER Experimental analysis

A series of critical experiments under collaboration between the USA and Japan has been performed at the Zero Power Plutonium Reactor (ZPPR). The program is called JUPITER which is the acronym of Japan and United States Program of Integral Test and Experimental Research. The analysis was performed by several Japanese organizations of atomic industry under the sponsorship of Power Reactor and Nuclear Fuel Development Corporation (PNC) as well as by the USA organizations. The analysis results[2,3] obtained in the USA and Japan were brought together and discussed in the JUPITER analysis meeting which was held by the two countries. We came across a problem that the C/E values of control rod worths increase with the distance of rod positions from the core center. Those of the reaction rate distribution also show the same tendency. For example in the ZPPR-10A and 10D assemblies, the C/E value of the outer ring control rod worth is 4 to 12 % higher than that of the core center. As for the ^{239}Pu fission rate distribution, 4 to 5 % space dependence is observed in the C/E values. Such a large space dependence of C/E values brings about difficulty in the accurate prediction of control rod worths and power distribution of the large LMFBR. That pushed us for the endeavor to make the C/E space dependence small.

As a method to investigate the cause of the C/E space dependence, we employed the cross-section adjustment method.[4] The adjusted cross-section set $\mathbf{T}'$ and the associated covariance matrix $\mathbf{M}'$ are obtained as was described in Eqs.(2) and (3). In the adjustment of the cross-sections, we employed the experimental data of criticality factor, reaction rate ratios as well as control rod worth and reactionrate distribution.

Table 1 shows the C/E values before and after the cross section

adjustments. Figure 1 compares the space dependence of control rod worth C/E values in the ZPPR-10D assembly for non-adjusted case and for the case, in which the cross-section adjustment method is employed. From the table and figure, we can see that the space dependence of C/E values for the control rod worth and reaction rate distribution has been reduced considerably.

Table 2 shows the amounts of cross section changes for important reactions in a large LMFBR neutronics calculations. It is interesting to see that the capture cross section of ^{238}U is decreased by 6 to 10 % below 100 keV, the fission cross section of ^{239}Pu is decreased by about 5 % between 800 to 100 keV and is decreased by about 2 % between 100 keV and 1 keV.

4. Reduction of Prediction Error of Burnup Core Performance Parameters by Use of the Cross-section Adjustment Method

Prediction accuracy of neutronics parameters of a large liquid-metal fast breeder reactor (LMFBR) is now remarkably being improved through the accumulation of nuclear data for cross-section evaluation, experimental data from critical facilities, and the refinement of calculational model. However, the direct experimental data for the quantities which are connected with burnup property are not obtained at zero power facility. The burnup properties such as burnup reactivity loss, breeding ratio, fissile inventory, and the change of power distribution during burnup are very important in the design of large LMFBRs. Under these circumstances, P. Hammer proposed an international benchmark problem[5] for the burnup characteristics of a 3000 MW(thermal) FBR at 1980 Nuclear Energy Agency committee on Reactor Physics (NEACRP), and many organizations had participated. One of the results is shown in Table 3. As seen in the table, the burnup reactivity varies largely from 0.5 to 1.9% $\Delta k/k$. The fact that no direct experimental value can be obtained for these burnup characteristics makes the situation difficult.

Under these circumstance, we want to decrese the prediction uncertainty of the burnup properties. In the followings, we show that the cross-section adjustment method is useful in decreasing the prediction uncertainty.[6]

We assumed a typical 1000-MWe LMFBR for the evaluation of prediction

error of burnup characteristics. The sensitivity coefficients for the burnup properties were calculated by the use of the generalized perturbation method developed by T. Takeda et. al.[7]

First, we evaluate the prediction error of burnup properties when our cross-section set is used in the prediction without any correction for the predicted value. The prediction error is calculated by Eq.(5). Table 4 shows the uncertainties for burnup reactivity loss, breeding ratio and fissile plutonium number densities.

The prediction error is about 30% for burnup reactivity loss, and about 5% for the breeding ratio. The prediction error for ^{239}Pu atomic number density is 1-2% in the core and 2-3% in the blanket, and that for ^{241}Pu atomic number density is 2-3% and about 15% in the core and blanket, respectively. These error values are larger than generally assumed in the design of a large LMFBR. Now, we evaluate how these error values can be decreased by utilizing the cross-section adjustment method.

The experimental data from ZPPR-9 shown in Table 5 were employed in the adjustment of our cross section set. Table 5 also includes the uncertainty of C/E value for each integral data. This uncertainty includes experimental error as well as the error encountered in the analysis.

The error in the case where an adjusted cross section is employed can be obtained by Eqs.(3) and (4). Here, we selected six cases as the pattern of the employment of experimental data. Table 6 shows the predicted errors of burnup properties for the above six cases. We find by comparing the results of cases 1 and 3 that the reaction rate ratio of $^{238}U(n,r)$ to $^{239}Pu(n,f)$ shows remarkable improvement in the prediction of burnup properties. Namely by the employment of the integral data, the prediction error is decreased from 29% to 20% for burnup reactivity loss and from 4.3% to 3.2% for breeding ratio. The error of ^{239}Pu atomic number density is also decreased.

Case 6, in which all the five types of integral data are utilized, shows that the prediction errors are 18% for burnup reactivity loss and 2.2% for breeding ratio. These values are about a half that of the case where nonadjusted cross section set is employed. The prediction error for ^{239}Pu atomic number density is also remarkably improved. On the other hand, that of ^{241}Pu atomic number density does not show any improvement because the data which works for the refinement of ^{241}Pu cross section are

not included in the integral data shown in Table 5.

5. The Utilization of the Cross-section Adjustment Method in the US and France

Recently in the United States of America, much attention is paid on the cross-section adjustment method as a useful tool to provide an accurate knowledge of the reactivity variation to enhance the passive safety in the transient over-power accidents in IFR. Members from ANL-east and -west started their adjustment study energetically, using various experimental data from ZPR, ZPPR, ZEBRA, FFTF, and others. Their work is featured by that the vast amount of data are employed in the adjustment. They used experimental data from 27 critical assemblies.[8,9] The data come from critical assemblies of large spectral range, various material compositions and sizes. One example of their results is shown in Table 7. The uncertainties of predicted values are decreased to one tenth by the cross-section adjustment. The biases of the calculated values before the adjustment are -0.5% for the plutonium fueled assemblies and 0.3 % for the uranium fueled assemblies. These are reduced to negligible values after the cross-section adjustment. The usefulness of the cross-section adjustment in burnup characteristics prediction are also investigated and showed that the uncertainty of burnup swing is decreased to about 1/2 through 1/3.[10]

French group is continueing their enthusiastic endeavor for the cross-section adjustment works.[11] From the programming stage of an experiment in critical facility, they consider the strategy of the data utilization in the cross-section adjustment and choose the best program which serves in the improvement of prediction accuracy. Their integral data include not only experimental data from MASURCA, but also extensive pin and sample iradiated data in PHENIX. In MASURCA, substitution worth of different Pu vector samples are measured, which is called BALZAC-HI experiment. In Phenix, irradiation experiment of separate pure sample (PROFIL) and MOX pins of different Pu compositions(TRAPU) are performed. Table 8 shows how the uncertainty of burnup reactivity swing is decreased by the employment of the cross-section adjustment method. From the table, we can see that the uncertainty is decreased to about one third by employing all the experimental data of BALZAC, PROFIL, TRAPU.

6. Concluding Remarks

As was described above, the cross section adjustment method gave us a fascinating lure. However, the cross-section adjustment works necessitate an enormous amounts of labour such as the evaluation of cross-section covariance file, calculation of sensitivity coefficients for neutronics properties, and the development of efficient method of adjustment. We would like to cooperate for our common target - **improvement of prediction accuracy** -.

- References -

(1) Dragt J.B., et al.: Nucl. Sci. Eng. 62, 117 (1977)
(2) Carpenter S., et al.: "Experimental Studies of 6000-litre LMFBR Cores at ZPPR", Proc. of the Topical Meeting - 1980 Advances in Reactor Physics and Shielding, 521-534, Sept 14-17, 1980, Sun Valley, Idaho, USA (1980).
(3) Yamamoto M., et al.: " Analysis of Large Conventional LMFBR Core Critical Experiments and Their Implication to Design Methods", Proc. of the Topical Meeting on Reactor Physics and Shielding, Volume II, 773-787, Sept 17-19, 1984, Chicago, Illinois, USA (1984)
(4) Kamei T. and Kato Y.: J. Nucl. Sci. Technol., 22[12],1025(1985)
(5) Hammer P.: "Proposal for Burnup Calculation Applied to the NEACRP Fast Breeder Benchmark", NEACRP-A-439, Nuclear Energy Agency Committee on Reactor Physics(1980)
(6) Kamei T. et al.: Nucl. Sci. Eng.,91,11(1985)
(7) Takeda T. and Umano T.: Nucl. Sci. Eng., 91, 1(1985)
(8) Poenitz W.P. and Collins P.J. :"Utilization of Experimental Integral Data for the Adjustment and Uncertainty Evaluation of Reactor Design Quantities", NEACRP Specialists' Meeting , Sept. 23-24, 1988, Jackson Hole, WY
(9) Collins P.J., et al.:"A Data Base for the Adjustment and Uncertainty Evaluation of Reactor Design Quantities", NEACRP Specialists' Meeting , Sept. 23-24, 1988, Jackson Hole, WY
(10) Khalil H. and Downar T. J.,"Uncertainty in the Burnup Reactivity Swing of Fast Reactors", NEACRP Specialists' Meeting , Sept. 23-24, 1988, Jackson Hole, WY
(11) D'Angel A. and Salvatores M.,"Recent Integral Experiments Designed to Improve Higher Actinide Data to Meet Design Target Accuracies",NEACRP Specialists' Meeting , Sept. 23-24, 1988, Jackson Hole, WY

Table 1 C/E values before and after cross section adjustment for various integral quantities

	Before Adjustment		After Adjustment	
	C/E	Space Dependence	C/E	Space Dependence
Criticality Factor				
ZPPR- 9	.9994		1.002	
ZPPR-10A	.9967		1.000	
ZPPR-10D	.9961		1.000	
Reaction Rate Ratio				
C^{28}/F^{49}	1.060		1.019	
F^{28}/F^{49}	.988		.992	
Control Rod Worth				
ZPPR-10A				
Central Rod	.951	1.000	1.029	1.000
1st Ring Rods	.947	.996	1.012	.983
2nd Ring Rods	.988	1.039	.993	.965
ZPPR-10D				
Central Rod	.943	1.000	1.034	1.000
1st Ring Rods	.954	1.012	1.036	1.002
2nd Ring Rods	1.003	1.064	1.048	1.014
3rd Ring Rods	1.064	1.128	1.062	1.027
^{239}Pu(n,f) Rate Distribution				
ZPPR-10A				
Core center	.981	1.000	1.002	1.000
Mid Inner Core	.980	1.012	1.009	1.007
Outer Core	1.016	1.037	1.002	1.000
ZPPR-10D				
Core center	.986	1.000	1.013	1.000
Mid Inner Core	.977	1.018	1.020	1.007
Outer Core	1.008	1.047	1.013	1.000

Table 2 Cross section changes of important reactions

(%)

Reaction	Group†	Cross section changes
σ_f^{49}	1	−2.4
	2	−5.1
	3	−2.2
	4	1.7
σ_c^{49}	1	2.8
	2	2.6
	3	−0.8
	4	−2.6
σ_f^{28}	1	−3.0
σ_c^{28}	1	−1.2
	2	−1.3
	3	−5.8
	4	−9.6
σ_{in}^{28}	1	−10.3
	2	−10.7

† Lower energy of each group: 800, 100, 1 keV and 0.025 eV

Table 3 Reactivity loss of 365-day burnup for a 3000-MW(thermal)LMFBR
- An international benchmark for burnup calculation -

Nuclear Data File	Reactivity Loss	Organization
JENDL-2	1.5% $\Delta k/k$	Japan Atomic Energy Research Institute
ENDF/B-IV	0.5 to 0.7	Swiss Federal Institute for Reactor Research, Comitato Nazionale per l'Energia Nucleare, Australian Atomic Energy Commission
ENDF/B-V	1.0	Argonne National Laboratory
KEDAK-3	1.9	Kernforschungszentrum Karlsruhe
CARNAVAL-IV	1.3	Commissariat à l'Energie Atomique

Table 4 Prediction uncertainty of 1000-MW(electric)core burnup Characteristics(Nonadjusted library)

Uncertainty for 292 EFPD Burnup

A. Burnup Reactivity and Breeding Ratio
Burnup Reactivity $2.557 \times (1 \pm 0.290)\%\ \Delta K/KK'$
Breeding Ratio $1.204 \times (1 \pm 0.043)$

B. Fissile Number Density [End of Equilibrium Cycle (EOEC)]

Region	^{239}Pu ($\times 10^{20}$ atom/cm^3)	^{241}Pu ($\times 10^{20}$ atom/cm^3)
Inner core	$8.435 \times (1 \pm 0.019)$	$1.271 \times (1 \pm 0.031)$
Outer core	$9.704 \times (1 \pm 0.012)$	$1.733 \times (1 \pm 0.021)$
Radial blanket-1	$1.874 \times (1 \pm 0.031)$	$0.001 \times (1 \pm 0.164)$
Radial blanket-2	$0.636 \times (1 \pm 0.016)$	$\sim 0 \times (1 \pm 0.162)$
Axial blanket-1	$2.286 \times (1 \pm 0.027)$	$0.004 \times (1 \pm 0.142)$
Axial blanket-2	$1.373 \times (1 \pm 0.019)$	$\sim 0 \times (1 \pm 0.146)$

Table 5 Integral data employed in the cross-section adjustment and the uncertainties (1σ)

	Error (%)
k_{eff}	0.5
C^{28}/F^{25}	3
F^{28}/F^{25}	4
F^{49}/F^{25}	3
Doppler (UO_2 sample)	5

Table 6 Prediction uncertainty of 1000-MW(electric)core burnup characteristics (Adjusted library)

Case Number	Integral Data Employed	Burnup Reactivity	Breeding Ratio	^{239}Pu Number Density at 292 EFPD Operation (%)			
				Inner Core	Outer Core	Radial Blanket (Core Side)	Axial Blanket (Core Side)
1	None	29.0	4.3	1.9	1.2	3.1	2.7
2	Only k_{eff}	25.4	3.1	1.4	1.0	1.6	1.6
3	Only C^{28}/F^{25}	19.8	3.2	1.4	0.9	2.1	1.8
4	C^{28}/F^{25}, F^{49}/F^{25}, F^{28}/F^{25}	19.1	2.6	1.1	0.8	1.5	1.4
5	k_{eff}, C^{28}/F^{25}, F^{49}/F^{25}, F^{28}/F^{25}	19.1	2.5	1.1	0.8	1.2	1.2
6	k_{eff}, C^{28}/F^{25}, F^{49}/F^{25}, F^{28}/F^{25}, Doppler	17.9	2.2	1.0	0.6	1.1	1.1

Table 7 One example of prediction of K_{eff} in the US

Assembly	Before Adjustment			After Adjustment	
	C/E-1,%	σ(C),%	σ(E,M)%	A/E-1,%	σ(A),%
Pu-fueled					
Jezebel	-0.2	1.8	0.2	-0.1	0.18
Jezebel-Pu	-0.8	1.6	0.3	-0.7	0.20
Flattop-Pu	0.7	1.6	0.2	0.4	0.14
ZPPR-12V	0.1	1.4	0.3	-0.1	0.14
ZPPR-12	-0.1	1.4	0.3	-0.2	0.12
ZPPR-15A	-0.5	1.6	0.3	0.2	0.14
ZPPR-15B	-0.5	1.7	0.3	0.1	0.14
Zebra-8B	1.0	3.2	0.4	0.7	0.25
ZPR-3/56B	-1.0	1.5	0.3	-0.5	0.16
Zebra-8E	-1.6	2.7	0.4	-0.7	0.21
ZPPR-13C	-0.7	1.6	0.3	0.0	0.12
Zebra-8D	0.1	2.6	0.5	0.7	0.20
ZPPR-17A	-0.7	1.6	0.3	0.0	0.12
Zebra-8C	-2.2	1.9	0.5	-0.4	0.27
ZPR-6/7	-0.8	1.6	0.3	-0.1	0.13
Zebra-8A	-1.4	2.0	0.7	-0.8	0.33
Zebra-8F	-0.3	1.9	0.5	0.5	0.33
Average	-0.5			-0.06	
U-fueled					
Godiva	-0.3	1.6	0.1	0.0	0.13
Flattop-25	0.4	1.2	0.1	-0.1	0.12
Big-10	1.6	2.0	0.3	0.1	0.17
ZPR-9/36	1.4	2.2	0.3	0.3	0.14
Scherzo	0.9	3.4	0.4	0.1	0.26
Zebra-8H	0.3	3.1	0.4	-0.4	0.20
ZPPR-15D	-0.7	1.1	0.3	-0.1	0.18
ZPR-6/6A	-1.2	1.2	0.3	-0.1	0.19
Average	0.3			-0.03	

σ(C) and σ(A): uncertainty due to cross-section error

σ(E,M) : combined uncertainty of the experimental value and method approximation

Table 8 Uncertainty in LMFBR reactivity loss per cycle

Case	A	B	C	D
BALZAC	NO	YES	YES	YES
PROFIL	NO	NO	YES	YES
TRAPU	NO	NO	NO	YES
Uncertainty	26 %	23 %	17 %	9 %

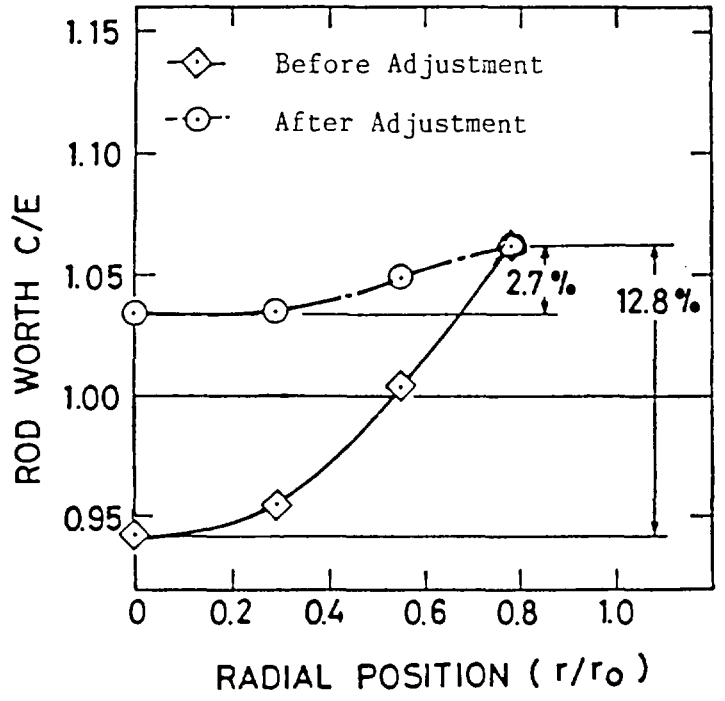

r : Radius of bank rods inserted
r_0: Core radius

Fig. 1 Spatial variation of control rod worth C/E values in ZPPR-10D assembly (before and after adjustment)

2.2.2 Application of Adjustment Method to JENDL-3T

Masanori Takamoto and Toshikazu Takeda

Osaka University, Department of Nuclear Engineering
Yamada-oka 2-1, Suita, Osaka, Japan

ABSTRACT

The integral data obtained from fast critical experiments have been utilized to adjust the 16 group cross section set produced from JENDL-3T. The diffusion coefficient, individual excitation levels of the ^{238}U inelastic scattering, β_{eff} and the fission spectrum were considered in the adjustment in addition to the conventional cross sections. The integral data we used are the multiplication factor, the reaction rate ratios, the reaction rate distributions and control rod worth of ZPPR-9, 10 and 13. The adjustment revealed that the ^{238}U capture cross section should be reduced by 2~10% over 1keV~1MeV.

I. INTRODUCTION

Recently the integral data for the large fast critical assemblies ZPPR-9,10 and 13 was utilized to adjust the 16 groups cross section set obtained from JENDL-2.[1] The changes of the ^{238}U capture and inelastic scattering cross sections, the ^{239}Pu capture and fission cross sections, and $\bar{\nu}$ value, and the diffusion coefficient were large, and had significant contribution to the improvement of k_{eff}, reaction rate ratio, control rod worth, and sodium void worth.

In this paper we apply the cross section adjustment to JENDL-3T to obtain some information for the final compilation of JENDL-3.

In Chap.II the analysis results of fast critical assemblies are described as C/E values which is the ratio of calculated to experimental values for JENDL-3T. The cross section adjustment results are shown in Chap.III

II. ANALYSIS OF INTEGRAL EXPERIMENTS

The joint physics large LMFBR core critical experiment program has been conducted between U.S. DOE and PNC, Japan, using the ZPPR facility at ANL-Idaho[2]. ZPPR-9 and -10 were conventional homogeneous two-zone cores of 650~850MWe-size. ZPPR-13 was a radial heterogeneous core. Physics parameters of these assemblies were measured, and analyzed in Japan by the method shown in Fig.1 using JENDL-2. A 70 group cross section set was produced from the JENDL-2 library using TIMS-1 and PROF-GROUCH-G2.[3] The base cell calculations are based on 1-D cell

calculations, and the base core calculations are based on 7-group diffusion calculations with Benoist's diffusion coefficients using one mesh point per drawer in the XY plane and ~5cm mesh intervals in the axial direction. The 7-group calculations were done for criticality, reaction rate and control rod worths, and the 18-group calculations were used for sodium void worths. The XYZ model was applied to all calculations except for control rod worths. For control rod worths, XY calculations were applied with axial buckling corresponding to the core height. As the corrections to the base calculation, the 2-D cell correction, cell interaction correction, 3-D transport correction, energy collapsing correction and mesh correction. The details of these corrections are shown in Ref.(4).

For the present adjustment of JENDL-3T, we made the new C/E values for JENDL-3T. We calculated the parameters using JENDL-2 and JENDL-3T by the diffusion core calculation for ZPPR-9,10D and 13A with xyz models , which included no correction. The difference between these two values for JENDL-2 and -3T was corrected to the C/E values obtained from JENDL-2. These corrected C/E values were used as those for JENDL-3T.

The C/E values are summarized in TABLE 1. The k_{eff} of JENDL-2 is predicted fairly well for all assemblies. But using JENDL-3T, the C/E values of k_{eff} become about 0.5% smaller than JENDL-2. The ^{239}Pu fission cross section gives a contribution of -1.4%dk/k and the ^{239}Pu ν value of 0.3%, the ^{238}U scattering of 0.7%, the ^{238}U capture of -0.2%, respectively as shown in TABLE 2.

The C/E value for control rod reactivity worth of ZPPR-10D had space discrepancy for JENDL-2: the C/E value becomes higher with core radius, and the C/E value for the outermost ring is 12% higher than that for the central rod. Using JENDL-3T, however, this space discrepancy was reduced to about 6%. This reduction is largely due to the ^{239}Pu fission and ν value.

As for the reaction rate ratio, the change of C/E values for 25F/49F(^{235}U fission/^{239}Pu fission), 28C/49F and 28F/49F are about -2%, 1.2%, 5.5% respectively. The discrepancy between C and E is smaller for 25F/49F but larger for the 28C/49F and the 28F/49F than for JENDL-2. For 28C/49F, the ^{238}U capture cross section gives a contribution of 0.6%, the ^{239}Pu fission cross section of 2% and the ^{238}U scattering cross section of -1%. For 28F/49F, the ^{238}U scattering cross section give a contribution of 6%, the ^{239}Pu fission cross section of 1.8% and the ^{238}U fission cross section of -2.4% respectively.

The cross section change from JENDL-2 to JENDL-3T is showed in Table 3 for main heavy nuclide. The ^{239}Pu fission cross section is decreased and ^{238}U capture cross section is increased and give negative contribution to k_{eff} or positive contribution to 28C/49F.

The reaction rate distribution of ^{239}Pu fission shows, for JENDL-2, a tendency of C/E value to becomes higher with core radius. The point-by-point C/E value become higher gradually with radius up to about 7% at the outer core relative to the core center for ZPPR-13A. For JENDL-2, however, this space discrepancy is reduced to ~3% as shown in TABLE 1.

III. ADJUSTMENT OF JENDL-3T

The 16-group cross section set obtained from JENDL-3T was adjusted using the C/E values of the core performance parameters of ZPPR-9, 10D and 13A. Sensitivity coefficients were calculated by the generalized perturbation theory code SAGEP based on diffusion theory on 2-D RZ geometry.[5] The cross section covariance matrix, except for ^{239}Pu, ^{235}U, ^{238}U and ^{240}Pu, was produced by modifying the covariance file evaluated by Drischler and Weisbin.[6] The variance of cross section of ^{239}Pu, ^{235}U, ^{238}U, and ^{240}Pu were produced by Nakagawa.[7] The standard deviations are listed in TABLE 4. The standard deviation for each excitation level of the ^{238}U inelastic scattering was taken as 10%, and that for diffusion coefficient as 5%.

The cross sections for the elements listed in TABLE 5 are adjusted. For the fission spectrum, JENDL-3T utilizes the Madland-Nix formula, but the sensitivity has not been calculated. So instead , the temperature of Maxwell distribution was chosen as the adjustment parameter. The diffusion coefficients were also adjusted because there is uncertainty in the P_1 scattering cross section Σ_{s^1} used in the definition of transport cross section $\Sigma_{tr}=\Sigma_{t}-\Sigma_{s^1}$. For the adjustment of the ^{238}U inelastic scattering cross section, 26 individual excitation levels and a continuum region were divided into four groups: the 1st group corresponds to the 1st and the 2nd levels, the 2nd group the 3rd to the 9th levels, the 3rd group the 10th to the 16th levels and the 4th group the continuum region as shown in TABLE 6. The scaling factor β_{eff} was also adjusted because the measured control rod worth is converted to k_{eff}. For the control rod worth, the method uncertainty is large because there is an error of about 4% in the estimated scaling factor β_{eff}. When we consider this large error in the adjustment of control rod worth for each rod pattern, the spatial dependence of the C/E values (not the C/E value itself) is not improved by the adjustment. Then, as utilized by Kamei and Kato[8], we took the ratio of control rod worths at the core center and off-center positions, and adjusted the ratio because there will be no scaling factor uncertainty.

The C/E values before and after the adjustment are also listed in TABLE 1. The cross section change is shown in TABLE 7.

The ^{238}U capture cross section is reduced by 2~10% in the energy of 1keV~1MeV. The element-wise contribution of improvement of C/E values is shown in TABLE 8. The underestimation k_{eff} of ~0.5% and the overestimation of 28C/49F of ~8% were improved by the adjustment. The main contribution is due to the ^{238}U capture cross section reduction.

The change of ^{239}Pu fission cross section is small, but the increase by 0.1~0.7% at the energy of 10keV~0.6MeV is important because this cross section has non-negligible sensitivity, and so remarkable contributions to the improvement for k_{eff} and reaction rate ratios.

The C/E values of 28F/49F on ZPPR-9, 10D were overestimated by 4~7%. To improve these values, the ^{238}U inelastic cross section was increased by ~2%. This is because the ^{238}U fission is the threshold reaction above 1MeV and so the

increase of inelastic scattering cross section make the neutron spectrum soft and reduce the ^{238}U fission reaction.

The ^{235}U fission cross section is decreased about~2% at the energy of 10keV~100keV and the ^{239}Pu capture cross section is increased about 6% at the energy of 100keV~1MeV. These change has large contribution of improvement of about 20% and 50%, respectively, for 25F/49F. The spatial discrepancy for the reaction rate distribution and the control rod worth was remarkably improved: The 6% discrepancy between the control rod worths at the core center and the core edge in ZPPR-10D was reduced to 2%. The increase of diffusion coefficient of about 4% has ~55% contribution.

Besides the diffusion coefficient, the ^{238}U capture cross section and the ^{239}Pu fission cross section have contributions of 53% and 5% to the improvement of the spatial discrepancy of control rod worth.

The above results was obtained when we took 10% uncertainty for the ^{238}U inelastic scattering cross section. If we assume the uncertainty as much as 30%, the contribution of the ^{238}U inelastic cross section and the fission spectrum changes become large. So we have to investigate the effect of uncertainty for the cross section adjustment in near future.

CONCLUDING REMARKABLE

The C/E values for JENDL-3T were calculated for the key core parameters in large fast critical assemblies. The results revealed that, the space dependency of control rod worth, which is about 12% for JENDL-2, is improved to 6%. The overestimation of 25F/49F, which is 3~6% in JENDL-2, is improved to 0.5~3%. However the k_{eff} was underestimated by 0.5~1% for JENDL-3T though near unity for JENDL-2. The 28C/49F and 28F/49F were overestimated about 2~10% for JENDL-3T. Using the C/E values, we have adjusted the 16 group cross section for JENDL-3T. The ^{238}U capture cross section is decreased by 2~10% at the energy of 1keV~1MeV which leads to the improvement of k_{eff}, 28C/49F, control rod worth. The space discrepancy of control rod worth of 6% is improved to 2% due to the ^{238}U capture cross section, the diffusion coefficient and ^{8}O scattering cross section. To improve large overestimation of 28F/49F, the ^{238}U capture cross section has a main contribution, and increase of inelastic scattering cross section has rather large contribution.

REFERENCES

1. T. TAKEDA et al.,"Prediction Uncertainty Evaluation Methods of Core Performance Parameters in Large LMFBRs", *Proc. 1988 International Reactor Physics Conference, Jackson Hole, Wyoming*, Sep. 18-22,1988.

2. M.YAMAMOTO et al.,"Analysis of Large Conventional LMFBR Core Critical Experiments and Their Implication to Design Methods", *Topical Mtg. on Reactor Physics and Shielding*,

Sep. 17-19, 1984, Chicago, USA.

3. H.TAKANO, A.HASEGAWA and K.KANEKO: "TIMS-PGG: A Code System for Producing Group Constants in Fast Neutron Energy Region", *JAERI-M 82-072* (1982).

4. T.TAKEDA et al., "Analysis of Large Liquid-Metal Fast Breeder Reactor Critical Experiments by Improved Methods," *Nucl.Sci.Eng.* 100, 538-548 (1988).

5. A.HARA, T.TAKEDA and Y.KIKUCHI, "SAGEP: Two-Dimensional Sensitivity Analysis Code Based on Generalized Perturbation Theory," *JAERI-M 84-065* (1984).

6. J.P.DRISCHLER and C.R.WEISBIN, *ORNL-5318* (1977).

7. Y.NAKAGAWA, *Private Communication* (1988).

8. T.KAMEI and Y.KATO, *J.Nucl.Sci.Technol.*, 22, 1025 (1985).

Table 1 C/E values of core performance parameters obtained JENDL-2 and JENDL-3T

Core Performance Parameters	C/E Value JENDL-2	JENDL-3T	Adjusted
ZPPR-9 k_{eff}	0.999	0.995	1.003
ZPPR-10D k_{eff}	0.996	0.991	0.999
ZPPR-13A k_{eff}	0.999	0.994	1.003
ZPPR-10D CR.Worth, Core Center	0.943	1.012	1.030
ZPPR-10D CR.Worth, 3rd CR Ring[1]	1.128	1.064	1.025
ZPPR-9 25F/49F[2]	1.027	1.005	0.998
ZPPR-9 25C/49F	1.070	1.084	1.024
ZPPR-9 28F/49F	0.988	1.045	1.008
ZPPR-10D 25F/49F	1.057	1.035	1.027
ZPPR-10D 28C/49F	1.088	1.103	1.042
ZPPR-10D 28F/49F	1.009	1.066	1.030
ZPPR-13A 25F/49F	1.033	1.010	1.002
ZPPR-13A 28F/49F	0.967	1.016	1.001
ZPPR-13A 28C/49F	1.058	1.071	1.010
ZPPR-9 RRD.49F, IC Midpoint[3]	1.009	1.007	1.006
ZPPR-9 RRD.49F, IC Edge	1.029	1.020	1.014
ZPPR-9 RRD.49F, OC Midpoint	1.041	1.015	1.006
ZPPR-10D RRD.49F, IC Midpoint	1.010	1.004	1.001
ZPPR-10D RRD.49F, IC Edge	1.019	0.993	0.996
ZPPR-10D RRD.49F, OC Midpoint	1.031	1.017	0.985
ZPPR-13A RRD.49F, 2nd Fuel Ring[4]	1.032	1.029	1.011
ZPPR-13A RRD.49F, 3rd Fuel Ring	1.069	1.030	1.011

1) CR Worth(3rd CR Ring)/CR Worth(Center CR)
2) Reaction rate ratio, F: fission, C: capture, 49: ^{239}Pu, 25: ^{235}U, 28: ^{238}U
3) Reaction rate distribution, ^{239}Pu fission rate, normalized to unity at core center, IC: inner core, OC: outer core
4) Normalized to unity at fuel ring 1

Table 2 Nuclide-wise change of core performance parameters from JENDL-2 to JENDL-3T

	k_{eff} ZPPR-9	CR Worth* ZPPR-10D	28C/49F ZPPR-9	28F/49F ZPPR-9	25F/49F ZPPR-9
^{239}Pu					
Fission	-1.4%	3%	2%	1.8%	2.5%
ν	0.3	1	0.0	0.0	0.0
Capture	0.2	0.5	0.0	-0.3	0.1
^{238}U					
Fission	-0.2	0.5	0.0	-2.4	0.0
Capture	-0.2	0.1	0.6	0.1	0.0
Scattering	0.7	-0.1	-1	6	-0.4
^{235}U					
Fission	0.0	0.0	0.0	0.0	-3.7
^{8}O					
Scattering	0.0	0.3	-0.1	0.0	-0.5
Total	-0.5	6	1.2	5.5	-2

* center control rod worth

Table 3 Cross section change from JENDL-2 to JENDL-3T

^{239}Pu fission (%)		^{238}U capture (%)	
energy group	(J3-J2)/J2	energy group	(J3-J2)/J2
1	3.3	1	-0.1
2	-0.3	2	8.3
3	-0.6	3	18.6
4	0.1	4	27.0
5	-1.2	5	6.9
6	-3.7	6	3.0
7	-4.0	7	5.0
8	-5.1	8	2.1
9	-4.9	9	0.1
10	-1.2	10	-0.5
11	-1.9	11	-1.6
12	-1.6	12	-2.4
13	2.0	13	-0.5
14	8.5	14	1.3
15	-9.6	15	0.1
16	-3.9	16	0.1

Table 4 Standard deviation of 16-group cross sections used in adjustment (%)

energy group	upper energy	^{8}O scat	^{11}Na cap	^{26}Fe cap	^{235}U cap	^{235}U fis	^{238}U cap
1	10.0 E+6	14.9*	50.0*	20.0*	69.3*	1.0**	50.0**
2	6.07 E+6	1.3	50.0	20.0	61.2	0.8	20.0
3	3.68 E+6	1.1	50.0	20.0	60.0	0.8	16.4
4	2.23 E+6	1.2	40.8	20.0	60.0	0.9	8.3
5	1.35 E+6	1.1	36.6	14.2	46.2	1.1	6.0
6	8.21 E+5	2.4	36.6	15.6	33.8	1.6	4.1
7	3.88 E+5	2.2	50.0	18.9	22.4	2.1	4.6
8	1.83 E+5	1.4	18.1	12.5	37.0	2.3	6.9
9	8.65 E+4	1.4	20.8	12.5	9.8	4.0	5.3*
10	4.09 E+4	1.4	13.6	9.2	8.8**	5.3	9.9
11	1.93 E+4	1.4	23.2	10.5	19.0	6.6	13.5
12	9.12 E+3	1.4	11.9	17.8	18.2	5.8	11.2
13	4.31 E+3	1.4	12.2	24.8	16.6	7.4	10.0
14	2.03 E+3	1.4	12.2	24.2	20.0	4.1	10.1
15	9.61 E+2	1.4	10.7	23.3	14.1	2.5	7.9
16	4.54 E+2	1.4	1.0	1.0	18.0	2.9	0.4

energy group	^{238}U fis	^{238}U ν	^{240}Pu cap	^{241}Pu fis	^{239}Pu cap	^{239}Pu fis	^{239}Pu ν
1	1.2**	0.4*	47.0**	1.9*	60.0*	1.3**	0.4**
2	0.9	1.1	47.0	4.4	60.0	1.2	0.6
3	0.9	1.4	47.0	3.4	60.0	1.1	0.5
4	1.1	1.6	40.0	3.7	60.0	0.9	0.4
5	1.7	1.6	34.0	4.6	37.8	0.9	0.4
6	6.6	1.6	24.0	7.5	20.0**	1.4	0.3
7	3.5*	1.6	17.0	7.5	18.0	1.7	0.4
8	7.9	1.6	16.0	4.1	18.0	1.8	0.6
9	7.9	1.6	9.6	2.7	10.0	5.0	0.7
10	108.0	1.6	8.0	4.0	9.1	5.2	0.7
11	109.6	1.6	7.9	5.1	13.0	5.4	0.7
12	109.6	1.6	7.4	5.3	8.6	5.2	0.7
13	0.0	0.0	10.0	9.3	10.0	4.8	0.7
14	109.7	1.6	10.0	12.9	12.0	7.3	0.7
15	109.6	1.6	10.0	12.6	8.0	4.1	0.7
16	109.5	1.6	10.0	0.7	7.5	3.5	0.5

scat: scattering cap: capture fis: fission ν: ν value
* Data by Drischler and Weibin
** Data by Nakagawa

Table 5 Cross sections used for adjustment

Nuclide	Capture	Fission	ν value	Scattering
^{235}U	◎	◎	◎	
^{238}U	◎	◎	◎	
^{239}Pu	◎	◎	◎	
^{240}Pu	◎			
^{241}Pu		◎		
^{26}Fe	◎			
^{11}Na	◎			
^{8}O				◎

Others
- β eff
- diffusion coefficient
- temperature parameter T of the Maxwell distribution for the ^{239}Pu fission spectrumχ
- excitation levels and the continuum region of the ^{238}U inelastic scattering

Table 6 Energy level structure of ^{238}U Inelastic scattering

Calculated Group	No.	Energy (MeV) JENDL-2	JENDL-3T
1	1	0.0447	0.0449
	2	0.148	0.148
2	3	0.301	0.307
	4	0.520	0.518
	5	0.680	0.680
	6	0.732	0.731
	7	0.790	0.776
	8	0.838	0.827
	9	0.939	0.927
3	10	0.968	0.950
	11	1.006	0.966
	12	1.047	0.993
	13	1.076	1.037
	14	1.100	1.060
	15	1.123	1.077
	16	1.150	1.107
	17	1.190	1.129
	18	1.210	1.150
	19	1.246	1.169
	20	1.274	1.223
	21	1.313	1.243
	22	1.361	1.270
	23	1.401	1.279
	24	1.437	1.290
	25	1.470	1.378
	26	———	1.415
4	Continuum region (above 1.5MeV)		

Table 7 Relative change of cross sections by adjustment of JENDL-3T (%)

Energy group	^{8}O sct	^{11}Na cap	^{26}Fe cap	^{235}U cap	^{235}U fis	^{238}U cap	^{238}U fis	^{240}Pu cap
1	-0.15	0.85	0.65	0.28	0.00	-16.92	-0.11	-1.84
2	-0.21	0.85	0.65	0.39	0.00	-2.65	-0.10	-2.07
3	-0.19	0.85	0.65	0.34	-0.01	-1.39	-0.12	-1.27
4	-0.19	0.22	0.65	0.34	-0.02	-2.91	-0.15	-1.38
5	-0.20	0.05	0.78	0.32	-0.04	-3.60	-0.17	-1.14
6	-0.63	0.15	0.71	0.27	-0.10	-2.40	-0.30	1.06
7	-0.59	0.31	1.21	0.22	-0.25	-2.55	-0.10	1.41
8	-0.29	0.15	0.87	0.34	-0.42	-4.25	-0.04	1.16
9	-0.29	0.14	0.71	0.14	-1.07	-3.64	-0.01	0.67
10	-0.29	0.07	0.54	0.15	-1.59	-8.16	-1.65	0.74
11	-0.29	0.08	0.53	0.29	-1.90	-11.01	-1.68	0.50
12	-0.29	0.13	0.85	0.30	-1.59	-8.33	-1.68	0.74
13	-0.29	0.15	0.55	0.29	-1.96	-6.60	0.00	0.95
14	-0.29	0.15	2.00	0.34	-1.07	-5.31	-1.68	0.81
15	-0.29	0.13	1.92	0.23	-0.55	-3.13	-1.68	0.70
16	-0.29	0.00	0.00	0.14	-0.54	-0.11	-1.67	0.07

Energy group	^{239}Pu cap	^{239}Pu fis	^{239}Pu ν	Dif.* Coef.	^{238}U inelastic scattering Lev.1	Lev.2	Lev.3	Lev.4
1	1.90	0.00	0.09	0.58	0.15	0.19	0.18	0.50
2	1.90	0.00	0.14	0.81	0.37	0.61	0.70	2.71
3	1.90	0.01	0.08	1.24	1.25	1.87	3.13	7.71
4	1.90	0.00	0.02	1.30	2.51	2.66	5.96	2.59
5	4.68	0.01	-0.12	1.15	1.31	0.95	0.96	0.00
6	5.96	0.04	-0.15	2.24	2.53	0.17	0.00	0.00
7	5.76	0.12	-0.17	2.46	1.03	0.06	0.00	0.00
8	5.66	0.18	-0.25	2.33	-0.29	0.00	0.00	0.00
9	0.80	0.65	-0.29	1.82	-1.14	0.00	0.00	0.00
10	4.12	0.77	-0.29	1.45	0.00	0.00	0.00	0.00
11	5.28	0.76	-0.29	1.10	0.00	0.00	0.00	0.00
12	3.98	0.61	-0.29	0.74	0.00	0.00	0.00	0.00
13	4.87	0.56	-0.29	0.54	0.00	0.00	0.00	0.00
14	6.19	0.86	-0.30	0.62	0.00	0.00	0.00	0.00
15	3.56	0.48	-0.28	0.55	0.00	0.00	0.00	0.00
16	0.16	0.41	-0.21	0.50	0.00	0.00	0.00	0.00

* diffusion coefficient
sct: scattering cap: capture fis: fission ν: ν value
Lev.1~4 : ^{238}U inelastic scattering, 1st-4th group (TABLE 6)

Table 8 Element-wise contribution to the C/E change due to Adjustment

(1) The Multiplication Factor of ZPPR-9

CROSS SECTION		ALTERATION (%)	CONTRIBUTION (%)
^{238}U	CAP	1.47	190
	Inel. Lev. 4*	-0.08	-11
^{239}Pu	FIS	0.22	28
	CAP	-0.26	-34
	ν	-0.16	-21
	Diffusion Coefficient	-0.23	-30
	Total	0.77	100.0

(2) The Reaction Rate Ratio 28C/49F of ZPPR-9

CROSS SECTION		ALTERATION (%)	CONTRIBUTION (%)
^{238}U	CAP	-5.2	94
^{949}Pu	FIS	-0.42	8
	Inel. Lev. 1*	0.08	-1
	Inel. Lev. 3*	0.11	-2
	Inel. Lev. 4*	0.08	-1
	Total	-5.5	100.0

(3) The Reaction Rate Ratio 28F/49F of ZPPR-9

CROSS SECTION		ALTERATION (%)	CONTRIBUTION (%)
^{238}U	CAP	-1.89	53
	Inel. Lev. 3*	-0.58	16
	Inel. Lev. 4*	-1.01	29
^{239}Pu	FIS	-0.29	8
	Total	-0.77	100.0

* Inel. Lev.1~4 : ^{238}U inelastic scattering, 1st-4th group (TABLE 6)

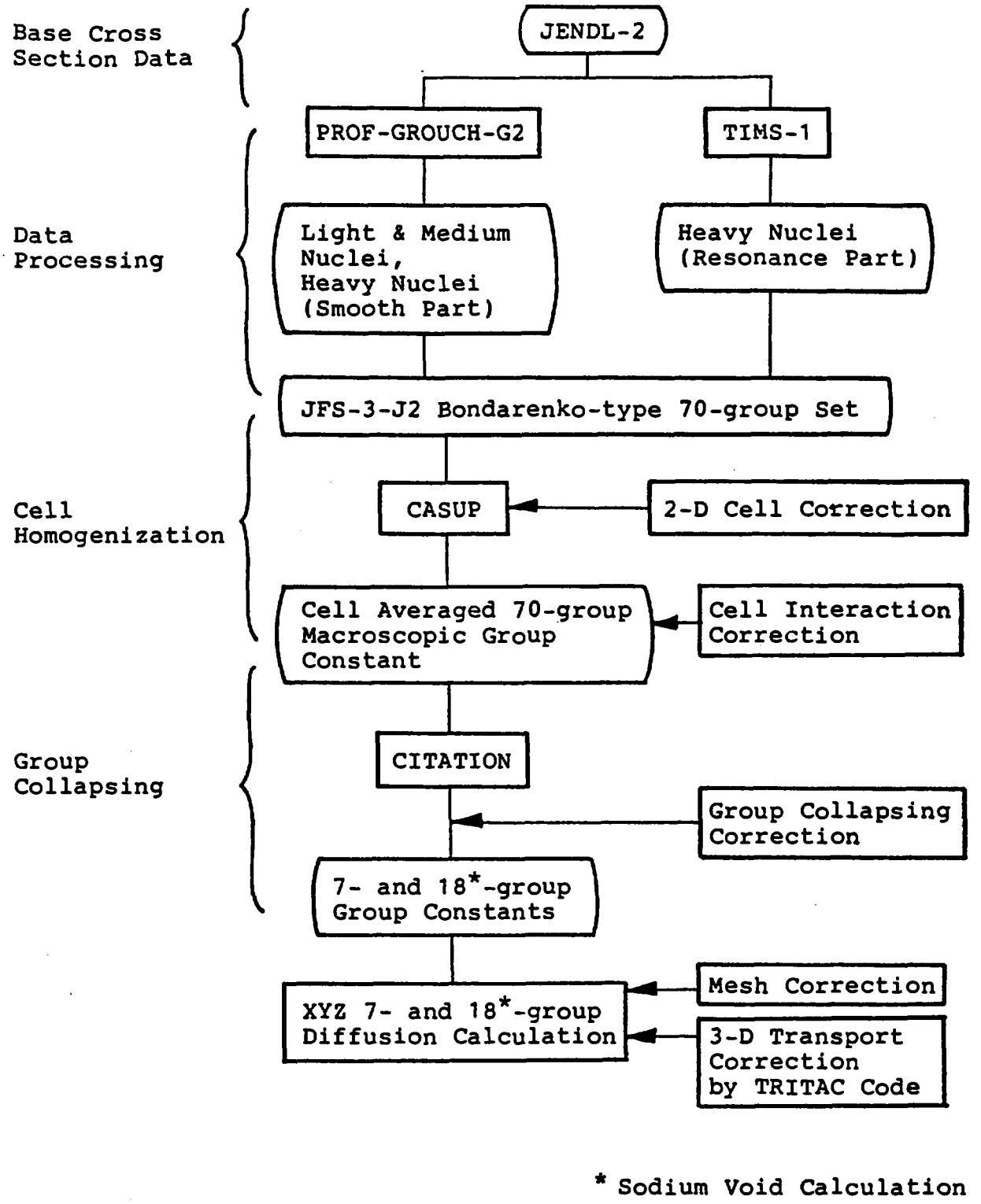

Fig. 1 Calculational flow of core performance parameters

2.2.3 Experimental Error on Integral Data of Reactor Physics Experiments at FCA

Toshitaka OSUGI and Susumu IIJIMA

Japan Atomic Energy Research Institute
Tokai-mura, Naka-gun, Ibaraki-ken 319-11, JAPAN

The procedures to estimate the experimental errors on integral data are discussed : Examples are taken from the measurements such as the criticality, the reactivity worth and the reaction rate ratio at FCA-XIV-1 core.

1. Introduction

Benchmark tests using the integral data are necessary to examine the availability of the nuclear data and computational methods in evaluating the nuclear characteristics. Moreover, the adjustment of the cross-section set is widely carried out on the basis of the benchmark results. In order to make these works efficient, it is important to get the knowledge of the uncertainty or experimental error associated with the integral data. For the purpose of the understanding of the experimental errors, the procedure to estimate them is explained using the measured data at the FCA-XIV-1 core as an example.

After a brief description for the FCA facility, the discussions are presented for the main sources in the experimental errors associated with the measured data such as the criticality, the reactivity worths and the reaction rate ratios.

2. FCA Facility

The JAERI Fast Critical Facility (FCA)[1),2)] is of the split-table type with horizontal matrix structure. Horizontally stacked on each of the two tables are 55.2 mm square, 1324.0 mm long, 1.0 mm thick stainless steel tubes, held in position by side and upper frames, forming a half matrix. Each half assembly contains usually four control-safety dual purpose rods of fuel removable type. One of the rods (or sets) in each half is used as control rod, and the rest as

safety rods.

The reactivity worth of the control rod is calibrated by the comparison method. The standard reactivity (ρ_o) is determined by a positive period measurement with the aid of the inhour equation. Delayed neutron data have been taken from Tomlinson's compilation[3]. In the excess reactivity range, the principal errors involved in the control rod calibration are those attributable to doubling time measurement and the delayed neutron data used in the inhour equation.

In the FCA facility, the reactivity effects of the changes of the core temperature and the gap width between the half assemblies are the main sources of the reactivity drift during the reactor operation. These effects should be known to correct the measured reactivity effects.

The temperature reactivity coefficient f_T was determined by measuring the reactivity change introduced by raising the core temperature about by 5°C.

The gap reactivity coefficient f_G was determined by measuring the curve of the reactivity vs. gap width between the half assemblies.

For the FCA-XIV-1 core, the following values were obtained ;

(1) standard reactivity (control rod insertion from 50 mm to 0 mm)

$\rho_o = 10.32 \pm 1.0\ \%\quad 10^{-4}\Delta k/k$

(only error in the doubling time measurement (±0.5 sec) is considered)

(2) temperature reactivity coefficient

$f_T = -0.69 \pm 0.02\quad 10^{-4}\Delta k/k/°C$

(3) gap reactivity coefficient

$f_G = -3.6 \pm 0.1\quad 10^{-4}\Delta k/k/mm\text{-}gap$

3. Excess Reactivity

The excess reactivity ρ_{ex} (20°C, 0.0mm) at the core temperature of 20°C and the gap width of 0.0 mm is defined by the equation

$$\rho_{ex}(20°C, 0.0mm) = \rho(R, T, G) + \Delta\rho(T \rightarrow 20°C) + \Delta\rho(G \rightarrow 0.0mm) + \Delta\rho(SS \rightarrow 0.0g), \quad (1)$$

where

$\rho(R,T,G)$ = measured excess reactivity

$R = (R_{C1}, R_{C2}, R_{S1}, \cdots, R_{S6})$ = rod positions

R_{C1}, R_{C2} = control rod positions

$R_{S1}, \cdots, R_{S6}$ = safety rod positions

$\Delta\rho(T \rightarrow 20°C)$ = reactivity correction by temperature from T to 20°C

$\Delta\rho(G \rightarrow 0.0mm)$ = reactivity correction by gap width from G to 0.0mm

$\Delta\rho(SS \rightarrow 0.0g)$ = reactivity correction by excess stainless steel between half assemblies from SS to 0.0 gram.

For the uncertainties in the rod positions, the core temperature and the gap width, we put

$$\delta R_{Ci} = \pm 0.1 \text{ mm } (i = 1,2)$$
$$\delta R_{Si} = \pm 0.01\text{mm } (i = 1, \cdots, 6)$$
$$\delta T = \pm 1.0 \text{ °C}$$
$$\delta G = \pm 0.3 \text{ mm}.$$

Using the values of ρ_0, f_T and f_G presented in Chapter 2, we get the componentwise experimental errors associated with the uncertainties in the rod positions, the core temperature and the gap width :

$$\delta\rho(R) = \pm \sqrt{2 \times 0.1^2\text{mm} + 6 \times 0.01^2\text{mm}} \times 10.32 \times 10^{-4}\Delta k/k \,/50\text{mm}$$
$$= \pm 0.030 \times 10^{-4}\Delta k/k$$
$$\delta\{\Delta\rho(T \rightarrow 20°C)\} = \pm 1.0°C \times 0.69 \times 10^{-4}\Delta k/k/°C$$
$$= \pm 0.69 \times 10^{-4}\Delta k/k$$
$$\delta\{\Delta\rho(G \rightarrow 0.0mm)\} = \pm 0.3mm \times 3.6 \times 10^{-4}\Delta k/k/mm\text{-gap}$$
$$= \pm 1.1 \times 10^{-4}\Delta k/k.$$

From the reactivity worth measurements of the stainless steel between half assemblies, we got

$$\delta\{\Delta\rho(SS \rightarrow 0.0g)\} = \pm 1.4 \times 10^{-4}\Delta k/k.$$

Then we get the total experimental error associated with the excess reactivity :

$$\delta\rho_{ex}(20°C,\ 0.0mm) = \pm\sqrt{\delta\rho(R)^2 + \delta\{\Delta\rho(T\rightarrow 20°C)\}^2 + \delta\{\Delta\rho(G\rightarrow 0.0mm)\}^2 + \delta\{\Delta\rho(SS\rightarrow 0.0g)\}^2}$$
$$= \pm\ 1.9\times 10^{-4}\Delta k/k$$

4. Reactivity Worth

4.1 Critical balance method

The reactivity worth $\Delta\rho_{I\rightarrow II}$ is defined by the difference of the excess reactivities, $\rho(R_I, T_I, G_I)$ and $\rho(R_{II}, T_{II}, G_{II})$ between two critical states, I and II, and the corrections for the core temperature and the gap width :

$$\Delta\rho_{I\rightarrow II} = \rho(R_{II}, T_{II}, G_{II}) - \rho(R_I, T_I, G_I) - \Delta\rho(T_I \rightarrow T_{II}) - \Delta\rho(G_I \rightarrow G_{II}) \quad (2)$$

The experimental error associated with the reactivity worth is expressed by the equation

$$\delta(\Delta\rho_{I\rightarrow II}) = \pm\sqrt{\delta\{\Delta\rho(\Delta R)\}^2 + \delta\{\Delta\rho(\Delta T)\}^2 + \delta\{\Delta\rho(\Delta G)\}^2}. \quad (3)$$

The degree of the uncertainty in the rod positions, the core temperatures and the gap widths depends on the experimental conditions or the experimental techniques.

(1) With separation of the assemblies

After measuring one critical state, the assemblies are separated for core modification, then, are reunited for measuring another critical state. In this case, we put

$$\delta R_{ci} = \pm\ 0.1\ mm \quad (i = 1, \cdots, 4)$$
$$\delta R_{si} = \pm\ 0.01\ mm \quad (i = 1, \cdots, 12)$$
$$\delta\{\Delta T\} = \pm\ 0.14\ °C$$
$$\delta\{\Delta G\} = \pm\ 0.014mm$$

The componentwise experimental errors associated with these uncertainties are calculated in a similar way of Chapter 3 :

$$\delta\{\Delta\rho(\Delta R)\} = \pm 0.042 \times 10^{-4}\Delta k/k$$
$$\delta\{\Delta\rho(\Delta T)\} = \pm 0.097 \times 10^{-4}\Delta k/k$$
$$\delta\{\Delta\rho(\Delta G)\} = \pm 0.050 \times 10^{-4}\Delta k/k$$

and the total experimental error

$$\delta\{\Delta\rho_{\mathrm{I}\rightarrow\mathrm{II}}\} = \pm 0.12 \times 10^{-4}\Delta k/k$$

(2) Without separation of the assemblies

When the measurements are made under stable core conditions, it is possible to reduce the uncertainties in the core temperature and the gap width between assemblies. To establish these core conditions, the assemblies have been kept united for more than two hours before the first criticality measurement and the core modifications are made without separation of the assemblies. The uncertainty in the rod positions is also reduced because the electric supply is not turned off.

In this case, we put

$$\delta R_{ci} = \pm 0.05 \ \mathrm{mm} \quad (i = 1, \cdots, 4)$$
$$\delta R_{si} = \pm 0.01 \ \mathrm{mm} \quad (i = 1, \cdots, 12)$$
$$\delta\{\Delta T\} = \pm 0.014 \ ^{\circ}\mathrm{C}$$
$$\delta\{\Delta G\} = \pm 0.0014 \mathrm{mm}$$

and

$$\delta\{\Delta\rho(\Delta R)\} = \pm 0.022 \times 10^{-4}\Delta k/k$$
$$\delta\{\Delta\rho(\Delta T)\} = \pm 0.0097 \times 10^{-4}\Delta k/k$$
$$\delta\{\Delta\rho(\Delta G)\} = \pm 0.0050 \times 10^{-4}\Delta k/k$$

then

$$\delta\{\Delta\rho_{\mathrm{I}\rightarrow\mathrm{II}}\} = \pm 0.025 \times 10^{-4}\Delta k/k \ .$$

(3) Oscillation method

The uncertainty in the rod positions can be reduced by using the fine control rod which has relatively small differential rod worth. Furthermore, the reactivity drift due to the changes of the core temperature and the gap width can be cancelled out with use of the sample oscillation method. In this

method, the reactivity worth of the sample is determined by measuring the reactivity changes caused by the sample oscillation, i.e., in-and-out sample movement. The effect of the reactivity drift on the sample reactivity worth can be minimized by repeating the measurements and by taking the average of the reactivity changes as the reactivity worth. This method has been used at FCA to measure the small reactivity worths of the actinide samples and the Doppler coefficient. The typical experimental errors of the reactivity worths associated with this method are estimated by, i.e. :

$$\delta\{\Delta\rho_{in-out}\} \approx \pm 0.1 \times 10^{-6} \sim 10^{-7}\ \Delta k/k$$

4.2 Source multiplication method

Using the source multiplication method, the sub-criticality ρ_1 is expressed by the equation

$$\rho_1 = \frac{A_0}{C_1} \cdot f_1 \tag{4}$$

where

$A_0 = \rho_0 C_0$

= constant determined by the known sub-criticality ρ_0 and the detector count rate C_0

C_1 = detector count rate

f_1 = calculated correction factor for the detector efficiency and the effective neutron source.

In the reactivity worth measurement for the simulated B_4C control rod at the FCA-XV-1 core, we got

$\delta A_0 = \pm 1.6\%$

$\delta C_1 = \pm 0.8\%$

$\delta f = \pm 1.0\%$

then

$\delta\rho(B_4C) = \pm 2.0\%$

$\delta\{\Delta\rho(\text{Void} \rightarrow B_4C)\} = \pm 2.2\%$

In this procedure, the A_0 value was determined by averaging the values of three known sub-critical states. The reactivity worth of the simulated B_4C control rod defined by the equation

$$\Delta\rho\,(\text{Void} \rightarrow B_4C) = \rho\,(B_4C) - \rho\,(\text{Void})$$

was obtained from the measurements using four independent detectors.

5. Reaction Rate Ratio

5.1 Micro fission counter

The fission rate F_m of m-nuclide is determined by the count rate of the micro fission counter inserted through the experimental hole :

$$F_m = \frac{R_M \cdot f_m}{k_M \cdot N_m} \tag{5}$$

where
- R_M = count rate of M-counter
- f_m = correction factor for impurities in M-counter
- k_M = counter efficiency of M-counter
- N_m = atom number density of m-nuclide in M-counter (effective atoms = $k_M N_m$).

The fission rates in uranium-235(F25), plutonium-239(F49) and uranium-238(F28) are measured at the FCA-XIV-1 core using the micro fission counters of Enriched U, Plutonium and Natural U listed in Table 1. The componentwise and total experimental errors on the reaction rates and reaction rate ratios are estimated :

Item	Experimental Error (%)		
	F25	F49	F28
δR_M	0.85	0.96	0.86
δk_M	2.0	2.0	2.0
δf_m	0.3	0.1	5.1
δF_m	2.2	2.2	5.5
δ {F49/F25} or δ {F28/F25}	-	3.1	6.0

Table 1 Effective atoms and isotopic compositions of fission counters

Counter name	Principal isotope	Effective number of fissile atoms	Isotopic composition (Atom %)			
Enriched U	^{235}U	$3.04 \times 10^{17} \pm 2.0\%$	^{234}U 0.95 ± 0.01	^{235}U 93.31 ± 0.05	^{236}U 0.41 ± 0.01	^{238}U 5.34 ± 0.04
Natural U	^{235}U	$4.16 \times 10^{17} \pm 2.0\%$	^{235}U 0.7204 ± 0.0007	^{238}U 99.23		
Plutonium	^{239}Pu	$7.10 \times 10^{17} \pm 2.0\%$	^{239}Pu 94.43 ± 0.02	^{240}Pu 5.22 ± 0.02	^{241}Pu 0.338 ± 0.002	^{242}Pu - 0.013
Neptunium	^{237}Np	$1.42 \times 10^{17} \pm 4.0\%$	^{237}Np 99.49	Pu* 0.506		

* Isotopic composition of the Pu is not known.

5.2 Activation foil

The reaction rate ratio of the captures in uranium-238(C28) to the fissions in uranium-235(F25) was measured using the enriched and depleted uranium foils. The thermal calibration was made by simultaneous irradiation of these foils in a thermal neutron field.

(1) Capture rate in uranium-238(C28)

The relative capture rates C28 in uranium-238 are obtained from the equation

$$C28 = \frac{R39}{\eta 39 \cdot f \cdot N28 \cdot k_c(t_r, t_c, t_m)} \quad (6)$$

where R39 = count rate of 277.6keV photo-peak for neptunium-239

$\eta 39$ = efficiency of Ge-detector for 277.6keV photo-peak of neptunium-239

f = correction factor for γ-self absorption in the activation foil

N28 = uranium-238 atoms in the activation foil

$k_c(t_r, t_c, t_m)$ = correction factor for the build-up and decay of neptunium-239 corresponding to the irradiation time (t_r), waiting time (t_c) and measuring time (t_m).

The experimental errors associated with the items in Eq.(6) were estimated :

δ R39 = ± 0.37 %

$\delta \eta 39$ = ± 0.95 %

δ N28 = ± 0.1 %

δk_c = ± 0.43 %

When the foils of the same specification are used in the measurements and the thermal calibration, the experimental error associated with the f-value in Eq.(6) is cancelled out. Additional uncertainty in the foil position in the cell is estimated to be about ± 0.5%, then

δ C28 = ± 1.2 %

(2) Fission rate in uranium-235(F25)

The relative fission rates F25i in uranium-235 measured by the photo-peak of i-fission product nuclide are obtained from the equation

$$F25_i = \frac{R_i}{y_i \cdot \eta_i \cdot N25 \cdot k_c(t_i, t_c, t_m)} \quad (7)$$

where R_i = count rate of the photo-peak for i-fission product nuclide

i = cerium-143(293.2keV), iodine-133(529.8keV), zirconium-97(745.0keV)

y_i = yield data for i-fission product nuclide

η_i = efficiency of Ge-detector for photo-peak of i-fission product nuclide

$N25$ = uranium-235 atoms in the activation foil

$k_c(t_i, t_c, t_m)$ = correction factor for the build-up and decay of i-fission product nuclide corresponding to the irradiation time(t_i), waiting time (t_c) and measuring time (t_m)

The experimental errors associated with the items in Eq.(7) were estimated :

Item	Experimental Error (%)		
	Ce-143	I-133	Zr-97
δR_i	1.55	3.63	2.09
δy_i [a]	-	-	-
$\delta \eta$	1.63	1.57	1.82
$\delta N25$	0.2	0.2	0.2
δk_c	1.37	1.25	0.90
δp [b]	0.7	0.7	0.7
$\delta F25_i$	2.73	4.21	3.00

$$\delta F25 = \pm 1.8\ \%$$

(a) When the signals from the same photo-peak are counted in the measurements and the thermal calibration, the experimental error associated with the y_i value in Eq.(7) is cancelled out

(b) Uncertainty in the foil position in the cell

(3) C28/F25

Considering the uncertainty (± 1.7%) in a correction factor for in-plate distribution, the experimental error associated with the reaction rate ratio C28/F25 is determined :

$$\delta \{C28/F25\} = \pm 2.8\ \%$$

6. Summary

The experimental errors associated with the integral data at the FCA-XIV-1 core are summarized in Table 2. In order to provide useful data in examing the availability of the nuclear data and computational methods, it is necessary to increase confidence of the data in the accuracy and to develop a new experimental technique. On the other hand, discussions should be concentrated on the items such as :

(a) target accuracies of the integral data requested from the point of view of the nuclear data evaluation

(b) measuring items which can be used to evaluate the specific nuclear data.

Acknowledgement

The authors wish to thank Messieurs S. Okajima and M. Ōbu for their valuable discussions.

References

1) Hirota J., et al. : J. Nucl. Sci. Technol. 6(1), 35 (1969).
2) Hirota J. : "Fast Critical Experiments in FCA and their Analysis," JAERI 1289 (1984).
3) Tomlinson L. : "Delayed Neutrons from Fission," AERE-R6993 (1972).

Table 2 Summary of experimental errors on integral data at FCA-XIV-1 core

Item	Experimental Error		
Excess reactivity	± 1.9	$\times 10^{-4}\Delta k/k$	a)
Reactivity worth			
(a) Critical balance method	± 0.12 ~ 0.025	$\times 10^{-4}\Delta k/k$	a)
(b) Oscillation method	± 0.01 ~ 0.001	$\times 10^{-4}\Delta k/k$	a)
(c) Source multiplication method	± 2.2 %		a)
Reaction rate ratio			
(a) F49/F25	± 3.1 %		b)
(b) F28/F25	± 6.0 %		b)
(c) C28/F25	± 2.8 %		c)

a) uncertainty in the delayed neutron data is not included

b) by micro fission counter

c) by activation foil

2.2.4 On Uncertainties of Evaluated Nuclear Data

Y.Kanda

Department of Energy Conversion Engineering,

Kyushu University, Kasuga, Fukuoka 816, Japan

Characteristics and estimated methods of the uncertainty of evaluated cross sections are discussed restricting to the evaluation of cross sections from differential experiments. The reason on the adoption of the differential data is described from the definition of the cross section. The evaluation is based on the assumption that the experimental data distribute in Gaussian distribution and the theory of error is applicable. The errors in a few typical experiments are shown to understand partial errors. The uncertainties associated with evaluation to are discussed.

1. Introduction

Evaluated nuclear data files have been widely used in nuclear application and, at present, are expected to compile uncertainties and correlation factors, which are represented as covariance matrices. Nuclear data evaluation is generally performed on the basis of differential measurements and then their availability for nuclear reactor design is examined by bench mark tests in which integral data are used. As both the differential and integral data referred in these procedures have experimental errors, the examination should be discussed taking account of their uncertainties. At present, however, there are not the evaluated nuclear data files having information about uncertainties enough

to calculate errors of integral quantities, because it is not easy to estimate evaluated nuclear data errors.

2. Nuclear Data Evaluation

The present discussion is limited to the uncertainties of cross sections evaluated from experimental data since major quantities in evaluated nuclear data files are neutron cross sections.

The cross section σ is defined as

$$n = \sigma \phi N \qquad (1)$$

where n is the number of reaction events, ϕ neutron flux and N the number of sample atoms. In order to determine experimentally, σ the other quantities n, ϕ and N in eq.(1) must be measured. A point to be emphasized about eq.(1) is that it is defined on condition that an incident neutron collides with sample nuclei one time at most and so the sample thickness must be smaller than the mean free path of a neutron in the sample material. Differential measurements can be physically distinguished from integral measurements on this view point: The former are experiments using a thinner sample than the mean free path and the latter are just the opposite. If the condition is not satisfied in a differential experiment, effect of multiple scattering must be corrected for experimental result. The integral experiments are extreme cases of them. The correction factor is estimated on the bases of a model which describe processes of neutron transport in the sample. Therefore, comparison between cross sections and integral measurements is performed through the model.

Since nuclear data evaluation is primarily the work in which the cross sections as physical constants should be determined, it is reasonable that the differential measurements should be based. From this

scenario, the uncertainties of the evaluated nuclear data can be computed from experimental errors of differential measurements used in the work.

It is assumed in theory of errors that distribution of measured data is Gaussian. In nuclear data evaluation it is followed also. The evaluated data are the most probable value and their uncertainties are standard deviations. There is a possibility that a measurement is biased by systematic errors which are not known by the experimenters. Such data must be excluded or given a small weight in the evaluation. This is one of the most essential and difficult procedures but the most important judgment in evaluation. The work of evaluators is selection of measurements which are not biased by systematic errors but distribute as Gaussian by statistical ones. Then, they can be averaged to obtain the most probable value. In this procedure, evaluators apply various techniques such as a least squares method, simultaneous evaluation method and others, but these are essentially similar to averaging of data.

3. Errors of Measurements

Experimental errors are estimated from uncertainties for n, ϕ and N in eq.(1), including those of correction factors for each quantity. It depends on a kind of cross section and an experimental method which quantity has a leading error in the measurement. Generally speaking, fission cross section measurements have difficulty to determine N because the sample thickness must be extremely thin and capture cross section measurements for fast neutrons have possibility to include a large error for n because of room background. Common difficulty in neutron cross section experiments is determination of ϕ, since neutron detection is not direct but is performed by induced-products of a neutron collision.

Typical error lists are shown in Table 1-7.

Table 1 shows an example of a total cross section measurement of ^{238}U and is a part of Tsubone et al.'s experiment[1], in which the Fe-filtered technique is applied. The list shown in Table 2 is quoted from Poenitz et al.[2] who measure capture cross sections of ^{238}U by using the activation method and $^{235}U(n,f)$ and $^{197}Au(n,\gamma)$ as reference cross sections. Table 3 is the list of $^{238}U(n,\gamma)$ cross section measurements of Lindner et al.[3] by using the activation technique and $^{235}U(n,f)$ as reference cross sections. Tables 4 and 5 are quoted from Behrens and Carlson's $^{238}U(n,f)$ measurements[4] which use a multi-foil fission chamber. In Table 6, the error list of Cance and Grenier[5] who measure absolutely $^{238}U(n,f)$ at 14 MeV by the associated particle method. Table 7 shows the errors in activation cross section experiments presented by Ikeda et al.[6], who measured the cross sections of 110 reactions for 26 elements by an intense neutron source.

Works of cross section measurement which do not give detailed information on experimental errors are less valuable because their objects should be presentation of quantitative results. Their weight in evaluation must be assumed less than any experiments whose errors are described in their reports.

4. Errors in Evaluation Procedures

If there are many available experiments at same energy, the weighted mean value of them is the evaluated one. The uncertainty of it can be computed by a manner of an ordinary error estimation. In this case, the errors are not added through the evaluation procedure. When an excitation function is evaluated, the cross section at a given energy which is chosen to take the evaluated value is estimated by interpolating the data

measured near the energy. In this case, selection of an energy is arbitrary to a certain extent and is performed taking account of situation of data distribution. The evaluated values depend on the selected energy. A typical example corresponding to this case is the simultaneous evaluation studied by the author[7,8] and the others[9,10]. The difference of the evaluated results for selection of the energy sets can be understood as systematic errors. Quantitative examples shown in Fig.1 are the systematic error in our simultaneous evaluation for $^{238}U(n,f)$ and $^{235}U(n,f)$[8]. The uncertainty of $^{238}U(n,f)$ cross section evaluated by the method is shown in Fig.2[8]. They can be estimated by the formulae developed in the evaluation method.

When nuclear model calculation is applied to evaluating an excitation function, the error can be estimated from the uncertainties of the parameters used in the model calculation. An example shows in Fig.3 quoted from de Saussure and Smith[10]. The uncertainty for model parameters is not usually given and they are very frequently applied so as to reproduce measurements by adjusting them. The author's group[12] has been tried to estimate quantitatively the uncertainties of model parameters associated with their adjustment to experimental data. It has been shown that they can be successfully estimated, if there are sufficient measurements to compare with the calculation.

5. Conclusion

The uncertainties of the nuclear data evaluated from differential measurements can be estimated from experimental errors but it is based on the assumption that the results of experiments distribute as Gaussian. The information on experimental errors enough to estimate them is

indispensable. The uncertainties associated with the evaluation procedures should be taken into account also.

References

1) I. Tsubone, Y. Nakajima, Y. Furuta, and Y. Kanda, Nucl. Sci. Eng. 88 (1984) 579.

2) W.P. Poenitz, L. F. Fawcett, Jr., and D. L. Smith, Nucl. Sci. Eng. 78 (1981) 239.

3) M. Lindner, R. J. Nagle, and J. H. Landrum, Nucl. Sci. Eng. 59 (1976) 381.

4) J. W. Behrens and G.W. Carlson, Nucl. Sci. Eng. 63 (1977) 250.

5) M. Cance and G. Grenier, Nucl. Sci. Eng. 68 (1978) 197.

6) Y. Ikeda et al. "Activation Cross Section Measurements for Fusion Reactor Structural Materials at Neutron Energy from 13.3 to 15.0 MeV using FNS Facility" JAERI-1312 (1988).

7) Y. Uenohara and Y. Kanda, Nucl. Data for Sci. and Tech. (Antwerp, 1982), K. H. Boeckhoff (ed.) (1983) p639.

8) Y. Kanda, Y. Uenohara, T. Murata, M. Kawai, H. Matsunobu, T. Nakagawa, Y. Kikuchi, and Y. Nakajima, Nucl. Data for Basic and Applied Sci. (Santa Fe, 1985), P. G. Young et al. (ed.) (1986) Vol. 2 p1567.

9) W. P. Poenitz, Proc. Conf. Nucl.Data Eval. Methods and Procedures (BNL, 1980), B. A. Magurno and S. Pearlstein (ed.) BNL-NCS-51363, Vol. I 1981) p249.

10) A. B. Carlson, W. P. Poenitz, G. M. Hale, and R. W. Peelle, Nucl.Data for Basic and Applied Sci. (Santa Fe, 1985), P. G. Young et al. (ed.) (1986) Vol. 2 p1429.

11) G. de Saussure and A. B. Smith, Nucl. Data for Sci. and Tech. (Antwerp, 1982), K. H. Boeckhoff (ed.) (1983) p9.

12) Y. Uenohara, H. Tsuji, and Y. Kanda, Nucl. Data for Sci. and Tech. (Mito, 1988), S. Igarasi (ed.) (1988) p 481.

Table 1 Total cross sections at Iron-filtered bands in the kiloelectron Volt region. (Quoted partially from Tsubone et al.[1])

E_f[a] (keV)	E_l[b] (keV)	E_h[b] (keV)	σ_t (b)	
			^{181}Ta	^{238}U
23.4	23.1	25.1	11.40 ± 0.05	13.65 ± 0.06
70.3	69.3	71.1	9.77 ± 0.16	12.69 ± 0.15
73.0	72.3	73.4	9.55 ± 0.23	13.18 ± 0.20
81.8	80.9	82.7	9.31 ± 0.05	12.21 ± 0.08
128.0	125.5	129.6	8.33 ± 0.04	11.52 ± 0.04
610.1	603.8	613.7	6.67 ± 0.03	7.89 ± 0.03
645.1	630.6	655.6	6.85 ± 0.02	7.87 ± 0.03
701.8	686.0	710.2	6.91 ± 0.03	7.63 ± 0.03
842.1	821.1	858.3	6.81 ± 0.05	7.31 ± 0.03
950.1	934.6	960.1	6.94 ± 0.03	7.09 ± 0.10

[a]The value E_f stands for the filter energy determined from the means of the neutron energy weighted by the neutron flux.

[b]The values E_l and E_h are energy boundaries used in deducing the total cross section and determining the filter energy.

Table 2 Error list for ^{238}U(n,γ) cross section measurements. (Poenitz et al.[2])

Source	Uncertainty (%)	Comment
Gamma detection efficiency	1.0	Common to all values
^{235}U sample mass	0.6	
Total fission-fragment absorption	0.5	
Half-life of ^{239}Np	0.2	
^{238}U sample mass	0.2	
^{235}U(n,f)cross section	2.0	
Statistics and reproducibility	0.7 to 23.1	Values are 0.7 to 3.0% <1 MeV
Neutron background	0.3 to 4.0	0.3% for most values except at higher energies and larger distances from the target
Second neutron group	0.1 to 1.2	Does not apply <800 keV
Scattering of neutrons in the counter, samples, and neutron source structural material	0.8 to 1.7	
Fission product decay	0.2 to 4.0	Does not apply <1 MeV

Table 3 Neutron capture cross sections from 0.1 to 3 MeV in mb. (Quoted partially from Lindner et al.[3])

Neutron Energy for Irradiation Number (MeV)				$\frac{\Delta E}{E_n}$	^{114}Cd[a]	^{181}Ta	^{197}Au	^{232}Th	^{238}U	^{237}Np
1	2	3	4							
0.121				0.36	40(10.9)	379(4.5)	320(0.8)	199(1.8)	160(0.6)	1033(7.0)
	0.121			0.44		343(0.7)		206(1.1)		1000(3.5)
0.154				0.41	37(8.7)	311(4.1)	297(0.9)	184(1.5)	139(0.6)	866(7.7)
	0.154			0.53		288(0.7)		187(0.6)		813(3.3)
0.198				0.43	44(7.3)	271(4.3)	273(0.7)	161(1.7)	129(0.6)	764(4.0)
	0.217			0.60		236(0.7)		153(0.6)		749(3.2)
0.264				0.44	42(6.6)	223(4.2)	235(0.7)	149(1.7)	122(0.6)	670(4.4)
		0.300		0.16		221(4.3)	217(0.4)	162(3.4)	133(0.8)	
	0.324			0.61		190(0.7)		139(0.7)		552(6.3)
		1.01		0.22		103(5.3)	77(0.8)	126(11)	126(0.9)	
			1.07	0.18	28(7.6)	111(2.1)	85(1.4)	127(1.3)	123(1.0)	114(18)
		1.24		0.19		93(6.3)	73(0.8)	114(5.7)	96(0.9)	
			1.44	0.18	17(18)	91(3.2)	72(1.6)	104(1.9)	80(1.3)	84(35)
		1.52		0.14		84(4.2)	71(0.5)		74(0.7)	
		1.66		0.10		78(3.5)	66(0.4)	95(4.0)	66(0.9)	
			1.90	0.15	16(18)	68(4.6)	57(2.7)	72(3.3)	54(2.4)	44(11)
			2.14	0.13	17(14)	57(4.6)	50(2.9)	57(3.4)	42(2.7)	59(11)
			2.37	0.11	18(9)	50(3.8)	39(2.4)	43(2.8)	33(2.2)	56(39)
			2.73	0.07			28(1.3)	30(1.5)	24(0.8)	39(44)
			2.82	0.06	16(5.1)	31(2.3)				

[a]The estimated standard deviations, in percent, are given in parentheses.

Table 4 Total systematic errors for fission cross section ratio measurements. (Behrens and Carlson[4])

Cross-Section Ratio	One Standard Deviation Total Systematic Error (%) for Various Neutron Energy Ranges (MeV)									
	0.1 to 0.3	0.3 to 0.5	0.5 to 1.0	1.0 to 1.75	1.75 to 4.0	4.0 to 7.0	7.0 to 10.0	10.0 to 15.0	15.0 to 20.0	20.0 to 30.0
$^{234}U:^{235}U$	0.6[a,b]	0.6[a]	0.2[a]	0.2[c]	0.3[a,c]	0.4[a,c]	0.7[a]	0.9[a]	1.4[a]	1.3[a]
$^{236}U:^{235}U$	0.2[a,d]	0.5[a]	0.8[a]	0.3[c,a]	0.4[c,a]	0.6[a,c]	0.7[a]	0.9[a]	1.2[a]	1.2[a]
$^{238}U:^{235}U$	0.9[d]	0.3[d]	0.4[a]	0.3[a,c]	0.2[c,a]	0.3[a,c]	0.4[a]	0.3[a,e]	0.6[a]	0.4[a,e]

[a]A major part of the error is from the time-shift effect.
[b]A major part of the error is from the time-independent backgrounds.
[c]A major part of the error is from the energy dependence of our fission chamber efficiencies (based on our two-parameter data).
[d]A major part of the error is from the impurities in the sample.
[e]A major part of the error is from the energy dependence of our fission chamber efficiencies (due to linear momentum).

Table 5 The $^{238}U:^{235}U$ fission cross section ratio. (Quoted partially from Behrens and Carlson[4])
a: one standard deviation rms sum of statistical errors, total systematic errors, and normalization errors.

E_n (MeV)	$\sigma_f{}^{239}U / \sigma_f{}^{235}U$	Statistical Uncertainty (%)	Total Uncertainty[a] (%)	E_n (MeV)	$\sigma_f{}^{238}U / \sigma_f{}^{235}U$	Statistical Uncertainty (%)	Total Uncertainty[a] (%)
0.1442	0.000043	28.3	28.3	4.835	0.5050	1.2	1.4
0.2467	0.000069	19.9	19.9	5.028	0.5203	1.2	1.4
0.3446	0.000167	14.2	14.2	5.177	0.5323	1.2	1.4
0.4171	0.000231	16.4	16.4	5.334	0.5319	1.1	1.3
0.4789	0.000247	13.1	13.1	5.497	0.5399	1.1	1.3
0.5348	0.000547	11.4	11.4	5.668	0.5489	1.1	1.3
0.5776	0.000545	10.7	10.7	5.847	0.5680	1.1	1.3
0.6253	0.000861	8.2	8.2	6.035	0.5676	1.1	1.3
0.6803	0.00140	6.1	6.2	6.232	0.5943	1.0	1.3
0.7260	0.00187	7.0	7.0	6.439	0.6253	1.0	1.3
0.7591	0.00274	5.6	5.7	6.657	0.6130	0.9	1.2
0.7944	0.00413	4.5	4.6	6.886	0.6017	0.9	1.2
0.8324	0.00558	3.9	4.0	7.127	0.5997	0.9	1.2
0.8574	0.00745	5.6	5.7	7.380	0.5876	0.9	1.2
0.8678	0.00835	5.1	5.2	7.648	0.5751	0.9	1.2

Table 6 Error list for absolute fission cross section measurements. (Cance and Grenier[5])

Effect	Uncertainty, %			
	^{235}U	^{238}U	^{235}U	^{239}Pu
Statistical	0.9	1.5	1.2	1.7
Extrapolation to zero pulse height	0.6	0.7	0.23	0.3
Loss of fissions	0.19	0.17	0.19	0.15
Number of atoms per cm^2	1.4	1.35	1.4	1.36
Neutron attenuation				
In target backing	0.36	0.36	0.36	0.36
In front face of fission chamber	0.3	0.3	0.3	0.3
Fissions due to other isotopes	0.2	0.4	0.2	0.17
Total uncertainty of the result	1.85	2.23	1.94	2.26
	$^{238}U/^{235}U$		$^{239}Pu/^{235}U$	
Total uncertainty of ratio	2.82		2.98	

Table 7 Error list for activation cross section measurements. (Ikeda et al.[6])

Items	Estimated error (%)
1. Statistics of γ-ray counts	0.3～5
2. Detector efficiency	2.0～3.0
3. Sample weight	＜0.1
4. Irradiation, cooling and measuring time	＜0.1
5. Self-absorption of γ-ray in a sample	＜0.5
6. Half-life (decay constant)	0.1～2
7. γ-ray emission probability	0.5～2
8. Correction factor for mean source position	＜0.1
9. Correction factor due to fluctuation of neutron flux during irradiation	＜0.1
10. Correction factor due to sum-peak of γ-ray	＜0.1
11. Standard reaction cross section	～3.0

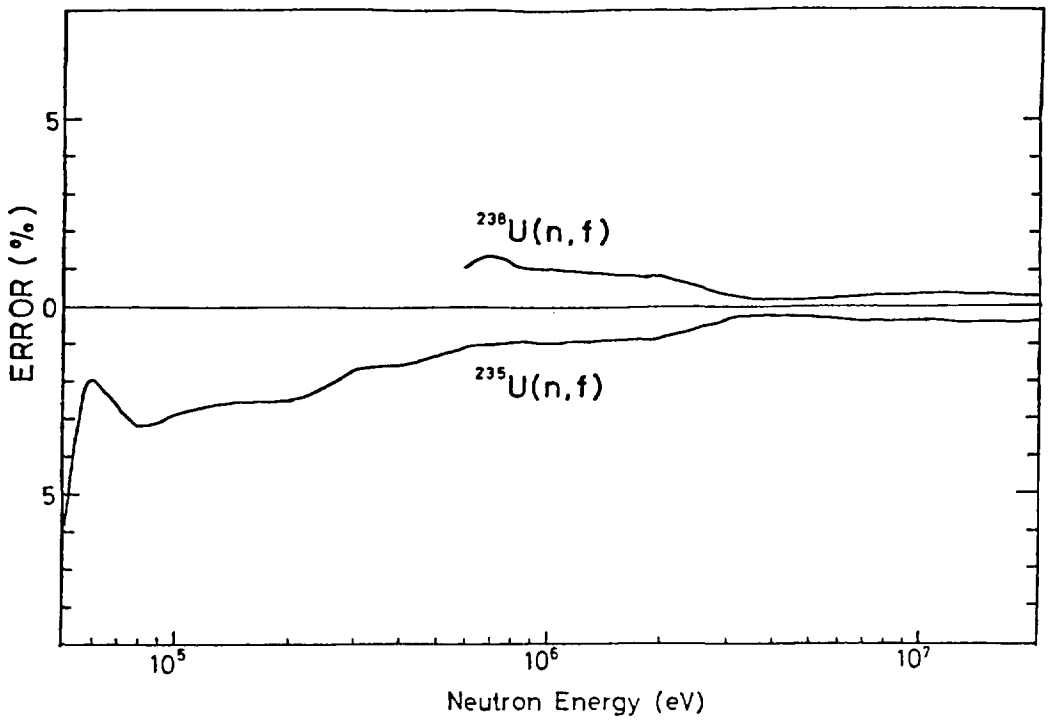

Fig. 1 Systematic errors for ^{238}U(n,f) and ^{235}U(n,f) in the simultaneous evaluation. (Y. Kanda et al.[8])

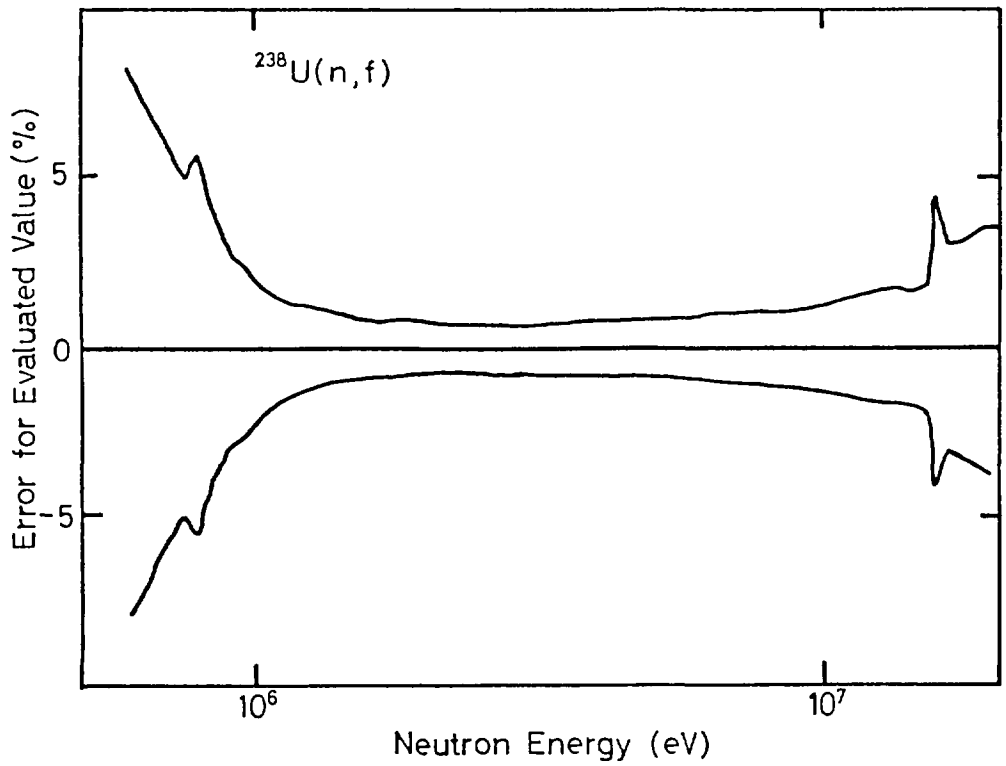

Fig. 2 Uncertainties for ^{238}U(n,f) estimated from diagonal elements in covariance matrices calculated in the simultaneous evaluation. (Y. Kanda et al.[8])

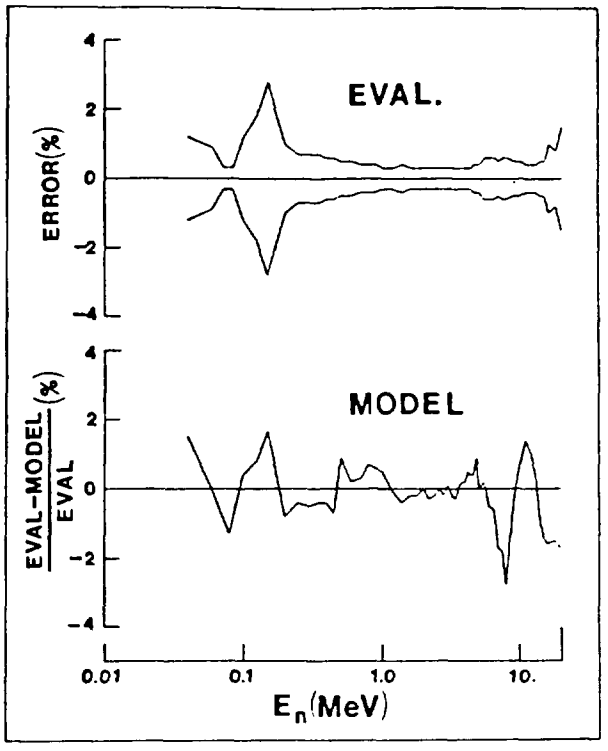

Fig. 3 ^{238}U total-cross-section-evaluation uncertainties (upper) and deviation of the evaluation from the model (lower). (de Saussure and Smith[11])

2.2.5 Comments on Uncertainty of Group Averaged Cross-sections

Masaharu Nakazawa
Department of Nuclear Engineering, University of Tokyo
7-3-1, Hongo, Bunkyo-ku, Tokyo 113, JAPAN

Many difficulties have been found when the uncertainties of group averaged cross-sections have been discussed, and here are given some remarks and some suggestions. One remark is the importantness of "energy resolution" of the uncertainty of original cross-section values, and some suggestions have been made. Second discussion has been made on the uncertainties of the weighting spectra, where special attention has been paid how to represent their range of uncertainty considering their discontinuity of spectrum.

1. Introduction

Practical neutron transport calculations such as ANISN or DOT codes are made by using the group-averaged cross-sections, and their present accuracies of calculations are depending on the uncertainty of the group averaged cross-section,[4] which is the starting point of present discussions.

Group averaged cross-section σg is defined like,

$$\sigma g \equiv \frac{\int \sigma(E)\,\phi(E)dE}{\int \phi(E)dE} \qquad \ldots(1)$$

where $\sigma(E)$, $\phi(E)$ are micro-cross section and neutron spectrum respectively, and integration interval by dE is [Eg, Eg+1] which is omitted here due to complicatedness.

The uncertainty of σg can be given like [1]

$$\frac{\overline{\Delta\sigma g \sigma k}}{\sigma g \cdot \sigma k} = \int\int dE dE' \{V(E,E')\,\phi(E)\,\phi(E') + D(E,E')\overline{\Delta\phi(E)\Delta\phi(E')}\}/F \qquad \ldots(2)$$

where

$$V(E,E') = \overline{\Delta\sigma(E)\Delta\sigma(E')}/\sigma(E)\cdot\sigma(E'),$$
$$D(E,E') = (\sigma(E)-\sigma g)(\sigma(E')-\sigma k)/\sigma(E)\sigma(E'),$$
$$F = \int\int dE dE' \phi(E)\phi(E')$$

two integral intervals are[Eg, Eg+1] and [Ek, Ek+1] for dE and dE' respectively.

Then the problem is attributed to obtain the uncertainties of $\sigma(E)$ and $\phi(E)$ functions.

2. Statistical random error of $\sigma(E)$ [2],[3]

If we consider the statistical uncertainty in the measurement of the cross-section $\sigma(E)$, they are uncorrelated with the different energy points, that is called here the random error. This random error gives pure diagonal components of the covariance matrix V(E,E'). And the first comment is related how to formulate this random error in the V(E, E') representation.

At first, if we simply adopt the following representation to mean the ε % random error of $\sigma(E)$,

$$V(E, E') = \begin{cases} \varepsilon^2 & \text{for} \quad E = E' \\ 0 & \text{for} \quad E \neq E' \end{cases} \qquad \cdots(3)$$

then it leads to wrong result, that can be understood easily when we calculate the uncertainty of the value I,

$$I \equiv \int_g^{g+1} \sigma(E)dE = \sigma g \cdot (Eg+1-Eg) \qquad \cdots(4)$$

where σg is the group averaged cross section. The uncertainty $(\Delta I)^2$ is given by

$$(\Delta I)^2 = \iint dE dE' \overline{\Delta\sigma(E)\Delta\sigma(E')}$$
$$= \varepsilon^2 \cdot \overline{\sigma g^2}(E_{g+1}-Eg) \qquad \cdots(5)$$

where $\overline{\sigma g^2}$ is mean value of $\sigma(E)^2$.
Then the relative error of I is given by

$$(\Delta I)^2/I^2 = \varepsilon^2 \cdot \overline{\sigma g^2}/\{\overline{\sigma g}^2 \cdot (Eg_{+1}-Eg)\}$$
$$\fallingdotseq \varepsilon^2/(Eg_{+1}-Eg) \qquad \cdots(6)$$

where it is assumed $\overline{\sigma g^2} \fallingdotseq \overline{\sigma g}^2$ for simplicity.

Looking into the eq.(6), the wrong point can be found in the inconsistency of dimension between the left and the right of the eq.(6). More clearly speaking, the left side means relative value (no dimension) although the right side depends on the inverse unit of Energy E (dimension of $(MeV)^{-1}$).

In order to avoid this kind of inconsistency, we should select the following form of the random error instead of eq.(3)

$$V(E,E') = \begin{cases} \varepsilon^2 \cdots & \text{for} \quad (E-E') < \delta/2 \\ 0 \cdots & \text{for the otherwise} \end{cases} \qquad \cdots(3)'$$

where the δ gives the energy resolution value to give the uncertainty of $\sigma(E)$.
Then relative error of I is modified like

$$(\Delta I)^2/I^2 \fallingdotseq \varepsilon^2 \cdot \delta/(Eg_{+1}-Eg) \qquad \cdots(6)'$$

and the dimension inconsistency mentioned in the eq.(6) has been solved in the eq.(6)' because the δ value is incorporated which has the same unit of Energy.

From these discussion, two conclusions can be obtained as

(1) when the statistical random error of $\sigma(E)$ is assigned as ε % at the Energy E, we must state the energy resolution δ simultaneously in this assignments.

(2) The products ($\varepsilon^2\delta$) of relative variance ε^2 and the energy resolution δ , are thought approximately unchanged in its value. In other words, relative random error ε is increased when the energy resolution δ to represent the cross-section $\sigma(E)$ is decreased, and if $\delta \to 0$, then relative error ε goes to infinite.

3. Neutron spectrum fluctuation due to the cross-section fluctuation [1]

As the weighting spectrum of eq.(1), we usually uses some simple form of

$$\phi(u) = \frac{1}{\xi\sigma(u)} \qquad \ldots(7)$$

where u is the lethargy and $\sigma(u)$ is the total cross-section of the neutron field materials.

The cross-section $\sigma(u)$ shows the fluctuation, especially in the resonance energy region, then the neutron spectrum $\phi(u)$ shows the same phenomena as is expected from the eq.(7). An example of this neutron spectrum fluctuation due to the cross-section fluctuation has been shown in Fig.1, where the neutron spectrum in the U-235 materials is described. And it is easy to understand that the averaged cross-section σg will be changed according to the degree of fluctuation of weighting spectrum.

Here, my second comment is that the degree of fluctuation of weighting spectrum is also dependent on the energy resolution to represent the neutron spectrum. In Fig.1, it is additionally given the smoothed neutron spectrum with the energy resolution of $\Delta E = 0.5$eV. The degree of neutron spectrum fluctuation is summarized in Table 1, as the value of relative uncertainty $\Delta\phi/\phi$ for each energy resolution value δ. It is very interesting that the product of relative uncertainty and the root of energy resolution is also unchanged for the practical ranges of δ.

In order to show the uncertainty of σg introduced by these weighting spectrum fluctuation, practical calculation of σg of Au-197(n, γ) reaction in the U-235 field have been made. In Fig.2, it is clearly shown the change of σg according to the energy resolution ΔE of the neutron spectrum representation.

In summary, two or three conclusive remarks can be obtained as

(1) the neutron spectrum has the random error according to the cross-section random error,
(2) if the smooth spectrum is applied as the weighting spectrum, like $\phi(u) = \text{const.}$, additional random error should be considered due to the cross-section fluctuation effect which is neglected, and
(3) the random error of weighting spectrum is also dependent on the energy resolution.

4. Neutron spectrum Covariance due to scattering process

Actual neutron spectrum is described as the stochastic process of the Fokker-Planck equation, and the expected value of neutron spectrum can be obtained from the usual Boltzmann equation which is derived from the Fokker-Planck equation. So, the covariance term of neutron spectrum due to its stochastic process can be obtained not from the Boltzmann equation, but

substantially from the original Fokker-Planck equation. The differences between the actual line spectrum and the expected spectrum from the Boltzmann eq. have been shown shematically in Fig.3.

At present, I have no idea to solve directly the Fokka-Planck equation for the neutron spectrum covariance which should be considered as the uncertainty of the weighting spectrum, but here is given simple idea to estimate the covariance from some physical model of neutron scattering process.

As for the neutron spectrum covariance in some materials, the parameter ξ , the average lethargy increase by collision is thought a good index to guess the collinsion number n in each lethargy group $\Delta u = ug - ug+1$, like $n = \Delta u/\xi$. Then my present idea to guess the uncertainty of σg due to the finite collision number n is given below

$$\Delta\sigma g = \frac{\Delta\sigma g(0)}{\sqrt{1+n}} = \frac{\Delta\sigma g(0)}{\sqrt{1+\Delta u/\xi}} \qquad \ldots(8)$$

where $\Delta\sigma g$ is the uncertainty of σg , and
$\Delta\sigma g\,(0)$ is the uncertainty of σg where the neutron collision is assumed once in the g-th group width,

From eq.(8) the uncertainty of group cross-section is guessed to be decreased so much in the heavy elements, which is equivalent to the wide resonance approximation in the resonance integral calculation.

5. Conclusion

In summary, the uncertainty of group averaged cross-section can not be obtained routinely, even if the covariance data of library cross-section can be completed because of lack of the knowledges of uncertainty of weighting spectrum. In order to gain such knowledges, here is given two ideas on the uncertainties of weighting spectrum,

(1) the random error should be considered using the energy resolution, and
(2) the covariance of the spectrum can be guessed using the average lethargy gain parameter ξ .

References

(1) NAKAZAWA, M., SEKIGUCHI, A., Several Applications of J1 Unfolding Method of Multiple Foil Data to Reactor Dosimetry, EUR 6813 EN-FR, 751 (1980)
(2) NAKAZAWA, M., A New Covariance Formulation Including the Energy Resolution Concept for the Neutron Dosimetry, Nuclear Data for Science and Technology, 441 (1983)
(3) NAKAZAWA, M., SEKIGUCHI, A., On the Uncertainty of Neutron Cross-Section for Reactor Dosimetry, JAERI-M-8769, 66 (1980)
(4) NAKAZAWA, M., Influences of the Covariance Matrices over Reactor Neutron Dosimetry, JAERI-M-9523, 113 (1981)

Table 1 Relative random error $\Delta\phi/\phi$ of neutron spectra of Fig. 1 for each energy resolution δ

energy resolution δ	relative uncertainty $\Delta\phi/\phi$	$\frac{\Delta\phi}{\phi} \times \sqrt{\delta}$
0.023*	0.584	0.089
0.069	0.498	0.13
0.162	0.389	0.16
0.208	0.356	0.16
0.254	0.329	0.17
0.485	0.234	0.16
0.943	0.166	0.16

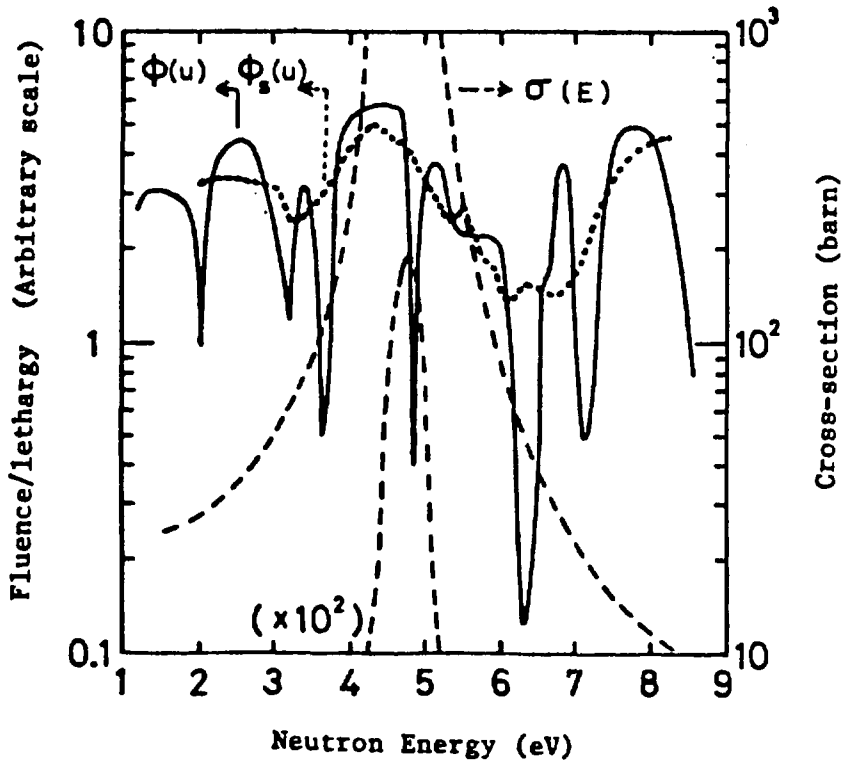

Fig. 1 Fluctuating neutron spectrum $\phi(u)$ in U-235 material $\phi_s(u)$ is smoothed with energy resolution of ΔE=0.5 eV.

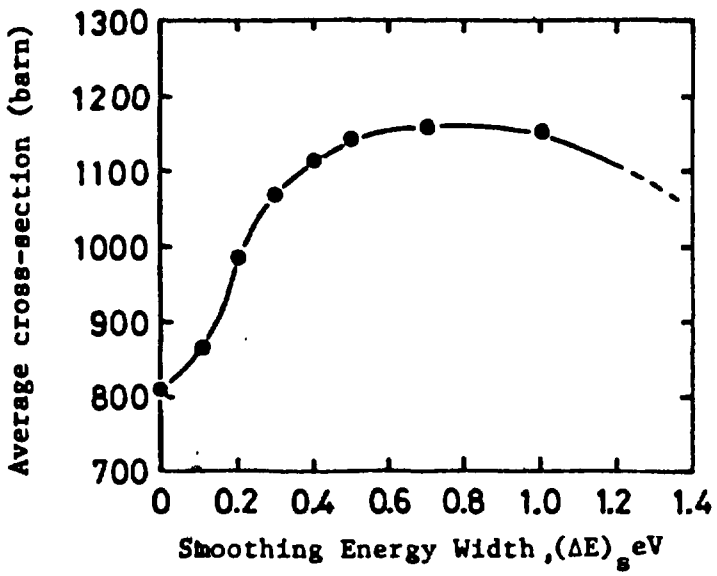

Fig. 2 Averaged cross-section of Au-197(n,γ) reaction in U-235 material.
$(\Delta E)_S$ means the energy resolution of the weighting spectrum.

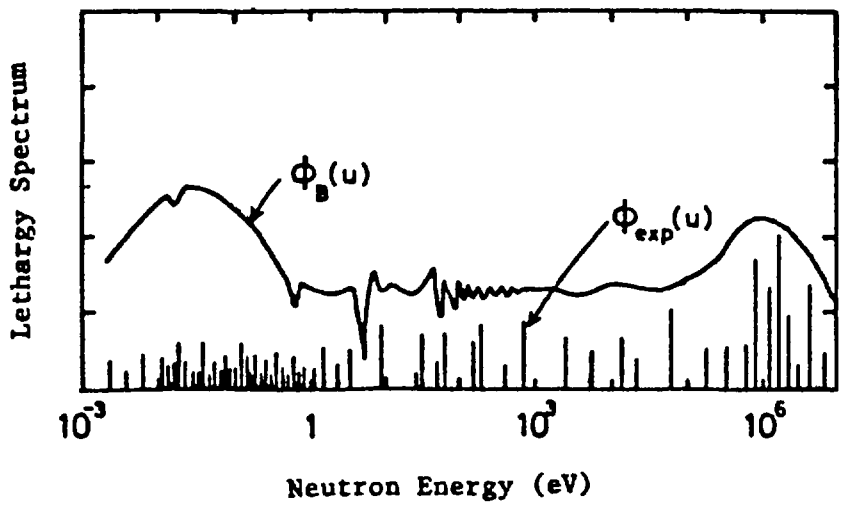

Fig. 3 Two schematic neutron spectra,
$\phi_{exp}(u)$ means actual stochastic process,
$\phi_B(u)$ means Boltzmann equation's spectrum.

2.3 Discussion

In this session, in order to supplement the previous session and to make a consensus for completion of JENDL-3, the following items were emphasized;

1) Uncertainty of method used for experiment analyses,
2) Some comments to cross section adjustment,
3) On the U-238 capture cross section and fission spectrum.

The first item was adopted for nuclear data evaluators in order to make clear the method uncertainties arisen from the method used for the experiment analysis. In this presentation and discussion, the origin of the interested errors, i.e. due to nuclear data or analysis method, was seriously discussed.

In the second item, some comments on the cross section adjustment was presented from the both viewpoints of differential and integral data adjustment.

The last item, which was significantly interested by about a hundred of participants, was motivated by recent work by F. H. Froehner for JEF-2 submitted to the 1988 International Reactor Conference held at Jackson Hole. In this work, he got the capture cross section of U-238 above 10 keV smaller than the values compiled in JENDL-2 , -3T and ENDF/B-IV. This cross section is the most important quantity for the reactor physics in relation to the criticality, conversion ratio, sodium void coefficients, and some authors have taken note the relation to the spatial dependence of E/C-values of control rod worths. As shown in the comment (2.3.4 by A. Hasegawa), the smaller capture cross section was preferable for FBR benchmark cores. Another topic in this term was the fission spectrum based on the Madland-Nix formula which was used for JENDL-3 data evaluation, and the discussion was focused on the harder spectrum predicted by their formula.

2.3.1 Comment: Method Error in Critical Experimental Analysis

Takanobu KAMEI
Nippon Atomic Industry Group Company, Ltd., NAIG Nuclear Research Laboratory
4-1 Ukishima-cho, Kawasaki-ku, Kawasaki-shi 210, Japan

Method error is evaluated for key neutronics parameters of large LMFBRs for a purpose of providing information of the C/E uncertainties of critical experimental analysis. The analysis error is compared with experimental error and cross-section error.

1. Introduction

In this afternoon session, measurement errors and cross-section evaluation errors were already presented by researchers of experimental side and cross-section evaluation side, respectively. When we discuss the quality of our cross-section library, we have to know method errors in the analysis of experimental data. Upon the request of the session chairman, the author delivered the following comment on the method error in the critical experimental analysis.

2. Method Error and the Comparison with Other Error Values

The method error is composed of several error sources such as processing error of nuclear data file to group constant, modeling error of drawer structure of a critical assembly, and the errors in the evaluation of neutron streaming, cell interaction and transport effect. Table 1 shows the categorized analysis errors for three key neutronics parameters.[1] These errors are considered random for each other, and the total error for each neutronics parameter is obtained by the square root of the sum of the square of each error.

The total error for criticality is 0.4%, and those for control rod worth and reaction rate distribution is 2.6% and 1.6%, respectively. In Table 2, these errors are compared with the experimental error in Jupiter experiment and with cross section error. The cross-section error in Table 2 was evaluated by use of the covariance matrix and sensitivity coefficients shown in Ref. 2. As for criticality factor prediction, the

error due to cross-section uncertainty is large compared to the other error sources. As for control rod worth prediction, errors of delayed neutron data and cross-section are larger than that of the method error. As for reaction rate distribution, the cross-section error seems to be larger than the method error and the experimental error.

- References -

(1) Takeda T. et al.:"Prediction Uncertainty Evaluation Methods of Core Performance Parameters in Large LMFBRs", Proc. the 1988 Int. Reactor Physics Conf.,Sept 18-22,1988, Jackson Hole, Wyoming, USA(1988)
(2) Kamei T., Yoshida T.:Nucl. Sci. Eng. 84, 83 (1983)

Table 1 Calculation uncertainty of key neutronics parameters

(in %, 1σ)

Error Item	Criticality	Control Rod Worth	Reaction Rate Distribution
Processing of Nuclear Data	0.3	1.5	1.0
Cell(Assembly) Modeling	0.2	1.4	0.4
Neutron Streaming	0.1	0.7	0.4
Cell Interaction	0.1	1.0	0.5
Core Calculation	0.1	1.0	1.0
Total(Method Error*)	0.4	2.6	1.6

* Excluding cross-section error

Table 2 Comparison of various error values

(in %,1σ)

Item	Criticality Factor	Control Rod Worth	Reaction Rate Distribution
Cross-section Error	3.2	4 - 6	2 - 3
Experimental Error	0.04	1.5	1.0
Delayed Neutron Error *	---	4	---
Method Error**	0.4	2.6	1.6

Note * Uncertainty of the conversion facter from inhour to k_{eff}

** Excluding cross-section error

2.3.2 Problems in Cross Section Data Adjustment

Iwao Otake
Data Engineering Inc.

Some problems in cross section data adjustment are presented on both sides of differential data and integral data adjustment.

The main purpose of the cross section data adjustment is, of course, to improve estimates of integral parameters in reactor design work, not to use integral data in the cross section evaluation process. The work of fitting differential data with integral data measured on critical assemblies have progressed since 1964. If we look at the process of progress in cross section data adjustment, we are able to recognize that it has proceeded in accordance with "materialistic dialectics". Although accuracy of differential data is fairly progressed in recent years, it will not be enough for users to apply it to reactor design calculations. So that, they should have to wait untill when appropriate time for its use comes (on the assumption that such time will comes),or they should conceive suitable methods to fit to the existing state of differential data. We can see the proper example by the following facts. For data adjustment concerned,we have experienced to apply AGLI system for the adjustment of the multi-group cross section set made from JENDL-1 and concluded that the state of differential cross section data was not appropriate for the adjustment. On the other hand, French adjusted multigroup cross section set, which has been developed since the 1970's and adopted different adjustment method, so-called parametrical approach, is used in present reactor designs. Problems still exist in cross section data adjustment are mostly on the side of differential data as follows.

The recent cross section data adjustment requires the variance -covariance matrices of all differential data used. The problem is that these matrices are not uniquely defined and dependent on cross section evaluation methods. So that, to make consistent covariance files, unified cross section evaluation method is required. Fortunately this seems to be satisfied by degrees in

the present JENDL files. But so far as covariance files concerned, they can not be acquired easily and even if acquired, values may be largely arbitrary. Because, works of making covariance files require a considerable amount of time and unified method of producing them does not seem to exist at present. Unified method of producing covariance files is strongly required to deal with the concept of systematic and statistical errors. Especially the method to define and deal with systematic error is inevitable to produce covariance files by the reason that it has a good deal of uncertainty and may hold a large portion of errors. Systematic error may be a main reason why we still find significant differences among major reaction cross sections in various evaluated data files.

Evaluation work of JENDL seems to be partly influenced by the adjusted data in recent years. For evaluators the position of application independent evaluation seems to be essential, but it has not been accepted by most of them unfortunately and this would be the reason we could not start from the old evaluation to make new files.

In order to achieve design accuracy, users sometimes require accuracies of differential data beyond nothing. The adjustment method like parametrical approach is effective in such circumstances. In accumulated integral data base we may meet much correlated data because of scarce experimental facilities. These data have to be dealed with caution in the data adjustment. Although the improvements of cross section uncertainties are obtained in the data adjustment process, they come in large part from compensations of large off-diagonal elements in the resulted covariance matrix. As these may be resulted from the correlation among differential data and integral data, precise investigation of the results will be necessary. If we could compare several adjusted data set with each other, we might meet the disagreement at present stage. We could take pragmatic way and use adjusted data sets.

2.3.3 Comments on Nuclear Data Evaluation of ^{238}U

Y. Kanda and Y.Uenohara

Department of Energy Conversion Engineering,

Kyushu University, Kasuga, Fukuoka 816, Japan

1. $^{238}U(n,\gamma)$ Cross Section

The $^{238}U(n,\gamma)$ cross section evaluated from differential measurements in the continuum region is a few percent larger than acceptable values in bench-mark tests. It has puzzled us for a long time. Several differential measurements have been conducted by various techniques to solve the problem. Few experiments of them presented smaller results but the average of them is not so small that the situation of $^{238}U(n,\gamma)$ cross section has not been changed. However, two remarkable reports were presented by Moxon, Sowerby, Nakajima and Nordborg and Froehner, at the International Reactor Physics Conference, Jackson Hole, Wyoming, September 1988. Their data are smaller than the early evaluations. In their reports, they derived Poenitz's studies that his results agree with their data. These are very interesting works. It is expected that the discrepancy between differential data and integral data is solved by these works. The detailed information of them is desired in order to know whether the evaluation procedures can be agreeable or not.

2. $^{238}U(n,n')$ Cross Sections

The evaluation of $^{238}U(n,n')$ cross sections is presented elsewhere by Uenohara and Kanda in these proceedings.

2.3.4 Comments on the U-238 capture cross section of JENDL-3 based on the FBR benchmark test between several recent evaluations

Akira Hasegawa

Japan Atomic Energy Research Institute
Tokai-mura, Naka-gun, Ibaraki-ken, 319-11 Japan

Abstract

Comments on the U-238 capture cross sections of JENDL-3TR1 are made in comparison with the recent evaluations of JEF-2 and ENDF/B-VI based on the benchmark test of FBRs, analyzing 21 cases of critical assemblies in one dimensional model. Discussions are limited only to the energy range from 10 keV to 300 keV(unresolved range). From the substitution of U-238 capture data of JENDL-3TR1 to JEF-2 or ENDF/B-VI, latter data showed better agreements than JENDL-3T in K_{eff} and spectral indices of U-238 capture related data such as C28/F25 or C28/F49. As a result, reconsideration will be needed in this energy range for JENDL-3TR1 data.

Status of U-238 capture data

Recently two new U-238 capture data are coming out, although these data are still candidates position, one is JEF-2 and the other ENDF/B-VI. These data are found in Frohner's paper/1/. In Fig. 1 and 2, these data are reproduced together with JENDL-3TR1/2/. The values of JEF-2 and ENDF/B-VI are only in graphical form. We read the values from the paper. we processed these data to group constants by PROF-GROUCH-G/B. The differences in group cross sections between JENDL-3TR1 and JEF-2 are also shown in the Figs. 1 and 2 as ratio data JEF-2 to JENDL-3TR1 just above the lower frame.

From the figure, two evaluations except JENDL-3TR1 are relatively close each other and they are traced considerably lower value of the capture cross sections among the experimental values. On the other hand, the data of JENDL-3TR1 are tracing the experimental value quite

well as shown in Figs. It traces about 10 % higher values compared with the JEF-2 and ENDF/B-VI. JENDL-3TR1 data are obtained by the simultaneous evaluations between major fission and capture cross sections, i.e. in principle least square fitting method is used between fission cross section for U-235, U-238, Pu-239, Pu-240, Pu-241 and capture cross section for U-238 and Au-197.

Benchmark test: Analysis of 21cases FBR critical assemblies

It has been recognized for a long time in the nuclear data community that there might be some discrepancy between the experimental data from the cross section measurement and the observation from the integral measurement. FBR analyst supposes relatively higher values are assigned to this reaction data, because the improper reproducibility for the central reaction rate ratio relating to this reaction, such as C28/F25 or C28/F49 (C28: capture reaction of U-238, F25: fission reaction of U-235, F49: fission reaction of Pu-239). These integral data are key parameters for the burn-up characteristics. Therefore it affects the performance of neutron economy of the reactor cores at the designing stage.

From the benchmark test for JENDL-3T/3/, the same conclusions has been made for the spectral indices of central reaction rate ratio C28/F25 and C28/F29. Therefore, JEF-2 and ENDF/B-VI data are thought more likely to diminish the long standing discrepancy observed in integral measurement than JENDL-3TR1. To test the performance of the new evaluations, We made the benchmark test by substituting of U-238 capture data of JENDL-3TR1 to JEF-2, for one dimensional model of FBR assemblies, following the same way as used in JENDL-2 and 3 test.

Results

In Fig.3, K_{eff} is shown. In Fig.4-7, spectral indices of C28/F25, C28/F49, F49/F25, F28/F25 respectively, are shown. In each figure, JEF-2 (U-238 capture cross sections) result is shown with JENDL-2, JENDL-3T and JENDL-3TR1 for the comparisons. In Table 1, K_{eff} of each assemblies are shown for these evaluations. In Table 2, summary of K_{eff} is shown.

K_{eff} (Criticality)

From Table 2, JENDL-2 results show the best agreements among the files, but it has been obvious that there were relatively large inconsistency in the evaluated data of JENDL-2 for major fission cross section and capture cross section. There are a big difference (more than 2 %) between U-core and Pu-core for JENDL-3T, this was due to especially nu value problem of U-235. In JENDL-3TR1, this fuel type difference considerably reduced, yet relatively lower criticality (0.991) is observed. If we use JEF-2 U-238 capture data (Frohner's data) in this JENDL-3TR1, the results are improved up to 0.994 as seen in the Table 2.

Table 2 Summary of K_{eff} (statistics)

	JENDL-2	JENDL-3T	JENDL-3TR1	JEF-2(Frohner)
Pu-core	0.998	0.990	0.992	0.995
U -core	1.000	1.011	0.989	0.993
All-core	1.000	0.996	0.991	0.994

Spectral indices

According to the lower value assignments between 10 keV to 300 keV, spectral indices relating to U-238 capture data, C28/F25, C28/F49 using JEF-2 data are relatively improved than JENDL-3 or 3TR1 as seen in Figs. 4 & 5. It is also pointed out that the results using JEF-2 evaluation approaches to the JENDL-2 results(see Fig.5). In any way, JEF-2 data predicts the integral experiments more accurately for U-238 related indices. And for the other spectral indices, such as F49/F25 or F28/F49 (F28: fission reaction of U-238), no significant changes are seen by JEF-2 U-238 capture evaluation(see Fig. 6,7).

Conclusion

From the integral point of view, it is concluded that U-238 capture data of JEF-2 or ENDF/B-VI evaluation have better predictability than JENDL-3TR1 for Keff and spectral indices relating to this reaction. However, up to now, not enough clear explanation are obtained for these new evaluations. We need some concrete reasons when we recommend these data in JENDL-3. Therefore we cannot recommend yet to adopt these new evaluations in JENDL-3. But we must recognize these data and we need further investigations why these new evaluation support the shocking low capture values(as much as 10 per cent).

References

/1/ Frohner: 'The Unresolved Resonance Range of U238,' Proc. Int. Reactor Physics Conf. Jackson Hole, pp III 171-182 (1988).

/2/ JAERI Nuclear Data Center: JENDL-3TR1 (1988).

/3/ A.Hasegawa : Proc. Int. Conf. on Nuclear Data for Sci. and Techn. Mito, pp445-454 (1988).

Table 1 Summary of K_{eff} (statistics)

* C/E OF K-EFFECTIVE
* PLUTONIUM FUEL

NO.	ASSEMBLY	EXPERIMENTAL	J3T (DIFFUSION)	J3TR1 (DIFFUSION)	FROHNER (DIFFUSION)	J2 (DIFFUSION)
1	VERA-11A	1.00000	0.97936 (-)	0.98014 (0.080)	0.98399 (0.473)	0.99498 (1.595)
4	ZEBRA-3	1.00000	0.97957 (-)	0.98225 (0.273)	0.99070 (1.135)	0.99979 (2.064)
6	SNEAK-7A	1.00000	0.99581 (-)	0.99750 (0.170)	1.00301 (0.723)	1.00579 (1.002)
8	ZPR-3-54	1.00000	0.96287 (-)	0.96460 (0.180)	0.96591 (0.316)	0.96355 (0.071)
9	ZPR-3-53	1.00000	0.99214 (-)	0.99395 (0.182)	0.99776 (0.566)	0.99588 (0.377)
10	SNEAK-7B	1.00000	0.99201 (-)	0.99520 (0.321)	1.00356 (1.165)	1.00379 (1.188)
11	ZPR-3-50	1.00000	0.99548 (-)	0.99865 (0.318)	1.00397 (0.853)	1.00030 (0.483)
12	ZPR-3-48	1.00000	0.99636 (-)	1.00027 (0.392)	1.00671 (1.038)	1.00632 (0.999)
14	ZPR-3-49	1.00000	0.99633 (-)	1.00066 (0.435)	1.00730 (1.101)	1.00903 (1.274)
15	ZPR3-56B	1.00000	0.99687 (-)	0.99876 (0.190)	1.00390 (0.705)	0.99631 (-0.057)
16	ZPR-6-7	1.00000	0.99304 (-)	0.99965 (0.663)	1.00721 (1.425)	0.99930 (0.629)
18	ZPPR-2	1.00000	0.99872 (-)	1.00318 (0.447)	1.00950 (1.080)	1.00577 (0.706)
19	MZA	1.01080	0.99304 (-)	0.99408 (0.105)	0.99915 (0.615)	0.99982 (0.683)
20	MZB(1)	1.00400	0.99218 (-)	0.99658 (0.444)	1.00328 (1.119)	0.99662 (0.448)
21	FCA-5-2	1.00000	0.98991 (-)	0.97595 (-1.410)	0.98273 (-0.725)	0.99275 (0.287)
* AVERAGE OF C/E			0.99025 (-)	0.99209 (0.187)	0.99791 (0.774)	0.99800 (0.783)
* AVERAGE(C/E)-1.0			-0.00975	-0.00791	-0.00209	-0.00200
* AVERAGE OF ABS(1.0-C/E)			0.00975	0.00845	0.00855	0.00613
* STND.DEV. OF C/E			0.00915	0.01074	0.01168	0.01030

SUMMARY OF BENCH MARK TEST (2)

* C/E OF K-EFFECITVE
* URANIUM FUEL

NO.	ASSEMBLY	EXPERIMENTAL	J3T (DIFFUSION)	J3TR1 (DIFFUSION)	FROHNER (DIFFUSION)	J2 (DIFFUSION)
2	VERA-1B	1.00000	1.00650 (-)	0.98432 (-2.204)	0.98850 (-1.788)	0.99954 (-0.692)
3	ZPR-3-6F	1.00000	1.02644 (-)	0.99855 (-2.717)	1.00437 (-2.150)	1.01283 (-1.326)
5	ZPR-3-12	1.00000	1.01451 (-)	0.99291 (-2.129)	1.00070 (-1.361)	1.00632 (-0.807)
7	ZPR-3-11	1.00000	1.01271 (-)	0.99369 (-1.878)	1.00425 (-0.836)	1.00500 (-0.762)
13	ZEBRA-2	1.00000	0.99777 (-)	0.97657 (-2.125)	0.98527 (-1.253)	0.99251 (-0.527)
17	ZPR-6-6A	1.00000	1.00916 (-)	0.98626 (-2.269)	0.99492 (-1.411)	1.00402 (-0.509)
* AVERAGE OF C/E			1.01118 (-)	0.98872 (-2.222)	0.99634 (-1.468)	1.00337 (-0.773)
* AVERAGE(C/E)-1.0			0.01118	-0.01128	-0.00366	0.00337
* AVERAGE OF ABS(1.0-C/E)			0.01193	0.01128	0.00677	0.00602
* STND.DEV. OF C/E			0.00868	0.00721	0.00744	0.00624

SUMMARY OF ALL ASSEMBLIES

* AVERAGE OF C/E	0.99623 (-)	0.99113 (-0.512)	0.99746 (0.124)	0.99953 (0.332)
* AVERAGE(C/E)-1.0	-0.00377	-0.00887	-0.00254	-0.00047
* AVERAGE OF ABS(1.0-C/E)	0.01037	0.00926	0.00804	0.00610
* STND.DEV. OF C/E	0.01307	0.00998	0.01067	0.00963

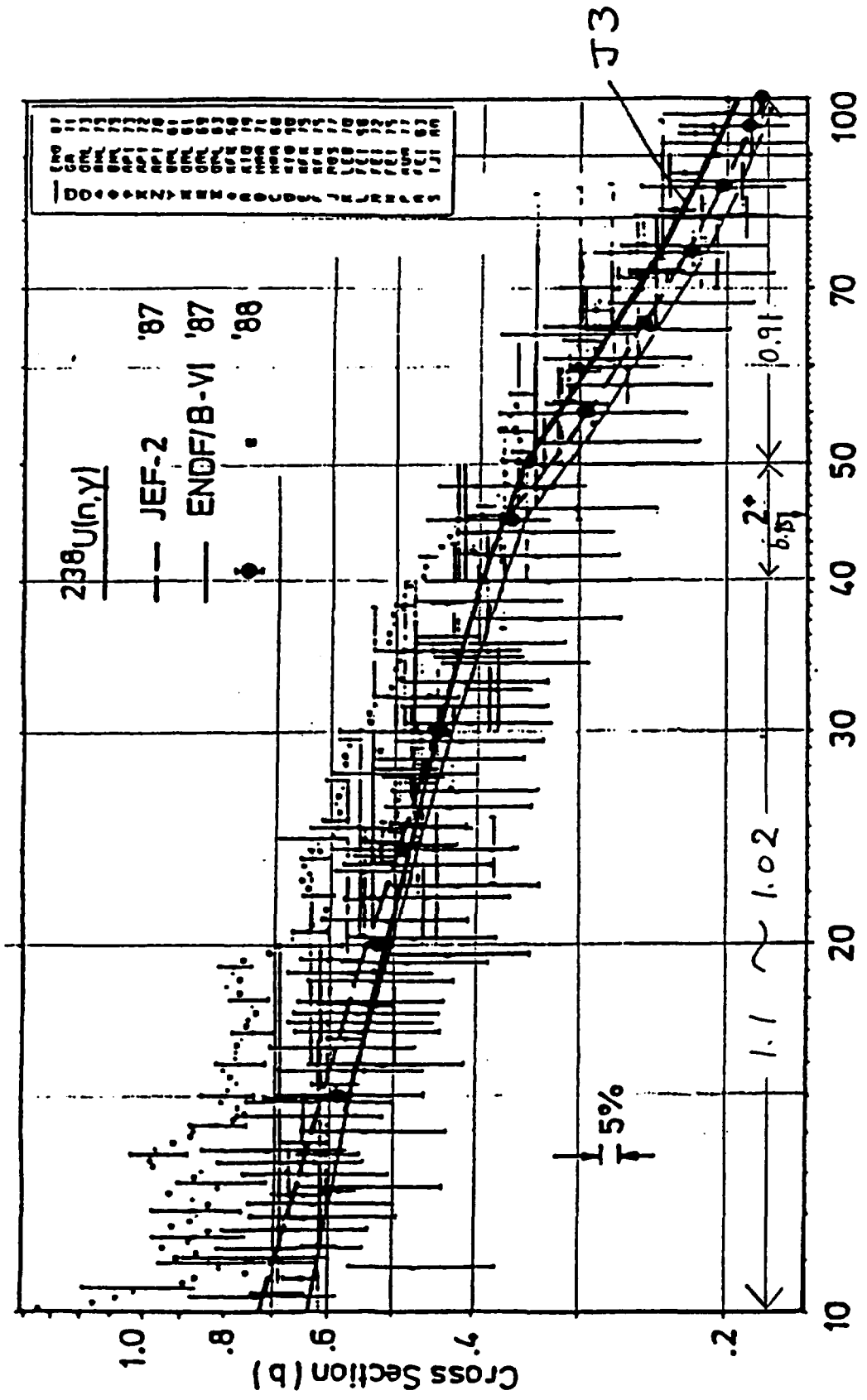

Fig. 1 U-238 capture cross sections (10 keV to 100 keV)

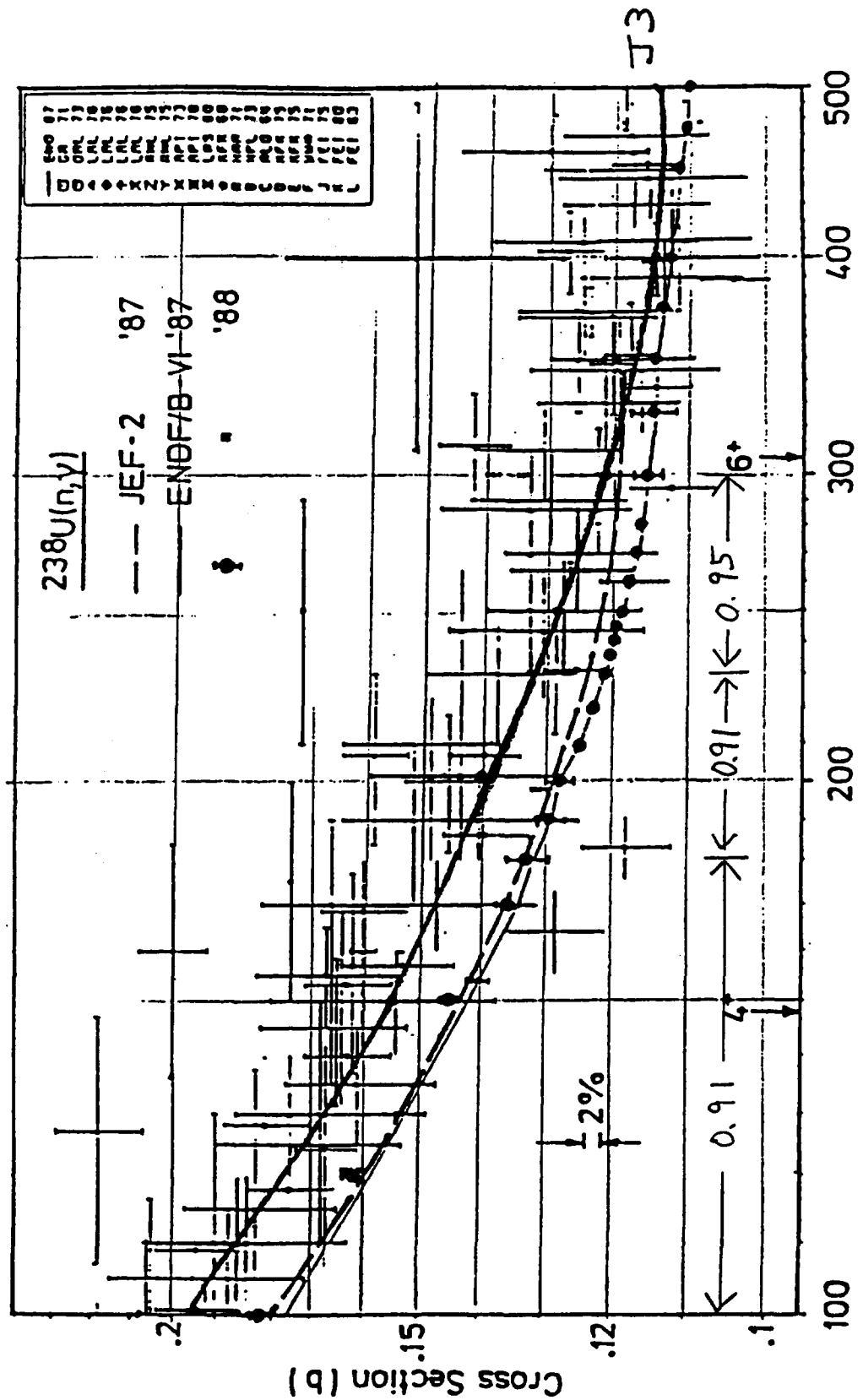

Fig. 2 U-238 capture cross sections (100 keV to 500 keV)

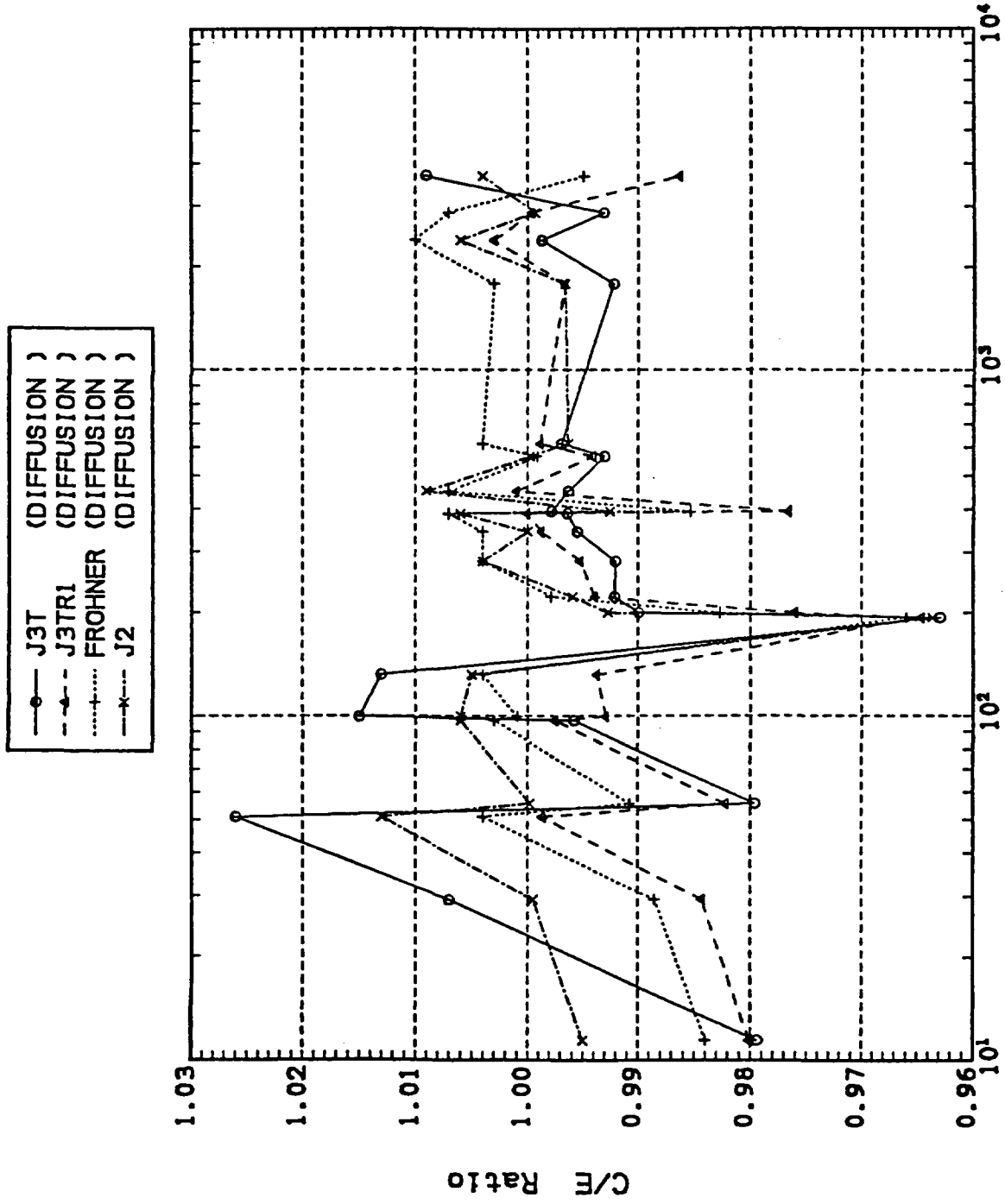

No	Core Name	Core Volume (l)
1	VERA-11A	11.45
2	VERA-1B	29.37
3	ZPR-3-6F	50.94
4	ZEBRA-3	55.56
5	SNEAK-7A	96.97
6	ZPR-3-12	99.64
7	ZPR-3-11	132.31
8	ZPR-3-54	193.61
9	FCA-5-2	199.23
10	ZPR-3-53	221.71
11	SNEAK-7B	281.16
12	ZPR-3-50	343.13
13	ZPR-3-48	387.97
14	ZEBRA-2	393.27
15	ZPR-3-49	449.77
16	MZA	565.06
17	ZPR-3-56	613.78
18	MZB	1777.61
19	ZPPR-2	2382.00
20	ZPR-6-7	2870.14
21	ZPR-6-6A	3668.11

Fig. 3 K-effective (JFS3J3U5N)

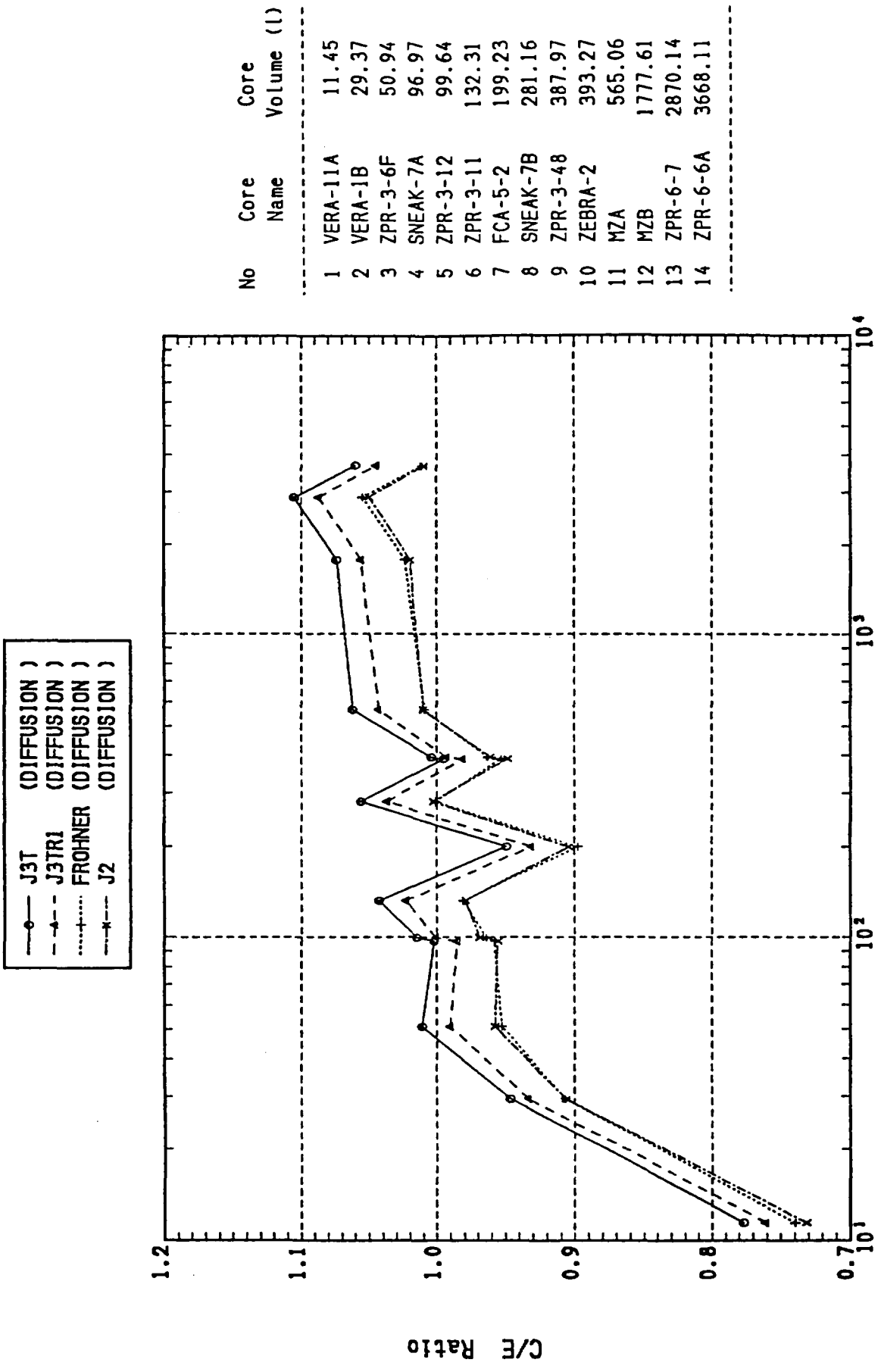

No	Core Name	Core Volume (l)
1	VERA-11A	11.45
2	VERA-1B	29.37
3	ZPR-3-6F	50.94
4	SNEAK-7A	96.97
5	ZPR-3-12	99.64
6	ZPR-3-11	132.31
7	FCA-5-2	199.23
8	SNEAK-7B	281.16
9	ZPR-3-48	387.97
10	ZEBRA-2	393.27
11	MZA	565.06
12	MZB	1777.61
13	ZPR-6-7	2870.14
14	ZPR-6-6A	3668.11

Fig. 4 C/E ratio of $\langle\sigma_c^{238}/\sigma_f^{235}\rangle$ (JFS3J3U5N)

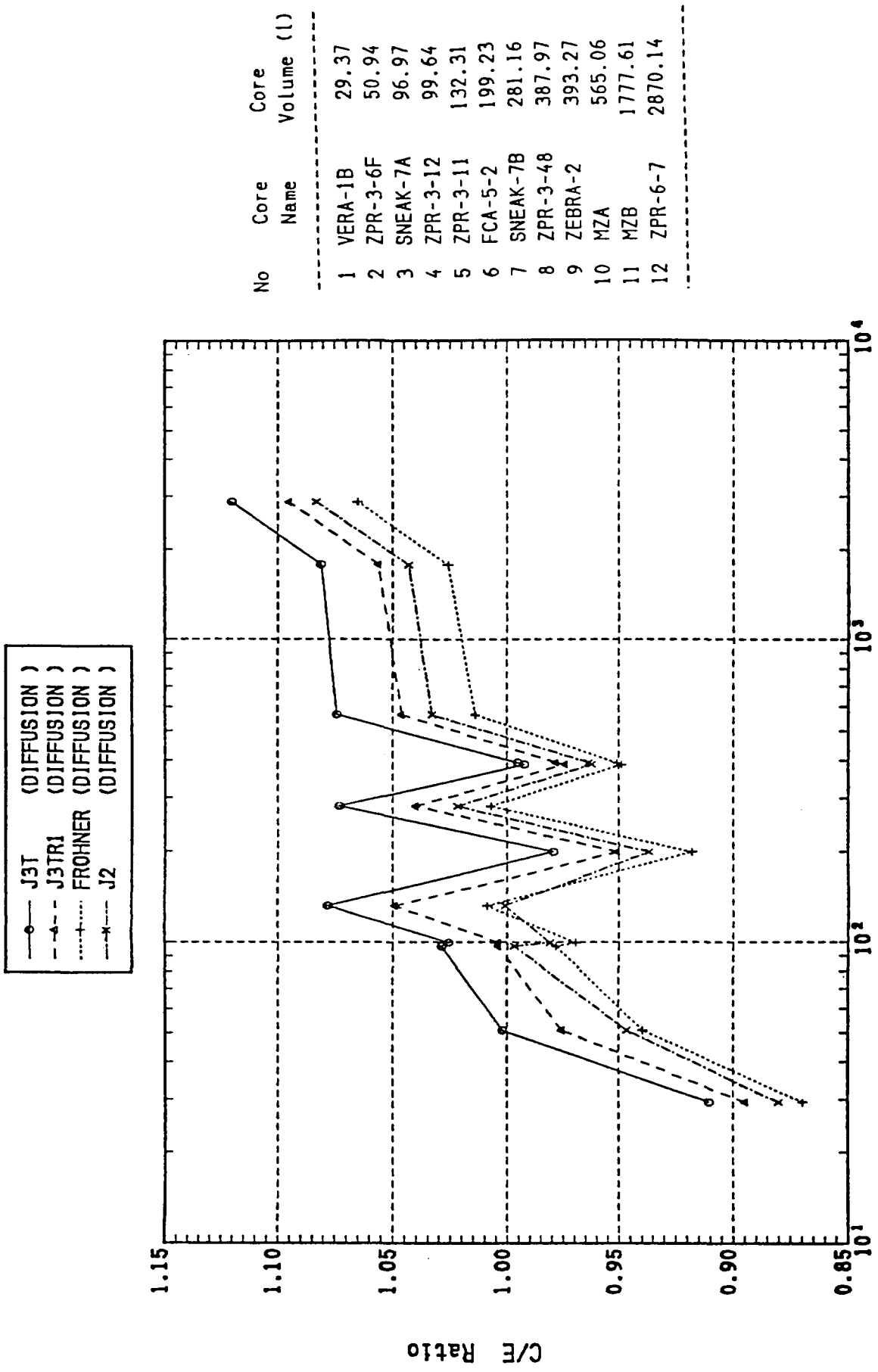

No	Core Name	Core Volume (l)
1	VERA-1B	29.37
2	ZPR-3-6F	50.94
3	SNEAK-7A	96.97
4	ZPR-3-12	99.64
5	ZPR-3-11	132.31
6	FCA-5-2	199.23
7	SNEAK-7B	281.16
8	ZPR-3-48	387.97
9	ZEBRA-2	393.27
10	MZA	565.06
11	MZB	1777.61
12	ZPR-6-7	2870.14

Fig. 5 C/E ratio of $\langle\sigma_C^{238}/\sigma_f^{239}\rangle$ (JFS3J3U5N)

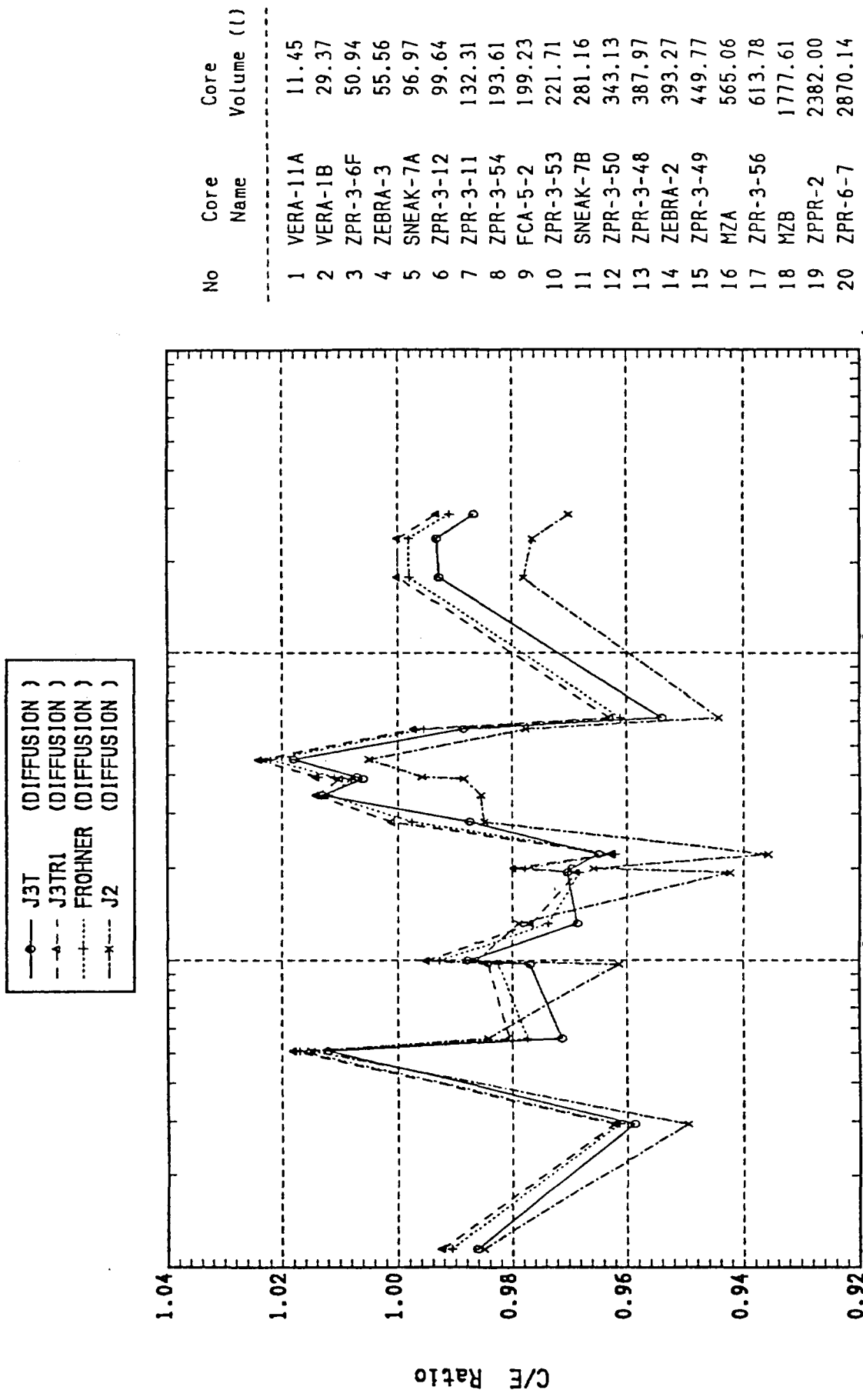

No	Core Name	Core Volume (l)
1	VERA-11A	11.45
2	VERA-1B	29.37
3	ZPR-3-6F	50.94
4	ZEBRA-3	55.56
5	SNEAK-7A	96.97
6	ZPR-3-12	99.64
7	ZPR-3-11	132.31
8	ZPR-3-54	193.61
9	FCA-5-2	199.23
10	ZPR-3-53	221.71
11	SNEAK-7B	281.16
12	ZPR-3-50	343.13
13	ZPR-3-48	387.97
14	ZEBRA-2	393.27
15	ZPR-3-49	449.77
16	MZA	565.06
17	ZPR-3-56	613.78
18	MZB	1777.61
19	ZPPR-2	2382.00
20	ZPR-6-7	2870.14

Fig. 6 C/E ratio of $\langle\sigma_f^{239}/\sigma_f^{235}\rangle$ (JFS3J3U5N)

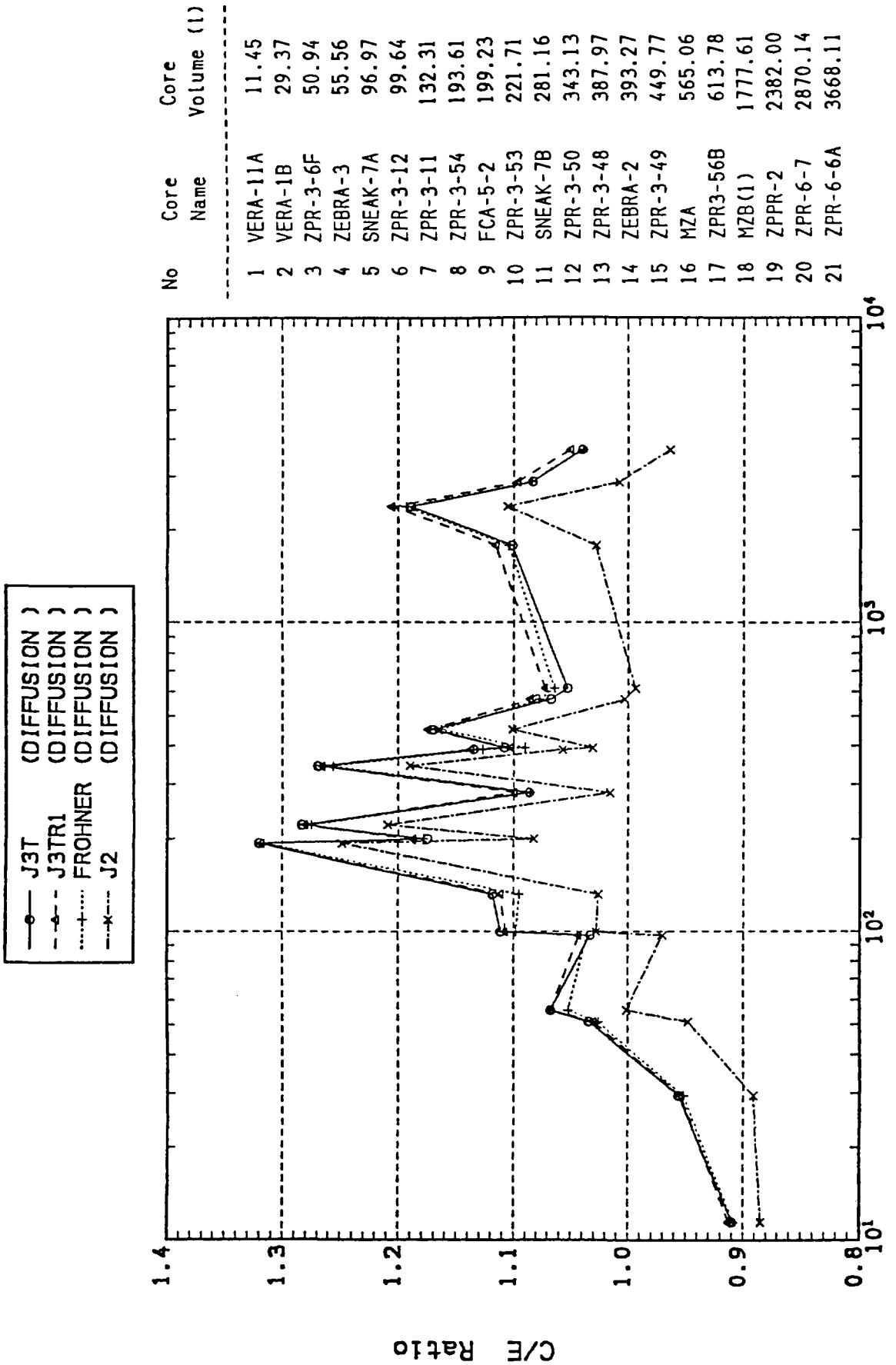

Fig. 7 C/E ratio of $<\sigma_f^{238}/\sigma_f^{235}>$ (JFS3J3U5N)

2.3.5 Analysis of FCA-IX Assembly Series by JENDL-3T/Rev.1

H.Takano and K. Kaneko
Department of Reactor Engineering
Japan Atomic Energy Research Institute
Tokai-mura, Naka-gun, Ibaraki-ken

The FCA-IX assembly series which were built to cover a wide of neutron spectrum shapes have been analysed to test the cross sections of higher actinides such as Np-237, Pu-240, Pu-242, Am-241 and Am-243 for the JENDL-2 and JENDL-3T/Rev.1 nuclear data. It was shown that the C/E-values for keff and central fission rate ratio obtained with JENDL-3T/Rev.1 depended strongly on the neutron spectrum shape.

Introduction

The FCA-IX assembly series consist of seven uranium fuelled cores which are built so as to cover the wide range of neutron spectrum shape and to test fission and capture cross sections of higher actinides.[1,2] The assemblies IX-1 to IX-6 were composed with 93 % enriched metal uranium, and diluent materials were graphite for the assemblies IX-1 to 3 and stainless steel for the assemblies IX-4 to IX-6. The assembly IX-7 was composed with 20 % enriched metal uranium without diluent materials. By analysing these assemblies we can investigate the relation between integral and nuclear data depending on neutron spectrum. The integral data measured in these assemblies are the effective multiplication factors, the central fission rate ratios of several actinide nuclides to uranium-235 and the central sample worths of actinide nuclides. In Refs.(1) and (2), the results obtained with the JENDL-2 and ENDF/B-IV nuclear data were discussed and the large discrepancies between the calculated and experimental values were shown especially for the fission reaction rate ratio of Am-243 to U-235 and the sample worths for Pu-240, Am-241 and Am-243.

In this report, the FCA-IX assembly series are analysed by using the JENDL-3T/Rev.1 nuclear data. For this purpose, the 70-group cross section library, JFS-3-J3T/Rev.1 [3] were generated with the processing code system TIMS-PGG.[4]

The effective cross sections were calculated by using the heterogeneous cell calculation code SLAROM.[5] The integral data obtained with two-dimensional diffusion calculations were corrected by the transport calculations.

Effective Multiplication Factor

The C/E-values of keff calculated with JENDL-2 and JENDL-3T/Rev.1 are shown in Table 1. The neutron spectra at core centre are compared in Fig. 1. The results obtained with JENDL-3T/Rev.1 are underestimated for neutron spectrum softening cores such as the assemblies IX-1 and -2. On the other hand, the results of JENDL-2 are overestimated for spectrum hardening cores. These are apparently observed from Figs. 2 and 3 in which the C/E-values of keff are shown as a function of spectral hardness of central fission rate ratios for U-238(n,f) to U-235(n,f).

Central Fission Rate Ratio

The central fission rate ratios of Pu-239, U-238, Np-237, Pu-238, Pu-242, Am-241 and Am-243 to U-235 were calculated for the JENDL-2 and JENDL-3T/Rev.1 nuclear data. Figures 4 - 10 show the C/E-values as a function of the assembly order which depends on the spectral hardness of U-238(n,f) to U-235(n,f). The experimental data were taken from the figures in Refs. (1) and (2). The results for JENDL-3T/Rev.1 are larger than those for JENDL-2 and overestimate considerably the measured data. Because the fission cross sections of U-235 for JENDL-3T/Rev.1 are smaller than those for JENDL-2 data. Furthermore, the C/E-values depend strongly on the spectrum hardness.

The Np-237, U-238, Pu-238, Pu-242, Am-241 and Am-243 are threshold fission reaction nuclides. It is wellknown that the results calculated for the threshold fission rate ratio overestimates the experimental data, such as seen for U-238 in Fig. 5. Then, it may be concluded that the results for Np-237, Pu-238 and Am-241 are in good agreement with the measured values, though they are overestimated for the soft spectrum cores.

Central Sample Worth

Figures 11 - 15 show the comparison of the sample worths of Np-237, Pu-238, Pu-242, Am-241 and Am-243 to Pu-239. The experimental

data were taken from the figure in Ref. (2). However, the data for Np-237, Am-241 and Am-243 measured at the assembly IX-3 were not considered in the present study, due to very small values. The agreement between the calculation and the measurement is not well generally. The Pu-240 sample worths calculated underestimate systematically the experimental data.

Concluding Remarks

The FCA-IX assembly series were analysed to test the cross sections of higher actinides by using JENDL-2 and JENDL-3T/Rev.1 nuclear data. The effective multiplication factors obtained with JENDL-3T/Rev.1 underestimated the experimental values for neutron spectrum softening cores. The central fission rate ratios for JENDL-3T/Rev.1 were larger than those for JENDL-2 and overestimated considerably the measured data. The large discrepancies between the calculations and experiments for the sample worths were observed.

Acknowledgements

The authors would like to express their appreciation to T. Mukaiyama and S. Okajima for supplying pleasantly the cell and composition data and the experimental data of keff.

References

1) T. Mukaiyama et al. : Actinide Integral Measurement in FCA Assemblies," Nuclear Cross Section for Technology, Proc. Inter. Conf., Santa Fe, May, 1985.
2) S. Okajima et al. :"Evaluation and Adjustment of Actinide Cross Sections Using Integral Data Measured at FCA," Nuclear Data for Science and technology, Proc. Inter. Conf., Mito, 1988.
3) H. Takano el al. : to be published
4) H. Takano et al.:" TIMS-PGG : A Code System for Producing Group Constants in Fast Neutron Energy Region," JAERI-M 82-072 (1982).
5) M. Nakagawa et al.: JAERI-1294 (1984).

Table 1 C/E values of k_{eff}

Assembly	JENDL-2	JENDL-3T/Revision-1
FCA-IX-1	0.9982	0.9732
FCA-IX-2	1.0004	0.9809
FCA-IX-3	1.0013	0.9861
FCA-IX-4	1.0172	1.0042
FCA-IX-5	1.0147	1.0038
FCA-IX-6	1.0038	0.9967
FCA-IX-7	1.0088	1.0004
average	1.0063	0.9922

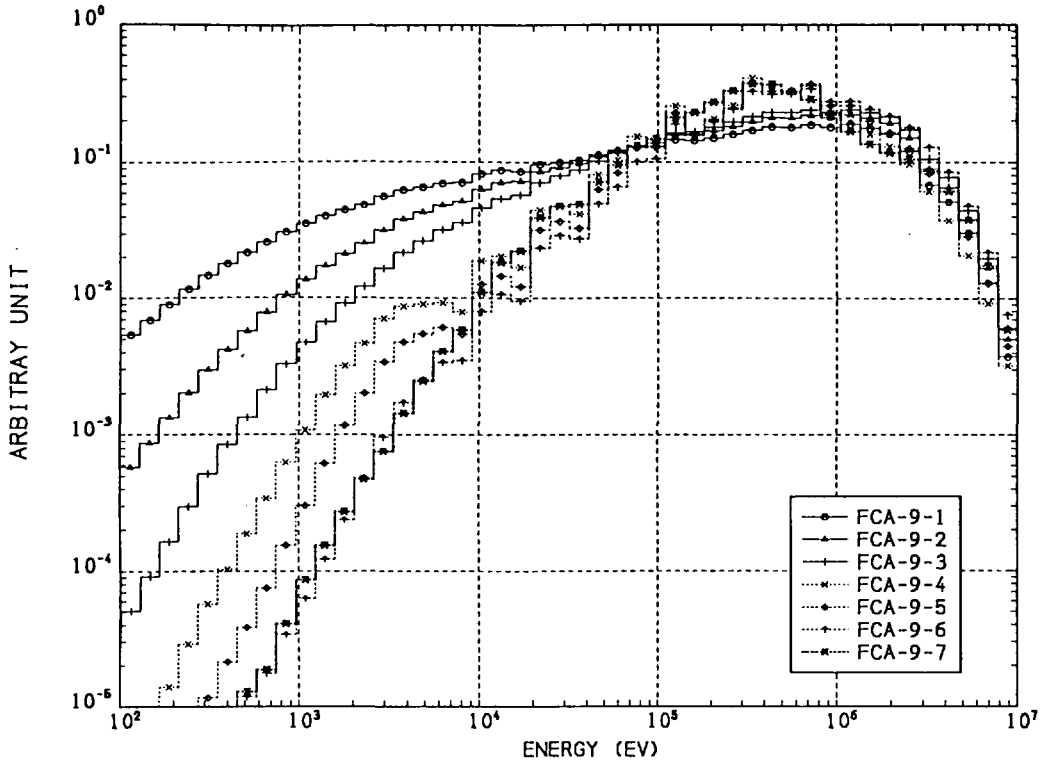

Fig. 1 Comparison of real neutron spectrum at core center (JFS3J2)

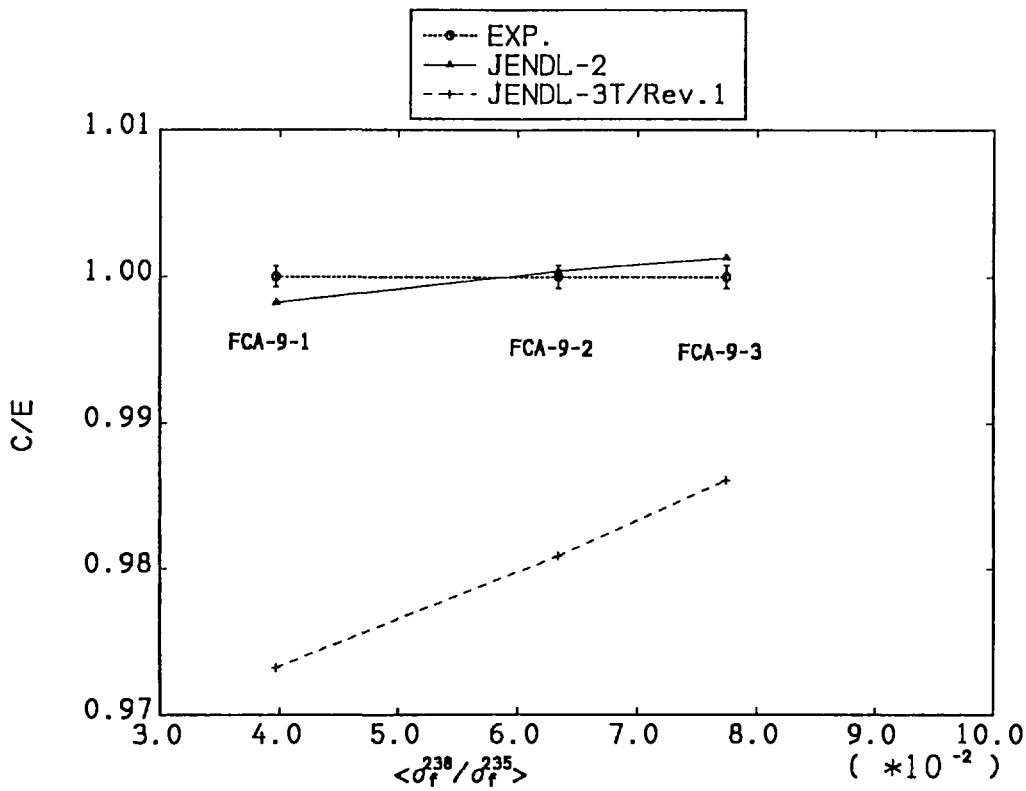

Fig. 2 C/E of k_{eff} for FCA-9-1, FCA-9-2, FCA-9-3 (Graphite Moderator)

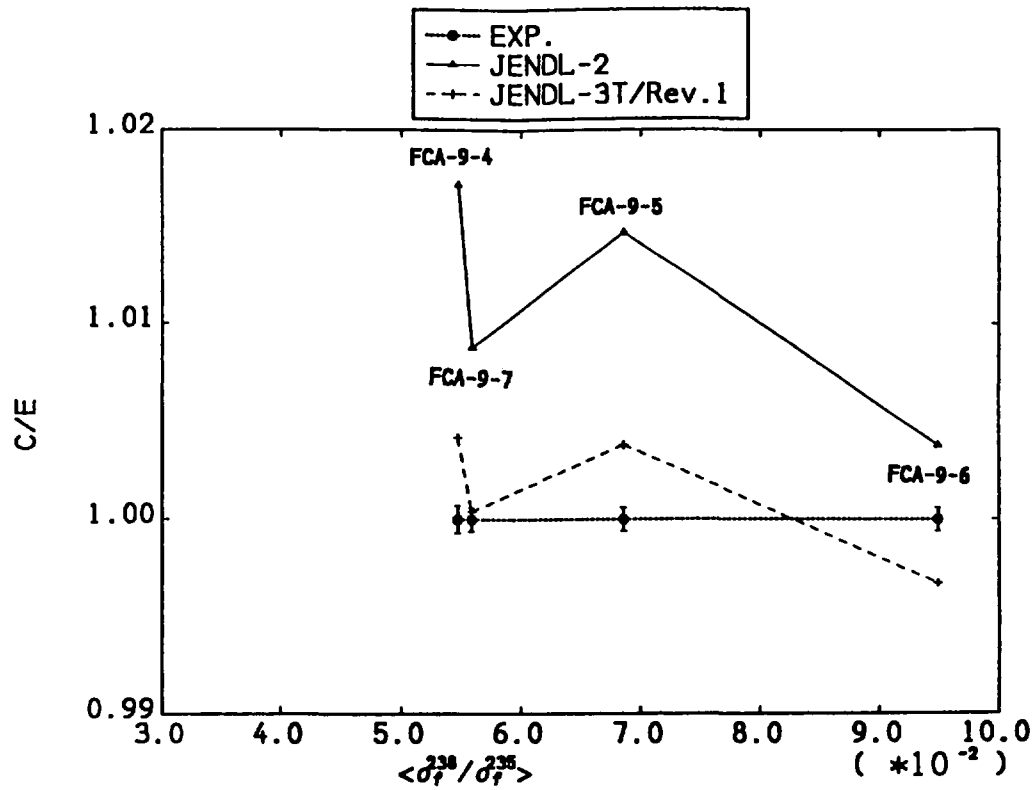

Fig. 3 C/E of k_{eff} for FCA-9-4, FCA-9-7, FCA-9-4, FCA-9-5 (SUS Moderator)

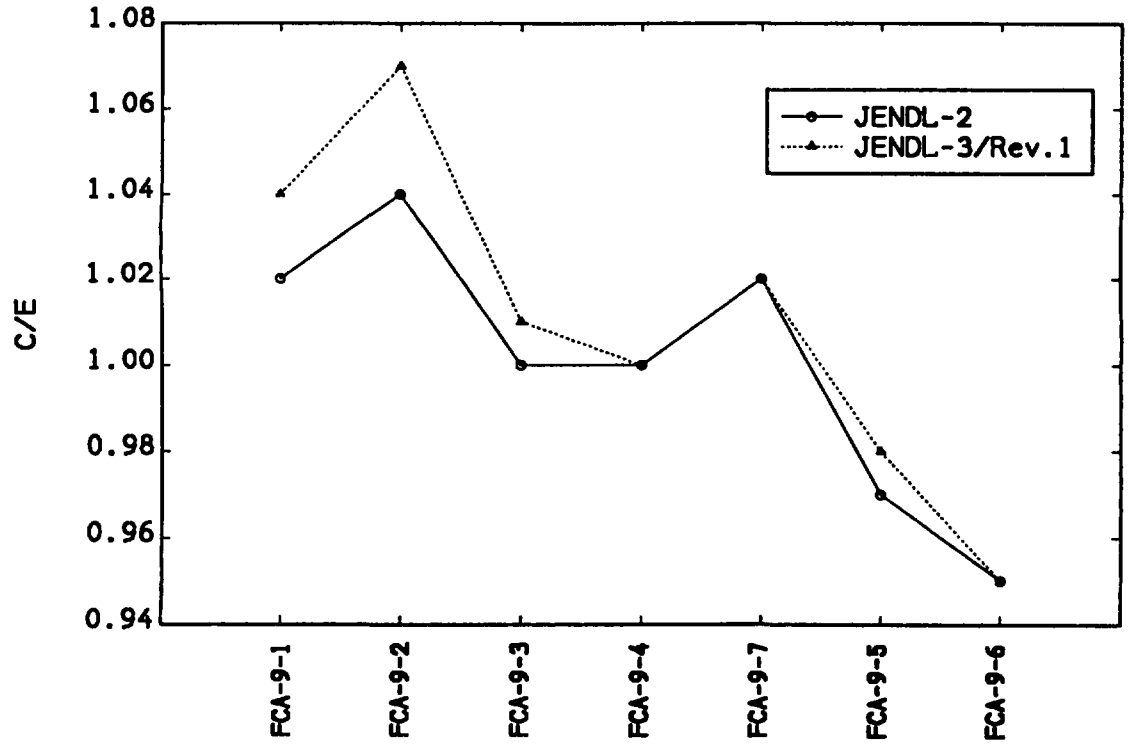

Fig. 4 ^{239}Pu fission rate ratio relative to ^{235}U fission

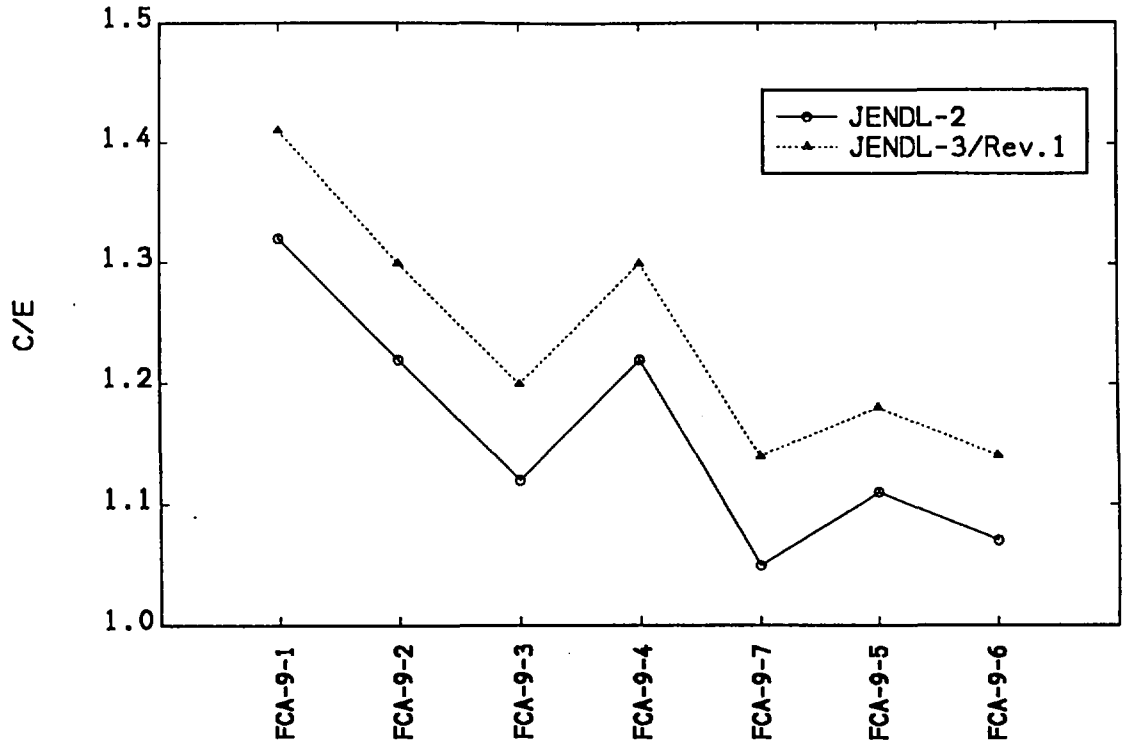

Fig. 5 ^{238}U fission rate ratio relative to ^{235}U fission

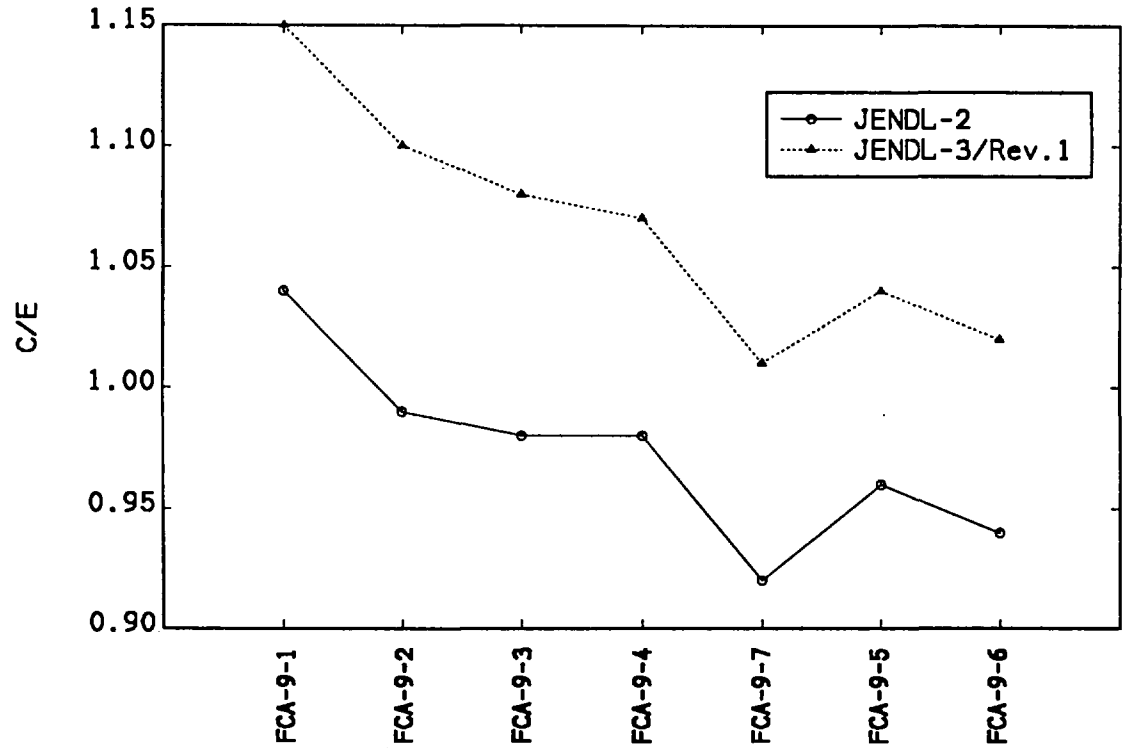

Fig. 6 ^{237}Np fission rate ratio relative to ^{235}U fission

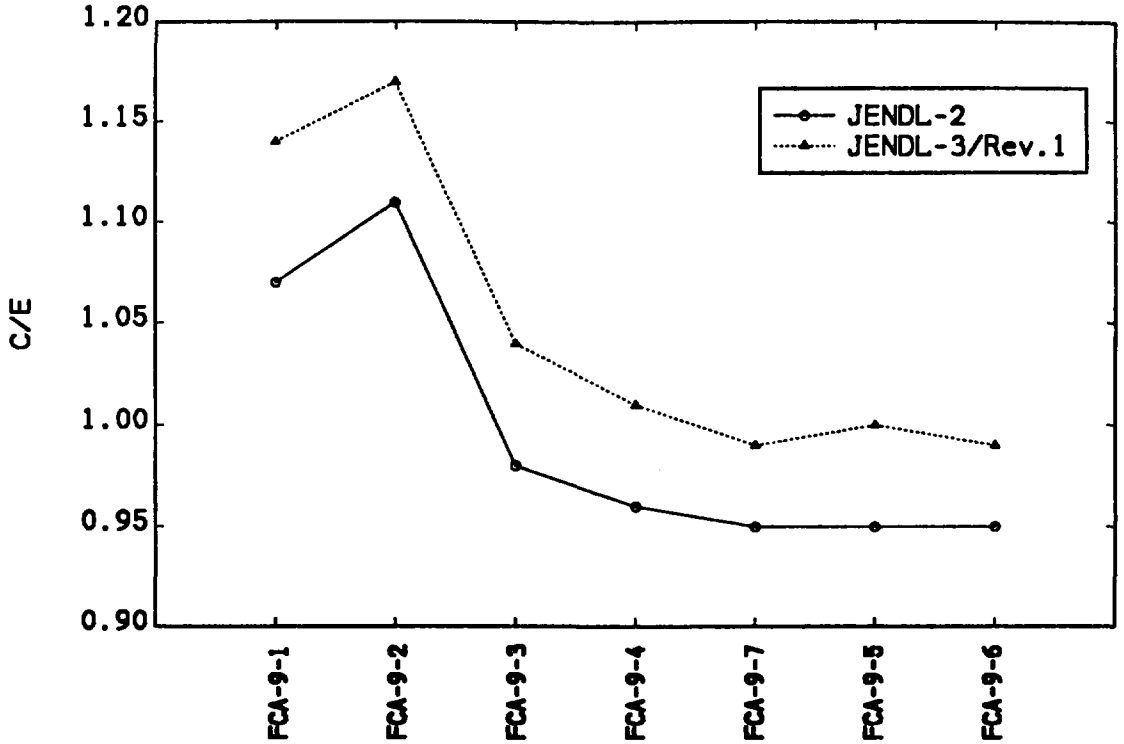

Fig. 7 ^{238}Pu fission rate ratio relative to ^{235}U fission

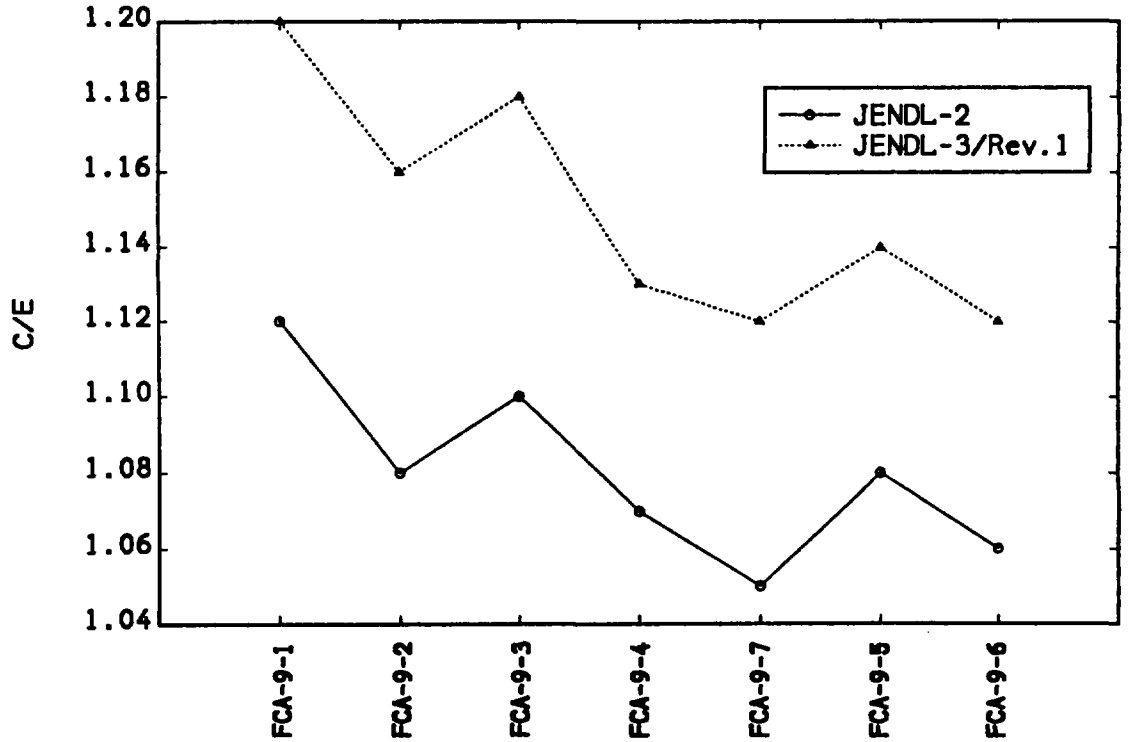

Fig. 8 ^{242}Pu fission rate ratio relative to ^{235}U fission

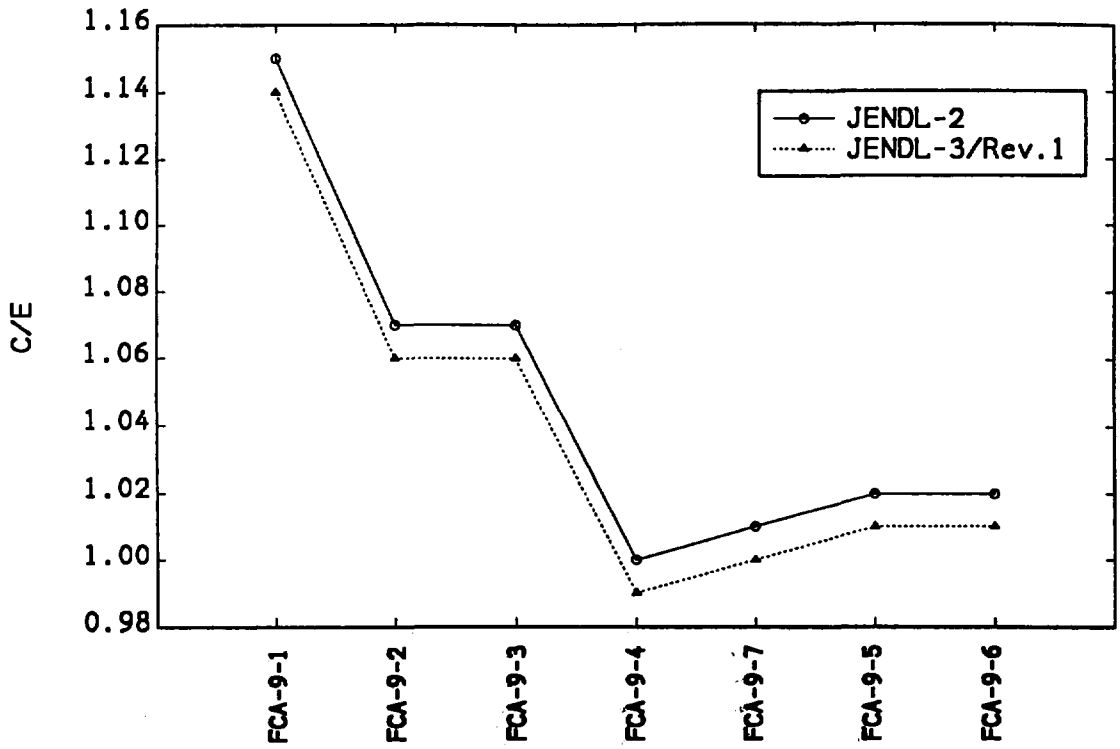

Fig. 9 ^{241}Am fission rate ratio relative to ^{235}U fission

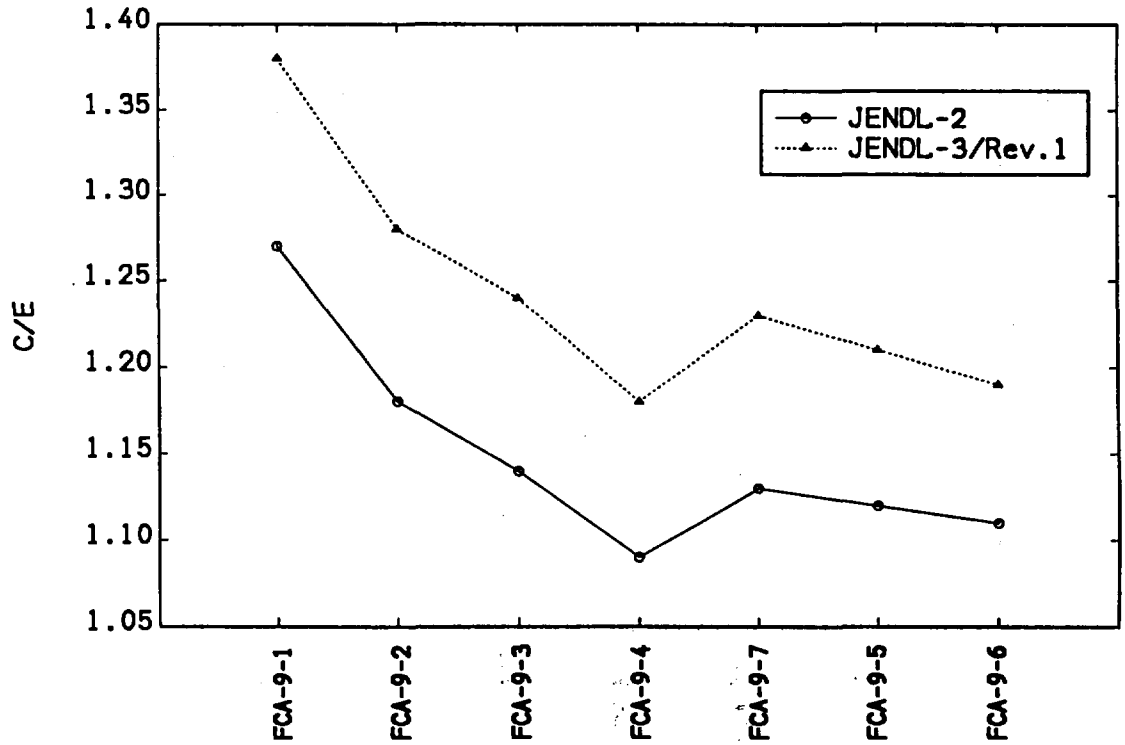

Fig. 10 ^{243}Am fission rate ratio relative to ^{235}U fission

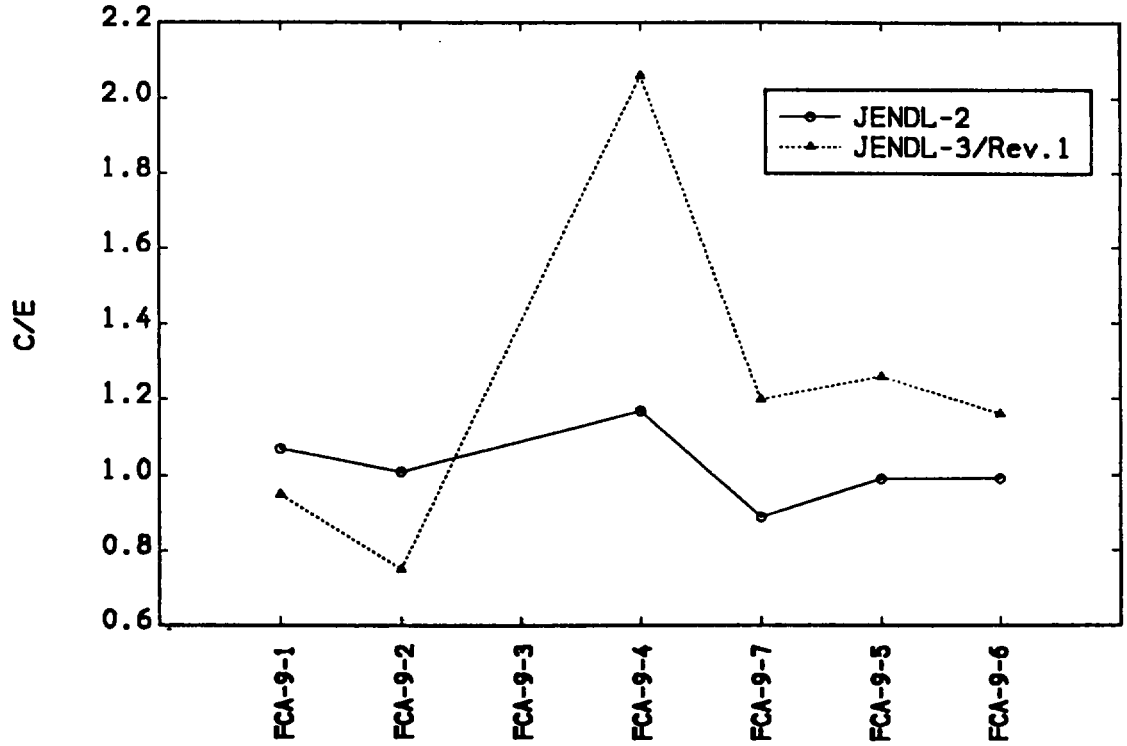

Fig. 11 ^{237}Np sample worth ratio relative to ^{239}Pu sample worth

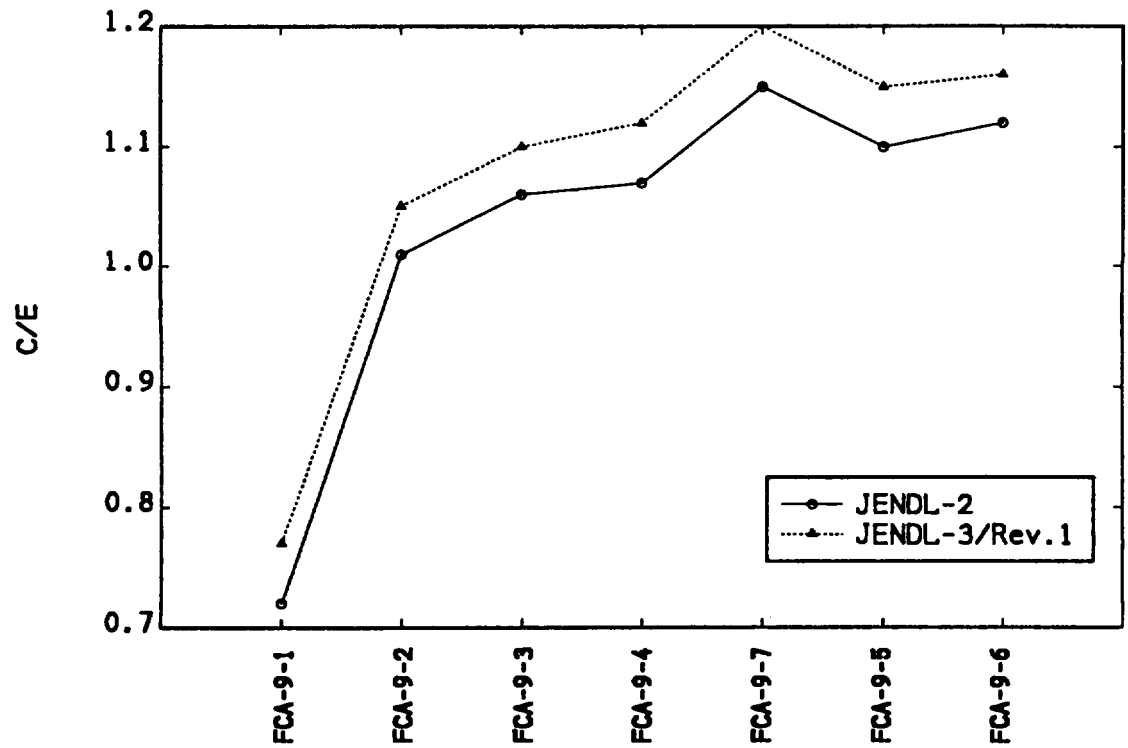

Fig. 12 ^{238}Pu sample worth ratio relative to ^{239}Pu sample worth

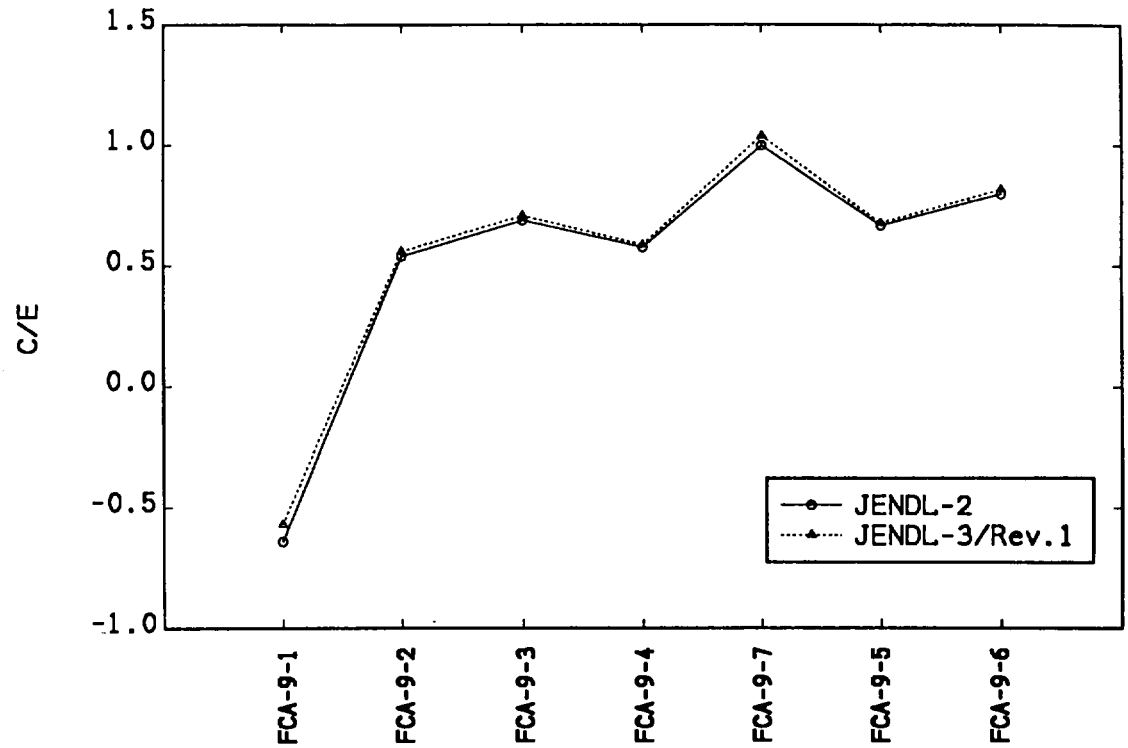

Fig. 13 ^{240}Pu sample worth ratio relative to ^{239}Pu sample worth

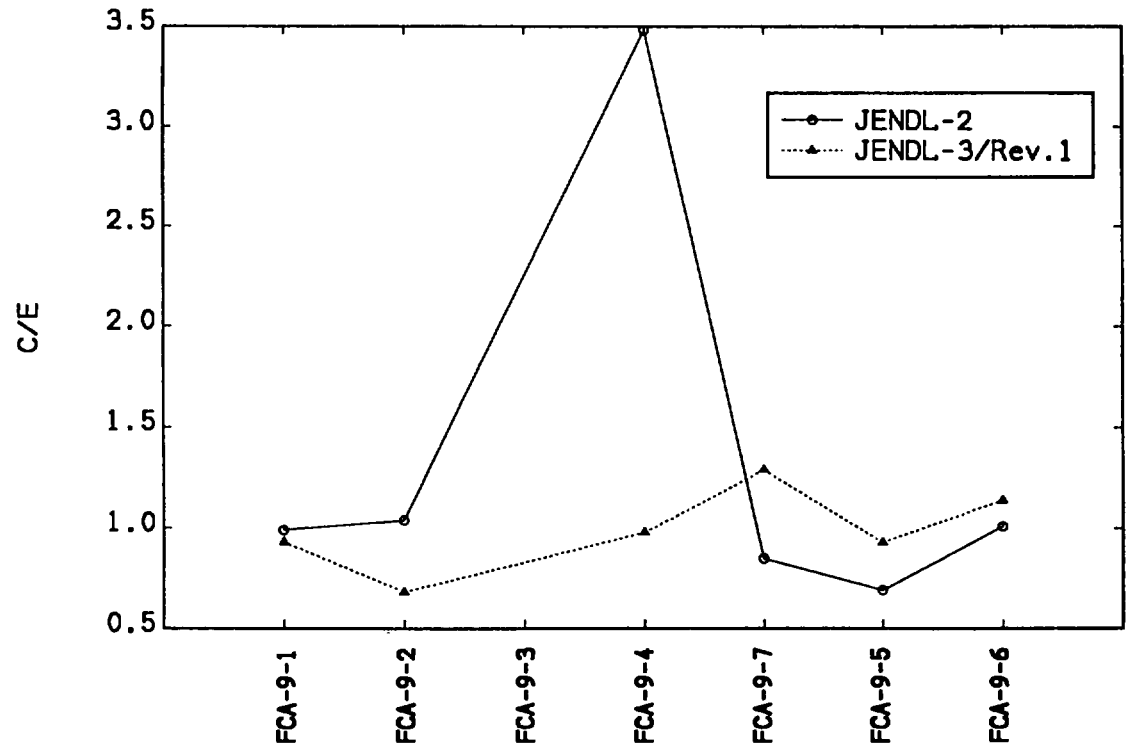

Fig. 14 ^{241}Am sample worth ratio relative to ^{239}Pu sample worth

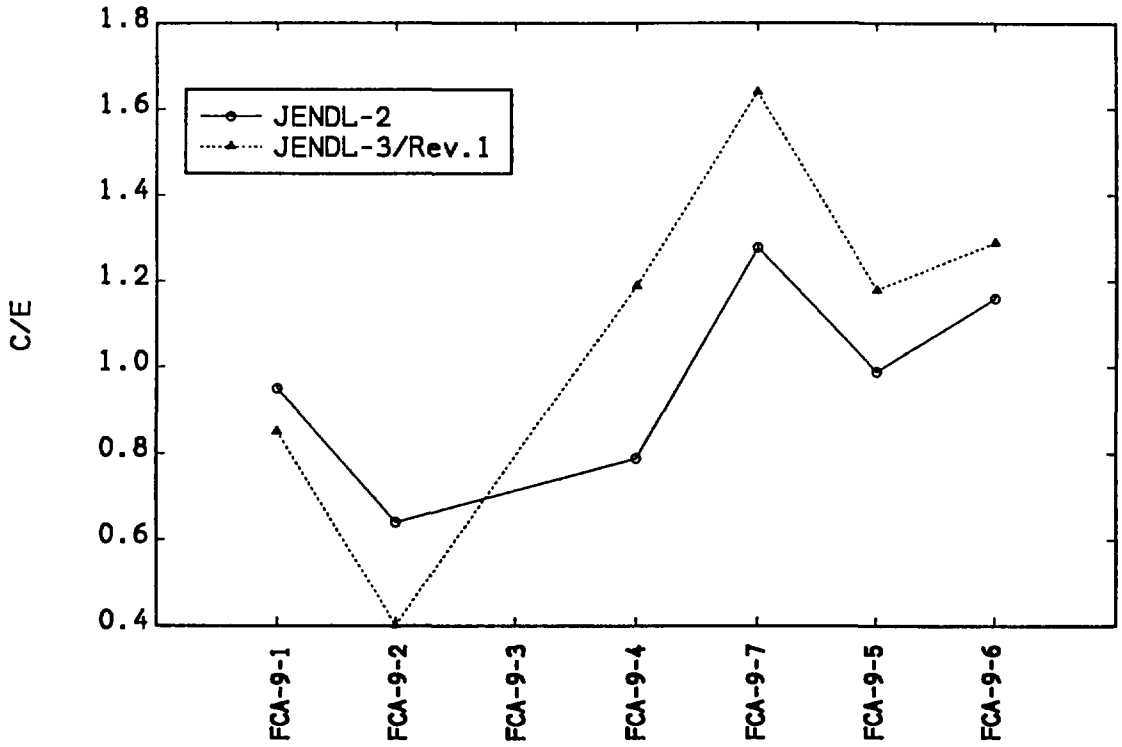

Fig. 15 ^{243}Am sample worth ratio relative to ^{239}Pu sample worth

2.3.6 On the Fission Neutron Spectrum for U-235 in JENDL-3T

Takaaki Ohsawa
Atomic Energy Research Institute, Kinki University
3-4-1 Kowakae, Higashi-osaka 577 Japan

Abstract: The fission neutron spectrum for U-235 contained in JENDL-3T was compared with those in JENDL-2 and ENDF/B-V. Verification of the spectrum was attempted by comparing the calculated and measured fission-spectrum averaged cross sections for 18 dosimetry reactions.

1. Introduction

The fission neutron spectrum of U-235 for JENDL-3T was evaluated on the basis of the Madland-Nix model[1]. In order to examine the appropriateness of the new evaluation, calculation was made of the spectrum-averaged cross sections for 18 threshold reactions using different spectrum shapes and they were compared with measured data.

2. Comparison of the Fission Neutron Spectrum in Different Files

In the earlier version of JENDL (JENDL-2), the fission neutron spectrum for the thermal-neutron-induced fission of ^{235}U was taken from ENDF/B-IV which was of the form of Maxwellian distribution with the average energy $\bar{E}$ = 1.985 MeV. In the newer version, ENDF/B-V, a harder spectrum, i.e. the Watt-type distribution with $\bar{E}$ = 2.032 MeV was adopted. The spectrum calculated with the method of Madland and Nix together with the input parameters given in ref.1) provided a distribution with $\bar{E}$ = 2.039 MeV which was almost the same value as that of the Watt spectrum in ENDF/B-IV but with a bit different shape. The main features of the three spectra are summarized in Table 1 and the shapes are compared in Fig.1. Note that the ratio of the spectrum to that of Maxwellian spectrum in JENDL-2 is plotted in this figure.

3. Verification of the Spectrum by Means of the Spectrum-Averaged Cross Sections

The fission-neutron averaged cross sections for 18 threshold reactions were calculated using these three spectrum. The dosimetry reactions with different thresholds were chosen so as to cover the wide energy regions of the spectrum. The horizontal bars in Fig.1 indicate the approximate energy intervals from which 90% of the corresponding total reaction response comes.

The cross section data were taken from JENDL-2 and ENDF/B-IV (The JENDL-3T dosimetry data were not used because the file was under compilation and the complete set of data for the chosen reactions were not available at the time of this calculation). The three spectra and two sets of cross section data provided six possible combinations.

Table 2 summarizes the calculated average cross sections for the six combinations. Experimental data are also shown in the last column, most of which were taken from the evaluation by Mannhart[2], supplemented with the works of Kobayashi and Kimura[3], Dezsoe et al.[4], and Fabry[5] for some of the reactions lacking in the work of Mannhart[2].

Figure 2 shows the calculation-to-experimental ratios (C/E) for the spectrum-averaged cross sections. The reactions were arranged with increasing order of threshold energy from top to bottom. It can readily be seen that the calculation agrees rather well, say within 15%, with experiments up to approximately 10 MeV for any of the three spectrum. An exception is the case for ^{47}Ti(n,p). Evidently this is due to the fact that the evaluated cross section for this reaction in ENDF/B-V is overestimated, since newer measurement by Mannhart et al.[6] yielded much lower data. At energies higher than 10 MeV, we can observe apparent deviations from unity to opposite directions, i.e. into the region of C/E>1 for Maxwellian spectrum (symbolized with open and closed triangles) and into the region of C/E<1 for Watt-type (squares) and Madland-Nix (circles) spectra. This fact suggests the possibility that the Maxwellian spectrum (JENDL-2, ENDF/B-IV) overestimates, and the Madland-Nix spectrum (JENDL-3T) and the Watt spectrum (ENDF/B-V) underestimate, the actual spectrum at energies above around 10 MeV.

4. Concluding Remarks

Comparing the general trends of the C/E-values for the three spectra, we can say that the Madland-Nix and Watt spectra represent the fission spectrum equally well than does the Maxwellian representation for thermal-neutron fission of ^{235}U. But the former two spectra tend to underestimate the actuall spectrum in the region above 10 MeV. This is not a region of no importance in reactor physics, since second- and third-chance fission raises the neutron importance in this region in fast reactors, and the rate of $^{237}Np(n,2n)$ reaction, which leads to production of ^{232}U in fuels, is affected by the high-energy component of the fission spectrum. Further detailed analysis of the dependence of the Madland-Nix spectrum on input parameters and possible amelioration of the model would be required.

Acknowledgments

The author is very indebted to Dr. Kobayashi of Kyoto University Research Reactor Institute for providing necessary information and data and for useful discussions. He is also very grateful to Prof. Kimura of Kyoto University for valuable suggestions.

References

1) D. G. Madland and J. R. Nix, Nucl. Sci. Eng. 81,213 (1982)
2) W. Mannhart, Proc. 5th ASTM-EURATOM Symposium on Reactor Dosimetry (1984) p.813
3) K. Kobayashi and I. Kimura, NEANDC(J)67, p.42 (1980)
4) Z. Dozsoe et al., Proc. Conf. on Neutron Physics, Kiev, 1977, p.32
5) A. Fabry, Neutron Cross Sections for Reactor Dosimetry, IAEA-208, Vol.I, p.233 (1978)
6) W. Mannhart, Proc. Int. Conf. on Nuclear Data for Basic and Applied Science, Santa Fe, 1985, Vol.1, p.577

Table 1 Comparison of main features of evaluated fission spectra for U-235. On the right hand side, the symbols used in Fig. 2 to distinguish the six combinations of spectra and cross section sets are shown.

File	Shape	$\bar{E}$ (MeV)	Cross Sections	
			JENDL-2	ENDF/B-V
JENDL-2 ENDF/B-IV	Maxwellian	1.985	▲	△
JENDL-3T	Madland-Nix	2.039	●	○
ENDF/B-V	Watt	2.032	■	□

Table 2 Comparison of the fission-spectrum averaged cross sections for thermal-neutron induced fission of U-235

Spectrum	JENDL-2 ENDF/B-IV (Maxwell)		JENDL-3T (Madland)		ENDF/B-V (Watt)		Exp'tal data (Mannhart)	
Cross Section	ENDF/B-V	JENDL-2	ENDF/B-V	JENDL-2	ENDF/B-V	JENDL-2		
$^{27}Al(n,p)^{27}Mg$	4.264	3.772	4.160	3.689	4.271	3.785	3.95±0.06	
$^{27}Al(n,a)^{27}Na$	0.8189	0.8310	0.6794	0.6929	0.7267	0.7402	0.706±0.028	
$^{46}Ti(n,p)^{46}Sc$	11.16		10.90		11.20		11.6±0.4	
$^{47}Ti(n,p)^{47}Sc$	21.67		22.52		22.48		17.7±0.6	
$^{48}Ti(n,p)^{48}Sc$	0.3180		0.2670		0.2846		0.302±0.010	
$^{55}Mn(n,2n)^{54}Mn$	0.3270	0.3335	0.1881	0.1920	0.2148	0.2192	0.202±0.001	*1
$^{54}Fe(n,p)^{54}Mn$	78.53	71.93	81.37	73.85	81.57	74.39	80.5±2.3	
$^{56}Fe(n,p)^{56}Mn$	1.119	1.162	0.9937	1.031	1.047	1.087	1.09±0.04	
$^{58}Ni(n,p)^{58}Co$	102.6	99.70	106.33	103.39	106.46	103.52	109.±3	
$^{58}Ni(n,2n)^{57}Ni$	0.00532	0.0052	0.00256	0.00251	0.00296	0.0029	0.00419±.00022	
$^{59}Co(n,a)^{56}Mn$	0.1711	0.1836	0.1450	0.1567	0.1543	0.1665	0.161±0.007	
$^{59}Co(n,2n)^{58}Co$	0.2977	0.2764	0.1684	0.1575	0.1926	0.1800	0.202±0.006	
$^{63}Cu(n,a)^{60}Co$	0.6087	0.5852	0.5422	0.5264	0.5703	0.5526	0.5±0.055	*2
$^{65}Cu(n,2n)^{64}Cu$	0.4809	0.4794	0.2853	0.2829	0.3246	0.3222		
$^{115}In(n,n')^{115}In$	173.2		181.5		179.3		190.3±7.3	
$^{127}I(n,2n)^{126}I$	1.730		1.129		1.270		1.04±0.06	*1
$^{19}F(n,2n)^{18}F$		0.0147		0.00792		0.0090		
$^{63}Cu(n,2n)^{62}Cu$		0.1499		0.0781		0.0900	0.122	*3

*1 Kobayashi and Kimura, ref.3.

*2 Dezsoe et al., ref.4.

*3 Fabry, ref.5.

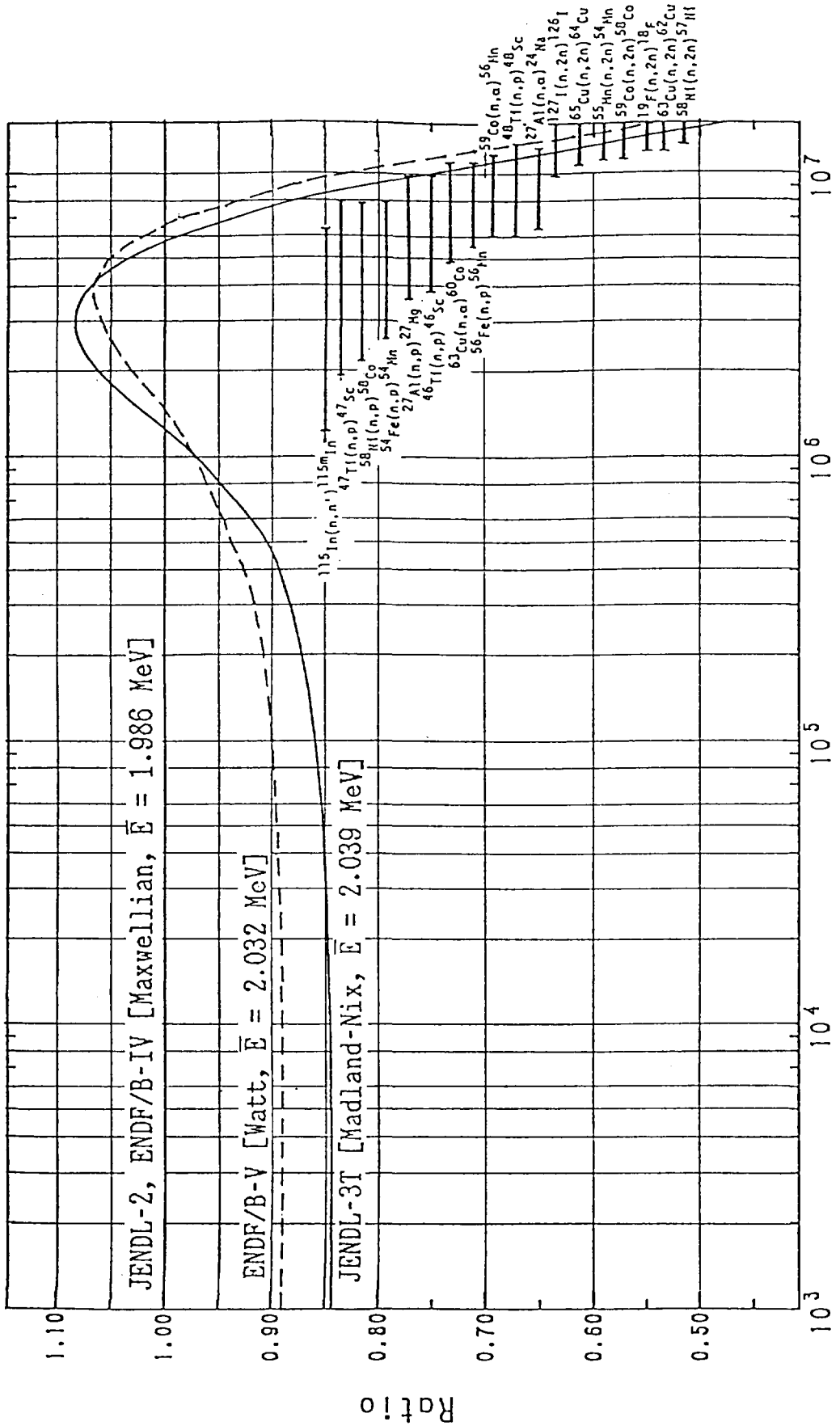

Fig. 1 Ratios of Madland-Nix(JENDL-3T) and Watt(ENDF/B-V) spectra relative to the maxwellian spectrum (JENDL-2, ENDF/B-IV).

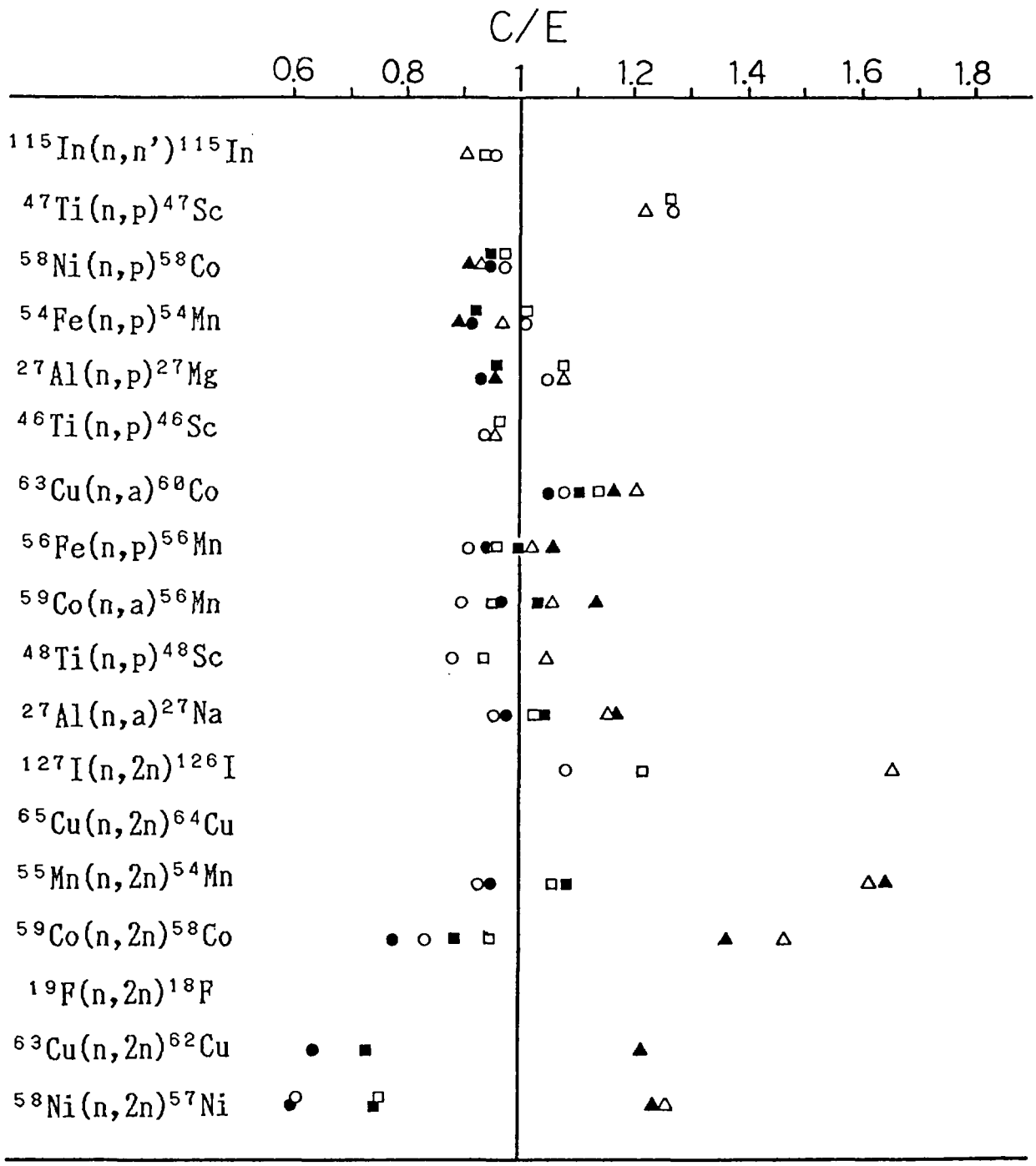

Fig. 2 C/E of fission-spectrum averaged cross sections for thermal-neutron induced fission of U-235. Experimental data were taken from Mannhart's evaluation (ref.2) if not otherwise stated.

2.4 Present Status and Future of Databases

2.4.1 Current Status of Database Development in JAERI

Y. Kikuchi
Japan Atomic Energy Research Institute
Tokai-mura, Naka-gun, Ibaraki-ken

In spite of the importance of database as a medium of scientific information exchange, most of databases currently used in Japan are imported ones. There is a movement to concern such a situation recently. JAERI is expected to have a function of database center in the field of nuclear technology. Responding to these requests, intensive discussion have been made in JAERI on the current status of database development, the problems encountered and the ways to resolve them.

JAERI has produced various kinds of data and some of them have been compiled as databases. Most of them, however, are at the laboratory memorandum level, and very few are widely used outside.

The following conditions should be fulfilled so that the outside users would like to use a database; (1) the data are complete and not lacking, (2) the DBMS is high-grade and user-friendly, (3) the user manual is well provided and (4) the status of development is announced to users.

It is difficult for a database of laboratory memorandum level to fullfill such conditions, because each laboratory has little incentive to such a service work and because it costs tremendous amount of man-power and money. Hence a special department, called Database Center, should be established and should develop, maintain, up-date high-grad databases (of information exchange level) and make a centralized service.

Various problems are now under discussion toward establishing the Database Center in JAERI.

1. Introduction

The importance of database becomes well recognized as a medium of scientific information exchange. Most of databases currently used in Japan are, however, imported ones. Such a situation is dangerous, because the advanced countries become reluctant to supply the scientific information to Japan. Furthermore, the domestically developed databases are essential to new and innovative research developments.

Recently in Japan there is a movement to concern such a situation. For example the scientific council pointed out the importance of databases in their 11th recommendation. Concerning the fact databases, it recommended that some special organization should collect, validate and file the original data and supply them as a database center.

JAERI should have a function of database center. This is clearly described in Long-Term Program for Development and Utilization of Nuclear Energy revised in 1987 as: JAERI is implementing a wide range of R & D and experiments in the field of nuclear energy and, furthermore, it also has the function of an integrated central research institution equipped with joint use facilities, data bases, etc.

Responding to these requests, an ad-hoc group was held in JAERI Tokai Research Establishment. The group discussed on the current status of databases developed in JAERI, the problems encountered and the ways to resolve them. This paper is an abstract of the report of the ad-hoc group.

2. Current Status of Existing Databases in JAERI

2.1 Current Status

JAERI has produced various kinds of scientific data through its research activity over 30 years. Some of these data have been compiled as databases with computer readable formats. The current status of these databases was investigated and the main results are given in Table 1.

Table 1 reveals that very few databases are prepared for open use. Most of databases have been developed for their own research purposes or as compilations of their research results. Different database management systems (DBMS) are used for different databases.

2.2 Analysis

In order to avoid confusion, the terminology "database" should be categorized in various aspects.

A. Grade of data processing

As is used in Table 1, the database can be categorized by grade of data processing as

1) Zeroth grade: Compilation of raw data without DBMS.
2) First grade: Compilation of raw or validated data with DBMS so that the data retrieval may be possible.
3) Second grade: Evaluated or recommended data.
4) Third grade: Data processed as input data library for a specific computer code.

B. Completeness from the viewpoint of utilization

1) Laboratory memorandum level

A database consists of the research results in a specific laboratory or of the data compiled for a specific research purpose. This type of database is aimed only to record their research activity. Hence the DBMS is often very simple one. Most of the databases existing in JAERI are at this level.

2) Information exchange level

One of the important role of the database is a medium of the scientific information exchange among different laboratories often in different countries. For this purpose, more general architecture and more flexible DBMS are required.

3. Ways to Accelerate the Database Activity

It is much required that the results of JAERI's research activity are provided as the databases of the information exchange level. As a matter of fact, however, very few databases currently existing are widely used even in Japan. There exists a large gap between the level of database required in the present era and the level of the databases so far developed in JAERI. Here are discussed the ways to resolve this gap.

3.1 Encouragement of Laboratory Memorandum Level Database

Many of the research results have been compiled as databases of laboratory memorandum level in JAERI. Some of important data, however, have not yet been compiled with computer readable formats. These data should be stored in computer as soon as possible before the records fade out.

In general, the following should be pointed out to encourage development of the databases of laboratory memorandum level.

1) Each researcher must have reform his sense; "the research work completes not at the time when the paper is published but at the time when the results are compiled as the database".
2) Enough budget and man-power should be provided to develop databases.
3) Database development should be well estimated as his research achievement.

3.2 Development of Information Exchange Level Database

Even if the databases of laboratory memorandum level are well developed and become open to outside utilization, it does not guarantee that these databases will be widely used. The reasons are as follows:

1) These databases are developed for special interests of a specific laboratory. Hence its contents look deviated or some important data are lacking from the viewpoint of outside users.

2) Their DBMS are often very primitive and do not satisfy the requests from the outside users.
3) The outside users are often not informed of the existence of the databases.

That is to say, the following conditions should be fulfilled so that the outside users would like to use a database; (1) the data are complete and not lacking, (2) the DBMS is high-grade and user-friendly, (3) the user manual is well provided and (4) the status of development is announced to users.

It is to be noted that these necessary conditions cannot be fulfilled easily by each laboratory where the database of laboratory memorandum level has been first developed. The reasons are:

1) The principle mission of each laboratory is naturally research activity. The works to fulfill the above conditions seem the service work which is not its mission. Hence there are no incentives to these works.
2) To fulfil the above conditions requires man-power and money of several times as much as those necessary to develop the original database. Each laboratory cannot afford it.
3) A high-grade DBMS should be developed with an unified policy over the institute. Such a work is not suitable to each laboratory.

Taking account of the situation, it can be concluded that a special department, called Database Center, should be established, in order to intensively develop the databases of the information exchange level in various fields. The database center make the development, maintenance, up-date and service of the databases as its own mission with a unified policy.

The merits of establishing the database center are summarized as follows:

1) The database development is its own mission.
2) The high-grade DBMS can be developed by considering various fields in the institute.

3) The budget and man-power can be concentrated to the center.
4) One definite channel is convenient to the outside users.
5) The data can be well controlled so that the copy right is protected and the illegal diffusion is prevented.

3.3 Relation between Database Center and Laboratories.

Even if the database center is established, the databases should be developed at the first stage in each laboratory. It becomes a duty of each laboratory to make its results computer readable databases. Further development depends on the character of laboratory. For example, nuclear data center has already a function of database center in the field of neutron nuclear data. On the other hand, most of experimental laboratories can make only the 0th databases.

Hence the relation between the center and laboratories are well defined for each database, so that the database center may function effectively. In establishing database center, some database developer may move from the laboratory to the center.

3.4 Research Activities in Database Center

The knowledge and judgement of specialists in the field of the data are essential in various stages of database development. Hence the database center must keep specialists in various fields. To keep their morals and assure the high quality of databases, the database center must have research activities relating to the databases. Candidates of the research activities are the data evaluation, the DBMS development, the AI approach to data handling and so on.

4. Present Movement for Establishing Database Center

Before establishing the database center in JAERI, a lot of problems should be discussed such as man-power, schedule, budget etc. For this purpose a special group consisting 6 part-timers was formed in the computer center. The group is studying the following problems.

1) Understanding the real status of database development in each laboratory.

2) Needs from outside users.
3) Availability of the data which JAERI cannot provide.
4) Scope and time schedule of development for each database.
5) Development of DBMS.
6) Network system with the other centers.

The items 1) to 4) will be finished in March 1989 and those 5) and 6) will be made in next year.

Table 1 Databases developed in JAERI

Name	Grade of Data Processing*	Data Size	Classification	Remarks
Material D.B.	1st, 2nd	30 MB	To be open	Fatigue, crack development, irradiation effect, creep etc. of structural materials for LWR, HTGR and fusion reactor
Fuel Behavior D.B.	1st	4 MB	Open	Fuel behavior data obtained in Studvik, Halden, Battel and JMTR projects.
NSRR Experiment D.B.	1st	100 MB	To be open	Fuel behavior during critical accidents
Thermohydraulic Experiments D.B.	0th, 1st	> 1,000 GB	To be open	ROSA-II, III, IV experiments, Reflooding experiments (classified), HCLWR thermo-hydraulic experiments etc.
Thermohydraulic Transient D.B.	1st, 2nd	10 GB	Open	Compilation of fundamental thermohydraulic experimental data and severe accident data for code verification
Nuclear Power Plant D.B.	1st	120 MB	Open	Specification of nuclear power plant taken from documents for licensing
Component Failure Probability D.B.	1st	3 MB	To be open	For PSA
Emergency Planning and Preparedness D.B.	1st, 2nd	200 MB	Classified	Computerized support system for emergency technical advisory body
Severe Accident D.B.	1st	650 MB	Classified	SFD, TMI-2, LACE project data
Nuclear Criticality Safety D.B.	1st	500 documents	Confidential	Criticality safety data in reprocessing plant

Name	Grade of Data Processing	Data Size	Classification	Remarks
Transfer Parameters in Environment	2nd	4 MB	Open	Transfer of radioactivity in the environment
Distribution of Agricultural Products and Population	1st	6.5 MB	Confidential	Population and agricultural product in each region of Japan
Weather D.B.	1st	8 MB	Confidential	Weather data in Tokai site
Personal Irradiation	1st	33.5 MB	Classified	Irradiation records of JAERI employees
Irradiation D.B. for Professionals	1st, 2nd	50 MB	Classified	Statistical records of irradiation for professional persons
Radiation Waste D.B.	0th, 1st	35 MB	Classified	Processing, mass, radioactive inventory, contamination etc.
JENDL	2nd	100 MB	Open	Evaluated nuclear data
NESTOR	1st	100 MB	Open	Experimental nuclear data
JEAMDL	2nd	8 MB	Open	Evaluated A & M data
AMSTOR	1st	17 MB	Open	Experimental A & M data
ENSDF	2nd	138 MB	Open	Evaluated nuclear structure and decay data
Decay Heat Library	1st	20 MB	Open	Decay data for residual heat calculation
Integral Experiment Data Bank	1st	1 MB	To be open	Critical experiments data
Sensitivity Analysis System (CATEX)	2nd, 3rd	10 MB	To be open	For sensitivity analysis of nuclear data

Name	Grade of Data Processing	Data Size	Classification	Remarks
Group Constants Library	3rd	1 GB (total)	Open with the code	Library for diffusion, transport and Monte Carlo codes; JFS-3, SRAC, BURMUDA, MGCL, JSD-1000, etc.
JT-60 Experiment D.B.	0th (1st)	20 GB	To be open	System control, plasma instrumentation, RF and NBI data
JT-60 Index File (DARTS)	1st	300 MB	To be open	Selected typical experimental data of JT-60 Experiments
JFT-2M Experiment D.B.	0th, 1st, 2nd	500 MB	Confidential	JFT-2M experimental data

* Grade of Data Processing
  0th: Compilation of raw data without DBMS.
  1st: Compilation of raw or validated data with DBMS so that the data retrieval may be possible.
  2nd: Evaluated or recommended data.
  3rd: Data processed as input data library for a specific computer code.

2.5 Theory and Evaluation of Nuclear Data

2.5.1 Current Topics of Electromagnetic Transitions in Neutron Capture Reactions

H. Kitazawa, M. Igashira and T. Uchiyama

Research Laboratory for Nuclear Reactors
Tokyo Institute of Technology

Strong primary gamma-ray transitions are given for neutron capture reactions passing through broad s-wave and p-wave resonances in the sd-shell nuclei ^{24}Mg, ^{28}Si and ^{32}S. These transitions are compared with valence model and particle-vibration coupling model calculations. Moreover, a systematics is shown on the energy and E1 sum-rule strength of the pygmy resonance which is found in gamma-ray spectra from neutron capture by heavy nuclei in the unresolved resonance region. This systematics is discussed in the framework of the shell model and hydrodynamical model. Several current topics are also presented of the isoscalar and isovector giant multipole resonance states in nuclei excited by polarized and unpolarized energetic neutron capture.

1. Introduction

Highly excited nuclear states are produced by neutron capture. Therefore, if detailed investigations are made on gamma-ray transitions from a capture state, it will be possible to obtain information on the nuclear structure of this state, using the well-known electromagnetic interaction.

Since the nuclear structure of low-lying states reflects strongly on broad resonances in the vicinity of the neutron emission threshold, our interest is aroused for gamma-ray transitions from these resonance states. And also, single-particle primary E1 transitions are often enhanced in neutron resonance capture reactions. This fact makes a striking contrast with the extreme retardation of most E1 transitions between bound states(1). A study of neutron resonance capture gamma rays will disclose a typical feature of electromagnetic transitions in nucleon capture reactions.

In the unresolved resonance region, pygmy resonances, which may be due to the E1 transition, have been observed in gamma-ray spectra from neutron capture by heavy nuclei. Probably, the pygmy resonance indicates the excitation of a new mode of the E1 collective vibrational motion in these nuclei.

Moreover, the radiative capture of energetic neutrons (> 5 MeV) excites various types of multipole resonances in nuclei. Therefore, gamma-ray transitions from these capture states would provide useful data concerning about the coupling between the single particle and the isoscalar or isovector field produced by these resonances.

2. Characteristic primary gamma rays from neutron capture

2.1 Neutron resonance capture reactions

Usually, some resonances with large reduced neutron width are observed at neutron energies below about 1.0 MeV. From the uncertainty principle, it is conceivable that these resonances consist of the simple particle-hole configuration. In fact, we can find strong single-particle gamma-ray transitions from broad s-wave and p-wave neutron resonances. There is also the possibility of extracting interesting information on the coupling between these transitions and the core excitation.

In table 1, a comparison is made between the calculated and observed partial radiative widths of the 84-keV $p_{3/2}$-wave resonance in ^{24}Mg[2]. The calculation was performed by the valence capture model[3] which assumed the single-particle E1 transition. The neutron effective charge was taken to be -Ze/A. It is noteworthy that the calculated widths for the 585-keV state and 2564-keV state transitions are in excellent agreement with the observed values, however the theoretical values for the ground state and 1965-keV state transitions are 2 to 3 times larger than the experimental ones. These results may be understood qualitatively by investigating details of the radial integral of the valence-transition matrix element. As is seen from fig. 1, the radial integral for the $2s_{1/2}$ state transition is preponderant in the nuclear external region due to the cancellation of the internal contribution and due to the extensive tail of the p-wave neutron orbit. Consequently, the $2s_{1/2}$ state transition is completely decoupled from the excitation of the isovector giant dipole resonance, while the $1d_{5/2}$-state transition is coupled to the resonance to a certain extent. This is the reason why the valence model is successful in predicting the partial widths for the 585-keV state and 2564-keV state transitions. Therefore, the smaller neutron effective charge should be used for the model calculation of the $1d_{5/2}$-state transition.

Strong transitions to low-lying states with large spectroscopic factor were also observed in the capture gamma-ray spectrum from the 103-keV s-wave resonance in ^{32}S, as shown in fig. 2. We notice that the enhanced M1 transition is found to the ground state, although the single-particle M1 transition to this state is l-forbidden. For this transition, account should be taken of the interaction between the valence

neutron and core nucleus. In table 2, the observed partial widths are compared with the valence model calculations[4]. In the model calculation, the partial width for the ground state M1 transition was calculated using the tensor operator

$$\sqrt{\frac{3}{4\pi}}\, k\mu_0 r^2 [Y_2 \otimes \sigma_1]^{(1)} \quad ,$$

where μ_0 is the nuclear magneton, and k(=0.71) was determined so as to make an agreement between the calculated and observed widths. The tensor operator, which was introduced by Bohr and Mottelson[5], is derived from the meson-exchange interaction or core-polarization configuration, and causes M1 transitions with $\Delta l=2$. What is it to generate the tensor interaction for primary electromagnetic transitions in neutron resonance capture reactions ? The question still remains in need of solution.

The calculated width for the 840-keV state M1 transition, which was obtained with the free nucleon g-factor, is much smaller than the observed one, because of the approximate orthogonality between the initial and final state radial wave functions. However, the remarkable discrepancy can be removed qualitatively by considering the excitation of the isovector M1 resonance in the core nucleus[4]. Furthermore, the valence model produces a satisfactory prediction of the partial width for the 3220-keV state E1 transition.

Here, it should be noted that the above M1 transitions are quite different from those in thermal neutron capture reactions[6]. Namely, the $1/2^+ \rightarrow 1/2^+$ and $1/2^+ \rightarrow 3/2^+$ transitions are extremely weakened for thermal neutron capture. Probably, it may be due to the fact that no direct M1 process exists for both single-particle transitions.

Deeply interesting results are found for E1 transitions from the 565-keV $p_{3/2}$-wave resonance in ^{28}Si[7]. In table 3, the observed partial radiative widths of this resonance are compared with model calculations. We pay special attention to the fact that the valence model calculation for the 1273-keV state with the large spectroscopic factor is much smaller than the observed value. This is because the $2p_{3/2} \rightarrow 1d_{3/2}$ valence transition is extremely weakened by the small vector coupling coefficient. In order to remove this discrepancy, we have performed the particle-vibration coupling model calculation (PV) of the radiative width of this resonance[8]. The resonance state wave function was obtained by coupling the 1d-, 1f-, and 2p-neutron single-particle states to the 2^+(1.78 MeV) and 3^-(6.88 MeV) one-phonon states in ^{28}Si. And also, the 2s- and 1d-neutron single-particle states were coupled to the 2^+

one-phonon state to calculate the wave functions of low-lying states. The resonance state wave function was approximated by a bound state wave function in the vicinity of the neutron emission threshold, the continuum nature of the wave function in the nuclear external region being neglected. As a result, excellent agreement was obtained between the calculated and observed widths, as shown in table 3. The calculation clarified that the radiative width for the 1273-keV state transition is determined predominantly by the $1f_{7/2} \rightarrow 1d_{5/2}$ single-particle transition with the 2^+ core-state excitation.

Moreover, we found that the core-excitation configuration in the model wave function, particularly the $(1f_{7/2} \otimes 2^+)$ component (18%) of the resonance state wave function and the $(1d_{5/2} \otimes 2^+)$ component of the wave functions of low-lying states in ^{29}Si are quite essential to explain the observed partial radiative widths, and also that the $(1d_{3/2} \otimes 3^-)$ configuration (81%) does not contribute to these radiative widths but it is the dominant component of the 565-keV resonance state wave function.

2.2 Pygmy resonance

In gamma-ray spectra from neutron capture by heavy nuclei in the unresolved resonance region, we often observe the strong gamma-ray transitions localized on a certain energy, which are named "anomalous bump". Since the energy of this bump does not depend on the incident neutron energy, it is conceivable that the bump is not caused by the irregularity of the nuclear level density, but caused by the resonance structure of the gamma-ray strength function. Although there exists no evidence that the bump is produced by E1 transitions, on several probable reasons it is interpreted as being due to the pygmy resonance structure of the E1 gamma-ray strength function.

In order to investigate the physical origin of the pygmy resonance, we have been measuring keV-neutron capture gamma rays from heavy nuclei since several years ago[9]. Figure 3 shows the capture gamma-ray spectra. In this figure, the bumps (depicted by oblique lines) in the gamma-ray spectra of Pr, Tb, Ho, Lu, Ta, and Au are found at the gamma-ray energies of 1.5, 2.5, 3.0, 3.5, 4.5 and 5.5 MeV, respectively. Furthermore, it was confirmed that the energy of the bump does not depend on the incident neutron energy.

Except the low-energy and high-energy components of discrete gamma rays, it is possible to extract the E1 gamma-ray strength function which reproduces the observed gamma-ray spectrum, using a spectrum fitting method. Thus, we determined the resonance parameters and E1 sum-rule strength of the pygmy resonance. In this analysis, the function of the Lorentz type was used as a trial

function for the gamma-ray strength function for the E1 giant resonance or pygmy resonance. The giant resonance parameters were taken from the work of Berman[10]. The nuclear level densities were calculated by the Gilbert-Cameron formula[11]. The level density parameters were obtained from a cumulative plot and the average level distance of s-wave resonances. As an example, the E1 gamma-ray strength function of ^{160}Tb is shown in fig. 4. The solid curve was obtained from the observed gamma-ray spectrum, and the dotted curve from the E1 gamma-ray strength function of the Brink-Axel type[12]. Figure 5 shows a dependence of the pygmy resonance energy and width on neutron number. The full circles show the resonance energy and the error bars show the resonance width. As seen from this figure, the resonance energy increases with neutron number in N=82-126, and reveals a distinct shell effect at N=82. Ratios of the pygmy resonance strength to the sum-rule value are shown in fig. 6. The E1 strength of the pygmy resonance is at most a few percent of the classical E1 sum rule, and increases sharply with neutron number, accompanying a severe discontinuity at N=82.

Some approaches were made to the elucidation of the pygmy resonance, using the shell model and hydrodynamical model. Harvey and Khanna[13] calculated the distribution of the E1 strength in ^{56}Ni, ^{90}Zr, ^{132}Sn and ^{208}Pb by diagonalizing Gaussian interaction matrix elements for the realistic particle-hole configuration. Consequently, it was shown that a few percent of the E1 strength concentrates at low energy, being decoupled from the excitation of the E1 giant resonance. For ^{208}Pb, such little E1 strength results principally from the neutron particle-hole configurations $(3p_{1/2}^{-1}4s_{1/2})$, $(3p_{1/2}^{-1}3d_{3/2})$ and $(3p_{3/2}^{-1}3d_{5/2})$, and from the proton particle-hole configuration $(3s_{1/2}^{-1}3p_{1/2})$. Thus, we can see that the single-particle states with small orbital angular momentum participate in these configurations.

On the other hand, Mohan et al.[14] described a nucleus by the incompressible, irrotational three fluids which are composed of the protons, the neutrons in the same orbits as protons (blocked neutrons), and the excess neutrons. In this model, protons are assumed to interact more strongly with blocked neutrons than with excess neutrons. Consequently, two vibrational eigen modes were found for ^{208}Pb at the excitation energies of 13.3 and 4.4 MeV. The former is the E1 giant resonance mode which is excited by the motion of the protons against the blocked neutrons and excess neutrons. The latter is produced by the motion of the excess neutrons against the protons and blocked neutrons, and it was considered as the pygmy resonance, although its calculated E1 strength was about ten times as large as the observed value.

From the above model calculations, we suppose that the pygmy resonance is a collective dipole state which is mainly formed by the neutron particle-hole states decoupled from the E1 giant resonance. In future, the detailed investigation of the

observed systematics for the pygmy resonance is expected to become an important problem in the physics of the nucleus with highly excess neutrons.

2.3 Neutron capture reactions in the giant resonance region

In the giant resonance region, strong discrete gamma rays originated from primary transitions to low-lying states of a residual nucleus are observed in neutron capture gamma-ray spectra. These transitions are well known as being due to the excitation of the E1 giant resonance and explained by the direct-semidirect model (DSD)[15]. In this model, the probability amplitudes of direct and semidirect process are added coherently. Here, in the direct process the incident particle makes transitions from unbound states to unfilled single-particle bound states without exciting the target nucleus, while in the semidirect process the giant resonance states in the target nucleus are excited through the interaction between the incident particle and target nucleus.

The DSD model produces the multipole transition matrix elements for neutron radiative capture reactions as follows:

$$T_{fi} = \langle \Psi_f | O^n | \Psi_i \rangle + \frac{\langle \Psi_f | O^t | \Psi_{int} \rangle \langle \Psi_{int} | H' | \Psi_i \rangle}{E_{\ell_i j_i} - E_{\ell_f j_f} - E_R + 1/2\, i\, \Gamma_R} ,$$

where Ψ_i, Ψ_{int} and Ψ_f are the initial, intermediate and final state wave functions, respectively. The quantities, E_R and Γ_R, are the energy and width of the multipole giant resonance in the target nucleus, and $E_{\ell_i j_i}$ and $E_{\ell_f j_f}$ are the initial and final state energies of the captured neutron. The operators for multipole radiation, O^n and O^t, operate on the incident particle and target nucleon, respectively, and H' is the coupling Hamiltonian between the incident particle and target nucleus.

Figure 7 shows the cross sections for primary gamma-ray transitions to low-lying states of residual nuclei in neutron radiative capture reactions[16]. The curves show DSD model and compound nucleus model (CN) calculations. In the DSD model calculation, the excitation of the E1 giant resonance was assumed in the intermediate state. The radial form factor of the coupling Hamiltonian was represented in terms of the complex function[17]

$$H' \propto r \left(V_1 f_r(r) - iW_1 4b \frac{df_i(r)}{dr} \right) ,$$

where V_1 and W_1 are the real and imaginary depths of the isospin-dependent optical potential, and $f_r(r)$ and $f_i(r)$ are the real and imaginary form factors of the Wood-Saxon type. As seen from the figure, overall agreement is obtained between the experimental and theoretical values.

Recently, the DSD model calculation for the $^{40}Ca(n,\gamma_0)^{41}Ca$ reaction has been performed by assuming that only the $T_<$ component of the E1 giant resonance with Γ_R=4.0 MeV located at E_R=18.1 MeV is excited and it exhausts 38% of the energy-weighted sum-rule, which is all of the estimated $T_<$ component[18]. The results give a poor description of the experimental data above the giant dipole resonance energy, as shown by a dot-dashed curve in fig. 8. Therefore, the $T_>$ component of the E1 giant resonance was included in the DSD model calculation, violating an isospin-conservation law. This resonance component was assumed to locate at E_R=20.6 MeV, to have the width Γ_R=4.0 MeV and to exhaust 12% of the energy-weighted sum-rule corresponding to 20% of the estimated $T_>$ component. The potential strengths, V_1 and W_1, were treated as free parameters and found to be V_1=120 MeV and W_1=40 MeV. As a result, remarkable improvement was obtained in the agreement between the experimental and theoretical values, as shown by a solid curve in fig. 8.

In addition to the isovector E1 giant resonance mentioned above, isoscaler (ISGQR) and isovector (IVGQR) giant quadrupole resonances were theoretically predicted and observed by electron, proton or alpha particle scattering on nuclei. However, these resonances have been never clearly identified by proton radiative capture reactions. It is because the proton effective charge for E2 transition (~ unit charge) is large. While, since the neutron effective charge (eZ/A^2) is extremely small, the asymmetry around 90° of the angular distribution of neutron capture gamma rays could be attributed to the interference between the E1 capture process and E2 giant resonance capture process.

The factor, A_1, representing the asymmetry around 90° of the angular distribution is defined as

$$A_1 = \frac{I(55°) - I(125°)}{I(55°) + I(125°)} ,$$

where $I(\theta)$ is the gamma-ray intensity at angle θ with respect to the neutron beam. Figure 9 shows the asymmetry factor for the $^{40}Ca(n,\gamma_0)^{41}Ca$ reaction[18]. Negative A_1 values at about 12-MeV neutron energy indicate the excitation of the isoscalar giant E2 resonance with Γ_R=4.0 MeV located E_R=18.4 MeV. The curves show the DSD model calculations. The strength of 60% of the energy-weighted sum-rule was

assumed for this resonance. And also, large positive A_1 values above E_n=20 MeV are interpreted as being caused by the isovector giant E2 resonance. This interpretation is supported by the DSD model calculations, in which the resonance energy and width were taken to be 32 MeV and 5 MeV, respectively. The isovector energy-weighted sum-rule strength exhausted by this resonance was taken to be 35%, which is the full $T_<$ resonance strength.

In the above DSD model calculation, the form factors of the coupling Hamiltonian for isoscalar and isovector E2 giant resonance were represented by

$$H' \propto -r \frac{d}{dr}(V_0 f_r(r) + iW_0 4b \frac{df_i(r)}{dr}) , \quad \text{(ISGQR)}$$

$$\propto r^2 (V_1 f_r(r) - iW_1 4b \frac{df_i(r)}{dr}) , \quad \text{(IVGQR)}$$

where the potential strengths, V_0 and W_0, were taken to be V_0=-50 MeV and W_0=10 MeV, which are close to those of a global optical potential.

Furthermore, the isovector M1 giant resonance has been observed by electron and proton scattering experiments. In this resonance such a highly collective mode as the E1 and E2 giant resonances mentioned above is scarcely expected. Usually, the resonance strength is observed, being split into fragments. Figure 10 shows the 90° analyzing powers of gamma rays from the polarized neutron capture in ^{13}C(22). In this experiment the distinct non-zero analyzing powers were found at neutron energies 9 MeV to 11 MeV, indicating the interference between the E1 process and the other process with different parity. These results were explained by the DSD model calculation which assumed two isovector M1 strengths at the excitation energies of 16.5 MeV and 17.5 MeV. In the model calculation the coupling Hamiltonian between the incident neutron and the isovector M1 resonance was expressed as

$$H' \propto V_{11} f(r) ,$$

where the potential strength V_{11} was taken to be 40 MeV estimated by Bohr and Mottelson. This is close to the value derived from recent studies of the giant Gamow-Teller states in medium nuclei(23).

According to the above discussion, we conclude that neutron radiative capture measurements could be a powerful means of the investigation of giant multipole

resonances, even when account is taken of the considerable difficulty in performing these measurements.

3. Summary

We have observed enhanced primary capture gamma rays from the 84-keV $p_{3/2}$-wave resonance in ^{24}Mg and the 103-keV s-wave resonance in ^{32}S with large reduced neutron width. In these gamma rays, E1 transitions are considerably well explained by the valence capture model. The good agreement between experimental data and model calculations originates from the fact that the nuclear internal contribution to the valence transition matrix element cancels out strongly and consequently these transitions are decoupled from the excitation of the isovector giant dipole resonance. In the M1 transition, however it was found that the core polarization in these neutron resonance states plays an important role.

For the 565-keV $p_{3/2}$-wave resonance capture reaction on ^{28}Si, we have shown that the E1 transitions from this resonance state to low-lying states are successfully described by the single-particle transitions with the core excitation of 2^+ and 3^- one-phonon states. Moreover, a systematics was obtained for the energy and E1 sum-rule strength of the pygmy resonance which was observed in capture gamma-ray spectra from heavy nuclei in the unresolved resonance region. The systematics shows remarkable shell effects at the neutron number N=82.

Current topics were also presented for the isoscalar and isovector giant multipole resonances excited by polarized and unpolarized energetic neutron capture, and it was concluded that these reactions are useful tools for the detailed investigation of giant resonances.

References

(1) Wilkinson, D.H.: Nuclear Spectroscopy, ed. F. Ajzenberg-Selove (Academic Press, New York, 1960) p. 867

(2) Uchiyama, T., Igashira, M., Kitazawa, H.: Proc. Int. Conf. on Nuclear Data for Science and Technology, Mito, 1988

(3) Lane, A.M., Mughabghab, S.F.: Phys. Rev. C, 10, 412 (1974)

(4) Kitazawa, H., Igashira, M.: J. Phys. G, 14, S215 (1988)

(5) Bohr, A., Mottelson, B.R.: Nuclear Structure, Vol. 1 (Benjamin, New York, 1969) p. 336

(6) Bird, J.R., Allen, B.J., Bergqvist, I., Biggerstaff, J.A.: Nuclear Data Tables, 11, 433 (1973)

(7) Shimizu, M., Igashira, M., Terazu, K., Kitazawa, H.: Nucl. Phys. A, 452, 205 (1986)

(8) Kitazawa, H., Ohgo, M., Uchiyama, T., Igashira, M.: Nucl. Phys. A, 464, 61 (1987)

(9) Igashira, M., Kitazawa, H., Shimizu, M., Komano, H., Yamamuro, N.: Nucl. Phys. A, 457, 301 (1986)

(10) Berman, B.L.: Atomic Data and Nuclear Data Tables, 15, 319 (1975)

(11) Gilbert, A., Cameron, A.G.W.: Can. J. Phys., 43, 1446 (1965)

(12) Axel, P.: Phys. Rev., 126, 671 (1962)

(13) Harvey, M., Khanna, F.C.: Nucl. Phys. A, 221, 77 (1974)

(14) Mohan, R., Danos, M., Biedenharn, L.C.: Phys. Rev. C, 3, 1740 (1971)

(15) Clement, C.F., Lane, A.M., Rook, J.R.: Nucl. Phys., 66, 273 (1965)

(16) Bergqvist, I.: Neutron Physics and Nuclear Data in Science and Technology, Vol. 3, Neutron Radiative Capture, ed. R.E. Chrien (Pergamon, New York) p. 33

(17) Potokar, M.: Phys. Lett. B, 46, 346 (1973)

(18) Bergqvist, I., Zorro, R., Hakansson, A., Lindholm, A., Nilsson, L., Olsson, N., Likar, A.: Nucl. Phys. A, 419, 509 (1984)

(19) Bergqvist, I., Drake, D.M., McDaniels, D.K.: Nucl. Phys. A, 231, 29 (1974)

(20) Wender, S.A., Roberson, N.R., Potokar, M., Weller, H.R., Tilley, D.R.: Phys. Rev. Lett., 41, 1217 (1978)

(21) Lindholm, A., Nilsson, L., Ahmad,M., Anwar, M., Bergqvist, I., Joly, S.: Nucl. Phys. A., 339, 205 (1980)

(22) Wright, M.C., Kitazawa, H., Roberson, N.R., Weller, H.R., Jensen, M., Tilley, D.R.: Phys. Rev. C, 31, 1125 (1985)

(23) Toki, H., Cha, D., Bertsch, G.: Phys. Rev. C, 24, 1371 (1981)

Table 1 Experimental and theoretical partial radiative widths of the 84-keV $p_{3/2}$-wave resonance in ^{24}Mg[2].

E_x(keV)	Γ_γ(eV)	
	Experiment	Valence
0.0(5/2+)	0.93±0.14	2.78
585(1/2+)	3.98±0.45	4.31
975(3/2+)	<0.16	0.10
1965(5/2+)	0.20±0.07	0.44
2564(1/2+)	0.68±0.14	0.69

Table 2 Experimental and theoretical partial radiative widths of the 103-keV s-wave resonance in ^{32}S[4].

E_x(keV)	Γ_γ(eV)	
	Experiment	Valence
0.0(3/2+)	0.85±0.11	0.85
840(1/2+)	0.87±0.13	0.007
3220(3/2-)	1.17±0.12	0.87

Table 3 Experimental and theoretical partial radiative widths of the 565-keV $p_{3/2}$-wave resonance in ^{28}Si[8].

E_x(keV)	Γ_γ(eV)		
	Experiment	Valence	PV
0.0(1/2+)	0.85±0.10	0.85	0.89
1273(3/2+)	0.40±0.06	0.06	0.46
2028(5/2+)	0.18±0.04	0.10	0.23
2426(3/2+)	0.18±0.04	0.00	0.32
3069(5/2+)	0.14±0.04	0.03	0.01

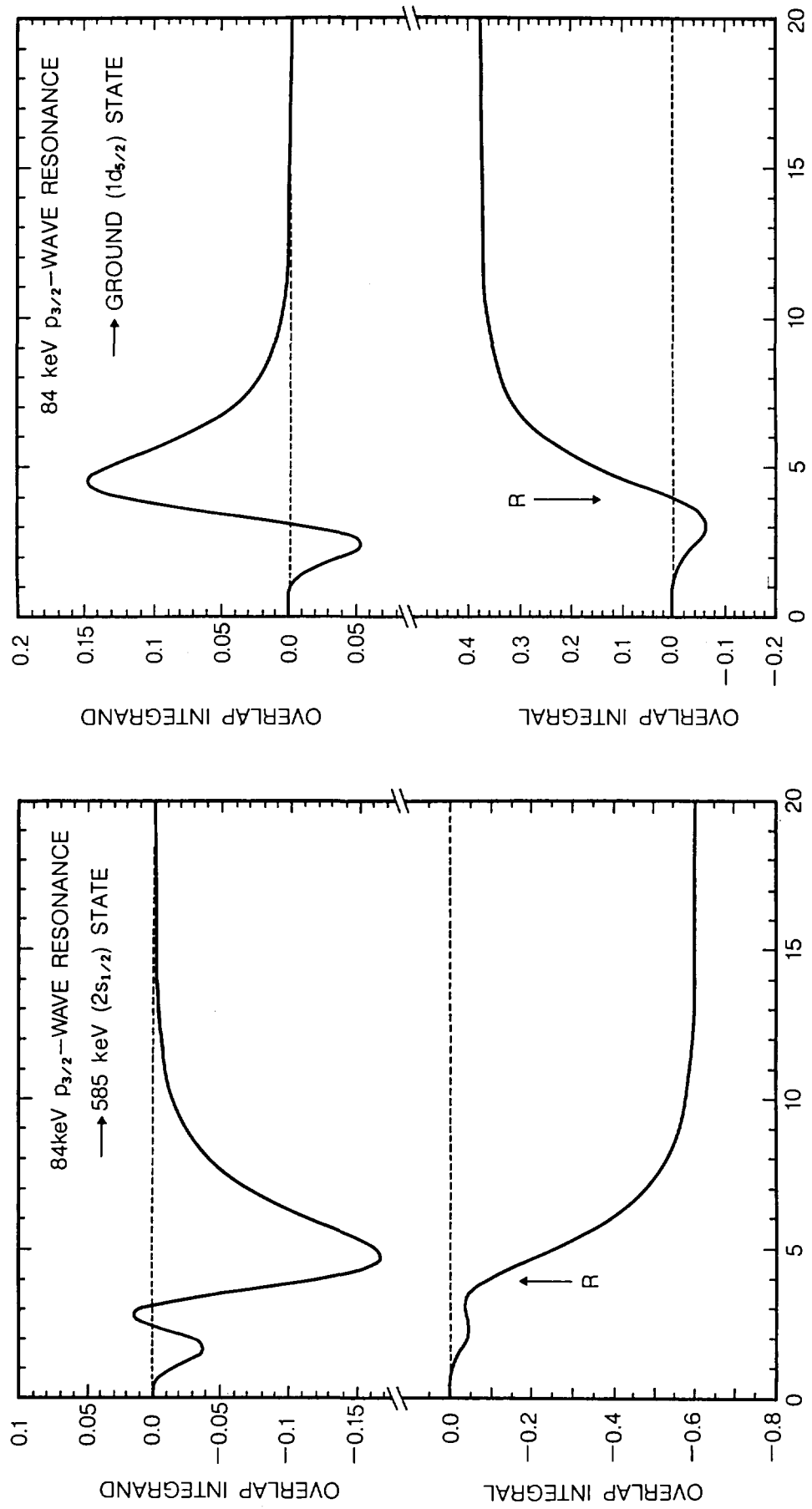

Fig. 1 Radial integrals of the valence capture matrix elements for the $2s_{1/2}$ and $1d_{5/2}$ state transitions from the 84-keV $p_{3/2}$-wave resonance in $^{24}Mg(2)$.

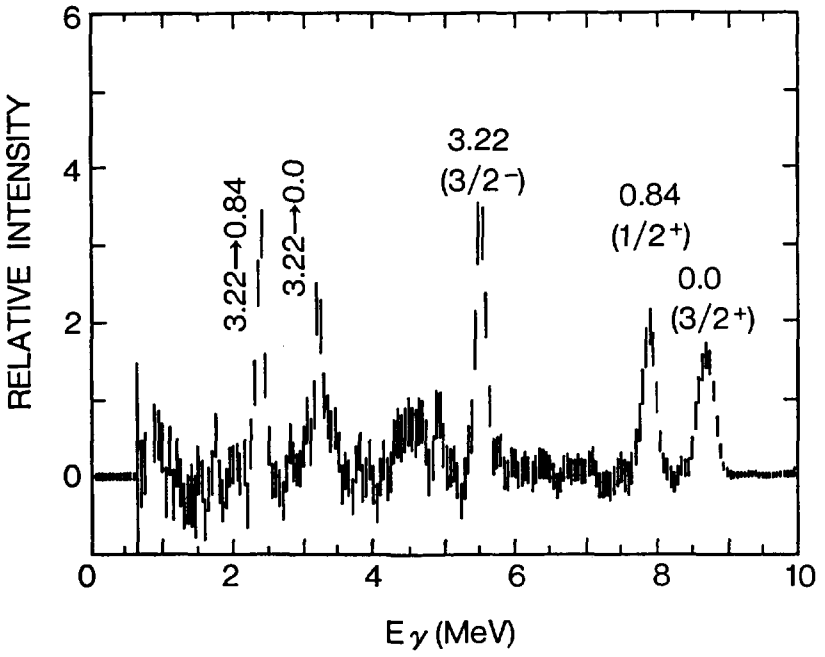

Fig. 2 Observed gamma-ray spectrum from the 103-keV s-wave resonance in $^{32}S(4)$.

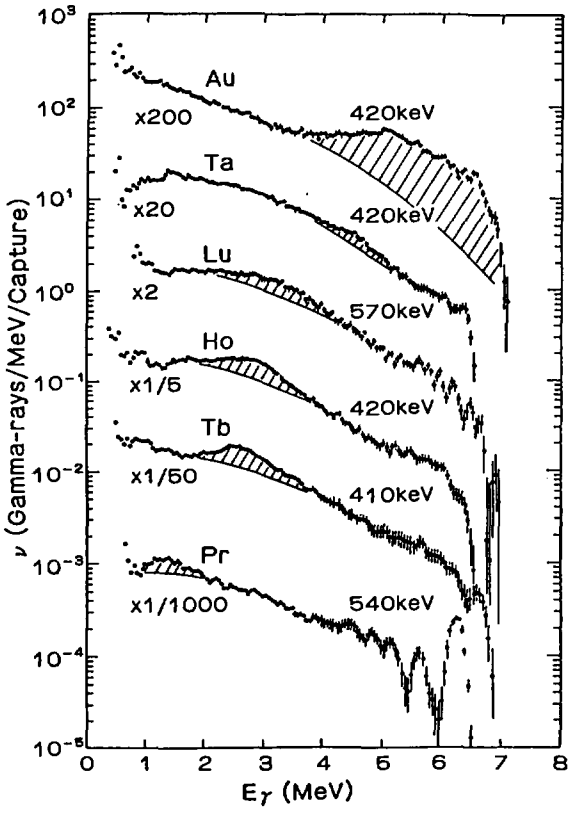

Fig. 3 Typical observed capture gamma-ray spectra of Pr, Tb, Ho, Lu, Ta and Au. The incident neutron energies are shown in the figure. The bumps depicted by oblique lines show the pygmy resonance(9).

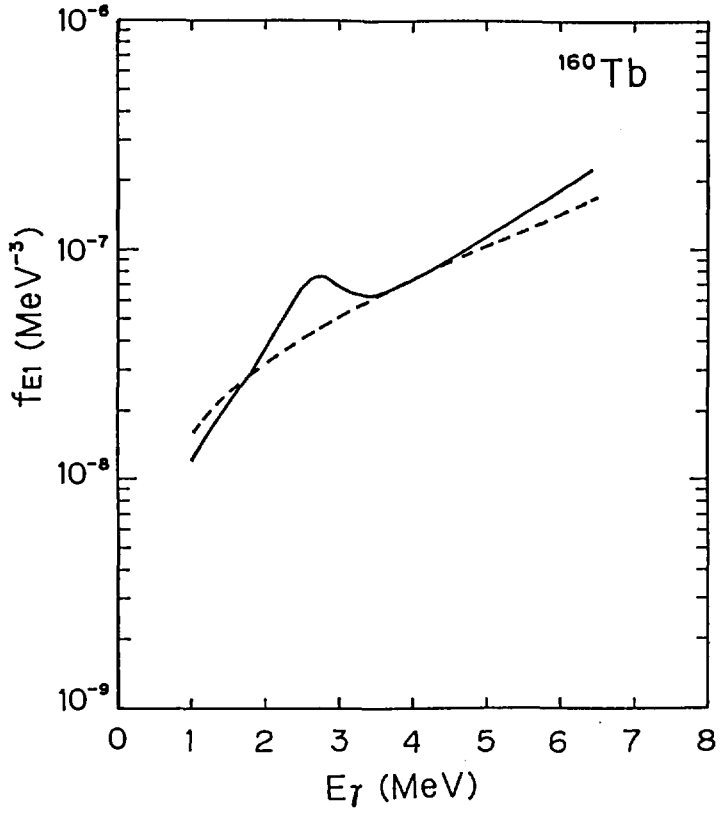

Fig. 4 E1 gamma-ray strength functions of ^{160}Tb. The solid curve was obtained from the observed gamma-ray spectrum, and the dotted curve from the E1 gamma-ray strength function of the Brink-Axel type.

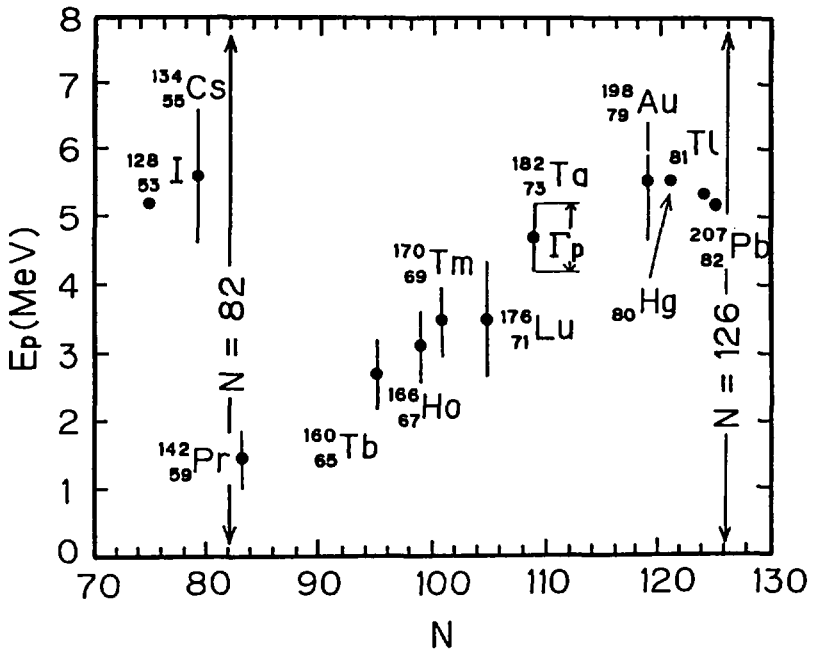

Fig. 5 Dependence of the pygmy resonance energy and width on neutron number[9].

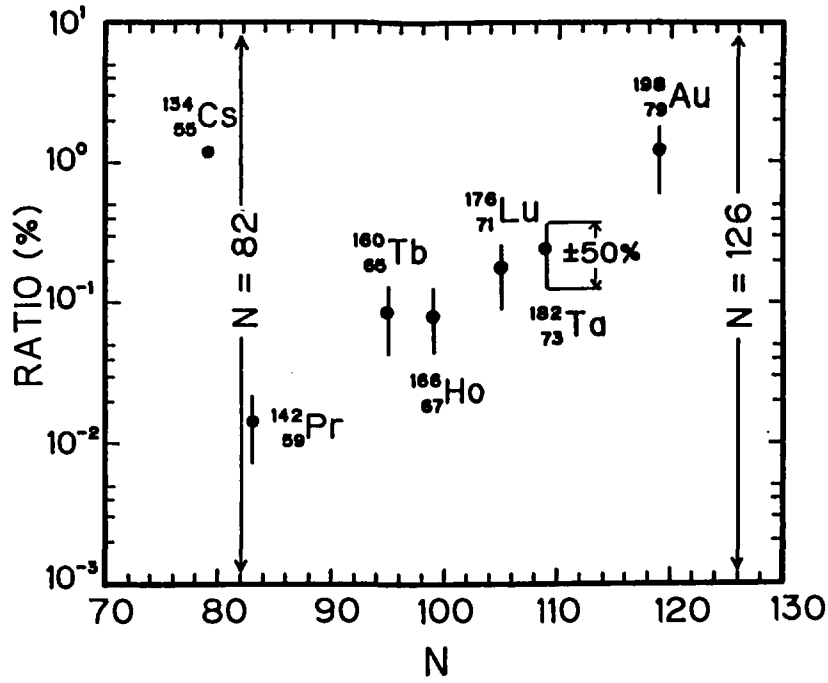

Fig. 6 Ratios of the electric dipole strength of the pygmy resonance to the classical sum-rule value as a function of the neutron number(9).

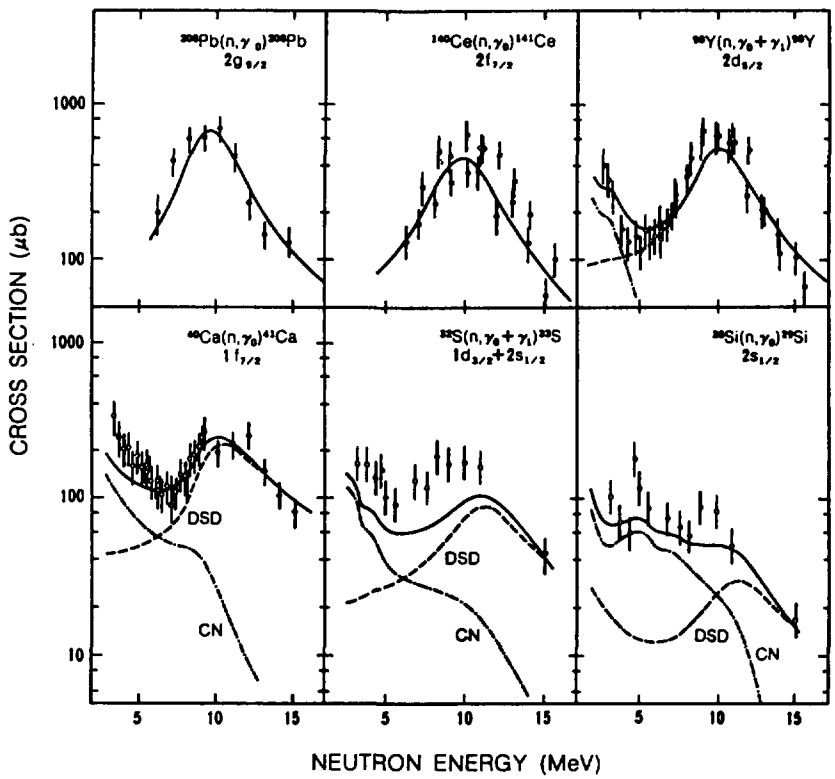

Fig. 7 Experimental and theoretical (n,γ_0) or $(n,\gamma_0+\gamma_1)$ cross sections in the giant resonance region. The full and open circles represent experimental results obtained at Los Alamos and Uppsals, respectively. The curves were calculated on the DSD model and the CN model(16).

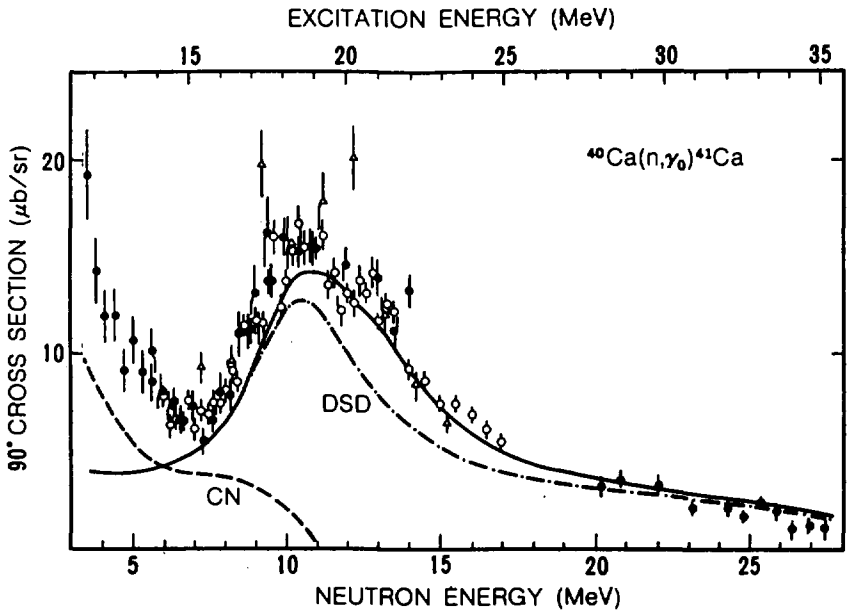

Fig. 8 90° cross sections of the $^{40}Ca(n,\gamma_0)^{41}Ca$ reaction. The experimental data are taken from ref. 19) (open triangles), ref. 20) (open circles), ref. 18) and ref. 21) (full circles). The solid and dot-dashed curves represent capture cross sections calculated on the DSD model. The dashed curve is the CN model capture cross section.

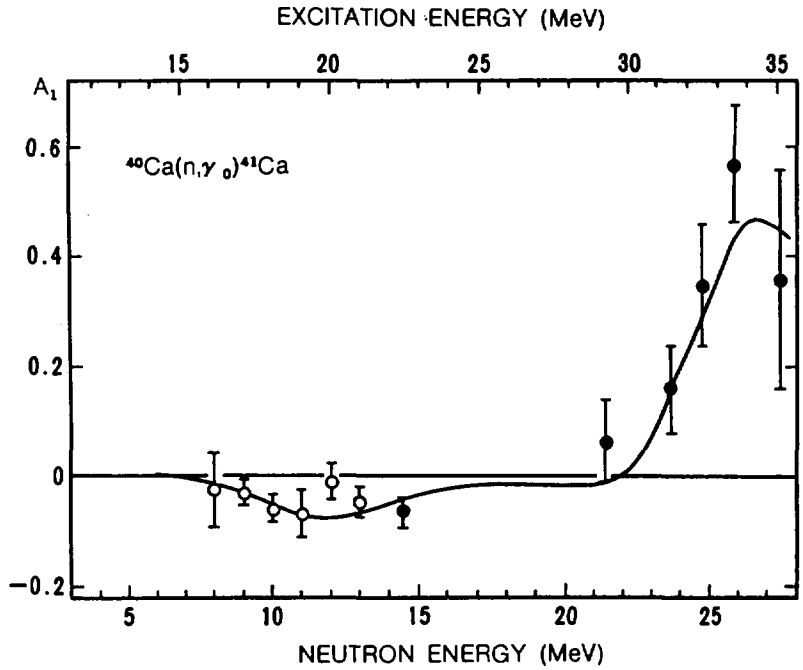

Fig. 9 Experimental and theoretical fore-aft asymmetries of the $^{40}Ca(n,\gamma_0)^{41}Ca$ reaction. The solid curve was calculated on the DSD model(18).

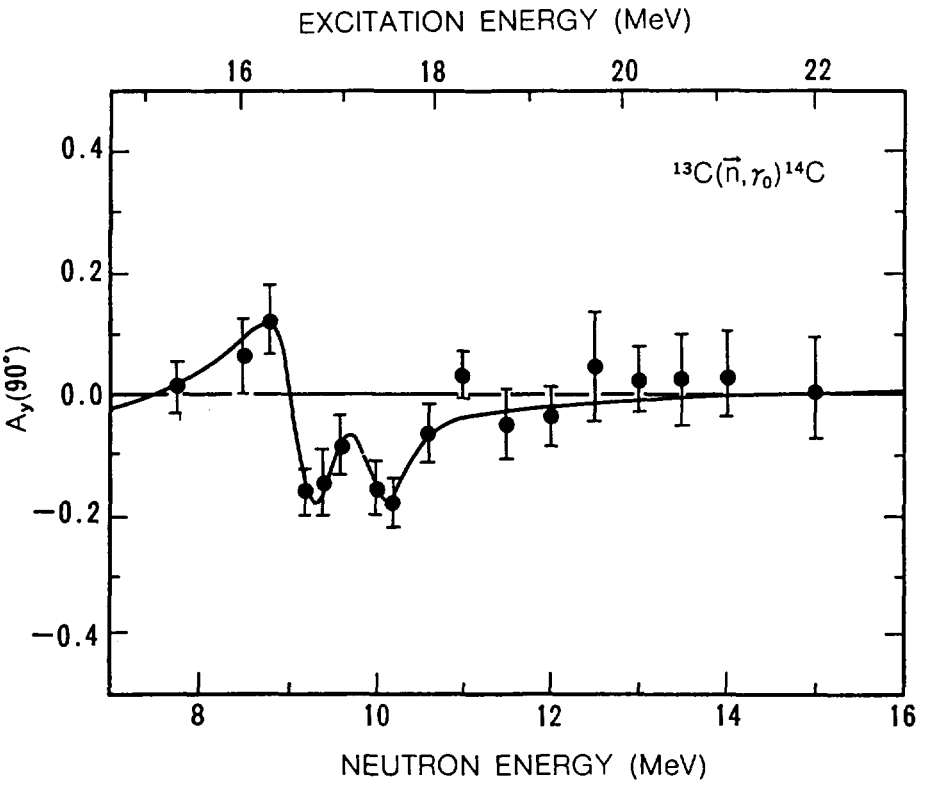

Fig. 10 90° analyzing powers as a function of the incident neutron energy for the $^{13}C(n,\gamma_0)^{14}C$ reaction. The solid curve represents the DSD model calculation which includes two narrow isovector M1 resonances at Ex=16.5 and 17.0 MeV[22].

2.5.2 JENDL Special Purpose Data Files and Related Nuclear Data

Shungo Iijima

NAIG Nuclear Research Laboratory
Nippon Atomic Insdustry Group Co., Ltd.
4-1 Ukishima-cho, Kawasaki-ku, Kasasaki, 210

The objectives of JENDL Special Purpose Data Files under development are the applications of nuclear data to the evaluation of the fuel cycle, nuclear activation, and radiation damage. The files in plan consist of 9 types of data, viz., the acitinide cross sections, the decay data, the activation cross sections, the (α,n) cross sections, the photo-reaction cross sections, the dosimetry cross sections, the gas production cross sections, the primary knock-on atom spectra and KERMA factors, and the data for standard.

The status of the compilation and the evaluation of these data are briefly reviewed. In particular, the features of the data required for the evaluation of the activation cross sections, (α,n) cross sections, photo-reaction crosss sections, and PKA data are discussed in some detail. The need for the realistic definition of the scope of the work is emphasized.

(Keywords : nuclear data, JENDL, special purpose data files, compilation, evaluation, fuel cycle, activation, radiation damge)

1. Introduction

After the completion of JENDL-3 scheduled in spring, 1989, the development of the Special Purpose Data Files is one of the primary targets of our nuclear data activity. The objectives are the applications to the evaluation of the fuel cycle, nuclear activation, and radiation damage. The JNDC activities for construcitng these files started from spring of 1987 and an increasing effort is being paid to these works.

The classification of files is given in Table 1 below.

Table 1 JENDL special purpose data files

File Name	Data Origin
Fuel cycle evaluation and nuclear activations	
(1) Actinide cross section file	JENDL-3
(2) Decay data file	ENSDF, JNDC FP file
(3) Activation cross section file	JENDL-3 + New
(4) (α,n) cross section file	New
(5) Photo-reaction data file	New
Radiation damage, dose and heat generations	
(6) PKA and KERMA data file	JENDL-3 + New
(7) Dosimetry cross section file	JENDL-3 + New
(8) Gas production cross ection file	JENDL-3
Data for standard	
(9) Standard data file.	Not yet fixed.

The files of actinide and gas production cross sections are to be made as soon as JENDL-3 is completed. The dosimetry cross section file was compiled and an integral test was performed using the data in fission spectrum field and the CFRMF.[1] Comments were sent to evaluators based on the test results. New evaluation is needed for several dosimetry cross sections not in JENDL. Covariance data are adopted from IRDF. For decay data files and standard files, the scopes are not yet determined.

In this paper, we discuss the status and the scope of the working group activities concerning the data files for activation cross sections, (α,n) reactions, photon-induced reactions, and the PKA/KERMA data. These fields are new to most of us. We already encountered with the fundamental problems, such as the collection of non-neutron nuclear data, the necessity for development of new theoretical codes, and the supply of needed nuclear data which are not in the general purpose file. Works involved seem to be really enormous unless the numbers of reactions are properly limited. The definition of the scope is probably the most urgent task.

2. Activation Cross Section file

Activation data file will contain about 1000 reactions as Priority 1 primarily for fusion applications. Applications to LWR's and FBR's are also taken into consideration but the fission products are excluded. Nuclides are limited to those constitute the normal candidate materials for reactors taking account of impurities. Reactions are limited to those of the threshold energies lower than 18 MeV and those producing the radioactive daughters having half-lives longer than 1 day. Exceptions are the production of Mn-56(2.579h) and some other isotopes which are of importance for LOCA analysis of fusion reactor. Also, the reactions are taken into acount where the daughters are short-lived but they in turn produce long-lived grand daughters by decay. The long-lived radioisotope targets of half-lives longer than 100 d are also taken into account.

Most of reaction cross sections can be edited from JENDL

General Purpose File and Fisssion Product Cross Section File. Emphasis is put on the new evaluation of isomer production cross sections.

Calculation of cross sections in MeV region is made with GNASH[2] and PEGASUS[3] code taking account of the systematics of experimental cross sections. The mass formula of Yamada et al.[4] is built in the program to calculate the mass excess of off-stable nuclides. Further, the input procedure to GNASH was greatly simplified by Yamamuro[5], faciliating an efficient calculation of cross sections. Figure 1 shows the comparison of calculation and experiment of ^{117m}In and ^{117g}In production cross sections from $^{117}Sn(n,p)$ reaction. The sytematics of isomer production cross sections is being investigated based on these calculation.

As reported at the last Mito conference, the REAC-ECN3 file of Hanford and ECN[6] is near completion and it contains about 9000 reactions. UKACT1 file of UK[7] contains about the same number of reactions. The scope of our file is being re-investigated to include the Priority II reactions.

An international cooperation and benchmark comparison of the activation data files for fusion applications is anticipated from the end of 1989. So, we must hurry up the evaluation.

3. (α,n) Cross Section File

The data concerning (α,n) reactions are used for the safety and economy evaluation of the storage and the transportation of spent fuel at nuclear plants and reprocessing plants. This is the primary purpose of the present file under development. The relevant alpha particle energy is below 10 MeV. The file will

contain microscopic (α,n) cross sections and neutron spectra for nuclides ranging from Li to Sn. Thick target yields and spectra will be also filed. A tabular and/or a parametrized form will be prepared to facilitate the users.

Evaluation has been made by Matsunobu (priv. comm.)for light nuclei,i.e., Li, Be, B, C, O and N, based on the experimental data and the statistical model calculation. Figures 2 to 4 show the (α,n) cross sections of nat. oxygen, the thick target yields and neutron spectra for UO_2, respectively. Calculation agrees fairly well with experiment. However, for carbon and boron, the calculated thick target neutron spectra are considerably different from the data of Jacobs[8], indicating that the goal is not yet near.

The charged particle data other than alpha particles are also required for the evaluation of induced activities at accelerators in laboratories, factories and hospitals. Incident energies up to about 50 MeV are concerned. Other apllications are the isotope productions for medical use, the activation techniques and radiobiology. Figure. 5 shows the comparison of the calculation (Yamamuro, priv.comm,) and the experiment of the cross section and yield for production of ^{61}Cu from Ni(α,p) reaction. This isotope is useful for medical purpose, having the life-time of 3.37h emitting 280 keV and 660 keV gamma-rays. Unfavorable isotope ^{64}Cu, half-life of 12.7h emitting 1.35 MeV gamma-rays, is also produced by Ni(α,p) reaction. The data are therefore useful for design of an efficient production of ^{61}Cu suppressing the production of ^{64}Cu.

The amount of future works depends critiaclly on the scope of the file, which has not been fixed yet in dedtail. Necessary minimum works are :

(1) Systematic collection of charged particle reaction data.
We expect much for the international channel to obtain these data. Domestically, Kyushu University is asked for the measurements.

(2) Treatment of resonance reactions and the associated neutron spectra for light nuclei. Murata at NAIG analyzed the data of oxygen and carbon.[9]

(3) Evaluation based on the combination of direct, precompound and the statitical model calculations is needed to include proton and other charged particle induced reactions for the energy range up to 50 MeV. Yamamuro is making calculations along this line.

4. Photo-reaction Data File

Photo-reaction data are required for the isotope productions for medical purpose and the evaluation of the induced activities and shielding design of accelerators. As to the isotope productions, the data for γ-ray energies up to about 50 MeV are requested. From the shilding design people of electron-synchroton, the data for inciden electrons of energies from 100 MeV to a few GeV are requested. Required data are the bremsstrahlung gamma-ray intensity and its spectrum, the thick target photo-neutron cross sections and neutron spectra.

The work is yet at the stage of planning. Since I am not an expert of theoretical nuclear physics, I sketch here only the global features of photo-reactions.

Photoneutron cross sections for ^{60}Ni are shown in Fig. 6, reproduced from Dietrich and Berman.[10] The Lorentzian fit is in underestimation for photon energies greater than about 25 MeV, indicating the existence of non-resonant direct reactions. This seems to be the case for other nuclides also.

Figures 7 and 8 show the Ni(γ,n) cross section and the neutron spctrum measured by brems. These were reproduced from Photonuclear Data-Abstract Sheets, NBS.[11] Fig. 7 shows also the calculation by Drechsel et.al.[12] based on the particle-hole excitation plus surface vibration taking account of the collective correlation (denoted by solide line c-c). Good agreement of caluclation and experimental data indicates that the photon absorption process is due to rather a simple mechanism (though the calculation requires the knowledge of expert). Fig. 8 reveals, however, the emitted neutron spectrum is described well by evaporation theory except at the high energy tail. This indicates that the energy absorbed in nucleus by a relatively simple mechanism is dissipated to complex nuclear modes and thermalized, eventually evaporating neutrons.

Fig. 9 is the alpha particle spectrum emitted from Al and Ni for monoenergetic gamma-rays of 120 MeV, reproduced from the NBS abstract, indicating that the alpha particle is emitted mostly from preequilibrium stage in contrast to the neutron emission.

In view of the above-stated examples, the developments of calculational codes may be directed to the following lines.

(1) Photon absorption cross sections may be best described by

the Lorentzian fit given by Dietrich and Berman, supplemented with the non-resonant direct reaction theory. Modern nuclear theoretical calculation of resonance absorption should be encouraged. But, at the present stage, it is probably not yet suited to the purpose of the nuclear data evaluation.

(2) Particle spectra may be described by the combination of direct reaction, preequilibrium process, and the multistep statistical thory. Since high excitation energy is to be treated, the preequilibrium cascade process is better taken into account. New codes have to be developed.

(3) Shielding people request the calculational formula for the intenstiy and spectrum of bremsstrahlung, and the range of validity of Schiff's formula. Thick target yields and neutron spectra for electron energy up to GeV are requested in the form of easy access, such as the fitting formula, a parametrization and tabular form, etc. The request is understood, but it is beyond the scope of the planned file and the man-power.

5. PKA Spectrum and KERMA Data File

The file is intended for applications to the the radiation damage study, the calculation of heat generation, and the neutron therapy. Incident neutrons are from 10^{-5} eV to 20 MeV covering elements of Z = 1 to 83. However, the KERMA factors for light elements up to 50 MeV are required from medical people.

The file will be divided in two files. The primary file will contain the neutron cross sections, the normalized PKA spectra, and some other derived basic quantities. The double differential PKA spectrum at neutron energy near 15 MeV will be included for

use of the computer simulation study of the radiation damage.

The double differential and the angle integrated PKA spectra for the 1st stage reactions are calculated from the cross sections in the center-of-mass system as :

$$\sigma(E_N,E_p,\theta_p) = (\frac{M}{m_1})^{3/2}\sqrt{\frac{E_p}{\varepsilon_c}}\,\sigma^{cm}(E_R,\varepsilon_c,\theta_c), \qquad (1)$$

$$\sigma(E_N,E_p) = \int_{\varepsilon_c(1)}^{\varepsilon_c(2)} d\varepsilon_c \frac{\pi M}{\sqrt{m_1 m_2}} \frac{1}{\sqrt{\varepsilon_c E_G}}\,\sigma^{cm}(E_R,\varepsilon_c,\theta_c(E_p,\varepsilon_c)) \qquad (2)$$

Here, (E_p,θ_p) and (ε_c,θ_c) are the energies and the angles of recoiled atom in lab. frame and of particle in c.m. frame, respectively. Other symbols are shown in the figure right. For the 2nd stage reactions, the Jacobians are applied twice. The calculations is a bit tedious but straightforward.

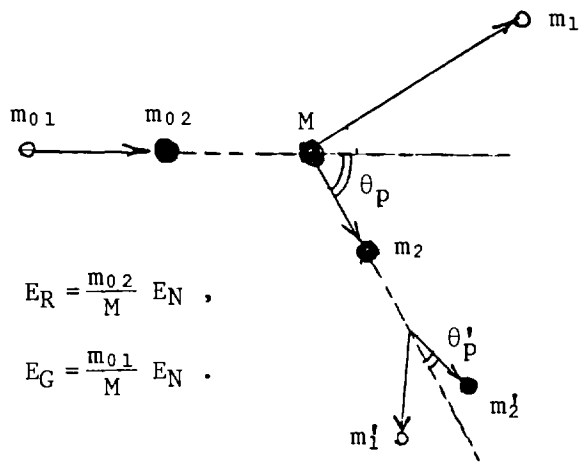

$$E_R = \frac{m_{02}}{M} E_N ,$$

$$E_G = \frac{m_{01}}{M} E_N .$$

Figure. 10 shows a demonstration of the calculated PKA spectrum from the 1st stage reactions with ^{58}Ni for 15 MeV neutrons. The elastic scatttering angular distributions are approximated by a forward peak and isotropic ones in backward directions. Direct in-elastic scattering cross sections were given by DWUCK code. Particle spectra were calculated with PEGASUS, normalizing the cross section values to that of JENDL-3.

The secondary file will contain the DPA cross sections and KERMA factors in group structure which are easily derived from

the data of the primary file. The DPA cross section is calculated based on the theory of Lindhard and Robinson[13] and the NRT model[14] as

$$\sigma_{DPA}(E_N) = \frac{0.8}{2\varepsilon_d} \int dE_p E_p / [1+kg(E_p)] \cdot \sigma(E_N, E_p). \quad (3)$$

Here, ε_d is the displacement energy and kg(Ep) the correction factor for the energy loss due to electronic excitation.

The KERMA for neutron elastic scattering and capture are calculated analytically. The recoil due to other reaction γ-rays is very small compared with the 1st recoil from particle emission and can be neglected. The KERMA factors for particle emissions are either calculated directly from the kinetic energies of recoil atom and the charged particles, Eq. (4), or from the energy balacne, Eq.(5) below. Summing over the reactions these are written by,

$$KF(E_N) \cong \frac{m_2}{M} E_G \sigma_R + \frac{m_1}{M} \bar{\varepsilon}_n \sigma_{n\text{-prod}}(E_N) + \sum_x^{p,\alpha,d,t} \bar{\varepsilon}_x \sigma_{x\text{-prod}}(E_N), \quad (4)$$

$$\text{or} \quad \cong \sum_x (E_N + Q_{n,x} - \bar{E}_n - Y_n - \bar{E}_\gamma \bar{Y}_\gamma)\, \sigma_{n,x}(E_N). \quad (5)$$

Here, in Eq.(4), σ_R is the non-elastic cross section, $\bar{\varepsilon}_x$ the average energy of particle x in c.m. system, and $\sigma_{x\text{-prod}}$ the particle production cross section. These are directly obtainable from,e.g.,the output of GNASH. Slight approximation has been used in deriving Eq.(4). In Eq.(5), $\bar{E}_n$ and $\bar{E}_\gamma$ are the average laboratory kinetic energies of the emitted neutrons and γ-rays, respectively. Y_γ is the γ-ray multiplicity and $Q_{n,x}$ the reaction Q-value.

As seen easily, when the charged particle emissions are not significant, the KERMA calculated from energy balnace is very senitive to the slight violation of the energy balance, i.e. to

the accuracy of the prediction of the emitted energies of neutrons and γ-rays.[14] The direct calculation by Eq.(4) is therefore more preferable.

The calculated KERMA factor for natural iron below 100 keV is shown in Fig. 11 in comparison with that of Howerton.[15] Figure 12 shows the KERMA for Fe-56 from 1 to 20 MeV based on the calculation using GNASH code with 0.25 MeV energy mesh. The direct method and the energy balance method are compared. The energy balance is violated by about 6 %, 3% and 1 % at 2 MeV, 5 MeV and 8 MeV, respectively, causing the discrepancy from the result of the direct calculation.

In fact, K. Maki at Hitachi noted that the KERMA factors calculated for natural iron using JENDL-3R1 and the energy balance have become negative above 5 MeV. In JENDL-3R1 the gamma-ray production cross sections of natural chromium, iron and nickel calculated with GNASH code were adjusted to reproduce the experimental data at ORNL without further compensating the neutron production cross sections.

The data for the double differential particle spectrum and especially the charged particle spectrum needed for calculation of PKA spectra are not in JENDL file. To be consistent with PKA spectrum data file , these data are better supplied to JENDL general purpose file in ENDF/B-6 formt. Finally, the calculation of KERMA factors for light nuclei requested from medical people pauses a very difficult problem when the breakup reactions occur. The lack of experimental data for neutron energy greater than 20 MeV severely limits the validity of theoretical calculation. Recent inelastic scattering experimental data on carbon and other

light nuclei up to 65 MeV by Finlay et al.[16] will be a very valuable source of data.

6. Concluding Remarks

Data files discussed here belong to the the new scope of JENDL which are not on the line of a straight extension of the previous activities. The works will have to be continued for a sizeable years with a considerable amount of man power. Hence, a new frame of working organization and a perspective should be given to these works. Also, an international collaboration in these new fields is very much desired.

Acknowledgement

Author is thankful to the working group members of the Special Purpose Nuclear Data and the Medium Weight Nucleus Nuclear Data of JNDC for contributions and discussions. He is especially indebted to N. Yamamuro at Data Engineering Inc. and H. Matsunobu at Sumitomo Atomic Industry Co. for providing him with their recent results of calculation.

References

(1) Anderl,R.A. : Specification for dosimetry Benchmark No.1, The coupled Fast Reactivity Measurements Facility(CFRMF) (1982)

(2) Young,P.G. and Arthur,E.D.. : GNASH: A Preequilibrium Statistical Nuclear Model Code for Calculation of Cross Sections and Emission Spectra, LA-6947(1977)

(3) Iijima,S.,Nakagawa,T.,Sugi,H.,Nishigori,T. :PEGASUS, A Pre-equilibrium and Multistep Evaporation Theory Code for Cross Section Calculation, JAERI Report (to be published)

(4) Tachibana, T., Uno, M., Yamada, M., Yamada, S.: Empirical Mass formula with Proton-Neutron Interaction, Atom.Data Nucl. Data Tables 39,251(1988)

(5) Yamamuro,N. :A Nuclear Cross Section Calculational System with Simplified Input -Format, Version 1,JAERI-M 88-140 (1988)

(6) Gruppelaar, H., et al.: The REAC-ECN-3 Data Library with Neutron Activation and Transmutation Cross Sections for Use in Fusion Reactor Technology, ECN-207 (1988)

(7) Forrest, R.A., et al.: The Data Library UKACT1 and the Inventory code FISPACT, Proc. Int. Conf. Nuclear Data for Science &Technoligy, Mito, 1988, p.1061Cross fI; Sowerby

(8) Jacobs,G.J.H., Liskien,H.: Ann. Nucl. Energy 10,541 (1983)

(9) Murata,T.: Neutron Emission from (,n) Reaction in Nuclear Fuel, JAERI-M 87-025 (1987) p.14

(10) Dietrich,S.S., Berman,B.L.: Photoneutron Cross Sections, Atom.Data Nucl.Data Tables 38,199 (1988)

(11) Fuller, E.G.,Gerstenberg, H.: Phtonuclear Data-Abstract Sheets 1955-1982, NBSIR 83-2742

(12) Drechsel,D., Seaborn,J.B., Greiner,W.: Pys.Rev.162,983(1967)

(13) Lindhard,J. et al.:Kgl.Danske VidenskSelsk.mat.-fys.Medd., 33,(1963),No.10.
Robinson,M.T.: Proc. B.N.E.S. conf. on Nuclear Fission Reactors, Culham 1969 (BNES,London) ,p.364

(14) Robinson,M.T.,Torrens,I.M. : Phys.Rev. B9,5008 (1974).
Recommendation for Displacement Calculations for Reactor/ Accelerator Stucies in Austenitic Steels, Nucl. Eng. & Design,33,91(1975)

(15) Howerton,R.J. : UCRL-50400, Vol.27,(1986)

(16) Finlay,R.W.,et al.:Nucl.Instr.Meth. Phys.Res.B10/11,296(1985)

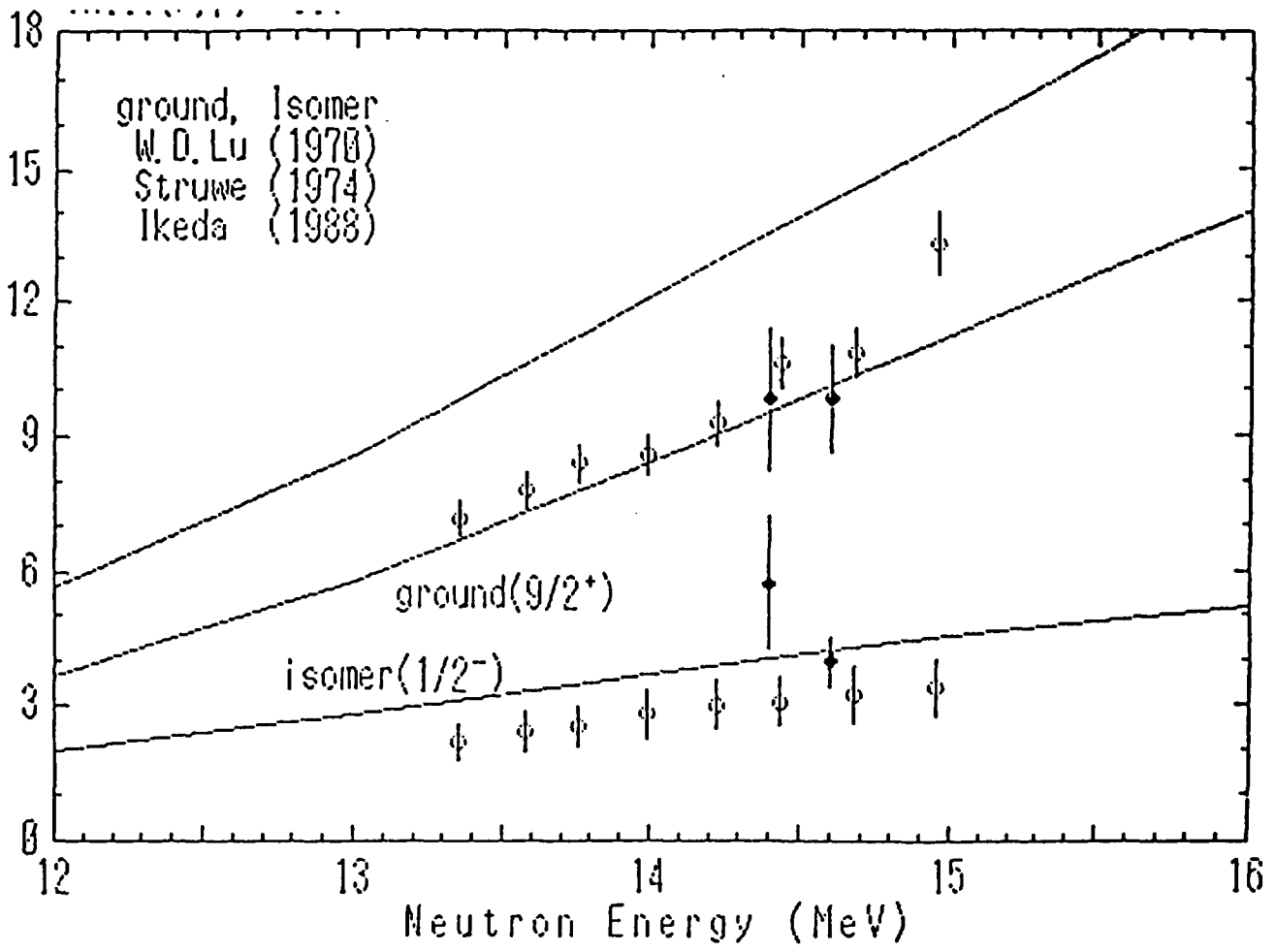

Fig. 1 ^{117m}In and ^{117g}In production cross sections from ^{117}Sn(n,p) Reactions. (comm. from N. Yamamuro)

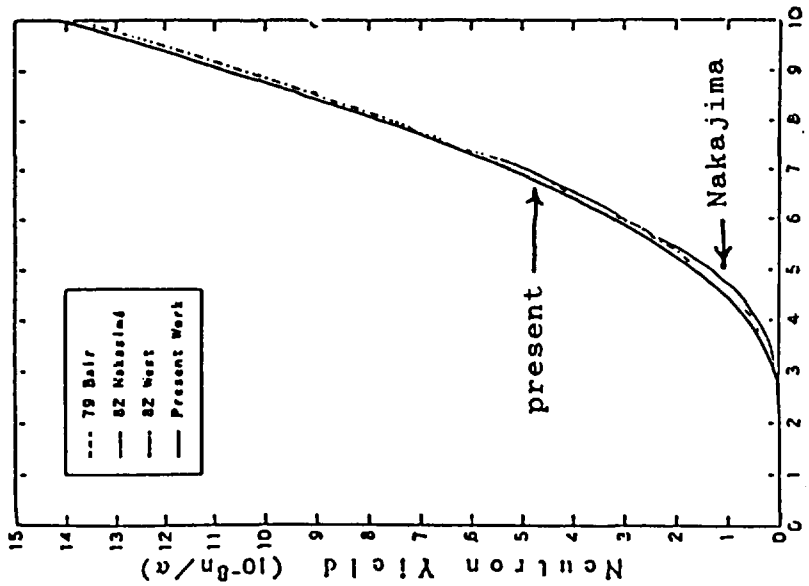

Fig. 3 Thick target (α,n) yield for uranium oxide. Comparison of the present calculation with experimental data and the calculation by R. Nakajima. (comm. by H. Matsunobu)

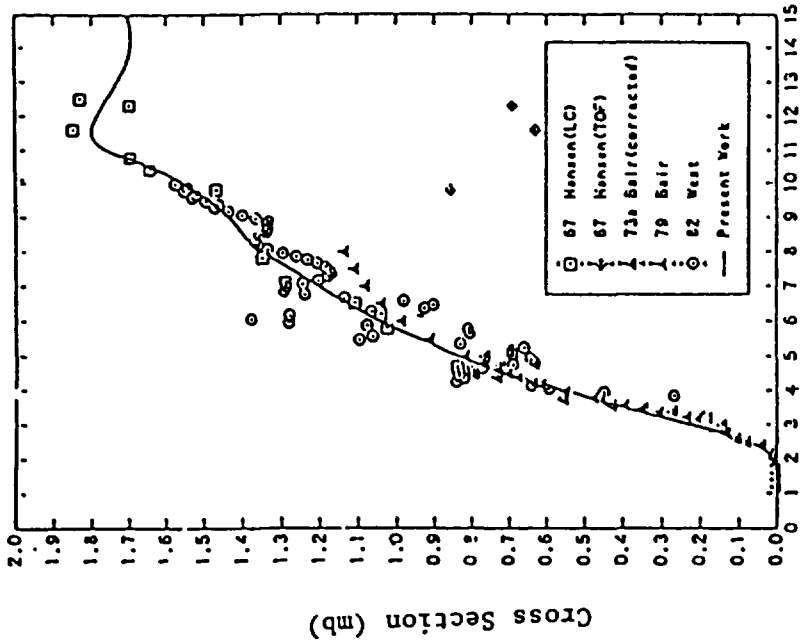

Fig. 2 (α,n) cross section for natural oxygen. Comparison of the statistical model calculation with experimental data. (comm. from H. Matsunobu)

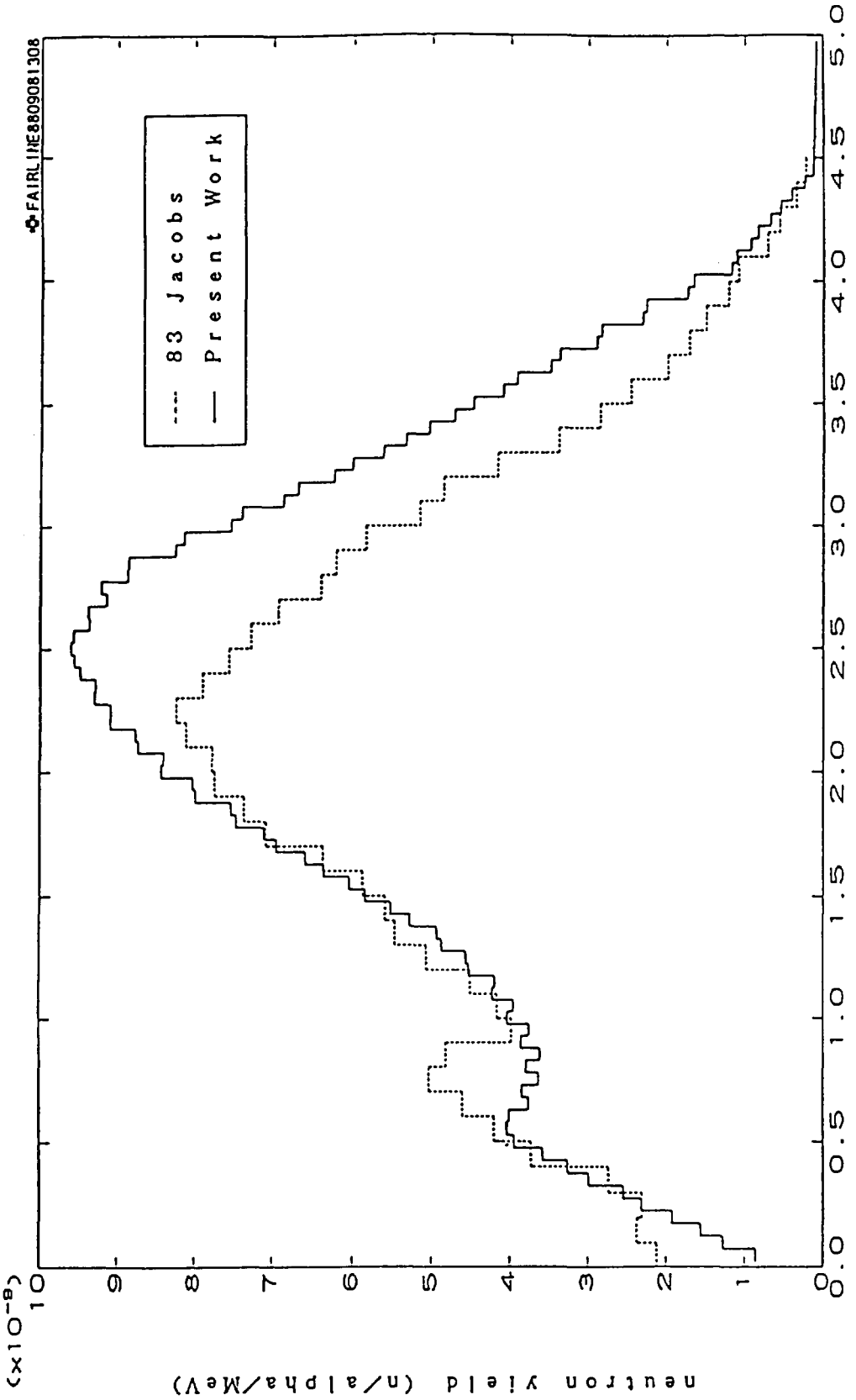

Fig. 4 (α,n) neutron spectrum from UO_2 for E_α=5.5 MeV
(comm. from H. Matsunobu)

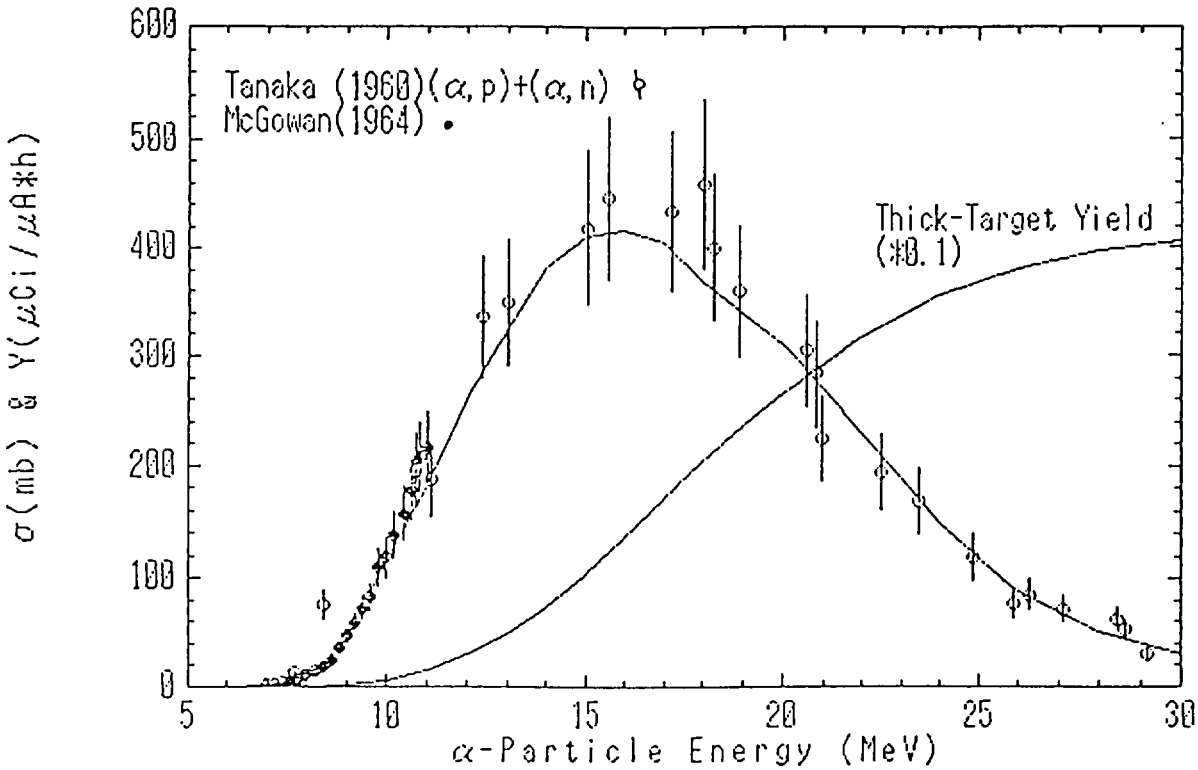

Fig. 5 Ni(α,p)^{61}Cu reaction cross section and thick target yield. (comm. from N. Yamamuro)

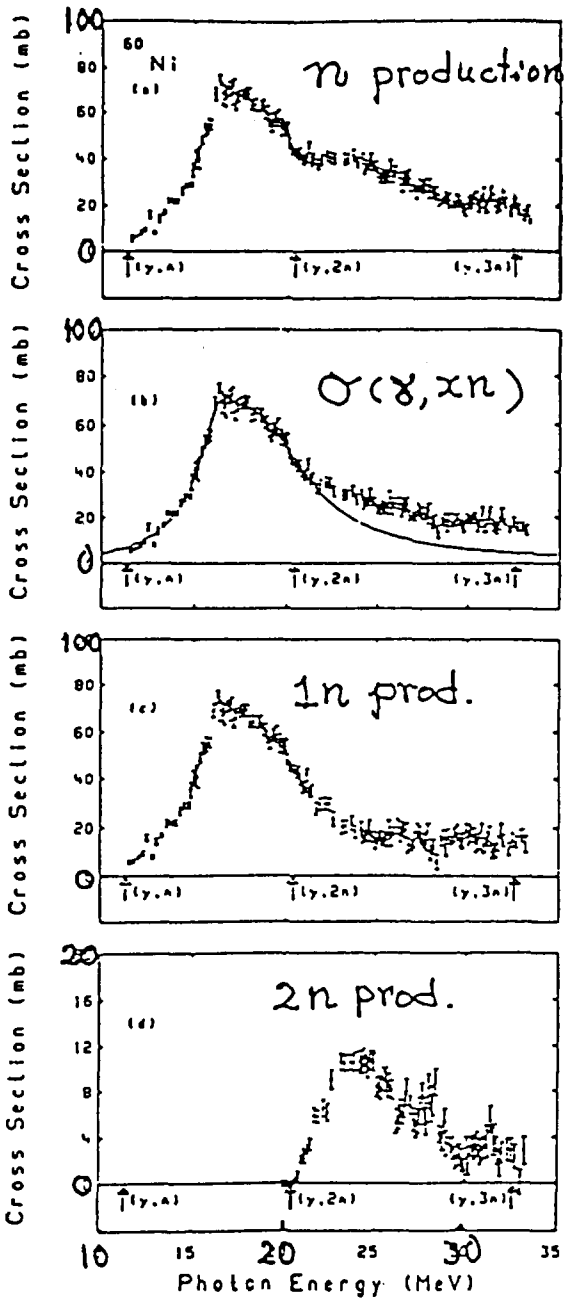

Fig. 6 Photo-neutron cross section for ^{60}Ni. (reproduced from Ref. 10.)

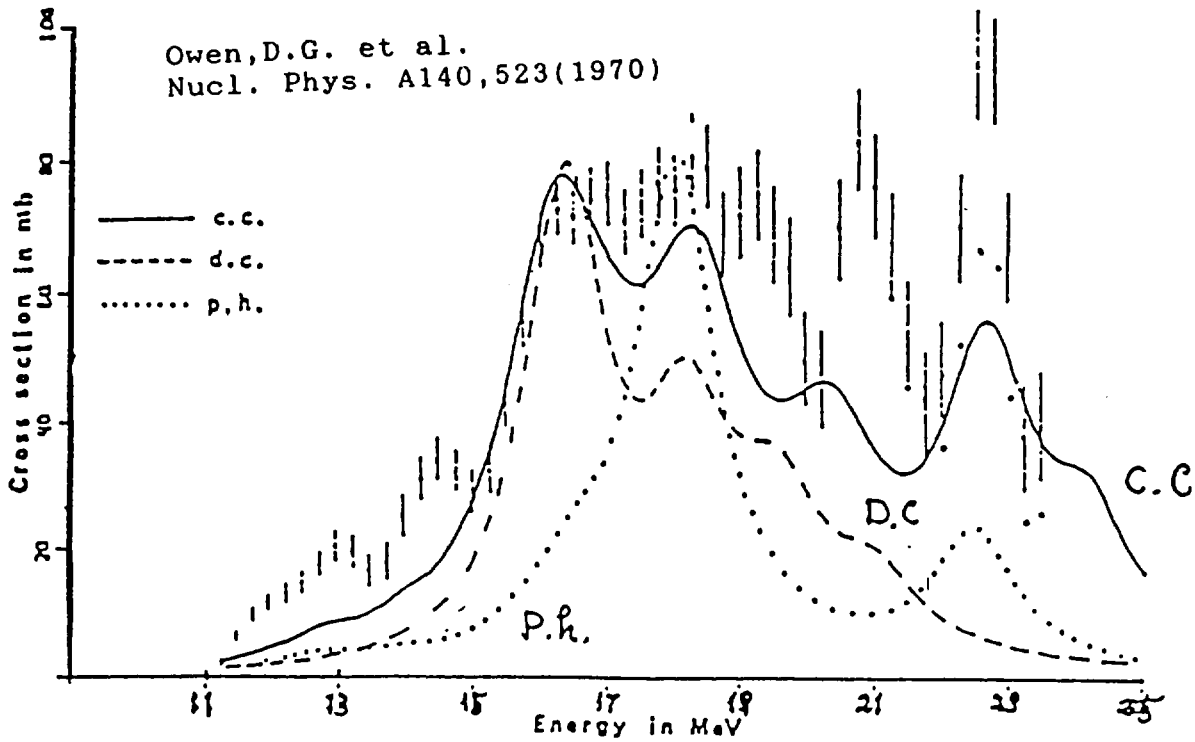

Fig. 7 ^{60}Ni(γ,xn) cross section. (reproduced from Ref. 11.)
Lines are calculation by Drechsel et al. (Ref. 13).
c.c : collective correlation, p.h. : particle-hole,
d.c.: dynamic collective theory.

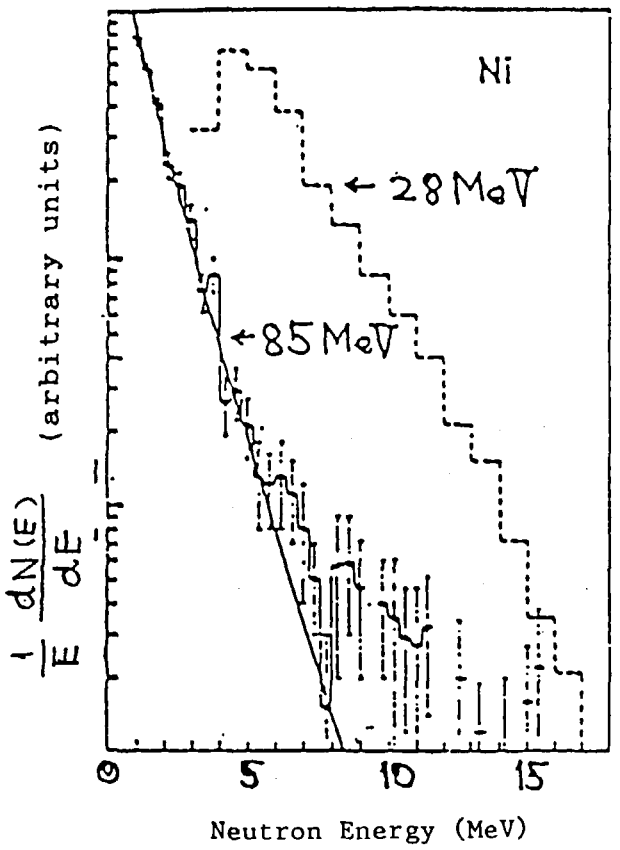

Garfagnini, R. et al.
Nucl. Phys. A122, 49 (1968)

Fig. 8 Neutron spectrum for Ni(γ,xn) with bremsstrahlungs of maximum energy 85 MeV. Straight line is the calculation by evaporation theory. (reproduced from Ref. 11.)

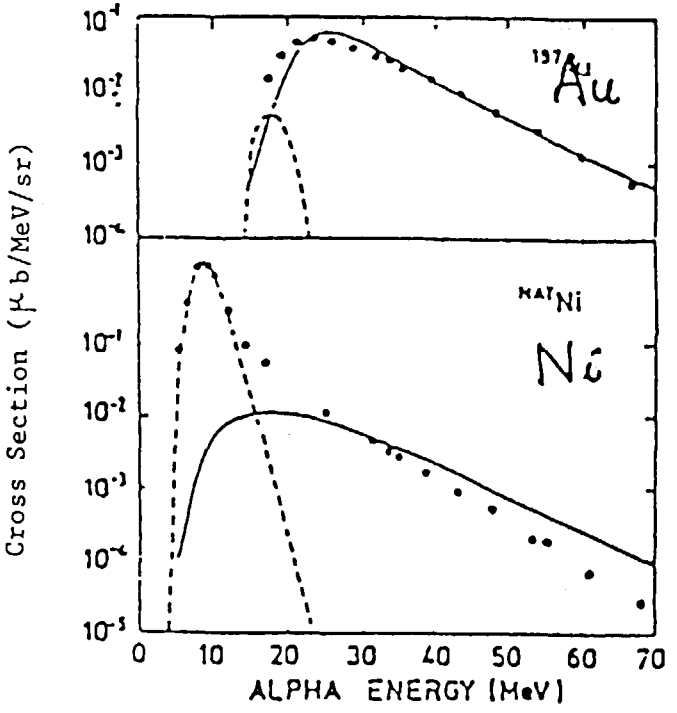

Flowers, A.G. et al.
Phys. Rev. Lett. 43, 323 (1979)

Fig. 9 Photo-alpha cross sections at 30° from Au and Ni with 120 MeV brems.
----- statistical component,
——— preequilibrium component.

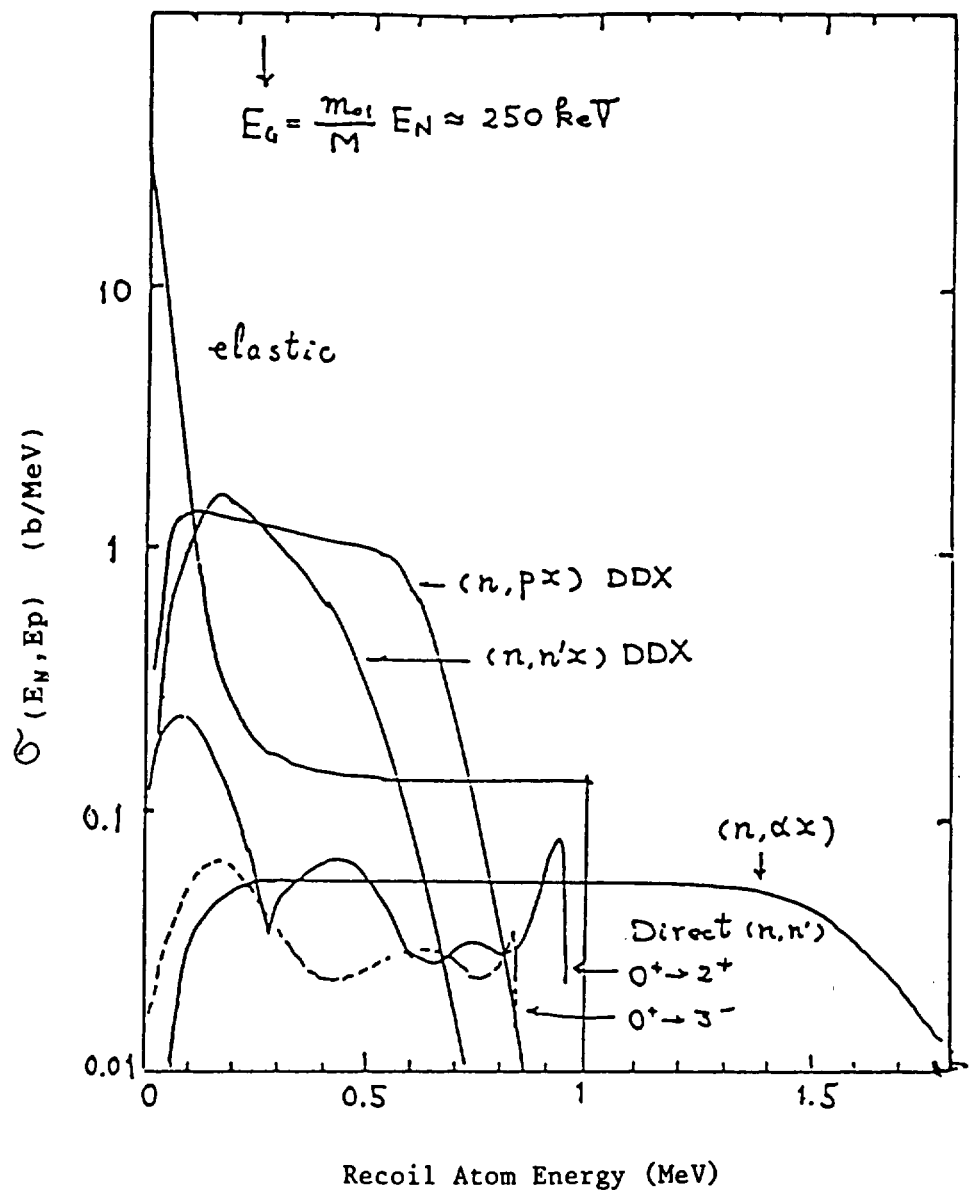

Fig. 10 Calculated PKA spectrum components from the first stage reactions with ^{58}Ni for 15 MeV neutrons.

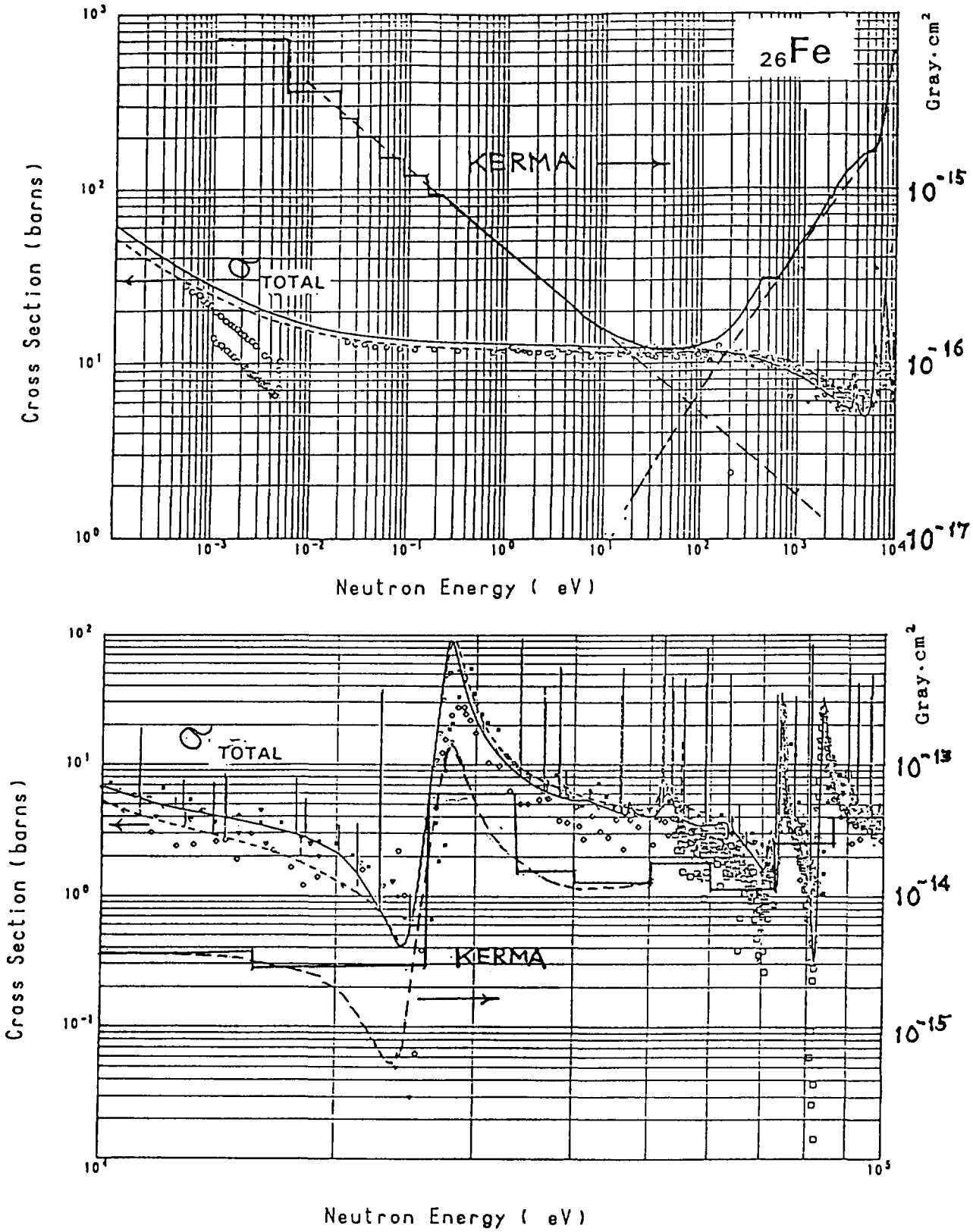

Fig. 11 Total cross section of natural iron and KERMA factor for neutron energy below 100 keV. Present calculation (dotted line KERMA) is compared with Howerton's calculation (solind line KERMA).

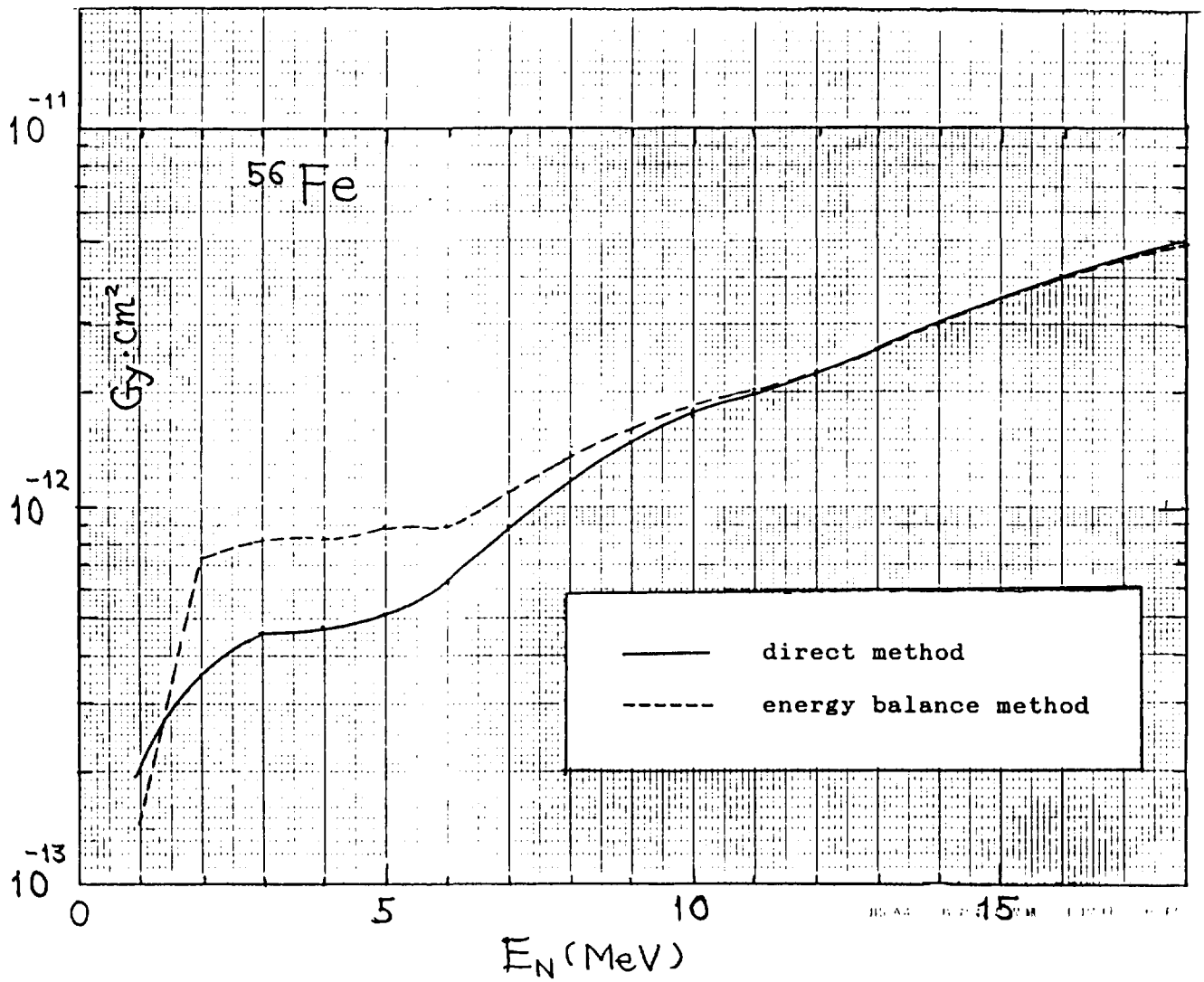

Fig. 12 KERMA factors for Fe-56 based on the calculation with GNASH code. Comparison of calculations by the direct method and the energy balance method. (See text)

2.6 Topics

2.6.1 Experimental Analyses by Use of JENDL-3T for Joint PNC/USDOE Criticality Safety Experiments

Nobuo Fukumura, Nagafumi Aihara[1], Tadakuni Matsumoto[2], Tomozo Koyama[3], Masuo Takami[4]

1) Oarai Engineering Center, PNC
Narita, Oarai, Ibaraki, 311-13
2) Tokai Works, PNC
Tokaimura, Ibaraki, 319-11
3) Head Office, PNC
Akasaka, Minato-ku, Tokyo, 107
4) Century Research Center,
Nihonbashi, Chuo-ku, Tokyo, 103

Abstract: Accuracy of evaluated nuclear data files of JENDL-3T are estimate using three critical experimental data of mixed plutonium and uranium nitrate solutions at a plutonium fraction of 0.4 and 0.5, and plutonium concentration of 42, 60 and 173 g/ℓ in cylindrical geometry. These data are obtained through Joint PNC/USDOE Criticality Data Development Program.

The calculational codes used for accuracy estimation are transport cell calculation code WIMS-E and monte-carlo core calculation code KENO-IV. The calculational accuracy using this code system is estimated by analysing the critical experimental data obtained by use of the heavy water moderated critical assembly (DCA). The critical accuracy is obtained within ±1%. This is almost the same value which is obtained by use of diffusion core calculation code CITATION.

After this evaluation the code system using JENDL 3T are applied for criticality safety experiments. The calculational error is within ±1%.

The same result is obtained even if JENDL 2 is substituted for JENDL 3T.

It is concluded that JENDL 3T is applicable for the mixed plutonium and uranium nitrate solution experimental system.

Introduction

JENDL 3T is the nclear data files which are now evaluated and compiled by the Japanese Nuclear Data Committee (JNDC). In order to estimate the validity of JENDL 3T it is necessary to choose the neutron energy spectrum which varies continuously from thermal neutron energy range to fast neutron energy range. But it is very difficult to choose the experimental system which has the wide range neutron energy spectrum change in the usual thermal nuclear reactor. In order to resolve this problem it is best to use the solution experimental system because the neutron energy spectrum changes continuously only by changing the nucler fuel material concentration in the solution. The critical experimental data of mixed plutonium and uranium nitrate solutions in cylindrical geometry are obtained by Joint PNC/USDOE Criticality Data Development Program[1]. The accuracy of JENDL 3T are estimated by analysing these experimental data using the sophistcated cell calculational code with transport theory WIMS-E.

Verification of Calculational Code

The cell calculational code WIMS-E is developed at winfrith in England[2]. The basic cross section library is in 69 groups with 14 fast groups (10 MeV ~ 9.118 keV), 13 resonace groups (9.118 keV ~ 4 eV) and 42 thermal groups (under 4 eV). The transport equation is solved by collision plobability method using up to 69 neutron energy groups.

By using this code we estimated the calculational error of plutonium isotopic composition of plutonium fuel after burn-up for the boiling-light-water-cooled, heavy-water-moderated reactor (ATR). Fugen is the proto type power reactor of ATR. Table 1 shows the design data of Fugen. For the PIE experimental analysis it is necessary to use the reactor operating history. Fig. 1 shows the history and Fig. 2 shows the fuel loading pattern. We used P_{06} plutonium fuel as shown in Fig. 2 for PIE. PIE data were obtained by JAERI.

In order to estimate the plutonium isotopic composition of plutonium fuel both the M-5 and O-22 plutonium fuel pins of fuel cluster was used as shown in Fig. 3. The measured points were shown in the same figure. For the experimental analysis we used the calculational model shown in Fig. 4. Fig. 5 or Fig. 6 shows the comparison between experiment and calculation.

It is clear from these figures that the calculational error of fissionable plutonium isotopic composition (^{239}Pu and ^{241}Pu) is up to 5%(3).

Table 2 shows the another result of comparison of micro-parameters between experiment and calculation. These experimental data have been obtained in the ATR type plutonium fuel pin pellets which were irradiated at Deuterium Critical Assembly (DCA). As shown in the figure the calculational error is up to 10%(4). The same value of calculational error is obtained as shown in Table 3. These experimental data were obtained by use of FFTR plutonium fuel pin according to Joing PNC/USDOE Criticality Data Development Program(5). The enrichment of plutonium is about 20 w/o. This is much higher than that of ATR plutonium fuel, but the calculational error is almost the same.

It is clear from these results that the cell calculational code is useful for the experimental analysis of the system using plutonium fuel pin.

Experimental Analysis Method of Mixed Plutonium and Uranium Nitrate Solution System

It is necessary to make the cross section library fitted to the WIMS code for the experimental analysis with use of the code. The procedure is shown in Fig. 7. This work was done by the CRC company. Table 4 shows the list of nuclear data files. We used JENDL-3T library of 21 nuclide. As for other nuclide the orginal library of WIMS code was used. By using this cross section library the experimental analysis for the mixed plutonium and uranium nitrate solution system was done according to Fig. 8.

The calculational model of the system is shown in Fig. 9. The experiments were done according to the Joint PNC/USDOE Criticality Data Development Program.(6) Three experimental conditions were shown in Table 5. The WIMS-E/KENO-IV code system is used for the analysis. The criticality by using the code system reproduces the experimental value within 1% in the case of critical experiment using DCA.

Results and Discussion

The analytical results are shown in Table 6. For the comparison the results by use of JENDL-2 library are also shown in the same table. As shown in Table 6 the criticality of the calculation reproduces the experimental results within 1% for both cases. But the result using JENDL-3T library is rather better than that using JENDL-2 library. For the comparison between JENDL-3T library and JENDL-2 library the relative deviation of JENDL-3T library based on JENDL-2 library is shown in Fig. 10 for the case of ^{239}Pu fission cross section. The figure shows that JENDL-3T library underestimates the ^{239}Pu fission cross section around the resonance neutron energy range compared with that of JENDL-2 library. This is one of the reason which JENDL-3T library is better than JENDL-2 library. Fig. 11 shows the neutron energy spectrum obtained by analysing the mixed plutonium and uranium nitrate solution system. The thermal neutron energy spectrum changes in a large way by changing the plutonium fuel concentration in the solution. But the criticality of calculation using the JENDL library reproduces the experimental results within 1%.

Conclusion

Experimental analyses using JENDL-3T nuclear data files have been done for the mixed plutonium and uranium nitrate solutions experimental system at a plutonium fraction of 0.4 and 0.5, and plutonium concentration of 42, 60 and 173 g/ℓ in cylindrical geometry.

From the present study the following are concluded:

1. The criticality of calculation using the code system WIMS-E/KENO-IV with JENDL-3T library reproduces the experimental result within 1%.
2. The same result is obtained by using JENDL-2 library, but the result using JENDL-3T is rather better than one using JENDL-2.
3. JENDL-3T library is useful for the analysis of critical experimental data using the mixed plutonium and uranium nitrate soltuions.

REFERENCES

(1) HACHIYA, Y., KOYAMA, T., SMOLEN, G.R., WHITESIDES, G.E.: "Joint United States/Japanese Criticality Data Development Program Plan", American Nuclear Society Topical Meeting on Criticality Safety and Storage of Fissile Material (1985).

(2) ASKEW, J.R., FAYERS, F.J., KEMSHELL, P.B.: "A General Description of the Lattice Code WIMS", J. Brit. Nucl. Energy Soc., 5, 564 (1966).

(3) AIHARA, N., FUKUMURA, N., KAWATA, N.: Fall Meeting of the Atomic Energy Society of Japan, E56 (1985).

(4) FUKUMURA, N.: J. Nucl. Sci. Technol., 18[4] (1981).

(5) BIERMAN, S.R., FUKUMURA, N.: Trans. Am. Nucl. Soc., 54 (198-200) (1987).

(6) SMOLEN, G.R., WHITESIDES, G.R., MATSUMOTO, T., FUNABASHI, H.: Proceedings ceedings of Int. Seminar on Criticality Safety, Tokyo, P.231 (1987).

Table 1 Design data of Fugen.

Parameter		Fugen
Electric Power	MWe	165
Thermal Power	MWt	557
Reactor		
Core Diameter	mm	4,053
Core Height	mm	3,700
No. of Channels		224
Control Rod (B_4C)		49
Lattice Pitch	mm	240
Fuel		
No. of Rods/Assembly		28
Pellet Diameter	mm	14.4
Moderator to Fuel Volume Ratio		8.24

Table 2 Comparison of reaction rate ratio in ATR lattice between experiment and calculation.

Fuel*	ρ^{28}**			δ^{28}**			δ_{25}^{49}**		
	Experiment (E)	Calculation (C)	C/E-1 (%)	Experiment (E)	Calculation (C)	C/E-1 (%)	Experiment (E)	Calculation (C)	C/E-1 (%)
5S Pu, 0% Void	0.823	0.923	12	0.109	0.106	−3	1.06	1.10	4
5S Pu, 100% Void	1.08	1.10	2	0.128	0.129	1	1.06	1.12	6
8R Pu, 0% Void	1.04	1.10	6	0.127	0.128	1	1.33	1.28	−4
8R Pu, 100% Void	1.39	1.31	−6	0.155	0.155	0	1.30	1.29	−1

* 5S Pu : 1.2 w/o fissile (92 w/o Pu fissile)
8R Pu : 1.4 w/o fissile (76 w/o Pu fissile)

** $\rho^{28} \equiv \dfrac{\int_{E_{cd}}^{\infty} \sigma_c^{28}(E)\phi(E)dE}{\int_0^{E_{cd}} \sigma_c^{28}(E)\phi(E)dE}$, $\delta^{28} \equiv \dfrac{N_f^{28}\int_{E_T}^{\infty} \sigma_f^{28}(E)\phi(E)dE}{N_f^{25}\int_0^{\infty} \sigma_f^{25}(E)\phi(E)dE}$, $\delta_{25}^{49} \equiv \dfrac{N_f^{49}\int_0^{\infty} \sigma_f^{49}(E)\phi(E)dE}{N_f^{25}\int_0^{\infty} \sigma_f^{25}(E)\phi(E)dE}$

where E_{cd} : Cd cut off energy, E_T : Threshold energy, N_f : Number density of fuel pellet.

Table 3 Comparison of reaction rate ratio between experiment and calculation in fuel pin of organic moderator

Pin No.	Nuclide	Reaction Rate Ratio		C/E − 1 (%)
		Calculation (C)	Experiment (E)	
2	$^{238}U_f/^{235}U_f$	1.53327×10^{-2}	1.40970×10^{-2}	8.8
	$^{239}Pu_f/^{235}U_f$	1.23089	1.20815	1.9
	$^{232}Th_f/^{235}U_f$	3.61708×10^{-3}	3.48662×10^{-3}	3.7
	$^{237}Np_f/^{235}U_f$	7.80839×10^{-2}	7.22344×10^{-2}	8.1

Table 4 List of nuclear data file

Nuclide	File	Resonance
H	JENDL-3T(ENDF-B/Ⅲ)	−
^{10}B	JENDL-3T	−
C	JENDL-3T(ENDF-B/Ⅲ)	−
N	JENDL-3T	−
O	JENDL-3T(ENDF-B/Ⅳ)	−
Al	JENDL-3T	−
Si	JENDL-2	−
Cr	JENDL-3T	−
Mn	JENDL-3T	−
Fe	JENDL-3T	−
Ni	JENDL-3T	−
Zr	JENDL-2	−
Mo	JENDL-3T	−
^{235}U	JENDL-3T	○
^{238}U	JENDL-3T	○
^{238}Pu	JENDL-2	○
^{239}Pu	JENDL-3T	○
^{240}Pu	JENDL-3T	○
^{241}Pu	JENDL-3T	○
^{242}Pu	JENDL-3T	○
^{241}Am	JENDL-3T	−

( ) : Scattering law

Table 5 Experimental condition

Case	Geometry	Reflector	Pu enrichment (%)	Pu concentration (g/L)
1	Cylinder	None	52	60
2	Cylinder	None	40	42
3	Cylinder	None	40	173

Table 6 Analytical results

Case	K_{eff}	
	JENDL-3T	JENDL-2
1	0.99970±0.00573	1.00997±0.00553
2	1.00084±0.00489	1.00485±0.00525
3	1.00654±0.00532	1.00901±0.00575
Ave.	1.00236	1.00794

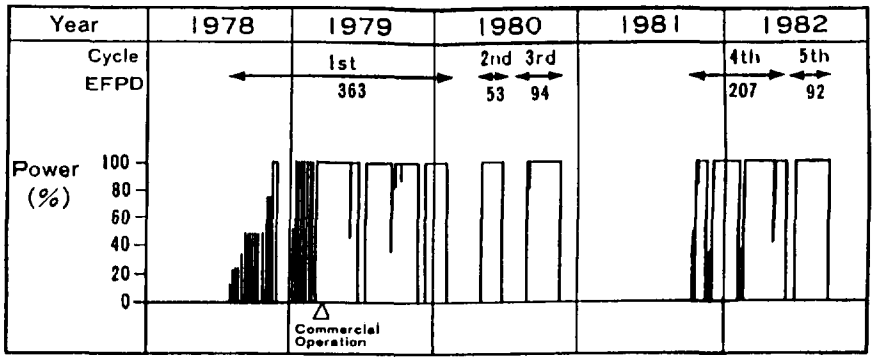

Cycle	1st	2nd		3rd		4th		5th	
	L	W	L	W	L	W	L	W	L
MOX Fuel	96	20	16	24	12	48	44	0	12
UO_2 Fuel	128	16	20	12	24	28	32	36	24

L: Loading W: Withdrawn

Fig. 1 Fugen operating history

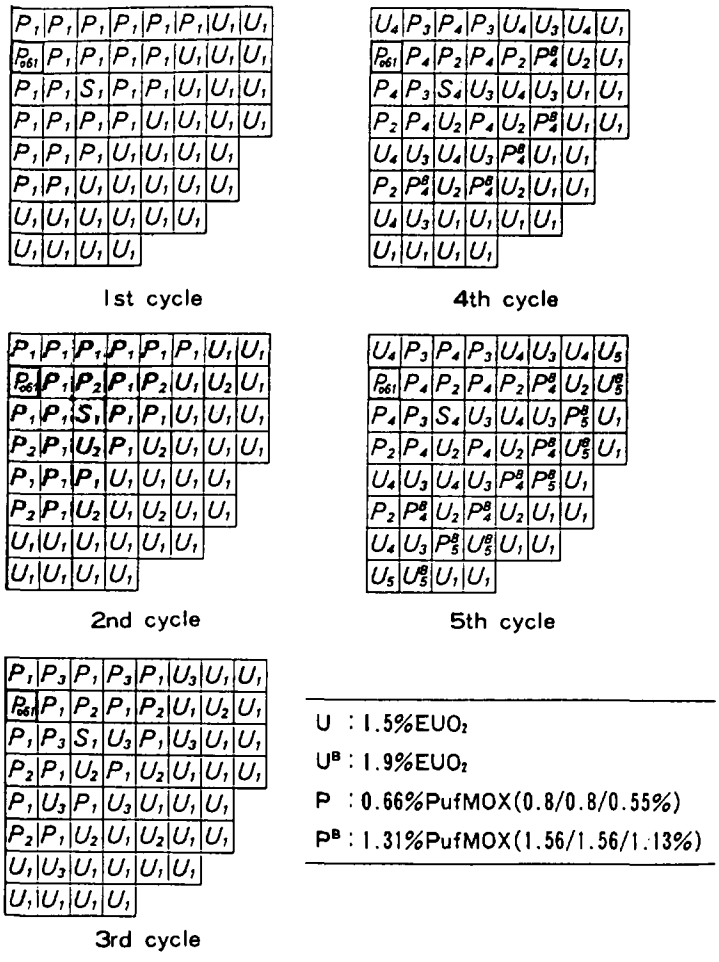

Fig. 2 Fuel loading pattern

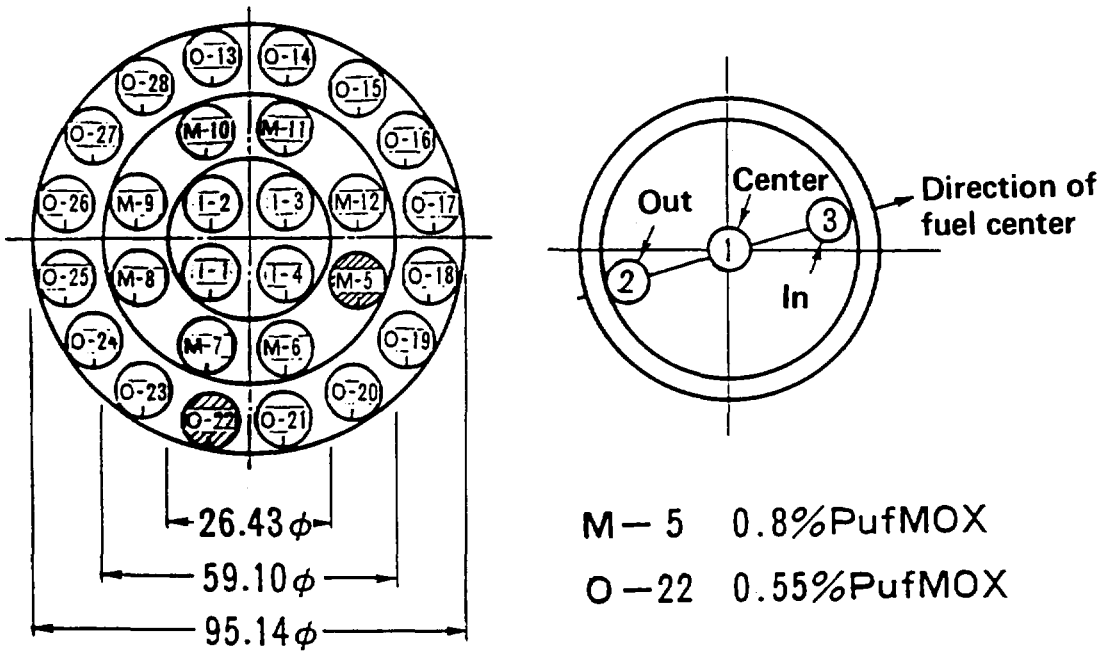

Fig. 3 Measured point of PIE

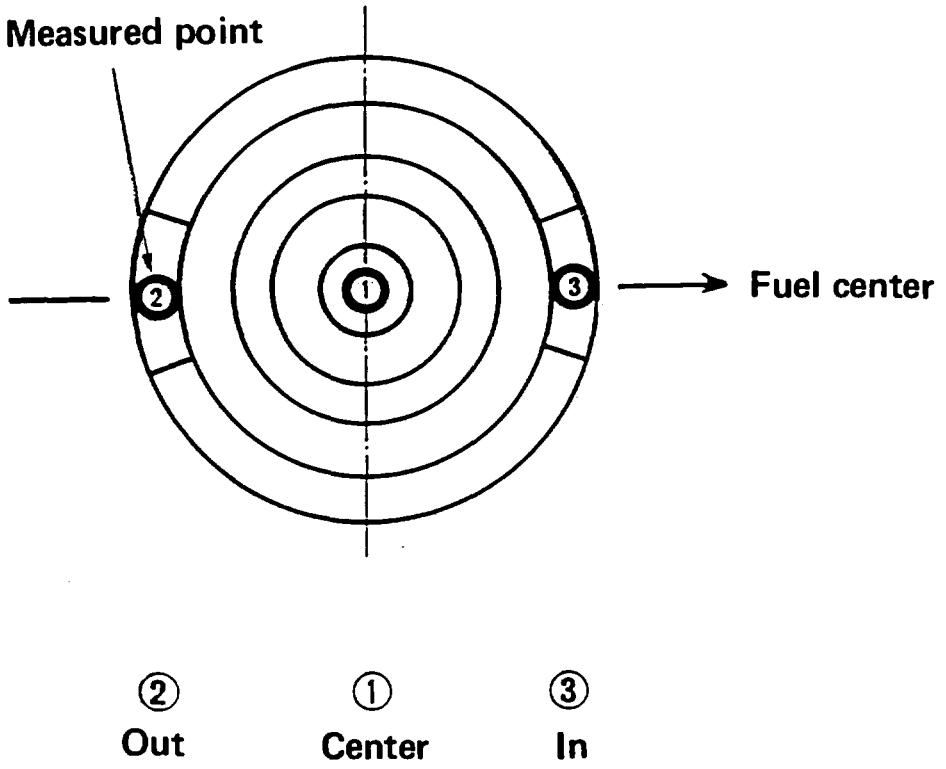

Fig. 4 Calculational model of PIE analysis

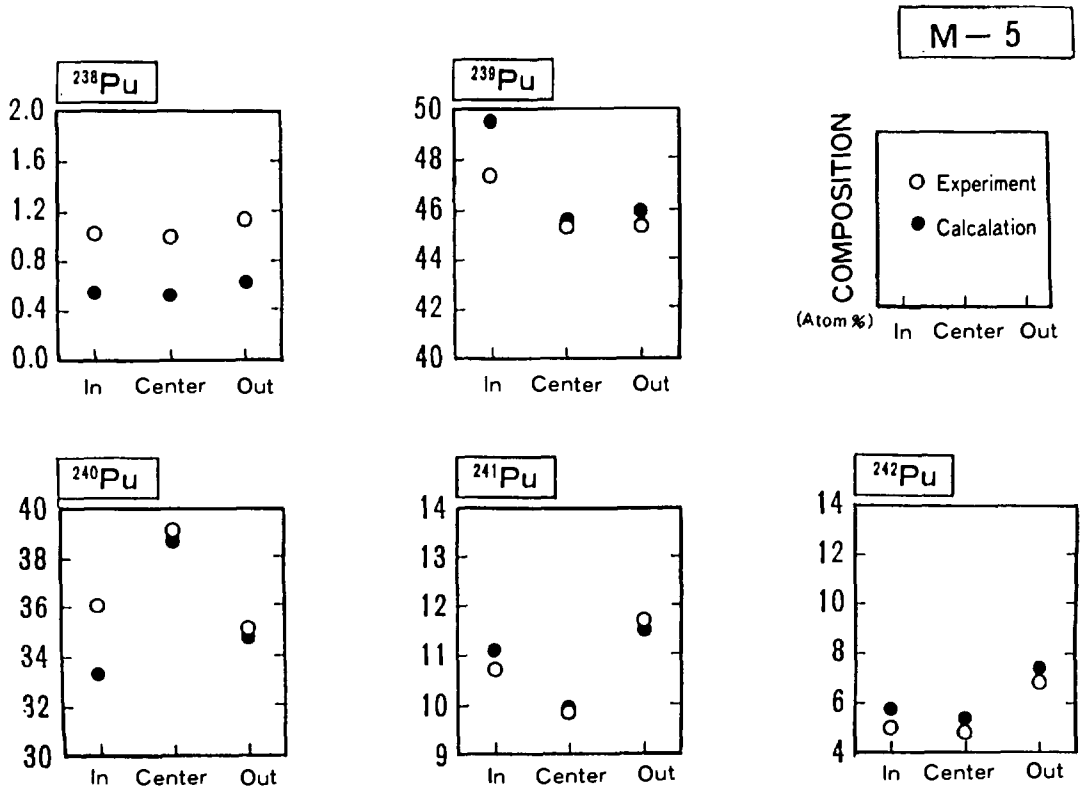

Fig. 5 Comparison of plutonium isotopic composition between experiment and calculation (M-5 pellet)

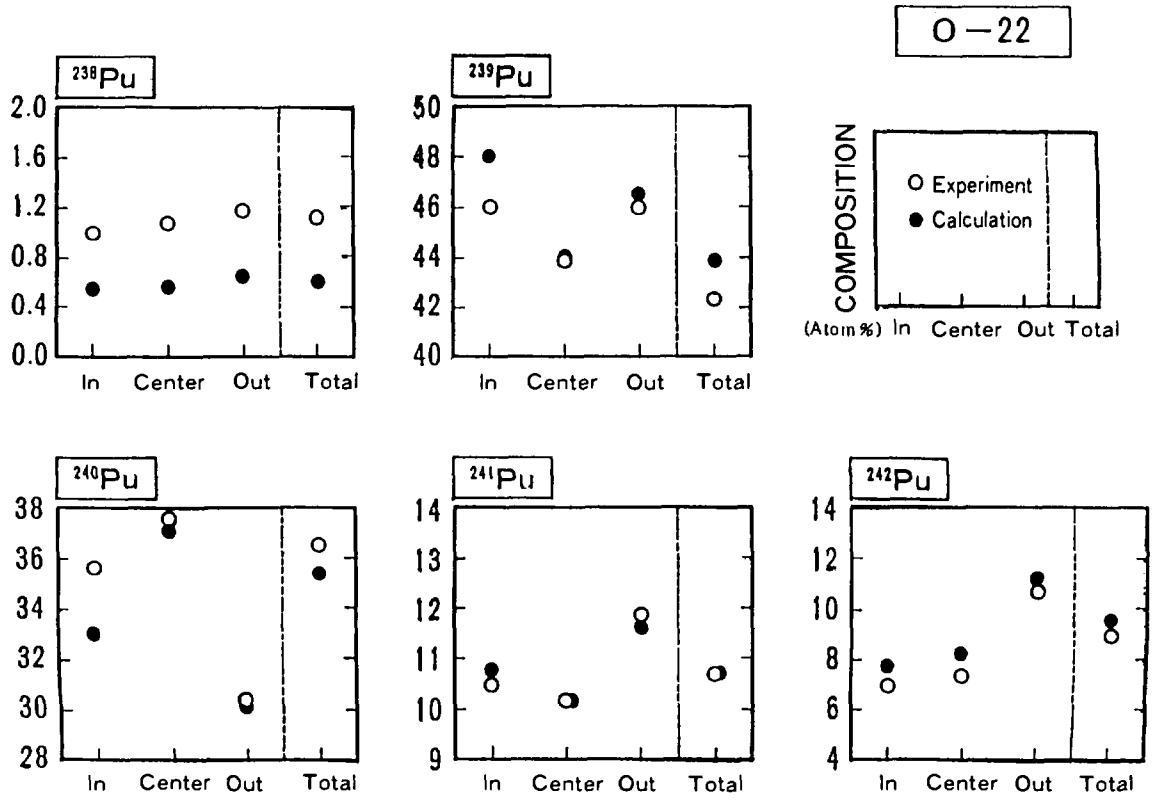

Fig. 6 Comparison of plutonium isotopic composition between experiment and calculation (O-22 pellet)

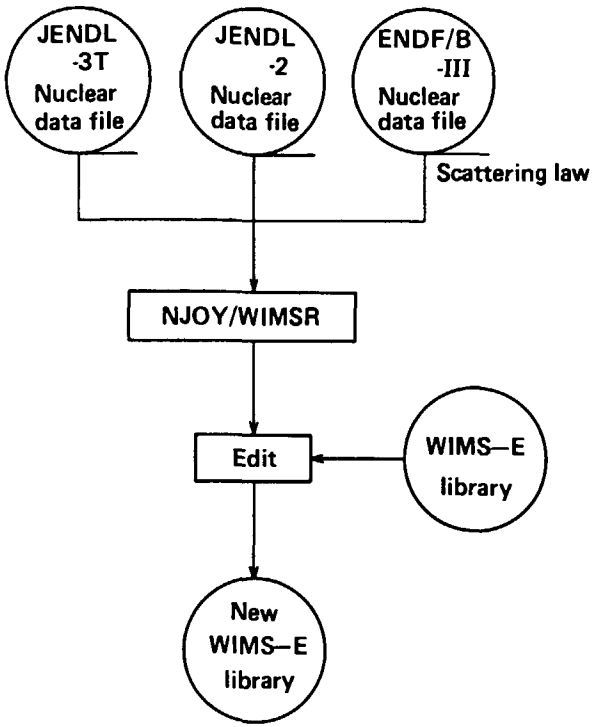

Fig. 7 Procedure of WIMS-E library production

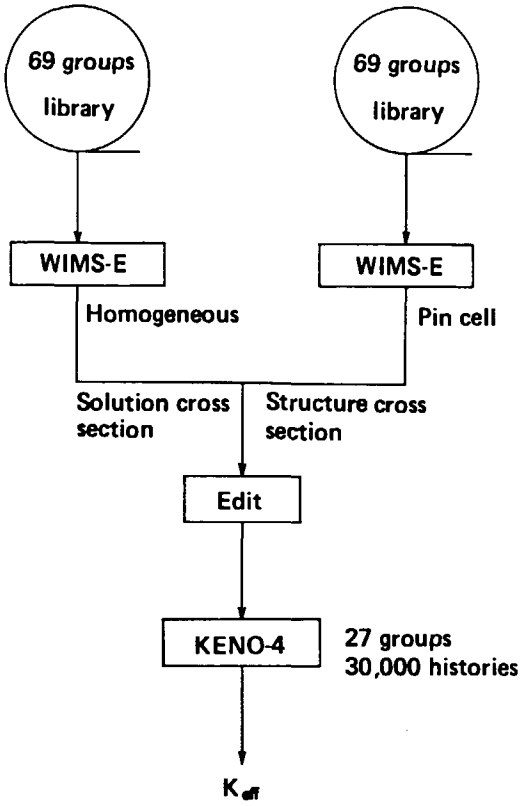

Fig. 8 Calculational method

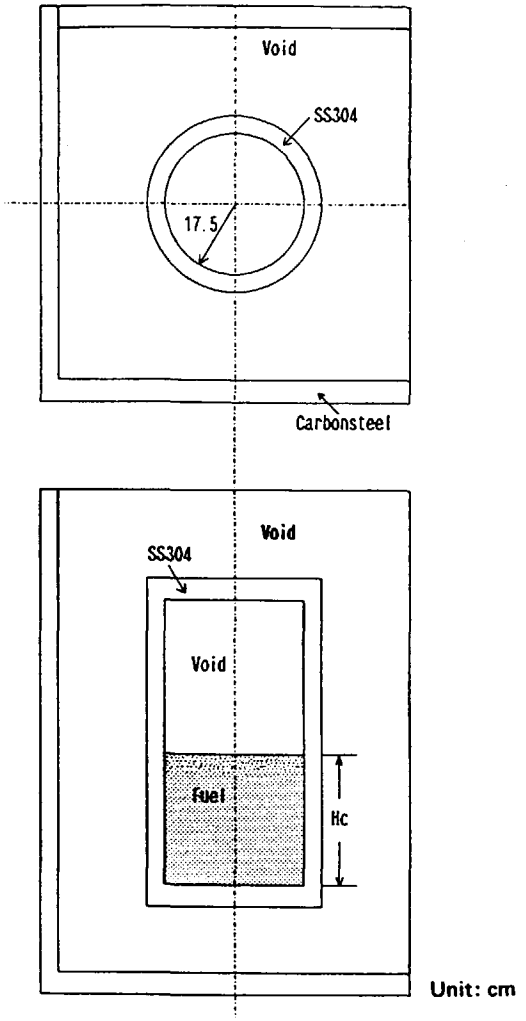

Fig. 9 Calculational model

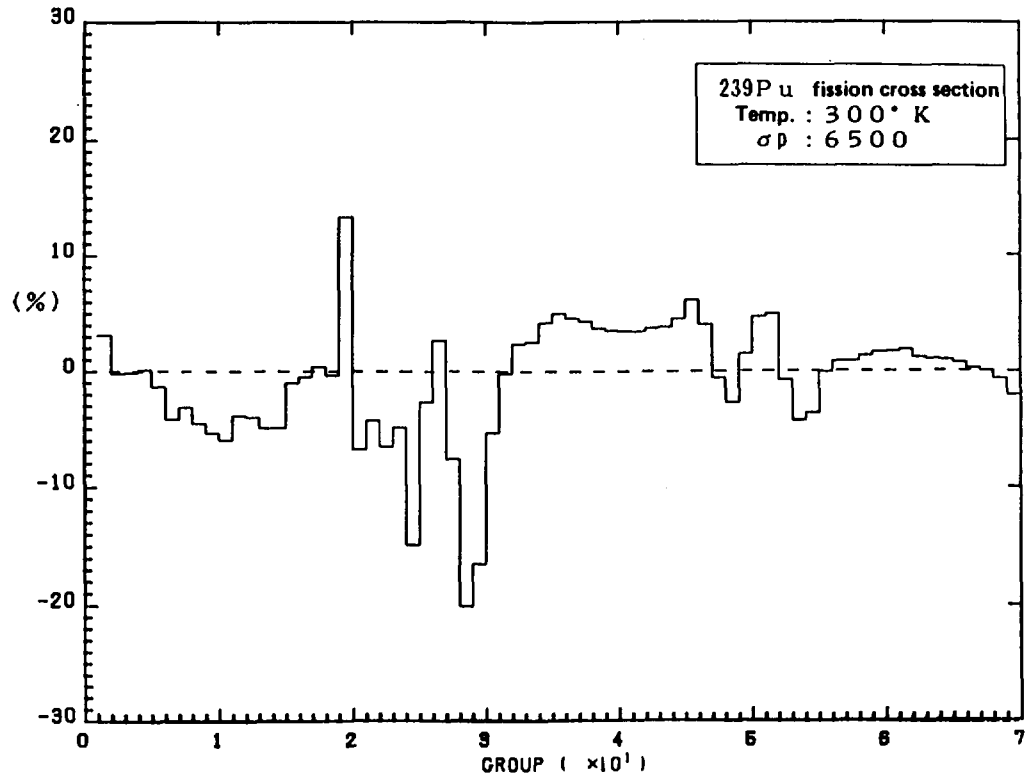

Fig. 10 Comparison between JENDL-3T and JENDL-2

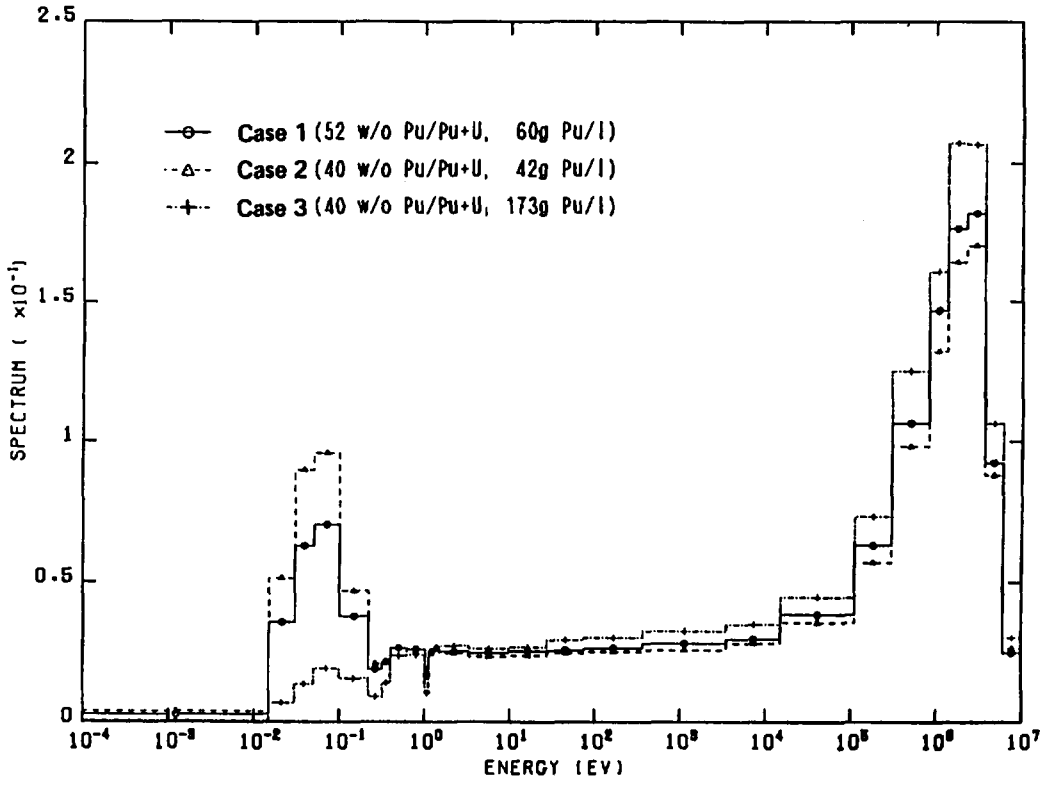

Fig. 11 Neutron energy spectrum of MOX nitrate solution

2.6.2 Synchrotron Radiation Project and Related Nuclear Data and Atomic and Molecular Data

Yohta Nakai

Atomic and Molecular Physics Laboratory, Department of Physics

Japan Atomic Energy Research Institute

Devolopement and construction of large synchrotron radiation project has been started in cooperation with Japan Atomic Energy Rsearch Institute and The Institute of Physical and Chemical Research Institute. The first photon beam of synchrotron radiation will be expected in 1995.

The synchrotron radiation system of this project consists of four main components; they are (1) Injection linear electron accelerator,(2) Synchrotron electron accelerator ring,(3) Synchrotron storage ring,and (4) Photon beam transport systems. A brief sketch and the design specifications are shown in Fig.1 and Table 1.

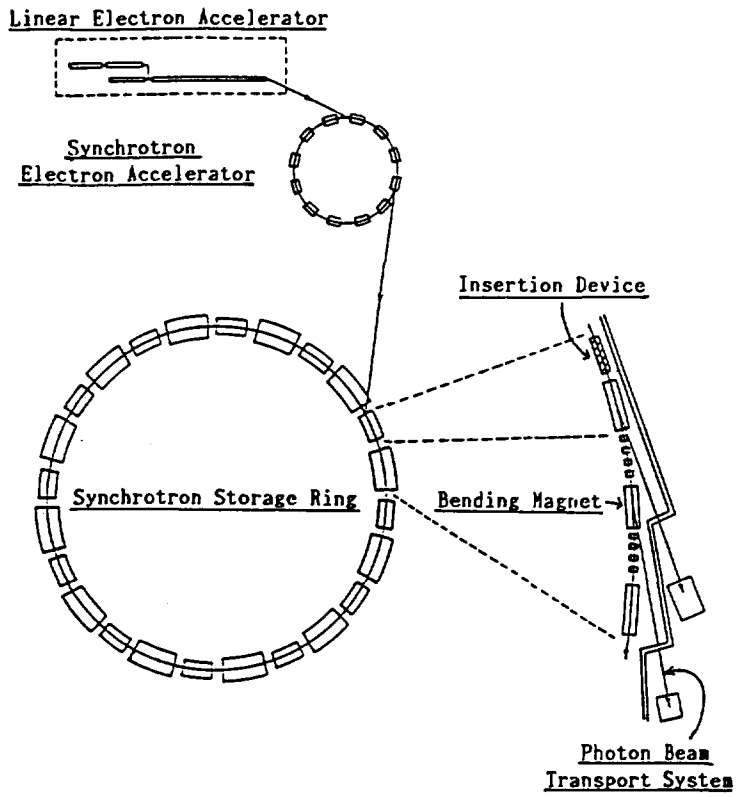

Fig. 1 Brief sketch of the syncrotron radiation system

Table 1 Design specifications of synchrotron radiation system

(1) Linear Electron Accelerator		
Injection Energy		1.5 GeV
Average Beam Current		18 μA
Length		150 m
Energy Width		1.0 %
Emittance		3.1×10^{-5} mrad
(Positron Energy)		250 MeV
(2) Synchrotron Electron Accelerator		
Injection Energy		8.0 GeV
Beam Current		10 mA
Bending Magnet Field		0.7 T
Circumference		471.5 m
Energy Width		0.1 %
Emittance	Horizontal	1.19×10^{-7} mrad
	Vertical	1.20×10^{-8} mrad
(3) Synchrotron Storage Ring		
Storage Energy		8.0 GeV
Storage Beam Current		100 mA
Bending Magnet Field		0.6 T
Circumference		1478.4 m
Energy Width		0.1 %
Emittance	Horizontal	4.89×10^{-9} mrad
	Vertical	0.49×10^{-9} mrad
RF Frequency		500 MHz

Synchrotron radiation has a number of outstanding properties:

(1) Continuum from the infrared out to the X-ray region.

(2) High intensities, storage rings are emitting 1 kW to several MW of synchrotron radiation.

(3) High degree of collimation.

(4) Polarization, completely linear in the plane of orbit.

(5) Elliptical polarization in the "wings" above and below the plane of the orbit.

(6) High brilliance of the source, because of the small cross section of the electron beam and the high degree of collimation of the radiation.

(7) Time structure, pulse duration as short as 50 ps.

(8) Quantitatively known characteristics.

(9) Clean environment (10^{-9} to 10^{-10} Torr) and high stability of the electron beam.

Thus, the synchrotron radiation bridges the large gap between the far UV and the X-ray range as well as being a unique X-ray source, and the unique combination of the above characteristics offers far-reaching possibilities for many fields of science and technology.

Fig. 2 presents the spectral distributions of brilliance of 8 GeV synchrotron radiation for the bending magnet, undulator and wigglar.

Nuclear data and atomic and molecular data related to the 8 Gev Synchrotron Radiation Project can be classified into two categories; one is for the machine side, other for the data production by using the synchrotron radiation.

Synchrotron electron accelerator and storage ring have 8 GeV and high current (10 and 100 mA respectively) electron beams. When these beams hit the materials such as constructive or surrounding ones, high energy Bremsstrahlung photons are produced with high

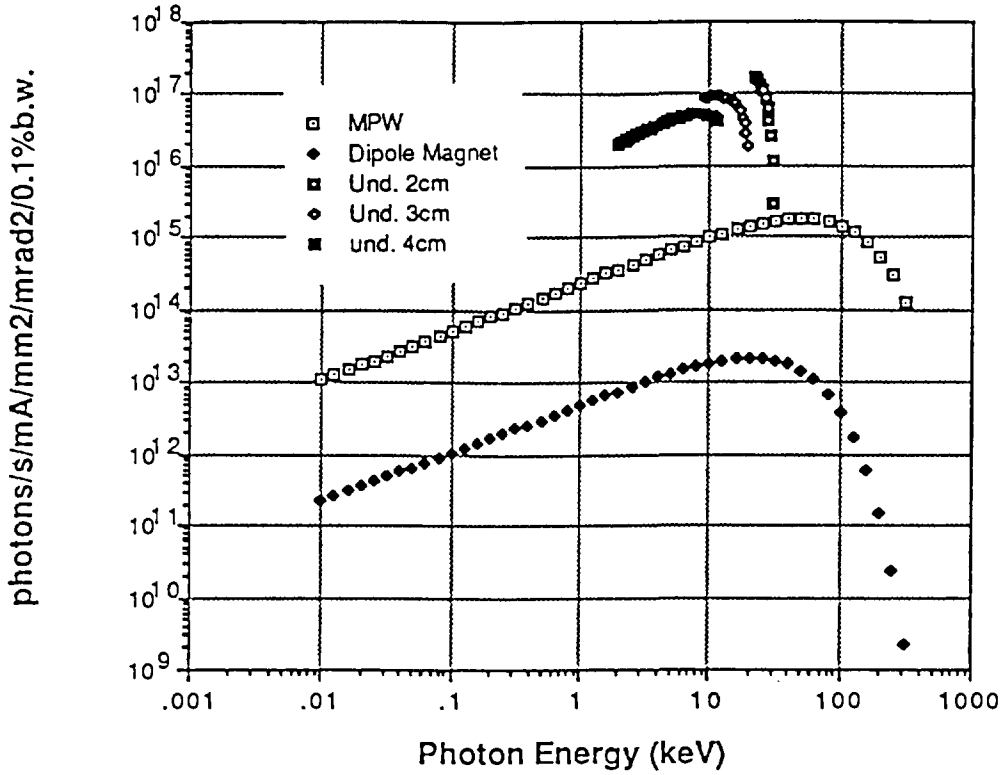

Fig. 2 The spectral distributions of brilliance of 8 GeV synchrotron radiation

conversion efficiencies. Fig.3 shows an example of Bremsstrahlung (radiation) yield for 10 keV to 10 GeV electron on iron target. And Fig.4 presents the photon attenuation coefficient data in iron which is needed to know the number and energy deposition in such materials.

Therefore, the photo nuclear data of these energy region is needed for safety and material reliability evaluation.

Electron stopping power and range data are also important for these problems. The examples of these data are shown in Figs.5 and 6.

We have been started to compile and evaluate these photon and electron data in related energy range for all kind of elements and important compounds, and some of these data are already stored in our computer.

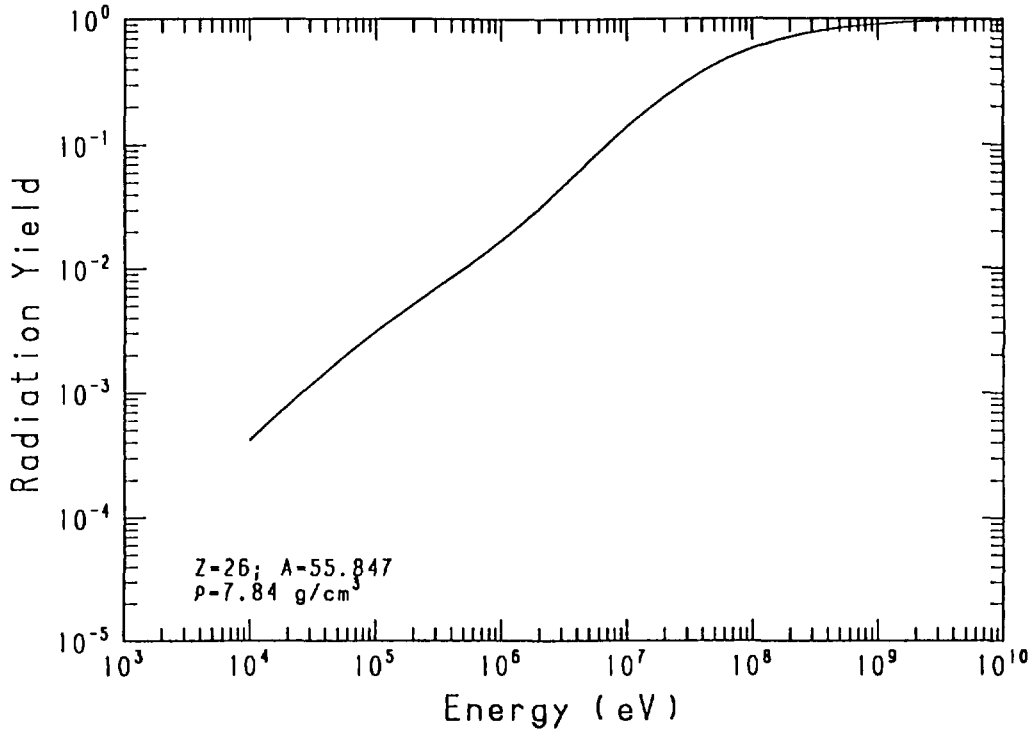

Fig. 3 Bremsstrahlung (radiation) yield for electron in Fe

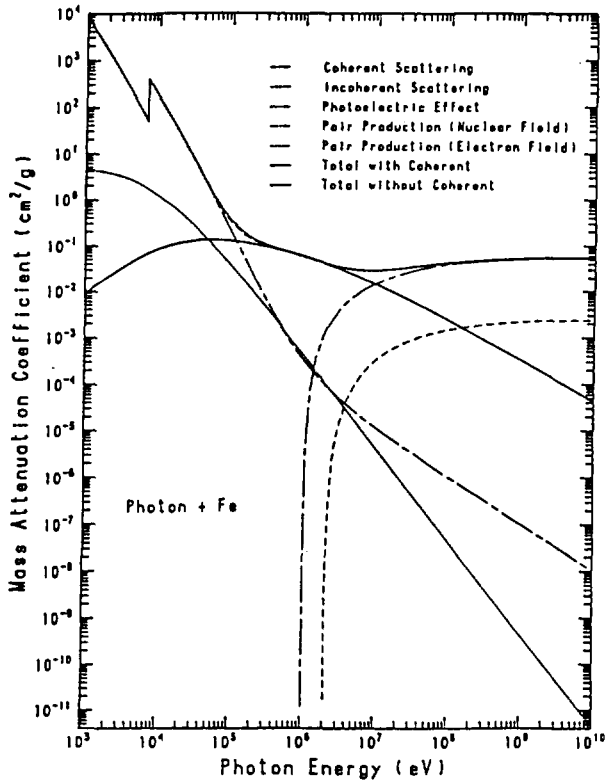

Fig. 4 Photon attenuation coefficient in Fe

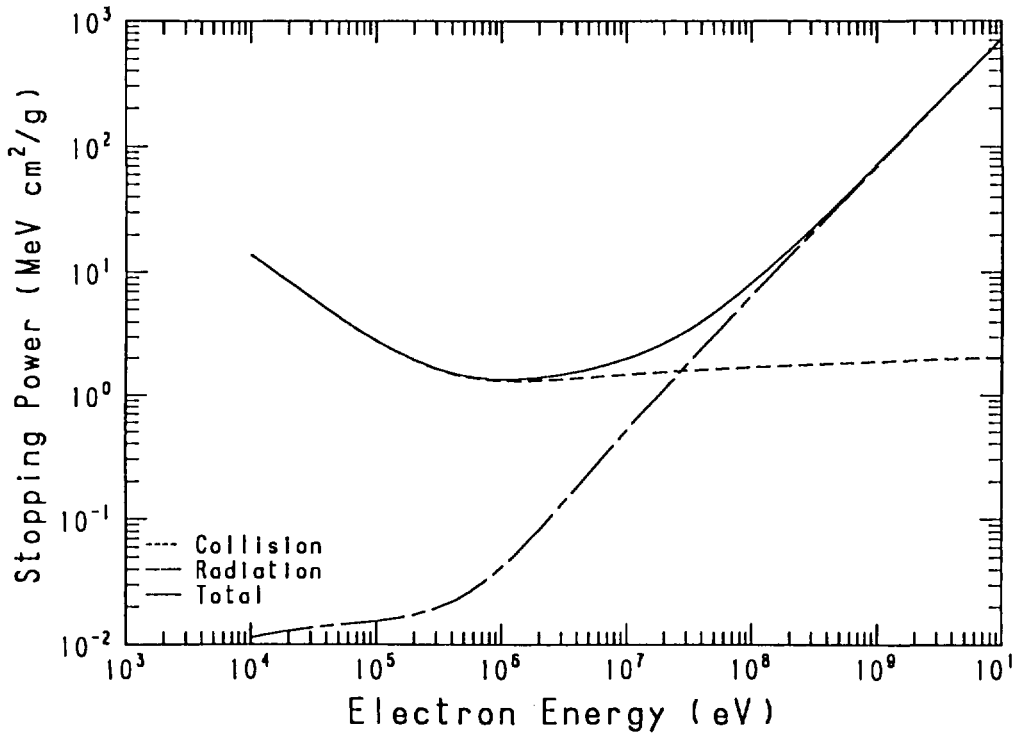

Fig. 5 Stopping power of electron in Fe

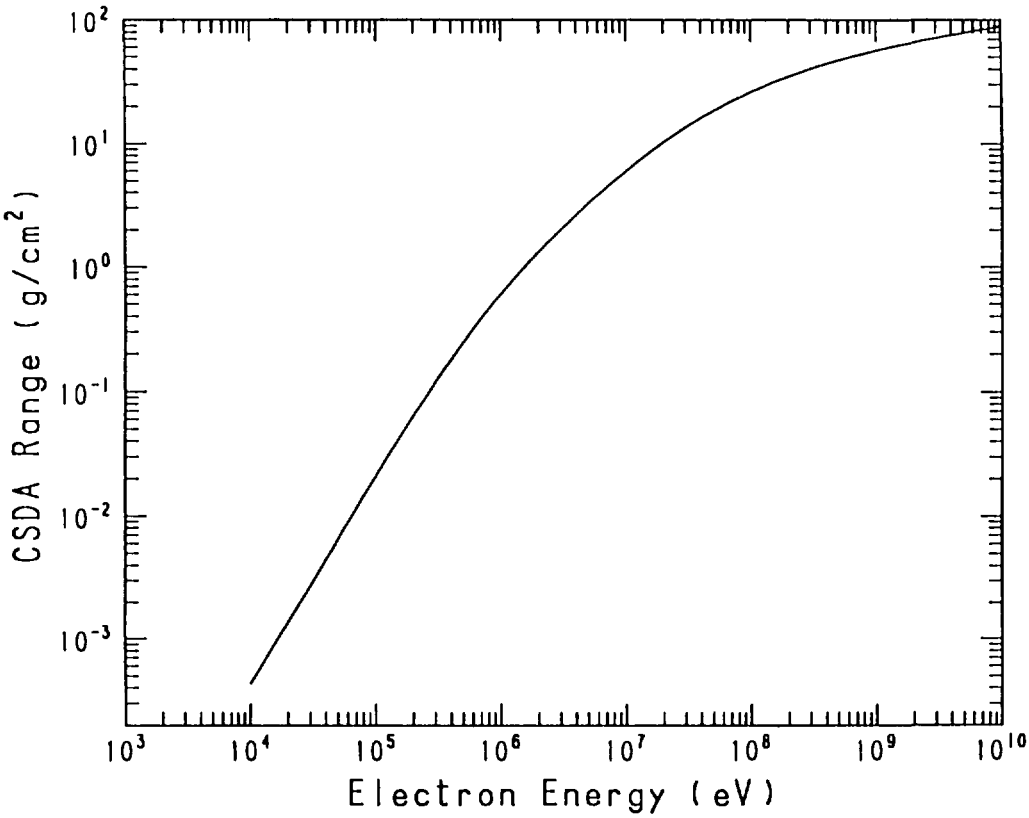

Fig. 6 Continuous slowing down range of electron in Fe

In atomic and molecular physics, the synchrotron radiations offer the unique possibilities to tune the excitation energy in optical or photoelectron emission experiments so as to optimally probe binding energies ranging from those of loosely bound outer electrons up to energies corresponding to the most tightly bound core levels as shown in Fig.7. The studies include ground state systems as well as highly excited and ionized states, which may provide useful informations for fusion plasma diagnostics.

Fundamental quantities,such as binging energies, their shifts in molecular enviroments, potential curves and photon energy dependent cross sections may be determined over extended energy range. In addition to the static properties determining the energetic structure of the system, dynamical processes, such as relaxation and energy transfer processes, are recieving increasing attention. All of these studies, which originate from the interaction between light and electronic charge, are the basis for further developements and refinements of theoretical models.

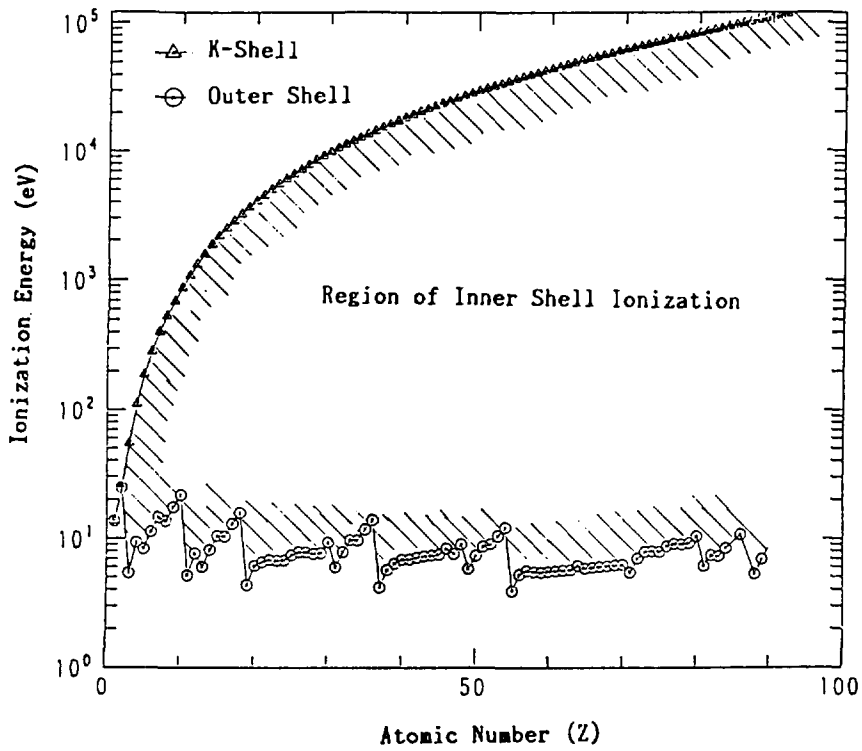

Fig. 7 Inner shell ionization energy of atoms

3. Papers Presented in Poster Session

3.1 Experimental Study of Resonance Interference between Th-232 and U-233

Y.Fujita, K.Kobayashi, S.M.Lee*
Research Reactor Institute, Kyoto University
and
I.Kimura
Faculty of Engineering, Kyoto University

Abstract

A preliminary result is reported for an experiment of the effective U-233 neutron cross section in its unresolved energy region shielded with the resonance structure of Th-232 in reactors. The experiment is an extension of the transmission and self-indication measurement which can determine the self-shielded cross section of a reactor material. In the present experiment, neutrons transmitted through thorium samples of several thicknesses are detected with the B-10(n,gamma) and U-233(n,absorption)reactions. The former is the transmission measurement and the latter may be called a mutual-indication measurement. Considerable improvements in the experimental technique are still needed to escape from the intense gamma-ray background come from the U-233 indication sample.

1. Introduction

The practical computational treatment of neutron absorption in fast reactors in the energy region of the unresolved resonances of core materials is characterized by several approximations. Some of these approximations are : statistical treatment of the unresolved resonances using mean resonance parameters, use of narrow resonance approximation and

---

Present address: Indira Gandhi Center for Atomic Research, Kalpakkam 603-102, India.

neglect of interference between resonances. The success of the practical computational methods shows that in general the overall effect of the approximations on the reactor integral parameters must be small. However, it is also known that the calculation of accurate self shielded cross sections in the unresolved resonance region and the calculation of parameters (like the Doppler coefficient) which depend on the temperature derivatives of the self shielding factors are affected significantly by the approximation made. In actual practice the cross section and its processing procedures are expected to be validated by reactor critical experiments. The critical experiments, however, are usually involve many materials in heterogeneous arrangement and the neutron flux exhibits complex spatial dependence. It consequently becomes difficult to evaluate the contribution of different effects to an overall discrepancy between experiment and calculation. There have been several measurements to directly determine self-shielding factors of neutron cross sections by making the transmission and self-indication measurement/1,2,3,4,5,6/. The nuclear data uncertainty and the cross section processing approximations are tested by escaping from the approximations in reactor geometry and neutron transport modeling. The results of these measurements would appear to serve more as benchmarks against which the basic cross section representations and processing methods can be tested rather than as input data for reactor computations.

We propose a transmission and mutual indication experiment as an extension of the transmission and self indication experiment. By the experiment, one can test the treatment of the overlap and interference between resonances of different nuclides. We attempt to apply the experiment to the case of U-233 and Th-232. It is presently in a preliminary stage and this report is of preliminary nature.

2. Mutual Indication Experiments

In multigroup cross section processing for reactor computations the gth group cross section of reaction x of isotope i in a particular region is derived from a ratio of integrals of the form:

$$\sigma^{i}_{xg} = \frac{\int_{\Delta Eg} \sigma^{i}_{x}(E)\ \phi(E)dE}{\int_{\Delta Eg} \phi(E)dE} \qquad (1)$$

Here $\phi(E)$ is the flux spectrum which varies from region to region in the reactor and has to be calculated from a slowing down equation approximate

to the reactor region and its fine spatial heterogeneities. For the calculation of the cross section in the resonance region and in the calculation of effective resonance integrals the group cross sections for a homogeneous reactor region are obtained from integrals of the form:

$$\sigma^i_{xg} = \frac{\int_{\Delta Eg} \frac{\sigma^i_x(E)}{\Sigma_t(E)} S(E)dE}{\int_{\Delta Eg} \frac{1}{\Sigma_t(E)} S(E)dE} \tag{2}$$

Here, $\sum_t(E)$ is the total macroscopic cross section and S(E) is the collision density in the concerned region. In practical fast reactor computations often further approximations are made in the computation of the above integrals as for example the ABBN procedure/7/.

The above integrals for cross sections of interest can be experimentally measured by time of flight measurements using a transmission sample of reactor composition to define $\sum_t(E)$, and indication sample defining $\sigma^i_x(E)$, as indicated schematically in Fig.1. Experimentally, one measures for various thicknesses of the transmission sample the transmission ratio given by,

$$T_g(t) = \frac{\int_{\Delta Eg} e^{-\Sigma_t t} S(E)dE}{\int_{\Delta Eg} S(E)dE} \tag{3}$$

Similarly, with the thin (no self shielding) indication sample and for various thicknesses of the transmission sample the indication ratio is obtained,

$$R_g(t) = \frac{\int_{\Delta Eg} \sigma^i_x(E)\, e^{-\Sigma_t t} S(E)dE}{\int_{\Delta Eg} \sigma^i_x(E)\, S(E)dE} \tag{4}$$

From the experimental measurement of $T_g(t)$ and $R_g(t)$ one can evaluate,

$$\int_0^\infty T_g(t)dt = \frac{\int_{\Delta Eg} \frac{1}{\Sigma_t(E)} S(E)dE}{\int_{\Delta Eg} S(E)dE} \tag{5}$$

$$\int_0^\infty R_g(t)dt = \frac{\int_{\Delta Eg} \frac{\sigma_x^i(E)}{\Sigma_t(E)} S(E)dE}{\int_{\Delta Eg} \sigma_x^i(E)\ S(E)dE} \tag{6}$$

Thus we get,

$$\frac{\int_0^\infty R_g(t)dt}{\int_0^\infty T_g(t)dt} = \frac{\int_{\Delta Eg} \frac{\sigma_x^i(E)}{\Sigma_t(E)} S(E)dE}{\int_{\Delta Eg} \frac{1}{\Sigma_t(E)} S(E)dE} \Bigg/ \frac{\int_{\Delta Eg} \sigma_x^i(E)\ S(E)dE}{\int_{\Delta Eg} S(E)dE} \tag{7}$$

Eq.(7) gives the ratio of the self shielded cross section of reaction x of isotope i approximate for reactor mixture $\sum_t(E)$, to the infinite dilution cross section for the same reaction. It is to be noted that the effects of overlap of resonances are automatically included in the above measured ratio. Generation of similar ratio from the evaluated nuclear data files by cross section processing codes will serve to validate their capability to determine accurate self shielded cross sections.

We attempt to apply the above measurements to determine the magnitude of resonance overlap between Th-232 and U-233 and to provide data which can be used to check the capability of existing evaluated nuclear data files and processing codes to compute this effect.

In the present study with thorium transmission sample and U-233 indication sample the measured ratio in Eq.(7) becomes:

$$\frac{\int_0^\infty R_g(t)dt}{\int_0^\infty T_g(t)dt} = \frac{\int_{\Delta Eg} \frac{\sigma_{c+f}^{U-233}(E)}{\sigma_t^{Th}(E)} \cdot \frac{dE}{E}}{\int_{\Delta Eg} \frac{1}{\sigma_t^{Th}(E)} \cdot \frac{dE}{E}} \Bigg/ \frac{\int_{\Delta Eg} \sigma_{c+f}^{U-233}(E) \cdot \frac{dE}{E}}{\int_{\Delta Eg} \frac{dE}{E}} \tag{8}$$

In the case the resonance overlap and interference is negligible the ratio will be near unity. The deviation of the ratio from unity indicates the degree of resonance overlap correction in the different energy groups. If there is appreciable overlap effect in some of the energy groups the the measured data provides useful information for testing the capability of the nuclear data files and the processing codes to reproduce this effect. Needless to say for processing procedures which neglect the overlap effect, like for example the ABBN procedure, the above ratio will be calculated as unity for all the energy groups.

3. Experiment and Preliminary Results

The experiment has been carried out using the neutron beam obtained by the neutron time of flight spectrometer installed at the electron linear accelerator facility of Kyoto University Research Reactor Institute. Essential part of experimental arrangement is shown in Fig.1. Photo neutrons were produced by a water-cooled tantalum target and were moderated to eV-keV energies by a water moderator. As the energy resolution is not essential in this experiment, a 6.5-m flight path of rather short length was employed to attain a better signal to background ratio. The transmission samples were stacked thorium metal plates and their thicknesses were varied from 0.5 mm to 3.81 cm. During the measurement, the samples were repeatedly changed with a few minutes interval by an automatic sample changer. The indication sample is a boron-10 powder sample canned in an aluminum case for the transmission measurement, and a 2 mm thick plate of U_3O_8-Al alloy for the indication measurements. The U-233 content in the plate is about 11 mg/cm^2. A pair of C_6D_6 scintillators, 10 cm in diameter and 3 cm in thickness, was used for the detector. The detector counts the fission and capture events in the U-233 sample and the 480 keV gamma rays in the B-10 sample.

Typical time of flight spectra are shown for B-10 and U-233 samples in Fig.2 (a),(b) respectively. The spectra were obtained with a 0.5 mm Cd overlap filter, and the background spectra were determined by the notch filter method using Na, Mn, Co and Ag filters. The high background level for U-233 comes from the gamma rays of the daughter nuclides in the U-decay chain.

Preliminary results of transmission and indication curves vs. the thickness of transmission samples are shown in Fig.3(a),(b),(c),(d). The case (a) is the energy region bunched between 4 and 30 keV which is the unresolved energy region for both of U-233 and Th-232. The transmission and indication curves are close and the ratio is near unity as a priori expected, since many resonances are involved in the energy interval and the statistical treatment is justified. The cases (b) and (c) are for energy regions, resolved for Th-233 and unresolved for U-233 in the evaluation of JENDL. The ratios deviate from unity in these cases, and the deviation may indicate that one cannot ignore the interference effect in the treatment of cross sections in this energy range. In other words, one needs to raise the lower energy limit, 100 eV, of the unresolved energy region of U-233 to a higher value. The case (d) is an example of curves in the energy where

dominant resonances of Th-232 and U-233 overlap.

The experiment is in a preliminary stage and the report is preliminary nature. The experimental error has not been examined and, naturally, the discussion of the results should be limited.

References

(1) Byoun T.Y., Block R.C. and Semler T.: CONF 720901, 1115(1972).
(2) Arnaud A. et al.: CONF 750303, 961(1975).
(3) Bakalov T. et al.: Proc. Conf. Nuclear Cross Sections for Technology, Knoxville p.692 (1979).
(4) Fujita Y., Kobayashi K., Yamamoto S., Kimura I. and Oigawa H.: Proc. Kiev Conf. on Neutron Physics, Vol.2, p.195, (1987).
(5) Vankov A.A., Ukraintsev V.F., Yaneva N., Tashkov S.,Mateeva A.: Nucl.Sci. Eng., 96, p.122 (1987).
(6) Bakalov T.,Ilchev G., Taskov S., Tran Khanh Mai, Janeva N., Vankov A.A., Grigoriev Yu.V., Ukraintsev V.F.: Proc. Int. Conf. Nuclear Data for Science & Technology, Antwerp,(1982).
(7) Abagyan L.P., Bazazyants N.O., Bondarenko I.I., and Nikolaev M.N.: Group Constants for Nuclear Reactor Calculations, Consultants Bureau, New York (1964).

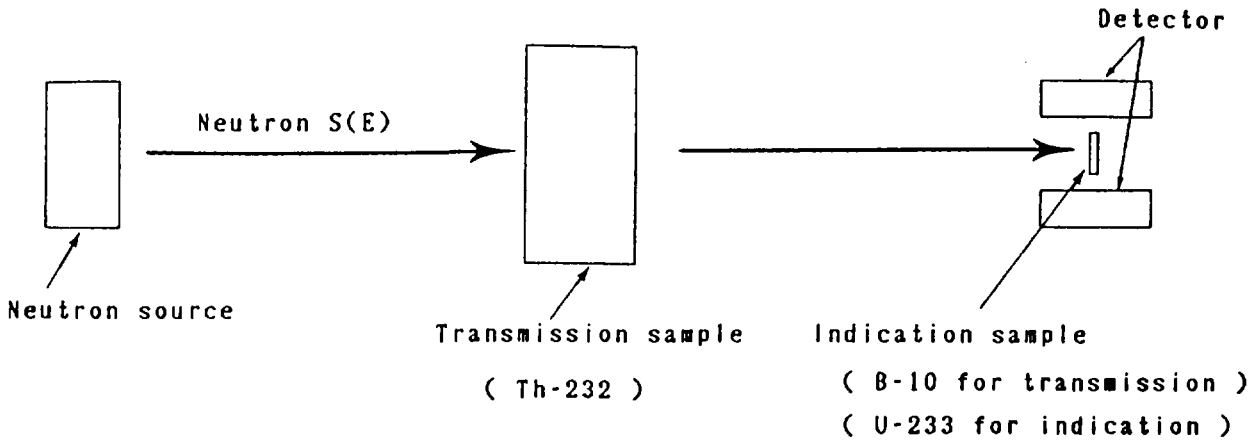

Fig. 1 Arrangement of the transmission and indication experiment.

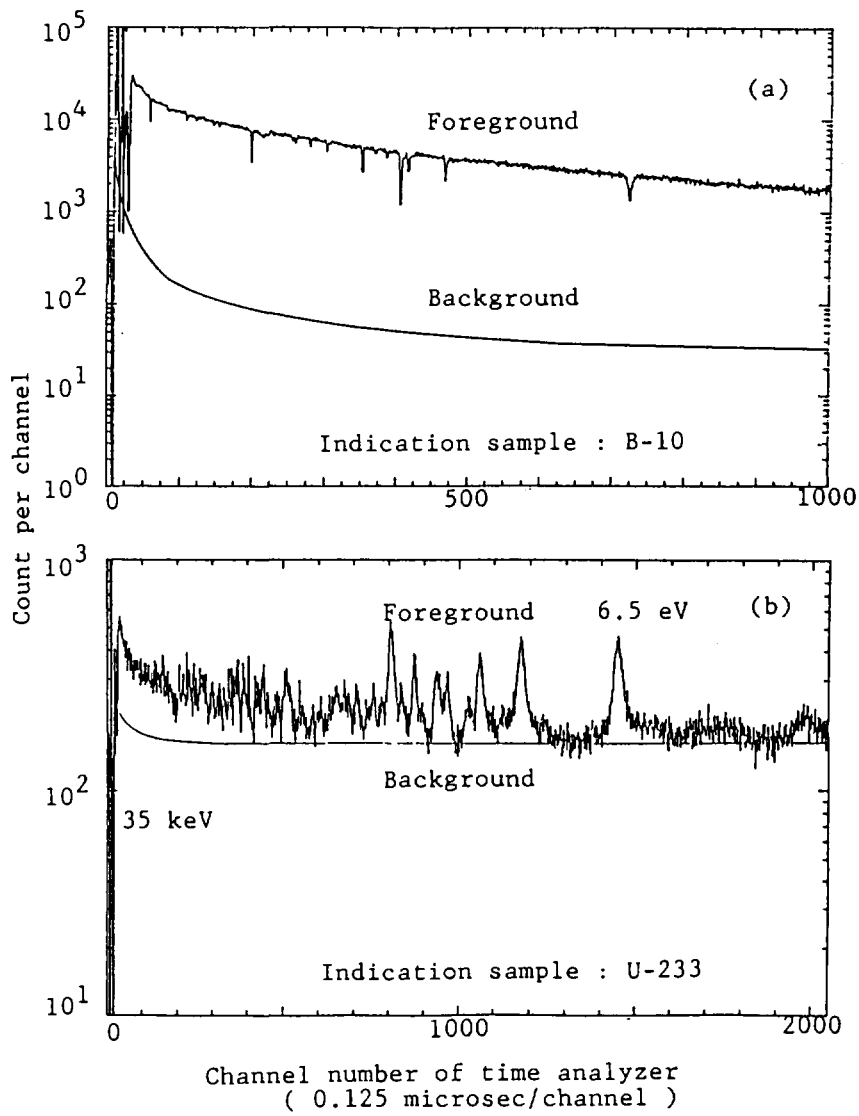

Fig. 2 Typical time of flight spectra of the C_6D_6 detector, (a) for B-10 and (b) for U-233 samples.

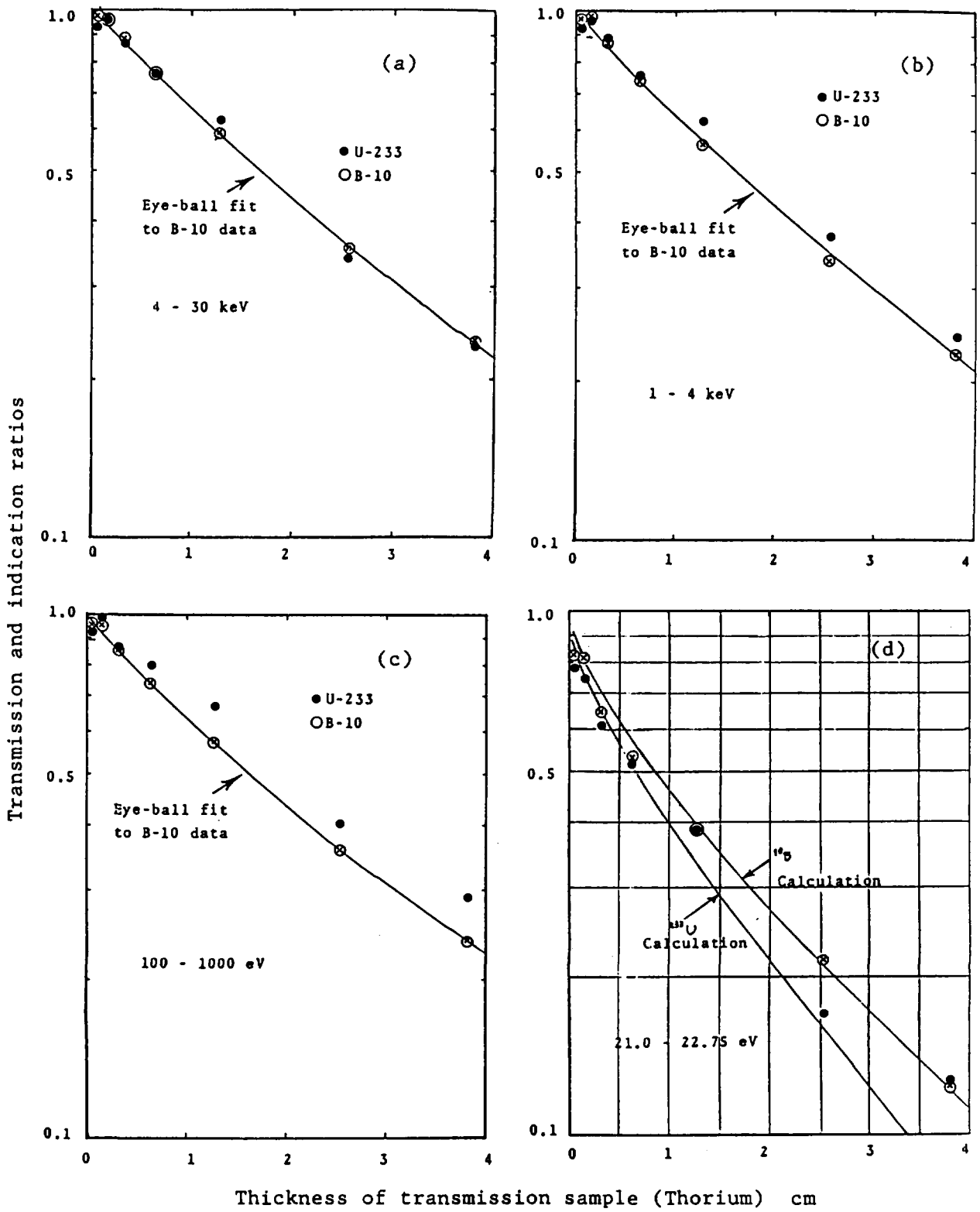

Fig. 3 Transmission and indication ratios vs. thicknesses of transmission sample, (a) for 4-30 keV, (b) for 1-4 keV, (c) for 100-1000 eV and (d) 21.0-22.75 eV.

3.2 Application of a Resonance Capture Detector to the Neutron Total Cross Section Measurements of Polyethylene and Lead

Katsuhei Kobayashi, Shuji Yamamoto and Yoshiaki Fujita
Research Reactor Institute, Kyoto University
Kumatori-cho, Sennan-gun, Osaka 590-04

A resonance capture detector, which is composed of eight pieces of BGO crystals and a capture sample of Ta, has been newly developed. This detector gave a good signal-to-noise ratio at the Ta resonances of 4.28, 10.4, 14.0, 23.9, 35.9 and 39.1 eV in the linac TOF spectrum.

At first, the detector has been used for the measurement of well decided neutron total cross section of polyethylene. The results obtained at the resonance energies showed quite a good agreement with those from the ENDF/B-IV data. This fact verified that the detector was usable for the TOF measurement of neutron total cross sections.

Next, the detection system has been applied to the measurement of neutron total cross section of lead at the above six energies. All of the results were about 11.2 b and constant with neutron energy. The accuracy of the measurement could be achieved with the standard deviation of 0.6 to 1.8 %. The present values are in good agreement with the ENDF/B-V data and with the measurements made by Waschkowski et al. and Adamchuk et al.

I INTRODUCTION

Precise measurement of nuclear data in the field of reactor physics is of great importamce for the safety design of nuclear reactors and for the evaluation of neutron flux density and/or energy spectrum around a reactor. From these points of view,

many efforts to obtain the accurate nuclear data have been made. One of the candidate techniques is that to use neutron flitered beams using such as thick Fe or Si material, which produces a well-isolated group of passed-through neutrons with an extremely low background of gamma-rays and off-energy neutrons[1,2].

We have paid attention to the signals from resonance captures which give high counts at the resonances and low counts in the off-resonance region. A resonance capture detector, which is composed of an adequate capture sample and $Bi_4Ge_3O_{12}$ scintillators, has been newly developed. When the detector is combined with a time-of-flight (TOF) measurement, the time spectrum shows a count peak corresponding to the each resonance for the capture sample. The spectral shape is very similar to that of the filtered neutrons, and it is expected that the good signal-to-noise ratio can be achieved in the resonance energy region.

In the present experiment, the detection system with a capture sample of Ta has been applied to the neutron total cross section measurement of polyethylene, at first, by the TOF method using an electron linear accelerator. By comparing the results at the Ta resonances from 4.28 to 39.1 eV with those from the evaluated nuclear data, the validity to use this resonance capture detector has been tested as a neutron detector for the TOF measurement. Thereafter, the neutron total cross section of lead has been measured with this detection system.

II RESONANCE CAPTURE DETECTOR

A $Bi_4Ge_3O_{12}$ (BGO) crystal has a high specific weight of about 7.13 g/cm^3 and it is expected to be applied to the measurement of capture gamma-rays as a total absorption detector. We have prepared eight pieces of BGO scintillators, each size 5 x 5 cm square and 7.5 cm, and assembled a scintillation bank to

have a through hole, 2.7 x 2.7 cm square, as shown in Fig. 1. Inside of the hole in the BGO scintillation bank was covered with enriched lithium-6 tiles of ^{6}LiF 3 mm thick, to absorb neutrons scattered by the capture sample. The characteristics of this detection system have been obtained and the applicability has been verified as a capture detector[3,4].

A Ta plate, 1.8 x 1.8 cm square and 1 mm thick, was placed as a capture sample at the center of the detector hole. The detector composed of the BGO scintillators and the Ta sample are sensitive to neutrons, especially at resonance energies for the Ta(n,r) reaction. Then, the detector gives high count peaks corresponding to the Ta resonances at 4.28, 10.4, 14.0, 23.9, 35.9 and 39.1 eV and so on in the time-of-flight (TOF) spectrum. In the off-resonance energy region, the event signals are quite low comparing to those at the resonances. Then, the TOF spectrum shape is very similar to that obtained from a neutron-filtered beam by the TOF method using such as thick Fe or Si materials[1,2]. A good signal-to-noise ratio can be expected in the resonance peak region with this neutron detector.

For the background measurement, a Ta plate of 2 mm thickness, which is same material as the capture sample, was inserted into the TOF beam. This is called self-indication measurement[5,6], which gives the background level at the Ta resonances as a saturated black region of signals in the TOF spectrum. Then, it could be possible to derive the background accurately.

The capture detection system consisted of eight pieces of BGO scintillators was separated into two parts; left half of the system by four pieces of scintillators and the other right half, as seen in Fig. 1. Coincidence measurement was made for these two segments of the detectors to reduce the background counts and improve the signal-to-noise ratio.

Neutron total cross sections of H and C are thought to be a well decided standard cross sections. In order to investigate

the validity of this resonance capture detector as a neutron detector for the TOF measurement, in the present study, total cross section of polyethylene has been measured firstly. Accurate results have been obtained and the values have been in good agreement with the expected data from ENDF/B-IV, so that the detection system has been verified to be superior in the precise total cross section measurement by the TOF method.

III EXPERIMENTAL METHOD

3.1 Transmission Samples

As the transmission samples, polyethylene and lead were selected; (1) two kinds of polyethylene samples were plate of 7 x 7 cm square and 0.5 cm thick each, and (2) three kinds of lead samples were in the form of metallic plates, each 5 x 5 cm square and 0.5 cm thick. The purity of the polyethylene sample was checked by the Chemical Inspection & Testing Institute, Japan, and they found that the purity was very high. The purity of the lead sample was 99.9993 % and the main impurities were 0.0006 % of Bi and 0.0001 % of Sb. The physical parameters of the transmission samples are given in Table 1.

3.2 Pulsed Neutron Source

The transmission measurements were made by the time-of-flight (TOF) method using the 46 MeV electron linear accelerator (linac) at the Research Reactor Institute, Kyoto University (KURRI). Bursts of fast neutrons were produced from the water-cooled photoneutron target, which was made of several sheets of Ta plates, 5 x 5 cm square with an effective total thickness of about 3.5 cm. This target was set at the center of an octagonal water tank, 30 cm diameter and 10 cm thick, to moderate the neutron energies. A Pb block, 7 cm diameter and 20 cm long, was placed in the neutron flight path in front of the target to

reduce the gamma-flash generated by the electron burst in the target.

During the experimental series for the TOF measurement, the KURRI linac was operated at the repetition rate of 300 Hz, with the pulse width of 68 nsec, electron energy 32 MeV and the peak current 2 A. A Cd filter of 0.5 mm thickness was placed in the neutron beam to suppress overlap of thermal neutrons from the previous pulses.

3.3 Experimental Arrangement

The experimental geometry is shown in Fig. 2. The flight path used in this experiment is in the direction of 135 degree to the linac beam. The neutron collimation system was mainly composed of B_4C, Li_2CO_3, and Pb maretials, and tapered from about 12 cm diameter at the entrance of the flight tube to 2 cm at the detector. The transmission samples, which were put on an automatic sample changer, were placed at the position of about 10 m from the Ta target. The cycle time was 12 min-period per one cycle, and the time was allotted to each sample so as to minimize the statistical error in the cross section obtained.

The neutron intensity was monitored during the experiment with a BF_3 proportional counter, which was inserted in the TOF neutron beam.

As mentioned above, a new type of resonance capture detector has been prepared as a neutron detector and used to measure the transmitted TOF neutrons. The detector was located at 12.7 m distant from the photoneutron target.

Background level could be easily determined by the self-indication measurement and the resultant level was verified by using notch-filters, such as Ag and Co. Coincidence technique was also useful to achieve a good signal-to-noise ratio.

3.4 Data Taking

The block diagram of the present measurement is illustrated

in Fig. 3. Output signals from the BGO scintillation bank are led to the coincidence circuit, which makes an output signal only when any signals from the left group of the four scintillators coincide with those from the other right group. By using this coincidence technique, signal-to-noise ratio could be improved by a factor of about two, comparing with the case without coincidence.

The coincidence signals from the BGO detection system were fed into a time digitizer, which was initiated by the KURRI-linac burst, and the TOF data were stored in a data aquisition system, Canberra's series 88 multi-parameter analyzer which was linked to a PDP-11/34 computer. The TOF analyzer was operated as four 2048-channel analyzers which corresponded to each sample "in" and "out" position. Another four 2048-channel analyzers were used for the TOF measurement using the BF_3 monitor system, which was used to normalize the neutron intensity between the experimental runs.

Each set of foreground and background runs with lead and/or polyethylene samples and open beam was carried out for about 15 hours and several series of transmission measurements were made by changing the transmission samples.

Energies of the TOF neutrons from the source to detector were checked by using the resonance energies of Ta mentioned above. The measured data showed a good agreement with the resonance energy.

IV DATA REDUCTION

We have prepared Fortran programs for the data processing. After dead time correction was performed, the data corresponding to each sample thickness were summed up by taking account of the monitor counts.

A typical example of the foreground and backgorund TOF

spectra for the open beam are displayed in Fig. 4. Foreground counts were taken from the peak region between the channels at full width at half maximum (FWHM), and background values from the saturated region of the time spectrum. Ratios of noise-to-sigral were obtained by calculating their counts per channel, and the values were 0.0058 to 0.0080 at the respective resonance energies from 4.28 to 39.1 eV.

The neutron transmission rate T_i corresponding to the i-th resonance region has been obtained from

$$T_i = \frac{\{I_i - IB_i\} / M}{\{O_i - OB_i\} / MB}$$

where I_i and O_i are the sample "in" and "out" foreground counts, IB_i and OB_i are the sample "in" and "out" background counts in the i-th resonance region, and M and MB are their monitor counts which were obtained by summing up the TOF data corresponding to the relevant energy region. The open data was commonly applied to each poltethylene and/or lead samples to derive the transmission rate data and the neutron total cross sections.

V RESULTS OF THE TOTAL CROSS SECTIONS

Two kinds of neutron total cross sections for polyethylene and lead have been obtained by the linac TOF method in the eV energy region, using a resonance capture detector newly developed. Firstly, we had a couple of experimental runs with polyethylene samples, which were materials made of H and C of the well known standard cross sections. The results of the neutron total cross sections at the Ta resonance energies of 4.28, 10.4, 14.0, 23.9, 35.9 and 39.1 eV are given in Fig. 5, and show a very good agreement with the data from the evaluated data file ENDF/B-IV. Then, we could decide that the resonance capture detector has been verified to be applicable to the TOF measurement as a

neutron detector.

Secondly, the resonance capture detector has been used to measure the neutron total cross sections of Pb. Eighteen runs have been made and the results are shown in Fig. 6. The experimental error for each datum is estimated to be about 1 %, which is similar to the fluctuation range among the data points. These data have been analyzed with a least squares processing and the final results are summarized in Table 2 and in Fig. 7, where the original drawing was taken from the literature[7]. Table 2 also shows the energy width and noise-to-signal ratio at FWHM of the each resonance peak for the open TOF beam. The uncertainties in the measurements are mainly due to the statistics in the transmission rate and to the sample thickness, and the resultant standard deviation is 0.6 to 1.8 %. The six points of present values are very close to each other so that one can realize the lead cross section is constant with neutron energy.

The present results show a very good agreement with the ENDF/B-V data, and with the experimental data by Waschkowski et al.[8] and Adamchuk et al.[9]. Some other experimental results in the relevant energy region seem to be close to the present values, although they are rather old. The JENDL-2 and ENDF/B-IV data are also in good agreement with the measurement.

VI CONCLUSION

A resonance capture detector composed of eight pieces of BGO scintillators and a capture sample of Ta has been developed and applied to the neutron total cross section measurement by the linac TOF method. The detector gave a high count peak and a good signal-to-noise ratio at the resonance energies of Ta of 4.28, 10.4, 14.0, 23.9, 35.9 and 39.1 eV in the TOF spectrum.

In order to investigate the validity to use the detector as

a neutron detector for the linac TOF method, at first, the detection system has been applied to the measurement of neutron total cross section of polyethylene whose data are well decided as a standard, and the results showed a good agreement with the ENDF/B-IV data. From the results obtained, it could be verified that the resonance capture detector is superior as a neutron detector for the linac TOF measurement.

With the resonance capture detector, secondly, neutron total cross sections of lead were measured by the same manner as those for polyethylene. All of the six points of data obtained were close to each other and about 11.2 b. An accurate determination of the cross section could be achieved with the standard deviation of 0.6 to 1.8 %. The present results are in good agreement with the ENDF/B-V and with the experimental data by Waschkowski et al. and Adamchuk et al.

References

1) R. C. Block, et al.: J. Nucl. Sci. Technol., 12, 1 (1975).
2) K. Kobayashi, et al.: J. Nucl. Sci. Technol., 18, 823 (1981).
3) S. Yamamoto, et al.: Nucl. Instr. Meth., A249, 484 (1986).
4) S. Yamamoto, et al.: Proc. of Int. Conf. on Nucl. Data for Sci. Technol., held at Mito, May 30-June 3, 1988, JAERI, p.375 (1988).
5) R. C. Block, et al.: Nucl. Sci. Eng., 80, 263 (1982).
6) Y. Fujita, et al.: Proc. of Int. Conf. on Neutron Physics, held at Kiev, Sept. 21-25, 1987, Vol.2, p.195 (1988).
7) V. McLane, et al.: "Neutron Cross Sections", Vol.2, Academic Press Inc., New York (1988).
8) W. Waschkowski, et al.: Zeitschrift F. Naturforschung, Sec.A, 31, 115 (1976).
9) Yu. V. Adamchuk, et al.: Proc. of Int. Conf. on Neutron Physics, held at Kiev, 1971, Vol.1, p.124 (1972).

Table 1 Transmission samples

Sample	Thickness	
	cm	atom/b
Lead	3	0.09858±0.00020
	4	0.13152±0.00026
	5	0.16478±0.00032
Polyethylene	0.5	0.02086±0.00004
	1	0.04080±0.00008

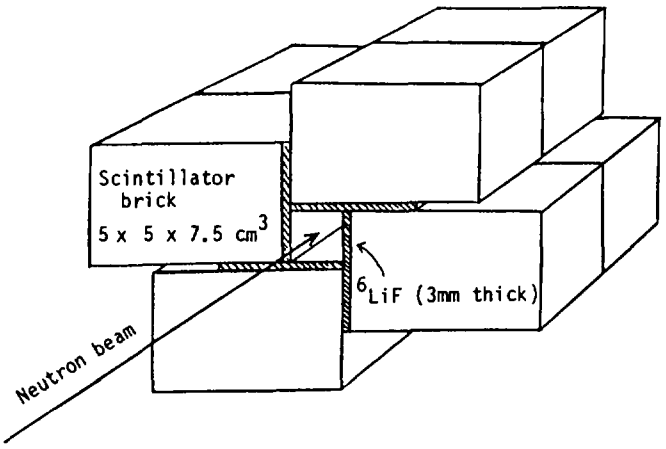

Fig. 1 Assembly of BGO scintillators.

Table 2 Neutron total cross section of lead.

Resonance energy (eV)	FWHM (eV)	Noise/Signal ratio [open beam]	Total cross section (barn)
4.28	0.30	0.0058	11.17 ± 0.025
10.4	0.34	0.0055	11.18 ± 0.036
14.0	0.26	0.0070	11.18 ± 0.051
23.9	0.54	0.0074	11.17 ± 0.040
35.9	1.17	0.0066	11.18 ± 0.037
39.1	1.11	0.0080	11.18 ± 0.045

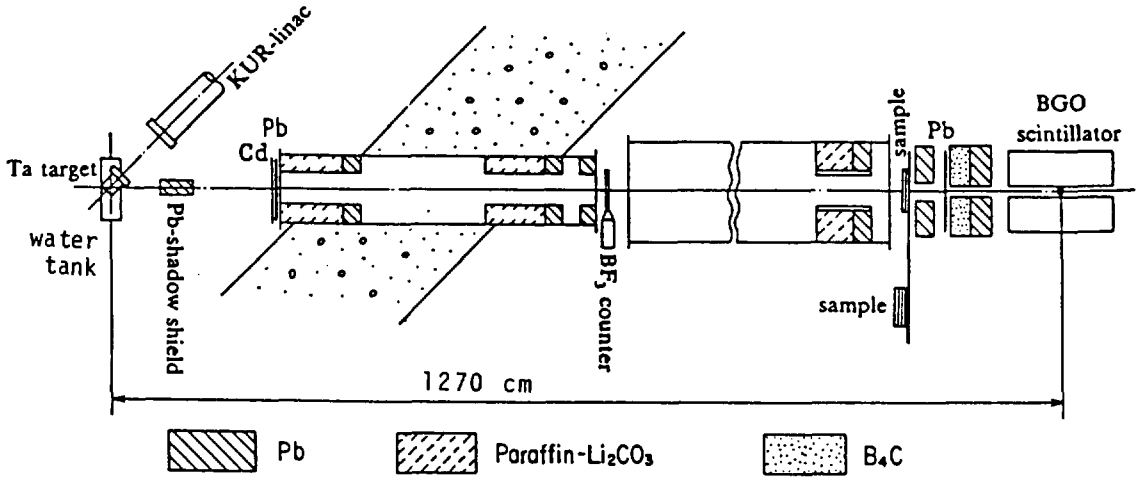

Fig. 2 Experimental arrangement for the transmission measurement.

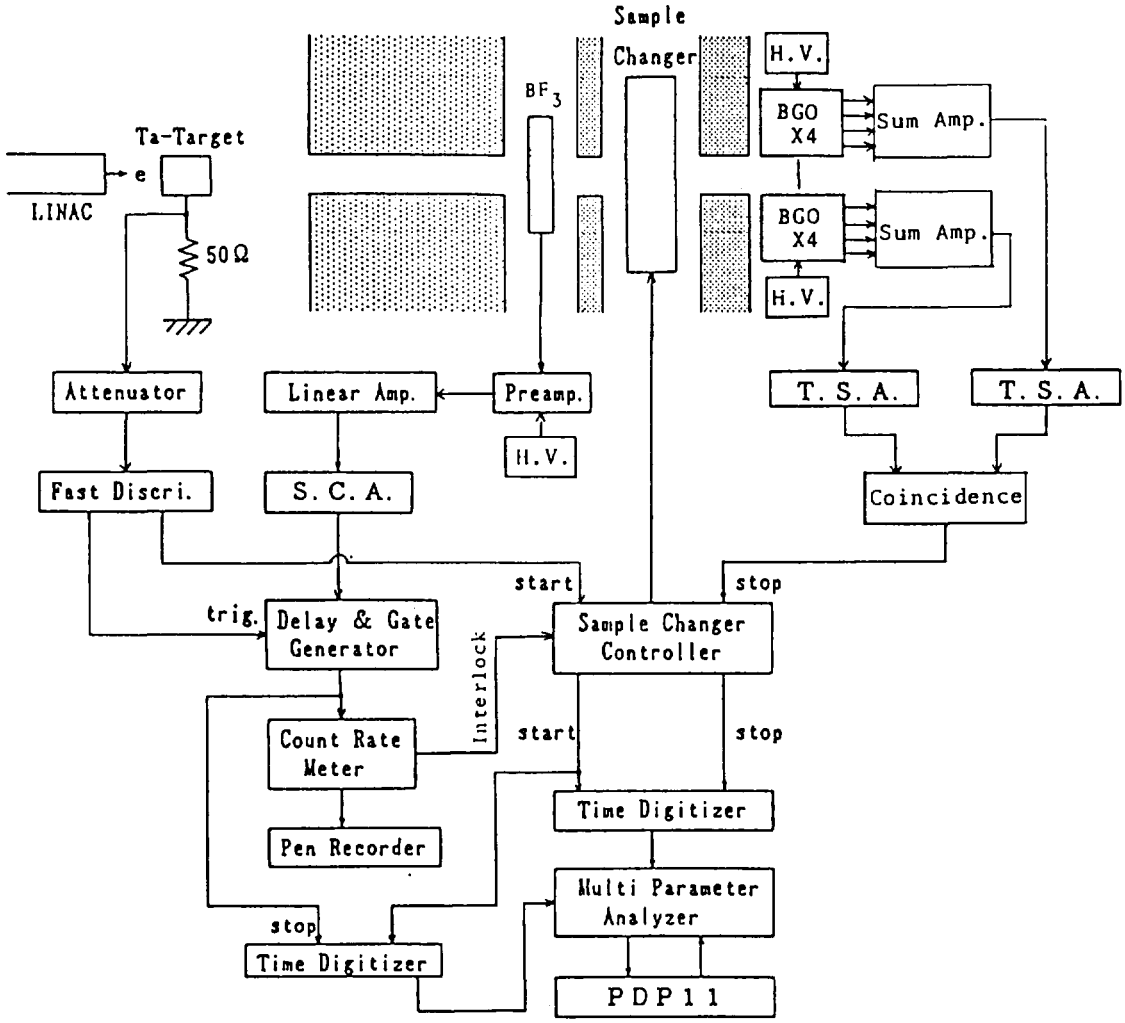

Fig. 3 Block diagram of the present measurement.

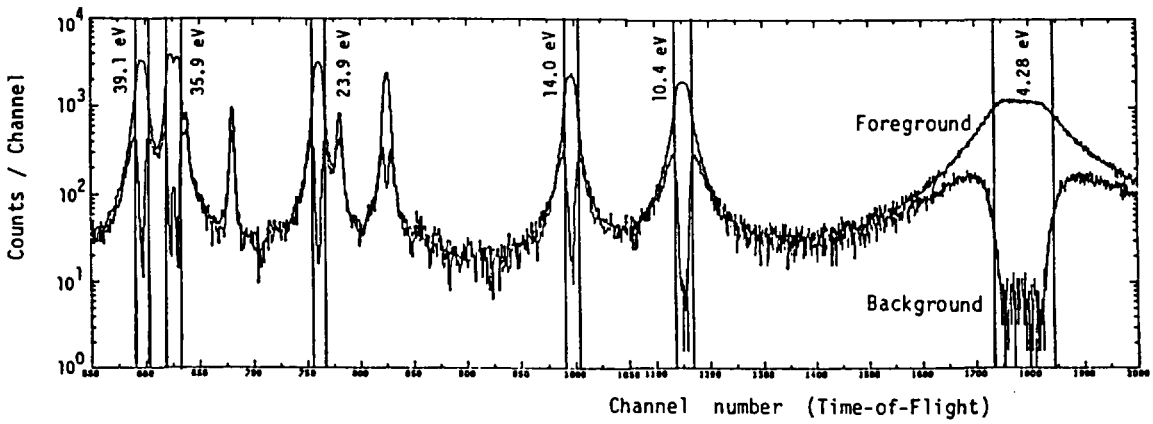

Fig. 4 An example of the foreground and background TOF spectra.

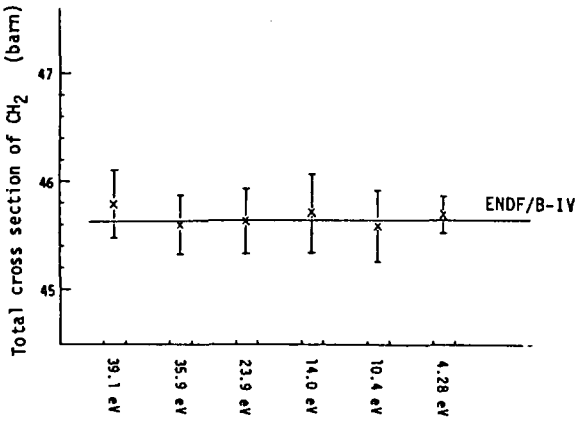

Fig. 5 Neutron total cross section of polyethylene.

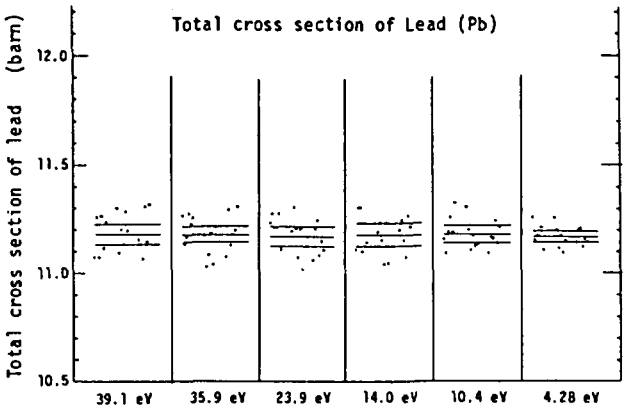

Fig. 6 Measured results of 18 runs for the neutron total cross section of lead.

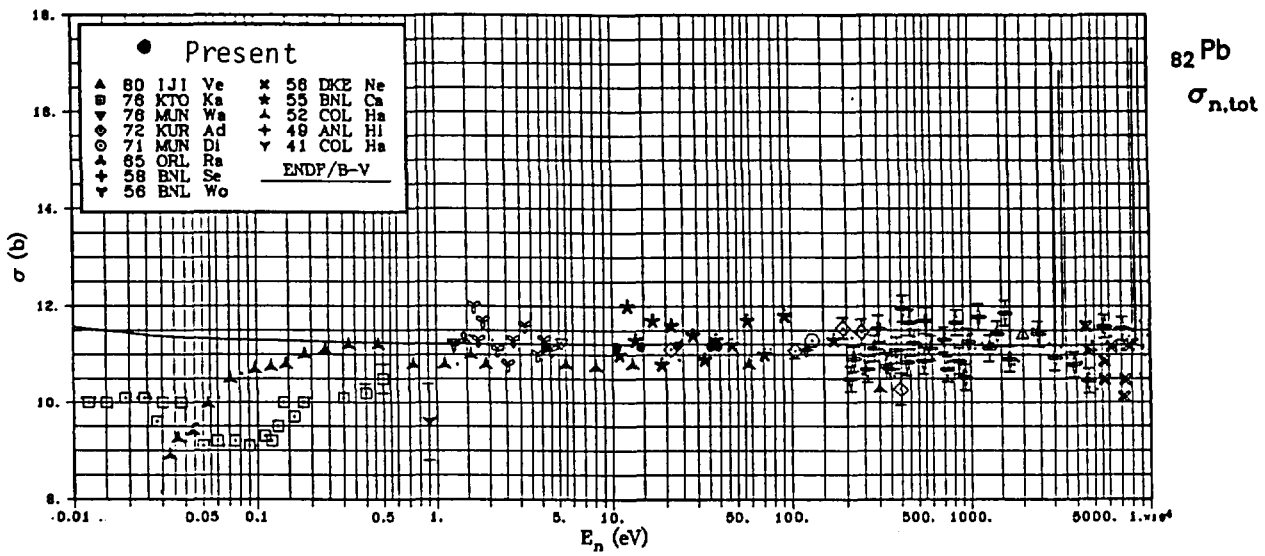

Fig. 7 Neutron total cross section of lead.

3.3 Resonance Integral Measurement with the Standard 1/E Neutron Spectrum Field

Itsuro Kimura
Department of Nuclear Engineering,
Faculty of Engineering, Kyoto University
Yoshida-honmachi, Sakyo-ku, Kyoto 606 Japan
and
Katsuhei Kobayashi, Shuji Yamamoto
Research Reactor Institute, Kyoto University
Kumatori-cho, Sennan-gun, Osaka 590-04 Japan
and
Ryota Miki and Tetsuo Itoh
Kinki University Atomic Energy Research Institute
3-4-1, Kowakae, Higashiosaka-shi, Osaka 577 Japan

The neutron spectrum at the center of the internal graphite reflector between the two-divided cores of a low power research reactor, UTR-KINKI, was verified to be very close to a standard 1/E shape from about 1 eV to a few hundreds keV, by (1) calculations with the SRAC code system, two dimensional diffusion (CITATION) and transport (TWOTRAN) codes, (2) unfolding multi-foil activation data by the NEUPAC code, and (3) measurement using the sandwich foil method.

Making use of this standard 1/E neutron spectrum field, fifteen kinds of resonance integrals were measured for the (n,γ) reactions of reactor materials, using the $^{197}Au(n,\gamma)^{198}Au$ reaction as a standard value. A Monte Carlo calculation was employed to correct the neutron self-shielding in the activation foils. In the uncertainty analysis, variance-covariance data were taken into account and a correlation matrix was given to the measured data.

The present results have been compared with the values evaluated by Mughabghab and the JENDL-2 data. General agreement between the measurement and the evaluated data has been seen except for Ti-50, Ni-64, Nb-93, Ag-109, and Ta-181.

I. INTRODUCTION

Recently, precise data of neutron resonance parameters for reactor materials have been required for designing intermediate spectrum reactors, such as a compact lattice PWR. For this purpose, not only the resonance parameters for each resonance but also the integral data for the parameters including the unresolved energy region are of great importance. The precise resonance integrals are requested for an integral check of resonance parameters and for neutron activation analysis, especially epithermal activation analysis[1]. In this work, the authors have tried to measured fifteen resonance integrals for reactor materials using a standard 1/E neutron spectrum field and to compare the measured values with two kinds of evaluated ones.

A good standard 1/E spectrum field is indispensable for the measurement of precise resonance integrals. There have been several works on the standard 1/E neutron field[2]. Most of the spectrum fields are rather complicated and do not have a very wide range of 1/E. The present authors have found that the neutron spectrum at the center of the 46 cm thick internal graphite reflector between the two-divided cores of UTR-KINKI, as shown in Fig. 1, is very close to a standard 1/E shape over five decades of neutron energy[3], although the absolute neutron flux there is relatively low. In the present work, first the neutron spectrum at the center of UTR-KINKI was obtained and verified to be close to a 1/E shape, by (1) the SRAC code system with the two dimensional (CITATION) and transport (TWOTRAN) codes, (2) unfolding multi-foil activation data, and (3) measurement using the sandwich foil method. Then, this standard 1/E neutron field was applied to resonance integral measurements.

II. NEUTRON SPECTRUM AT THE CORE CENTER OF UTR-KINKI

2.1 Calculation

The neutron energy spectrum at the center of the internal graphite reflector of UTR-KINKI has been calculated using the

SRAC code system[4], which includes cross section libraries, auxiliary processing codes, and other various routines and calculation parameters. One hundred and twentytwo group constants were produced from ENDF/B-IV data. In this calculation, geometrical conditions were assumed to be that the 46 cm-separate cores with MTR-type enriched uranium fuels closely resembled a cylindrical ring. The calculations were carried out with the two dimensional diffusion code (CITATION) and two dimentional transport code (TWOTRAN) on X-Y and R-Z geometries[5,6], to obtain the neutron spectrum in the central void region of 9.5 x 9.5 cm square and 66 cm height space for a vertical graphite stringer which was taken out during the foil irradiation. The result of the neutron spectrum is shown in Figs. 2(a) and 2(b). The calculated spectrum satisfactorily agrees with a standard 1/E neutron spectrum field from about 1 eV to a few hundred keV.

2.2 Spectrum Unfolding

The neutron spectrum at the center of UTR-KINKI has been measured by unfolding multi-foil activation data for the $^{197}Au(n,\gamma)$, $^{115}In(n,\gamma)$, $^{63}Cu(n,\gamma)$, $^{59}Co(n,\gamma)$, $^{23}Na(n,\gamma)$, $^{115}In(n,n')$, $^{58}Ni(n,p)$, $^{27}Al(n,p)$, and $^{27}Al(n,\alpha)$ reactions. The NEUPAC code[7,8], which was successfully applied to the neutron spectrum measurements[3,8,9,10], has been employed to obtain the neutron spectrum. This code contains energy dependent group cross section libraries for main important neutron dosimetry reactions in ENDF/B-V. We adopted 144 energy groups from 0.01 eV to 16.4 MeV. Variance and covariance data were produced from the above nine kinds of reaction rate data as input data for the NEUPAC calculation, in a similar manner to the authors previous method[11]. The initial guess spectrum for the NEUPAC calculation was taken from the calculation obtained above. The result of the unfolded spectrum is shown in Figs. 2(a) and 2(b). It is clear that the neutron spectrum at the core center gives a good standard 1/E shape in the relevant energy range.

2.3 Epithermal Neutron Flux Measurement with Resonance Foils

The sandwich method using resonance foils[12,13] has been used to measure epithermal neutrons at the main resonances only. In this work, (n,γ) reactions for In-115, Au-197, W-186, and Mn-55 have been employed and their induced activations have been measured by a Ge detector. Five resonance foils for each reaction have been put one upon another in a packet with a Cd-cover 0.5 mm thick. The reaction rate of a foil is divided into two parts; (1) one due to the strong resonances and (2) the other due to weak resonances and the 1/v cross section. The difference in reaction rate between the outer and the center foils of the sandwich is expressed as[13];

$$\Delta A = \varepsilon N \sum \phi(u_i) x_i$$

where ΔA is the remaining difference in reaction rate due to the strong resonance contributions, ε is detection efficiency, N is number of target atoms, and $\phi(u_i)$ and x_i are neutron lethargy flux and the sandwich foil cross section at the i-th resonance, respectively. In this measurement, each x_i value for the main resonance(i=1) was referred to the data by Nakazawa[14] except for the Mn data which were obtained by a Monte Carlo calculation to be mentioned later. Neutron fluxes at 1.46, 4.94, 18.8, and 337 eV resonances of In-115, Au-197, W-186, and Mn-55 have been measured and displayed in Fig. 2(a). These results are in satisfactory agreement with a standard 1/E spectrum and the unfolded spectrum.

III. MEASUREMENT OF RESONANCE INTEGRAL

The resonance integral is defined by the relation;

$$I_x = \int_{E_{Cd}}^{\infty} \sigma_x(E) / E \, dE$$

where $\sigma_x(E)$ is cross section as a function of energy E and E_{Cd} is a Cd cut-off energy. In the present measurement, thickness of the Cd-cover is 0.5 mm, which corresponds to a cut-off energy of about 0.5 eV.

Most of the samples were metallic foils of 12.7 mm diameter and less than 0.3 mm thickness. However, Na and Ga samples were

prepared by absorbing the aqueous solution into a filter paper and drying it. The sample and gold foils with Cd-covers were stuck on an aluminum holder, and were set at the center of the internal graphite reflector. These samples were irradiated for 20 to 180 minutes at the nominal power of 1 W at UTR-KINKI, when the absolute thermal neutron flux was about 2×10^7 n/cm^2/sec. Induced activities from the irradiated samples were measured with a Ge detector, whose detection efficiency had been calibrated with standard gamma-ray sources.

The unknown cross section was measured relative to that for the ^{197}Au(n,γ) reaction as a standard value of 1550±28 barn[15]. The relevant resonance integral I_x to be measured is given as follows;

$$I_x = I_{Au} \frac{\varepsilon_{Au}}{\varepsilon_x} \frac{R_x}{R_{Au}} \frac{S_x}{S_{Au}}$$

where I_{Au} is a standard value of the gold resonance integral, ε, R, and S are detection efficiency, reaction rate, and self-shielding correction, and the subscripts Au and x mean the data for gold and sample, respectively.

The neutron self-shielding correction in the sample foils was obtained from a Monte Carlo calculation using the VIM code[16]. This correction method was verified by comparing the calculated spatial distribution of the reaction rates in the foil with that obtained experimentally. A good agreement between the calculated and measured results was found.

IV. RESULTS AND DISCUSSION

After the neutron spectrum at the core center of the research reactor UTR-KINKI was verified to be a standard 1/E shape, fifteen kinds of resonance integral were measured there. The results have been normalized to a standard value of 1550±28 barn for the ^{197}Au(n,γ) reaction[15], and summarized in Table 1. By taking into account the variance-covariance data in the measurement, experimental errors and their correlation coefficients have been obtained.

We have investigated the effect that changing the Cd cut-off energy has on the resonance integral, and found that a 10 % change in energy results in only a 0.2 % shift in the integral, if the cross section around 0.5 eV is assumed to exhibit 1/v behaviour. Moreover, the neutron spectrum with which the actual irradiations are carried out may deviate from the ideal 1/E spectrum. The contribution from this non-1/E behavior to the resonance integral, especially at energies below 1 eV, was estimated and corrected by using the spectrum calculated at the core center.

Comparing the evaluated data in the literature[15] and JENDL-2 data with the present measurements, general agreement has been obtained except for the following; more than 20 % differences between the evaluated and the measured data can be seen in the data for Ni-64, Nb-93, and Ta-181 in JENDL-2 and in the data for Ti-50, Nb-93, and Ag-109 in the literature. Especially for Ni-64, Nb-93, and Ta-181, there exist more than 10 % differences between the Mughabghab and JENDL-2 evaluated data.

REFERENCES

1) K. Tomuta, IAERU-8502, p.3 (1984).
2) J. Grundl and C. Eisenhauer, Proc. IAEA Consultants' Meeting on Integral Cross Section Measurements in Standard Neutron Fields for Reactor Dosimetry, Vol.1, p.53, IAEA-208 (1978).
3) K. Kobayashi, et al., Ann. Rept. Kinki Univ. Atomic Energy Res. Inst., Vol.25, in print.
4) K. Tsuchihashi, et al., JAERI 1285 (1983).
5) R. Miki, et al., Ann. Rept. Kinki Univ. Atomic Energy Res. Inst., Vol.23, p.33 (1986).
6) R. Miki, et al., Ann. Rept. Kinki Univ. Atomic Energy Res. Inst., Vol.24, p.39 (1987).
7) M. Nakazawa and A. Sekiguchi, Proc. 2nd ASTM-Euratom Symp. on Reactor Dosimetry, NUREG/CP-0004, Vol.3, p.1423 (1977).
8) T. Taniguchi, et al., NEUT Res. Rept. 83-10 (1983).

9) K. Kobayashi, et al., Ann. Rept. Res. Reactor Inst., Kyoto Univ. Vol.20, p.1 (1987), and KURRI-TR-287 (1987).
10) K. Kobayashi and I. Kimura, Proc. Int. Conf. on Nuclear Data for Science and Technology, May 30 - June 3, 1988, Mito, Japan, Edited by S. Igarasi, JAERI, p.261 (1988).
11) K. Kobayashi, et al., J. Nucl. Sci. Technol. 19, 341 (1982).
12) A. Weitzberg, ANL-7320, p.535 (1966).
13) M. Nakazawa, KURRI-TR-69, p.38 (1969).
14) M. Nakazawa, Private communication (1985).
15) S. F. Mughabghab, "Neutron Cross Sections", Vol.1, parts A & B, Academic Press Inc. (1984).
16) R. N. Blomquist, et al., ORNL/RSIC-44 (1980).

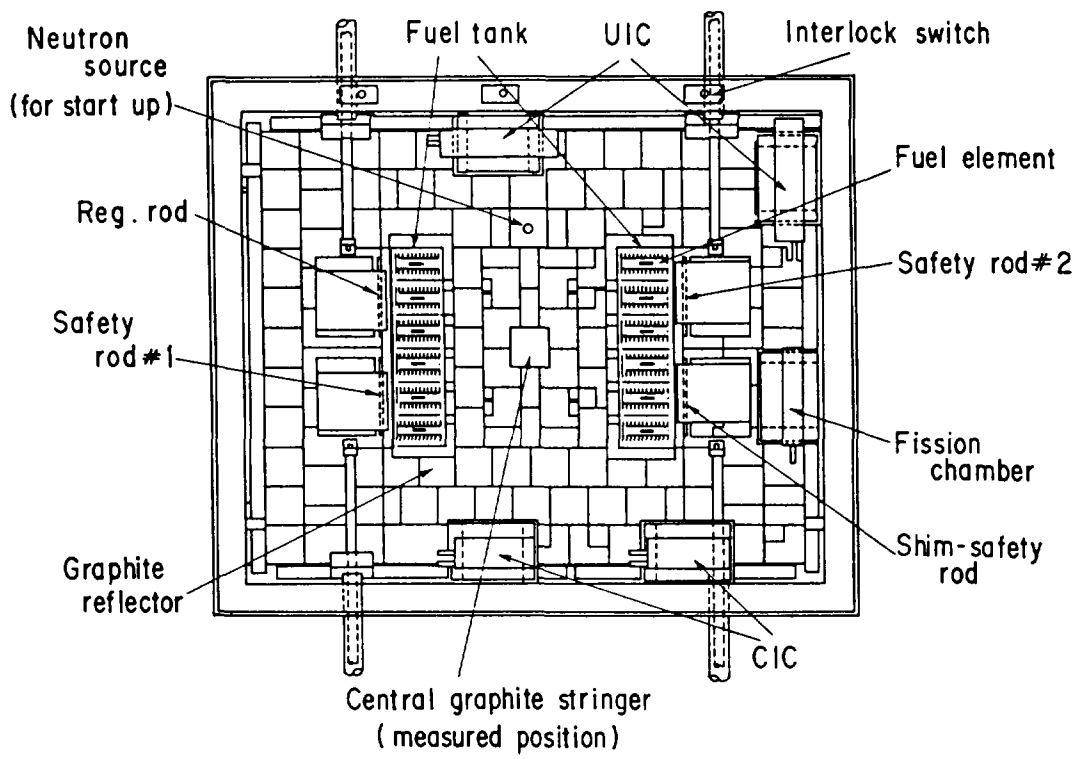

Fig. 1 Cross sectional view of UTR-KINKI.

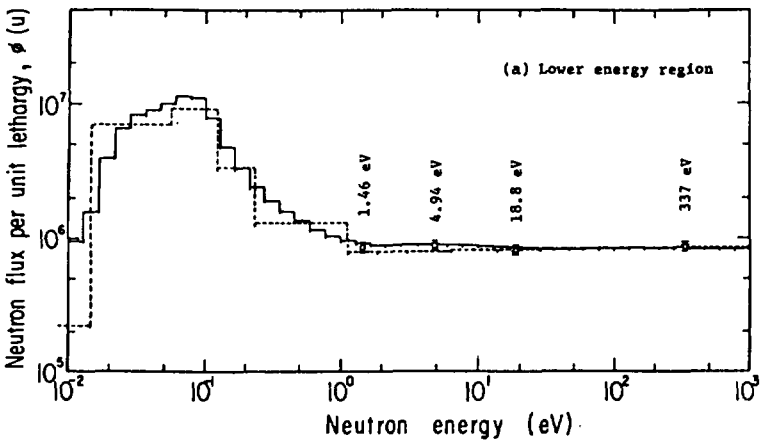

Fig. 2(a) Neutron energy spectrum in the central graphite region of UTR-KINKI.
——— NEUPAC unfolding
---- SRAC code system calculation
○□△▽ sandwich foil method by In, Au, W and Mn, respectively.

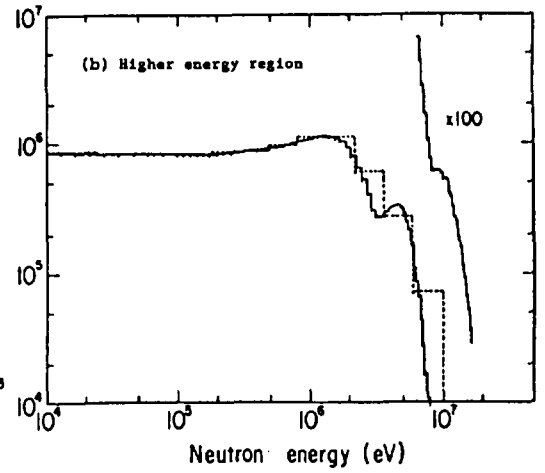

Fig. 2(b) Neutron energy spectrum in the central graphite region of UTR-KINKI.

Table 1 Summary of the present measurements of resonance integrals and comparison with the evaluated data

Reaction	Present measurement			Evaluated value (b)	
	Cross section (b)	(%)	Correlation matrix, (x 100)	JENDL-2	Mughabghab*
$^{197}Au(n,\gamma)^{198}Au$	1550	1.81	100	- - -	1550 ± 28
$^{23}Na(n,\gamma)^{24}Na$	0.3197	4.14	43 100	0.329	0.311±0.010
$^{50}Ti(n,\gamma)^{51}Ti$	0.1414	6.42	28 19 100	- - -	0.118±0.011
$^{51}V(n,\gamma)^{52}V$	2.799	5.99	30 27 25 100	2.534	2.7 ± 0.1
$^{55}Mn(n,\gamma)^{56}Mn$	13.90	2.94	60 35 20 22 100	14.63	14.0 ± 0.3
$^{59}Co(n,\gamma)^{60}Co$	73.34	4.91	37 32 30 37 27 100	75.65	74 ± 2
$^{64}Ni(n,\gamma)^{65}Ni$	0.9238	6.48	28 24 24 29 21 34 100	0.819	0.98 ± 0.15
$^{71}Ga(n,\gamma)^{72}Ga$	30.26	5.65	32 27 15 16 26 20 15 100	- - -	31.2 ± 1.9
$^{93}Nb(n,\gamma)^{94m}Nb$	6.246	6.10	29 22 22 25 22 30 23 16 100	9.59	8.5 ± 0.5
$^{107}Ag(n,\gamma)^{108}Ag$	106.4	6.73	27 22 25 20 20 29 23 14 21 100	- - -	100 ± 5
$^{109}Ag(n,\gamma)^{110m}Ag$	56.89	4.98	36 28 32 33 27 41 32 20 30 34 100	- - -	72.3 ± 4
$^{115}In(n,\gamma)^{116m}In$	2695	5.75	31 23 16 13 24 17 14 46 15 15 18 100	- - -	2650 ± 100
$^{181}Ta(n,\gamma)^{182}Ta$	655.4	4.24	43 29 33 40 31 46 37 22 36 32 46 20 100	743.4	660 ± 23
$^{186}W(n,\gamma)^{187}W$	510.7	4.76	38 25 32 32 28 40 29 20 31 30 39 20 44 100	- - -	485 ± 15
$^{232}Th(n,\gamma)^{233}Th$	85.71	3.43	53 29 17 19 71 22 17 21 18 16 23 20 26 23 100	79.93	85 ± 3
$^{238}U(n,\gamma)^{239}U$	274.8	4.09	44 25 15 16 66 19 15 18 16 14 19 17 22 20 64 100	279.0	277 ± 3

* cited from "Neutron Cross Sections", Academic Press, Inc. (1984).

3.4 Sensitivity Analysis Method of Resonance Parameters to Nuclear Performance Parameters

Atsushi ZUKERAN and Yuichi MORIMOTO
Energy Research Laboratory, Hitachi Ltd.
1168 Moriyama-cho, Hitachi-shi, Ibaraki-ken, Japan

I. INTRODUCTION

The "simultaneous evaluation method" has been employed for JENDL-3 nuclear data evaluation. The method, however, is restricted to the higher energy region above the unresolved resonance. Present work has been motivated to examine possibility of the sensitivity analysis of resonance parameters as a basis for such a evaluation method.

2. METHOD

Reactor core performance parameters such as $K\infty$ are function of the reaction rate denoted by $\langle \Sigma_x \phi \rangle$ for reaction x, where Σ and ϕ mean the macroscopic cross section obtained by a linear combination of microscopic cross sections σ_x's, and neutron flux, respectively. By using the Nordheim expression for an effective cross section, the reaction rate can be shown by

$$\langle \Sigma_x \Phi \rangle = C_0 \sum_i \sum_k \frac{N^i \Delta V}{E^i_{0,k}} \frac{\Gamma^i_{n,k} \Gamma^i_{x,k}}{(\Gamma^i_k)^2} D^i_k \qquad (1)$$

where the function D^i_k indicates the reaction rate of the reaction x with unit peak cross section, i.e.,

$$D_k = \int_0^\infty \Psi(x^i, \theta^i)\, \Phi(E)\, dE \qquad (2)$$

and the parameters used above show the following meanings, c_0: constant/ N^i : atom density of i-th isotope/ ΔV : volume element/ $\Gamma^i_{n,k}, \Gamma^i_{x,k}, \Gamma^i_k$: neutron, reaction x and total widths respectively at resonance energy $E^i_{0,k}$ of the k-th resonance/ $\psi(\chi^i, \theta^i)$: Doppler broadening function as the function of resonance energy measured from $E^i_{0,k}$ with Γ^i_k-unit and temperature variable θ^i, respectively.

As shown in eq.(1) and (2), the reaction rate $\langle \Sigma_x \phi \rangle$ are expressed in terms of the resonance parameters and the neutron flux. Consequently, the sensitivity coefficients can be obtained by the partial derivatives with respect to the resonance parameter. For instance, the sensitivity coefficient of the neutron production reaction rate is

$$S^{p,i}_{x,k} = \delta_{x,n} + \delta_{x,f} - 2\delta_{x,t} + \frac{\Gamma^i_{x,k}}{D_k}\left(\frac{\partial D_k}{\partial \Gamma^i_{x,k}}\right) \tag{3}$$

where no correlations among the resonance parameters are assumed.

The fractional change of K-infinite can be shown by the sensitivity coefficient as shown below

$$\left(\frac{\delta K_\infty}{K_\infty}\right)_f = \sum_i \sum_k \{\widehat{S}^{p,i}_{f,k} + \widehat{S}^{a,i}_{f,k} + S^{d,i}_{f,k} + \sum_j \sum_l S^{p,ij}_{f,l}\}\left(\frac{\delta \Gamma^i_{f,k}}{\Gamma^i_{f,k}}\right) \tag{4}$$

where

$$\widehat{S}^{a,i}_{f,k} = \frac{\langle \Sigma_a \Phi\rangle^{r,i}_k}{\langle \Sigma_a \Phi\rangle} S^{a,i}_{f,k} \qquad S^{a,i}_{f,k} = \frac{\Gamma^i_{f,k}}{\langle \Sigma_a \Phi\rangle^{r,i}_k}\frac{\partial \langle \Sigma_a \Phi\rangle^i_k}{\partial \Gamma^{r,i}_{f,k}} \qquad S^{p,ij}_{f,l} = \frac{N^i \overline{\nu^i} \sigma^j_{f_0 l}}{N^i \overline{\nu^i} \sigma^i_{f_0 k}} \frac{\Gamma^i_{f,k}}{D^i_k}\left(\frac{\partial D_l}{\partial \Gamma^i_k}\right)$$

$$\widehat{S}^{p,i}_{f,k} = \frac{\langle \nu\Sigma_f \Phi\rangle^i_k}{\langle \nu\Sigma_f \Phi\rangle} S^{p,i}_{f,k} \qquad S^{p,i}_{f,k} = \frac{\Gamma^i_{f,k}}{\langle \nu\Sigma_f \Phi\rangle^i_k}\frac{\partial \langle \nu\Sigma_f \Phi\rangle^i_k}{\partial \Gamma^i_{f,k}} \qquad S^{d,i}_{f,k} = \frac{\Gamma^i_{f,k}}{D^i_k}\frac{\partial D^i_k}{\partial \Gamma^i_{f,k}}$$

when the magnitude of fission width Γ_f is changed. In eq.(4), the subscripts p,and a mean the production term and absorption one, and d indicates the interference term, respectively.

The sensitivity coefficients for the correlated cases can be also obtained in the similar expressions. Under the condition that the fission area (A^*_f)obtained in the transmission measurement is conserved, the fission width can be expressed in terms of the toatl and neutron widths, and fission area. Cosequently, the sensitivity coefficients defined by eq.(3) becomes

$$S^{p,i}_{n,k} = -\left[1 + \frac{A^{*i}_{f,k} + \Gamma^i_{\gamma,k}}{\Gamma^i_k}\left(\frac{\Gamma^i_{n,k}}{\Gamma^i_n - A^{*i}_{f,k}}\right)^2 - \frac{\Gamma^i_{n,k}}{D_k}\frac{\partial D_k}{\partial \Gamma^i_{n,k}}\right] \tag{5}$$

where the last term indicates the correlation term between the neutron flux and resonance parameters,i.e., the change of neutron flux through resonance parameters. As shown by eq.(2), the D function is the intergrated bilinear function of Doppler broadening function and neutron flux as function of resonance parameters and thus it can be partially differentiated by an interested resonance parameter as

$$\frac{\partial D}{\partial \Gamma_x} = \int \Psi\Phi\left\{\frac{\Psi'}{\Psi} + \frac{\Phi'}{\Phi}\right\} dE \tag{6}$$

Therefore, the sensitivity function for the interference term be-

tween neutron flux and resonance parameters defined by the last term of eq. (5) can be more simpler form as shown below,

$$S^{d,i}_{x,k}=\frac{\Gamma^i_{x,k}}{D_k}\frac{\partial D_k}{\partial\Gamma_{x,k}}=[1-\frac{1}{4\theta\sqrt{\theta}}+\int\{\frac{1+x^2}{4\theta}\Psi\Phi+\Gamma\Psi(\frac{\partial\phi}{\partial\Gamma})\}dE/D^i_k]\frac{\Gamma^i_{x,k}}{\Gamma^i_k}(\frac{\partial\Gamma^i_k}{\partial\Gamma_{x,k}}) \quad (7)$$

When zero temperature Doppler broadening function can be acceptable, the above equation is approximated by

$$S^{d,i}_{x,k}=[1-\frac{1}{4\theta\sqrt{\theta}}+\int\{\frac{\Phi}{4\theta}+\Gamma\Psi(\frac{\partial\Phi}{\partial\Gamma_x})\}dE/D^\Gamma_k]\frac{\Gamma^i_{x,k}}{\Gamma^i_k}(\frac{\partial\Gamma^i_k}{\partial\Gamma^i_x}) \quad (8)$$

As expected from the previous description, the present theory basis on the so-called the first order perturbation theory assuming that the change of the neutron flux is small when the magnitude of resonance parameters are changed.

3. EXAMPLE

In prior to the numerical examination of the present theory described above, the direct evaluation of the sensitivity against the change of resonance parameters is performed by using multigroup Monte Carlo neutron transport code based on the Nordheim theory for effective cross sections. The result of this direct calculation provides the reference values of the sensitivity coefficients for the present theory.

The sensitivity analysis of the capture width of Pu240 first resonance was made for NEA CRP Benchmark (HCR) core by using the 190 group Monte Carlo code. The change of the neutron balances, as absorption rates normalized to production rates, from the reference are shown in Table 1 in the three group structure condensed from 190 group. In the table, the case-A means when the capture area is conserved and in the case-B no correlation among the resonance parameters of Pu240 is not taken into account.

As shown in Table 1, the change of Pu240 capture width contributes so as to reduce the K-infinite while contrarily the U238 terms acts. The same trends are observed in the U235, Pu239 and Pu242 terms. It seems that this phenomena are likely due to the change of neutron flux expected from the interference terms D function in present theory. Comparing the case-A and B, significant differences of isotopic total contributions are found in the odd mass nuclides such as Pu239, which may be due to cancel-

lation of production (fission) and absorption terms. In order to confirm this different contribution depending on cases, preliminary investigation has been attempted by using the present theory. However, the statistical fluctuation of neutron flues obtained by Monte Carlo code prevented the present theory from getting the decided results. It indicates that conventional determistic methods are preferred for provision of basic date required for present theory.

In Fig. 1, the relative change of k-infinite is shown as a function of the relative change of 240Pu fission width with the sensitivity coefficient based on the direct calculation. The sensitivity coefficient of PU240 capture width is -0.033 %⊿K/k.

Table 1 Change of neutron balance (%Δk/k)

Isotope	Case[1]	Energy Group 1	2	3	Total
U235	A	-0.0005	-0.0135	-0.0002	-0.0143
	B	-0.0015	-0.0077	-0.0003	-0.0095
U238	A	-0.0724	-0.1713	0.0049	-0.2388
	B	-0.0987	-0.1211	0.0051	-0.2193
Pu239	A	-0.0237	-0.4099	0.1287	-0.3049
	B	-0.0330	-0.0902	0.0614	-0.0618
Pu240	A	-0.0060	-0.0368	0.2612	0.2184
	B	-0.0056	-0.0289	0.2613	0.2268
Pu241	A	-0.0047	-0.0552	-0.0048	-0.0647
	B	-0.0066	0.1370	-0.0037	0.1267
Pu242	A	-0.0015	-0.0031	-0.0429	-0.0476
	B	-0.0017	-0.0025	-0.0080	-0.0122
	A	-0.1088	-0.6898	0.3469	-0.4519 ±0.0030[2]
	B	-0.1471	-0.1134	0.3158	-0.0507 ±0.0032

1) A: Pu240 Capture width increased by 8% under area = constant
B: Pu240 Capture width increased by 8% without correlation

2) Monte Carlo statistical error

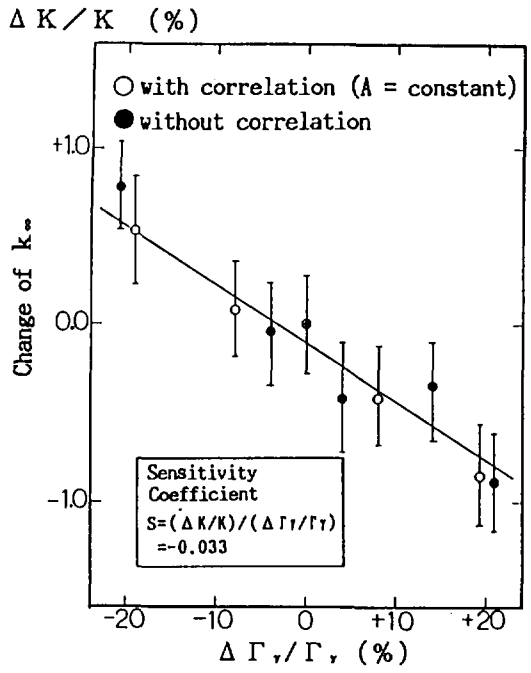

Fig. 1 K_∞ as a function of ^{240}Pu capture width.

4. CONCLUDING REMARKS

1) Formula for the sensitivity coefficients of the resonance parameters has been derived from the reaction rate expression in terms of the resonance parameter and neutron flux.
2) The sensitivity coefficients can be expressed in the terms due to the resonance parameter and due to correlation with neutron flux through Doppler broadening function.
3) Slight non-linearity has been observed in an example made for ^{240}Pu first resonance capture width.

3.5 The Measurement of Leakage Neutron Spectra from Various Sphere Piles with 14 MeV Neutrons

Chihiro Ichihara, Shu A. Hayashi, Katsuhei Kobayashi
Research Reactor Institute, Kyoto University
Kumatori-cho, Sennan-gun, Osaka 590-04, Japan

Itsuro Kimura
Dept. Nuclear Engineering, Fac. Engineering, Kyoto University
Yoshida, Sakyo-ku, Kyoto, Kyoto 606, Japan

Junji Yamamoto and Akito Takahashi
Dept. Nuclear Engineering, Fac. Engineering, Osaka University
Yamada-oka, Suita, Osaka 565, Japan

Abstract

In order to check the neutron cross section data of several kinds of materials which will be used for fusion reactors, fast reactors and semiconductor devices, leakage neutron spectra from sphere piles of six different materials have been measured using the intense pulsed neutron source OKTAVIAN at Osaka University and time-of-flight techniques. Measured samples include LiF, TEFLON:$(CF_2)_n$, Ti, As, Se, and Zr. The thicknesses of the piles were 0.4 to 3.5 mean free paths for 14MeV neutrons. The obtained data were compared with the theoretical calculations using a Monte Carlo transport code, MCNP and the evaluated nuclear data files, ENDF/B-IV, ENDL-85 etc. except for selenium. The general shapes of these calculated spectra agree with the measured ones, but in details calculation show some discrepancies in the energy range between few hundred keV and 14 MeV where the secondary neutrons through (n,2n) reactions or inelastic scatterings are dominant.

1 Introduction

An integral experiment plays an important roll for the verification of the nuclear data files and the calculational method. We have studied the leakage neutron spectra from the sphere piles of various kinds of the candidate materials for fusion reactors and fast reactors [1].

In the present paper, the leakage neutron spectra from six different sample piles are studied. The samples, lithium fluoride and TEFLON(polytetrafluoroethylene) are chosen to check the cross section data for Fluorine which is the main component of some compound (for instance FLIBE) used for fusion rectors and fast reactors.

Electronic devices are also considered to suffer from neutron dose in the fusion reactors. Therefore it is important to check the neutron reaction cross sections of the semi-conductor component elements as it gives the basic information for the irradiation damage of the electronic devices. Two kinds of semiconductor element, arsenic and selenium were chosen as the sample piles.

Titanium and zirconium were picked up as both of them will be used widely in the fusion reactors and fast reactors.

2 Experiment

2.1 Sample Piles

All sample piles were formed as spherical so as to place the tritium target at their centers. The samples include lithium fluoride, TEFLON:$(CF_2)_n$, titanium, arsenic, selenium and zirconium. Those samples were packed into spherical shells made of stainless steel or normal steel. Table-1 shows the list of the measured sample piles, where pile diameter and sample thickness (in unit of cm and mean free paths for 14 MeV neutrons) of each pile are given. The geometries of the piles are shown in Fig.1.

2.2 Experimental Set up

The experiment has been performed by the time-of-flight(TOF) technique using the intense 14 MeV neutron source facility OKTAVIAN [2] of Osaka University. The experimental arrangement in the OKTAVIAN facility is shown in Fig.2. A tritium target is placed at the center of each pile. The energy of the incident deuterons was about 250keV. A cylindrical liquid scintillator NE-218 (5in-diam. × 2in-long) was used as a neutron detector. The detector was located at the angle of 55deg with respect to the incident deuteron beam. Neutron flight path was about 11 m from the center of the tritium target to the surface of the detector. A pre-collimator system made of polyethylene-iron multi-layers was set between the pile and the detector to reduce the neutron background. The

aperture size of this collimator was determined so that the whole surface of the piles facing to the detector could be viewed.

3 Data Processing

The detector efficiency was determined by combining the value calculated with a Monte Carlo code and the relative efficiency derived from the TOF measurements of ^{252}Cf spontaneous fission spectrum and the leakage spectrum from a 30 cm graphite Sphere.

Niobium activation foils were irradiated to monitor the source neutron strength during the measurements. By using these monitor values and measured source neutron spectra, the neutron leakage current spectra from the sample surface were determined by the method stated elsewhere [3].

4 Calculation

A point Monte Carlo transport code MCNP [4] was used for the theoretical calculations. Continuous energy cross section file, BMCCS1 (mostly from END/B-IV) and ENDL-85 which are attached with this code were used for the calculation. As the cross section data for selenium were not available from these libraries, no calculation was done for this pile. The surface current tally from the outer surface of the piles was employed to compare with the experimentally obtained spectra. The overall calculational error was about 0.3% and 0.7% at 14 MeV and 0.1MeV, respectively.

5 Result

The measured and calculated spectra are shown in Figs. 3 through 8 together with the ratio of the calculated and measured values(C/E) except for selenium pile. In Table-1, listed are the cross section data used for the calculation.

5.1 Lithium fluoride and TEFLON

The predicted spectra for both LiF and TEFLON show considerable underestimation in the range 0.2 MeV< E_n <10 MeV(Fig.3 and 4). The study of the neutron leakage spectrum from a 40 cm lithium sphere ([5]) showed considerable good agreement between experiment and calculation. And the cross section value for carbon is considered as the cross section standard below about 2 MeV. Consequently, the disagreement observed for these two piles is mainly caused by the problem of the fluorine cross sections, possibly too small inelastic scattering cross sections of ENDF/B-IV.

5.2 Titanium

The Fig.5 shows the experimental and calculated leakage spectrum from the titanium pile. The predicted spectrum gives underestimation above 3 MeV and considerable overestimation under that. This implies the problem in the non-elastic cross section values of ENDF/B-IV such as (n,2n) or inelastic continuum cross sections.

5.3 Arsenic

Quite different result from the experiment was obtained by the calculation using ENDL–85 data (Fig.6). Complete re- evaluation will be necessary for this element.

5.4 Zirconium

The ENDL–85 prediction gives large difference for the energy region 1 MeV< E_n <14 MeV, while it agrees well below 1MeV (Fig.8). It will be necessary to re-evaluate (n,2n) and inelastic scattering cross sections.

6 Acknowledgment

Part of this work has been supported by a Grant-in-Aid for Scientific Research of the Ministry of Education, Science and Culture, Japan, and undertaken with the framework of the co- operative research program of the OKTAVIAN facility. We are grateful to Prof. K. Sumita of Osaka University for his continuous support to this work.

References

[1] C. Ichihara et al.:*Proc. Int. Conf. Nucl. Data for Sci. & Tech.*, Mito (1988)

[2] K. Sumita, et al.:*Proc. 12-th SOFT*, vol.1, 687(1982), Juelich

[3] A. Takahashi, et al.:*OKTAVIAN Report*, C-83- 02(1983).

[4] J. F. Briesmeister ed.:*MCNP-A General Monte Carlo Code for Neutron and Photon Transport*, LA-7396-M, Rev.2, (1986)

[5] K.Sugiyama et al.:OKTAVIAN Report C-86-02 (1986)

Table 1 Characteristic parameters of the piles, calculation codes and nuclear data files used.

Pile	Dia.	Sample cm	Thick. MFPs	Calc. code	Data Libraries
LiF	61	27.5	3.5	MCNP	^{6}Li:LASL
					^{7}Li:B-IV
					F:B-IV
TEFLON	40	9.8	0.7	MCNP	C:LASL
					F:B-IV
Ti	40	9.8	0.4	MCNP	B-IV
As	40	9.8	0.8	MCNP	ENDL-85
Se	40	9.8	0.6	--	--
Zr	61	27.5	2.0	MCNP	ENDL-85

LASL: LASL subset, B-IV: ENDF/B-IV
FSX: FSX125G/J3T1, GICX: GICXFNS

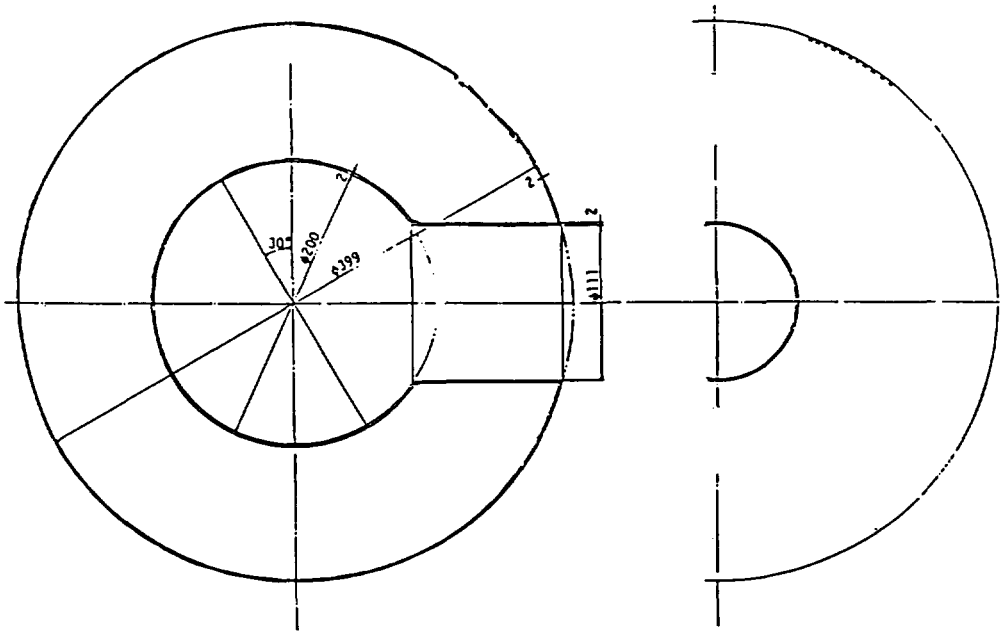

(a)

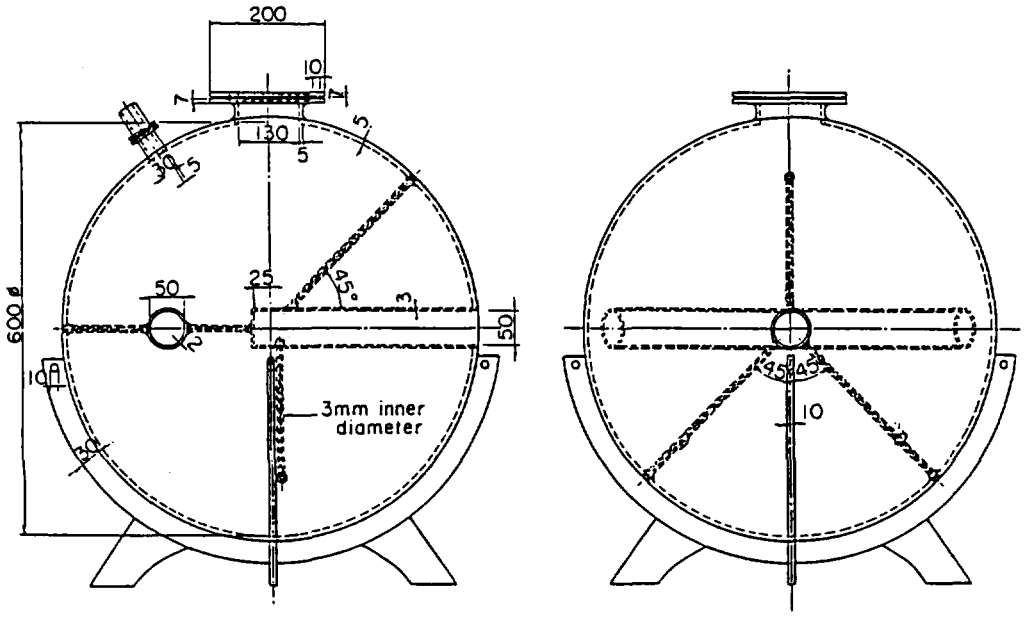

(b)

Fig. 1 The geometries of the sample piles.
(a) 40 cm diameter sphere for use with TEFLON, Ti, As and Se pile.
(b) 60 cm diameter sphere for use with LiF and Zr pile.

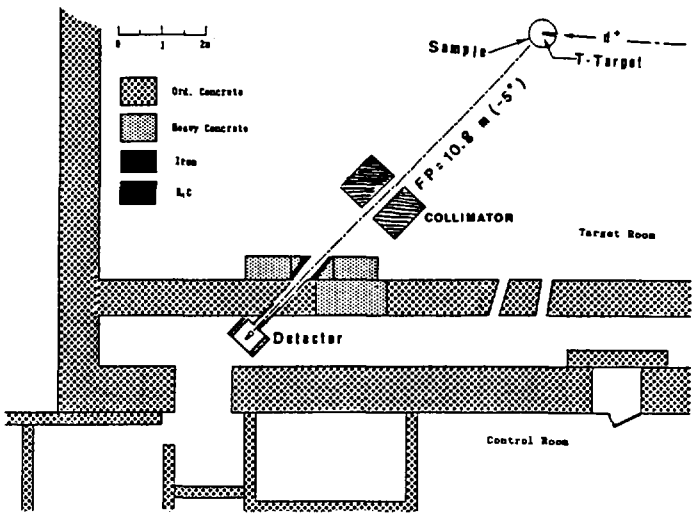

Fig. 2 Experimental arrangement at OKTAVIAN facility.

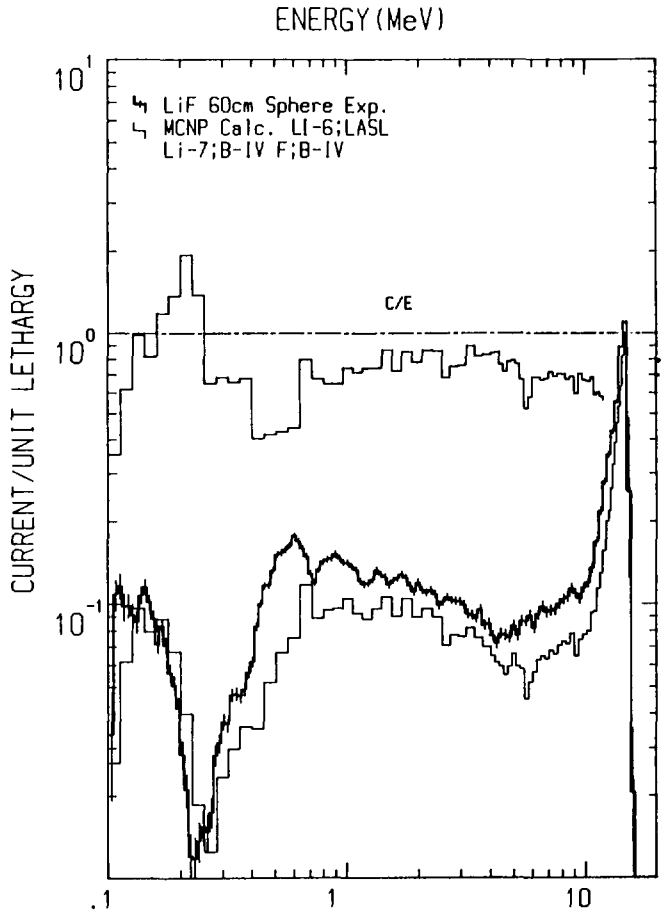

Fig. 3 Experimental and calculated spectra from lithium fluoride 60 cm sphere

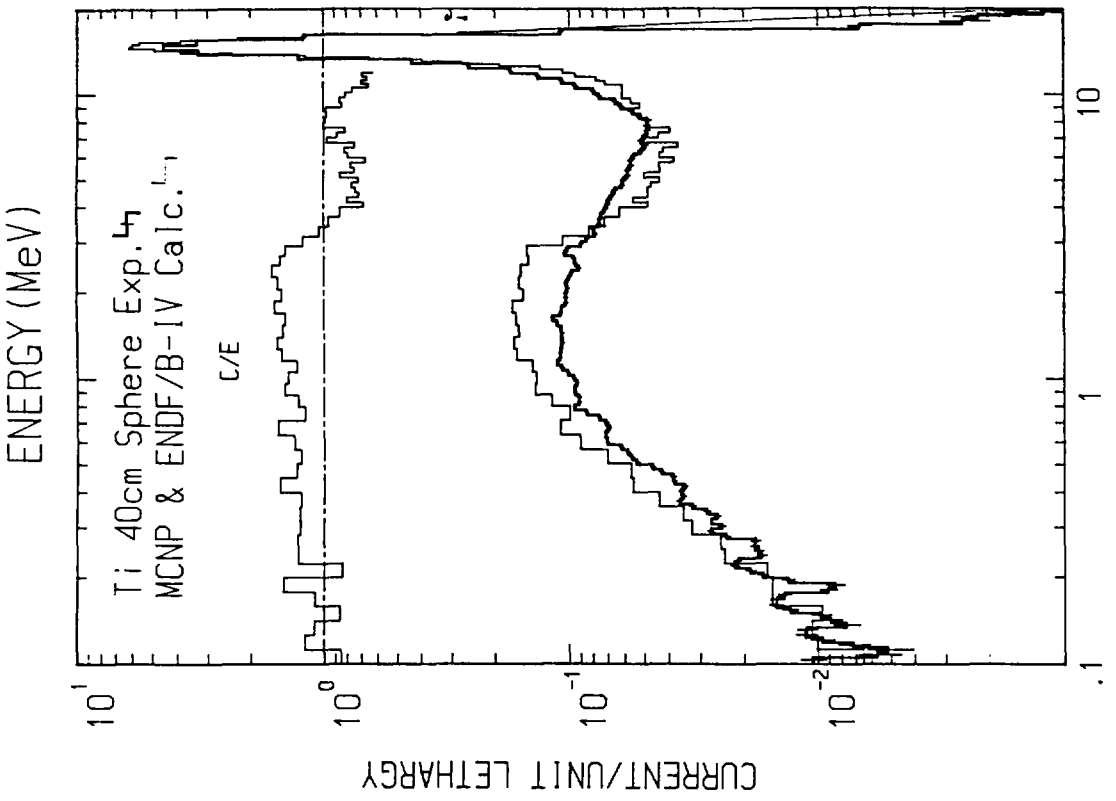

Fig. 5 Experimental and calculated spectra from titanium 40 cm sphere

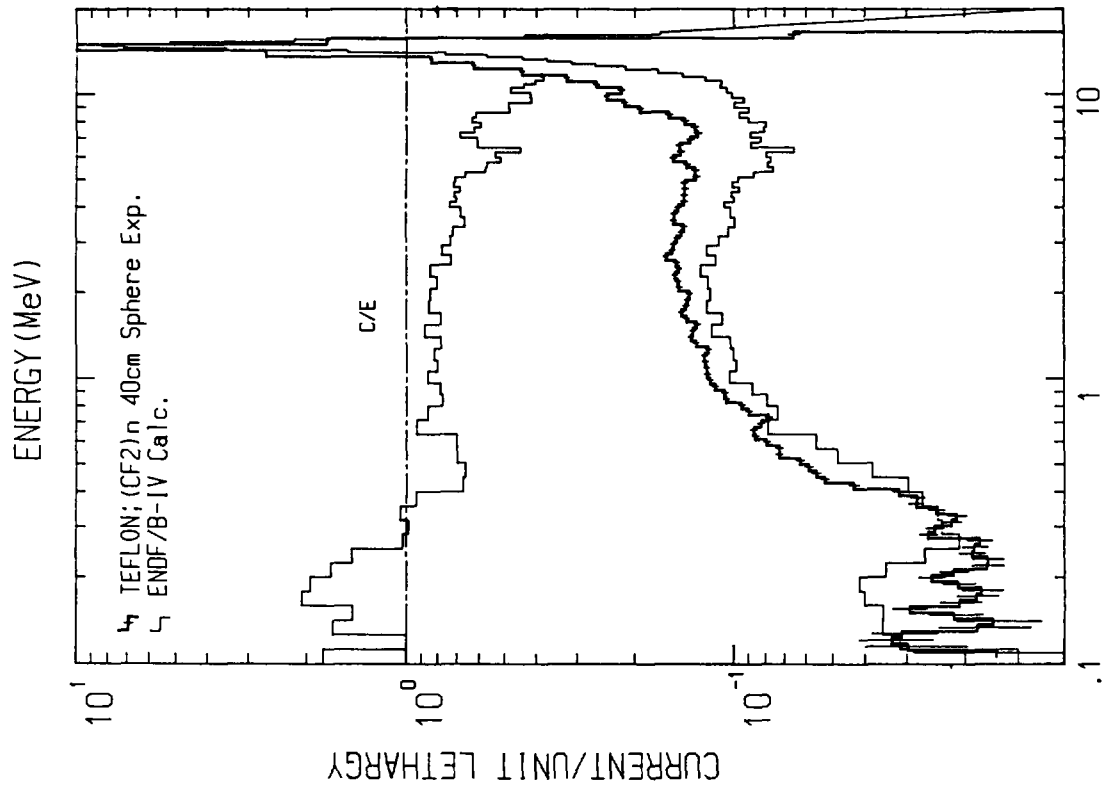

Fig. 4 Experimental and calculated spectra from TEFLON: $(CF_2)_n$ 40 cm sphere

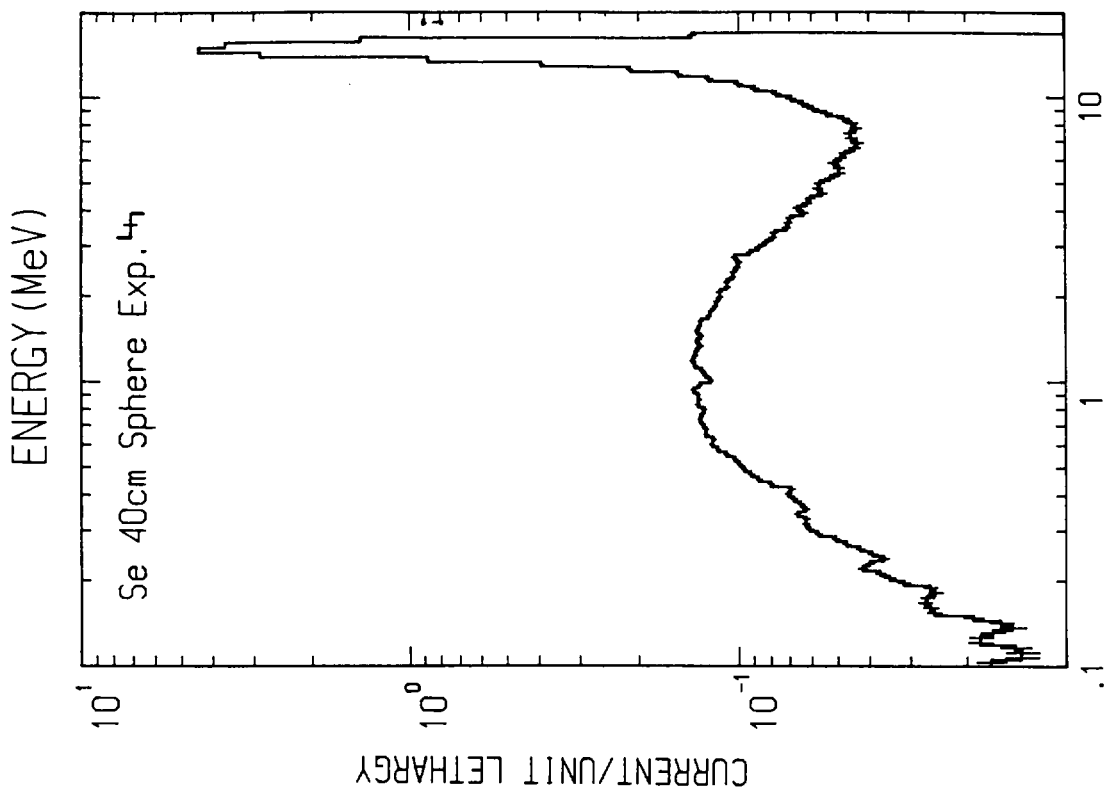

Fig. 7 Experimental and calculated spectra from selenium 40 cm sphere

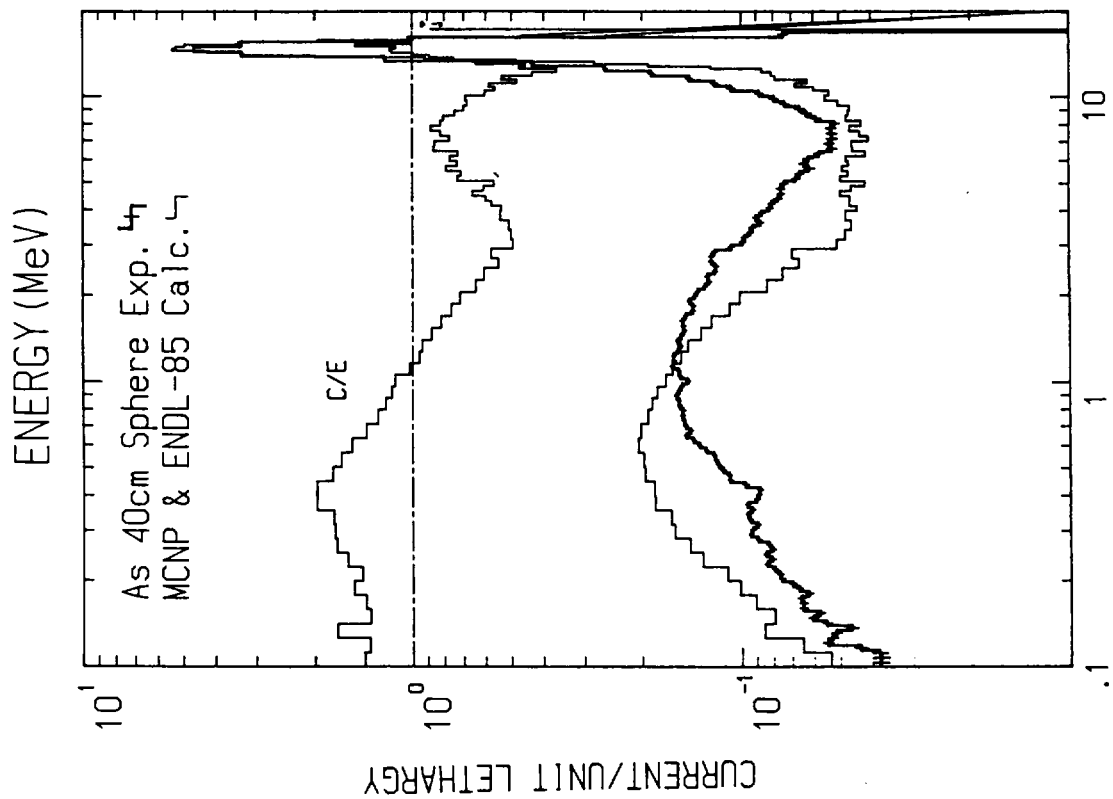

Fig. 6 Experimental and calculated spectra from arsenic 40 cm sphere

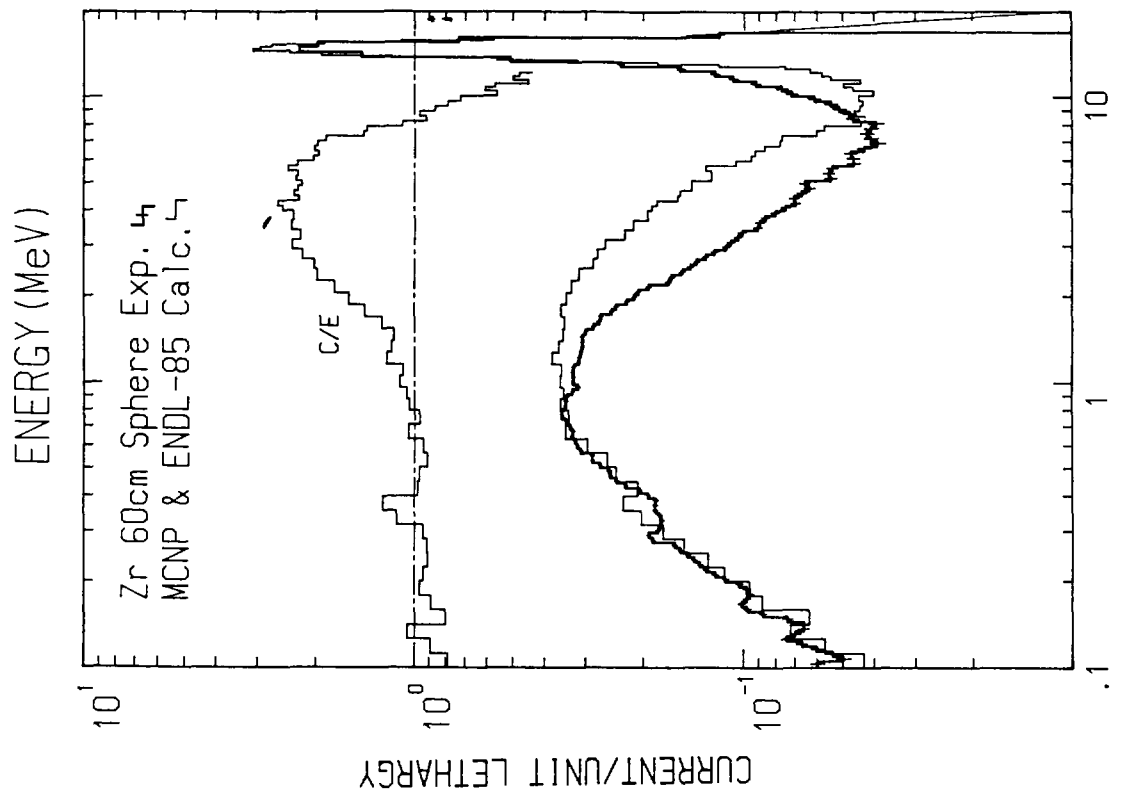

Fig. 8 Experimental and calculated spectra from zirconium 60 cm sphere

3.6 Gamma-Ray Emission Spectra from Spheres with 14 MeV Neutron Source

Junji Yamamoto, Takeshi Kanaoka, Isao Murata*
Akito Takahashi and Kenji Sumita

Department of Nuclear Engineering, Osaka University
2-1 Yamada-oka, Suita, Osaka 565, Japan

Energy spectra of neutron-induced gamma-rays emitted from spherical samples were measured using a 14 MeV neutron source. The samples in use were LiF, Teflon:$(CF_2)_n$, Si, Cr, Mn, Co, Cu, Nb, Mo, W and Pb. A diameter of the sphere was either 40 or 60 cm. The gamma-ray energy in the emission spectra covered the range from 500 keV to 10 MeV. Measured spectra were compared with transport calculations using the nuclear data files of JENDL-3T and ENDF/B-IV. The agreements between the measurements and the JENDL-3T calculations were good in the emission spectra for the low energy gamma-rays from inelastic scattering.

1. Introduction

Nuclear data for gamma-ray productions have been newly compiled in JENDL-3 [1]. Experiments associated with neutron-induced gamma-rays have been made using 14 MeV sources [2,3] in order to test the cross section data needed in the nuclear calculations for fusion neutronics studies. A series of experiments is under way at the OKTAVIAN facility of Osaka University. Main objective of the present work is to obtain the benchmark data for the assessment of the gamma-ray nuclear data in JENDL-3. Energy spectra have been measured with respect to the gamma-rays which were produced from (n,x γ) reactions in spheres and emitted from the spheres. The energy spectra for neutron emission have been already measured by using the same spheres and neutron source [4]. The information from the two emission spectra of neutrons and gamma-rays will be therefore useful in the assessment of the nuclear data through the transport calculations. We have

---

*Present affiliation : Japan Atomic Energy Research Institute

been also carrying out the measurements of gamma-ray production cross sections at 14 MeV [5], so that we intend to make the integral experiment the second approach for the assessment of the gamma-ray nuclear data in addition to the differential experiment.

A variety of spherical samples were available in the present experiment: eleven samples of lithium fluoride, Teflon:$(CF_2)_n$, silicon, chromium, manganese, cobalt, copper, niobium, molybdenum, tungsten and lead, since some of the spheres had been used in the measurements of angular dependent neutron spectra at KURRI-LINAC [6] and five spheres of Teflon, silicon, chromium, cobalt and tungsten were prepared for the measurements of neutron emission spectra at OKTAVIAN.

2. Experimental Procedure

The materials except lead were contained in respective spherical shells made of stainless steel due to either powdered or granular samples. Elements of Li, Si, Cr, Cu, Mo, W and Pb were in natural abundance. The configuration of each sphere is illustrated in Ref.4. The diameters were 60 cm for lithium fluoride, silicon, manganese, copper and molybdenum and 40 cm for Teflon, chrominum, cobalt, tungsten and lead, respectively. Only the niobium sphere was 28 cm in diameter.

Figure 1 shows the arrangement of the experiment. 14 MeV neutrons were generated at the center of the sphere and the gamma-rays were produced from neutron-induced reactions in the sphere. A gamma-ray detector was a cylindrical NaI crystal of 7.62 cm in diameter by 7.62 cm in length. The detector was located at 5.8 m distance from the neutron source and counted the gamma-rays emitted at 55° direction with respect to the OKTAVIAN D^+ beam line. Time spectra of neutrons and gamma-rays from the sphere were measured simultaneous with pulse-height spectra by means of a TOF technique. This manner was a conventional one to discriminate the desired gamma-rays from a neutron background. OKTAVIAN was run in the pulsed mode with the repetition frequency of 500 kHz. The pulse width was 3 nsec in FWHM and the difference in flight times between the 14 MeV neutrons and the prompt gamma-rays was about 90 nsec from the sphere to the detector. Those were enough to separate the gamma-rays from the neutron background in the TOF spectra.

A radioactivation method was applicable to the fluence monitor of the 14 MeV source neutrons. A cylindrical cup of niobium of 5 cm in diameter,

5 cm in length and 0.05 mm in thickness was mounted at the neutron source in every run. After irradiation the fluence was determined from radioactivity induced by ^{92}Nb(n,2n) reaction.

The gamma-ray pulse-height spectra were unfolded using the FERDOR code [7] to produce energy spectra. The response matrix of the NaI detector for monoenergetic gamma-rays was obtained from the calculations with a Monte Carlo code which was developed in our facility [8]. In the response calculations, the code could successfully analyze the response by the following photons as well as the monoenergetic incident photons into the NaI crystal: Photons scattered inside the collimator, photons backscattered from the shield surrounding the detector and photons scattered in aluminum case mounting the NaI crystal. The calculated matrix was compared with the measured one using some gamma-ray sources [6] and the good agreement could be obtained.

3. Results

Figure 2 shows the gamma-ray emission spectra from the spheres of silicon, cobalt and Teflon, respectively. Each energy spectrum was obtained as total leakage current per a source neutron. The gamma-ray energy covered the range from 500 keV to 10 MeV. The energy-resolution of the NaI spectrometer was good enough to analyze the prominent discrete gamma-rays: in the silicon spectrum 585 keV gamma-rays from ^{28}Si(n,α) reaction and two peaks at 1.8 and 2.8 MeV from ^{28}Si(n,n') reaction. The transport calculations will be done using standard group constants [9] that will be newly produced from JENDL-3T(R1) after the release of it. The work is now in progress, so that some of the preliminary results of the MCNP [10] calculations are presented in this report. The processing code NJOY [11] generated from either JENDL-3T [12] or ENDF/B-IV [13] the pointwise cross section set supplied for MCNP.

The measured and calculated emission spectra from the copper sphere are shown in Fig.3. In the energy below 3 MeV the JENDL-3T calculation agrees fairly well with the measurement. JENDL-3T is more accurate than ENDF/B-IV in the evaluation for the low energy discrete gamma-rays. That follows the conclusion in the previous measurement of energy differential cross sections at 14 MeV [14], in which it has been confirmed that the production cross sections from ^{63}, ^{65}Cu(n,n') reactions in JENDL-3T agree with the measured values in the low energy region. The calculated spectra

however deviated from the measured one in the energy range more than 6 MeV, where the captured gamma-rays appeared by the interaction of low energy neutrons with the copper and the outer shell of stainless steel. Specially the gamma-rays from $^{56}Fe(n,\gamma)$ in the outer shell were dominant in the range from 7 to 8 MeV.

In the molybdenum spectra shown in Fig.4, the JENDL-3T evaluation was better than the B-IV one in the energy range below 2 MeV. The present situation for the accuracy of gamma-ray production data would be fairly good for molybdenum in JENDL-3T, considering that the reaction channels for producing the gamma-rays are complex in molybdenum due to many isotopes and that the (n,n') reactions are in competition with the (n,2n) reactions having the large cross section values.

Figure 5 shows the energy spectra emitted from the lead sphere. Most of neutron-induced gamma-rays were distributed below 6 MeV, since lead has a large values of the cross section for (n,2n) reaction. (Q-value is -6.73 MeV and the (n,2n) value is 2.04 barns at 14.0 MeV in JENDL-3T to 5.4 barns of the total cross section.) The discrete gamma-rays appear sharply at the energies of 0.8 and 2.6 MeV. A broad peak is however found at 0.8 MeV in the JENDL-3T calculation. The discrete gamma-ray productions were evaluated in ENDF/B-IV but the B-IV calculation underestimated the measured values over most of gamma-ray energies. That would be consistent with the experimental result on the neutron multiplication for the lead sphere [15], in which the multiplication factor calculated with B-IV was smaller by 10 % than that obtained from the measured spectrum of emission neutrons. Figure 6 points out another consistency between the results of gamma-ray and neutron emissions. In Fig.6(b) the B-IV calculation considerably overestimates the measured emission spectrum in the energy range below 4 MeV. The overestimation of the B-IV calculation can be also observed in the neutron emission spectrum shown in Fig.6(a). It was understandable that the discrepancy resulted from the insufficient evaluation with regard to inelastic scattering cross sections since the emissions of 1.4 MeV gamma-rays are the transitions from 2.676 to 1.434 MeV excited level and 1.434 to the ground state of ^{52}Cr induced by the (n,n') reaction.

The thickness of outer wall of the shell was 4.5 mm for the 60 cm-diam. sphere and 2 mm for the 40 cm-diam. one, respectively. The emission gamma-rays from the materials were shielded by the outer wall and the unnecessary gamma-rays were produced by the interaction of neutrons with

the wall of stainless steel. As shown in Fig.7(a), the emission spectrum through the shell slightly differs from the spectrum without the shell. Figure 7(b) indicates the magnitude of the distortion as a ratio between the spectra with and without the shell. The peak at 800 keV was due to the emission of 847 keV gamma-rays from the first level excitation of ^{56}Fe produced from the (n,n') reaction and the peak around 7 MeV resulted from ^{56}Fe(n,γ) reaction induced by the slowing down neutrons in the copper layer. The gamma-ray fluxes decreased by 10 % between 1 and 6 MeV. The magnitude of the decrement was constant. This is because the gamma-ray production by (n,n') reaction and the gamma-ray shield by the 4.5 mm-thick wall compensated each of the other. As for the gamma-ray production at the neutron source, the contamination of the emission spectra with the source gamma-rays was quite small for the spheres as copper and molybdenum.

In the present experiment the period to measure the prompt gamma-rays from the sphere was 60 to 80 nanoseconds after the source neutrons generating, so that it was necessary to compute the gamma-ray fluxes in the spheres by using time-dependent transport calculations. However, steady state transport calculations have been done under the compatible condition with the experimental manner by a simple method, in which the neutron-mean-emission times from the sphere were investigated as a function of neutron energy to estimate neutron slowing down times in the spheres. A full detail of the method will be mentioned elsewhere.

4. Summary

The gamma-ray emission spectra from the spherical samples could be successfully measured as well as the neutron emission spectra. Both the data of neutron and gamma-ray were compared with the transport calculations using JENDL-3T and ENDF/B-IV. It was concluded that the gamma-ray production data in JENDL-3T are more accurate than those of ENDF/B-IV in the emission spectra for low energy gamma-rays. This is mainly because JENDL-3T has made an advance in the data evaluation for (n,n') reactions as can be found in the neutron emission spectra.

Acknowledgment

Part of this work has been supported by the Grant-in-Aid for Scientific Promotion of Fusion Research from the Ministry of Education, Science and Culture.(No.63050012) Most of the spheres have been provided

at the Research Reactor Institute of Kyoto University. The authors would like to thank Mr. C. Ichihara and Dr. S. Hayashi of the institute and Prof. I. Kimura of Kyoto University for their cooperation.

References

1) Asami,T.:"Compilation of JENDL-3", Proc. the 1987 Seminar on Nuclear Data, JAERI-M 88-065, 4(1987)
2) Hansen,L.F.:"Integral Measurements and Calculations of Neutron and Gamma-ray Emission at 14 MeV and Overview of the New Multi-User Tandem at LLNL", UCRL-97188(1987)
3) Shin,K. et al.:"Measurements of Backscattered Neutrons and Secondary Gamma-Rays from Stainless Steel and Limestone Concrete for 14 MeV Source Neutrons", J. Nucl. Sci. Technol., 25(4), 333(1988)
4) Ichihara,C. et al.:"Measurement of Leakage Neutron Spectra from Various Sphere Piles with 14 MeV Neutrons", Proc. the 1987 Seminar on Nuclear Data, JAERI-M 88-065, 263(1987)
5) Yamamoto,J. et al.:"Differential Cross Sections for Gamma-Ray Production by 14 MeV Neutrons", Proc. the 1987 Seminar on Nuclear Data, JAERI-M 88-065, 374(1987)
6) Hayashi,S. et al.:"Measurement and Analysis of Fast Neutron Spectra in Iron, Nickel and Chromium", J. Nucl. Sci. Technol., 24(9), 702(1987)
7) Harris,L. et al.:"An Introduction to the Principles and Use of the FERDOR Unfolding Code", GA-9882, Gulf Radiation Technology(1970)
8) Murata,I. et al.:"Measurement of Energy Dependent Efficiency and Response Function for the NaI Detector by Activation Method", Preprint 1987 Fall Meeting of the Atomic Energy Society of Japan, C10(1987)
9) Maekawa, H.:"Fusion Neutronics Integral Test for JENDL-3T", Proc. the 1987 Seminar on Nuclear Data, JAERI-M 88-065, 198(1987)
10) Los Alamos Radiation Transport Group(X-6):"MCNP-A General Monte Carlo Code for Neutron and Photon Transport", LA-7396-M, Rev.(1981)
11) MacFarlane,R.E. et al.:"The NJOY Nuclear Data Processing System, Volume 1: User's Manual", LA-9303-M, vol.1(ENDF-324)(1982)
12) JENDL Compilation Group (Nuclear Data Center, JAERI): JENDL-3T, private communication(1987)
13) ENDF/B Summary Documentation, BNL-NCS-17541(ENDF-201), 2nd Edition(1975)

14) Murata,I. et al.:"Measurements of Gamma-Ray Production Cross Sections from Silicon and Copper by 14 MeV neutrons",Preprint 1988 Annual Meeting of the Atomic Energy Society of Japan, E29(1988)

15) Yamamoto,J. et al.:"Determination of the Tritium Breeding Ratio in a Pb-Li Spherical Blanket by Leakage Neutron Spectra", Proc. International Symposium on Fusion Nuclear Technology(Tokyo 1988), J. Fusion Engineering and Design, to be published.

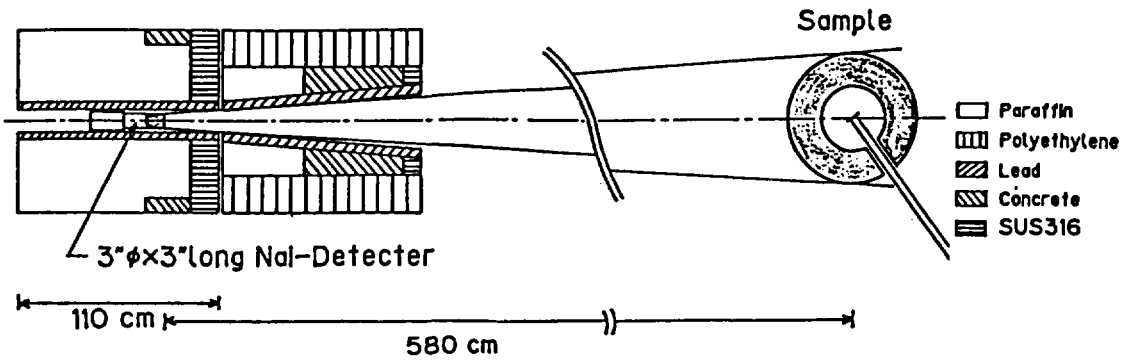

Fig. 1 Experimental arrangement.

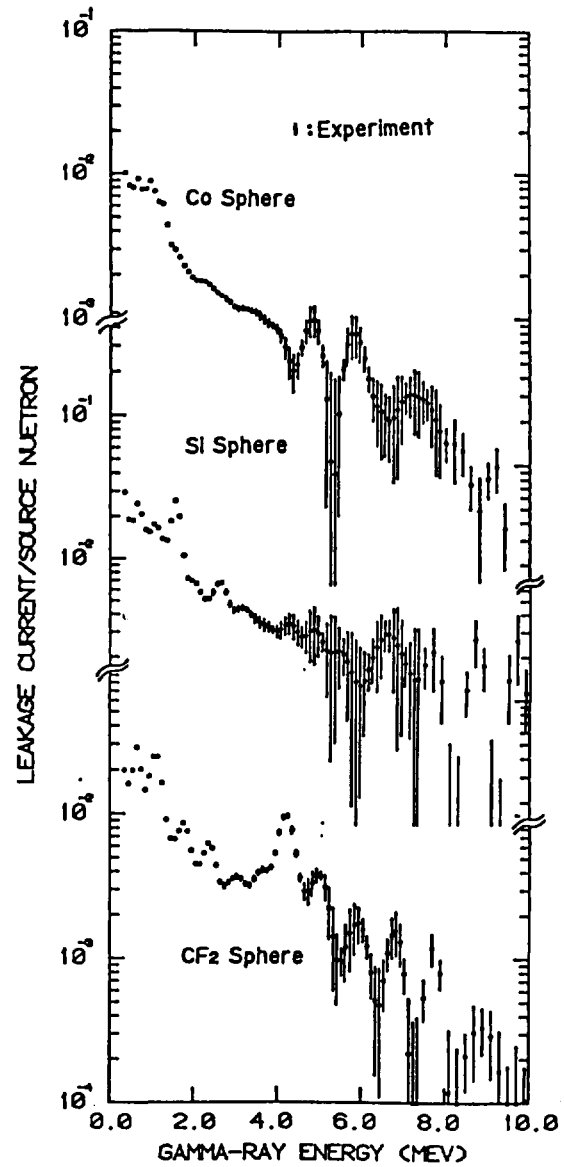

Fig. 2 The gamma-ray emission spectra from the spheres of cobalt, silicon and Teflon (CF_2).

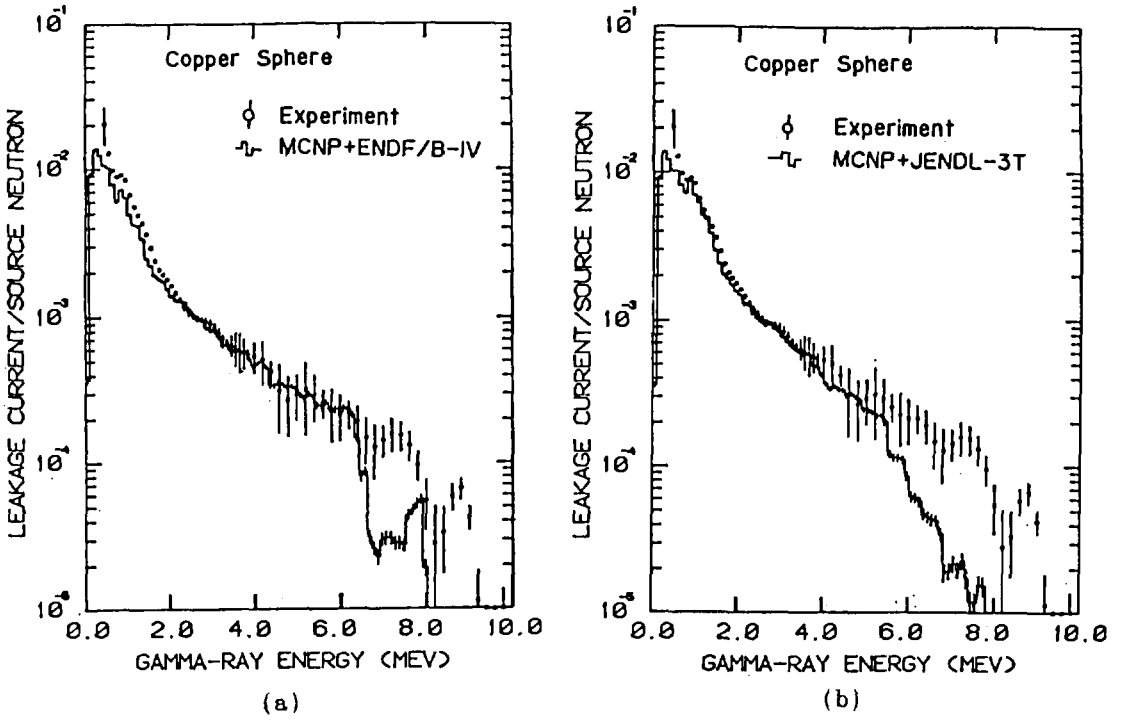

Fig. 3 The emission spectra from the copper sphere, in comparison with the ENDF/B-IV calculation (a) and the JENDL-3T one (b).

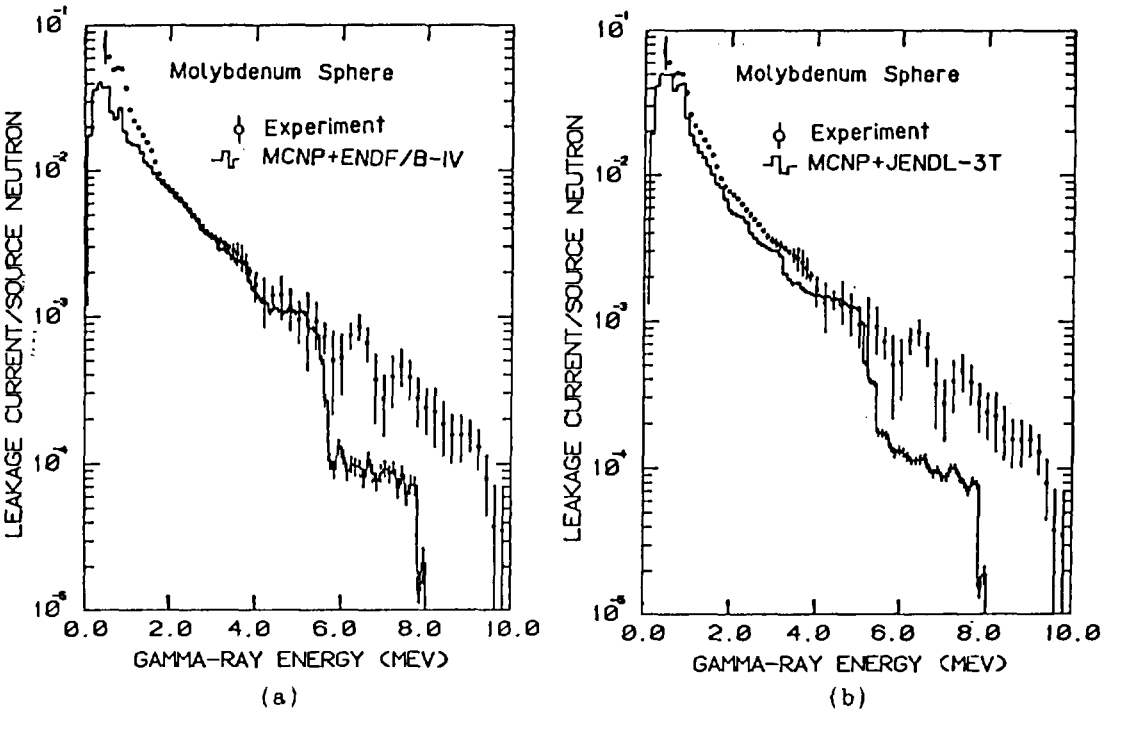

Fig. 4 The emission spectra from the molybdenum sphere, in comparison with the ENDF/B-IV calculation (a) and the JENDL-3T one (b).

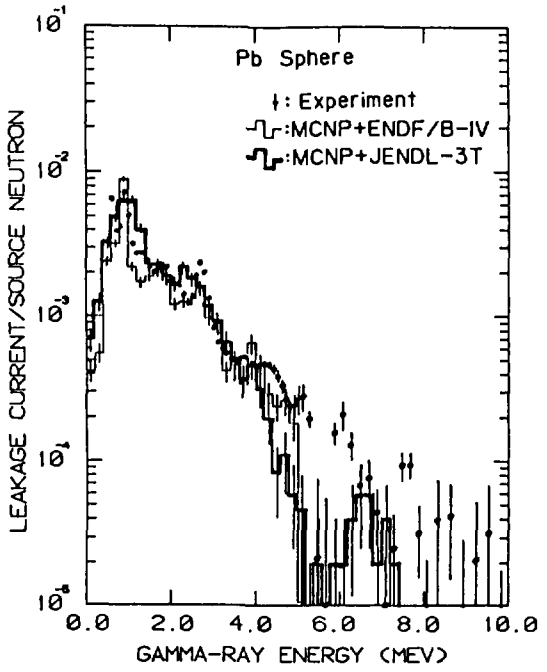

Fig. 5 The emission spectra from the lead sphere.

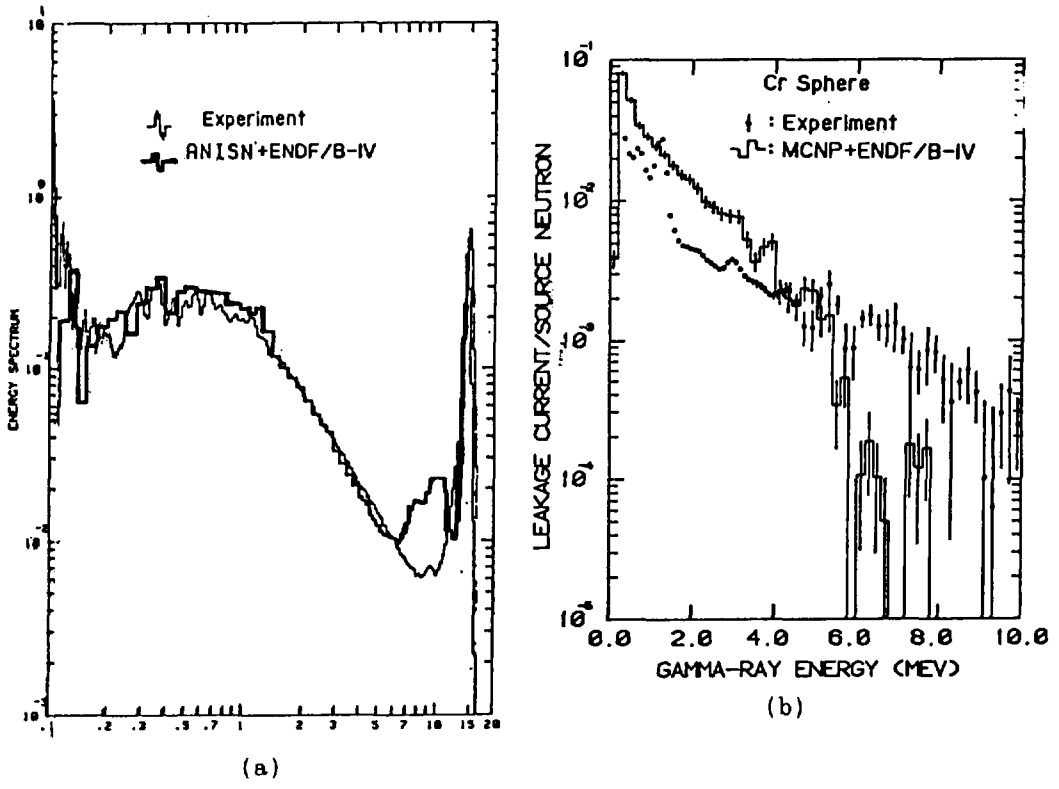

Fig. 6 The energy spectra of neutrons (a) and gamma-rays (b) emitted from the chromium sphere.

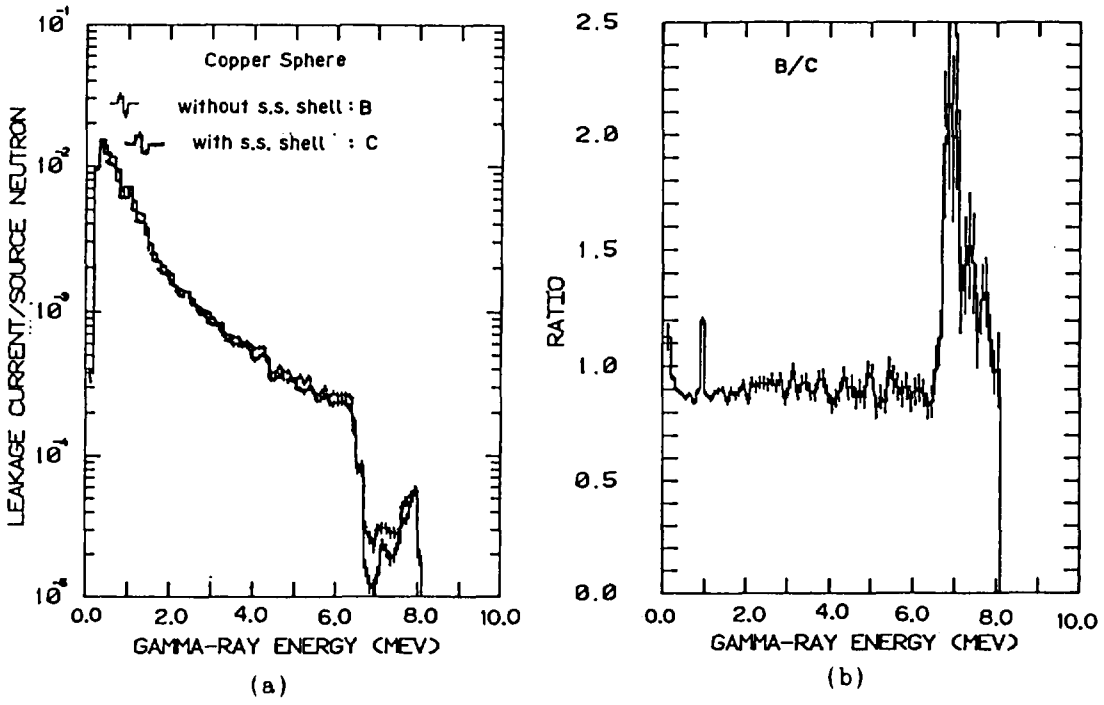

Fig. 7 The calculated gamma-ray spectra emitted from the copper sphere with the stainless steel shell or without one (a) and the ratio between the two spectra (b).

3.7 Systematics and Parametrization of Continuum Angular Distributions

Isao Kumabe, Yukinobu Watanabe,
Yoshimitsu Nohtomi and Mitsuru Hanada

Department of Nuclear Engineering,
Kyushu University, Fukuoka 812

In order to improve Kalbach and Mann's systematics for the application to the continuum angular distributions for the reactions induced by 14 MeV neutrons, we have carried out the reparametrization of their parameters, based on the values of the parameters derived from the fits to the 18 MeV and 25 MeV (p,n) data and the 18 MeV (p,p') data. For the (n,α) reaction we have also carried out the reparametrization, based on the values of the parameters derived from the fits to the 18~25 MeV (p,α) data. The calculated anglar distributions using the present parameters show excellent agreement with those for 14 MeV (n,n'), (n,p) and (n,α) reactions.

1. Introduction

Many theoretical approaches for calculating continuum angular distributions have been proposed. However they involve some serious approximations and / or computational complexities.

There are two approaches[1,2] which are based on the direct reaction models and are most successful. Unfortunately, the calculations are quite complex and the theory has not been much compared with experimental data.

Kalbach and Mann[3](K & M), therefore, decided to approach the problem phenomenologically, studying the systematics of a wide variety of experimental angular distributions and then finding a convenient way to parametrize them. They have studied a large number of experimental angular distributions for particles emitted

into the continuum in preequilibrium nuclear reactions in order to study their systematics. For pure multistep direct reactions it has been found that to first order the shapes of these angular distributions are determined by the energy of the outgoing particle. The formulation has been shown to have significant predictive ability for light ion reactions.

Although the angular distributions calculated by this systematics are in fairly good agreement with the experimental ones for the reaction induced by 14 MeV neutrons, this prediction shows slight underestimation at backward angles. K & M have performed the parametrization on the basis of the values of the parameters derived mainly from the fits to the 62 MeV (p,p') data. Therefore we have undertaken to carry out the reparametrization based on the values of the parameters derived from the fits to the data of the 18 and 25 MeV (p,n) reactions[4] and the 18 MeV (p,p') reaction recently measured.

As will be described in section 4, for the (p,α) and (n,α) reactions, the calculated angular distributions using the present parameters show not so good agreement with the experimental ones. Therefore we have carried out the reparametrization based on the values of the parameters derived from the fits to the data[5] of 18, 20, and 25 MeV (p,α) reactions.

2. Systematics and parametrization performed by Kalbach and Mann

K & M[3] assumed that the angular distributions are described in terms of Legendre polynomials for the reaction (a,b).

$$\frac{d^2\sigma}{d\Omega\, d\epsilon}(a,b) = a_0(\mathrm{tot}) \sum_{l=0}^{l_{max}} b_l P_l(\cos\Theta). \qquad (1)$$

The general idea of statistical multistep direct (MSD) and statistical multistep compound (MSC) processes seems useful.

In the case where the MSD/MSC distinction is a meaningful one, K & M assumed that the two components will show the same systematics in the reduced polynomial

coefficients, except that only the even order polynomials will contribute to the MSC part. Thus the cross section of Eq.(1) becomes

$$\frac{d^2\sigma}{d\Omega\, d\epsilon}(a,b) = a_0(\mathrm{MSD}) \sum_{l=0}^{l_{max}} b_l P_l(\cos\Theta) + a_0(\mathrm{MSC}) \sum_{\substack{l=0 \\ \Delta l=2}}^{l_{max}} b_l P_l(\cos\Theta). \qquad (2)$$

The various a_0 values are obviously related by $a_0(\mathrm{tot}) = a_0(\mathrm{MSD}) + a_0(\mathrm{MSC})$.

They have studied a large number of experimental angular distributions for particles emitted into the continuum in preequilibrium nuclear reactions in order to study their systematics.

They demonstrated the following systematics in the region where the cross section should be nearly pure MSD:

(1) The angular distributions are not sensitive to the incident energy.

(2) The angular distributions do not depend on target mass.

(3) Results for different outgoing particles agree when compared for the same outgoing energy ε.

(4) There is a possible dependence of the shapes of the angular distributions on the nature of the projectile, with complex projectiles leading to more forward peaked curves.

By analogy to the weighted transmission coefficients for a parabolic barrier, K & M have assumed that

$$b_l(\epsilon) = \frac{(2l+1)}{1+\exp[A_l(B_l-\epsilon)]}, \qquad (3)$$

where A_l and B_l are free variables.

The fit with experimental data gives the dependences:

$$A_l = 0.036\ \mathrm{MeV}^{-1} + 0.0039\ \mathrm{MeV}^{-1}\, l(l+1), \qquad (4a)$$

$$B_l = 92\ \mathrm{MeV} - 90\ \mathrm{MeV}\, [l(l+1)]^{-1/2}. \qquad (4b)$$

3. Reparametrization I

-(p,p'), (p,n), (n,n') and (n,p) reactions-

Recently Scobel et al.[4] have measured the neutron energy and angular distributions for the (p,n) reaction on isotopes of Zr and Mo with 18 and 25 MeV protons. The

numerical data[4] are available. More recently we have measured the energy spectra and the angular distributions of protons emitted from (p,p') scattering for ^{90}Zr, ^{93}Nb, ^{92,94,96,98,100}Mo, ^{106}Pd and Ag at an incident energy of 18 MeV. We have chosen the reactions in the energy region in which the contribution of the compound process is negligibly small.

The procedure of parametrization is similar to that performed by K & M. A nonlinear least squares fitting routine was used to optimize the values of A_ℓ and B_ℓ in Eq.(3). The results of the least squares fittings give the following dependence,

$$A_\ell = 0.0561 + 0.0377\ell \quad (\mathrm{MeV}^{-1}) \qquad (5a)$$

$$B_\ell = 47.9 - 27.1\ \ell^{-1/2} \quad (\mathrm{MeV}) \qquad (5b)$$

4. Reparametrization II

-(p,α) and (n,α) reactions-

For the (p,α) and (n,α) reactions the calculated angular distributions using the present parameters of Eq.(5) show not so good agreement with the experimental ones as shown in Fig.7. Therefore we have also carried out the reparametrization for the (p,α) and (n,α) reactions.

Recently we have measured the energy spectra and the angular distributions of α-particles emitted from the (p,α) reaction for ^{112}Cd, ^{118}Sn, ^{120}Sn, Sb, ^{128}Te and ^{130}Te at an incident energy of 18 MeV. Ferrero et. al.[5] have reported measurements of the energy spectra and the angular distributions of α-particles emitted from the (p,α) reaction for ^{93}Nb, ^{107}Ag, ^{118}Sn, ^{165}Ho and ^{169}Tm at incident energies of 20~44 MeV. We have chosen our 18 MeV data and 20~25 MeV data[5] for ^{118}Sn in the energy region in which the contribution of the compound process is negligibly small.

The procedure of parametrization is similar to that by K & M. The results of the least squares fittings give the following dependence,

$$A_\ell = 0.0526 + 0.0081\,\ell\,(\ell+1) \qquad (6a)$$

$$B_\ell = 61.2 - 42.2\ell^{-1/2} \qquad (6b)$$

K & M have assumed that the MSD and MSC components will show the same systematics in the reduced polynomial coefficients, except that only the even order polynomials will contribute to the MSC part. However it has no theoretical base that the MSC component can describe by the second term in Eq.(2). Therefore we assumed that the MSC component can be replaced by the evaporation cross section and calculated it by means of the standard Hauser- Feshbach theory. In this calculation, we used the TNG code[6] with the cut-off parameter $\sigma^2 = 0.0888(aU)^{1/2}A^{2/3}$.

For the 18 MeV (p,α) reaction b_2 values calculated for various target nuclei are shown by circles in Fig.1. Since b_ℓ values for $\ell \geq 4$ are very small, they were neglected.

Next, we have undertaken to carry out the parametrization of b_2 values. The results of the least squares fittings give the following dependence,

$$b_2 = 0.215\exp[-0.0410A+(0.691\times10^{-3}A+0.188)\varepsilon], \qquad (7)$$

and are shown by solid curves in Fig.1.

For the 14 MeV (n,α) reaction b_2 values calculated for various target nuclei are shown by circles in Fig.2. The results of the least squares fittings give the following dependence,

$$b_2 = 0.288\exp[-0.046A+0.0703A^{0.32}\varepsilon], \qquad (8)$$

and are shown by solid curves in Fig.2.

5. Comparison with data

To test the usefulness of the empirical parametrization derived here, comparisons of calculated angular distributions with 14 MeV (n,n') and (n,p) data are presented. In this calculation the division of the cross section into a multistep direct part and a multistep compound part was replacecd by the conventional division into a preequilibrium part and an equilibrium part, respectively. Namely, we assumed that the angular distributions for multistep direct reactions are approximately valid for all preequilibrium particles and the

angular distributions for multistep compound reaction correspond to those for the evaporation part. Therefore the experimental angle-integrated energy spectra were divided into the preequilibrium and evaporation parts, and the values of a_0(MSD) and a_0(MSC) were determined.

Comparisons of calculated angular distributions with 14 MeV (n,n')[7] and (n,p)[8] data are shown in Fig.3. The solid and dashed curves are the calculated angular distributions using the present and K & M's parameters, respectively. The calculated angular distributions using the present parameters show excellent agreement with the experimental ones.

For the (p,α) and (n,α) reactions, angular distributions were calculated using Eqs.(3) and (6) for the first term in Eq.(2), and Eq.(7) or (8) for the second term. Comparisons of calculated angular distributions with 18 MeV (p,α) and 14 MeV (n,α) data[9] are shwon in Figs. 4 and 5, respectively. The solid curves are the calculated angular distributions using the present parameters. The calculated angular distributions using the present parameters show excellent agreement with the experimental ones.

More recently Kalbach[10] developed new systematics. The dashed curves in Figs. 4-6 are the angular distributions calculated using the new Kalbach's systematics. As is shown in Fig.6, this prediction for the (n,n') reaction shows slight underestimation at forward angles although the understimation of the angular distributions at backward angles calculated by K & M's parameters is improved.

References

1) TAMURA, T., et.al. : Phys. Lett. 66B, 109 (1977)
2) FESHBACH, H. et.al. : Ann. Phys., 125, 429 (1980)
3) KALBACH, C. and Mann, F.M. : Phys. Rev. 23 112 (1981)
4) SCOBEL, W. et.al. : Phys Rev. C30, 1480 (1984), Lawrence Livermore National Laboratory Report No. UCID-20101, 1984 (unpublished)
5) FERRERO, A.M. et.al. : INFN Report, INFN/BE 78/6 (1978)

6) SHIBATA, K. and FU, C.Y. : ORNL/TM-10093 (1981)
7) IRIE, Y. et.al. : Mem. Fac. Eng. Kyushu Univ., 37, 19 (1977)
8) TRAXLER, G. et.al. : Nucl. Sci. and Eng. 90, 174 (1985)
9) FISCHER, R. et.al. : Phys. Rev. C30, 72 (1984), Phys. Rev. C34, 460 (1986)
10) KALBACH, C. : Phys. Rev. C37, 2350 (1988)

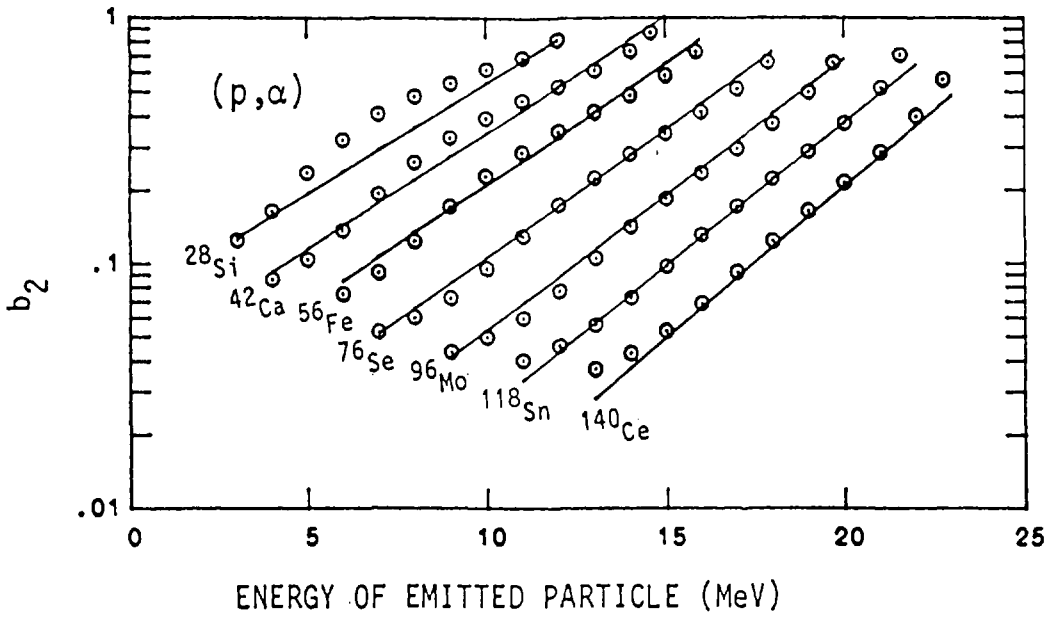

Fig. 1 Systematics of reduced Legendre coefficient b_2 values for 18 MeV (p,α) reaction. Circles represent the values calculated using the Hauser-Feshbach theory. The solid curves are the results of least squares fitting to circles.

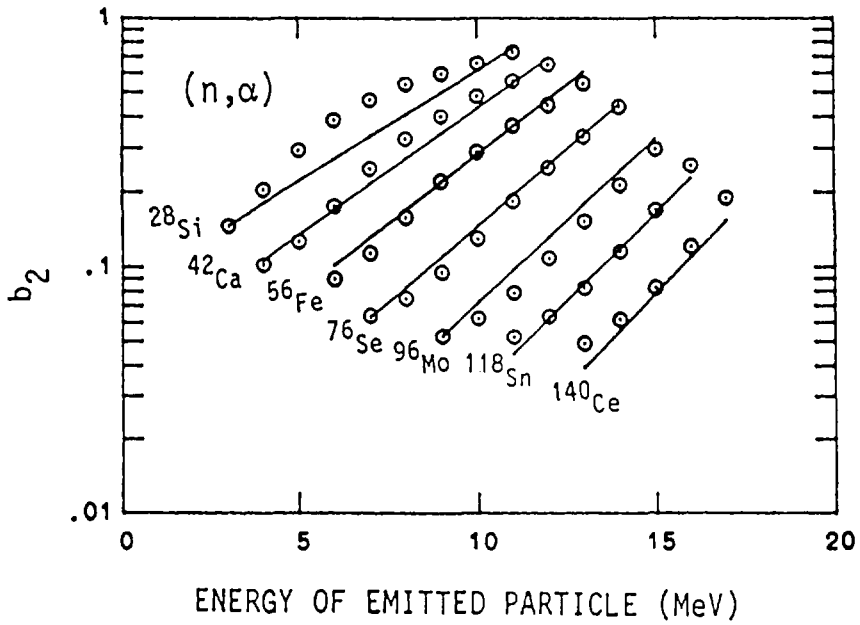

Fig. 2 Systematics of reduced Legendre coefficient b_2 values for 14 MeV (n,α) reaction. Also see the caption of Fig. 1.

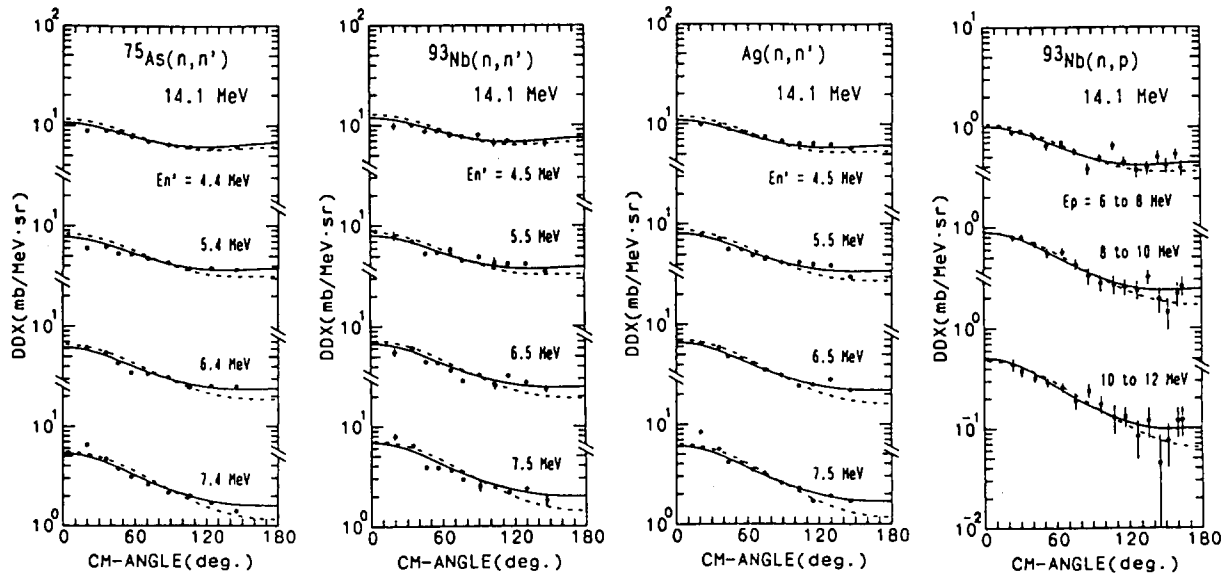

Fig. 3 Comparisons of calculated angular distributions with 14 MeV (n,n') and (n,p) data. The solid and dashed curves are the calculated angular distributions using the present and K & M's parameters, respectively.

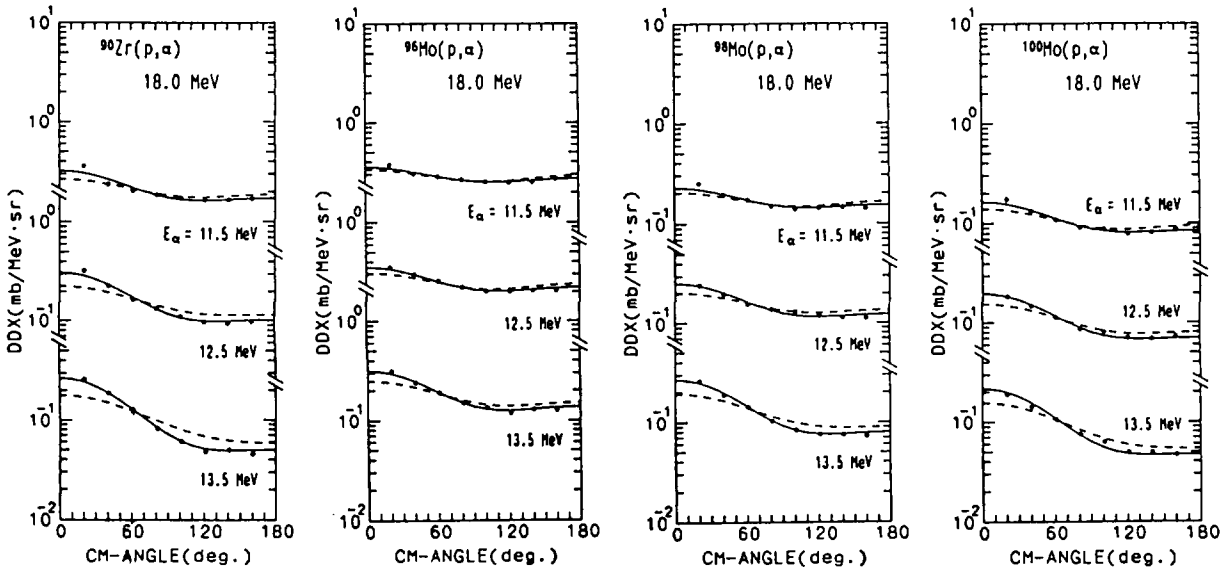

Fig. 4 Comparisons of calculated angular distributions with 18 MeV (p,α) data. The solid and dashed curves are the calculated angular distributions using the present (Eq.(6)) and Kalbach's parameters, respectively.

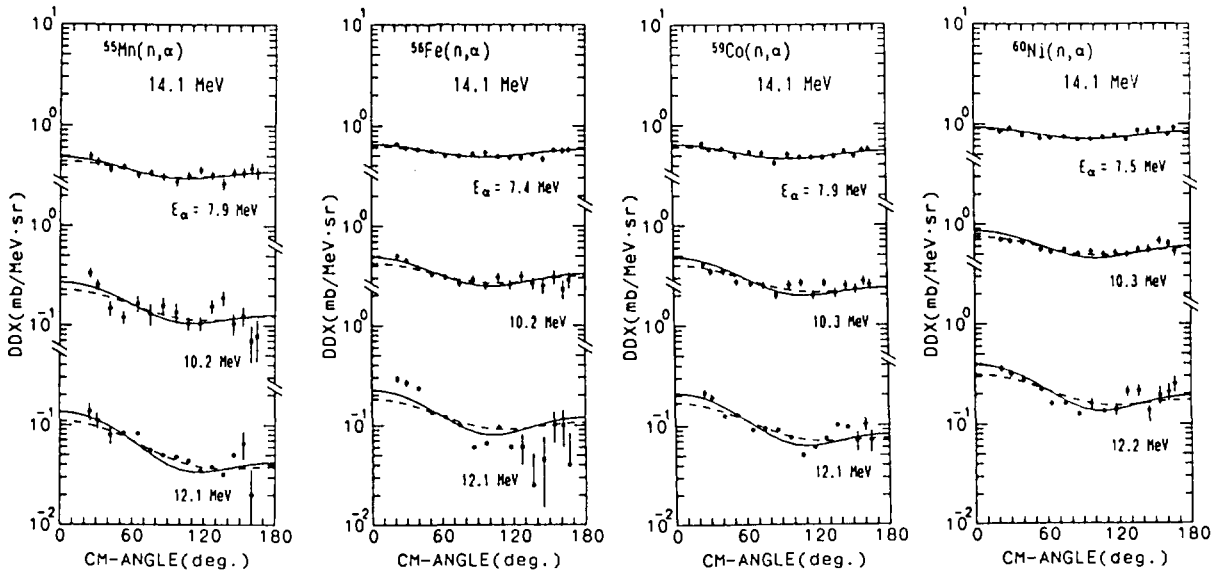

Fig. 5 Comparisons of calculated angular distributions with 14 MeV (n,α) data. Also see the caption of Fig. 4.

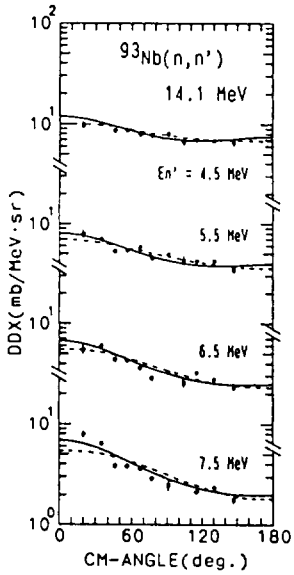

Fig. 6
Comparisons of calculated angular distributions with 14 MeV (n,n') data. The solid and dashed curves are calculated angular distributions using the present (Eq.(5)) and Kalbach's parameters, respectively.

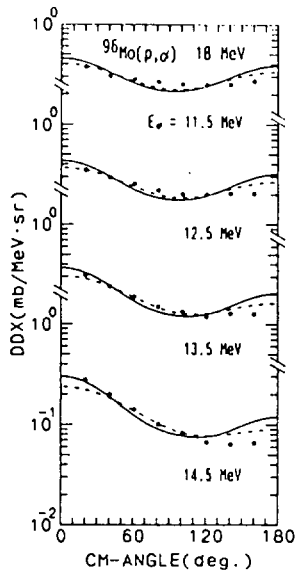

Fig. 7
Comparisons of calculated angular distributions with 18 MeV (p,α) data. The solid and dashed curves are calculated angular distributions using the present (Eq.(5)) and K & M's parameters, respectively.

3.8 Measurement of Neutron Emission Spectra from Neutron Induced Fission and Scattering of U-238

M.Baba, H.Wakabayashi, N.Ito, K.Maeda and N.Hirakawa
Department of Nuclear Engineering, Tohoku University
Aoba, Aramaki, Sendai 980, Japan

We have measured the double-differential neutron emission spectra from fast neutron interaction with ^{238}U and obtained the data for

1) prompt fission neutron spectrum for 2-MeV incident neutrons, and
2) double-differential neutron scattering cross sections for 1.2, 2.0, 4.2, 6.1 and 14.1 MeV neutrons.

The results of fission spectrum is observed to be softer significantly than both evaluation by JENDL-3T and ENDF/B-IV. The Maxwellian temperature deduced from the experimental spectrum is 1.257 MeV and is lower than that of ENDF/B-IV; the average energy of fission neutrons deduced from the temperature is markedly lower than JENDL-3T value.

The experimental neutron emission spectra from inelastic scattering differ markedly from JENDL-3T in the energy region of Q=-0.9 and -1.2 MeV levels, and continuum for MeV incident neutrons, and in high energy region for 14 MeV incident neutrons.

1. Introduction

The data for energy distribution of prompt fission neutrons and inelastically-scattered neutrons from ^{238}U are of prime importance for design of fast reactors and hybrid reactors /1/. However, there are marked differences between the current evaluated data files. The situation will be attributable to the scarcity of experimental data as well as the difficulty in theoretical calculation.

In this study, we measured neutron emission spectra of ^{238}U and deduced

1) prompt fission neurons spectrum for 2-MeV incident neutrons, and
2) double-differential neutron scattering cross sections for 1.2, 2.0, 4.2, 6.1 and 14.1-MeV neutrons.

In the study, we put emphasize to measure the emission spectra from

high-lying and continuum levels, since there are very few experimental data for them despite of the importance for neutron moderation in the reactors.

we discuss the results in comparison with other experimental and evaluated data.

2. Experiments and Data Analyses

Experiments were performed using Tohoku university Dynamitron T-O-F spectrometer. The method of experiments and data analyses is almost same as in our previous studies /2-4/, then only outlines are described here.

2.1 Experimental Apparatus

The primary neutrons were obtained via the T(p,n), D(d,n) and T(d,n) reactions for 1.2 & 2 MeV, 4.2 & 6.1 MeV, and 14.1 MeV measurements, respectively, using solid Ti-T and deuterium gaseous targets. The energy dispersions of primary neutrons were about 100, and 300 keV for the T(p,n) and D(d,n), T(d,n) reactions, respectively. The 14.1 MeV neutrons were obtained at emission angle of 97.5-deg..

The sample was a solid cylinder of elemental uranium, 2 cm in dia. and 5 cm long, and encased in an aluminum can. It was placed 10 cm or 12 cm from the neutron producing target for fission neutrons or scattered neutrons measurements, respectively.

The neutron detector was a NE213 scintillator, 14 cm in dia. and 10 cm thick, or 5" in dia. and 2" thick, equipped with two-bias pulse shape discriminators; the smaller one was employed in measurements for 1.2 to 6 MeV neutrons to reduce time dispersion due to detector thickness. The detector bias was set at about 2 MeV and 0.3 MeV for high- and low-bias system, respectively, while the latter was lowered to 0.1 MeV at 1.2 and 2 MeV measurements. The energy dependence of neutron detector efficiency was determined to 5% by combining the calculation with O5S code /5/, and measurements of ^{252}Cf fission spectrum and hydrogen scattered neutron yields. The overall timing resolution was 1.8 to 2.5 ns.

The measurements were performed separately for fission neutrons and scattered neutrons to optimize the experimental conditions for each quantity.

2.2 Fission Spectrum Measurement

The fission spectrum was measured for 2 MeV neutrons at two emission angles, 90- and 135-deg., to inspect the angle dependence of the spectrum.

The fight path was 3.86 m long as a compromise between the energy resolution and signal to background ratio; this is relatively long compared with previous authors /6,7/ to improve the data quality at higher emission energy.

Cares were taken to reduce the background level by adopting tight collimation and sufficient gamma-ray rejection in the detector. Consequently, the backgrounds observed by measurements for empty can and lead sample, were entirely time independent, and their magnitudes could be estimated unambiguously.

The measurements were divided into cyclic runs with one or two hour duration for the uranium sample, and lead sample or empty can, monitoring the stability of counting system.

The measured T-O-F distribution at 135-deg. is shown in Fig.1; fission neutrons are observed clearly with favorable signal to background ratio. The T-O-F data were corrected for the effects of 1) sample-out background, 2) sample activity including delayed neutrons and gamma-rays, 3) multiple-scattering and 4) distortion due to finite energy resolution and detector thickness.

2.3 Scattered Neutron Spectrum

The measurements were done at 6 to 8 angles at flight path length around 5 m. This flight path length allowed the observation of gross structure of the emission spectrum, while it was not possible to resolve the very closely spaced individual levels.

The absolute value of scattering cross section was determined relative to the hydrogen scattering cross sections.

The data correction was made similarly as in the fission neutron measurements; nonetheless, the backgrounds caused by parasitic components in the source neutrons were considered additionally by using gas-out data for D(d,n) neutrons and Monte Calro calculations for T(p,n) and T(d,n) neutrons.

3. Results and Discussion

3.1 Fission Spectrum

We compare the experimental results with evaluated data using the Maxwellian distribution function as the reference spectrum for normalization between the spectra; this manner has been used in the data comparison of standard spectrum of ^{252}Cf.

Figure 2 illustrates the experimental results at 135-deg. divided by square root of emission energy. The Maxwellian temperature T_M deduced from

the fit to the experimental spectrum is 1.257 MeV, while the experimental data deviate downwards from the fitted curve at higher neutron energy. This deviation is similar as that reported for the cases of ^{252}Cf /8/ and ^{235}U /9/. As shown in Fig.3, this value of Maxwellian temperature is lower markedly than ENDF/B-IV (T=1.33MeV), but is closer to the experimental values by Barnard et al. at 2 MeV /6/ and Batchelor et al. at 3 to 7 MeV/7/.

In Fig.4, the present results are compared with JENDL-3T* evaluation based on Madland-Nix model /8/ calculation, in the form of ratio to the best fit Maxwellian spectrum. The spectrum given by JENDL-3T is fairly close in shape to JENDL-3T above a few MeV, but is much lower than Maxwellian distribution that fits the experimental data. This feature between the Maxwellian and Madland-Nix model calculation is also similar as the case of ^{252}Cf /8/.

On the other hand, the Watt distribution function provides better reproduction of the experiments as shown in Fig.5; this is also the cases of ^{252}Cf /10/ and ^{235}U /9/, and is reasonable because of more realistic assumption in the Watt function than in Maxwellian.

The results at 90-deg. showed slight but appreciable change in shape and emission probability; the spectrum is softer (T_M=1.247 MeV) and emission rate is smaller as suggested from the effect of fragment anisotropy with respect to the incident beam.

3.2 Scattered Neutron Spectrum

Figure 6 presents the experimental results of scattered neutron spectra in comparison with those reproduced from JENDL-3T and ENDF/B-IV. The present results are in good agreement with both evaluations at 1.2 MeV; however, they show marked differences at higher incident energies.

In comparison with other experiments, the present data are in general agreement with those by Batchelor et al. /7/ at MeV region, and with those by Shen et al. /11/ at 14 MeV (Fig.7).

For MeV incident energies, the present values are smaller than JENDL-3T at levels around Q=-0.9 and -1.2 MeV, and is larger at higher levels and/or continuum region.

At 14 MeV incident energy, the present results are much larger than JENDL-3T especially at forward angles in high energy region where precompound neutron emission will be dominant.

High energy neutrons show strong forward rising as seen generally in other elements. The angle dependence are compared with the systematics by Kalbach-Mann /12/ and Kalbach /13/. In this comparison, the fraction of precompound reaction was estimated by fitting the angle integrated experimental

compound reaction was estimated by fitting the angle integrated experimental spectrum with superposition of three components corresponding to fission spectrum, cascade neutron spectrum and exciton spectrum. The fission neutrons were assumed to have spectrum by JENDL-3T and be isotropic in the laboratory frame. The results, shown in Fig.8, indicate the experimental data are interpreted more consistently by Kalbach systematics; similar result was observed also for thorium by our study. This is contrast to the general trends observed for lighter and non fissioning elements /4, 14/ and should be traced further by considering the effects of spectrum and angular distribution of fission neutrons.

4. Summary and Conclusion

We have measured double-differential neutron emission spectrum from ^{238}U, for incident neutrons between 1.2 and 14.1 MeV, and obtained the results for

1) prompt fission neutron spectrum for 2-MeV neutrons, and
2) double-differential neutron scattering cross sections for 1.2, 2.0, 4.2, 6.1 and 14.1 MeV neutrons.

The results were compared with other experiments and evaluation.

The experimental data for fission spectrum suggests the spectrum by ENDF/B-IV and JENDL-3T will be too hard.

For the inelastic scattering cross sections, the data indicates JENDL-3T overemphasizes the excitation of the levels around Q=-0.9, -1.2 MeV, and inversely underpredicts the high-lying and/or continuum levels at MeV incident energies, and neutrons due to pre-compound process at 14 MeV.

* JENDL-3T is a temporary file for testing the evaluated data for JENDL-3. The data in JENDL-3T may be partly revised in JENDL-3.

References:

1. WRENDA 87/88; World Request List for Nuclear Data, INDC(SEC)-095/URSF, IAEA(1980)
2. S.Chiba et al., J.Nucl.Sci.Technol.,22(10) 771 (1985)
3. M.Baba et al., Technology Report, Tohoku University 50(1) 1 (1985)
4. M.Baba et al., Proc.Int.Conf. "Nuclear Data" 1988 Mito, pp.209 & 291
5. R.E.Textor & V.V.Verbinski, ORNL-4160 (1965)

6. E.Barnard et al., Nucl.Phys., 65 236 (1965)
7. R.Batchelor et al., Nucl.Phys., 71 228 (1965)
8. D.G.Madland et al., Nucl.Sci.Eng., 81 213 (1982) and LA-UR-88-2340 (1988)
9. P.I.Johansson et al., Nucl.Sci.Eng., 62 695 (1977)
10. F.Frohner, IAEA Consultant Meeting "Physics of Neutron Emission in Fission" (Mito, 1988) No.9-1
11. G.Shen et al., Proc.Int.Conf. "Nuclear Data" 1988 Mito, pp.201
12. C.Kalbach & F.M.Mann, Phys.Rev., C23(1) 112 (1981)
13. C.Kalbach, Phys.Rev., C37(6) 2350 (1988)
14. I.Kumabe, 1988 Ann. Meeting of Atomic Energy Society of Japan, B23 and private communication.

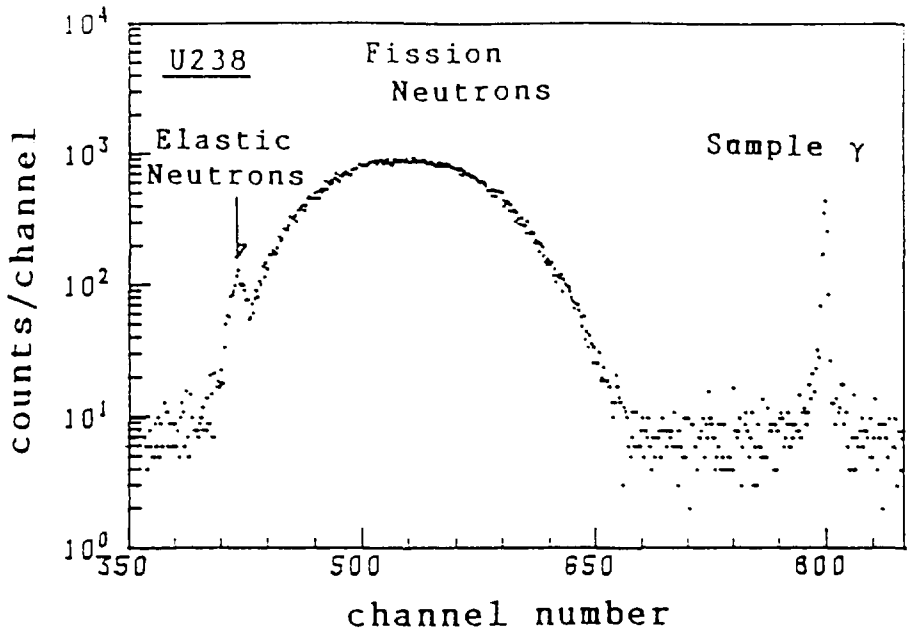

Fig. 1 T-O-F spectrum for neutron induced fission of 2-MeV neutrons on ^{238}U, measured by high-bias system at 135-deg. emission angle.

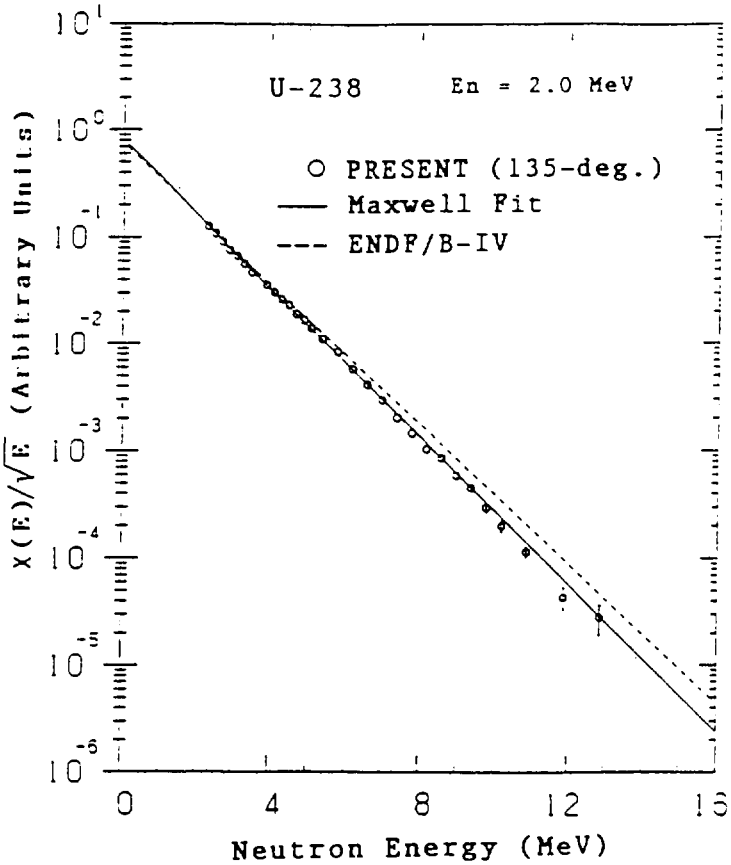

Fig. 2 Fission neutron spectrum for 2-MeV neutrons at 135-deg., divided by square root of emission energy, compared with the Maxwellian fit.

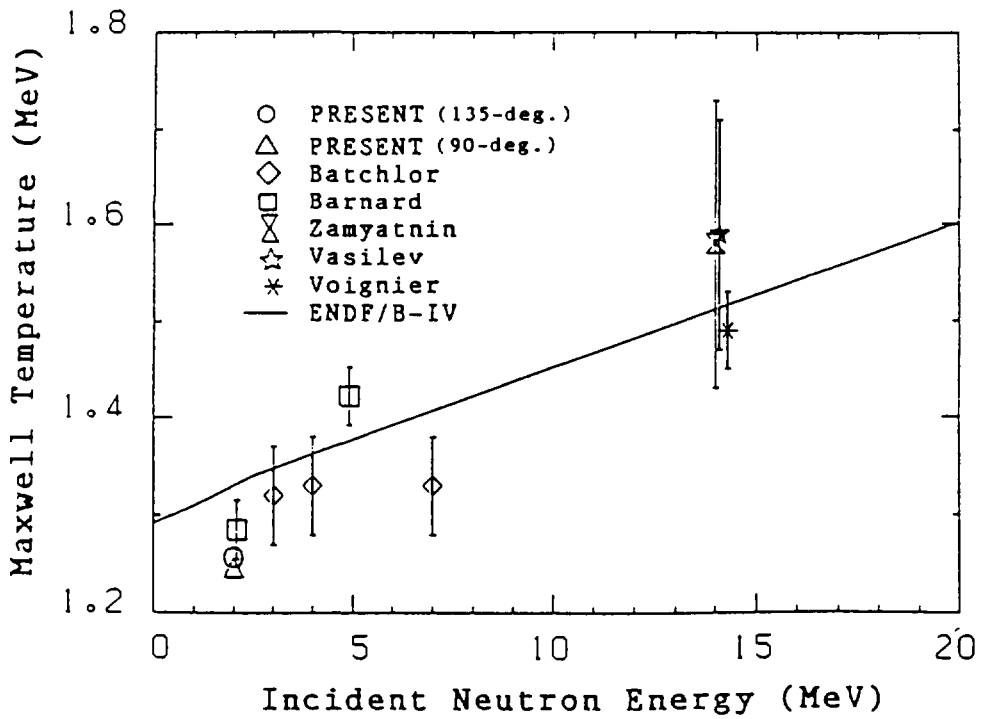

Fig. 3 The Maxwellian temperature of fission neutrons from ^{238}U.

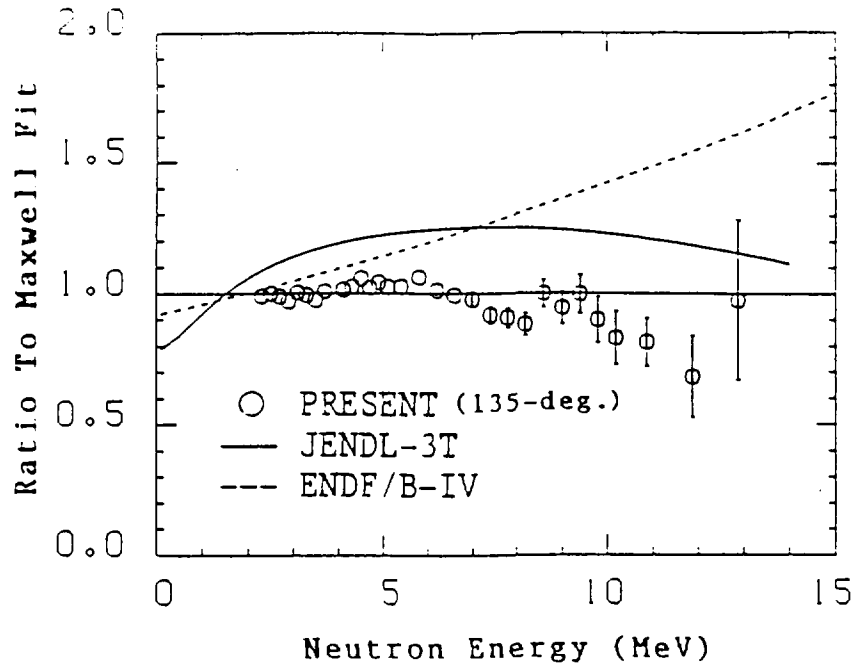

Fig. 4 Comparison between ^{238}U fission spectrum data, in the form of the ratio to the Maxwellian distribution that fits the experimental data.

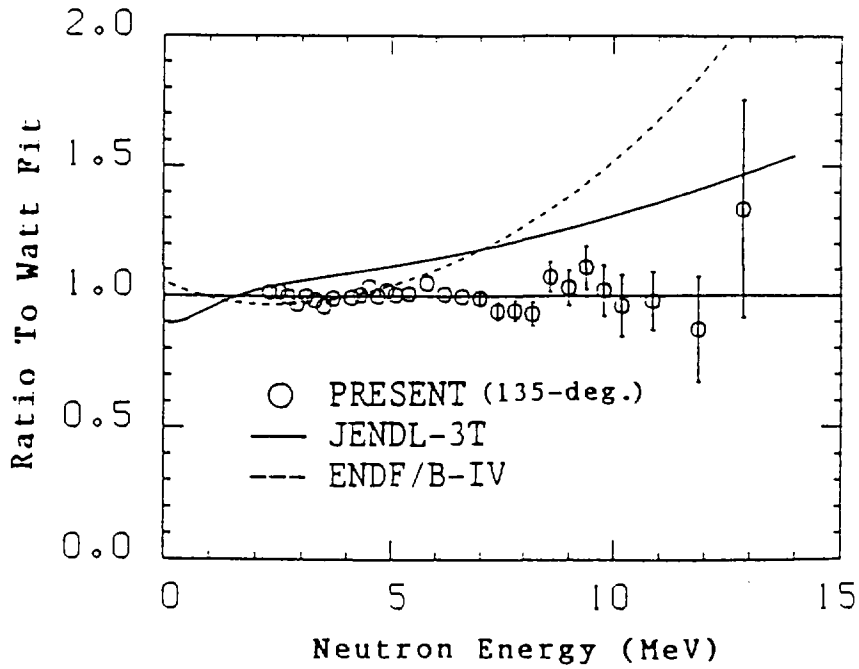

Fig. 5 The ratio of ^{238}U fission spectra to the Watt distribution function that fits the experimental data.

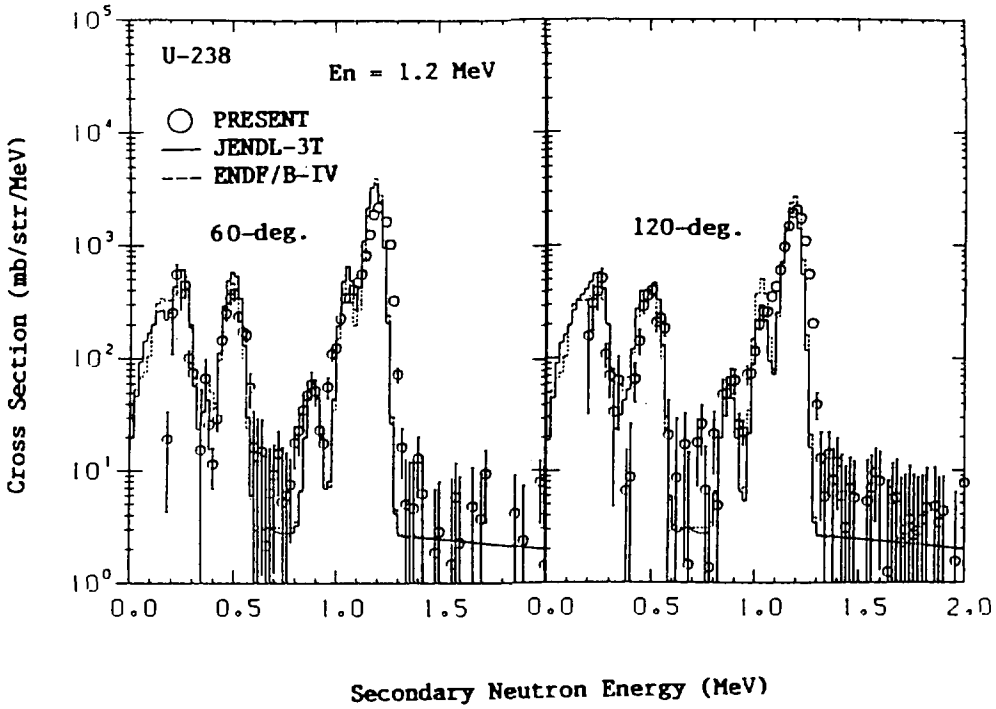

Fig. 6(a) Neutron emission spectrum of ^{238}U for 1.2-MeV neutrons.

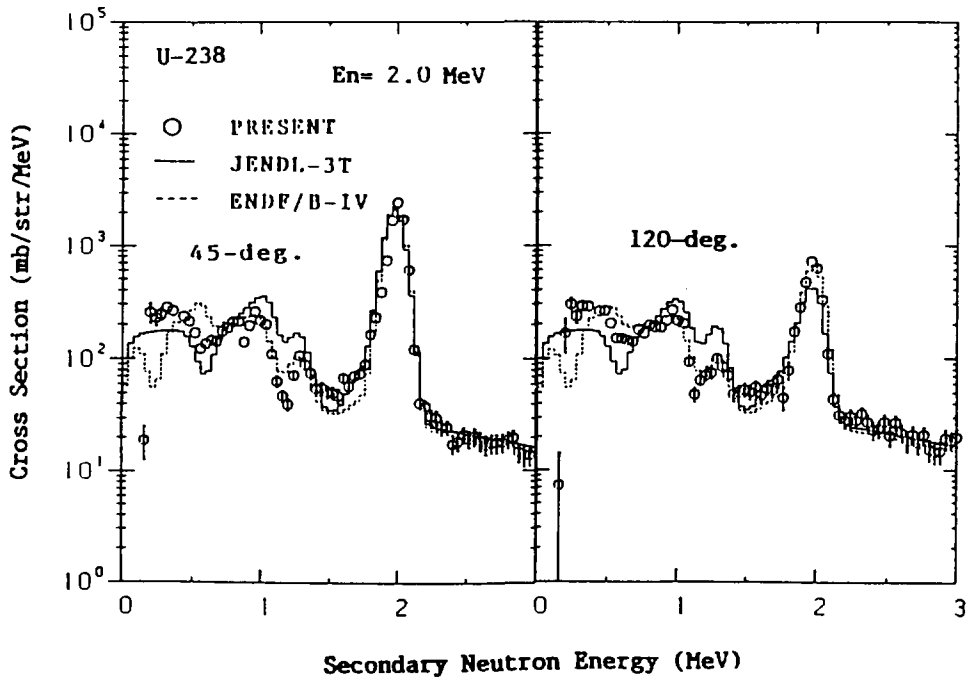

Fig. 6(b) Neutron emission spectrum of ^{238}U for 2.0-MeV neutrons.

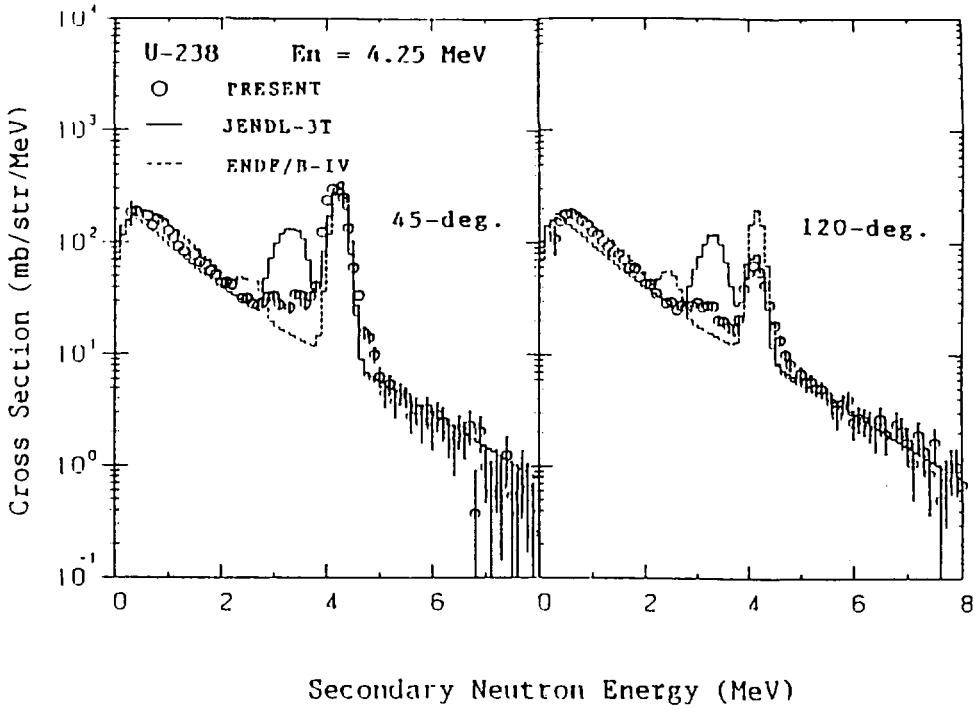

Fig. 6(c) Neutron emission spectrum of ^{238}U for 4.2-MeV neutrons.

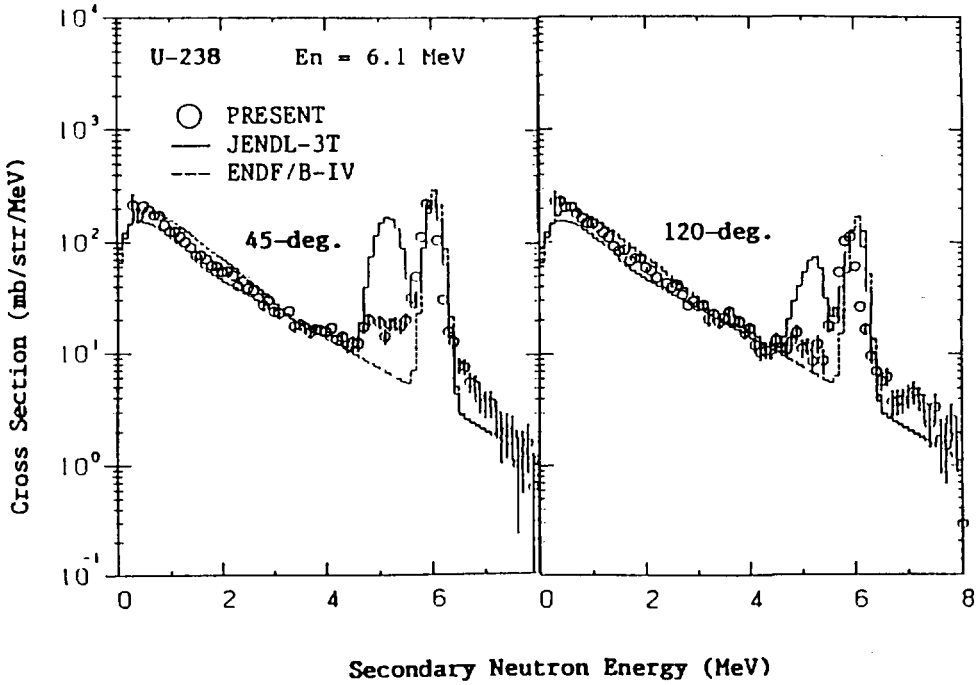

Fig. 6(d) Neutron emission spectrum of ^{238}U for 6.1-MeV neutrons.

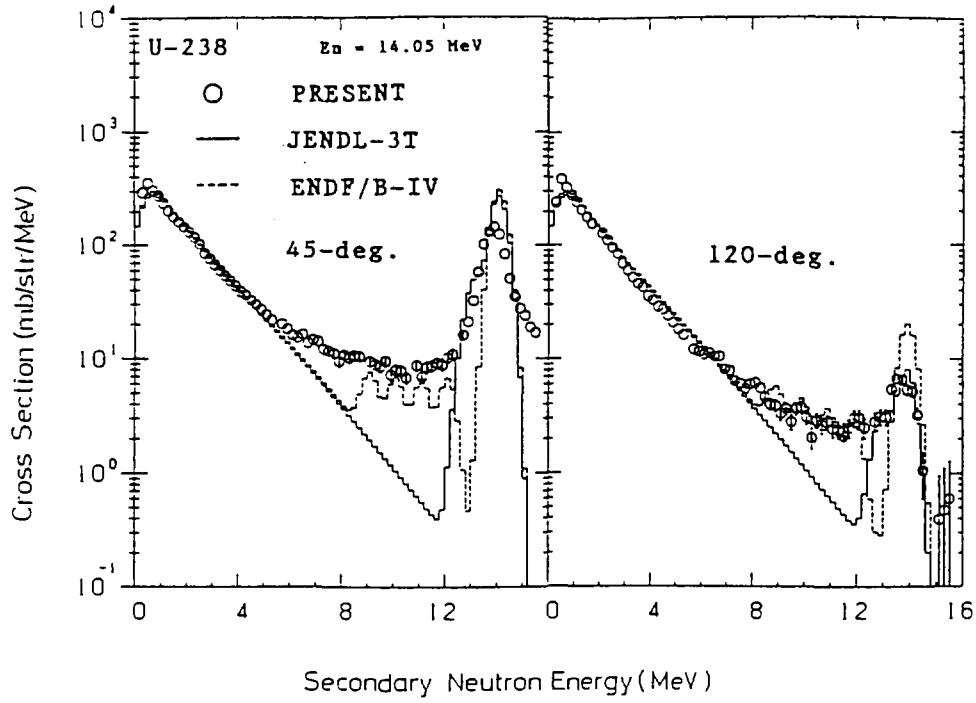

Fig. 6(e) Neutron emission spectrum of ^{238}U for 14.1-MeV neutrons.

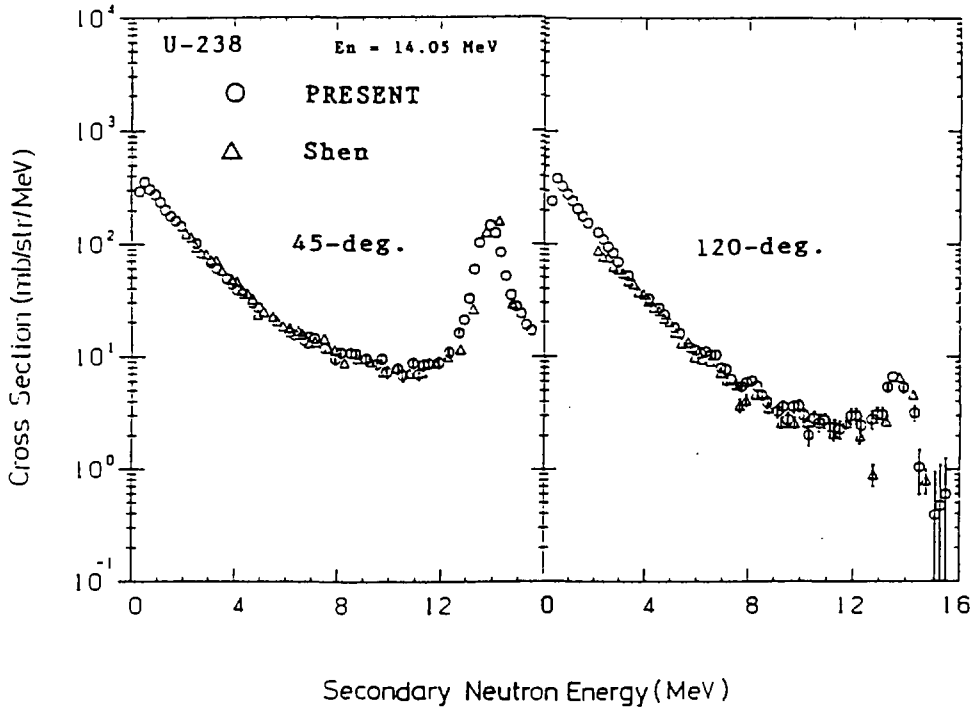

Fig. 7 Comparison of neutron emission spectrum from ^{238}U at 14.1-MeV incident energy.

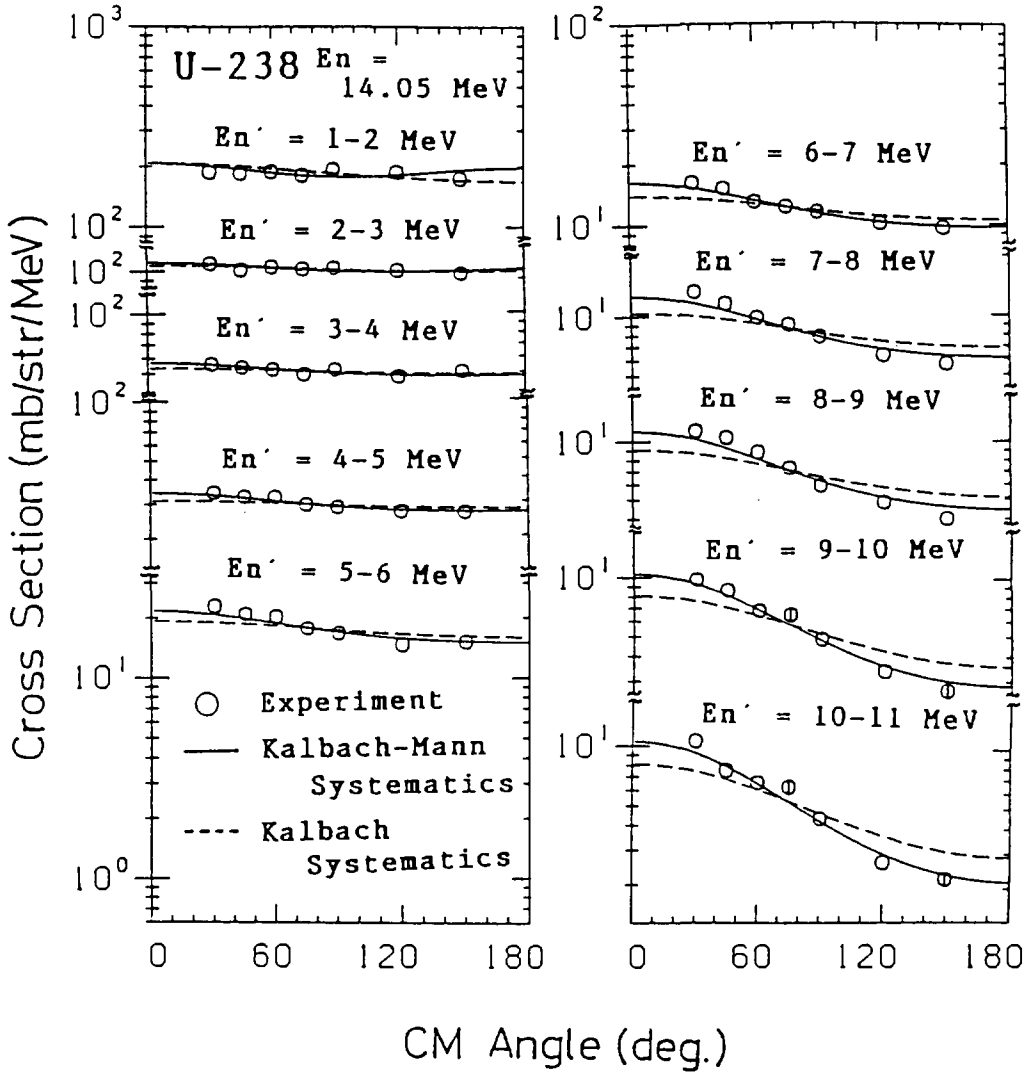

Fig. 8 Angular distribution of emission neutrons, compared with the calculation based on the systematics by Kalbach-Mann and Kalbach.

3.9 Evaluation of $^{238}U(n,n')$ Cross Sections

Yuji Uenohara and Yukinori Kanda

Department of Energy Conversion Engineering, Kyushu University
Kasuga, Fukuoka 816, Japan

Abstract

We evaluated the (n,n') cross sections for the 26 discrete levels and continuous region. In the present evaluations, direct reaction components for the discrete levels were evaluated by using coupled channel model code ECIS and DWBA code DWUCK4, and normalized to current measurements. The compound nucleus reaction components were done by using the statistical model code CASTHY. The more realistic evaluation results were obtained because of the employment of direct reaction models. The present evaluation results became larger than JENDL-2.

1. Introduction

Inelastic cross sections of ^{238}U are very important quantities for design of fast breeder reactors. The previous evaluation, JENDL-2, of inelastic cross sections for discrete levels were inaccurate above neutron energy of 3 MeV because of lack of experimental data. Recently, the inelastic cross sections for some discrete levels have been measured above neutron energy of several MeV. These experimental data are larger than JENDL-2.

In the present evaluation, the coupled channel model code ECIS and DWBA code DWUCK4 are used for the calculations of direct reaction components for the discrete levels. The compound nucleus reaction components are done by using the statistical model code CASTHY. The (n,n') cross sections for the twenty six

discrete levels and continuous region are included.

2. Status On Current Measurements of Inelastic Cross Sections

Before about 1980, the $^{238}U(n,n')$ cross sections were almost measured below incident neutron energies of two MeV. After about 1980, several measurements[1,2,3,4] were performed in higher energy regions. They were measured with $(n,n'\gamma)$ or (n,n') measurements. Olsen et al.[1] measured the inelastic cross sections for levels from 680- to 1224-keV in the incident neutron energy range from 0.5- to 5-MeV with $(n,n'\gamma)$ measurements. Beghian et al.[2] did those for first and second levels in the energy range from 0.9- to 3.1 MeV with (n,n') measurements. Haouat et al.[3] did those for the first and second levels from 0.7- to 3.5- MeV with (n,n') measurements. Shao et al.[4] measured those for levels from 680- to 1530-keV in the energy range between 0.9- and 2.2-MeV with both of $(n,n'\gamma)$ and (n,n') measurements. Olsen et al.'s data are very important and interest us since they give many information on inelastic scattering in high energy region, where measurements are scarce. However, Shao et al. suggest the discrepancy between $(n,n'\gamma)$ and (n,n') measurements.

3. Evaluation

Neutron inelastic scattering cross sections are evaluated as the excitation curves of discrete, and as those of a continuum of unresolved states. The level informations are given in Table I. At neutron energies of a few MeV, both of direct and compound processes contribute to inelastic scattering. The latter are small in the neutron energy of above 3 MeV. The experimental data measured in the high energy region become important to evaluate inelastic cross sections. We, therefore, evaluated the inelastic cross sections by normalizing the results of model calculations to new measurements.

The compound nucleus formation cross sections were calculated by using the coupled channel model code ECIS and wit the parameters shown in Eqs.1 to 4. They include cross sections for compound elastic scattering, direct and compound processes of inelastic scattering, (n,2n), (n,3n), fission, and capture. The cross sections for (n,2n), (n,3n) had been evaluated from the available experimental data. The fission and capture cross sections are taken from the results of the simultaneous evaluation.

We calculated the excitation curves of direct inelastic scattering processes using the coupled channel model and the distorted wave Born approximation and, then, normalized them to available experimental data.

The coupled-Channel model code ECIS was used for the first and second levels. The optical potential parameters[3] are

Real: $V_0=46.2 - 0.3E$, (1)
$r = 1.26$, $a = 0.63$,

Imaginarly: $W_s = 3.6 + 0.4E$ (Surface Absorption), (2)
$r_s = 1.26$, $a_s = 0.52$,

Spin-Orbit: $V_{so} = 6.2$, (3)
$r_{so} = 1.12$, $a_{so} = 0.47$,

and

Deformation: $\beta_2 = 0.198$, $\beta_4 = 0.057$. (4)

The calculated cross sections were normalized by referring the available experimental data[2,3,5]. The evaluated cross sections are shown in Figs.1 and 2.

For the 3rd through 26th levels, the excitation curves were

calculated with the distorted wave Born approximation code DWUCK4. The optical potential parameters[6] are

$$\text{Real} \qquad V_0 = 50.378 - 0.354E - 27.073(N - Z)/A, \qquad (5)$$
$$r = 1.264, \quad a = 0.612,$$

$$\text{Imaginarly: (Surface-Absorption)} \quad W_s = 9.265 - 0.232E + 0.03318E^2 - 12.666(N - Z)/A,$$
$$r_s = 1.256, \; a_s = 0.553 + 0.0144E, \qquad (6)$$

and

$$\text{Spin-Orbit} \qquad V_{so} = 6.2, \qquad (7)$$
$$r_{so} = 1.1, \; a_{so} = 0.75.$$

Above 3 MeV, Olsen et al.'s data, which were measured by detecting γ-ray from (n,n'γ), are available for the evaluations. However, we found that the results of Olsen et al. are higher than from Shao et al.'s results, in which emitted neutrons from (n,n') were detected. It is natural that neutron detection is more suitable than γ-detections. For the 6, 8, and 9th levels, the (n,n') cross sections were evaluated by comparing with Shao et al.'s measurements. The normalization constants for other levels were estimated from these normalizations.

The compound processes are calculated using the Hauser-Feshbach model code CASTHY.

The evaluated cross sections are shown in Figs.1 through 6 by the solid lines. The present evaluation's components are compared with the total inelastic cross sections of JENDL-2, in Fig. 7.

4. Conclusion

We have evaluated the inelastic cross sections of ^{238}U from thresholds to 20 MeV. The more realistic evaluation results have been obtained because of the employment of direct reaction models. The present evaluation results are larger than JENDL-2.

References

1) Olsen D.K. et al.,Proc.Int.Conf. Nuclear Cross Sections for Technology,Knoxville, USA, Oct. 1979 p.677

2) Beghian L.E. et al.: Nucl. Sci. Eng., 69, 191 (1979)

3) Haouat G. et al.: Nucl. Sci. Eng., 81, 491 (1982)

4) Shao J.Q., Nucl. Sci. Eng., 92, 350 (1986)

5) Guenter P.: ANL-NDM-16 (1975)

6) Madland D.G. and Young P.G.:"Neutron Nucleus Optical Potential for the actinide region" IAEA-190, P.251 (1978)

7) Nuclear Data Sheets 38 277 (1983)

Table 1 Level scheme of ^{238}U[7)]

No.	Energy[MeV]	J^{π}
0	0	0^+
1	0.0449	2^+
2	0.1484	4^+
3	0.3072	6^+
4	0.5178	8^+
5	0.6801	1^-
6	0.7319	3^-
7	0.7757	10^+
8	0.8271	5^-
9	0.927	0^+
10	0.95	2^-
11	0.9663	2^+
12	0.9983	2^+
13	1.0373	2^+
14	1.0595	3^+
15	1.0765	12^+
16	1.1056	3^+
17	1.127	4^+
18	1.1503	9^-
19	1.169	3^-
20	1.2239	2^+
21	1.243	4^-
22	1.27	6^+
23	1.2785	2^-
24	1.290	5^-
25	1.3784	11^-
26	1.4153	14^+

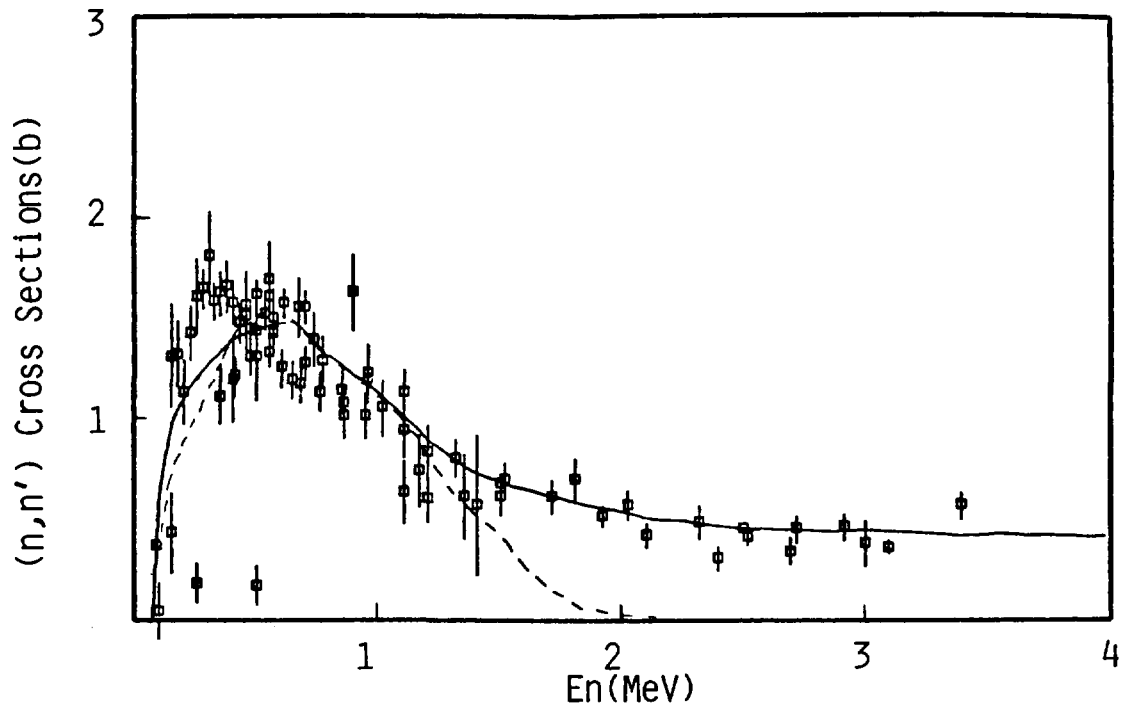

Fig. 1 Inelastic cross sections for discrete level (45 keV 2^+). Solid and dashed lines indicate present and JENDL-2 evaluations, respectively.

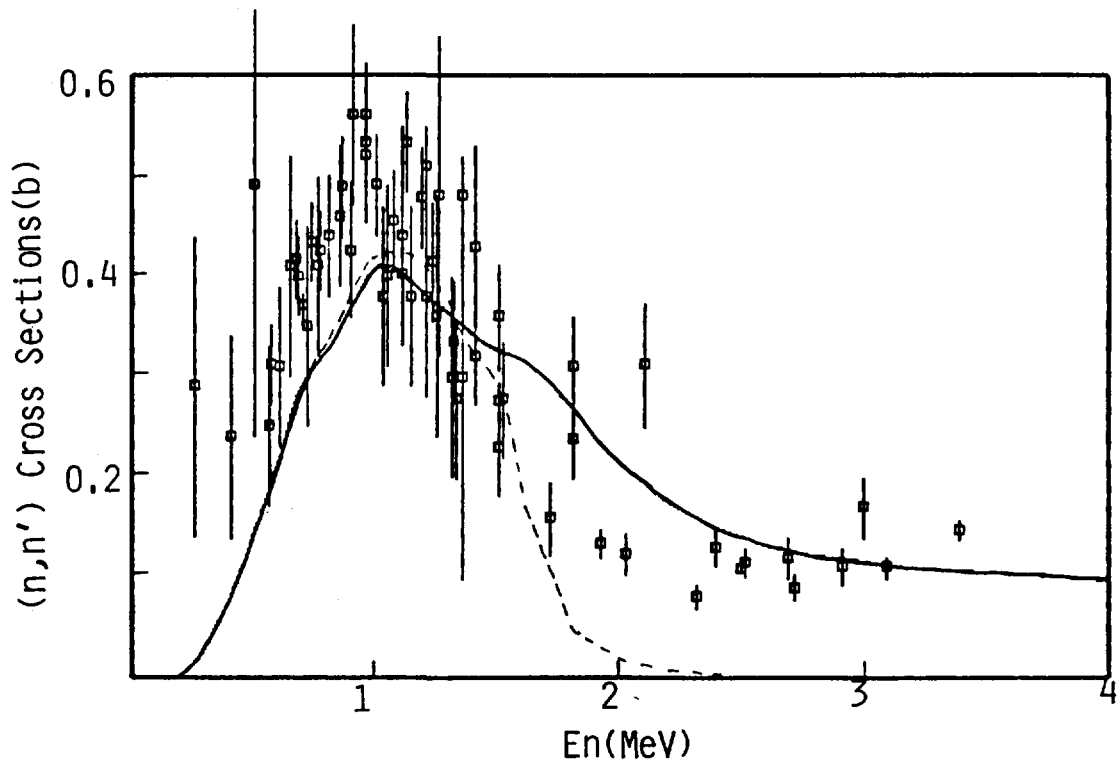

Fig. 2 Inelastic cross sections for discrete level (148 keV 4^+). The line type meanings are same as Fig. 1.

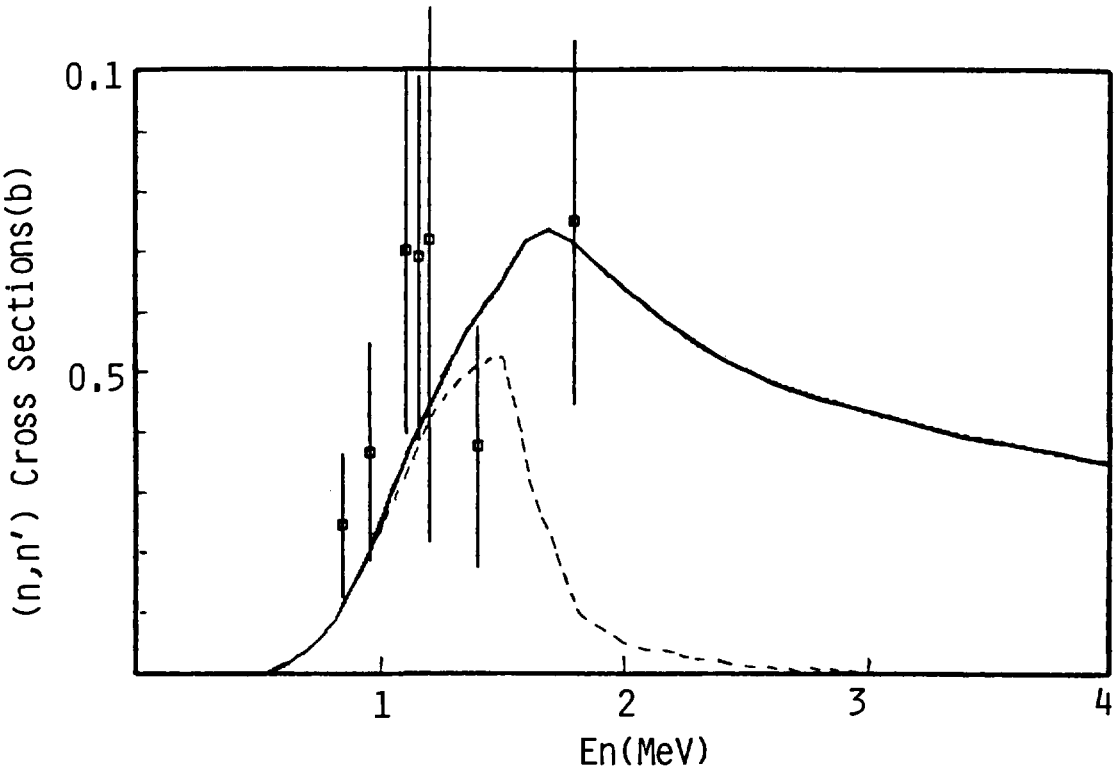

Fig. 3 Inelastic cross sections for discrete level (308 keV 6^+). The line type meanings are same as Fig. 1.

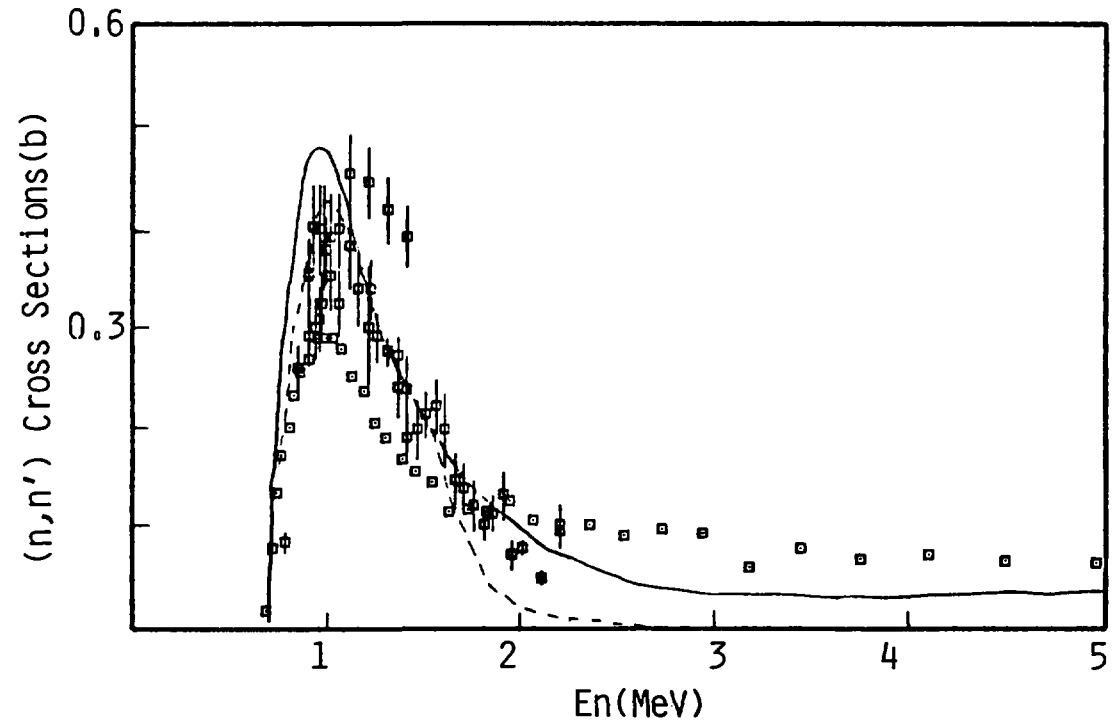

Fig. 4 Inelastic cross sections for discrete level (680 keV 1^-). The line type meanings are same as Fig. 1.

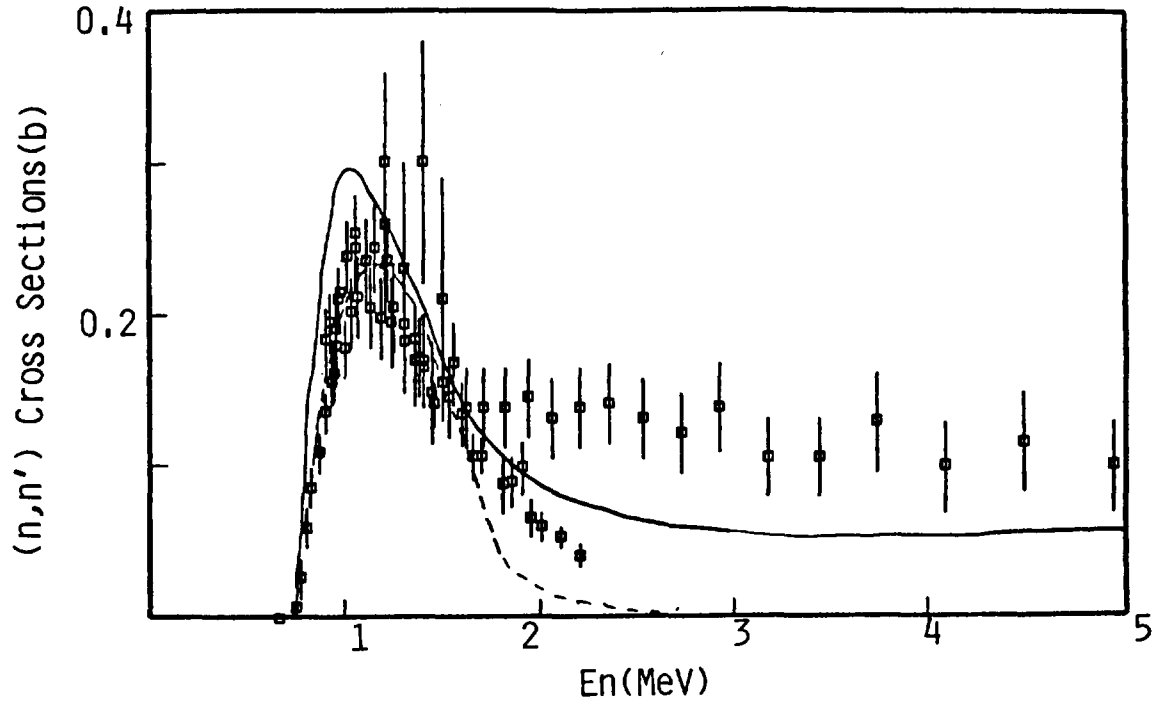

Fig. 5 Inelastic cross sections for discrete level (732 keV 3^-). The line type meanings are same as Fig. 1.

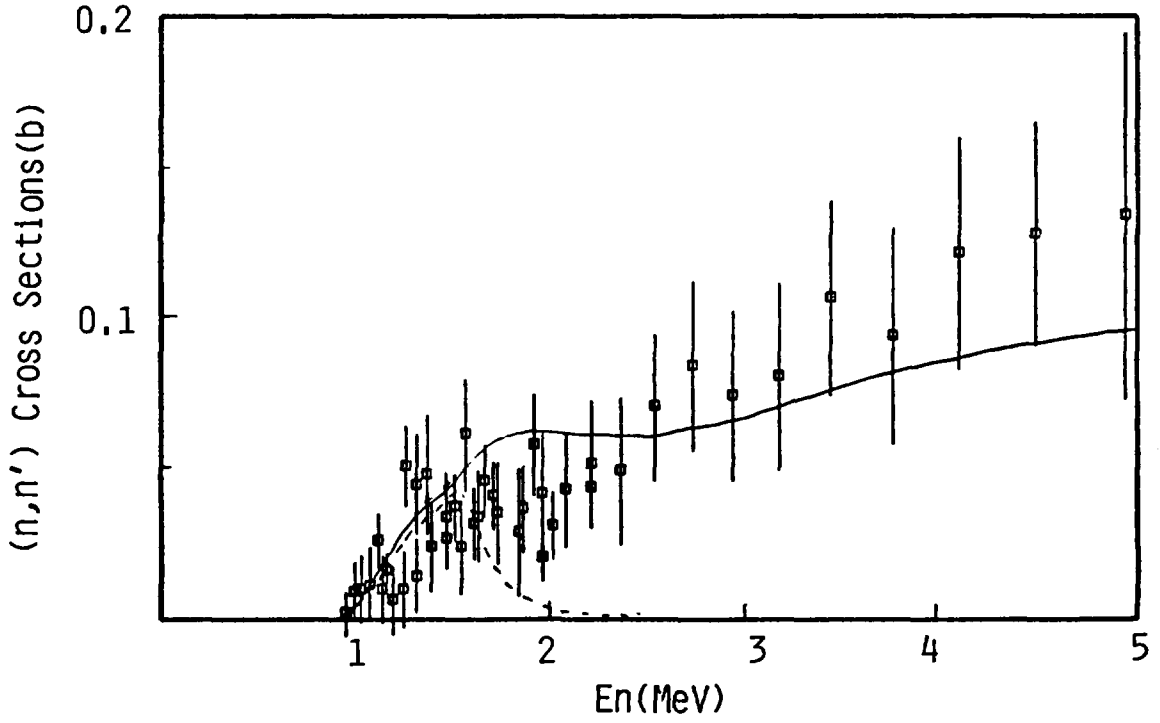

Fig. 6 Inelastic cross sections for discrete level (827 keV 5^-). The line type meanings are same as Fig. 1.

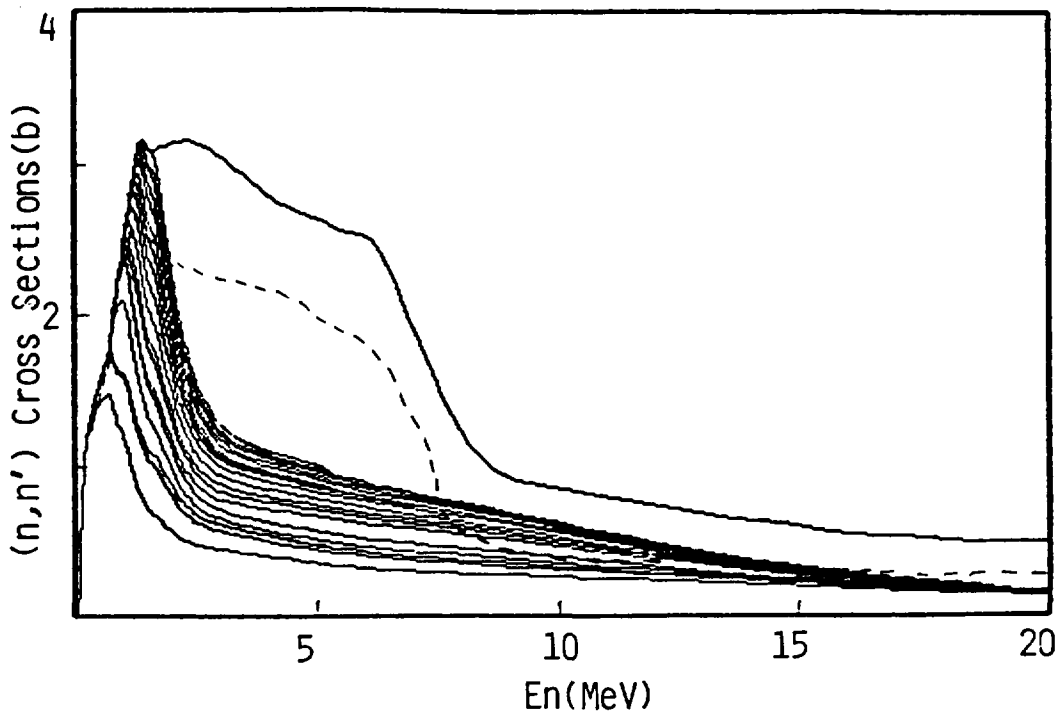

Fig. 7 Cumulative sum of the present evaluation's components culminating in the total inelastic cross sections. (Solid lines) The dashed line indicates the total inelastic cross sections of JENDL-2.

3.10 Adjustment of Evaluated Fission Neutron Spectrum by Integral Data

Toshihiko KAWANO, Yuji UENOHARA, and Yukinori KANDA
Department of Energy Conversion Engineering,
Kyushu University, Kasuga, Fukuoka 816, Japan

ABSTRACT : Fission spectra of both Madland-Nix's ^{235}U and Mannhart's ^{252}Cf are adjusted by Bayesian method, so that integral data are consistent with differential data. Six cross sections, $^{27}Al(n,p)$, $^{27}Al(n,\alpha)$, $^{54}Fe(n,p)$, $^{56}Fe(n,p)$, $^{59}Co(n,\alpha)$ and $^{56}Ni(n,p)$, are chosen for the bases of adjustment procedure. An effect of an *a priori* covariance matrix is also examined. Spectrum averaged cross sections reduce after adjustment of the spectrum.

1. INTRODUCTION

A prompt fission neutron spectrum is important not only as a nuclear data but also for a confirmation of an evaluated differential cross section by comparing with a fission spectrum averaged cross section. The differential cross sections are measured in a monoenergetic neutron field. On other hand, measurements of the fission spectrum averaged cross sections are performed in well-known neutron fields like $^{235}U(n,f)$ and ^{252}Cf (spontaneous) fission neutron spectrum. And the integral data must be consistent with the differential data.

The fission neutron spectra should be accurate and be consistent with experimental data. As concerns the ^{235}U fission neutron spectrum, there are, however, some discrepancies between the integral data and calculated spectrum averaged cross sections by means of the fission spectra of contemporary files, namely, Maxwellian type, Watt type, and Madland-Nix type fission neutron spectrum.

In the present work, the ^{235}U and the ^{252}Cf fission neutron spectrum are modified by Bayesian method in order to become good mediators between the integral and the differential data. Six cross sections - $^{27}Al(n,p)$, $^{27}Al(n,\alpha)$, $^{54}Fe(n,p)$, $^{56}Fe(n,p)$, $^{59}Co(n,\alpha)$ and $^{59}Ni(n,p)$ - are chosen for the bases of adjustment procedure, since their cross sections are determined relatively well.

2. METHOD OF CALCULATION

Before adjustment of a fission neutron spectrum, both fission neutron spectrum averaged cross section and differential cross section are estimated by experimental integral and differential data, respectively. The evaluated differential cross section is given by following equations.

$$\theta = (\Psi^t V^{-1} \Psi)^{-1} (\Psi^t V^{-1} Y) \quad (1)$$

where the vector Y is composed of logarithms of the experimental values including absolute and relative measurements, and the matrix V is a covariance matrix of the vector Y. The parameter vector θ is approximately equal to product of a design matrix Ψ and the vector Y. The design matrix is made up so as to interpolate an interval of evaluation energy points.

Spectrum adjustment is performed as follows.

$$\chi_1 = \chi_0 + M_0 \Phi^t(\Phi M_0 \Phi^t + V)^{-1} (I - \Phi \chi_0) \quad (2)$$

$$M_1 = M_0 - M_0 \Phi^t(\Phi M_0 \Phi^t + V)^{-1} \Phi M_0 \quad (3)$$

$$\chi = \chi_1 + M_1 C^t(C M_1 C^t)^{-1} (1.0 - C \chi_1) \quad (4)$$

$$M = M_1 - M_1 C^t(C M_1 C^t)^{-1} C M_1 \quad (5)$$

where

χ_0 : *a priori* parameter vector composed of fission neutron spectrum,
M_0 : *a priori* covariance matrix of parameter χ_0,
χ : *a posteriori* parameter vector,
M : *a posteriori* covariance matrix of parameter χ,
I : vector of experimental data,
V : covariance matrix of the experimental data I,
Φ : design matrix ($\Phi \chi_0$=I),
C : design matrix for normalization of the spectrum χ_1 ($C\chi_1$=1.0).

The spectrum of ^{235}U in JENDL-3T[1] calculated by Madland and Nix's formula and the spectrum of ^{252}Cf evaluated by Mannhart[2] are employed as the *a priori* parameters χ_0. As to ^{235}U, An effect of an a priori covariance matrix has to be investigated, since the *a priori* covariance matrix M_0 is not given. In this study, standard error of the spectrum at every energy point is assumed to be 5 %, and correlation factors between different energy points are assumed to be nothing in one case and 50 % in another case.

3. RESULTS AND DISCUSSION

An adjusted fission neutron spectrum of ^{235}U is shown in Fig. 1 when the correlation factors are all 0 %. In this figure, the solid line indicates the *a posteriori* spectrum, the dotted line indicates the *a priori* spectrum of JENDL-3T. And the ratio of the *a posteriori* to the *a priori* spectrum is also shown in this figure. Bayesian estimation so acts on the spectrum as to reduce it, since the spectrum averaged cross sections tend to become larger than experimental values when the evaluated differential cross sections employed in the present study are averaged by the *a priori* spectrum, as seen in Fig. 5. On the other hand, because of a small sensitivity of the differential cross sections of the 6 reactions in a low energy region, spectrum reduction is executed at a high energy region where influence of the differential data upon the spectrum averaged cross sections is effective. In addition, the spectrum must be normalized. Consequently, the adjusted spectrum increases below about 3 MeV in order to compensate the reduction of the spectrum in the high energy region.

Fig. 2 is also the ^{235}U fission neutron spectrum, though the correlation factors are all 50 %. The tendency and the feature are similar to the adjusted spectrum discussed on Fig. 1. The modification, however, spreads over the energy because of an existence of the correlation.

The differential cross section has an effective energy region where the spectrum averaged cross section is contributed up to 90 % when the spectrum is adjusted to it. The lower limit of the energy region is about 2 MeV of $^{58}Ni(n,p)$ reaction, and the upper limit is about 15 MeV of $^{27}Al(n,\alpha)$. Because of a lack of an information in the outside of the region, it cannot be mentioned that the spectrum is determined firmly

there. If spectrum adjustment must cover a wide range of neutron energy, different reactions that the marginal energy region is covered with their effective energy regions must be employed.

Adjusted spontaneous fission neutron spectra of ^{252}Cf are demonstrated in Figs. 3 and 4. The dotted line is an *a priori* spectrum evaluated by Mannhart. As seen in Figs. 1 and 2, an influence of the covariance is small except for assumptions of extreme correlations. Hence, the same assumptions with that of ^{235}U fission spectrum adjustment is applied to Mannhart's spectrum, as it has own covariance matrix. Differential cross sections averaged by Mannhart's spectrum are consistent with the experimental integral values, and a variance is small.

In Figs. 5 and 6, ^{235}U and ^{252}Cf fission spectrum averaged cross sections are shown, respectively. In these figures, the solid line is the adjusted cross section when a correlation is 0 %, the dotted and dashed line is the case of 50 % correlation, and the dotted line is calculated with the *a priori* spectrum.

In Fig. 5, the adjusted cross sections of $^{27}Al(n,\alpha)$ and $^{59}Co(n,\alpha)$ reactions are below weighted averaged values of experimental integral data. These two reactions have relative high threshold energies. And above the threshold energies, adjusted spectrum is less than the original. The over-reduction then takes place, though the adjusted cross sections approach to the experimental integral data.

Although, it is possible to modify the evaluated differential cross sections in order to adjust the spectrum averaged them to integral data[3], adjustment of the evaluated differential cross sections cannot be recommended, because they include so many experimental informations. Hence, it may be said that the spectrum adjustment is reasonable because a small modification brings a desirable consistency.

4. CONCLUSION

Fission spectra of both ^{235}U in JENDL-3T and Mannhart's ^{252}Cf are adjusted, so that integral data are consistent with differential data. The spectra are reduced dominantly at the neutron energy of from 3 MeV to 15 MeV where the differential data are effective.

There are little difference of the *a posteriori* spectra between the case of 0 % correlation assumption and the case of 50 %.

REFERENCES

[1] JENDL Compilation Group (Nuclear Data Center,JAERI):JENDL-3T Private Communication (1987).

[2] W.Mannhart, "Evaluation of the Cf-252 Fission Neutron Spectrum between 0 MeV and 20 MeV", 6th ASTM/Euratom Symposium on Reactor Dosimetry, Jackson Hole, Wyoming USA, June 1987.

[3] Y.Kanda, Y.Uenohara, "Evaluation of Some Activation Cross Sections Measured by Monoenergetic and Fission Neutrons", International Conference on Nuclear Data for Science and Technology, Mito Japan, May 1988.

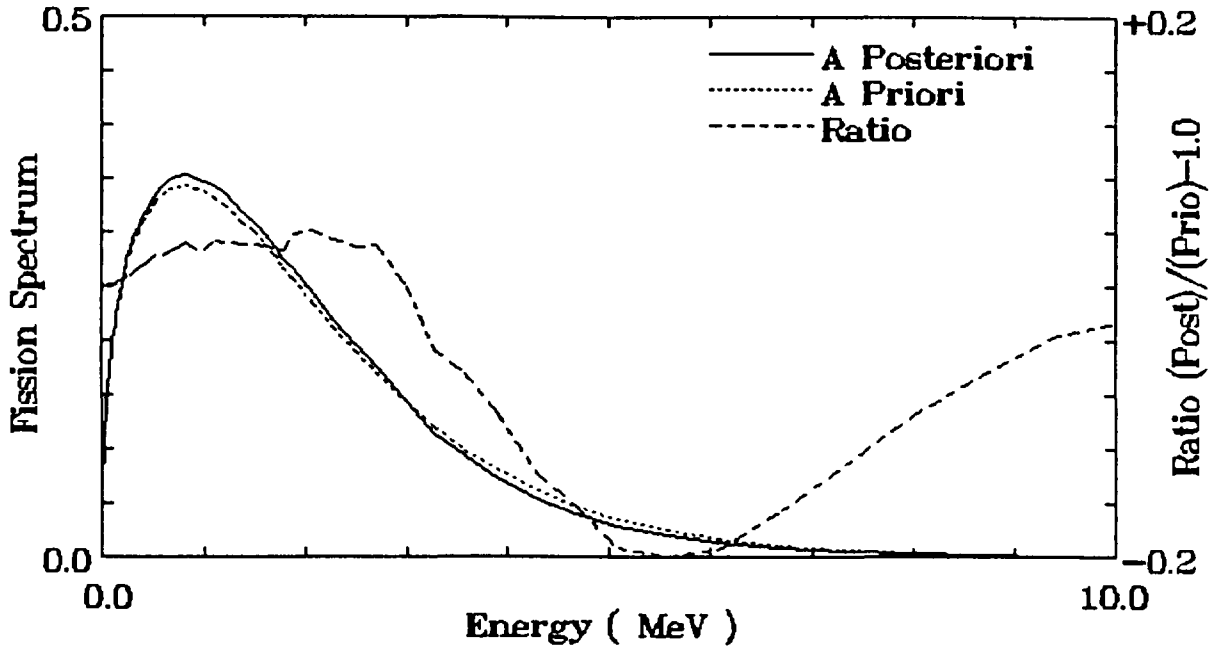

Fig. 1 Fission neutron spectrum of ^{235}U when correlation is 0 %
solid line : a posteriori spectrum
dotted line: a priori spectrum (JENDL-3T)

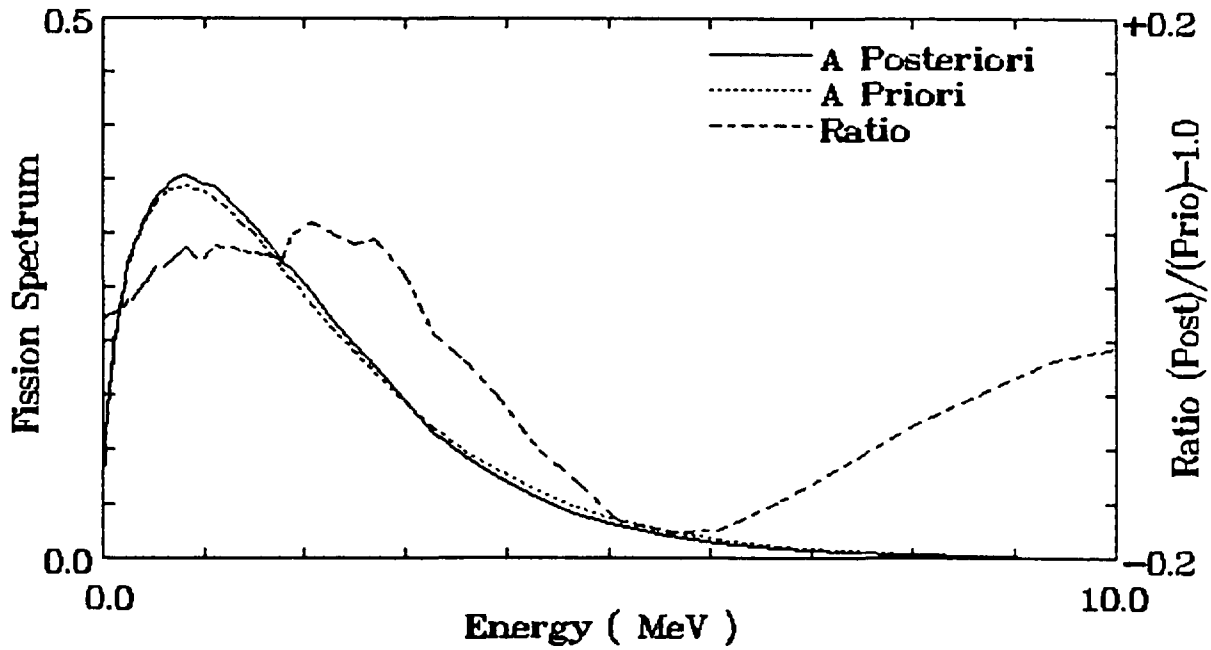

Fig. 2 Fission neutron spectrum of ^{235}U when correlation is 50 %
solid line : a posteriori spectrum
dotted line: a priori spectrum (JENDL-3T)

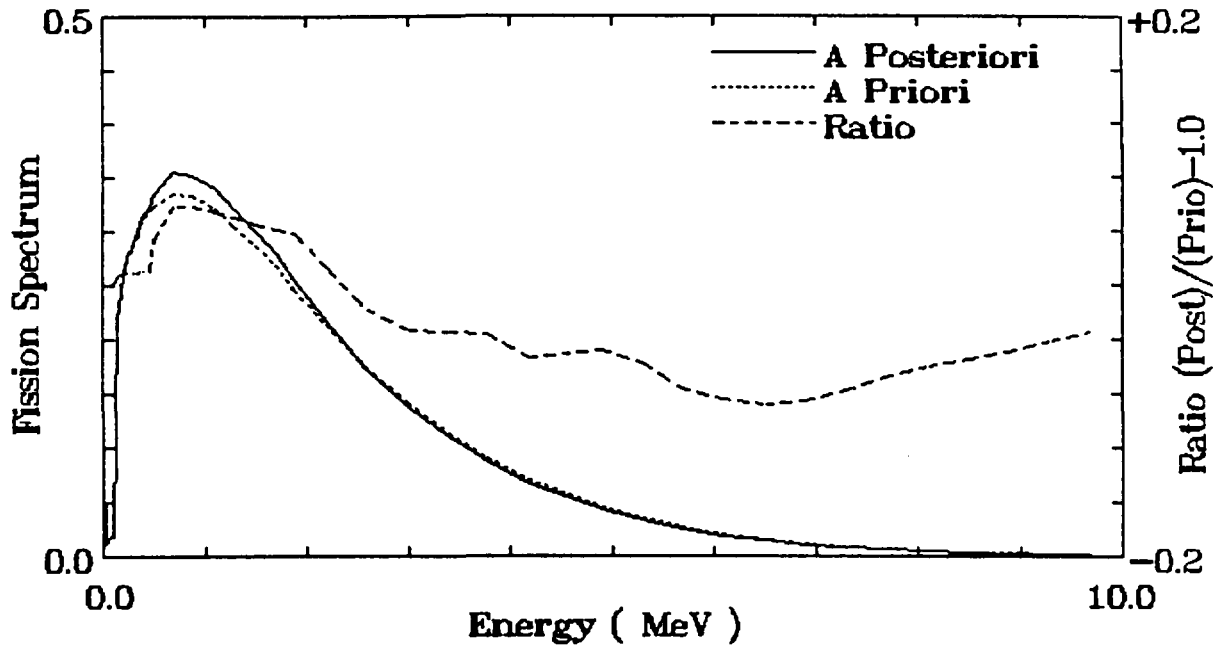

Fig. 3 Fission neutron spectrum of ^{252}Cf when correlation is 0 %
solid line : a posteriori spectrum
dotted line: a priori spectrum (Mannhart)

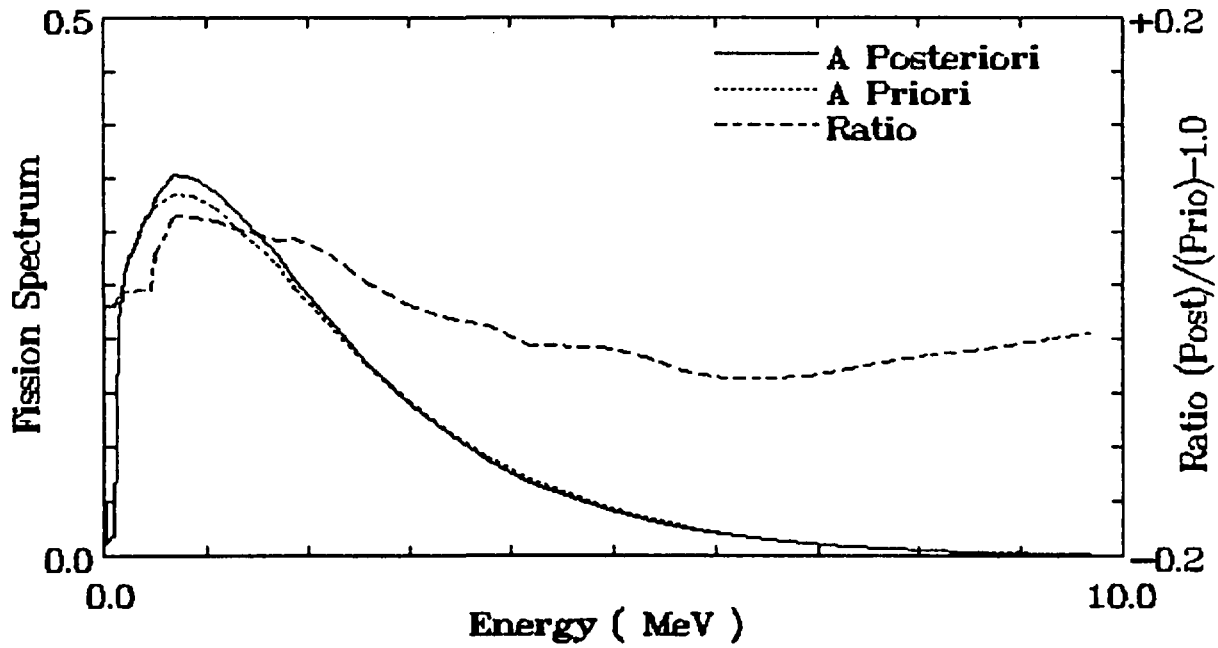

Fig. 4 Fission neutron spectrum of ^{252}Cf when correlation is 50 %
solid line : a posteriori spectrum
dotted line: a priori spectrum (Mannhart)

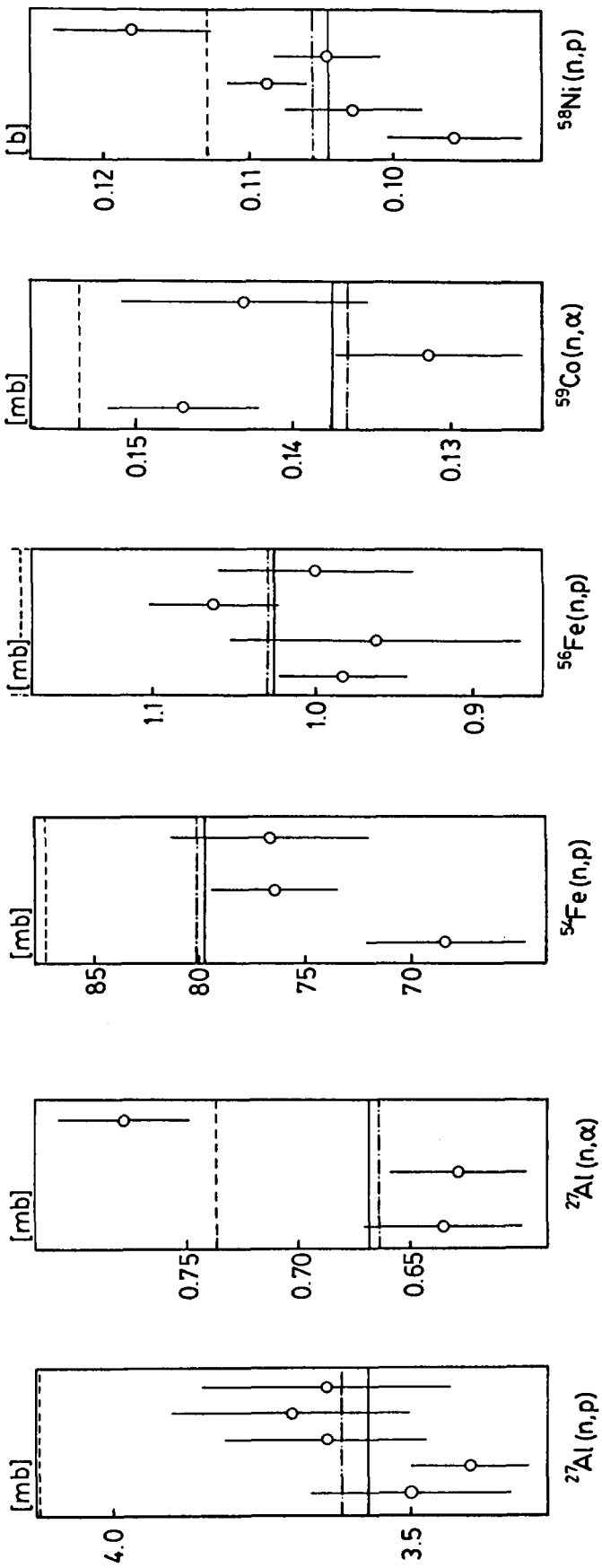

Fig. 5 ^{235}U fission spectrum averaged cross sections
solid line: adjusted spectrum averaged cross section when correlation is 0 %
dotted and dashed line: when correlation is 50 %
dotted line: a priori spectrum averaged cross section

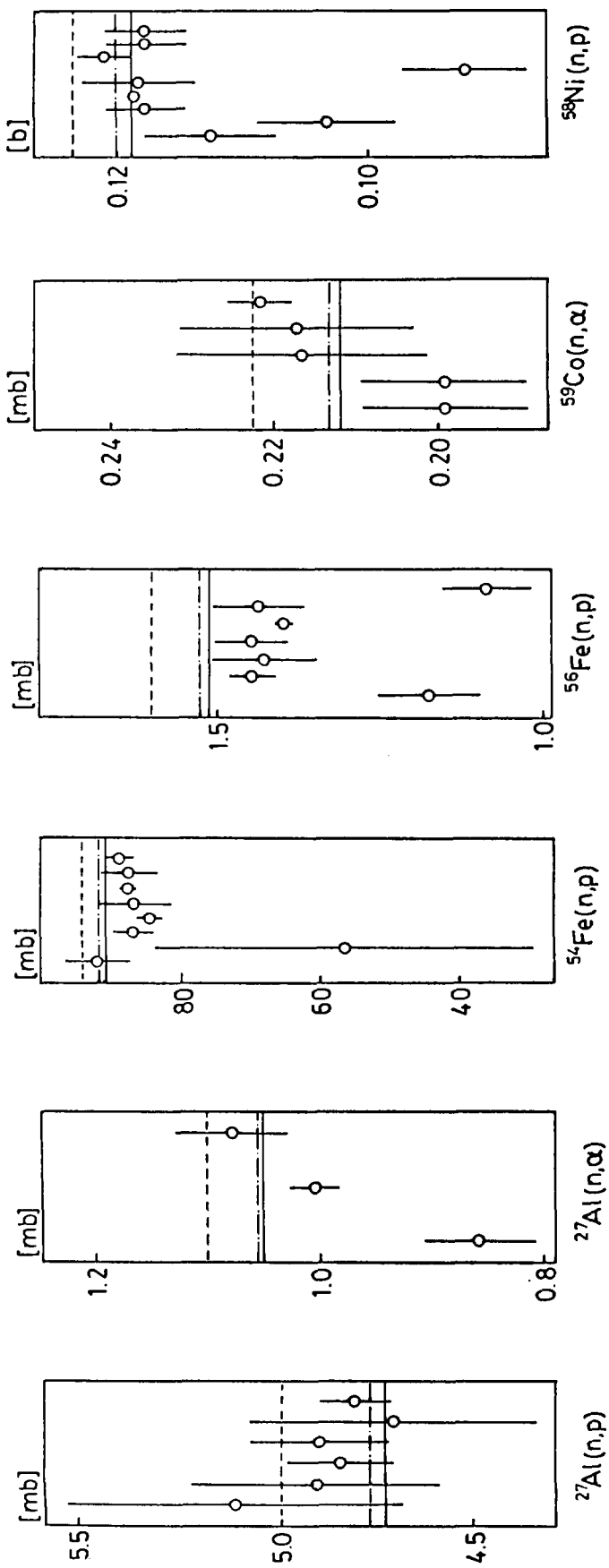

Fig. 6 ^{252}Cf fission spectrum averaged cross sections
solid line: adjusted spectrum averaged cross section when correlation is 0 %
dotted and dashed line: when correlation is 50 %
dotted line: a priori spectrum averaged cross section

3.11 Compilation of MCNP Data Library Based on JENDL-3T and Test through Analysis of Benchmark Experiment

K. Sakurai, N. Sasamoto, K. Kosako, T. Ishikawa, O. Sato,
Y. Oyama, H. Narita, H. Maekawa, K. Ueki
Research Committee on Reactor Physics of JAERI,
MCNP Data Library Compilation Subworking Group
Japan Atomic Energy Research Institute,
Tokai-mura, Naka-gun, Ibaraki-ken

Based on an evaluated nuclear data library JENDL-3T, a temporary version of JENDL-3, a pointwise neutron cross section library for MCNP code is compiled which involves 39 nuclides from H-1 to Am-241 which are important for shielding calculations. Compilation is performed with the code system which consists of the nuclear data processing code NJOY-83 and library compilation code MACROS. Validity of the code system and reliability of the library are certified by analysing benchmark experiments.

1. Introduction

More than five years have already passed since introduction of a continuous energy model Monte Carlo code MCNP[1] to Japan. At present, the MCNP has become widely utilized mainly in a field of radiation shielding. Since the nuclear cross sections to be used in MCNP are the pointwise ones, we are free from computational errors based on group averaging process, such as errors due to self-shielding factors, energy group structures, etc. This is the reason why MCNP is considered to be suitable for benchmark test on nuclear data.

The only pointwise cross section library being used for MCNP calculations in Japan is the one compiled at LANL(Los Alamos National Laboratory) mainly based on ENDF/B-4 files. On the other hand, the Japanese evaluated nuclear data library JENDL is available in Japan and its latest version, JENDL-3, is scheduled to be released. In advance of its release, JENDL-3T[2], a temporary nuclear data library of JENDL-3, has been compiled for various benchmark test calculations. The benchmark tests are now in progress, based on transport calculations with DOT-3.5 and MORSE codes using group constants library from JENDL-3T. Then, in order to carry out benchmark tests using pointwise cross section data, a pointwise neutron cross section library for MCNP was compiled based on JENDL-3T, including 39 nuclides from H-1 to Am-241 which are usually used for shielding calculations. Compilation was made at MCNP Data Library Compilation Subworking Group (SWG) of Research Committee on Reactor Physics of JAERI.

2. Compilation of MCNP Library Based on JENDL-3T

The present system consists of the nuclear data processing code system NJOY-83, a modified version of NJOY, and the compilation code MACROS with which the pointwise data generated with NJOY-83 are arranged to the library to be adaptable to MCNP. Schematic flow of the present system is given in Fig.1. The MACROS includes the following functions : 1) compiling new cross section library, 2) adding new cross section data to the library, 3) deleting stored data from the library, 4) replacing new data with the stored ones, 5) rearranging order of stored data and 6) printing stored data. Original data from JENDL-3T are referred to generate pointwise neutron cross sections in ACE format for every 39 nuclides, which are then stored on a temporary file. When generation for every nuclides is completed, the data generated are transferred to MACROS code to compile pointwise cross section library, together with their directory file for MCNP.

The library includes 39 nuclides as given in Table 1. Most of them are those from JSD1000[3], the standard shielding group constant library in Japan and the rest from the nuclides specific in fusion neutronics field. Therefore the present library is considred to cover almost all nuclides necessary for shielding design calculations of any kinds of facilities. The pointwise data of some nuclides are generated based not only on JENDL-3T but on ENDF/B-4. The pointwise data based on ENDF/B-4 using the present code system are to be compared with ENDF/B-4 based data by LANL to certify validity of the present compilation system. As for secondary gamma-ray production cross sections, only those of 23 nuclides among 39 are included in JENDL-3T and those of the rest nuclides are replaced by those from ENDF/B-4.

Although the present library includes only neutron transport and secondary gamma-ray production cross sections, at the time when JENDL-3 is released for general use, we have a plan to generate and compile final version of JENDL-3 based library by adding $S(\alpha,\beta)$ data and gamma-ray transport cross sections to the present system.

3. Analysis of Iron Benchmark Experiments

Compilation method of pointwise cross section library for MCNP with NJOY-83/MACROS was verified by the following procedures. At first neutron transport calculations with MCNP were carried out for all nuclides considered in the library using an imaginary spherical geometry with the radius of 10 cm containing 14 MeV neutrons at its center. As a result, it was shown that the directory file and cross section data library are adequately read in by MCNP and that although not so rigorously certified, neutron transport calculations are performed properly. As a second stage of verification, we calculated several benchmark experiments with MCNP using both ENDF/B-4 based library compiled by our system [ENDF/B-4(SWG)] and

also ENDF/B-4 based one by LANL [ENDF/B-4(LANL)]. The calculational results show that the calculations with two ENDF/B-4 based libraries agree with each other within FSDs (fractional standard deviations) of the MCNP calculations. After verifying the present compilation method, we then moved on to analysis of the benchmark experiments with MCNP using JENDL-3T based library. Among many calculations performed, only the results for some iron benchmark experiments [4,5,6] are presented in the paper. The results were compared with the measurements and the calculations using ENDF/B-4 based library to investigate reliability of the JENDL-3T data.

3.1 Analysis of KfK Iron Experiment[4]

Measurements were made for leakage spectra from spherical surface covering the energy range from 60 keV to 5 MeV for the configuration of iron sphere with a radius of 20 cm, involving Cf-252 neutrons at its center. MCNP calculations were made using 30,000 histories with an energy and space dependent weight-window method, assuming a surface crossing estimator on the actual surface of the sphere, resulting in FSD values of 3 - 6 % on energy spectra for the entire energy region of interest. In Fig.2 is given a comparison of the calculated spectra with the measured ones. The two calculations using the ENDF/B-4 based libraries are found to agree with each other within their FSD values. Besides, their agreement with the calculations using JENDL-3T based library are also excellent : no meaningful differences are observed above 1 MeV, the calculations agree generally well with the measured spectrum.

3.2 Analysis of LLL Iron Sphere Experiment[5]

Measurements were made for neutron leakage spectra from a spherical iron sample ranging from 2 - 15 MeV. Experimental configurations were modeled by three-dimensional spheres because of anisotropic distribution of D-T neutrons. Figure 3 provides comparison of the calculated and measured spectra from iron sphere.MCNP calculaitons were performed using 10,000 histories with energy and space dependent weight-window method with a point estimator defined at the actual detector positions, resulting in energy spectra with FSD value of less than 5 % except for the region of 6 - 12 MeV where FSD value is 10 -15 % because of relatively low flux distribution. JENDL-3T based spectrum apparently underestimates the other ENDF/B-4 based calculations at 7 - 10 MeV and 11- 13 MeV, especially the underestimate at the latter region is prominent. Although we obtained good agreement among the three calculaitons at 13 - 14 MeV, they underestimate the measurement. In spite of the disagreement at higher energy region, the excellent agreement is obtained among all the spectra below 6 MeV.

3.3 Analysis of Winfrith Iron Penetration Experiment[6]

Measurements were made of penetrated neutron spectra through very

thick iron slab up to about 110 cm in depth. Calculations with 130,000 histories were performed with the space and energy dependent weight-window method using both JENDL-3T based library and ENDF/B-4 based one by LANL. An estimator NESXE[7] was also employed in order to improve FSD. In Figs.4 through 6 are given comparisons of the MCNP calculated neutron spectra and the measured ones. As a whole, their agreement is satisfactory. But the measured spectra agree with the ENDF/B-4 based spectra apparently better than those based on JENDL-3T above the iron 24 keV resonance region where JENDL-3T based spectra generally underestimate the measurements. It is worth noticing, however, that they agree well at every positions considered, that is, calculational errors do not depend on penetration depth.

4. Summary and Discussion

Pointwise neutron cross section library for MCNP was compiled with NJOY-83/MACROS code system based on JENDL-3T. Almost all technical difficulties on processing JENDL-3T with NJOY-83 were resolved, with some exceptions left unresolved yet.

The energy spectra of fast neutrons having penetrated through iron media were calculated with MCNP using both JENDL-3T and ENDF/B-4 based libraries and they were compared with the measured spectra. As a result, it was seen that as a whole their agreement is rather satisfactory, though there appear meaningful differences between the two calculations.

It is important for MCNP calculations to improve its FSD values for obtaining solutions with accuracy high enough to be utilized for nuclear data evaluation. For the purpose, we introduced a newly developed estimator NESXE (Next Event Surface Crossing Estimator) to MCNP for the Winfrith iron penetration experiment. This estimator was found to provide far more accurate solution than that by built-in estimators.

References

1) MCNP : Monte Carlo Neutron and Photon Transport Code, CCC-200, (1983).
2) JENDL Compilation Group (Nuclear Data Center, JAERI) : JENDL-3T, private communication, (1987). JENDL-3T is a temporary file for testing the evaluated data which are for JENDL-3. The data in JENDL-3T will be revised in JENDL-3.
3) YAMANO, N., JAERI-M 84-038, (1984).
4) WERLE, H., et al., NEACRP-U-73, (1976).
5) TANAKA, S., JAERI-M 7843, (1978) (in Japanese).
6) CARTER, M. D., NEACRP-U-73, (1976).
7) UEKI, K., et al., Nucl. Sci. Eng., 84, 271 (1983).

Table 1 Contents of MCNP-V3 data library based on JENDL-3T

Nuclide	ZAID	Nuclear Data Based on	Nuclide	ZAID	Nuclear Data Based on
H-1	1001.30	JENDL-3T	Cr	24000.30 24000.20	JENDL-3T JENDL-2
D-2	1002.30	JENDL-3T	Mn-55	25055.30 25055.20	JENDL-3T JENDL-2
T-3	1003.40	ENDF/B-IV	Fe	26000.35 26000.40	JENDL-3T ENDF/B-IV
Li-6	3006.30	JENDL-3T	Co-59	27059.30	JENDL-3T
Li-7	3007.30	JENDL-3T	Ni	28000.30 28000.40	JENDL-3T ENDF/B-IV
Be-9	4009.30 4009.40	JENDL-3T ENDF/B-IV	Cu	29000.30	JENDL-3T
B-10	5010.30	JENDL-3T	Zr	40000.30	JENDL-3T
B-11	5011.30	JENDL-3T	Nb	41093.30 41093.20	JENDL-3T ENDF/B-IV
C-12	6012.30 6012.40	JENDL-3T ENDF/B-IV	Mo	42000.30	JENDL-3T
N-14	7014.30	JENDL-3T	Cd	48000.30 48000.40	JENDL-3T ENDF/B-IV
O-16	8016.30	JENDL-3T	W	74000.30	JENDL-3T
F-19	9019.30 9019.40	JENDL-3T ENDF/B-IV	Pb	82000.30 82000.20	JENDL-3T JENDL-2
Na-23	11023.30 11023.40	JENDL-3T ENDF/B-IV	U-235	92235.30 92235.40	JENDL-3T ENDF/B-IV
Mg	12000.30	JENDL-3T	U-238	92238.30 92238.40	JENDL-3T ENDF/B-IV
Al-27	13027.30	JENDL-3T	Pu-239	94239.30	JENDL-3T
Si	14000.30 14000.40	JENDL-3T ENDF/B-IV	Pu-240	94240.30 94240.20	JENDL-3T JENDL-2
K	19000.30	JENDL-3T	Pu-241	94241.30	JENDL-3T
Ca	20000.30 20000.40	JENDL-3T ENDF/B-IV	Pu-242	94242.30 94242.20	JENDL-3T JENDL-2
Ti	22000.30 22000.40	JENDL-3T ENDF/B-IV	Am-241	95241.30	JENDL-3T
V-51	23000.30 23000.40	JENDL-3T ENDF/B-IV			

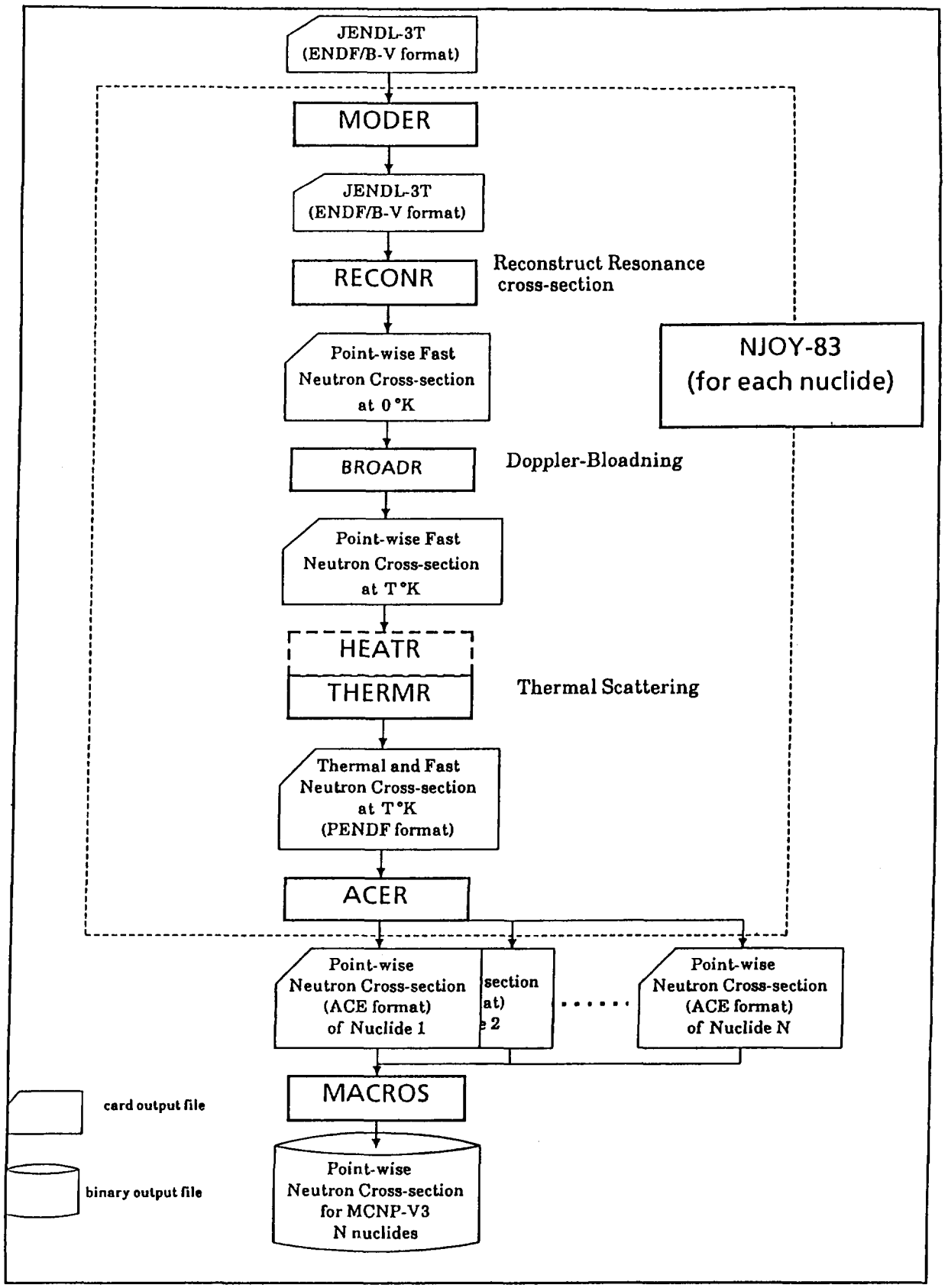

Fig. 1 Compilation code system of MCNP data library

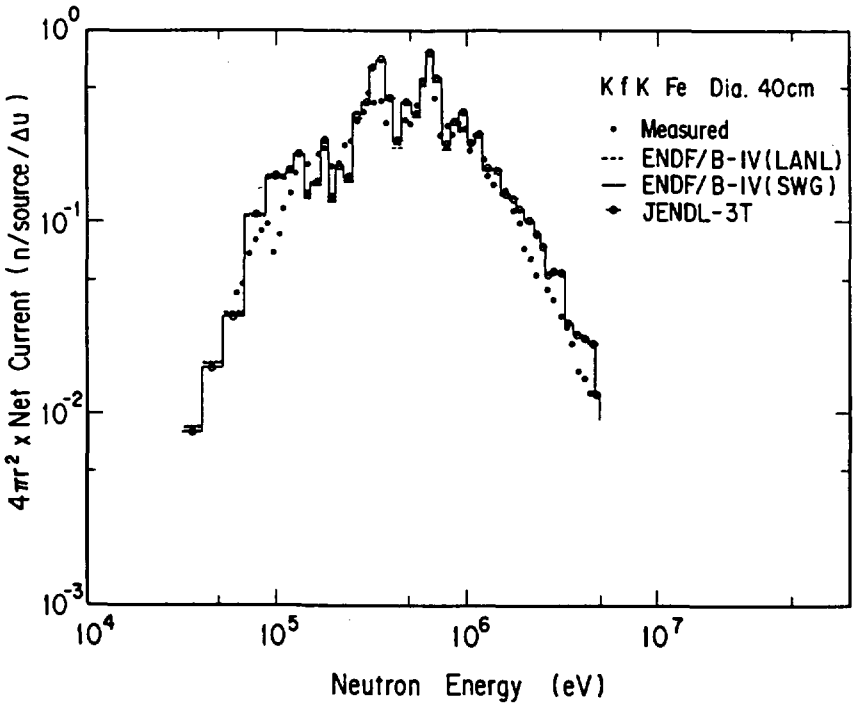

Fig. 2 Leakage neutron spectra from KfK iron sphere with Cf-252 neutrons

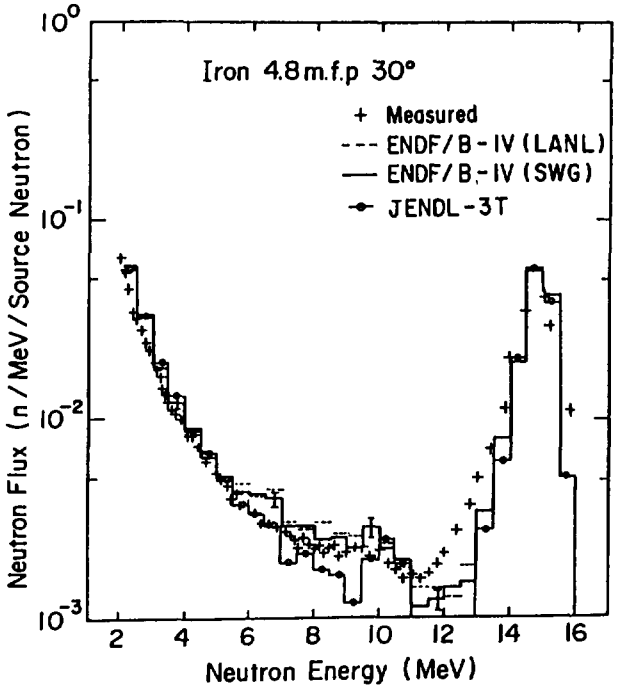

Fig. 3 Leakage neutron spectra from LLL iron sphere with D-T neutrons

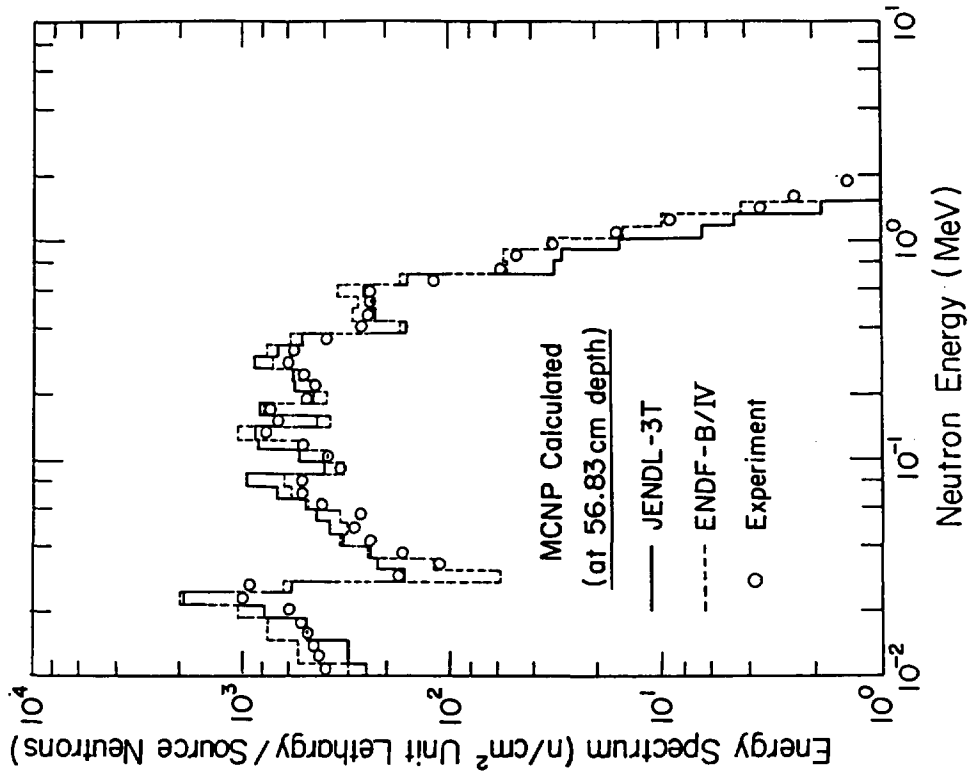

Fig. 5 Neutron spectra within Winfrith iron slab at 56.84 cm in depth

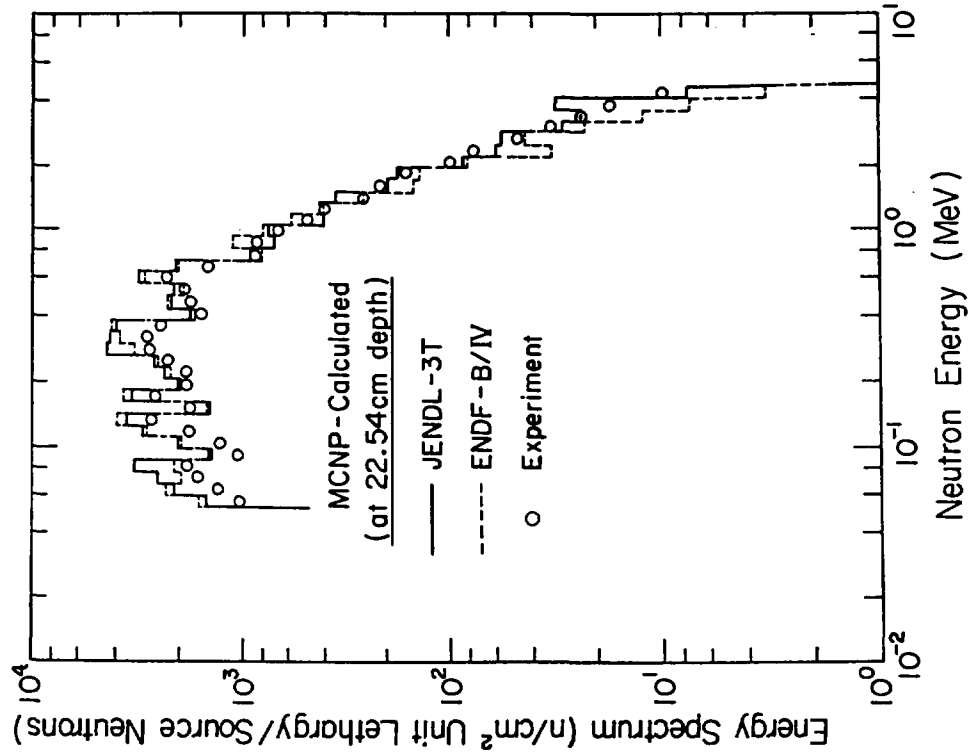

Fig. 4 Neutron spectra within Winfrith iron slab at 22.54 cm in depth

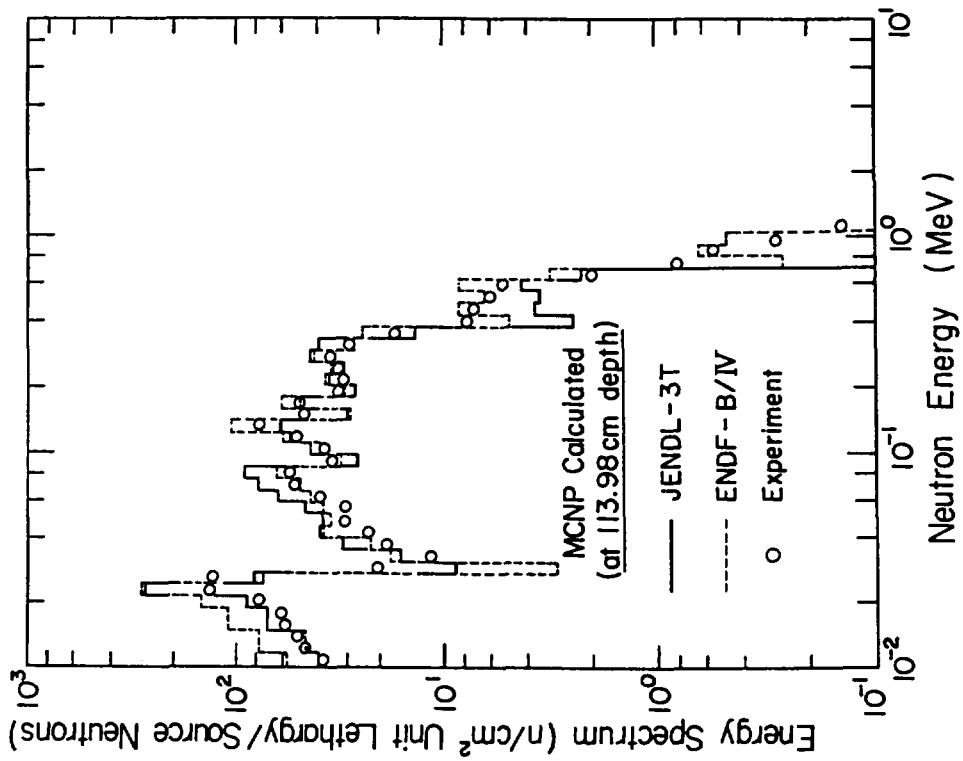

Fig. 6 Neutron spectra within Winfrith iron slab at 113.98 cm in depth

3.12 Measurement of Formation Cross-sections of Short-lived Nuclei Produced by 14 MeV Neutron (II)

Akihiko Osa, Hiroyuki Yoshida, Masahide Miyachi, Koki Kato, Akio Hosoya, Michihiro Shibata, Hiroshi Yamamoto, Kiyoshi Kawade, Toshio Katoh, *Toshiyuki Iida and *Akito Takahashi
Department of Nuclear Engineering, Nagoya University
*Department of Nuclear Engineering, Osaka University

Abstract:

Neutron activation cross sections have been measured at energy range from 13.4 to 14.9 MeV for nine reactions; $^{54}Fe(n,2n)^{53g}Fe$, $^{60}Ni(n,p)^{60m}Co$, $^{62}Ni(n,p)^{62m,62g}Co$, $^{63}Cu(n,\alpha)^{60m}Co$, $^{94}Zr(n,p)^{94}Y$, $^{92}Mo(n,p)^{91g}Mo$, $^{97}Mo(n,p)^{97m}Nb$ and $^{98}Mo(n,n'p)^{97m}Nb$.

1. Introduction

Measurement of formation cross-sections of short-lived nuclei (with half-lives between 1 min. and about 20 min.) produced by 14 MeV neutron irradiation has been done by the activation method. Irradiated sample materials were Mo, Zr, Cu, Ni and Fe. The energy range of neutron was from 13.4 to 14.9 MeV. The amount of induced activities was determined from the gamma-ray intensities.

The amount of some positron emitting nuclei which emitted nearly no gamma-ray was obtained from the intensities of the annihilation gamma-rays of 511 keV.

2. Experiment and results

Experiments were performed at the Intense 14-MeV-Neutron Source Facility (OKTAVIAN) of Osaka University. For the activation of samples, pneumatic tubes were set at 6 directions (between 0° and 155°) for the incident deuteron beam direction. The distances between the T-target and the irradiation points were 15 cm. The induced activities were measured by two Ge detectors at an equivalent distance of 5 cm. The annihilation gamma-rays from positron emitting nuclei were emasured by

setting the irradiated samples between two 10 mm thick acrylic plates. The broadening of gamma emitting points in the plates was examined by using the 514 keV gamma-ray from ^{85}Sr. The neutron energies were determined by the Zr/Nb method. The neutron flux at the irradiation points was monitored by using two aluminum foils (purity: 99.2%, 1 cm x 1 cm x 0.2 cm). The reference reaction for the flux measurement was the $^{27}Al(n,p)^{27}Mg$(9.46 min) reaction, which was determined referring to the standard $^{27}Al(n,\alpha)^{24}Na$ reaction (ENDF/B-V). Separated isotopes or natural samples were used for irradiation samples. The amoount of samples were from 30 mg to 100 mg.

Corrections were made for time variation of neutron flux, thickness of samples, self absorption and others. Accuracies of the obtained cross-sections were around 5% in case of the good statistics. The effect of broadening of gamma emitting points in the absorber for positron can be neglected for the positron energies less than 3 MeV, within the present experimental errors of about 2%. The measured reactions and associated decay dare are shown in Table 1 and the obtained results are in Table 2. The experimental errors of neutron energies are estimated to be less than 100 keV. Some examples of the results are shown in Figs. 1-5.

REFERENCES

(1) Ryves, T. B., et al.: J. Phys. G; Nucl. Phys. 4(1978)1783.
(2) Bormann, M., et al.: Z. Phys. A277(1976)203.
(3) Sigg, R. A., P. K. Kuroda: J. Inorg. Nucl. Chem. 37(1975)631.
(4) Qaim, S. M.: Nucl. Phys. A185(1972)614.
(5) Molla, N. I., S. M. Qaim: Nucl. Phys. A283(1977)269.
(6) Ikeda, Y., et al.: JAERI-1312(1988).
(7) Marcinkowski, A., et al.: Z. Phys. A323(1986)91.
(8) Amemiya, S., et al.: J. Nucl. Sci. Technol. 19(1982)781.
(9) Rao, C. V. S., et al.: Phys. Scripta 24(1981)935.
(10) Lu, W. D., et al.: Phys. Rev. C1(1970)350.

Table 1 Reactions measured and associated decay data

Target Nucleus	Reaction	Product	Half-life	Gamma-ray Energy(keV)	Branching Ratio(%)	Q-value (MeV)
^{54}Fe	(n,2n)	^{53g}Fe	8.51m	378	42	-13.38
^{60}Ni	(n,p)	^{60m}Co	10.47m	59	2.0	-2.46
^{62}Ni	(n,p)	^{62m}Co	13.91m	1163	67.6	-4.48
	(n,p)	^{62g}Co	1.50m	1129	13.1	-4.46
^{63}Cu	(n,α)	^{60m}Co	10.47m	59	2.0	1.69
^{94}Zr	(n,p)	^{94}Y	18.7m	919	56	-4.10
^{92}Mo	(n,2n)	^{91g}Mo	15.49m	511*	187.4	-12.68
^{97}Mo	(n,p)	^{97m}Nb	60s	743	97.9	-1.89
^{98}Mo	(n,n'p)	^{97m}Nb	60s	743	97.9	-8.39

* annihilation γ-ray

Table 2 Activation Cross-sections

Energy	$^{54}Fe(n,2n)^{53g}Fe$	$^{60}Ni(n,p)^{60m}Co$	$^{63}Cu(n,\ )^{60m}Co$
14.87 MeV	10.6 ± 0.8 mb	148 ± 15 mb	16 ± 5 mb
14.64	8.8 ± 0.7		21 ± 7
14.35	5.2 ± 0.6		16 ± 7
14.02	2.1 ± 0.3	190 ± 19	17 ± 6
13.70	0.2 ± 0.2		28 ± 6
13.40		201 ± 20	18 ± 4

Energy	$^{62}Ni(n,p)^{62m}Co$	$^{62}Ni(n,p)^{62g}Co$	$^{94}Zr(n,p)^{94m}Y$
14.87 MeV	17.4 ± 1.2 mb	20 ± 4 mb	6.6 ± 0.8 mb
14.64	16.3 ± 1.3	25 ± 6	7.7 ± 0.8
14.35	14.9 ± 1.1	19 ± 4	5.6 ± 0.7
14.02	15.6 ± 1.0	16 ± 3	5.7 ± 0.6
13.70	10.6 ± 1.3	13 ± 5	5.3 ± 0.7
13.40	11.7 ± 0.9	12 ± 3	4.2 ± 0.5

Energy	$^{92}Mo(n,2n)^{91g}Mo$	$^{97}Mo(n,p)^{97m}Nb$	$^{98}Mo(n,n'p)^{97m}Nb$
14.87 MeV	216 ± 11 mb	4.9 ± 0.6 mb	1.2 ± 0.4 mb
14.64	198 ± 10	3.4 ± 0.7	1.0 ± 0.4
14.35	172 ± 9	4.2 ± 0.7	0.5 ± 0.2
14.02	133 ± 7	3.4 ± 0.6	
13.70	87 ± 5	3.3 ± 0.7	
13.40	45 ± 3	3.6 ± 0.7	

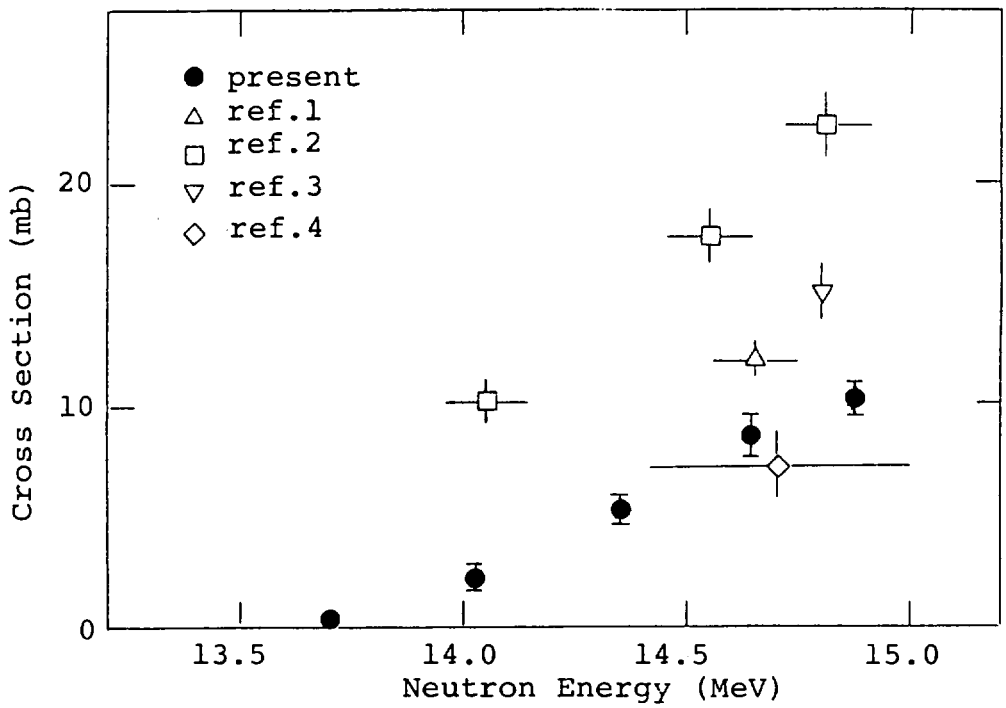

Fig. 1 Cross sections of $^{54}Fe(n,2n)^{53g}Fe$

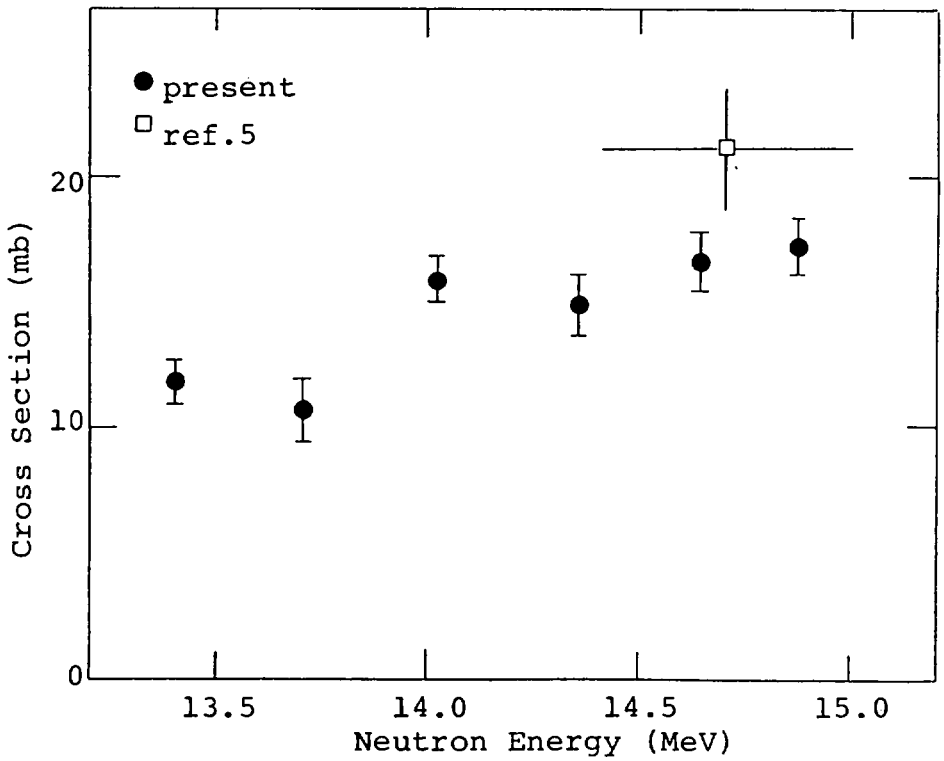

Fig. 2 Cross sections of $^{62}Ni(n,p)^{62m}Co$

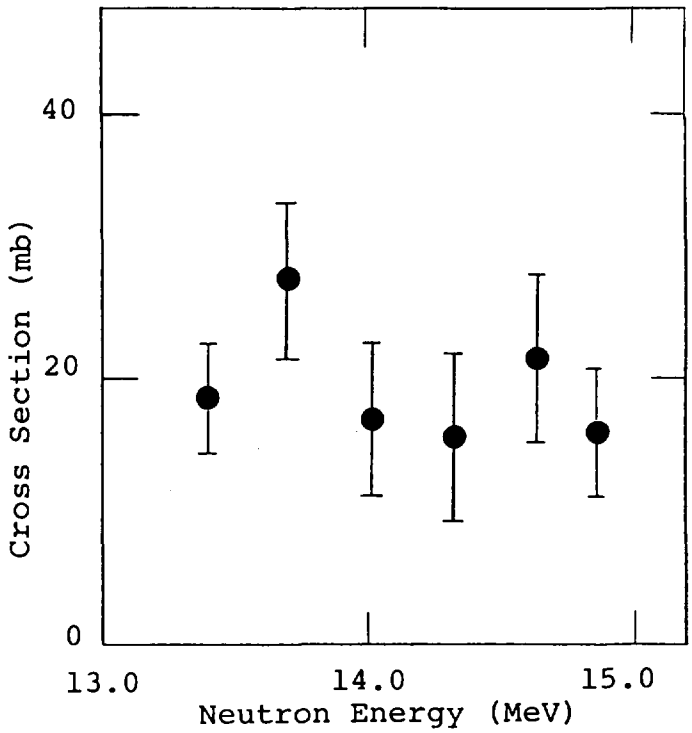

Fig. 3 Cross sections of $^{63}Cu(n,\alpha)^{60m}Co$

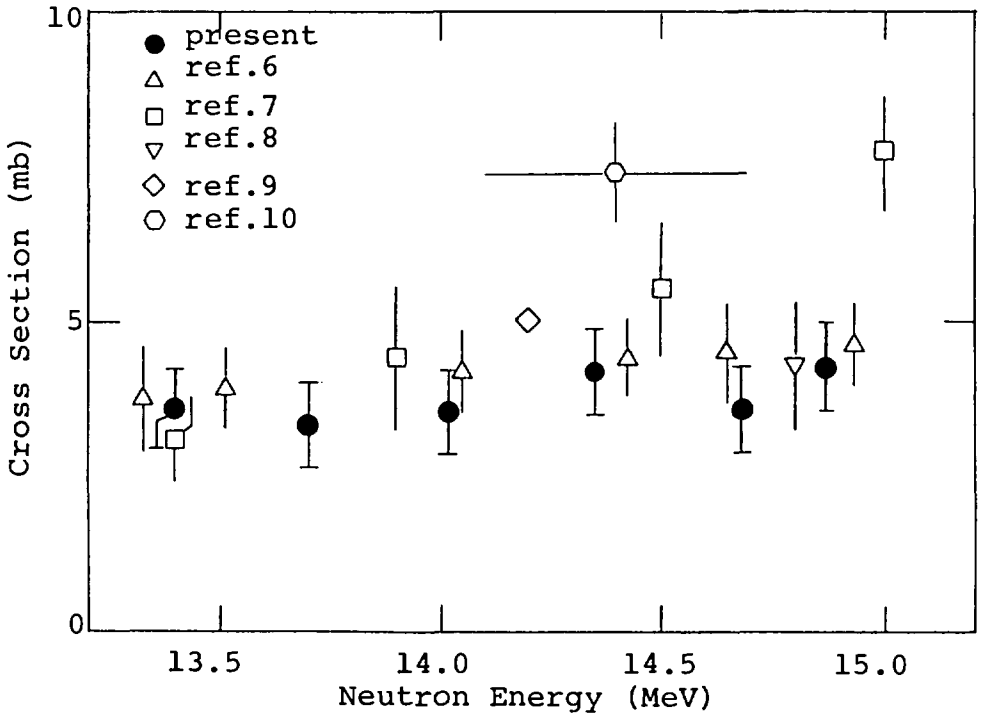

Fig. 4 Cross sections of $^{97}Mo(n,p)^{97m}Nb$

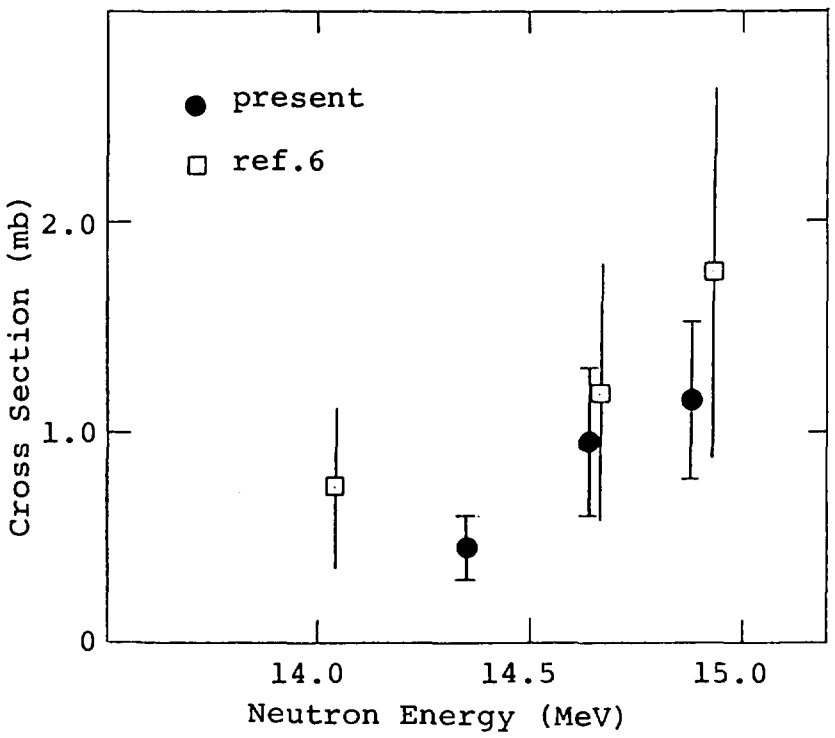

Fig. 5 Cross sections of $^{98}Mo(n,n'p)^{97m}Nb$

3.13 Incident Energy Dependence of Preequilibrium Process in Nucleon-Induced Reactions

Y. Watanabe, K. Kodaka, Y. Kubo, N. Koori,
M. Eriguchi, M. Hanada and I. Kumabe

Department of Nuclear Engineering, Kyushu University, Fukuoka

Proton energy spectra from (p,xp) reactions on ^{98}Mo and ^{106}Pd have been measured at incident energies of 12, 14, 16, and 18 MeV to investigate the incident energy dependence of preequilibrium process. The spectra were compared with a calculation based on the exciton model in which the squared average transition matrix element $|M|^2$ was assumed to be $KA^{-3}E^{-1}$ and isospin conservation was taken into account. The calculated spectra using a constant K-value were in good agreement with all the measured ones. Proton spectra from the ^{54}Fe(p,xp) reaction at 29 and 39 MeV and (n,xn) spectra for several target nuclei at 14-26 MeV were also analyzed by the exciton model and the evaporation model to examine the application of the model and the parameters used to the reactions induced by 10-40 MeV nucleon.

1. INTRODUCTION

In reactions induced by several tens of MeV nucleon, preequilibrium process contributes significantly to particle emissions with relatively high outgoing energies. Recently, in the field of nuclear data evaluation for fusion energy development, some nuclear model calculation codes[1] in which preequilibrium process is taken into account, have been developed and have been utilized in the evaluation of nuclear data in the incident energy and target mass regions where available experimental data lack.

As far as neutron-induced reactions are concerned, most of the experimental data on energy spectra of emitted particle are those for a 14 MeV neutron, and the data except for 14 MeV are quite little. It is, therefore, important to enhance the reliability of the model parameters used in the calculation as well as the nuclear modeling in evaluating the nuclear data over a wide range of incident energies.

On the other hand, the experimental data of proton-induced reaction which is analogous to neutron-induced reaction are superior to those of the latter in terms of good counting statistics. Proton experiments also have an

advantage that incident energy can be more easily changed than in the neutron experiments.

In the present work, we pay attention to inelastic scattering in nucleon-induced reactions. First, energy spectra from (p,xp) reactions were measured systematically at 12, 14, 16, and 18 MeV to investigate the incident energy dependence of preequilibrium process in the nucleon-induced reaction in terms of the exciton model. In addition, proton spectra from the ^{54}Fe(p,xp) reaction at 29 and 39 MeV and several neutron data except for 14 MeV were analyzed by the exciton model, and the application of the model and the parameters used to reactions at incident energies of 10-40 MeV was examined.

2. EXPERIMENT

The experiment was performed using protons with incident energies of 12, 14, 16, and 18 MeV from the tandem Van de Graaff accelerator at Kyushu University. Targets were self-supporting metallic foils(^{98}Mo and ^{106}Pd), and their thickness were 0.45 and 1.02 mg/cm^2, respectively. The experimental procedure and data processing have been described in detail elsewhere[2] with the data for 18 MeV.

3. EXPERIMENTAL RESULTS

Figure 1 shows double differential proton emission cross sections measured at 70° for ^{106}Pd. For each incident energy, continuum portion is observed in outgoing energies lower than a large elastic peak and pronounced structures corresponding to the direct collective excitation, such as the lowest 2^+ and 3^- levels. The angular distributions in continuum portion of more than 6 MeV are peaked forward as shown in Fig.2. This suggests that preequilibrium proton emissions, especially proton emissions from states with an initial configuration n=3, are dominant in this portion. The similar experimental result was obtained for ^{98}Mo.

Angle-integrated energy spectra for the four incident energies are shown by histogram in Figs. 3 and 4. Note that the portion of the spectra corresponding to residual excitations of 4 MeV or less is excluded in these figures.

4. ANALYSIS AND RESULTS

4.1 (p,xp) SPECTRA

In proton-induced reactions, analog states($T_>$ states) of a composite

nucleus are excited. It is known that proton emissions from the composite nucleus are more enhanced than neutron emissions because of suppression of neutron emissions from the $T_>$ states[3]. Isospin conservation was, therefore, considered in the exciton model for preequilibrium process and the Hauser-Feshbach model for equilibrium process. The formulation of the exciton model and the details of the model calculation have been described in Ref.[2].

In the exciton model, the transition rate from the n-exciton state to the m-exciton state is given by

$$\lambda_{n\to m} = \frac{2\pi}{\hbar} |M|^2 \rho_f , \qquad (1)$$

where ρ_f is the final state density and $|M|^2$ the squared average transition matrix element. In the present analysis, $|M|^2$ has been assumed to be the empirical value as follows[4]:

$$|M|^2 = K A^{-3} E^{-1} , \qquad (2)$$

where A is the mass number of composite nucleus and E is its excitation energy and K is the adjustable parameter which is determined so as to reproduce the absolute value of experimental spectra.

The empirical value[4] given by Eq.(2) was derived from the exciton model analysis of several (p,p'), (p,n), and (α,p) data at incident energies larger than 20 MeV. Since the result contains large uncertainty in the derived K-value, it is unknown whether Eq.(2) with a constant K-value is applicable to nucleon-induced reactions over a wide range of incident energies. We have, therefore, investigated the incident energy dependence of the K-value through the analysis of (p,xp) spectra.

In the present calculation, the K-values have been fixed to be 405 and 430 MeV^3 for ^{98}Mo and ^{106}Pd, respectively. The same values were applied to all the incident energies from 12 to 18 MeV. The calculated spectra are compared with the measured ones in Figs.3 and 4. The other parameters used in this calculation were the same as those in Ref. [2]. As shown in Figs.3 and 4, the calculated spectra are in excellent agreement with the experimental ones for 12-18 MeV. This indicates no incident energy dependence of the K-value in the Mo-Pd region for the (p,xp) reaction induced by 12-18 MeV protons.

Next, in order to test the application of the model and parameters used

in above-mentioned calculation, we calculated proton spectra from the $^{54}Fe(p,xp)$ reaction at incident energies of 29 and 39 MeV. The results are shown in Fig.5 together with the experimental data by Bertrand et al.[5]. In this calculation, the K-value was fixed to be 430 MeV^3. Note that only preequilibrium component was calculated for the reaction at 39 MeV and compared with the experimental data. The calculated spectra show good agreement with the experimental ones in outgoing energies less than 20 MeV. Disagreement seen in higher outgoing energies is expected to be due to the contribution of direct process which has not been considered in the present analysis.

4.2 (n,xn) SPECTRA

Several data on (n,xn) reactions at incident energies except for 14 MeV were analyzed on the basis of the similar theoretical model as mentioned above; the data are (n,xn) spectra on Fe, Cu and Zr at 18 MeV[6,7] and those on Fe and Cu at 25.7 MeV[8]. Isospin was not considered as a quantum number because the analog states(the $T_>$ states) are not excited in neutron-induced reactions. To simplify the model calculation, the evaporation model[9] was used for the compound process calculation in place of the Hauser-Feshbach model. In the evaporation model calculation, an excitation energy dependent level density parameter a(U) was introduced according to the Ignatyuk model[10].

Comparisons between the calculated results and the experimental data are shown in Figs.6-8. In the calculation for 14 MeV, the K-value was fixed to be 550 MeV^3 that is the same value used in the previous analysis of the 14.1 MeV (n,xn) reactions on nuclei in the tin region[11]. As shown in Fig.6, good agreement between the calculated and experimental spectra was obtained for Fe, Cu and Zr in continuum portion where preequilibrium process is dominant. The 25.7 MeV (n,xn) spectra for Fe and Cu were calculated using the same parameters. The results also reproduce satisfactorily the experimental values as shown in Fig.8.

On the other hand, the results of a calculation of 18 MeV (n,xn) spectra for both Fe and Cu required a K-value (700 MeV^3) larger than the above-mentioned value(550 MeV^3) to fit the experimental ones. The results are shown in Fig.7. For the Zr(n,xn) reaction at 18 MeV, however, the K-value was set to be 550 MeV^3 to reproduce the experimental data. Additional accumulation and analysis of (n,xn) data for 18 MeV will be necessary to investigate the

difference of the K-value derived from the present analysis of 18 MeV(n,xn) spectra.

5. SUMMARY

The proton spectra from the ^{98}Mo and ^{106}Pd(p,xp) reactions at 12, 14, 16, and 18 MeV have been measured in order to investigate the incident energy dependence of preequilibrium process in nucleon inelastic scatterings. The (p,xp) spectra were analyzed on the basis of the exciton model and the Hauser-Feshbach model in which isospin conservation was taken into account. In the exciton model calculation, the squared average transition matrix element $|M|^2$ was assumed to be the empirical value $KA^{-3}E^{-1}$. The calculated results using a constant K value(405 MeV^3 for ^{98}Mo and 430 MeV^3 for ^{106}Pd) showed good agreement with the experimental spectra for all incident energies of 12-18 MeV.

We have also examined the application of this model to the reactions at higher incident energies. The continuum spectra of the ^{54}Fe(p,xp) reactions at 29 and 39 MeV were reproduced by the calculation using the similar model with K=430 MeV^3. From these analyses, it was found that the K-value has no incident energy dependence for the (p,p') scattering at incident energies of 10-40 MeV.

In addition, the calculation using the similar model was applied to the (n,xn) reactions on Fe, Cu , and Zr at incident energies of 14-26 MeV. The result using K=550 MeV^3 showed good agreement with the experimental energy spectra except for the 18 MeV(n,xn) spectra for Fe and Cu; a different K-value(700 MeV^3) was required for both spectra.

Finally, the K-value derived from the analysis of the (p,xp) and (n,xn) reactions indicated a possible dependence on the kind of incident nucleon. The dependence has not been discussed in this paper, but this would be one of important questions that should be addressed in the exciton model.

The authors would like to thank members of the Nuclear Physics Laboratory of the Department of Physics, Kyushu University, for their assistance in operating the accelerator.

References

[1] SARTORI, E.: *in Proceedings of a Specialists' meeting on Preequilibrium Nuclear Reactions,* Semmering, Austria, 1988, edited by B. Strohmaier,(NEANDC-245 'U',1988), p 257.

[2] WATANABE, Y. et al.: Phys. Rev. C **36**, 1325 (1987).

[3] KALBACH-CLINE, C. et al.: Nucl. Phys. **A222**, 405 (1974);
KALBACH, C. et al.: Z. Phys. A **295**, 175 (1975).

[4] KALBACH, C. : Nucl. Phys. **A210**, 590 (1973).

[5] BERTRAND, F.E. and PEELE, R.W. : Phys. Rev. C **8**, 1045 (1973).

[6] YABUTA, N. and BABA, M. et al. : Progress Report No. NETU-47, Fast Neutron Laboratory, Tohoku Univ. (1985);
KIKUCHI, T. and BABA, M. et al. : ibid. Report No. NETU-49 (1986).

[7] BABA, M. : private communication.

[8] MARCINKOWSKI, A. et al.: Nucl. Sci. and Eng. **83**, 13 (1983).

[9] WEISSKOPF, V.F. and EWING, D.H. : Phys. Rev. **57**, 472 (1940).

[10] IGNATYUK, A.V. et al. : Sov. J. Nucl. Phys. **21**, 255 (1976).

[11] WATANABE, Y. et al. : Phys. Rev. C **37**, 963 (1988).

[12] VONACH, H. et al. : BNL-NCS-51245, Brookhaven National Laboratory (1980) Vol.1, p 343.

[13] HERMSDORF, D. et al. : Zentralinstitut fur Kernforschung Report No. ZfK-277.

[14] STENGL, S. et al. : Nucl. Phys. A **290**, 109 (1977).

[15] IRIE, Y. et al. : J. Phys. Soc. Jpn **39**, 537 (1975).

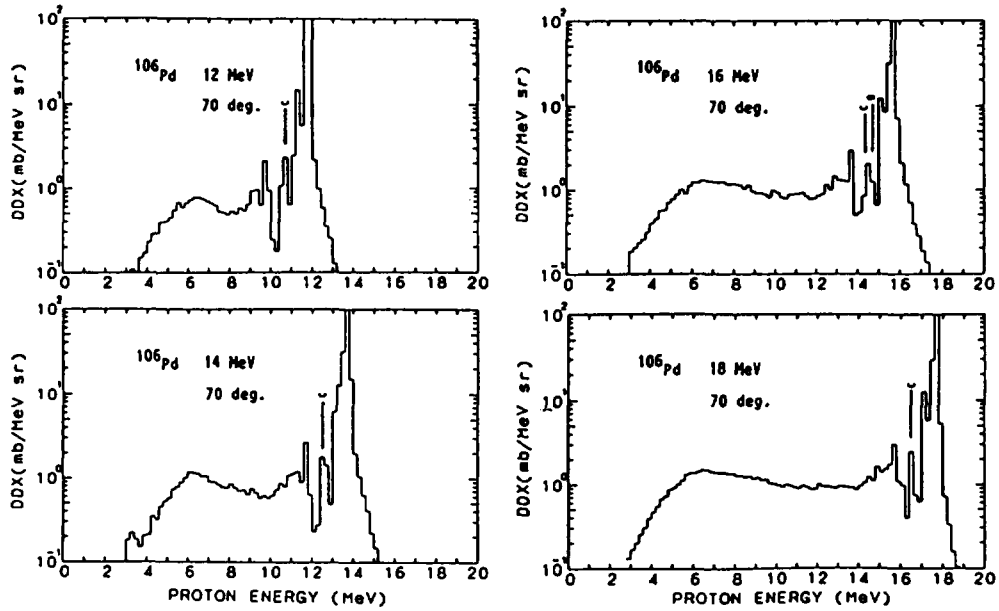

Fig. 1 Double differential proton emission cross sections measured at 70° for the ^{106}Pd(p,xp) reactions at incident energies of 12, 14, 16, and 18 MeV. The peaks labeled C and O correspond to elastic scattering from impurities ^{12}C and ^{16}O.

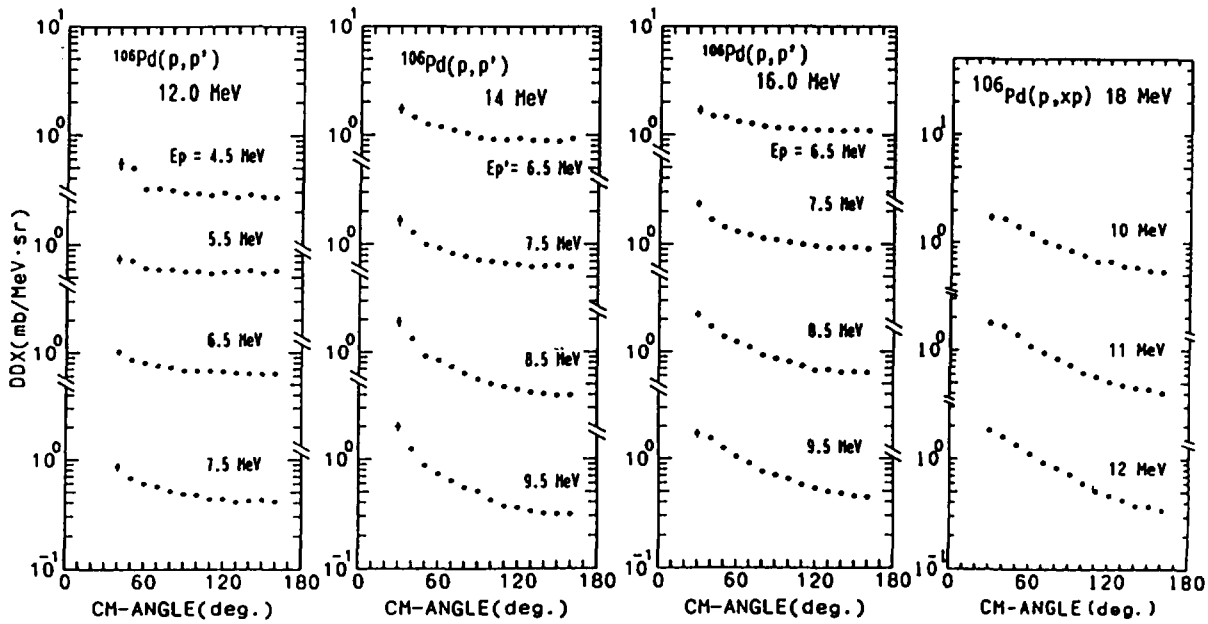

Fig. 2 Measured angular distributions of protons emitted from the ^{106}Pd(p,xp) reactions at incident energies of 12, 14, 16, and 18 MeV.

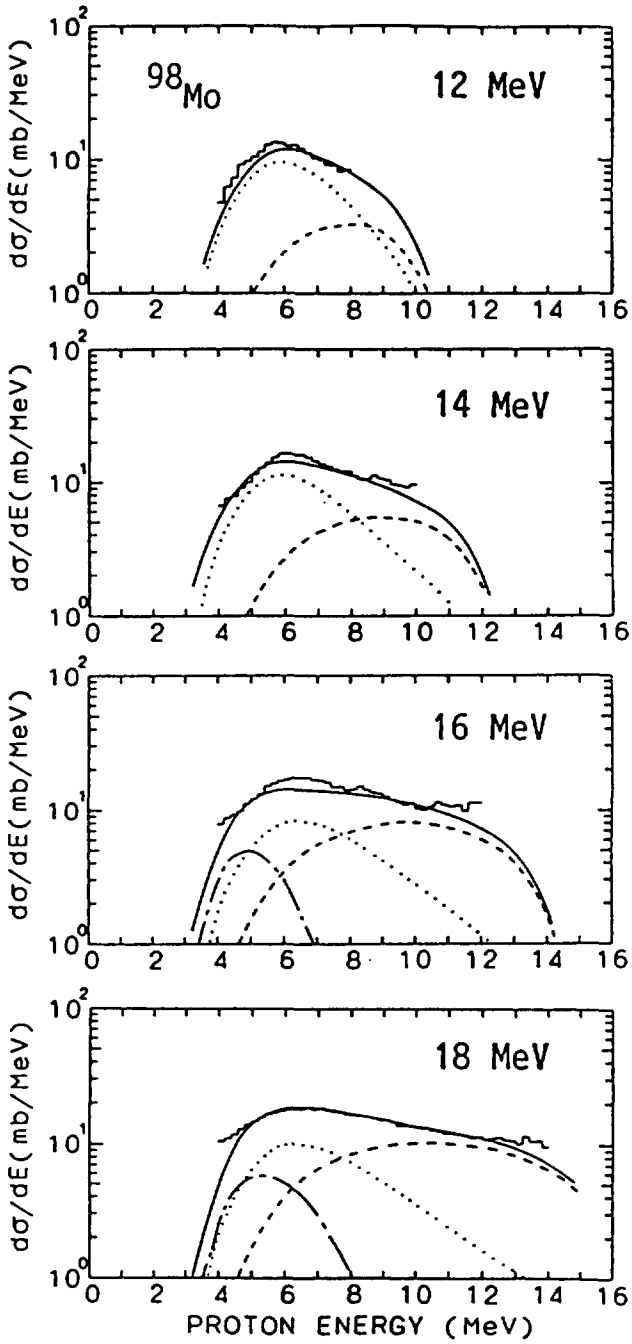

Fig. 3 Experimental and calculated (p,xp) spectra for ^{98}Mo. Histograms represent the experimental angle-integrated spectra. Solid curves are the total calculated energy spectra. Dashed curves are $T_<$ components of the calculated preequilibrium energy spectra using the exciton model; dotted curves are $T_>$ components of them. Dashed-dotted curves show the calculated equilibrium spectra using the Hauser-Feshbach model.

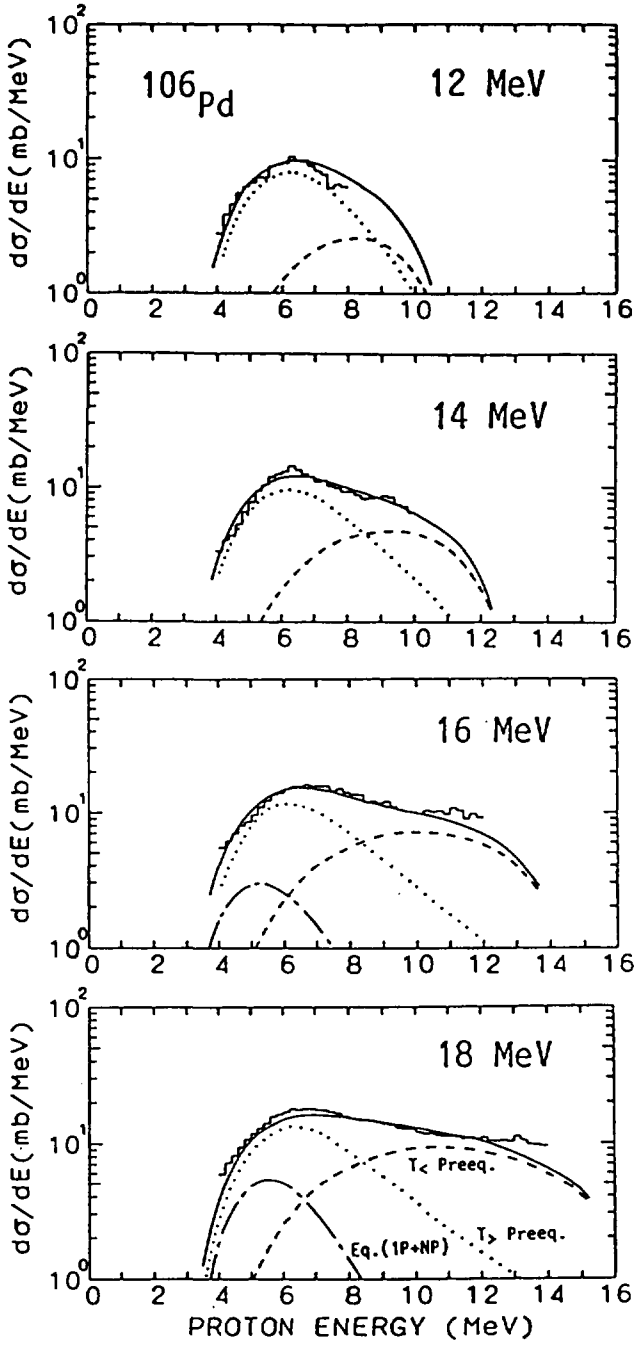

Fig. 4 As in Fig. 3 for ^{106}Pd.

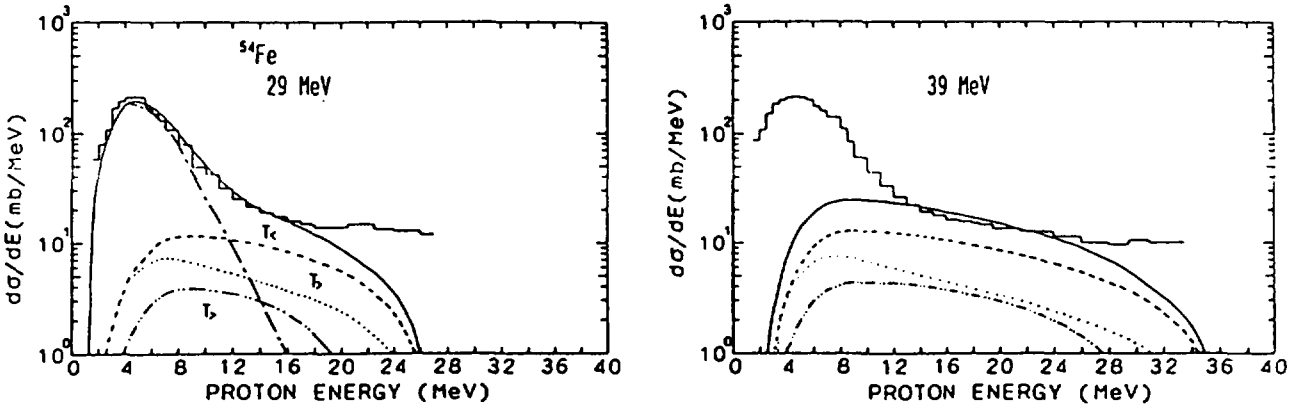

Fig. 5 Calculated and experimental (p,xp) spectra for ^{54}Fe at incident energies of 29 and 39 MeV. The experimental data are taken from Ref.[5]. Calculated results are as in Fig. 3. Dashed-dotted-dotted curves represent T> components for the decay from T> states in the composite nucleus (^{55}Co) to T> states in the residual nucleus (^{54}Fe).

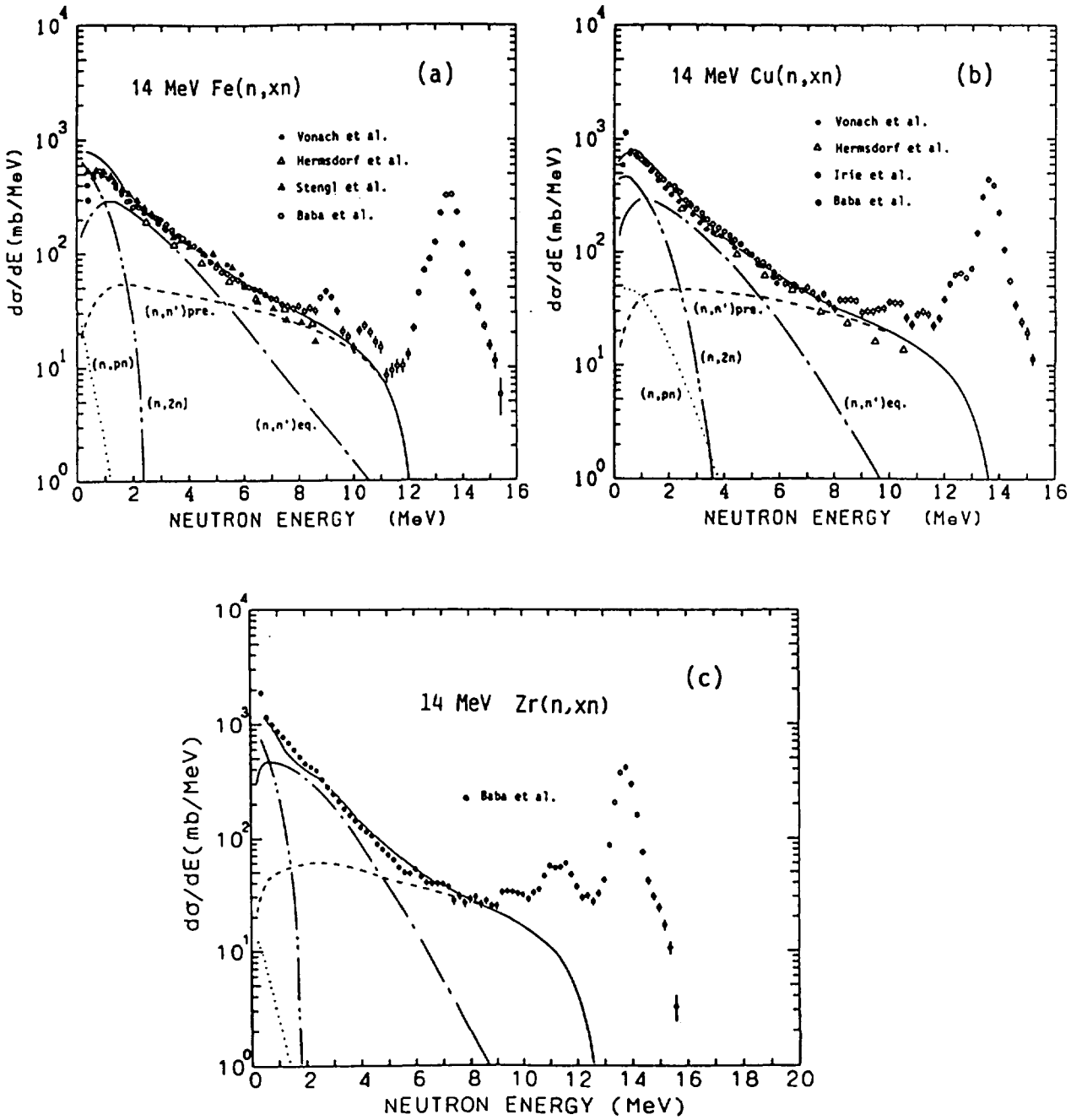

Fig. 6 Calculated and experimental 14 MeV (n,xn) spectra for Fe, Cu, and Zr. Dashed curves are the calculated preequilibrium components using the exciton model. Dashed-dotted, dashed-dotted-dotted, and dotted curves show the calculated evaporation spectra from (n,n'), (n,2n), and (n,pn) reactions, respectively. Experimental data are from Refs.[6,11,12,13] in (a); Refs.[6,11, 12,14] in (b); Ref.[6] in (c).

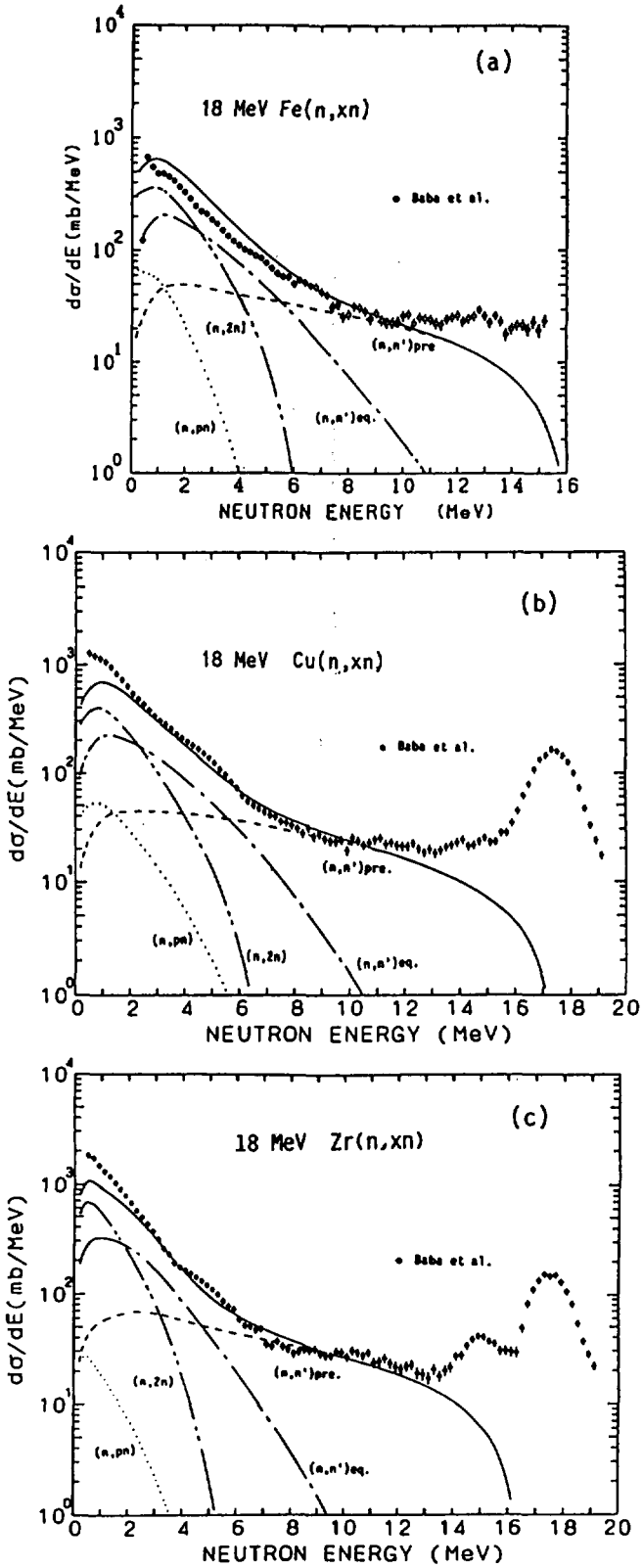

Fig. 7 As in Fig. 6 for an incident neutron energy of 18 MeV. Data are taken from Refs.[6,7].

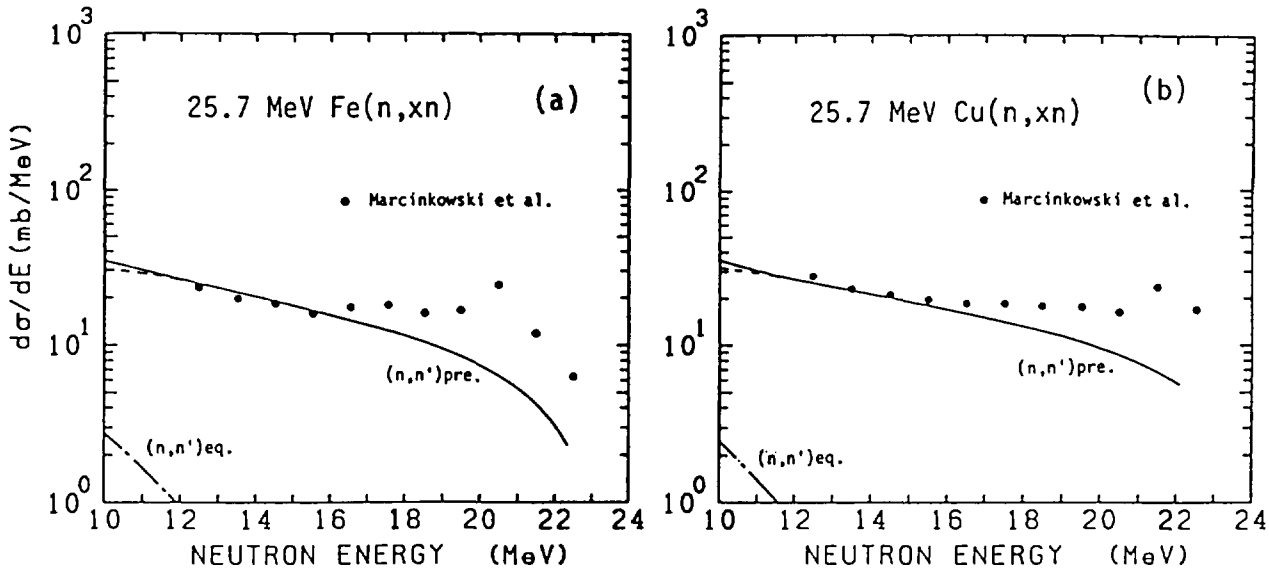

Fig. 8 As in Fig. 6 for 25.7 MeV (n,xn) spectra for Fe and Cu. Data are from Ref.[8].

3.14 Development of a Supporting System for Nuclear Data Evaluation in a 32-bit Workstation Using Artificial Intelligence Technology (SENDAI)

S. Iwasaki, N. Odano, M. Kitamura, and K. Sugiyama

Department of Nuclear Engineering, Tohoku University
Aramaki-Aza-Aoba, Sendai 980, Japan

Outline of a supporting system for the nuclear cross section calculation under development in a 32-bit workstation at Tohoku University and the knowledge representation used in the system are described.

The system consists of five subsystems: knowledge base which has a key role to control the whole of the system; the system of the cross section calculation codes; and data bases for the various kinds of nuclear parameters as the initial input values to these codes, for the experimental data which should be fitted by the calculations, and for the evaluated nuclear data libraries to be compared with the calculated results.

The knowledge base system based on an expert tool, would guide users showing the sequence of the calculation, how to select the candidate of the input parameters and to determine the best parameters by fitting process. The guidance knowledge is acquired from several literatures, and the authors experiences of the actual calculations, then converted to the rules and input to the system.

1. Introduction

An expert system in the field of the nuclear data evaluation is considered to be one of the solutions to the rapidly increasing requests on the nuclear data for various applied fields in Japan in spite of deficiency of the man-power for the evaluation after the completion of JENDL-3.

If a collection of various kinds of knowledge about the nuclear data evaluation process in which the evaluators manipulate codes and various kinds of nuclear cross section data are systematized and implemented in a computer system (knowledge base), it would be very convenient for unskilled persons, and even for the experts themselves. Also, the knowledge base system would have high flexibility to update and modification according to the progress of the theories, techniques and development of codes.

In the present paper, a planning of making a supporting system for neutron nuclear cross section calculation by a set of nuclear codes is described. We have assumed that the objective area of the nucleus in the system is limited to the region of the medium weight elements (20 < range of atomic number < 82)

and the incident neutron energy range of above unresolved resonance energy. The knowledge sources of the present system were proceedings of several recent meetings /1/, /2/, /3/, /4/, /5/ and papers /6/,/7/,/8/,/9/,/10/,/11/, and additional authors experiences of calculations/12,13/. Among them, the Yamamuro's paper/11/ is the important knowledge source in the present system. The knowledge has been implemented in the form of rules of the methods of the evaluation.

2. Structure of the System

Conventionally, evaluators use a couple of nuclear data calculation codes which are provided in a large computer system and run each code after preparation of respective input parameter files in a different format. Usually the initial input parameters are not given by default, and must be determined by consulting and referring various literatures, and then a input parameter file is made for the calculation. They compare the result with the corresponding experimental data which are stored in another file system or other literatures. If they do not get good fit, they will modify some parameters of the input file and try again. They repeat this process until they get satisfying result and would take much time.

We have proposed a supporting system for the nuclear data calculation /14/ in which these data and code are provided in the same memory area together with a knowledge base system. The proposed system which is being developed in a engineering workstation is shown in Fig. 1. We called the system as an integrated one which consists of the following subsystems:

- .Knowledge base system
- .Nuclear calculation Code system
- .Data base for the various input parameters for the codes
- .Data base for the experimental data
- .Data base for the evaluated nuclear data libraries.

The data and codes are dynamically connected in the evaluation process. This evaluation process is controlled by the knowledge base which is the essential part of the present system. In the present study, we use a commercial tool in order to construct this knowledge base.

We assumed that there may be three levels in the degree of nuclear cross section calculation for the evaluation or other purposes. The first level is for unskilled persons who want to calculate certain cross sections for some purposes, e.g., checking of their experimental cross sections using the parameters of default in the system.

The second level is for the initial stage of the evaluation, where the input parameters are selected among several candidate and fitted locally to the given cross sections.

The third level is for the usual cross section evaluation process in which the input parameters should be fitted from the local and global point of view.

The limit of the model calculation should be considered if the fitting is not satisfied and sometimes the experimental data for certain cross sections would be adopted in place of the calculation. In the fitting process, the quality of the experimental data should be checked, and a reliable data must be selected from the experimental data base. Many steps of the modification of the parameters, calculation and comparison should be repeated. Also, there would be many exceptional conditions to a given target nucleus.

In the present study, we have taken the aim as the construction of a second level system, considering the difficulty of the third level system as a goal of the phase of our development plan.

In the second level system, we assumed the code system covers the following five codes, ELIESE-3/15/, CASTHY/16/, GNASH/17/, DWUCK/18/, and ECIS79/19/ (in near future). These code have been used in many evaluators for the JENDL-3 libraries and revised for convenience sake of the neutron cross section calculations. Therefore, the characteristics of the codes are rather well known.

Data base for the input parameters are important in the system. Following parameters are now considered as data base quantities: the optical potential parameters for light particles of local and global sets; the SPR values/20/; the giant-dipole resonance parameters; the level density parameters; the capture cross section data; the precompound reaction related parameter values/11/; the level structure and gamma-decay data given by ENSDF, etc.; the deformation parameters of the lower levels, etc.

It is vast work to compile these parameter data, and is difficult for such a small research group. Therefore, we are compiling one by one for given target nuclei. The complete and systematic compilation works should be done at JAERI Nuclear Data Center (JAERI-NDC).

The experimental cross section data base is based on the EXFOR data file. However, the format of the EXFOR data is inconvenient to access respective data, the format of the data base will be changed to that one like NESTOR system of JAERI-NDC.

As the evaluated nuclear data base, the JENDL and ENDF/B libraries are also available and used for the comparison.

3. Development Environment of the System

Hardware environment of the system development is the following: a 32-bit engineering work station by Hewlett Packard, Co. HP-9000 360CH with a new CPU, M68030(25MHz) and floating point co-processor, M688882. The computing performance the system is about 5MIPS. Capacity of the main memory unit is 8Mbytes. A high resolution color bit map display, a mouse interface and a 304Mbyte-hard disk data storage are associated to the system. Operating system is HP-UX which provides a environment of multi-tasks, multi-users, multi-languages and LAN. The 360CH forms a LAN with a SONY-830 workstation and

a NEC PC-9800VX, and the LAN is also connected to the system, ACOS2000 of the large computer center of the university.

In this system the all codes and their parameters data base and experimental data base related to the objective nucleus can be stored in the hard disk. These data bases can be retrieved from the mass storage devices of the ACOS2000. We are able to compute cross sections and other physical quantities using the codes in the workstation and to get results within a reasonable turn-around time.

The knowledge base should be constructed in a proper development environment. In the present study, we determined to use a software tool in order to develop the system as soon as possible and not to use knowledge-oriented language. As the tool, Nexpert Object by Neuron Data Inc., (U.S.A.) was chosen because this provides production system and also frame like representation with rather high performance, and good human interfaces for development and editing the knowledge base.

A feature of Nexpert Object/21/ is to adopt the symmetrical production rules which can be used in both backward and forward inferences. In Fig.2, the rules structure is shown. Various kinds of operators are provided for both condition part and action part. Execution of external routines and access to the data base can easily be done.

Class/object representation of the knowledges is another feature of Nexpert Object. These can be used to describe a layered knowledge of some objects. A class is a collection of instance (a-kind-of relation), object, which exists in the real world. A class is able to possess subclasses. Higher class is for general and common, and lower subclasses present more special ones. A object is divided into some components or constituents which are sub-objects (a-part-of relation). All classes and objects are able to be associated with any number of attributes, properties, whose slots contained some numbers or property values, etc. The properties and their values can be inherited both downward and upward according to designer's strategy. Fig.3 show structure of the classes and objects. The class and objects can be compiled by the editor independently from the rules, and/or can be created or deleted dynamically by the rule during the inference. The properties and their values can also be accessed and modified by the rule's conditions and actions.

Notebook type editors of the rules and class/objects and network representation function for editing, compilation and navigation of knowledge base are provided as user and designer interface.

4. Outline of the Rules in the System

The supporting system is consisted of two parts. The first part corresponds to the set up the condition for the target nucleus and calculation level, and the second one to the parameters determination, calculation and comparison with experimental data.

In the first part, the system ask to user what nucleus/nuclei he/she wants to calculate in what calculation level among two levels discussed in the previous section. The system initializes several parameters in the knowledge base according to the answers.

The second part is the main part of the system. In Fig.4, tree diagrams of the second part of higher (closer to the final goal) rules are shown, and their lower rules are not shown. Note that the rules in the figure is different from the actual rule representation in the system for the sake of easy understanding. The respective item in each box is the rule. The Nexpert Object automatically connected each rule through the backward reasoning according to the corresponding the operators of the condition part of a rule and hypothesis of another rule, and constructed the tree structures like as shown in Fig. 2 (b).

The second part is divided into rather independent five rule blocks, which corresponds to a code. The first is the block for the neutron OPM parameters selection using CASTHY code based on the SPRT criterion/22/ of the n-OPM. The second block is for the transmission coefficients calculation of the six light particles, i.e., n, p , d , t, h and α. The calculated transmission data are stored in a file, FILE_28. which will used in the GNASH code. The third one is the block for the direct reaction calculation of the neutron discrete inelastic by use of the DWUCK-4 code. The output of the cross section is stored in a file, FILE_33 for the next GNASH code.

The forth block is for the calculation of the various cross sections using the GNASH code. In the first part of this block, the particle emission spectra at 14MeV and excitation cross sections for several threshold reactions are calculated, and several input parameters are adjusted by comparing the experimental data. The output of the GNASH code is used for the competing reaction cross sections of the next CASTHY code calculations. In the last block, the inelastic and capture cross sections are evaluated according to the reliable experimental capture data and calculate the gamma-ray transmission coefficients. The results of the CASTHY code again will be input to the GNASH code, and the cross sections are calculated in the entire energy range, and finally checked by comparison with experimental data base. The result will be converted in the ENDF/B format and output in order to be compared with other evaluated data libraries.

Lower level part of the system corresponds to the selection of each parameter. When some parameters are selected in a rule, the rule's action writes the data values in the corresponding property slot of para_objl, for example.

Double square boxes shown in the figure indicate the revision processes of the parameters when the fitting is not good, and their exact rules are not shown. Briefly, for example, after 14MeV cross section calculation by GNASH code, emission spectra for neutron, proton, deuteron and alpha-particle should be compared with the experiment. If the fitting for the proton emission

spectrum is unsatisfactory, the comparison rule's action write the judgment of the fitting, NG, into the slot of the property of the par_obj1, 14MeV_fit_p_sp. In this case, the initial parameters for the level density could be improper. The comparison rule 'reset'/21/ the hypothesis, PARTICLE_SPEC_at_14_MeV. Then the lower hypotheses which support the PARTICLE_SPEC_at_14_MeV will also be set as 'unknown'. Because the only level density parameters are not good in this case, after the reset, the rule sets other parameter selection rules as 'true' again. Then the system asks to user to change the level density parameters and proceeds to calculation step by the new set of parameters.

When the parameters are modified, a new parameter object, para_obj2 is created by the rule action. The properties and their values of the new object are the same as the old one except for the modified ones. Unmodified values are inherited from the old one. After the calculation and comparisons, the comment for the new judgment fitting will be written into the slot of the property, 14MeV_fit_p_sp of the para_obj2.

Thus, if all sets of parameter values are compiled with the comments of the fittings in the knowledge base, the compiled data are very important and useful for the analysis of the fitting process and also in the case of reuse of the parameter sets.

5. Summary

Plan of the development of a supporting system for the second level of nuclear cross section calculation in the 32-bit workstation is described. We have assumed that the man-power for the development the system is about 2men x a half year. In order to approach to the third (highest) level system, it is necessary to gain various kinds of knowledge from the much experienced evaluators directly by interview technique, etc. Even though, there are many problems to be solved. As already mentioned in section 2, the main problems are judgment of the fitting, assignment of the most sensitive parameters to the fitting, the limit of the fitting or model calculation, and the judgment of the experimental data quality.

These concept are all difficult to be implemented into a rule base, because no definite description of these concept is given in a written form. Thus, the study on these problems would give some impacts on the development of the methodology for the nuclear data evaluation conversely.

Acknowledgment

This work is supported by a Grant for Scientific Research from the Ministry of Culture, Science and Education in 1988FY. Drs. Y. Nakagawa and N. Yamamuro are acknowledged for their grate helps and valuable discussions.

REFERENCES

1. Proc. of Consultants' Meeting on the use of Nuclear Theory in Neutron Nuclear Data Evaluation, vol.I & II, IAEA-190, Trieste, 8-11 Dec. 1975 (IAEA, Viena 1976).
2. Proceedings of Workshop on Evaluation Methods and Procedures,BNL, Upton NY BNL, 22-25 Oct., 1980 (Upton, 1980).
3. Proc. NEANDC/NEACRP Specialist's Meeting on Fast Neutron Capture Cross Sections, April 20-23, 1982 ANL, ANL-83-4 (Argonne 1983).
4. Proc. of a Advisory Group Meeting on Basic and Applied Problems of Nuclear Level Densities, Upton NY, 11-15 April, 1983, BNL-NCS-51694, M.R. Bhat(Ed.), (IAEA and USDOE 1983).
5. Proc. on Specialist Meeting on Use of the Optical Model for the Calculation of Neutron Cross Sections below 20 MeV, Paris, Nov. 13-15, 1985 (OECD 1986).
6. Arthur, E.D and Young, P.G.: LA-8626-MS(ENDF-304),UC-34c ,LANL (1980).
7. Arthur, E.D.: Proceeding of Consultants' Meeting on Structural Materials (IAEA), Vienna, Austria, November 2-4, (1983), and LA-UR 83-3137 LANL (1983).
8. Prince, A.: Proc. International Conference on Nuclear Data for Science and Technology, Antwerp, Sep. 6-10, 1982, pp, ECSC,EEC,EAEC,Brussels and Luxembourg (1983).
9. Strohmaier, B and Uhl, M.: ibid., pp552-555.
10. Hetrick, D.M., Fu, C.Y. and Larson, D.C.:ORNL/TM-9086 ENDF-337(ORNL 1984).
11. N. Yamamuro, N.: JAERI-M88-140(1988).
12. Iwasaki, S. ,Odano, H, Tanaka, S., Dumais, J.R., and Sugiyama, K.:Proc. Int. Conf. Nucl. Data Sci. Tech., Igarashi, S. (Ed),p229, Mito, Saikon Pub. Co. (Tokyo 1988).
13. Iwasaki, S. Odano, and Sugiyama, K.: 15th. Int. Symp. Fusion Tech., E13, Utrecht, 19-23 Sep. 1988.
14. Iwasaki, S. Odano, N. Kitamura, M. and Sugiyama, K.: Fall Meet.Jap. Atom. Energy Soc., C4 Oct.1988.
15. Igarashi, S.: JAERI 1224 (1972).
16. Igarashi, S.: J. Nucl. Sci. Technol., 12, 67 (1975).
17. Young, P.G. and Arthur, E.D.: LA-6947, LASL (1977).
18. Kunz, P.D.: DWUCK, University of Colorado Report (1974).
19. Raynal, J: IAEA-SMR-9/8 & 9/9 (1972).
20. Mughabghab, S.F., Divadeenam, M.and Holden, N.E.:"Neutron Cross Sections, vol1&2 Neutron Resonance Parameters and Thermal Cross Sections, Part A:Z=1-60 ", Academic Press (New York, 1981).
21. Nexpert Object manual, Neuron Data Inc. (1988).
22. Delaroche, J.P., Lagrange, Ch., and Salvy, J.: p251 in ref. 1.

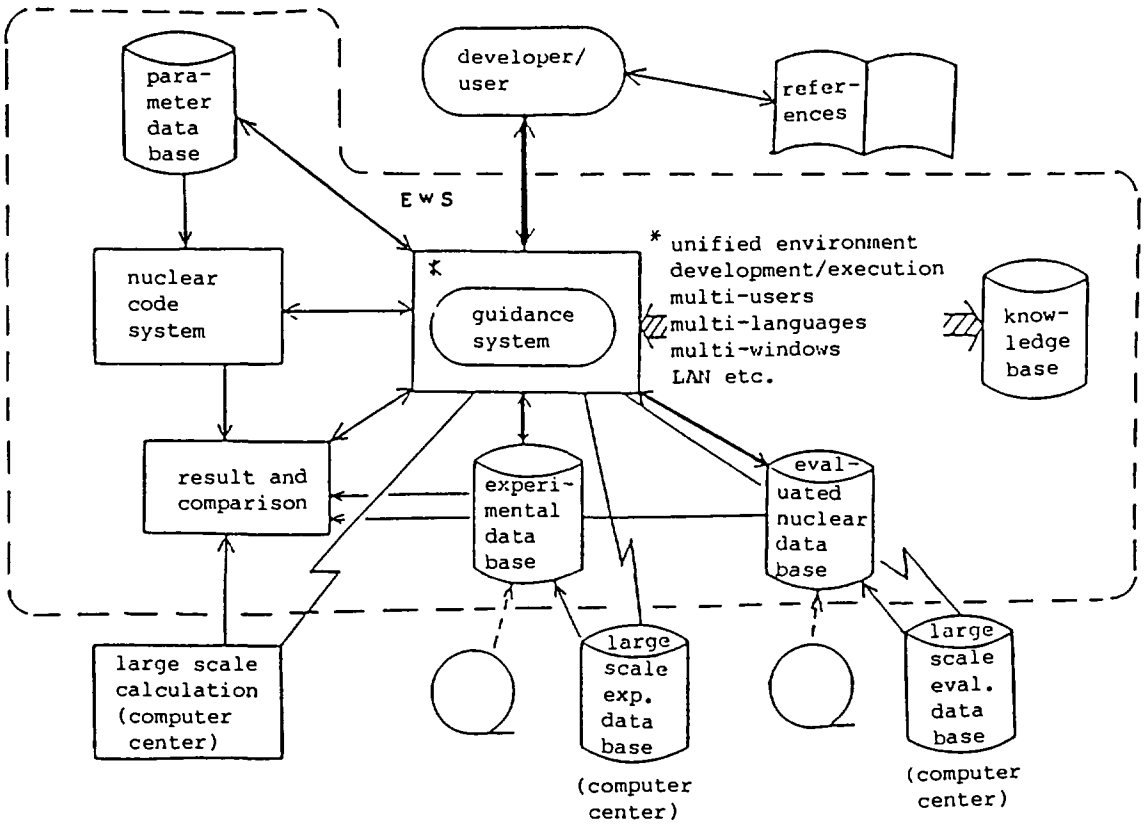

Fig. 1 Proposed supporting system for the nuclear cross section calculation developed in a 32-bit engineering workstation /14/.

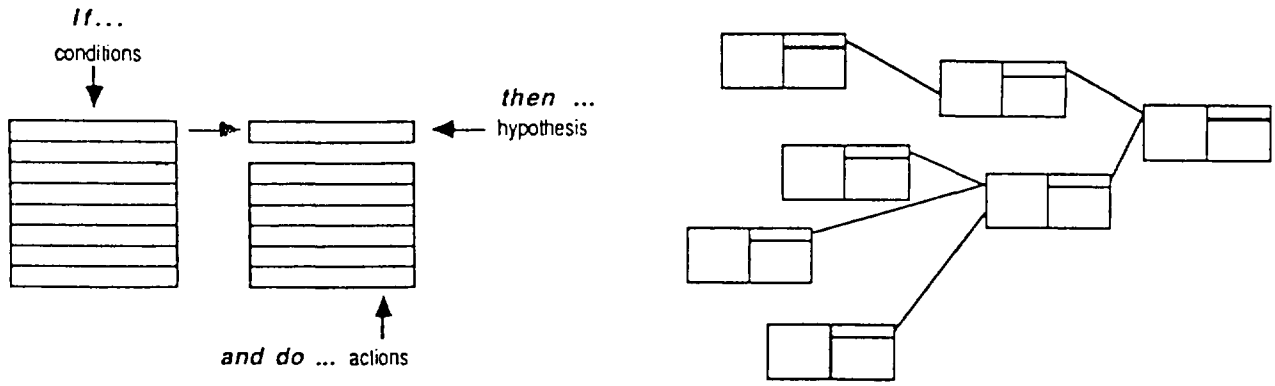

Fig. 2 The elements of a rule (a), and tree structure of the rules (b) in the Nexpert Object /21/.

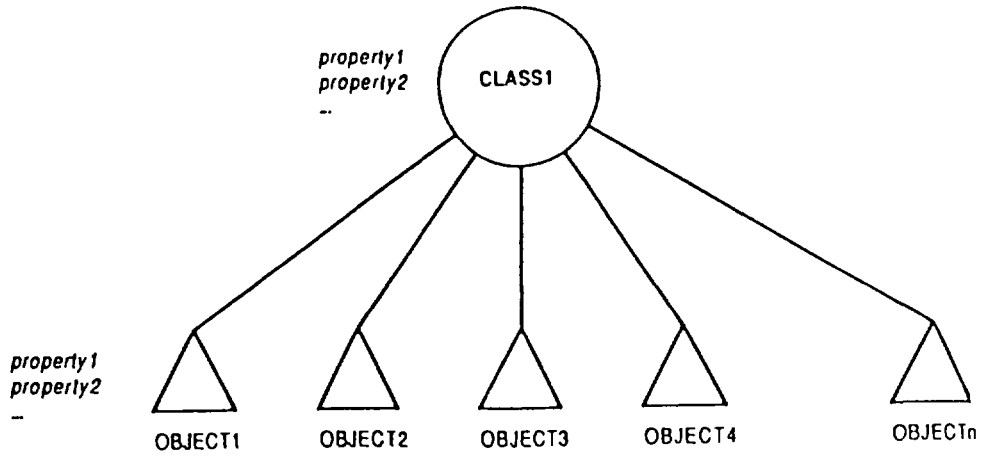

(a)

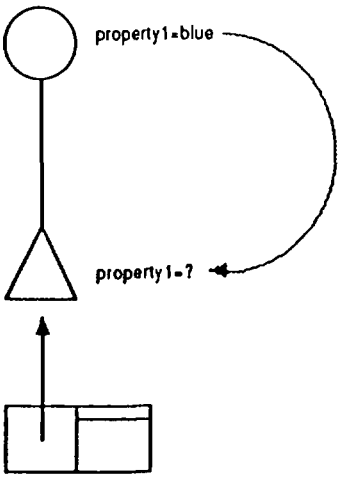

(b)

Fig. 3 Concept of class and objects in the Nexpert Object /21/. (a): objects and their class, (b): a rule reads an object.property1 which is obtained from the class by the inheritance mechanism of the property.

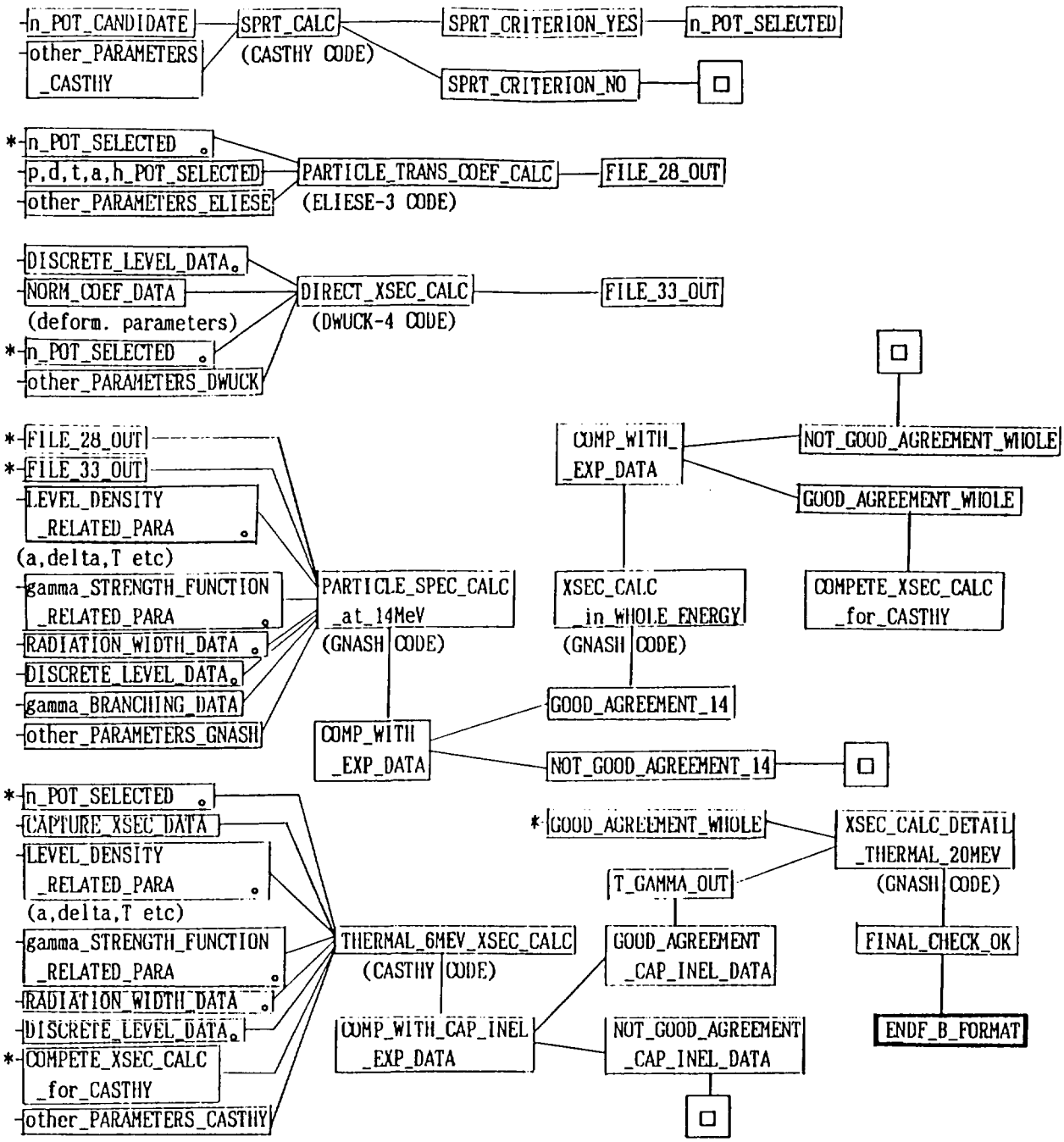

Fig. 4 Tree structure of the upper part rules of the supporting system which corresponds to the calculation process using code. Lower parts rules (input parameter selection parts) are not shown. Each block corresponds to a code system. Four double boxes indicate the modification process of the input parameters and are not shown in the figure. Symbols (*) and (○) mean that the lower parts of the rule are presented elsewhere in the figure, and the same hypothesis exists elsewhere in the figure, respectively.

3.15 Kerma factors for neutrons with energies above 20 MeV

K. Kitao

National Institute of Radiological Scienses

9-1, Anagawa-4-Chome, Chiba-Shi 260, Japan

Abstract

A short review is presented concerning the calculation of kerma factors for neutrons with energies above 20 MeV. Using the program ALICE, the light particle spectra from neutron-induced reaction and kerma factors for C, N, O and tissue have been calculated. The spectra are also compared with experimental results by Romero et al. at 27.4, 39.7 and 60.7 MeV neutron energy.

1. Introduction

Recent X-ray therapeutic apparatuses with energies tens of MV have provided the percent depth dose of 50% at 21 cm deep for a 10 cm x 10 cm field. For to achieve the level of depth dose in fast neutron teletherapy, the neutron beam have to be produced from the (p,n) reaction on beryllium with bombardment of protons with energy more than 70 MeV. Figure 1 shows values of the percent depth dose have been measured at some high energy accelerator em-ployed fast neutron therapy. The energy distribution of Be-p neutrons is varied with thickness of the beryllium target, backing materials and filter materials. In any case, calculations of neutron kerma factors for materials of biomedical importance have to extend for neutrons up to 100 MeV.

Neutron kerma factor for a given material is equal to the initial kintic energies of all the charged particles liberated by neutrons in a volume element of material. Then, kerma per unit fluence K(E), for monoenergetic neutrons with energy E, is defined by

$$K(E) = \Sigma_J \Sigma_I \langle E_{JI}(E) \rangle \sigma_J(E), \qquad (1)$$

where $\langle E_{JI}(E) \rangle$ is average energy transferred to the kinetic energy of Ith charged particle in Jth reaction, $\sigma_J(E)$ is the Jth reaction cross section at

particle energy E.

Cross section $\sigma_J(E) = \int d\sigma$ and $\langle E_{JI}(E) \rangle = (\int E_I d\sigma)_J / \int d\sigma$, then kerma factor is given by,

$$K(E) = \Sigma_J \Sigma_I \int E_I \, d\sigma_J,$$
$$= \Sigma_J \Sigma_I \int E_I (d\sigma/dE)_{JI} dE, \quad (2)$$

where $(d\sigma/dE)_{JI}$ is the spectrum of emitted Ith light charged particles from Jth reaction, and this is equal to the angle-integrated differential cross-section. Romero et al./1/ had made the measurements of neutron-induced charged particle (protons, deuterons, tritons, helium-3 and alpha particles) cross sections on tissue elements at 27.4, 39.7 and 60.7 MeV.

In this work, we assume C with a composition of 100% 12C, N with 100% 14N and O with 100% 16O, and compare charged particle emission spectra for C, N and O calculated by ALICE code/2/ with experimental spectra by Romero et al./1/ And, we have calculate kerma factors for C, N, O and ICRU muscle tissue, using the calculated spectra and the recoil kerma from that cited by Romero et al./1/

2. Status on kerma calculations

As it is shown in the table 1, since 1977 kerma factors for neutrons with energies above 20 MeV have been calculated for light elements by several groups (Alsmiller and Barish/3/, Wells/4/, Behrooz/5,6/, Caswell and Coyne/7/, Dimbylow/8,9/, Brenner/10/) based on calculated neutron cross sections or evaluation of limited experimental data. Therefore, there are significant discrepancies in the results.

Brenner/10/ had pointed out that all the nuclear models used in calculation of the neutron cross sections are quite adequate for the heavier elements in tissue but not suitable for low-mass nuclei. Experiments have predict that assumption of statistical evaporation as a means of de-excitation is reasonable for heavy and medium mass nuclei, but not for carbon. And assumption of an analytic form for the density of nuclear levels, as used in the pre-equilibrium model, cannot be justified for low-massnuclei,too.

3. Code ALICE and experimental spectra

We have used the code ALICE(ALICE/LIVERMORE 82)/2/, to calculate the

particle spectra emitted from the neutron induced reaction. Nobody hitherto have used this code for kerma calculation. For multiple particle emission, the ALICE code performs equilibrium (compound nucleus) decay calculations using the Weisskopf-Ewing evaporation model. Precompound decay is treated by the hybrid model. Emitted particle may be either neutron; n and p; n, p and α; n, p, α and d.

Spectra calculated by ALICE code for p, α and d from C at 27.7 MeV neutron energy, and form N at 39.7 MeV, have been compared with those measured by Romero et al./1/ And the spectra from O at 60.7 MeV compared with those of Dimbylow/9/. These results are shown in Figure 2 to 5. The calculated and experimental spectra are in agreement at 27.4 MeV.(Fig.2) However, deuteron spectra show disagreement all over the energy of emitted particles from N at 39.7 MeV, and from O at 60.7 MeV. At higher d-energies, ~15 MeV or more at 39.7 MeV and ~20 MeV or more at 60.7 MeV the calculated spectra are higher than experiment. At lower energy region, the calculated d spectra, as well as p, are lower than experiment. The trend can see in alpha spectra from O at 60.7 MeV.

In table 2, comparison between the calculated kerma values for light particles and the experimental values by Romero et al./1/ is presented. The calculated carbon kerma factors, included the recoil kerma factor cited by Romero et al./1/, are shown in table 3 together with those calculated by other authors. Using kerma factor calculated for C, N and O, kerma values for ICRU muscle tissue(with a composition of 10.1% H, 11.1% C, 2.6% N and 76.2% O by weight) have been derived at 27.4, 39.7 and 60.7 MeV neutron energy. Where the hydrogen kerma factors have used those of Bassel and Herling/11/. Figure 6 illustrates these results and compares with the values of other authors.

4. Conclusion

It is important to improve the reliability of the kerma calculation there are measurements of double differential cross sections for emitted charged particles from tissue and dosimeter elements bombarded by neutrons. Some discrepancies between the calculated kerma by the ALICE and the experimental values suggest to be need for a search for suitable parameter in application of the ALICE code.

References

1. Romero,J.L.,Brady,F.P. and Subramanian,T.S.: Proc. Int. Conf., Santa Fe, 1985, p.687.
2. Blann,M.and Bisplinghoff,J.: Lawrence Livermore National Laboratory Report UCLD-19614 (1982) unpublished.
3. Alsmiller,R.G. and J.Barish,J.: Health Phys. 33, 98 (1977).
4. Wells,A.H.: Rad. Res. 80, 1 (1979).
5. Behrooz,M.A.,Gillespie,E.J. and Watt,D.E.: Phys. Med. Biol. 26, 507 1981).
6. Behrooz,M.A. and Watt,D.E.: Radiat. Prot. Dosim. 1, 291 (1982).
7. R.S.Caswell et al.: Radiat. Res. 83, 217 (1980).
8. Dimbylow,P.J.: Phys. Med. Biol. 25, 637 (1980).
9. Dimbylow,P.J.: ibid. 27, 989 (1982).
10. Brenner,D.J.: ibid. 29, 437 (1983).
11. Bassel,R.H. and Herling, G.H.: Radiat. Res. 69, 210 (1977).

Table 1 A summary of kerma factor calculations.

Author	neutron energy	model or method
Alsmiller(1977)	<70 MeV	Intranuclear cascade model
Wells(1979)	<80	Intranuclear cascade + evaporation model
Caswell(1980)	20-30	Optical model
Dimbylow(1980)	<50	Continuous evaporation model
Behrooz(1981,82)	<60	---
Dimbylow(1982)	<50	NOPTIC(optical model) + GNASH + DWUCK
Brenner(1983)	<80	Intranuclear cascade model + optical model
Present work(1988)	<60	ALICE

Table 2 Comparison between the experimental values* and calculated kerma values by ALICE for emitted light particles. (in 10^{-15} Gy m^2)

	En = 27.4 MeV		39.7 MeV		60.7 MeV	
element	exp.	cal.	exp.	cal.	exp.	cal.
C	3.2(1)	2.73	3.6(1)	3.95	5.3(2)	5.77
N	2.3(2)	2.91	3.7(1)	4.09	5.8(6)	6.29
O	2.0(1)	2.22	2.9(1)	3.28	4.8(5)	5.13

* from ref./1/.

Table 3 Carbon kerma factor (in 10^{-15} Gy m^2)

Author	Neutron energy (MeV) 27.4	39.7	60.7
Werlls/4/	3.86	4.12	4.75
Dimbylow/8/	4.64	5.48	
Behrooz/5/	3.08	3.65	6.8
Behrooz/6/	3.25	3.82	6.4
Dimbylow/9/	3.7	4.1	5.4
Brenner/10/	3.72	3.87	4.71
Romero et al./1/	3.9(1)*	4.4(1)*	6.2(2)*
Present work	3.46+	4.74+	6.45+

* 4.0(1) means 4.0 ± 0.1.

+ value included the elasic and non-elastic recoil kerma from ref./1/.

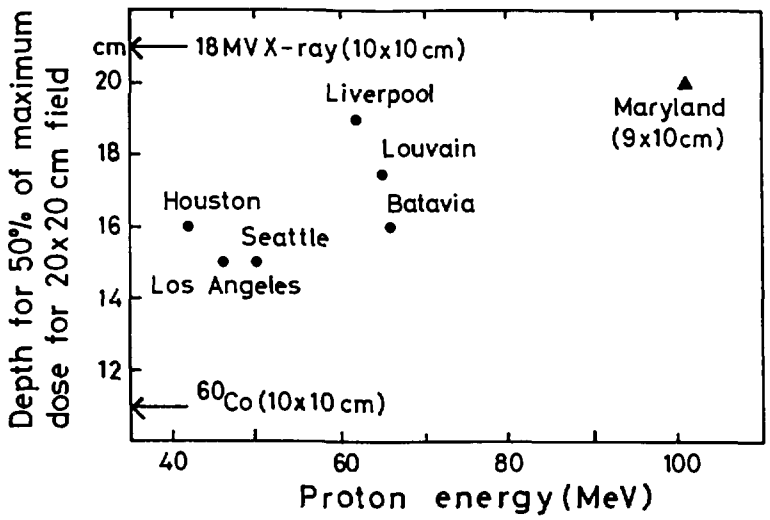

Fig. 1 Measured depth for 50 % maximum dose obtained by neutrons from thick beryllium target bombarding with protons.

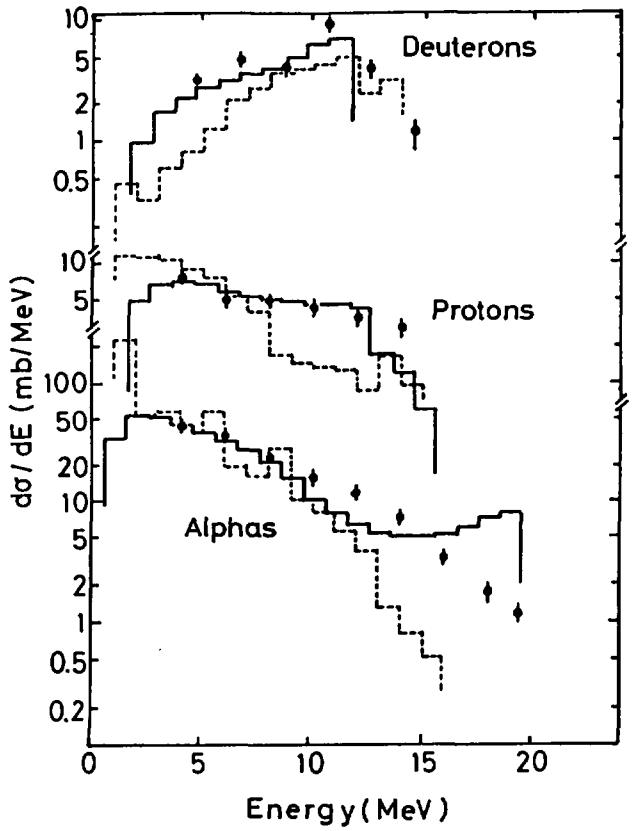

Fig. 2 A comparison between calculated and experimental charged particle spectra produced by 27.4 MeV neutrons incident on C. ——, ALICE (present work); ..., GNASH + DWUCK (Dimbylow/9/); ●, experiment (Romero et al./1/)

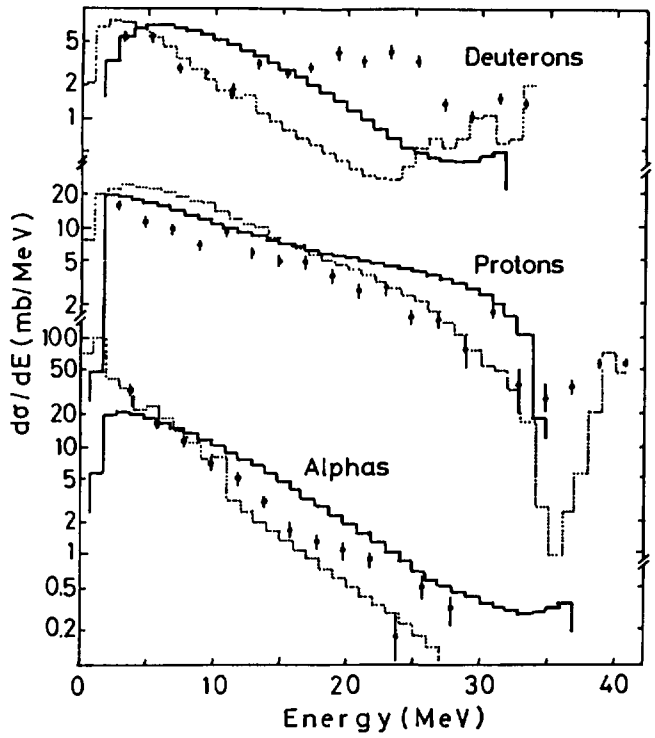

Fig. 3 A comparison between calculated and experimental charged particle spectra produced by 39.7 MeV neutrons incident on N. ——, ALICE (present work); ..., GNASH + DWUCK (Dimbylow/9/); ●, experiment (Romero et al./1/)

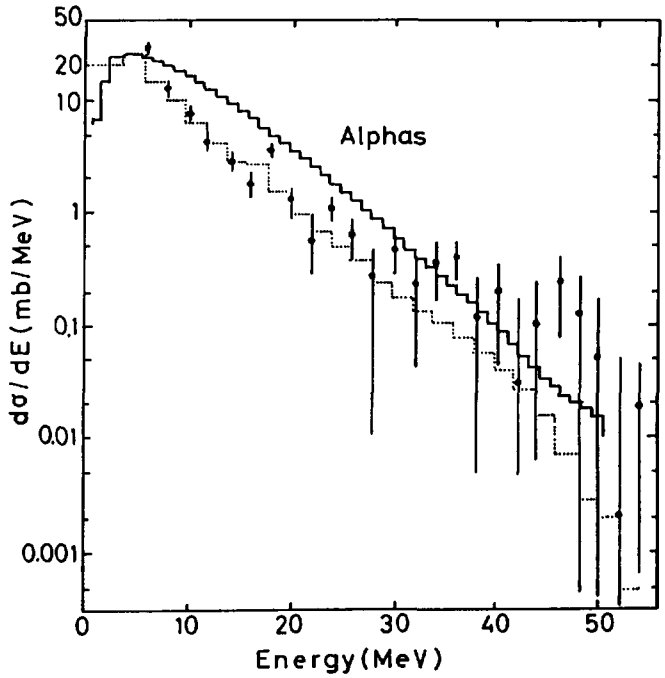

Fig. 4 A comparison between calculated and experimental alpha particle spectra produced by 60.7 MeV neutrons incident on O. ——, ALICE (present work); ..., GNASH + DWUCK (Dimbylow/9/); ●, experiment (from Dimbylow/9/)

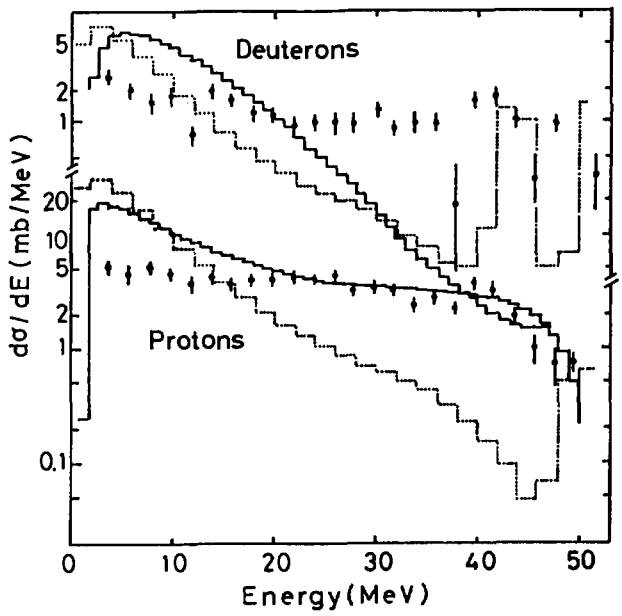

Fig. 5 A comparison between calculated and experimental proton and deuteron spectra produced by 60.7 MeV neutrons incident on O. ——, ALICE (present work); ..., GNASH + DWUCK (Dimbylow/9/); ●, experiment (from Dimbylow/9/)

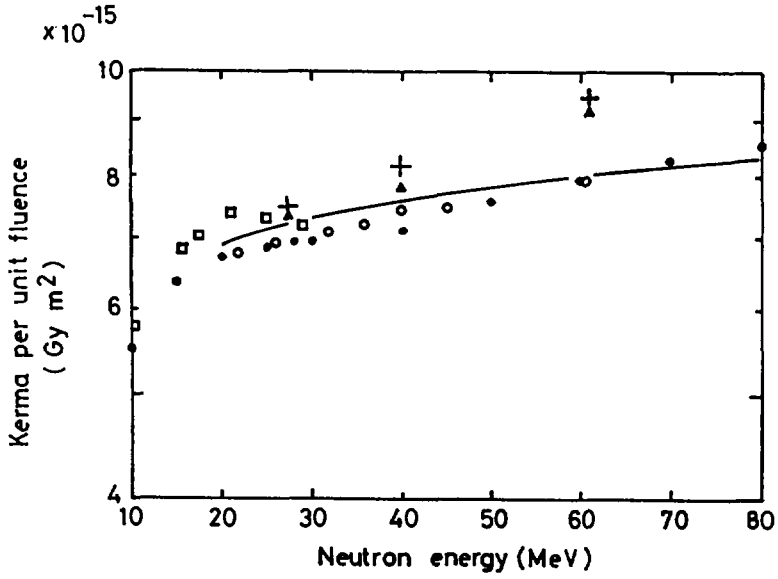

Fig. 6 Kerma per unit fluence for ICRU muscle tissue (see text, for its composition). +, Present work; △, ref./1/; ●, ref./9/; o, ref./4/; □, ref./7/ and ——, ref./10/.

3.16 Evaluation of $^{93}Nb(n,n')^{93m}Nb$ Cross Sections for JENDL Dosimetry File

K. Sakurai, Y. Ikeda, T. Nakagawa, T. Iguchi,
S. Iijima, K. Kobayashi, S. Iwasaki, and M. Nakazawa

JNDC Dosimetry Sub-working Group

Cross sections for $^{93}Nb(n,n')^{93m}Nb$ reaction are evaluated for JENDL Dosimetry file. C/E's of averaged cross section for U-235 fission spectrum are 1.105 in IRDF-82, 0.924 in Lippincott, and 0.994 in this data, respectively.

JENDL dosimetry file is under development, some cross sections in the file are evaluated by benchmark tests.

$^{93}Nb(n,n')^{93m}Nb$ reaction is available for reactor pressure vessel dosimetry, because of low threshold energy of this reaction, 0.1 MeV, and long half life time, 16.1 years, of the isomer, ^{93m}Nb. This reaction, fundamental studies were began in Europe, has become of major interest. And irradiation experiments have been carried out positively in USA and Japan since last ten years. The initial evaluated data of this reaction was included into International Dosimetry File of IAEA, IRDF-82.[1] By the request of dosimetry users, the cross sections have been measured actively, and decisive data for evaluation has been published.

Because cross sections in IRDF-82 are unsatisfactory data, Lippincott[2], HEDL in USA, proposed the evaluated data based on measured data that presented at Nuclear Data Meeting at Santa Fe by D.B.Gaythe r et al.[3] At Nuclear Data Meeting at Mito, Japan, Gaythe r et al. have presented the data, including near 3 MeV region data that became subject at issue, by means of to add measured points.[4] In this paper, we have determined the evaluated data and its covariance matrix based on this data. C/E's of averaged cross section for U-235 fission spectrum are 1.105 in IRDF-82, 0.924 in Lippincott, and 0.994 in this data, respectively. The experimental value measured by J.G.William et al.[5] is used. IRDF-82 data is overestimated the cross sections in the range of 1-3 MeV, on the other hand, Lippincott data is underestimated one. Though Lippincott disregards measured data above 6 MeV, that dosimetry is not affected very much, this data is more realistic because of regarding the measured data of 14 MeV by T.B.Ryves et al.[6]

References

1) D.E.Cullen, N.Kocherov and P.M.McLaughlin : The International Reactor Dosimetry File (IRDF-82), IAEA-NDS-41/R, (1982).
2) E.P.Lippincott : private communication, (1987).
3) D.B.Gaythe r et al. : Proc. Int. Conf. on Neclear Data for Basic and Applied Science and Technology, Santa Fe, (1985), Vol.1, 521, Gordon and Breach Science Publishers, (1986).
4) D.B.Gaythe r et al. : Proc. Int. Conf. on Neclear Data for Science and Technology, Mito, (1988), 1049, Saikon Publishing Co., Ltd., (1988).
5) J.G.Williams et al. : Measurements of Fission Spectrum Averaged Cross Sections for the ^{93}Nb(n,n')^{93m}Nb reaction, 6th ASTM-EURATOM Symp. on Reactor Dosimetry, Jackson Hole, (1987).
6) T.B.Ryves et al. : Nucl. Phys., 7 (1981) 529.

3.17 A Test of JENDL-3T/R1 Dosimetry Cross Sections by Using Integral Experimental data at FNS

Y. Ikeda and C. Konno

Japan Atomic Energy Research Institute

Tokai-mura, Naka-gun, Ibaraki-ken

Some dosimetry cross sections prepared for the JENDL-3T/R1 special purpose file have been tested by using integral data obtained at FNS. The main focus of this test was placed on the examination of the adequacy of the cross sections in the fusion dosimetry application. The reactions tested are $^{27}Al(n, \alpha)^{24}Na$, $^{56}Fe(n, p)^{56}Mn$, $^{54}Fe(n, p)^{54}Mn$, $^{58}Ni(n, 2n)^{57}Ni$, $^{58}Ni(n, p)^{58}Co$ and $^{90}Zr(n, 2n)^{89}Zr$. The neutron spectra in the Phase-II experimental systems of JAERI/USDOE collaborative program were used in the present test because the systems simulate the D-T fusion neutron field. The comparison between JENDL-3T/R1 and ENDF/B-V was made. The consistency of the cross sections for the 14 MeV neutron was discussed.

1. Introduction

A dosimetry file will be newly implemented in the JENDL-3 nuclear data file as one of special purpose files. Before it is open to be used, the data should be examined concerning the adequacy and reliability through the integral test. Although there have been significant improvements in the dosimetry cross section evaluation, such as ENDF/B-V dosimetry file[1], it is often quoted that there are inconsistencies among the cross sections, especially for 14 MeV neutron energy region.[2] This paper reports the integral test of some dosimetry cross sections in JENDL-3T/R1 dosimetry file by using integral experimental data at FNS.[3] The main focus of this test is placed on the examination of the adequacy of the data for the fusion application. The reactions tested are $^{27}Al(n, \alpha)^{24}Na$, $^{56}Fe(n, p)^{56}Mn$, $^{54}Fe(n, p)^{54}Mn$, $^{58}Ni(n, 2n)^{57}Ni$, $^{58}Ni(n, p)^{58}Co$ and $^{90}Zr(n, 2n)^{89}Zr$.
These reactions are considered to be important indices and the standard ones for high energy neutron dosimetry. The D-T neutron fields in the Phase-II

systems of JAERI/USDOE collaborative program on the fusion blanket neutronics [4] were used for the present test. It was expected that the spectra in the system reasonably simulated the fusion reactor blanket configuration. The comparison between JENDL-3T/R1[5] and ENDF/B-V was made on the reaction rates of interest and the consistency of the cross sections for the 14 MeV neutron was also discussed through the comparison of the reaction rates with experimental data.[6]

2. Dosimetry cross sections

The reactions tested here are $^{27}Al(n, \alpha)^{24}Na$, $^{56}Fe(n, p)^{56}Mn$, $^{54}Fe(n, p)^{54}Mn$, $^{58}Ni(n, 2n)^{57}Ni$, $^{58}Ni(n, p)^{58}Co$ and $^{90}Zr(n, 2n)^{89}Zr$.

The JENDL-3 data for these reactions were taken from partial cross sections in the general purpose file of JENDL-3T/R1. The data of the ENDF/B-V dosimetry file were also tested because the dosimetry file has been used widely as the standard data. The cross section data with 125 energy groups were prepared for the present test in order to match the neutron energy groups used in the spectrum calculation.

3. Neutron spectra

In the test we employed the spectra in the two different systems of Phase-II of JAERI/USDOE collaborative program for the fusion blanket experiment. It was expected that the systems could simulated well the D-T fusion blanket configuration and the spectra in the system were appropriate for this testing purpos. Basically, the systems consisted of a 60 cm thick blanket test zone enclosed by a 20 cm thick Li_2CO_3 zone with a 5 cm thick polyethylene insulator zone. The D-T neutron source was located inside of the enclosure. The cross sectional view of the system configuration is shown in Fig. 1. In the first system, only lithium oxide (Li_2O) was stacked in the testing zone. In the other system, a Be layer of 5 cm thick was lined up on the inside wall of the enclosure and first 5 cm thick of the testing zone. This Be makes the incident neutrons on the testing zone very soft. We called these two systems as "Reference" and "Be-lined", respectively.

The spectra at positions of 0.0, 10.0 and 30.0 cm in the "Reference" system and 0.0, 20.0 and 40.0 cm in the "Be-lined" System were calculated by DOT 3.5 with JENDL-3PR2.[7] The spectra are shown in Figs.2.1 and 2.2. The dashed lines in the spectra indicate ranges of uncertainty deduced from spectrum adjustment by STAY'SL[8] with multiple-foils activation data.

4. Comparison of JENDL-3T/R1 with ENDF/B-V

Figure 3 shows the ratios of reaction rates in the both systems calculated with JENDL-3T/R1 to those with ENDF/B-V. There are large differences in the reactions of $^{58}Ni(n, 2n)^{57}Ni$ and $^{58}Ni(n, p)^{58}Co$ at front positions. Since the 14 MeV neutron dominates the spectrum on the surface, these differences imply that cross sections of JENDL-3T/R1 are higher and lower by 10 % than those of ENDF/B-V for the reactions of $^{58}Ni(n, 2n)^{57}Ni$ and $^{58}Ni(n, p)^{58}Co$, respectively. At deeper positions, however, the differences decrease to be within ± 4 %. The JENDL-3 always gives smaller and larger values for $^{27}Al(n, \alpha)^{24}Na$ and $^{56}Fe(n, p)^{56}Mn$ by 2.5 % and 3% than the ENDF/B-V.

5. Comparison of reaction rates calculated with those measured

Figures 4.1 and 4.2 show the ratio of reaction rates calculated to those measured (C/E) in both "Reference" and "Be-lined" systems, respectively. At the front positions in both system, the ENDF/B-V gives overestimations and underestimations for $^{58}Ni(n, p)^{58}Co$ and $^{58}Ni(n, 2n)^{57}Ni$ by 10 to 18 % and 15 % , respectively, whereas the JENDL-3T/R1 shows reasonable agreements within ± 6 % with experiments. These large disagreements in ENDF/B-V decrease as the depth increases. Considering the neutron spectrum change with the depth in the system, there seems to be problems for the cross section data at 14 MeV region in ENDF/B-V. In this regard, the JENDL-3T/R1 seems to be adequate. For the other reactions, the C/E values are within the range from 0.95 to 1.05 at all positions. This fact gives the good consistency of the reaction rate as long as D-T neutron spectrum is concerned.

6. Summary

From the present integral test, it is clearly demonstrated that the accuracy of the JENDL-3T/R1 has been improved very much in comparison with ENDF/B-V. It is also pointed out that the JENDL-3T/R1 shows the good consistency among different reaction rates for the D-T neutron fields.

References

1. ENDF/B-V dosimetry file: "Evaluated Neutron Data file, ENDF/B-V", ENDF/B Summary Documentation, Compiled by R. Kinsey, ENDF-201, 3rd Edition, Brookhaven National Laboratory (1979).

2. Y. Ikeda, et al.: "Activation Cross Section Measurements for Fusion Reactor Structural Materials at Neutron Energy from 13.3 to 15.0 MeV Using FNS Facility", JAERI-1312 (1988).
3. T. Nakamura et al.: "Present Status of The Fusion Neutronics Source (FNS), "Proc. 4th Symp. on Accelerator Sci. Technol., RIKEN, Saitama, Nov. 24-26, 1982, pp 155-156.
4. T. Nakamura and M. A. Abdou, "Overview of JAERI/USDOE Collaborative Program on Fusion Blanket Neutronics Experiments," Proc. of Int. Symp. on Fusion Nucl. Technol., Tokyo, Apr. 11-15 (1988).
5. JENDL-3T/R1: "Japanese Evaluated Nuclear Data Library, Version-3 Testing version Rivision 1,"
6. Y. Oyama et al.:"Experimental Neutronics Parameter Measured in Phase-II of JAERI/USDOE Collaborative Program on Fusion Blanket Neutronics," ibid. (1988).
7. JENDL-3PR2 :"Japanese Evaluated Nuclear Data Library, Version-3 Preliminary-2," JAERI-M 86-029 (1986).
8. F. G. Perey :"Least-Squares Dosimetry Unfolding: The Program STAY'SL," ORNL/TM-6062 (1977)

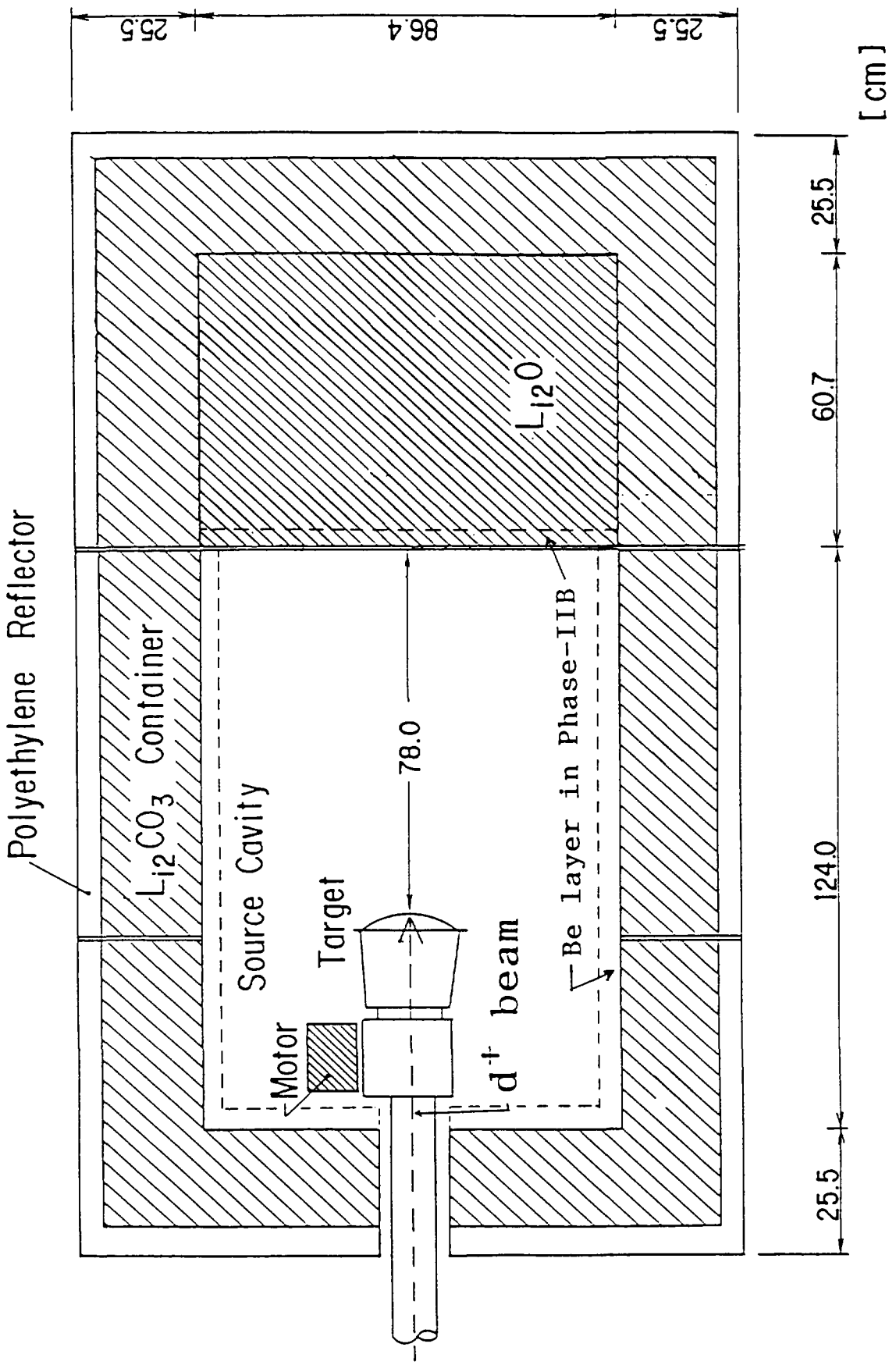

Fig. 1 Experimental system configuration for the JAERI/USDOE collaborative program on fusion blanket neutronics.

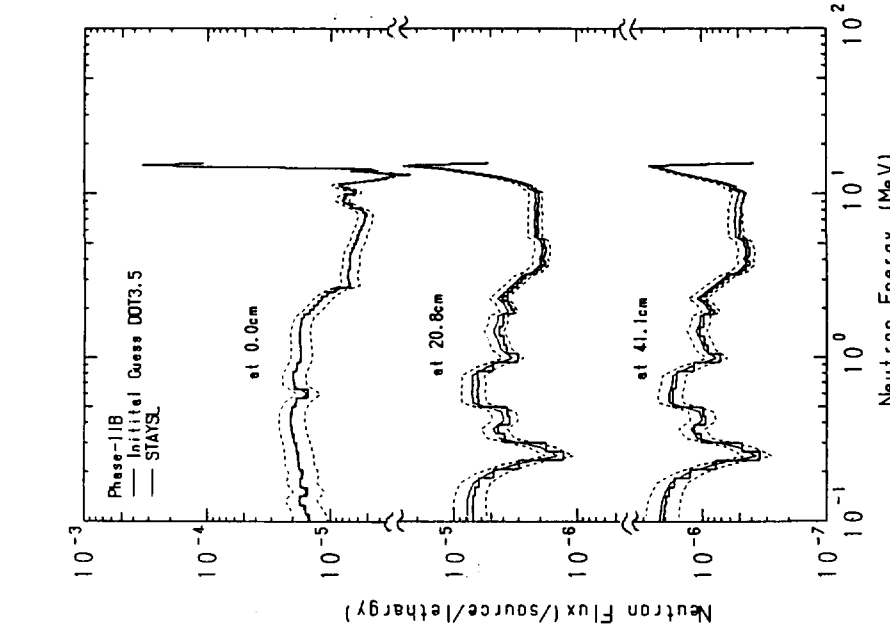

Fig. 2.2 Adjusted neutron spectra and DOT3.5 calculation in the "Be-lined" system. The uncertainty ranges are shown by dashed line.

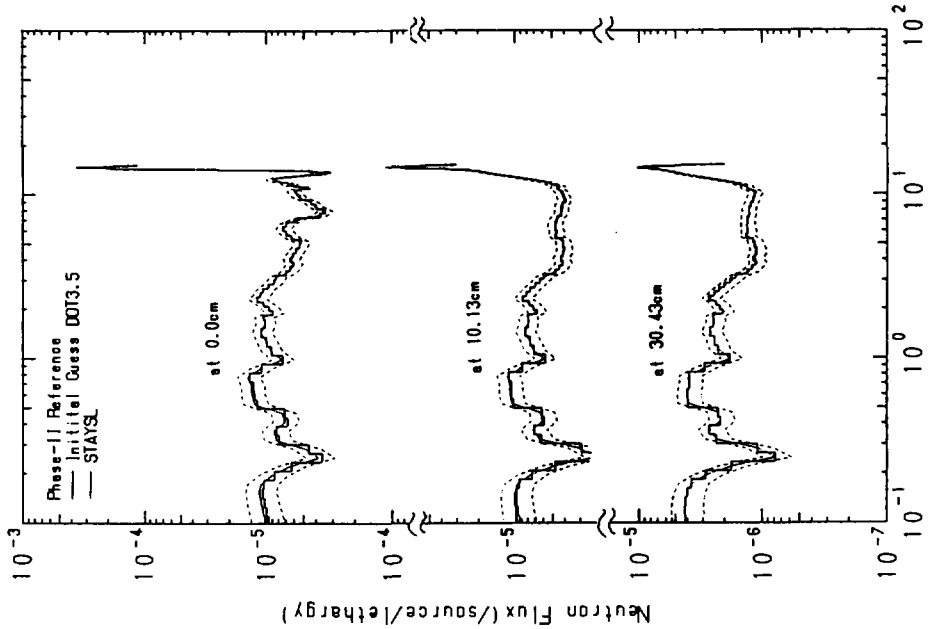

Fig. 2.1 Abjusted neutron spectra and DOT3.5 calculation in the "Reference" system. The uncertainty ranges are shown by dashed line.

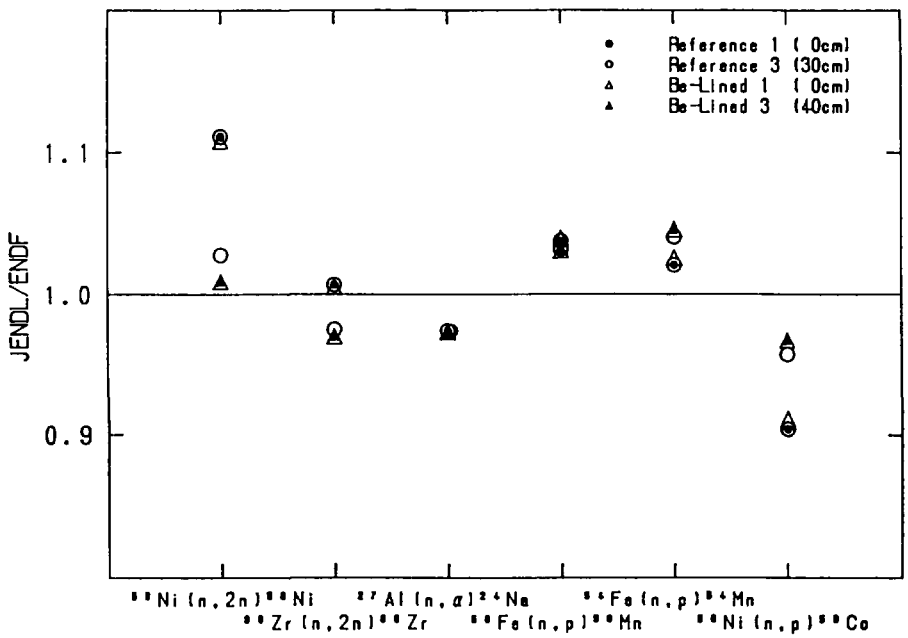

Fig. 3 Comparison of reaction rates between JENDL-3T/R1 and ENDF/B-V.

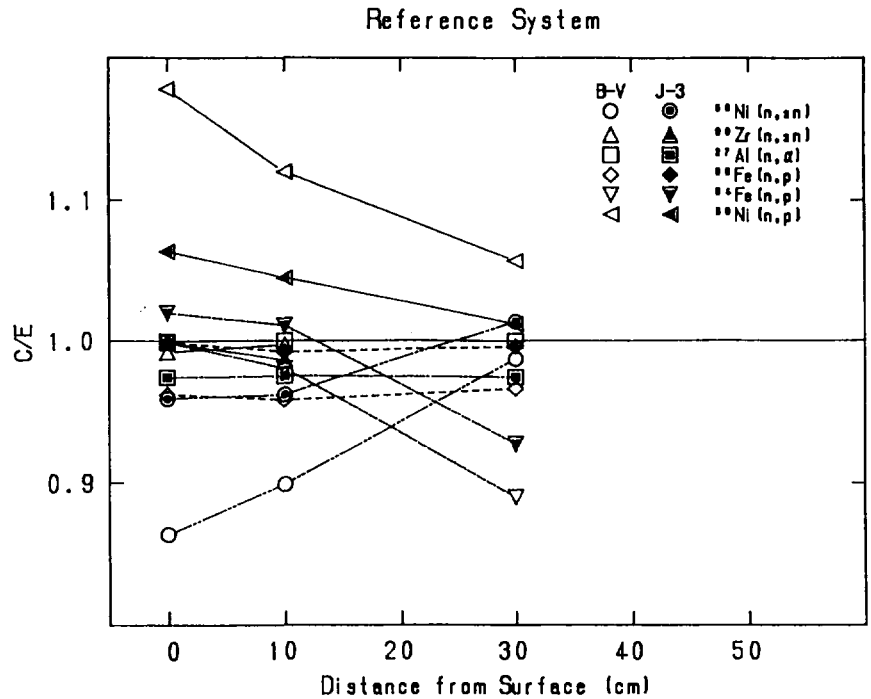

Fig. 4.1 C/Es of reaction rates in "Reference" system.

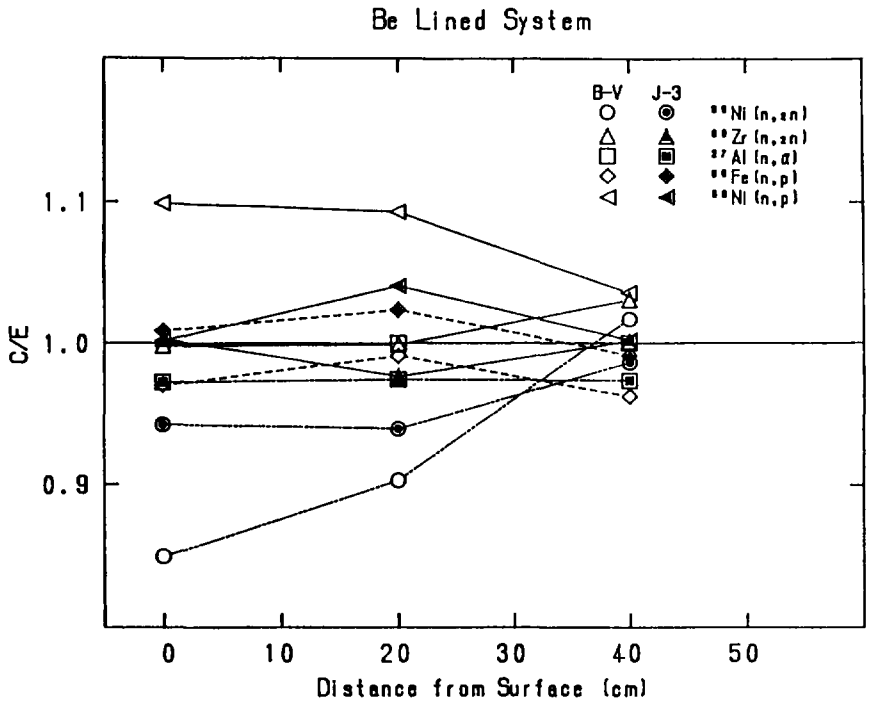

Fig. 4.2 C/Es of reaction rates in "Be-lined" system.

3.18 Comparisons of Neutron Radiation Damage Parameters Obtained by Using JENDL-3T and ENDF/B-IV Libraries

Takeo ARUGA
Department of Fuels and Materials Research, JAERI,

Kensuke SHIRAISHI
Takasaki Radiation Chemistry Research Establishment, JAERI

Neutron spectrum weighted displacement cross sections and energy spectra of primary knock-on atoms (PKA) have been compared for JENDL-3T[1)]* and ENDF/B-IV nuclear data files. The discrepancies between the results calculated by using the both files are less than 10 % for displacement cross sections of Fe, Cr, Ni, Al, Si and C irradiated with fission and fusion reactor neutrons. The inelastic scattering contributions to displacements are smaller in JENDL-3T calculation for Cr, Ni and Al than ENDF/B-IV, for fusion reactor neutron irradiations. The significance of the discrepancies are discussed in view of the damage analysis for neutron irradiated materials.

1. Introduction

It is well established in the materials community studying radiation damage to fusion reactors to use a unit of displacement per atom (dpa) to correlate irradiation effects to materials property. Energy spectra of primary knock-on atoms (PKA) also have been considered to be of importance in understanding the fundamentals of radiation damages produced under different neutron energy spectra. Since PKA energy spectra and dpa calculations depend on nuclear reaction data and nuclear kinematics models to be applied, it is worth while to examine systematic variations, if existing, between nuclear data files which have been independently evaluated, for the damage analysis of

---

*) JENDL-3T is a temporary file for testing the evaluated data which are for JENDL-3. The data in JENDL-3T will be partly revised in JENDL-3.

neutron irradiated materials. In the present study, the neutron irradiation damage parameters of displacement cross sections and PKA energy spectra, both weighted by several neutron spectra, have been calculated for major constituents in steels and also for lighter elements in ceramic materials to be used for a future fusion reactor, using evaluated nuclear data files of JENDL-3T and ENDF/B-IV. The results obtained for different neutron spectra are compared between the both data files used, and the significances of discrepancies are discussed in terms of an anlysis of the radiation effects data of materials.

2. Calculational procedures.

The present calculations are performed using a code already developed for an estimation of PKA spectra and defect productions in a stainless steel irradiated with breeder reactor neutrons[2]. The calculational model or nuclear kinematics applied in the code are based on those found in a number of papers[3)-7)]. The reaction types considered are (n,n) elastic scattering, (n,n') inelastic scattering, (n,2n), (n,p), (n,α) and (n,γ). In the first place, the energy transfer kernels $\sigma_i(E)K_i(E,T)$ are calculated, where $K_i(E,T)$ describes the probability that an i-type nuclear reaction at energy E will produce a PKA of energy T. The energy transfer kernel for (n,n) is calculated straightforwardly by using a elastic scattering cross section and energy-dependent Legendre coefficients resulting from Legendre expansions of the scattered neutron angular distributions in the center-of-mass system. Inelastic scattering is treated separately for the nuclear excitation to resolved levels and unresolved continuum. For resolved level excitations, the kernel is calculated by using fractional cross sections to the total inelastic cross section and corresponding level excitation energies or the reaction Q-values, with isotropic emissions of neutrons in the center-of-mass system from the excited levels being assumed. The charged-particle emission reactions of (n,p), (n,α) and also the unresolved inelastic scatterings are treated under the assumption that the particle is emitted from the compound nucleus isotropically in the center-of-mass system with an energy distribution described by the evaporation model using an energy-dependent nuclear temperature, which is given as a function of effective Coulomb barrier energies[8)] for (n,p) and (n,α) reactions. For (n,2n) reaction, the kinematics is simply

approximated by the unresolved inelastic scattering model described above, or one neutron model, except for accounting the cross section and the reaction Q-value. The approximation is reported to be reasonable after a comparison with the rigorous Monte Carlo procedure[3]. Neutron energy dependent gamma-ray spectra, which are filed in the data libraries, from descrete and/or continuous levels are assumed to be emitted independently and simply used to calculate the kernel by (n,γ) reactions, with influences of sequential emission of gamma-rays and momentum balance being ignored; the effects on the approximation are reported to be moderate[7),9)]. The calculation of PKA spectrum by (n,γ) reaction is added to the code for the present revision.

Displacement cross sections are calculated by integration of the product of $\sigma(E)K(E,T)$ and $\nu(T)$ over possible energies of T, where $\nu(T)$ represents displacement production function of a PKA with energy of T ,recommended as being $0.8T_{dam}/2E_d$ for $T > E_d$[10)]. E_d is a displacement threshold energy and T_{dam} is the total kinetic energy imparted to subsequently recoiled atoms after PKA, which is determined from Robinson's fitting formula[11)]. On the other hand, integration of the product of $\sigma(E)K(E,T)$ and an irradiating neutron spectrum Φ(E) over the neutron energy gives the PKA energy spectrum in the irradiated material. Since the calculations described above are carried out in the framework of multi-group structure both in the transfer energy and the neutron energy, the group averaged nuclear cross sections are prepared by the SUPERTOG[12)] program after the resonance parameters for (n,n) and (n,γ) reactions are processed by the RESENDD[13)] code. The neutron spectra used for obtaining the neutron spectrum weighted average values of displacement damage parameters are considered to be representative of fission reactor neutrons for JMTR[14)] and JOYO-II[15)], and of typical fusion reactor first wall neutrons for JXFR(Japan Experimental Fusion Reactor)[16)], which are plotted in Fig. 1. The JMTR neutron spectrum is given for neutron energies above 0.4 eV and the JXFR flux corresponds to a wall loading of 0.17 MW/M^2. The elements investigated in the present study are natural elements of Fe, Cr, Ni as major elements in stainless steels, as well as Al, Si, C as lighter elements used in ceramic materials for a variety of applications such as fusion reactors.

3. Result and discussion.

The PKA spectra produced by 42-th group neutrons in the energy range of 13.7-14.9 MeV, which is identical to the energy transfer kernel giving the probability for 42-th group neutrons to produce PKAs of energy T, are shown for Fe in Fig. 2 and 3, as calculated by using JENDL-3T and ENDF/B-IV, with contributions of each reaction type being superposed. Here, Fe is taken as an example for presenting the calculated results graphically, since it is most interested by the practical applications. The figures above show that the both nuclear data libraries give similar PKA spectra for neutrons of the above group. The neutron energy dependence of PKA energy spectra will be well illustrated in three-dimensional plotting; examples are shown in Fig. 4 in a log-scale axis for Fe irradiated with fission neutrons for (n,α) reaction and summed total from all contributions. On the other hand, integration of $\Phi(E)\sigma(E)K(E,T)$ over neutron energies gives the neutron spectrum weighted PKA spectrum, examples of which are given for Fe irradiated with JXFR spectrum, in Fig. 5 by using JENDL-3T and in Fig. 6 by ENDF/B-IV. Although the PKA distributions for summed total are calculated to be very similar between the two results, the contribution from inelastic scattering by JENDL-3T is found to have much PKAs of lower energies compared with that by ENDF/B-IV, from the figures.

The neutron energy dependent displacement cross sections, as obtained by integration of $\sigma(E)K(E,T)\nu(T)$ over the possible PKA energies, are shown also for Fe in Fig. 7 for JENDL-3T and in Fig. 8 for ENDF/B-IV, compared with that given in ASTM standard[10] for summed total in fine 642 group structure. From Fig. 7, the displacement cross section calculated by using JENDL-3T agrees fairly well with the ASTM standard which is based on ENDF/B-IV, although inelastic scatterings are calculated to have contributions by neutrons with energies below 1 MeV, where the results by ENDF/B-IV show no contributions from inelatic scattering(Fig. 8). The inelastic scattering which produces displacement by neutrons with energies below 1 MeV will result in producing PKAs with lower energies than those obtained by ENDF/B-IV, as shown in Fig. 5 and 6. The general trend of good agreement is also noted for the result by ENDF/B-IV and ASTM standard (Fig. 8). However, the displacement cross section by (n,γ) is considerably larger than the standard. This will be ascribed to the fact that in the standard,

gamma-ray spectrum of themal neutron captures is used, independent of neutron energies. The fact is further illustrated by the result obtained by using the TENJIN2 code and ENDF/B-IV, in which the thermal neutron capture gamma-ray spectrum is used, as shown in Fig. 9. The code TENJIN2 has been revised from TENJIN1[17] by adding the contributions of (n,p) and (n,α), in which displacement cross sections are directly obtained by integration over the PKA energy or angular distributions of recoil atoms, without calculating the PKA spectrum. It is noted that the (n,γ) displacement cross section becomes zero above a few hundreds of keV in neutron energies(Fig. 7 and 8), if neutron energy dependent gamma-ray spectrum in the files is used; whereas the cross section obtained by using the thermal capture gamma-ray spectrum decreases gradually up to several MeV of neutron energies(Fig. 9).

Comparisons of general trends in the displacement damage calculations based on the two libraries will be best made by neutron spectrum weighted averages such as displacement cross sections, average PKA energies. PKA production and displacement cross sections averaged over the above described neutron spectra are given in Table 1 for Fe,Cr, Ni, and in Table 2 for Al, Si, C. In the tables, fractions of elastic scattering (n,n) contribution in PKA production cross section and also in displacement cross section are compared, as well as average PKA energies for both total PKAs and PKAs produced by (n,n) only; PKA energies are averaged above each displacement threshold energy, which is used 40 eV for Fe, Cr, Ni[18], 25 eV for Al[18] and Si[19] and 31 eV for C[20]. The results in Table 1, 2 show that the the discrepancies in PKA production (item 1 in the tables) or simply neutron-spectrum-averaged nuclear cross sections of reactions which produce PKAs, are less than 10 % between JENDL-3T and ENDF/B-IV for most of the combinations of the elements and irradiating neutron spectra. The largest discrepance is for Cr irradiated with fusion neutrons, where the PKA production cross section by JENDL-3T is 9 % smaller than that by ENDF/B-IV. The results for C agree well between the both.

As for neutron spectrum dependence, the discrepancies in PKA production cross sections seem to be in an descending order of fusion reactor, JMTR and JOYO-II; showing that the harder the spectrum, the larger the discrepancies between the two libraries. Whereas, the values themselves of the PKA production cross sections for Fe, Cr and Ni are

in an descending order of fusion reactor, JOYO-II and JMTR. On the other hand, the discrepancies in displacement cross sections generally become smaller than those in PKA production cross sections, except for the case of Ni irradiated with fusion reactor neutrons, where the avereaged displacement cross section by JENDL-3T is smaller by 10 % than that by ENDF/B-IV.

The discrepancies of fractions of (n,n) in the displacement cross sections (Table 1,2) for Cr, Ni and Al irradiated with fusion reactor neutrons are found to be larger compared with other combinations of element and neutron spectrum, with the fraction obtained by JENDL-3T being larger by more than 10 % compared with those by ENDF/B-IV. The facts are attributed to the smaller fractions of inelastic scattering contribution, when other non-elastic reactions contribute to almost the same fraction between the results from the two libraries. In fact, the fraction of (n,n') is smaller by 6 % for Cr, Al and by 8 % for Ni than that by ENDF/B-IV, which are resulted from both the smaller farction in PKA production cross section and the lower (n,n') PKA energy; 280 keV by JENDL-3T versus 320 keV for the fusion reactor neutron spectrum weighted average PKA energy for (n,n') scattering for Cr, for example. The relatively smaller fractions of (n,n) scattering PKAs for JMTR spectrum is resulting from (n,γ) reactions by a larger population of low energy neutrons and the fraction is reduced further when thermal neutrons of energies below 0.4 eV are taken into the consideration.

Generally speaking, discrepancies between the displacement cross sections obtained by using JENDL-3T and ENDF/B-IV is less than 10 % for the combinations presently investigated. The significance of the discrepancies, which possibly originate from the difference in the data libraries, apart from uncertainties involved in displacement model and nuclear kinematic models, is discussed in view of the major objective of evaluating the displacement damage parameters. Usefulness of the displacement cross section is best exhibited in presenting the radiation effects data of materials irradiated with different neutron spectra. The present situation of studying the radiation effects for materials to be used in fusion reactors is forcing an unit of dpa for an irradiation dose unit, toward establishing the radiation damage model applicable to predict behaviors of materials irradiated with different neutron

spectra. This is mainly because presently 14 MeV fusion neutron sources for materials irradiation testing have much far less intensity, compared with anticipated fusion reactor irradiations. Therefore, current studies on radiation damages for the materials must be made by fission neutron irradiations.

The first step of establishing the model for predicting materials behaviors under irradiations of different neutron spectra will be made by compilations of radiation effect data as a function of dpa. For this purpose, neutron energy dependent displacement cross sections have been calculated and saved in the data base and are used in converting fluences to dpa. An example of compilating the property data for irradiated materials is given in Fig. 10 for Type 316 stainless steel irradiation data appeared in published papers, after converting to dpa. The data have been compiled in the relational data base system FMDB-J, which has been developed based on the previous work[21]. In the system, the materials properties data are expressed in property name like swelling and numerical values as a function of experimental variables such as specimen preparations, irradiation and testing conditions. The interrelated data structure is inevitable for expressing the irradiation properties data, since the radiation effects data are strongly influenced by conditions of specimens and experiments. Examples of specimen data and irradiation /testing data as retrieved in relation to data in Fig. 10 are given in Fig. 11 and 12. Based on these data and confining the specimen and irradiation conditions like irradiation temperatures, dpa dependence of the property is investigated. As shown, however, in Fig. 13, which gives an example of obtaining a fitting equation describing the swelling of Type 316 stainless steel as a function of dpa[22], a vast scattering of the data is existing. The scattering of the data on mechanical and dimensional properties of irradiated materials is likely to be inherent to materials irradiation tests, because of uncontrollable nature of inhomogeneity of microstructure, effects of minor elements, non-uniform treatment history, for testing samples and uncertainties for irradiation and testing conditions. Currently, the world wide efforts to reduce the scattering of radiation effects data are being made by adding other factors like helium atom production rate and effects of PKA energy related cascade structure, based on theoretical studies, as well as by

measuring neutron spectra and fluences as precisely as possible.

The present study shows the good agreement between the two libraries for displacement cross sections, as far as inter-comparisons of radiation effects data as a function of dpa are concerned. The precise evaluation of PKA spectrum is increasingly important recently in undersatanding the fundamentals of radiation damages through comparisons between the theoretical and experimental studies.

Acknowledgement

The authors would like to thank Dr. S. Iijima of NAIG for important comments given to the calculations, and Drs T. Nakagawa, Y. Komuro and J. Katakura of JAERI for instructions and usage of RESENDD and SUPERTOG codes.

References

1) JENDL Compilation Group(Nuclear Data Center, JAERI): JENDL-3T, Private communication(1987).
2) Ishino, S., Iwata, S., Matsutani, Y., Tanaka, S., Shiraishi, K. and Aruga, T.: "Radiation Effects in Breeder Reactor Structural Materials", AIME, p. 879 (1977).
3) Odette, G. R. and Doiron, D. R.: Nucl. Technol.,29,346(1976)
4) Jenkins, J. D.: Nucl. Sci. Eng.,41,155 (1970).
5) Doran, D. G. : Nucl. Sci. Eng.,49,130 (1972).
6) Parkin, D. M. and Goland, A. N.: Radiation Effects, 28, 31(1976).
7) Gabriel, T. A., Amburgey, J. D. and Greene, N. M.: Nucl. Sci. Eng., 61, 21(1976).
8) Kikuchi, K. and Kawai, M.: "Nuclear Matter and Nuclear Reactions", Elsevier Pub. Co., (1968).
9) Smither, R. K. and Greenwood, L. R.: NUREG/CP-0029, 793 (1982).
10) Annual Book of ASTM standards, Volume 12.02, E693-79, p.375 (1986).
11) Robinson, M. T.:"Radiation Induced Voids in Metals", p.397 (1972).
12) Wright, R. Q., Greene, N. M., Lucius, J. L. and Graven, C. W.: ORNL-TM-2679 (1969).
13) Nakagawa, T., JAERI-M 84-192 (1984).
14) Iida, H., JAERI, private communication (1973).
15) Iwanaga, H., PNC, private communication (1977).
16) Seki, Y., private communication (1977).

17) Sone, K. and Shiraishi, K.: JAERI-M 6358 (1976).
18) Annual Book of ASTM Standards, Volume 12.02, E521-83, p.248 (1983).
19) Kirk, M. A. and Greenwood, L. R.: J. Nucl. Mater., 80, 159 (1979).
20) Iwata, T. and Nihira, T.: J. Phys. Soc. Japan., 31, 1761 (1972).
21) Ishino, S. and Iwata, S.: J. At. Energy Soc. Jpn., 23, 489 (1981).
22) Horie, T., Aruga, T., Miki, N., Minato, A,, Seki, M., Shiraishi, K. Tsujimura, K., Watanabe, T. and Tone, T.: Proc. in IAEA-TCM on Lifetime predictions for First Wall and Blanket Structure of Fusion Reactors, Karlsruhe (1985).

Table 1 Comparisons of neutron spectrum weighted PKA and displacement parameters obtained by using JENDL3T and ENDF/B-IV for Fe, Cr and Ni.

Neutron spectrum	Fusion (JXFR)			FBR (JOYO-II)			JMTR		
Element / Parameter	a. JENDL3T	b. ENDF/B-IV	(a-b)/b.	a.	b.	(a-b)/b.	a.	b.	(a-b)/b.
Fe									
1. PKA production cross section(b)	4.6	4.9	-0.067	4.2	4.4	-0.057	3.1	3.3	-0.063
2. Displacement cross section(b)	512	521	-0.018	400	409	-0.021	364	371	-0.020
3. Fraction of (n,n) in PKAs (%)	94.5	94.0		95.1	95.3		90.1	88.9	
4. Fraction of (n,n) in displacements (%)	44.0	46.0		74.6	73.3		70.7	68.5	
5. av. PKA energy (keV)	21.0	20.0		14.8	14.2		18.5	17.8	
6. av. PKA energy of (n,n) (keV)	8.4	8.4		11.2	10.5		14.2	13.4	
Cr									
1.	4.4	4.8	-0.090	4.2	5.0	-0.066	3.4	3.7	-0.083
2.	505	542	-0.068	441	468	-0.057	382	417	-0.083
3.	95.5	95.2		97.0	96.6		92.3	92.1	
4.	52.4	46.4		82.1	80.5		77.3	76.0	
5.	22.4	21.4		16.3	16.3		18.0	18.1	
6.	10.5	8.8		13.4	13.1		14.8	14.7	
Ni									
1.	9.2	8.7	+0.056	7.3	6.8	+0.078	5.7	5.4	+0.055
2.	521	584	-0.106	478	458	+0.044	407	387	+0.051
3.	98.0	97.4		98.2	97.9		94.9	94.8	
4.	58.6	49.0		84.5	81.2		78.5	73.9	
5.	10.1	12.3		9.7	10.0		11.1	11.1	
6.	5.2	5.2		8.1	8.1		8.9	8.4	

Table 2 Comparisons of neutron spectrum weighted PKA and displacement parameters obtained by using JENDL3T and ENDF/B-IV for Al, Si and C.

Neutron spectrum	Fusion			FBR (JOYO-II)			JMTR		
	a. JENDL3T	b. ENDF/B-IV	(a-b)/b.	a.	b.	(a-b)/b.	a.	b.	(a-b)/b.
Element / Parameter									
Al									
1. PKA production cross section(b)	3.4	3.4	0.0	4.2	4.0	+0.044	2.5	2.4	+0.025
2. Displacement cross section(b)	754	821	-0.081	930	917	+0.013	1168	1184	-0.014
3. Fraction of (n,n) in PKAs (%)	96.7	95.5		98.3	98.1		96.0	95.8	
4. Fraction of (n,n) in displacements (%)	73.4	64.9		91.6	90.6		87.2	86.4	
5. av. PKA energy (keV)	45.9	53.2		28.2	29.5		40.8	43.2	
6. av. PKA energy of (n,n) (keV)	24.5	23.3		24.8	25.7		35.2	37.0	
Si									
1. PKA production cross section(b)	2.6	2.4	+0.086	3.4	3.2	+0.067	2.24	2.15	+0.064
2. Displacement cross section(b)	760	776	-0.021	845	883	-0.043	456	478	-0.047
3. Fraction of (n,n) in PKAs	95.3	94.7		98.5	98.4		96.7	96.7	
4. Fraction of (n,n) in displacements	66.1	64.8		92.2	92.3		88.3	88.4	
5. av. PKA energy (keV)	63.6	69.0		30.9	35.1		40.3	46.1	
6. av. PKA energy of (n,n) (keV)	28.6	30.3		27.5	31.3		35.1	40.3	
C									
1. PKA production cross section(b)	3.5	3.5	0.0	3.5	3.5	.0.0	2.6	2.6	0.0
2. Displacement cross section(b)	512	526	-0.027	708	712	0.0	591	592	0.0
3. Fraction of (n,n) in PKAs	98.2	97.8		99.9	99.9		99.8	99.8	
4. Fraction of (n,n) in displacements	92.4	90.9		99.7	99.7		99.5	99.5	
5. av. PKA energy (keV)	83.6	94.1		67.1	67.5		83.6	84.0	
6. av. PKA energy of (n,n) (keV)	58.0	59.2		66.3	66.7		82.6	83.0	

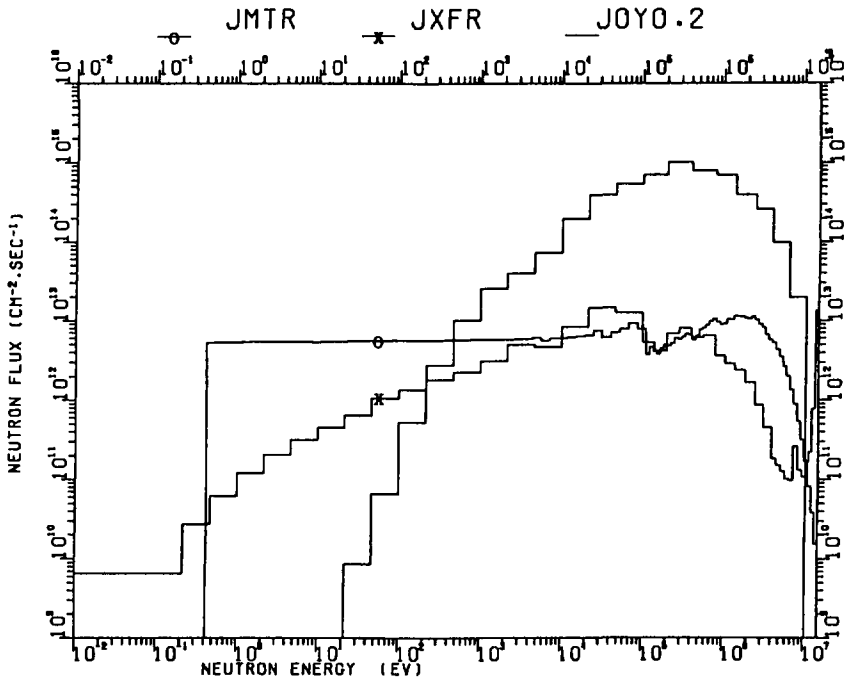

Fig. 1 Neutron spectra used for obtaining spectrum weighted averages of displacement cross section and PKA energy spectrum.

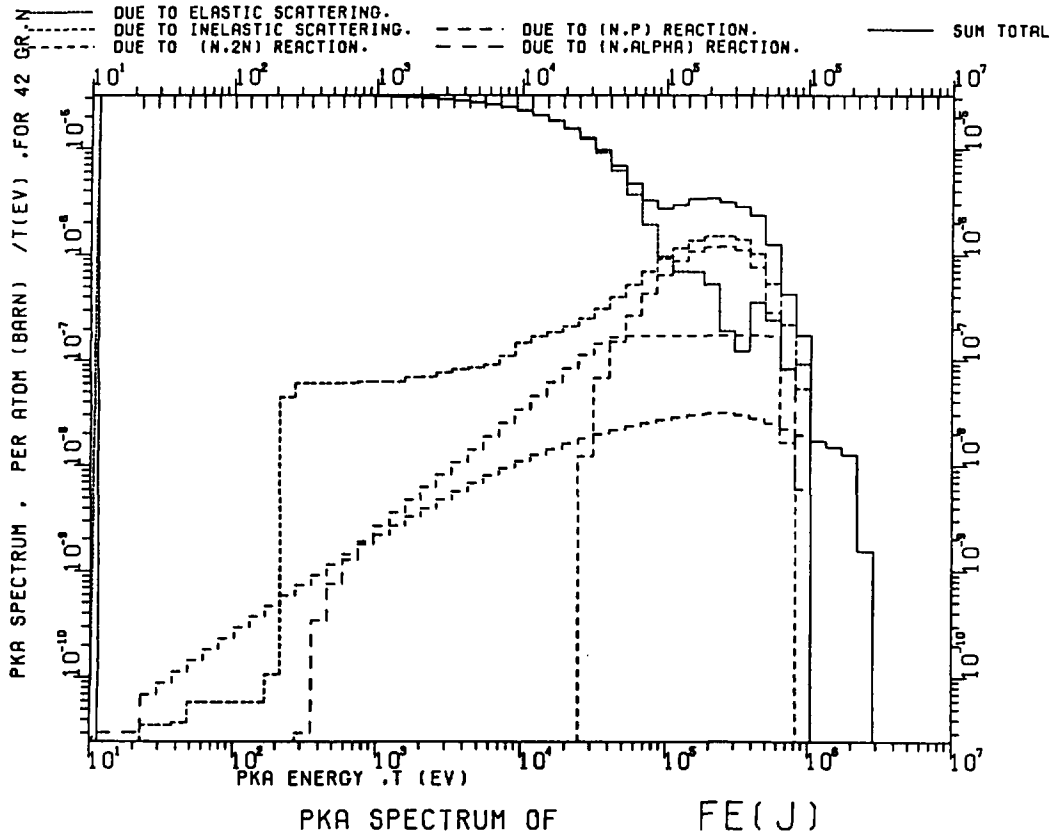

Fig. 2 PKA spectrum produced by a neutron of energy range of 13.7-14.9 MeV for Fe, as calculated by using JENDL-3T.

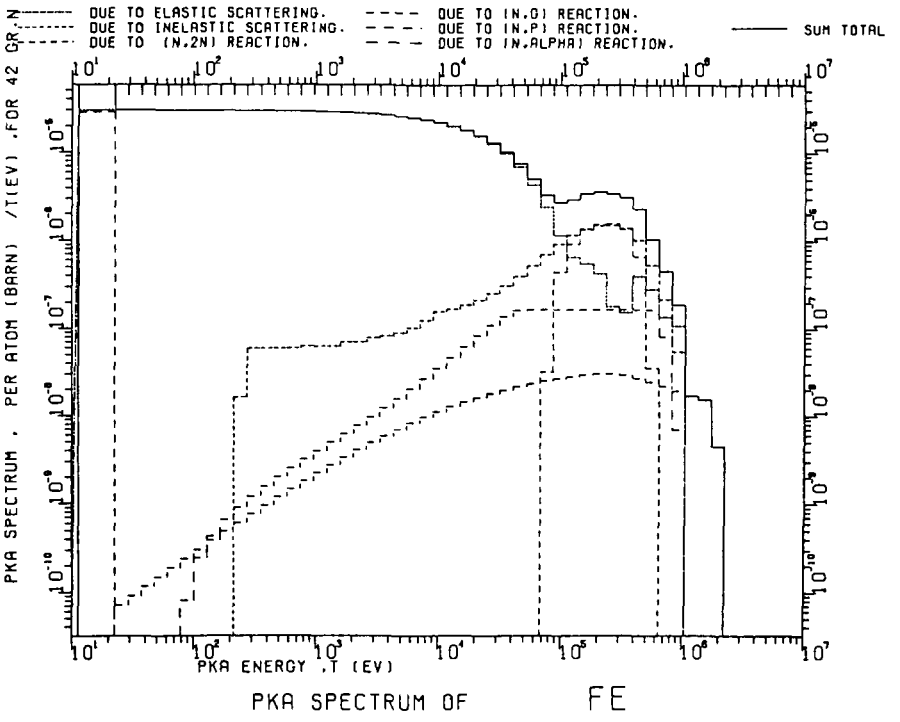

Fig. 3 PKA spectrum produced by a neutron of energy range of 13.7-14.9 MeV for Fe, as calculated by using ENDF/B-IV.

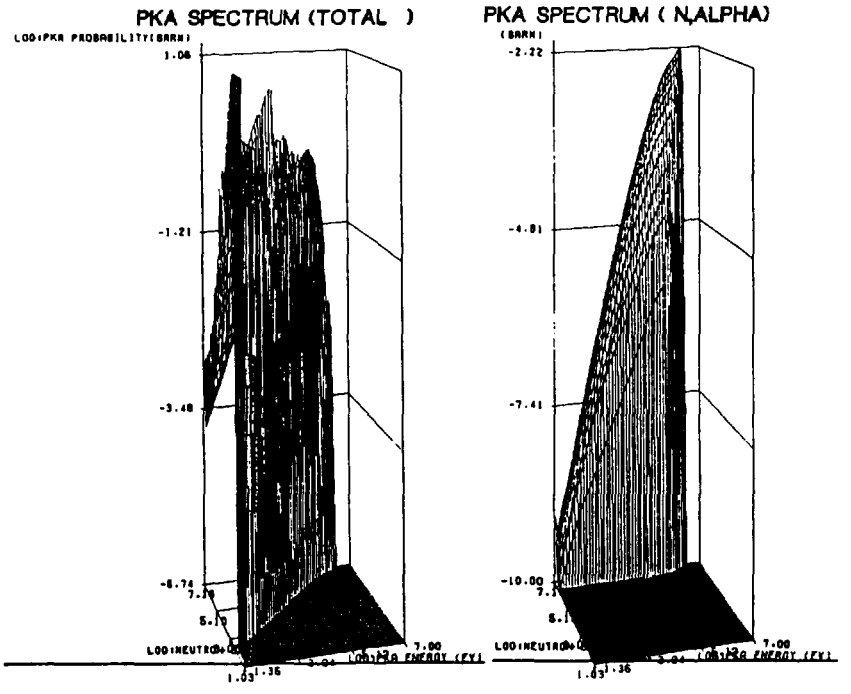

Fig. 4 Three-dimensional illustrations of PKA spectra of summed total of contributions from other reactions and of (n,α) reaction for Fe irradiated with fission neutrons.

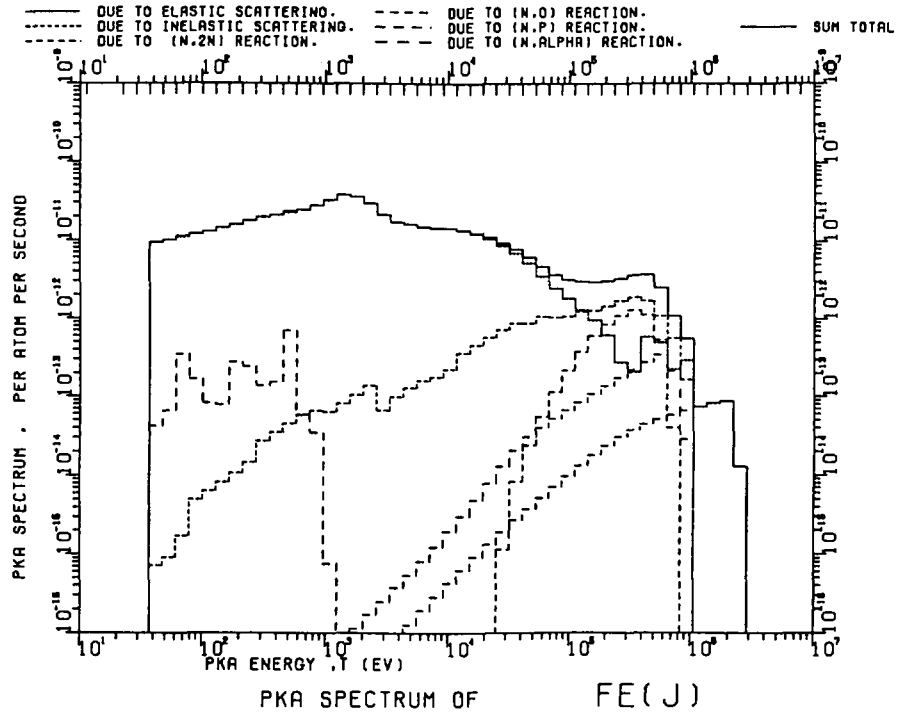

Fig. 5 PKA spectrum in Fe irradiated with fusion reactor neutrons obtained by using JENDL-3T, with contributions from each reaction.

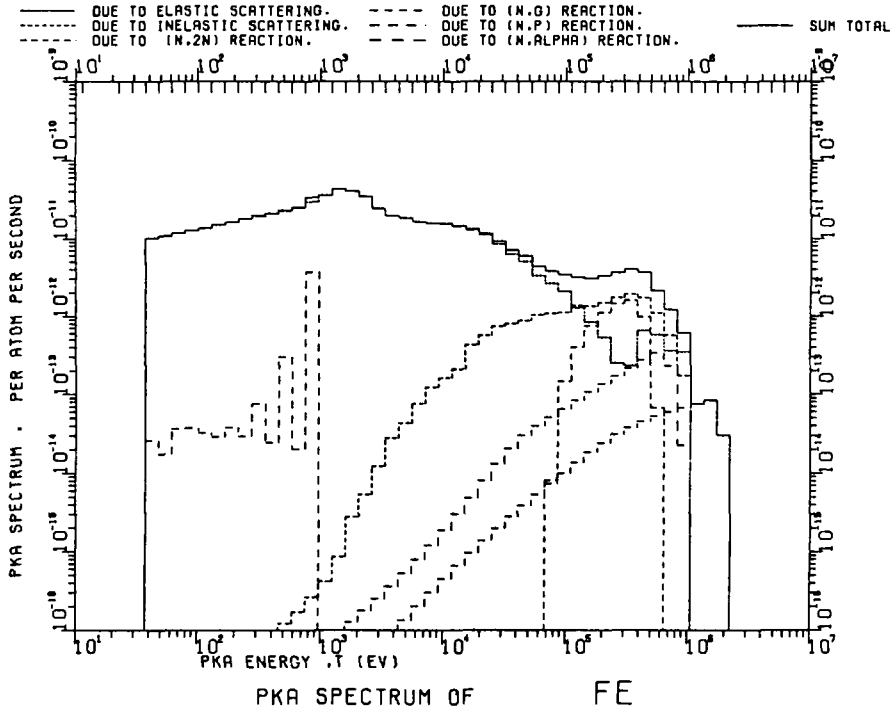

Fig. 6 PKA spectrum in Fe irradiated with fusion reactor neutrons obtained by using ENDF/B-IV.

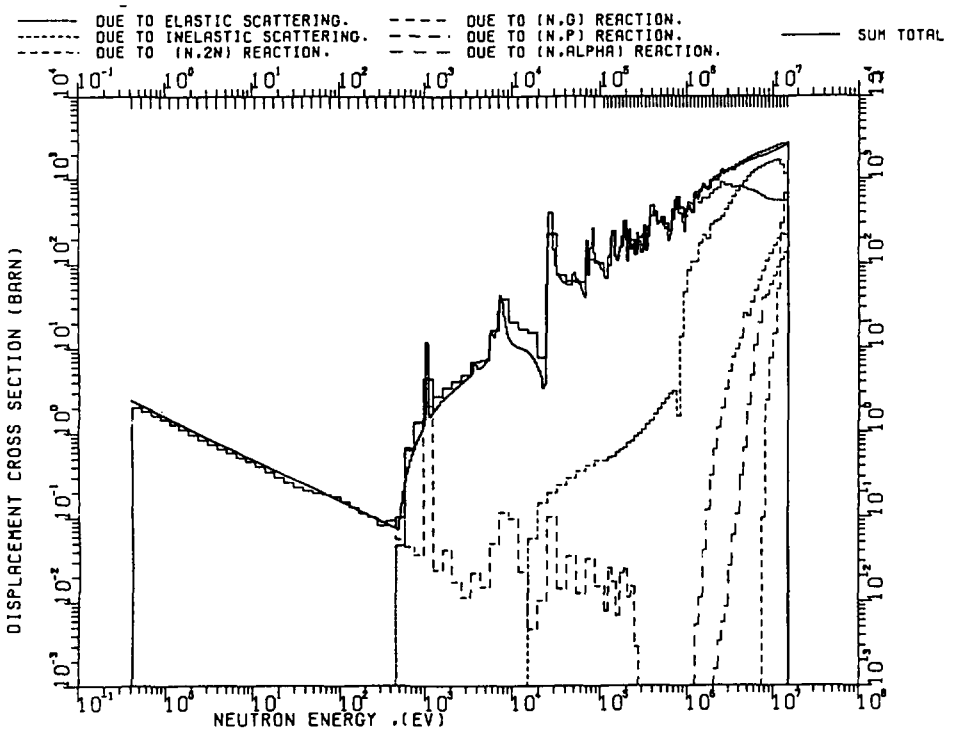

Fig. 7 Displacement cross sections of Fe as calculated by using JENDL-3T with contributions from each reaction. Total cross section is compared with ASTM standard given in finer group structure.

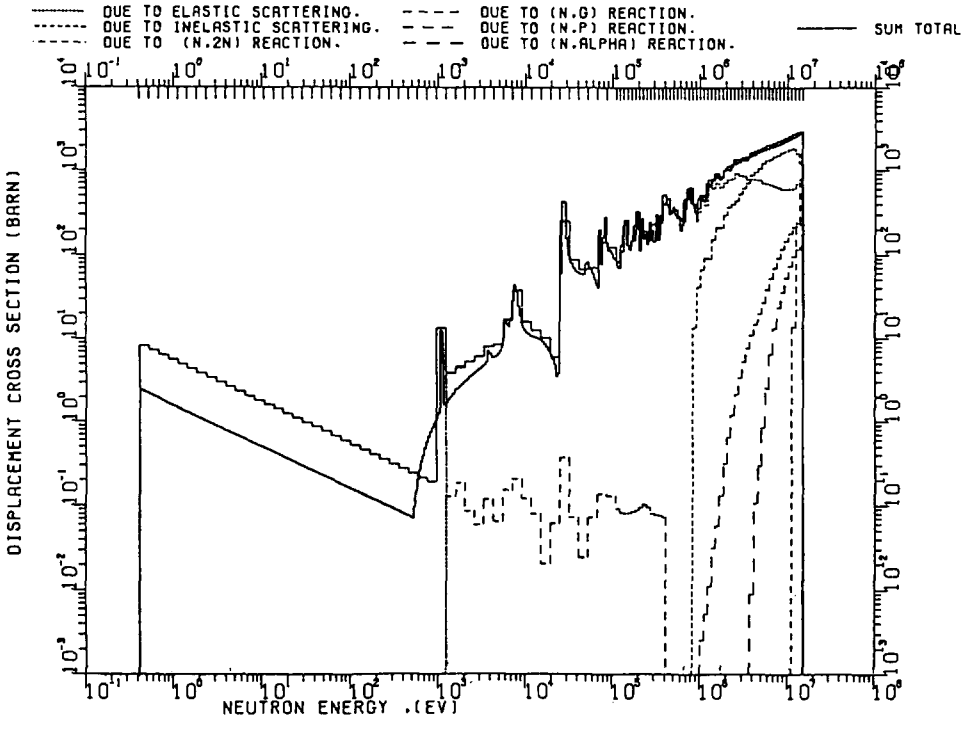

Fig. 8 Displacement cross sections of Fe as calculated by using ENDF/B-IV with contributions from each reaction. Total cross section is compared with ASTM standard given in a finer group structure.

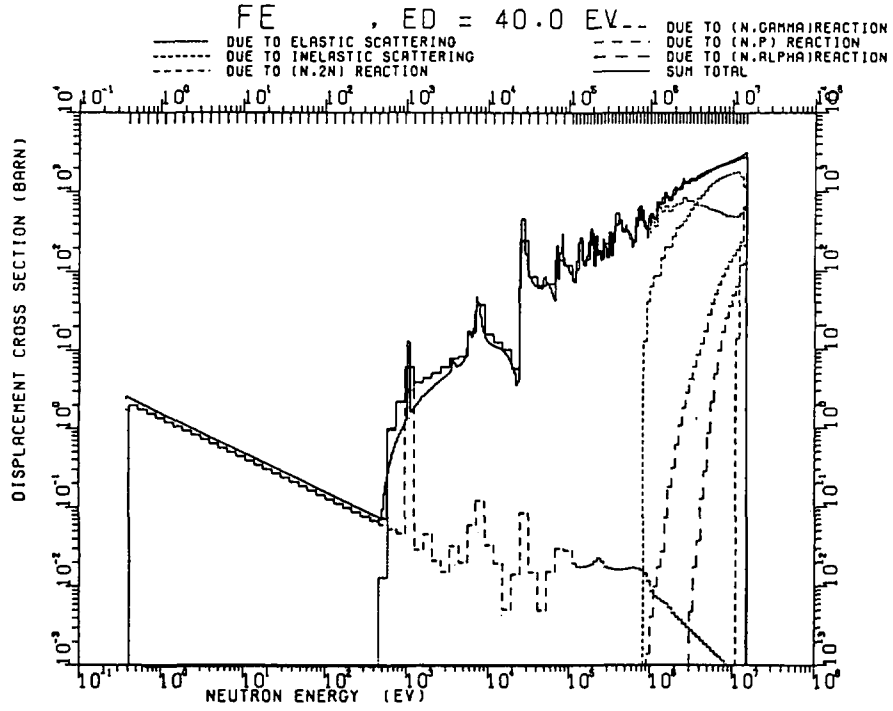

Fig. 9 Displacement cross sections of Fe obtained by using TENJIN2 code and ENDF/B-IV. Total cross section is compared with ASTM standard given in a finer group structure.

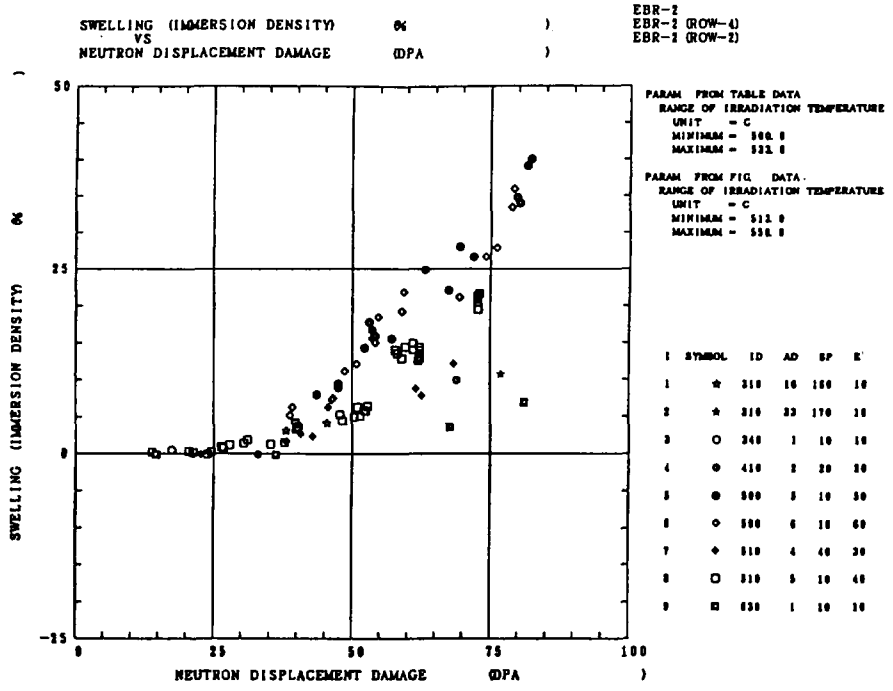

Fig. 10 Example of data retrieval from the data base for illustrating the radiation effects data as a function of dpa. Each data point is related to cited paper ID, data group AD in the paper, specimen and experiment condition, SP, E.

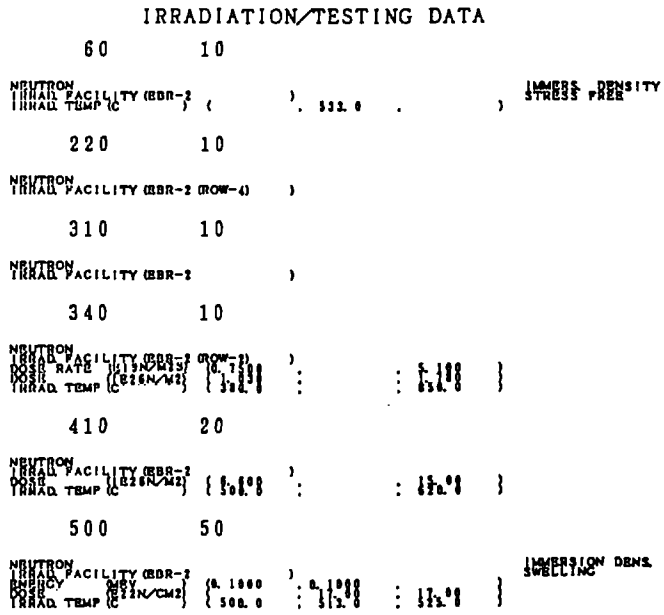

Fig. 11 Example of data retrieval from the data base, related to data given in Fig. 10 for experimental conditions.

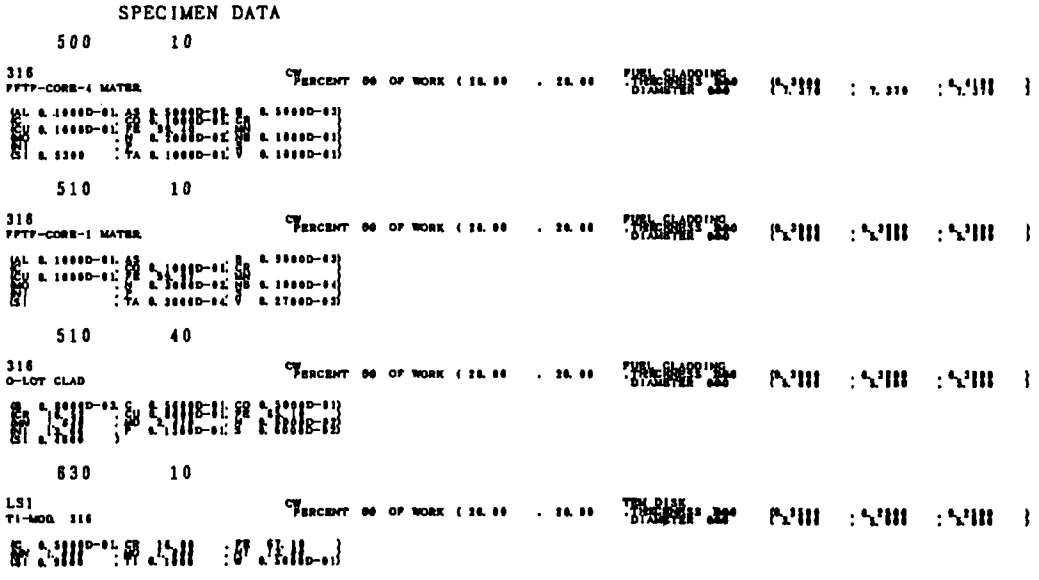

Fig. 12 Example of data retrieval from the data base, related to data given in Fig. 10 for specimen conditions.

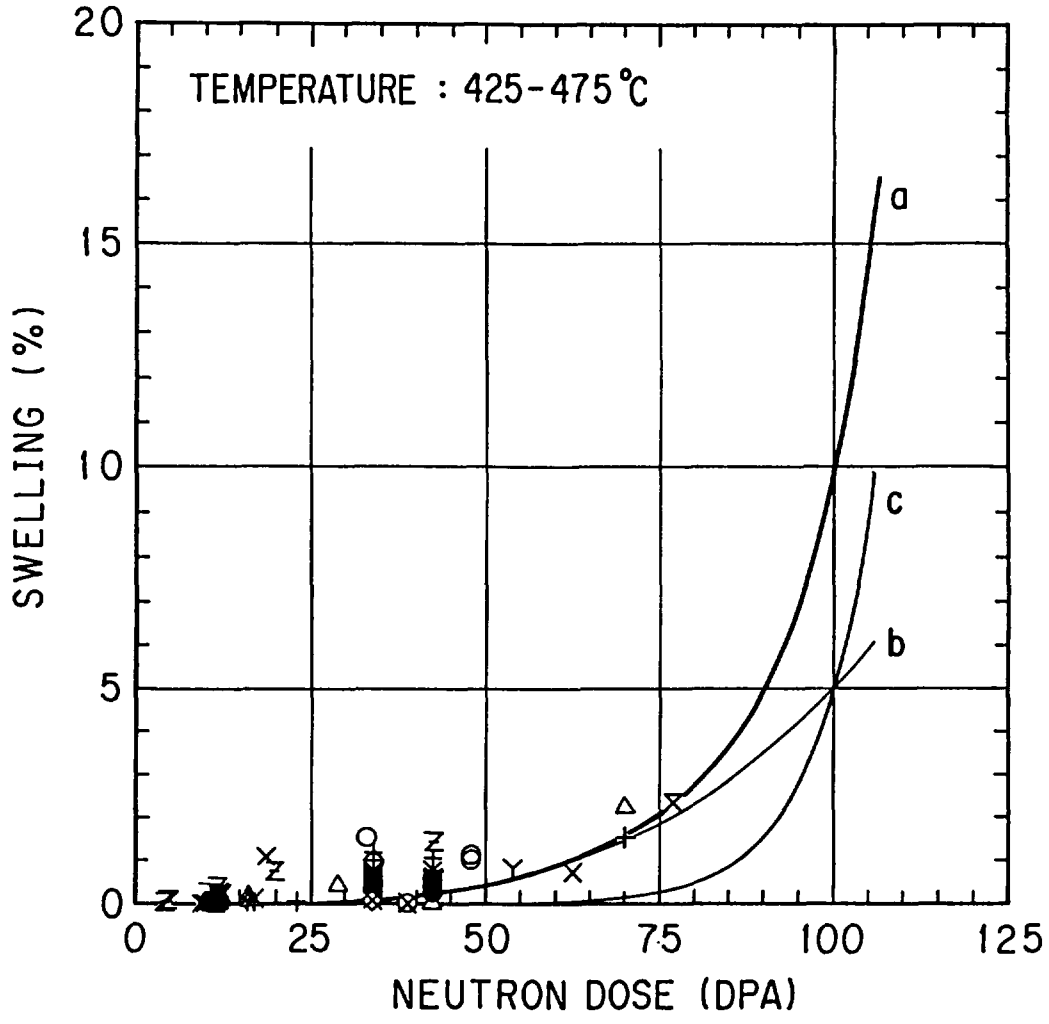

Fig. 13 Example of finding a fitting equation curve describing swelling as a function of dpa.

国際単位系 (SI) と換算表

表 1　SI 基本単位および補助単位

量	名称	記号
長さ	メートル	m
質量	キログラム	kg
時間	秒	s
電流	アンペア	A
熱力学温度	ケルビン	K
物質量	モル	mol
光度	カンデラ	cd
平面角	ラジアン	rad
立体角	ステラジアン	sr

表 2　SI と併用される単位

名称	記号
分，時，日	min，h，d
度，分，秒	°，′，″
リットル	l，L
トン	t
電子ボルト	eV
原子質量単位	u

1 eV = 1.60218 × 10^{-19} J

1 u = 1.66054 × 10^{-27} kg

表 5　SI 接頭語

倍数	接頭語	記号
10^{18}	エクサ	E
10^{15}	ペタ	P
10^{12}	テラ	T
10^{9}	ギガ	G
10^{6}	メガ	M
10^{3}	キロ	k
10^{2}	ヘクト	h
10^{1}	デカ	da
10^{-1}	デシ	d
10^{-2}	センチ	c
10^{-3}	ミリ	m
10^{-6}	マイクロ	μ
10^{-9}	ナノ	n
10^{-12}	ピコ	p
10^{-15}	フェムト	f
10^{-18}	アト	a

表 3　固有の名称をもつ SI 組立単位

量	名称	記号	他の SI 単位による表現
周波数	ヘルツ	Hz	s^{-1}
力	ニュートン	N	m·kg/s^2
圧力，応力	パスカル	Pa	N/m^2
エネルギー，仕事，熱量	ジュール	J	N·m
工率，放射束	ワット	W	J/s
電気量，電荷	クーロン	C	A·s
電位，電圧，起電力	ボルト	V	W/A
静電容量	ファラド	F	C/V
電気抵抗	オーム	Ω	V/A
コンダクタンス	ジーメンス	S	A/V
磁束	ウェーバ	Wb	V·s
磁束密度	テスラ	T	Wb/m^2
インダクタンス	ヘンリー	H	Wb/A
セルシウス温度	セルシウス度	℃	
光束	ルーメン	lm	cd·sr
照度	ルクス	lx	lm/m^2
放射能	ベクレル	Bq	s^{-1}
吸収線量	グレイ	Gy	J/kg
線量当量	シーベルト	Sv	J/kg

表 4　SI と共に暫定的に維持される単位

名称	記号
オングストローム	Å
バーン	b
バール	bar
ガル	Gal
キュリー	Ci
レントゲン	R
ラド	rad
レム	rem

1 Å = 0.1 nm = 10^{-10} m

1 b = 100 fm^2 = 10^{-28} m^2

1 bar = 0.1 MPa = 10^5 Pa

1 Gal = 1 cm/s^2 = 10^{-2} m/s^2

1 Ci = 3.7 × 10^{10} Bq

1 R = 2.58 × 10^{-4} C/kg

1 rad = 1 cGy = 10^{-2} Gy

1 rem = 1 cSv = 10^{-2} Sv

(注)

1. 表 1　5 は「国際単位系」第 5 版，国際度量衡局 1985 年刊行による。ただし，1 eV および 1 u の値は CODATA の 1986 年推奨値によった。
2. 表 4 には海里，ノット，アール，ヘクタールも含まれているが日常の単位なのでここでは省略した。
3. bar は，JIS では流体の圧力を表わす場合に限り表 2 のカテゴリーに分類されている。
4. EC 閣僚理事会指令では bar，barn および「血圧の単位」mmHg を表 2 のカテゴリーに入れている。

換　算　表

力	N(=10^5 dyn)	kgf	lbf
	1	0.101972	0.224809
	9.80665	1	2.20462
	4.44822	0.453592	1

粘度　1 Pa·s(N·s/m^2) = 10 P(ポアズ)(g/(cm·s))

動粘度　1 m^2/s = 10^4 St(ストークス)(cm^2/s)

圧力	MPa(=10 bar)	kgf/cm^2	atm	mmHg(Torr)	lbf/in^2(psi)
	1	10.1972	9.86923	7.50062 × 10^3	145.038
	0.0980665	1	0.967841	735.559	14.2233
	0.101325	1.03323	1	760	14.6959
	1.33322 × 10^{-4}	1.35951 × 10^{-3}	1.31579 × 10^{-3}	1	1.93368 × 10^{-2}
	6.89476 × 10^{-3}	7.03070 × 10^{-2}	6.80460 × 10^{-2}	51.7149	1

エネルギー・仕事・熱量	J(=10^7 erg)	kgf·m	kW·h	cal(計量法)	Btu	ft·lbf	eV
	1	0.101972	2.77778 × 10^{-7}	0.238889	9.47813 × 10^{-4}	0.737562	6.24150 × 10^{18}
	9.80665	1	2.72407 × 10^{-6}	2.34270	9.29487 × 10^{-3}	7.23301	6.12082 × 10^{19}
	3.6 × 10^6	3.67098 × 10^5	1	8.59999 × 10^5	3412.13	2.65522 × 10^6	2.24694 × 10^{25}
	4.18605	0.426858	1.16279 × 10^{-6}	1	3.96759 × 10^{-3}	3.08747	2.61272 × 10^{19}
	1055.06	107.586	2.93072 × 10^{-4}	252.042	1	778.172	6.58515 × 10^{21}
	1.35582	0.138255	3.76616 × 10^{-7}	0.323890	1.28506 × 10^{-3}	1	8.46233 × 10^{18}
	1.60218 × 10^{-19}	1.63377 × 10^{-20}	4.45050 × 10^{-26}	3.82743 × 10^{-20}	1.51857 × 10^{-22}	1.18171 × 10^{-19}	1

1 cal = 4.18605 J (計量法)
= 4.184 J　(熱化学)
= 4.1855 J　(15 °C)
= 4.1868 J (国際蒸気表)

仕事率　1 PS (仏馬力)
= 75 kgf·m/s
= 735.499 W

放射能	Bq	Ci
	1	2.70270 × 10^{-11}
	3.7 × 10^{10}	1

吸収線量	Gy	rad
	1	100
	0.01	1

照射線量	C/kg	R
	1	3876
	2.58 × 10^{-4}	1

線量当量	Sv	rem
	1	100
	0.01	1

(86 年 12 月 26 日現在)

WANG DAPAI, PH.D.
NUCLEAR DATA SECTION
- IAEA